Immunomodulatory effects of distinct bioactive lipid groups on T lymphocytes within the obesity-induced inflammatory microenvironment

by

Salih Kucuk

A thesis submitted to the University of Birmingham for the degree of

DOCTOR OF PHILOSOPHY

Institute of Inflammation and Ageing

College of Medical and Dental Sciences

University of Birmingham

August 2023

UNIVERSITY OF
BIRMINGHAM

University of Birmingham Research Archive

e-theses repository

This unpublished thesis/dissertation is copyright of the author and/or third parties. The intellectual property rights of the author or third parties in respect of this work are as defined by The Copyright Designs and Patents Act 1988 or as modified by any successor legislation.

Any use made of information contained in this thesis/dissertation must be in accordance with that legislation and must be properly acknowledged. Further distribution or reproduction in any format is prohibited without the permission of the copyright holder.

Abstract

Diet-induced obesity (DIO) is a global pandemic with an increasing trend in all age groups around the world. Overconsumption of energy dense obesogenic diets, with a high fat content, induce and escalate obesity-linked low grade chronic inflammatory microenvironment (OIIM). The OIIM is one of the main immune dysfunctions which induces and contributes to many obesity-associated diseases such as cardiovascular diseases, type-II diabetes and autoimmune diseases. Distinct bioactive fatty acids (FAs): palmitate and stearic acid, found within the high fat diet, augment the OIIM via their pro-inflammatory immunomodulatory effects. This pro-inflammatory biasing immunomodulation by bioactive FAs can lead to functional, epigenetic, developmental and migratory cellular modulations. Considering the critical contributions of T cells to OIIM, we have investigated the OIIM at two different stages by using early-DIO (3-weeks) and fully established-DIO (14-weeks) models. The aim of this thesis was to investigate the critical immunomodulatory potential of bioactive lipid groups that could potentially both alleviate or aggravate the OIIM.

WD-feeding in early-DIO model illustrated a profound bias towards pro-inflammatory Th17 phenotype with a codominant reduction of anti-inflammatory regulatory T cells which are key modulators of OIIM. Importantly, omega-3 supplementation into obesogenic WD significantly reverted the obesity-induced distortion in Th17/Treg balance and alleviated the OIIM.

Furthermore, consistent with the background literature, 14-week HFD-feeding in an fully-established DIO model was shown to induce a profound elevation towards pro-inflammatory $CXCR3^+$ and LFA-1^+ $CD44^+$ EM $CD4^+$ T populations compared to CD control. Interestingly, introduction of dieting and weight loss (WGWL model), illustrated the same exacerbated potential for the expansion of pro-inflammatory EM populations even after the weight loss. This preserved HFD-driven priming phenotype was further associated with epigenetic alterations driven by bioactive saturated-FAs. Importantly, utilisation of *in vitro* experiments further identified the potential functional alterations including autophagy and senescence which are associated with the epigenetically modified genes STK26 and CDKN1C. Altogether this work identified various obesogenic diet-derived bioactive lipid inducing DIO-linked alterations on distinct T cell populations that prone a persistent pro-inflammatory phenotype inducing the OIIM pathophysiology.

Dedication

To Mine Ağdıran

July 1963- June 2014

Acknowledgements

Firstly, I would like to thank all of my supervisors: Prof. Simon W. Jones, Dr. Jorge Caamano and Prof. Claudio Mauro for their support and guidance during my PhD. However, a special thanks goes to my main supervisor and mentor Prof. Mauro for believing in me from beginning, always being open minded and always providing me the opportunity to become a better scientist. It has been a true inspiration to work with him who taught me that scientific research is a journey, whilst you are climbing towards your next challenge, you always should look back and appreciate how far you've come.

Additionally, I would also like to thank to Dr Jennifer Niven for her kind guidance, help, and endless support, including her incredible flow cytometry skills in which she kindly supervised me and taught me that there is no such thing as too many controls. Dr Niven has always motivated (stressed me) and pushed me to be better scientist, for whom I will be always thankful for everything she taught me thought my PhD .

Another special thanks goes to Dr Michelangelo Certo for always being there and guiding me to become a better scientist. Along so many other things, Dr Certo has always supported me with his excellent figure illustration and lab skills but I would like to specially thank him for his wise advice in both lab and life which always turn out to be true (*$p<0.05$). Grazie mille per tutto! I also owe massive thanks to Dr. Abdullah M.A. Alghamdi (T.B.C.) whom has been no better than a brother for me in the lab and UoB. I would like to greatly thank him for generously sharing all of his extensive knowledge on human $CD4^+$ T cells and single-gene mutations. He was simply a source of energy throughout my PhD. I will miss our deep conversations!

Another special thanks goes to another special person Miss Chloe Lockwood for everything she did to help me within a year that made this possible. She has always been an endless source of motivation and encouragement, such as believing in me that I can write 50,000 words and then also believing that I can cut 20,000 words in a week.

I would also like to thank all the past and present members of the Mauro lab especially Dr. Alba Llibre and Miss Atrayee Gope, for their contributions and support throughout my PhD project. I am also grateful for all the support and kindness I received from members of both lab 3 and 1 whom made this journey enjoyable. Specifically, I would like to thank to Dr. Sally

Clayton and Dr. John O'Neil for always being around and kindly helping me. Also to Dr. Hussein Farah for always being there by rescuing me from countless times of stress/panic and providing endless encouragement and moral support. I am greatly thankful for Mr Mohammad Alqahtani's kind, helpful support whom taught me a lot in blood processing and tissue culture.

Finally, I would like to thank to my whole family specially my father and aunties whom brought me up to this day with their endless support and also would like to specifically "thank" to my sister KK for always being herself and KKing around.

It was an honour to work along these inspirational people. Lastly, I would like to my funders the Centre for Musculoskeletal Ageing Research (CMAR) for their support.

Table of Contents

Abstract ..... **II**

Dedication ..... **III**

List of Figures ..... **XI**

List of Tables ..... **XVII**

Publications ..... **XVIII**

Abbreviations ..... **XIX**

Chapter 1) INTRODUCTION **1**

1. Obesity *1*

1.1. Biological hallmarks of obesity *1*

1.2. Obesity-associated diseases *3*

1.3. Role of obesogenic diets on obesity and its comorbidities *5*

1.4. Lipotoxicity: Linking high fat intake to obesity associated pathophysiology *7*

1.5. Fatty acids *7*

1.5.1 Saturated fatty-acids 8

1.5.1.1 Palmitic acid (PA) 8

1.5.1.2 Stearic Acid (STE) 10

1.5.2 Unsaturated fatty-acids 10

1.5.2.1 Monounsaturated FA: Oleic acid (OA-OLE) 11

1.5.2.2 Polyunsaturated FAs: Omega-3 (ω−3) & Omega-6 (ω−6) 12

1.6. Complex bioactive lipids- Sphingolipids *14*

1.6.1. Ceramides 14

1.6.1.1 Ceramide biosynthesis and metabolism 15

1.6.1.2. Interventions to ceramide biosynthesis 17

1.6.1.2.1. Myriocin 18

1.6.1.2.2. Fingolimod (FTY720) 18

1.6.1.2.3. Fumonisin b_1 (FB_1) 20

1.6.1.3. Molecular actions of bioactive ceramides 22

1.7. Immune cells involved in obesity-induced inflammatory microenvironment (OIIM) *26*

1.7.1. Adaptive immune system 27

1.7.1.1. T cells 27

1.7.1.1.1. $CD4^+$ T cell origins and development 28

1.7.1.1.2. $CD4^+$ T cell activation 29

1.7.1.1.3. $CD4^+$ TCR signalling pathways 30

1.7.1.1.4 Differentiation of $CD4^+$ T cell into effector lineages 31

1.7.1.1.4.1. Th1 31

1.7.1.1.4.2. Th2 32

1.7.1.1.4.3. Th17 33

1.7.1.1.4.4. Regulatory T cells (Tregs) 34

1.8. Immunomodulatory actions of bioactive lipids on $CD4^+$ T cells *36*

1.8.1. Palmitic (PA) and Stearic (STE) SFAs 36

1.8.2. Oleic acid (OA) MUFA 38

1.8.3. Omega-3 (ω−3) PUFA 38

1.8.4. Ceramides 40

1.8.4.1 Immunomodulatory actions of ceramides on $CD4^+$ T cell differentiation 42

Chapter 2) MATERIALS AND METHODS 44

Materials 44

2.1 In vivo murine diet experiments 44

2.2 In vitro cell culturing 44

2.3 Flow cytometry 47

2.4 RNA isolation and RT-qPCR 50

2.5 Western blotting 50

2.6 ELISA 51

Methods 52

2. 7 In vivo diet experiments 52
2.7.1 3-week early DIO omega-3 supplementation murine models 52
2.7.2 FTY720 inhibitor on 3-week early DIO murine model 54
2.7.3 14-week DIO weight-gain weight-loss (WGWL) murine model 54
2.7.4 Murine tissue collection and processing 54
2.7.4.1 Murine fat tissue digestion and lymphocyte isolation 54
2.7.4.2 Murine secondary lymphoid organ tissue digestion and lymphocyte isolation 55

2.8 Isolation of ex vivo CD4⁺ T cells from murine and human samples 55
2.8.1 Isolation of mouse CD4⁺ T cells from the SLO lymphocytes 55
2.8.2 Isolation of human CD4⁺ T cells from human PBMCs 56

2. 9 In vitro experimental protocols 57
2.9.1 Primary cell culture conditions 57
2.9.2 *In vitro* ceramide treatment of murine and human CD4⁺ T cells 58
2.9.2.1 Solubilisation of ceramides 58
2.9.2.2 Ceramide treatment during *in vitro* CD4⁺ T cell differentiation 58
2.9.3 In vitro time-course activation of human CD4⁺ T cells pre-treated with ceramides 60
2.9.4 Overnight lipid pre-treatment of human CD4⁺ T cells *in vitro* with palmitic, stearic and oleic acid .. 60
2.9.4.1 Solubilisation and optimisation of lipotoxicity of palmitic, stearic and oleic acid lipids 61
2.9.4.2 Overnight lipid pre-treatment of human CD4⁺ T cells *in vitro* 61

2.10 RNA isolation and cDNA synthesis 62

2.11 Real time quantitative PCR (RT-qPCR) 63

2.12 Western blotting 64

2.13 Lipidomics analysis 65

2.14 Flow cytometry 66
2.14.1 Extracellular staining 66
2.14.2 Intracellular staining (ICS) 66
2.14.3 Annexin and PI staining 67
2.14.4 Autophagy LC3-II detection by flow cytometry 67
2.14.5 Flow cytometry controls 68

2.15 Enzyme-Linked Immunosorbent Assays (ELISA) 69

2.16 Epigenetic analysis on differential methylation 70

2.17 Data handling and statistics 71

Chapter 3) Omega 3 supplementation can ameliorate the OIIM in an early-DIO murine model 72

3.1. Introduction 72
3.1.1. Effector T cell populations in OIIM 74
3.1.2. Obesity-associated T cell exhaustion and senescence 75
3.1.3. Aims and hypotheses 76

Results ... *77*

3.2. Optimisation of the alloimmunisation protocol for the in vivo diet experiments ... *77*

3.3. Characterising the effects of different obesogenic diets and n-3PUFA supplementation on the CD4⁺ T lymphocyte populations ... *79*

3.4. WD induced pro-inflammatory alterations in the memory CD4⁺ T lymphocyte populations ... *82*

3.5. Dissecting the alterations in specific effector CD4⁺ T helper cell subsets induced by WD and ω−3 supplementation ... *86*

3.6. Investigating the pro-inflammatory effects of WD and homeostatic effects of n-3PUFA on CD8⁺ T lymphocytes in OIIM ... *91*

3.7. Dissecting the alterations in specific cytotoxic CD8⁺ T lymphocyte subsets induced via WD and ω−3 supplementation ... *95*

3.8. n-3PUFA supplementation to the WD 'boosts' the anti-inflammatory CD4⁺ and CD8⁺ Foxp3⁺ Treg population frequencies in vivo ... *99*

3.9. Discussion ... *103*

Chapter 4) Bioactive C24 biases Foxp3⁺ Treg differentiation towards pro-inflammatory RORγt⁺ Th17 fate in both *in vivo* and *in vitro* models ... **108**

4.1. Introduction ... *108*
4.1.1 The delicate balance between Treg/Th17 CD4⁺ T cell differentiation ... 108
4.1.2 Pro-inflammatory immunomodulatory potentials of ceramides on CD4⁺ T cells ... 111
4.1.3 Aims and hypotheses ... 112

Results ... *113*

4.2. N-3PUFA supplementation to diet reduces the WD-induced ceramide synthesis and concentration in 3-week early DIO murine model ... *113*

4.3. Pharmacological inhibition of CerS2 reduced the C24 synthesis without alleviating the WD-induced effector memory phenotype ... *117*

4.4. Pharmacological inhibition of C24 synthesis boosted Foxp3⁺ Treg populations in SLOs ... *123*

4.5. Optimisation of ceramide lipotoxicity on murine and human CD4⁺ Treg polarisation in vitro models ... *129*

4.6. C24 ceramide directly interferes with Foxp3⁺ Treg differentiation of both murine and human CD4⁺ T cells ... *132*

4.7. C24 ceramide induces the secretion of Th17 effector CD4⁺ T cell fate specific IL-17 and reduces IL-10 cytokine secretion ... *137*

4.8 In vitro supplementation of omega-3 to the ceramide treated CD4⁺ T cells did not ameliorate the pro-inflammatory effect of C24 ... *144*

4.9 Bioactive C24 alone is not responsible for the WD-induced cellular senescence on CD4⁺ T cells ... *147*

4.10 Potential molecular mechanisms underpinning the pro-inflammatory immunomodulation of C24 against CD4+ Treg fate and biasing towards RORγt+ Th17 ... *149*

4.11 Discussion ... *158*
4.11.1 *In vivo* inhibition of C24 alleviated the Th17/Treg CD4⁺ T cell balance ... 158
4.11.2 *In vitro* C24 treatment enhanced the RORγt⁺ Th17 differentiation with concomitant inhibition of Foxp3⁺ Treg differentiation of naïve human and murine CD4⁺ T cells ... 161
4.11.3 Secretory profile and capacity of *in vitro* C24 treated CD4⁺ T cells ... 161
4.11.4 Molecular mechanism of bioactive C24 inducing Th17 differentiation ... 162
4.10.5 Systemic effect of n-3PUFA supplementation ... 164
4.11.6 Limitations and additional experimental plans ... 165

Chapter 5) HFD-induced long-lasting epigenetic changes alters the autophagy and senescence in EM T cells of formerly obese mouse model 167

5.1. Introduction 167
5.1.1 Bioactive lipid groups 168
5.1.2 Autophagy in T cells under obese conditions 170
5.1.3 Senescence in obesity pathophysiology 173
5.1.4 Aims and hypothesis 174

Results 175

5.2. Establishment and characterisation of the in vivo 14-week HFD fed DIO murine model T lymphocytes 175

5.3. HFD induces a persistent bias in CD4⁺ T cell differentiation towards pro-inflammatory effector memory subset 178

5.4. HFD-induced past history of obesity primes the differentiation of CD4⁺ T cells towards CXCR3⁺- LFA-1⁺ pro-inflammatory effector memory phenotype 183

5.5 HFD-induced alterations in distinct effector CD4⁺ and cytotoxic CD8⁺ T cell subsets 189

5.6. Exogenous in vitro exposure of bioactive saturated fatty acids recapitulates the HFD-induced pro-inflammatory effector memory bias in human CD4⁺ T cells 190

5.7. HFD promotes epigenetic modification of critical genes that may underpin the long-lasting bias in pro-inflammatory effector memory phenotype 196

5.8. Hypomethylation of STK26 and CDKN1C by HFD-derived bioactive PA and STE induces elevation of gene expression and protein levels 199

5.9. Potential functional cellular alterations on T lymphocytes associated with HFD-driven hypomethylation-linked upregulation of STK26 and CDKN1C 207
5.9.1. Modulations in autophagy flux capacity within *ex vivo* murine CD4 T cells isolated from SLOs of different diet groups 207
5.9.2 Modulations in autophagy flux capacity within *in vitro* lipid treated human CD4⁺ T cells 209
5.9.3. Modulations in cellular senescence of *ex vivo* murine and *in vitro* human CD4⁺ T cells 212

5.10. Discussion 218
5.10.1 Potential molecular mechanisms and drivers of the obesogenic memory phenotype in T lymphocytes 222
5.10.2 Bioactive SFAs can recapitulate the HFD-induced alterations in cellular functions linked with STK26 and CDKN1C 224

Chapter 6) DISCUSSION 227

6.1. Addressing the hypotheses and overall findings 227

6.2 Ceramides and n-3PUFA as active mediators of T cell lineage plasticity 230

6.3 Potential molecular links between bioactive C24 and n-3PUFA in mediating the Th17/Treg balance 232

6.4 Proposed model of C24-driven Th17 differentiation under DIO conditions and outstanding questions .. 234

6.5 Experimental limitations and future work 236
6.5.1 Limitations of *in vivo* DIO murine models 237
6.5.1.1 Sexual dimorphism in DIO models 237
6.5.1.3 Time of recovery in the WGWL DIO murine models 238
6.5.2 Limitations of *in vitro* lipid treatment of CD4⁺ T cells 239
6.5.2.1 Human leukocytes cones 240
6.5.3 Dissecting the functional changes in autophagy and senescence profiles of CD4⁺ T cells following SFA exposure 241
6.5.3.1 Investigating the immunometabolism of T cells following the bioactive lipid treatment 241
6.5.3.2 Autophagy flux capacity 241
6.5.3.3 Senescence profile 242

6.6 Investigating the clinical obese human samples *243*
6.7 Potential crosstalk between autophagy and senescence *244*
6.8 Cellular lipid bilayer membrane order *246*
6.9 Conclusions and implications *247*

REFERENCES **250**

SUPPLEMENTARY MATERIAL **286**

List of Figures

1) **Introduction**		
Figure 1.1)	The hallmarks of obesity	2
Figure 1.2)	Biosynthesis of MUFAs from *De novo* synthesis of FAs	12
Figure 1.3)	Metabolism of Omega fatty acids	13
Figure 1.4)	Sphingolipid metabolism and ceramide biosynthesis pathways.	16
Figure 1.5)	Conventional inhibitors used to inhibit the *de novo* ceramide biosynthesis pathway	18
Figure 1.6)	Cellular and molecular mechanisms of bioactive ceramides	23
Figure 1.7)	Schematic representation of T cell activation signalling pathways	30

2) **Materials and Methods**		
Figure 2.1)	Murine splenocyte population CD4% prior to isolation isolated from spleen and LNs and following the $CD4^+$ T cell isolation via Stemcell EasySep kit.	55
Figure 2.2)	Isolation of human naïve $CD4^+$ T cells from fresh human blood cones.	56
Figure 2.3)	Representative flow cytometry gating strategy used for *in vitro* murine $CD4^+$ T cell polarisation analysis	60
Figure 2.4)	Optimisation of cell viability	62
Figure 2.5)	Working principles of Guava LC3-II autophagy detection kit	68
Figure 2.6)	Full spectrum of BD LSR Fortessa X-20 flow cytometry with 4-laser setup	69
Figure 2.7)	Experimental schematic of the RRBS sequencing of $CD4^+$ T cells isolated from 14-week DIO murine models	71

3) **Dietary omega-3 can ameliorate the OIIM in an early-DIO murine model**		
Figure 3.1)	Representative flow cytometry plots of main gating strategy for population of interests in the optimisation trial for the allogeneic injection via i.p	78
Figure 3.2)	Allogeneic splenocyte injection via i.p induced polyclonal T cell response and established T cell memory in a dose-dependent manner	79
Figure 3.3)	Different diets tested did not alter body weight of mice groups throughout the extent of the experiment	80
Figure 3.4)	Representative flow cytometry gating strategy used as the main gating throughout the experiment.	80
Figure 3.5)	Effect of different diets on total live $CD4^+$ and $CD8^+$ T cell populations within SLOs and fat tissues	81

Figure 3.6)	WD and n-3PUFA supplementation alters the distribution of main T cell subsets including naïve, CM and EM populations	83
Figure 3.7)	n-3PUFA supplementation into WD reduces the $CD44^+$, $LFA\text{-}1^+$ and $CD44^+$, $CXCR3^+$ frequencies in pLN	84
Figure 3.8)	n-3PUFA supplementation into WD reduces the pro-inflammatory effector memory phenotype observed in 3-week early DIO murine model	85
Figure 3.9)	WD-induced elevation in pro-inflammatory $CD4^+$ effector T cell subsets can be abrogated via dietary n-3PUFA supplementation	88
Figure 3.10)	WD induces $CD4^+$ T cell exhaustion and senescence in SLOs	90
Figure 3.11)	Dietary n-3PUFA supplementation into WD alleviates the pro-inflammatory T follicular helper populations	91
Figure 3.12)	WD and n-3PUFA supplementation alters the distribution of main T cell subsets including naïve, CM and EM populations in SLOs and fat tissues	93
Figure 3.13)	n-3PUFA supplementation into WD reduces the pro-inflammatory cytotoxic memory $CD8^+$ T cell population frequencies in 3-week early DIO murine model	95
Figure 3.14)	Obesogenic diets and n-3PUFA supplementation did not altered cytotoxic $CD8^+$ T cell subsets in 3-week early DIO murine model	97
Figure 3.15)	n-3PUFA supplementation into WD ameliorated the WD-induced elevation $CD8^+$ Tfh population	99
Figure 3.16)	Representative flow cytometry plots showing the gating and modulation on Treg population between CD and WD+n-3PUFA groups.	100
Figure 3.17)	n-3PUFA supplementation boosts the $Foxp3^+$ $CD4^+$ Treg populations within SLOs and fat tissue	101
Figure 3.18)	n-3PUFA supplementation into WD increases $Foxp3^+$ $CD8^+$ Treg populations within spleen and mLN tissues	102

4) <u>Bioactive C24 biases $Foxp3^+$ Treg differentiation towards pro-inflammatory $ROR\gamma t^+$ Th17 fate in both *in vivo* and *in vitro* models</u>		
Figure 4.1)	Representation of the classical molecular pathways regulating the fragile balance of Th17 and Treg differentiation	110
Figure 4.2)	n-3PUFA supplementation attenuate the WD-induced elevation thein pro-inflammatory associated ceramides	115
Figure 4.3)	Effect of WD and n-3PUFA+WD diets on distinct ceramide species detected in fat tissues and plasma	117
Figure 4.4)	The ceramide synthase 2 (CerS2) inhibitor FTY720 reduces plasma ceramide concentration in plasma	118

Figure 4.5)	Effect FTY720 inhibitor on total live $CD4^+$ and $CD8^+$ T cell populations within SLOs and fat tissues	120
Figure 4.6)	Pharmacological inhibition of CerS2 via FTY720 did not attenuate the WD-induced distribution of memory $CD4^+$ T cell subsets	121
Figure 4.7)	Pharmacological inhibition of CerS2 via FTY720 did not attenuate the pro-inflammatory effector memory $CD4^+$ T cell phenotype induced by WD	122
Figure 4.8)	CerS2 inhibitor FTY720 attenuates the pro-inflammatory $ROR\gamma t^+$ Th17 $CD4^+$ effector T cell subset in SLOs	124
Figure 4.9)	CerS2 inhibitor FTY720 increases the $Foxp3^+$ and $CD25^+$ $Foxp3^+$ $CD4^+$ Treg populations within the SLOs of WD-fed murine groups	126
Figure 4.10)	CerS2 inhibitor FTY720 increases the BCL-2 expression on the $Foxp3^+$ and $CD25^+$ $Foxp3^+$ $CD4^+$ Treg populations within the SLOs	128
Figure 4.11)	Foxp3 expression of in vitro iTreg differentiated human $CD4^+$ T cells	131
Figure 4.12)	Representative flow cytometry plots of key effector $CD4^+$ T cell lineage-defining transcription factors	133
Figure 4.13)	C24 0.1µM reduces the $Foxp3^+$ Treg differentiation in both murine and human *in vitro* $CD4^+$ T cell Treg differentiation models	134
Figure 4.14)	C24 0.1µM increases the $ROR\gamma t^+$ Th17 differentiation in both murine and human *in vitro* $CD4^+$ T cell Treg differentiation models	136
Figure 4.15)	C24 0.1µM treatment reduces the IL-10 cytokine levels in both murine and human *in vitro* $CD4^+$ Treg differentiation models	138
Figure 4.16)	C24 0.1µM downregulated the $IL\text{-}10^+$ Treg population in human *in vitro* $CD4^+$ T cell Treg differentiation model	139
Figure 4.17)	C24 0.1µM treatment increases the IL-17A cytokine levels in both murine and human *in vitro* $CD4^+$ Treg differentiation models	140
Figure 4.18)	C24 0.1µM reduces the $IL\text{-}13^+$ Th2 population in human *in vitro* $CD4^+$ T cell Treg differentiation model	141
Figure 4.19)	Exogenous ceramide treatment illustrated no modulatory effect on IFNγ expression within murine $CD4^+$ T cell Treg differentiation model	143
Figure 4.20)	EPA supplementation down regulates the C24-induced RORγt expression in human $CD4^+$ T cells under in vitro Treg differentiation conditions	145
Figure 4.21)	Effect of 3-week WD and n-3PUFA supplementation on the gene expression of ceramide biosynthesis enzymes, CerS2, 5 and 6 in murine fat tissue	147
Figure 4.22)	Exogenous *in vitro* C24 treatment shows no effect on cellular senescence of human $CD4^+$ T cells under Treg differentiation conditions	148
Figure 4.23)	*In vitro* C24 treatment does not affect the early proximal signalling components of TCR signalling	150

Figure 4.24)	*In vitro* C24 treatment reduces the downstream components of TCR signalling in human $CD4^+$ T cells	151
Figure 4.25)	Exogenous C24 0.1μM increases the CD39, STAT-3 and HIF-1α expression within the human *in vitro* $CD4^+$ T cell Treg differentiation models	153
Figure 4.26)	Representative flow cytometry plots of key effector $CD4^+$ T cell lineage-defining transcription factors in human $CD4^+$ T cells under Treg differentiation conditions	154
Figure 4.27)	Representative flow cytometry plots of HIF-1α and RORγt human $CD4^+$ T cell populations $CD4^+$ T cells under *in vitro* Treg differentiation conditions	156
Figure 4.28)	Exogenous C24 0.1μM increases the CD39, STAT-3 and HIF-1 expression specifically within RORγt$^+$ Th17 $CD4^+$ T cells even under Treg differentiation conditions	157

5) HFD-induced long-lasting epigenetic changes alters the autophagy and senescence in EM T cells of formerly obese mouse model		
Figure 5.1)	A schematic of the main canonical autophagy pathway	171
Figure 5.2)	Obesity-driven senescence profile on $CD4^+$ T cells	174
Figure 5.3)	14-week HFD feeding increased the total body weight and fat content in murine model	177
Figure 5.4)	Effects of HFD and HFD-RE (WGWL) on naive $CD4^+$ T cell populations within SLOs and fat tissues	178
Figure 5.5)	Effects of HFD and HFD-RE (WGWL) on CM $CD4^+$ T cell populations within SLOs and fat tissues	179
Figure 5.6)	Exposure to HFD induces a long-term increase in the $CD4^+$ T cell EM population frequencies	180
Figure 5.7)	Exposure to HFD induces a long-term increase in the $CD8^+$ T cell CM population in pLN of HFD-RE (WGWL) group	182
Figure 5.8)	Exposure to HFD induces an increase in the $CD8^+$ T cell EM population in pLN	183
Figure 5.9)	Representative flow cytometry plots of pLN tissues obtained CD, HFD and HDF-RE groups	185
Figure 5.10)	Exposure to HFD induces a long-term increase in the pro-inflammatory $CXCR3^+$ and LFA-1^+ $CD44^+$ $CD4^+$ T cell EM populations	186
Figure 5.11)	Exposure to HFD induces a long-term increase in the pro-inflammatory $CXCR3^+$ and LFA-1^+ $CD44^+$ $CD8^+$ T cell EM populations	188
Figure 5.12)	HFD feeding induced elevation of Tbet$^+$ Tc1 cytotoxic $CD8^+$ T cell subsets	190
Figure 5.13)	Exogenous SFA (PA and STE) pre-treatment induces elevation of human EM $CD4^+$ T cell population *in vitro*	193
Figure 5.14)	Foxp3^+ Treg population within human $CD4^+$ T cells on 3-day *in vitro* lipid treatment assay	195

Figure 5.15)	Past DIO by 8-weeks of HFD exposure induces a persistent epigenetic alteration in methylation structure of murine $CD4^+$ T cells inducing a long-term reprogramming	197
Figure 5.16)	Past DIO by 8-weeks of HFD exposure induced a persistent hypomethylation of STK26 and CDKN1C within murine $CD4^+$ T cells	198
Figure 5.17)	STK26 gene expression in human and murine $CD4^+$ T cells	200
Figure 5.18)	HFD-feeding increases the STK26 protein levels within pLN tissues of the 14-wk DIO murine model	201
Figure 5.19)	STK26 mRNA expression within human $CD4^+$ T cells on 3-day *in vitro* lipid pre-treatment assay	202
Figure 5.20)	Palmitate pre-treatment of human $CD4^+$ T cell *in vitro* induces upregulation of STK26 protein	204
Figure 5.21)	CDKN1C ($p57^{KIP2}$) gene expression in human $CD4^+$ T cells	205
Figure 5.22)	CDKN1C mRNA expression within human $CD4^+$ T cells on 3-day *in vitro* lipid pre-treatment assay	206
Figure 5.23)	Exposure to HFD induces a long-term increase in the autophagy flux within the EM $CD4^+$ T cell populations of formerly obese mice group	208
Figure 5.24)	Detection of autophagosome-bound intracellular LC3-II within *in vitro* human $CD4^+$ T cells pre-treated with bioactive lipids	210
Figure 5.25)	Donor to donor variance in LC3-II expression within *in vitro* human $CD4^+$ T cells pre-treated with bioactive lipids	211
Figure 5.26)	Expression of exhaustion and senescence markers on SLO $CD4^+$ T cells of 14-week DIO mouse model	213
Figure 5.27)	HFD feeding induced an elevation in senescence markers of EM $CD4^+$ T cell populations	214
Figure 5.28)	In vitro SFA (PA and STE) pre-treatment of human $CD4^+$ T cell phenotype induces an exhaustion and senescence phenotype	216
Figure 5.29)	Secretory phenotype of human $CD4^+$ T cell pre-treated with bioactive *lipids in vitro*	218

6) <u>Discussion</u>		
Figure 6.1)	A schematic of the main outcomes of the 3-week early DIO model with the critical immunomodulatory effects of bioactive lipids	228
Figure 6.2)	A schematic summary of the proposed Th17/Treg differentiation pathways modulated by bioactive C24 in inducing the Th17	229
Figure 6.3)	Obesity-linked factors mediating the fragile Th17/Treg balance	236
Figure 6.4)	Direct alterations of cellular lipid bilayer following the *in vitro* bioactive lipid treatment of human $CD4^+$ T cells	246

Supplementary Material		
Figure S1)	Pharmacological inhibition of CerS2 via FTY720 did not attenuate the WD-induced distribution of memory $CD8^+$ T cell subsets	286
Figure S2)	Pharmacological inhibition of CerS2 via FTY720 did not attenuate the pro-inflammatory effector memory $CD8^+$ T cell phenotype induced by WD	287
Figure S3)	Effect of CerS2 inhibition on senescent T cell populations within SLOs	288
Figure S4)	Representative flow cytometry gating strategy for Annexin V and PI staining.	289
Figure S5)	Survival plots of human and murine $CD4^+$ T cell for assessing the lipotoxicity of ceramides *in vitro* cultures	289
Figure S6)	Validation of AnnexinV/PI assay via Near IR live/dead marker	290
Figure S7)	Effect of exogenous EPA supplementation on the viability of human $CD4^+$ T cell *in* vitro ceramide treatment model	291
Figure S8)	IL-6 cytokine concentrations within *in vitro* C24-treated murine $CD4^+$ T cells under Treg differentiation conditions	291
Figure S9)	Representative flow cytometry plots illustrating the full gating strategy utilised to analyse *in vitro* C24-treated human $CD4^+$ T cells under Treg differentiation condition model	292
Figure S10)	Effects of HFD and HFD-RE (WGWL) on total live $CD4^+$ and $CD8^+$ T cell populations within SLOs and fat tissues	293
Figure S11)	Effects of HFD and HFD-RE (WGWL) on naive $CD8^+$ T cell populations within SLOs and fat tissues	294
Figure S12)	HFD feeding induced alterations in main effector $CD4^+$ T cell subsets	295
Figure S13)	Cell viability of human $CD4^+$ T cells on 3-day *in vitro* lipid treatment assay	296
Figure S14)	Activation status of human $CD4^+$ T cells on 3-day *in vitro* lipid treatment assay with 48hrs of CD3 and CD28 stimulation	297
Figure S15)	IL-2Rα (CD25) mRNA expression within human $CD4^+$ T cells on 3-day *in vitro* lipid treatment assay	298
Figure S16)	Optimisation of autophagy flux detection within mouse splenocytes by quantifying autophagosome -bound intracellular LC3-II via Guava kit	299
Figure S17)	Optimisation of autophagy flux detection within human PBMCs by quantifying autophagosome-bound intracellular LC3-II via Guava kit	301
Figure S18)	Optimisation the dose- and time- response of CQ in autophagy flux detection within human PBMCs by quantifying autophagosome-bound intracellular LC3-II via Guava kit	302

List of Tables

Chapter 1

Table 1.3.1) Macronutrient composition of Western diet (WD), High fat diet (HFD) and Mediterranean diet (MD)
Table 1.5.1) Nomenclature of prominent fatty-acids including their isomer formula as commonly used in the literature
Table 1.6.1) Intervention methods to target the *de novo* ceramide biosynthesis pathways

Chapter 2

Table 2.1.1) DIO *in vivo* murine model
Table 2.2.1) General *in vitro* and *ex vivo* cell culture reagents
Table 2.2.2) $CD4^+$ T cell isolation and activation
Table 2.2.3) Cytokines and stimulants
Table 2.2.4) Bioactive lipid groups
Table 2.3.1) Flow cytometry antibodies used for both *in vivo* and *in vitro* assays
Table 2.4.1) RNA isolation and cDNA synthesis reagents
Table 2.5.1) Western blotting reagents
Table 2.5.2) Western blotting antibodies
Table 2.6.1) ELISA reagents
Table 2.7.1) Nutritional composition of experimental diets
Table 2.9.1) Cell culture seeding densities
Table 2.9.2) CD4+ T cell activation reagents
Table 2.9.3) Cytokines used for the *in vitro* differentiation optimisation experiments
Table 2.10.1) cDNA synthesis reaction cocktail content
Table 2.10.2) cDNA synthesis reaction thermocycler settings
Table 2.11.1) Specific primers designed for the candidate genes identified in the preliminary data.
Table 2.15.1) ELISA dilution factors of the samples

Chapter 5

Table 5.1) Differentially methylated genes between the diet groups
Table 5.2) Differentially methylated genes between HFD-RE vs. CD compared to HFD vs. CD group

Publications

Kucuk, S., Niven, J., Caamano, J., Jones, S. W., Camacho-Muñoz, D., Nicolaou, A., & Mauro, C. (2021). *Unwrapping the mechanisms of ceramide and fatty acid-initiated signals leading to immune-inflammatory responses in obesity*. *The international journal of biochemistry & cell biology*, *135*, 105972. https://doi.org/10.1016/j.biocel.2021.105972

*Camacho-Muñoz, D., *Niven, J., ***Kucuk, S.**, Cucchi, D., Certo, M., Jones, S. W., Fischer, D. P., Mauro, C., & Nicolaou, A. (2022). *Omega-3 polyunsaturated fatty acids reverse the impact of western diets on regulatory T cell responses through averting ceramide-mediated pathways. Biochemical pharmacology*, *204*,115211. https://doi.org/10.1016/j.bcp.2022.115211

*Niven, J., ***Kucuk, S.**, Gope, A., Certo, M., Macchi, C., Wijesinghe, S., Sadaf, A., Sharma-Oates, A.,Chiamaka, C., Cucchi, D.,Smith, J., Scibior-bentkowska, D., Ladoukakis, E., Grundler, F., Mesnage, R., da Silva Xavier, G., Caamano, J., Nicolaou, A., Lord, J., Jones, W. S., Ruscica, M., Jones, N., Makarova, M., Hiwot, G. T., Nedjai, B., Hogan, A., Mauro, C. *Stk26-induced autophagy and cdkn1c-induced senescence crosstalk to maintain CD4+ T cell-mediated inflammatory programs upon weight loss*- Manuscript in preparation.

Abbreviations

Acid sphingomyelinase (ASM)
Adenosine diphosphate (ADP)
Adenosine triphosphate (ATP)
AMP-activated protein kinase (AMPK)
Cardiovascular diseases (CVD)
Central memory (CM)
Chemokine (C-X-C motif) receptor 3 (CXCR3)
Chow diet (CD)
Diet-induced obese (DIO)
Effector memory (EM)
Fatty acids (FA)
Fluorescein isothiocyanate (FITC)
Fluorescence minus one (FMO)
Forkhead box P3 (Foxp3)
Forward scatter (FCS)
G-protein coupled receptor (GPCR)
GATA Binding Protein 3 (GATA-3)
High fat diet (HFD)
Hypoxia-induced factor 1α (HIF-1α)
Immunoreceptor Tyrosine-based activating motifs (ITAM)
Interleukin (IL)
Kawasaki disease (KD)
Killer cell lectin-like receptor subfamily G member 1 (KLRG1)
Lymphocyte function antigen-1 (LFA-1)
Lymphocyte-Specific protein tyrosine Kinase (LCK)
Mammalian target of rapamycin (mTOR)
Mean Fluorescence Intensity (MFI)
Mediterranean diet (MD)
Mesenteric lymph node (mLN)
Monounsaturated FAs (MUFAs)
Multiple Sclerosis (MS)
Nod-like receptor 3 (NLRP3)
Nuclear factor-kappa B (NF-κB)
Obesity-induced inflammatory microenvironment (OIIM)
Oleic acid (OA)
Omega-3 (n-3PUFA)
Palmitic acid (PA)
Perigonadal fat (p.fat)
Peripheral Blood Mononuclear cell (PBMC)
Peripheral lymph node (pLN)
Phorbol 12-myristate 13-acetate (PMA)
Phosphate Buffered Saline (PBS)
Phosphatidylinositol-3-kinase (PI3K)
Polymerase chain reaction (PCR)
Polyunsaturated FAs (PUFAs)
Programmed cell death protein-1 (PD-1)

Protein kinase B (AKT)
Reactive oxygen species (ROS)
Retinoic acid receptor-related orphan receptor gamma-T (RORγt)
Rheumatoid arthritis (RA)
Saturated FAs (SFA)
Secondary lymphoid organs (SLOs)
Signal transducer and activator of transcription-3 (STAT3)
Sphingosine 1-phosphate (S1P)
Stearic Acid (STE)
Subcutaneous fat (s.fat)
T cell receptor (TCR)
T regulatory cells (Treg)
T-box expressed in T cells (T-bet)
Terminally differentiated effector memory (TEMRA)
Toll-like receptor (TLR)
Transcription factors (TF)
Tumour necrosis factor-alpha (TNF-α)
Type 2 Diabetes (T2D)
Western diet (WD)
Zeta-Chain-Associated Protein Kinase 70 (ZAP70)

Chapter 1) INTRODUCTION

1. Obesity

Obesity is one of the major worldwide health concerns of the 21st century. The World Health Organisation (WHO) defines obesity as excessive fat accumulation that poses health risks. The global prevalence of obesity almost tripled between 1975 and 2016 [2]. According to WHO's report (2016), 650 million people (13% of adults) were classified as obese and 1.9 billion (39% of adults) were at risk of obesity, classified as overweight [2]. Epidemiological reports illustrated an increasing prevalence of obesity among children. In 2016, >340 million children (aged 5-19) were reported as overweight or obese, highlighting the undeniable health risks for near future [3, 4].

Obesity aetiology simply, driven by persistent positive energy balance where dietary energy intake exceeds expenditure of the body. However, obesity is a multifactorial disease developing over time through associations with various genetic and environmental factors. Recent researches highlights that the current obesity epidemic is majorly driven by environmental factors such as nutritional-diet, lifestyle, socioeconomic status and industrialisation [5, 6]. Developed countries with sedentary lifestyle and high-calorie diets were shown to suffer more from obesity and obesity-associated diseases [6].

1.1. Biological hallmarks of obesity

Obesity drivers various deleterious alterations in vital cellular functions leading to reduced physiological functionality and increasing the risk of various diseases leading to a reduced life span [7]. It is crucial to identify the hallmarks and the extensive network of pathological sequelae of obesity. Importantly, obesity shares multiple critical hallmarks with other complex pathophysiologies such as ageing and cancer [7, 8]. The main hallmarks of obesity could be summarised as genomic instability, deregulated cellular metabolism/energetics, epigenetic alterations, mitochondrial dysfunction, cellular senescence and low-grade chronic inflammation with altered immunity (**Figure 1.1**).

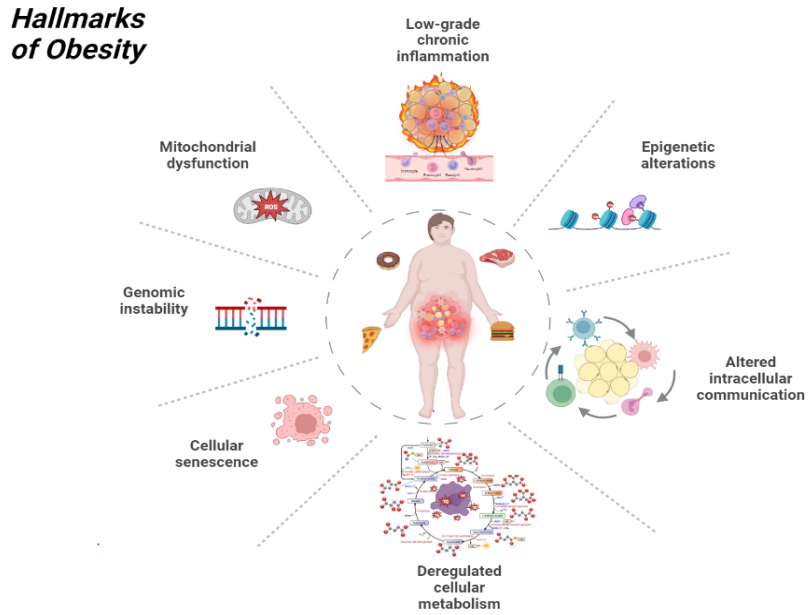


Figure 1.1) The hallmarks of obesity
Seven major hallmarks of obesity have been suggested by the literature; Low-grade chronic inflammation, epigenetic alterations, altered intracellular communication, deregulated cellular metabolism, cellular senescence, genomic instability and mitochondrial dysfunction

Obesity-driven oxidative stress is known to be the main driver of genomic instability in obesity [9]. Oxidation of excessive fatty acids (FAs) creates reactive oxygen species (ROS), leading to oxidative stress-induced DNA damage and decrease antioxidant capacity in the obese microenvironment [10]. Additionally, obese ROS production through glycation is another major mechanism of DNA damage [11]. Interestingly, inflammation mechanisms and ROS production are well known to augment each other. As surplus ROS production is shown to induce inflammatory pathways, inflammatory cells themselves are also shown to contribute to persistent ROS production in adipose tissue– causing the eventual impairment of both DNA and RNA [8, 12].

Mitochondrial dysfunction is another highly important hallmark of obesity. Obesity-induced excessive ROS production has also been shown to increase mitochondrial damage leading to reduced mitochondrial biogenesis, reduced oxidative capacity and increased glucose dependence for energy generation [13, 14]. This obesity-induced mitochondrial dysfunction is correlated with increased cellular apoptosis, low-grade chronic inflammation and metabolic alterations [14].

Dysregulated cellular metabolism and nutrient sensing are two interrelated hallmarks of obesity. Obesity is known to interrupt two major pathways of cellular metabolism; the insulin/insulin-like growth factor signalling (IIS) pathway and the mammalian target of rapamycin (mTOR) signalling pathway. Both of these pathways play crucial roles in multiple

vital cellular functions including: protein synthesis, lipid synthesis, autophagy and mitochondrial biogenesis/metabolism [15, 16]. Any dysregulation of these pathways leads to a deregulated cellular metabolism resulting in major systemic effects on anabolism, reproduction and survival [15, 17]. Obesity is also shown to promote the over-activation of these pathways in adipose tissues leading to hyperlipidemia and insulin resistance [16]. However, both IIS and mTOR pathways are also disrupted in other tissues such as skeletal muscle and liver – leading to the alteration of various consequential/downstream pathways such as PI3K/AKT signalling [8, 16]. Deregulated cellular metabolism and altered intracellular signalling are shown to play a crucial role in the pathophysiology of various diseases, especially contributing to obesity-induced low-grade inflammation [7, 18].

Obesity-induced low-grade chronic inflammatory microenvironment (OIIM) is the most common hallmark of obesity. Obesity-related low-grade chronic inflammation has been shown to induce, escalate or associate with most of the pathological sequelae of obesity. All hallmarks of obesity are known to contribute OIIM either directly or indirectly [7, 18]. Obesity-linked cellular senescence and epigenetic alterations will be address in the further sections of this thesis. It should be noted that nutritional diet is another undeniable component of obesity that will be also further detailed in relation to obesity-associated pathophysiologies.

1.2. Obesity-associated diseases

Obesity is known to dysregulate many key systems such as the immune system, cellular metabolism and signalling pathways. Obesity-induced metabolic dysregulation and low-grade chronic inflammation are the main hallmarks of obesity that could directly trigger diseases such as type II diabetes, cancer, cardiovascular diseases (CVDs), musculoskeletal diseases, osteoarthritis, non-alcoholic fatty liver disease, chronic renal failure, metabolic syndrome (MetS) and autoimmune diseases [19]. Following smoking, obesity is the second cause of premature deaths around the world, responsible of 2.8 million deaths annually [20].

Type 2 diabetes (T2D) is highly associated with obesity and is documented to be the most common metabolic disease in the world [21]. Obesity contributed to T2D through worsening the physiological parameters by dysregulating insulin signalling and inducing the OIIM [22]. Hotamisligil et al. 1996, illustrated that inflammatory cytokines can directly trigger insulin resistance via altering insulin signalling [23]. Additionally, increased lipolysis and high serum-

free FAs have been shown to impair insulin receptor signalling leading to apoptotic β-cells [24]. Recent studies also illustrated the critical role of obesogenic diet-induced epigenetic modifications on insulin signalling genes augmenting the pathology of T2D [21, 25]. Interestingly, differential DNA methylation in blood leukocytes has been associated with obesity-associated T2D [25]. Recent large-scale epigenetic studies highlighted the differential methylation of certain CpG sites (cytosine-guanine) in $CD4^+$ T cells associated with BMI and obesity-associated T2D [26].

Additionally, obesity is known to significantly increase the risk of CVDs morbidity and mortality [27, 28]. Obesity alters physiological parameters including elevation in adiposity, high blood glucose levels, lipoprotein and cholesterol accumulation due to dyslipidemia [29]. These pathophysiological parameters have been shown to drive systemic hypertension, altered contractility and accelerate arterial and cardiac injuries - leading to CVDs [30].

Furthermore, MetS is another pathology which is also associated with obesity through patients exhibiting insulin resistance, dysglycaemia, hyper tension and hyperlipidemia. MetS patients have an increased risk for T2D, non-alcoholic fatty liver disease, Alzheimer's and CVDs [31, 32]. Interestingly, in western countries 35% of the population have MetS [33, 34]. The western diets consumed within these countries is thought to play a role in evoking MetS and other obesity associated diseases.

Recently, obesity is also shown to aggravate other critical diseases such as severe-acute respiratory-syndrome coronavirus-2 (SARS-CoV-2/COVID-19) [35]. Meta-analysis of SARS-CoV-2 patients documented that obesity increases COVID-19 infection risk by 46%, hospitalisation risk by 113% and death rate by 48% [36]. Interestingly, obesogenic diets are suggested to exacerbate the disease severity of COVID-19 due to the OIIM where high-fat, high-sugar diet is shown to trigger systemic immune and metabolomic dysregulation in the Syrian hamster model infected with SARS-CoV-2 [37, 38]. Dysregulated immunity in OIIM is documented to induce, escalate or be associated with multiple obesity-linked diseases [39]. Therefore, it is pivotal to identify the main players driving OIIM, the link between obesogenic diets and molecular mechanisms driving OIIM in obesity-linked pathologies.

1.3. Role of obesogenic diets on obesity and its comorbidities

The nutritional dietary content is certainly the most critical environmental factor in the pathophysiology of obesity and associated diseases. It is known that the prevalence of obesity is critically high in the modern Western world [2, 40]. This is mainly linked to the consumption of energy-dense WD composed of high saturated fat, sugar and salt content with low fibre leading to increased weight and adiposity [2, 40]. Literature has identified direct causative links between obesity and nutrition/diet were dietary intake can directly interfere with hallmarks of obesity by disrupting signalling pathways, altering epigenetic landscape and modulating the immune response [41].

There are several diets highly common in the world, each with different macro and micronutrient content (low-fat, high-protein, low-carbohydrate, Mediterranean (MD) and vegan/vegetarian diets) [42]. The high-fat diet (HFD) and Western diet (WD) are identified as the two main obesogenic diets.

High-fat diets are energy-dense diets (~35-50% of the energy from fat) consisting of sucrose, maltodextrose, starch, soybean oil or lard and cellulose [43]. Although the exact biochemical parameters might vary among cultures and studies, the traditional factor is to simply exchange carbohydrate-derived calories with fat-derived calories [44].

Although the HFD is traditionally used to induce obesity and its comorbidities in murine models, more recently the WD is also used to trigger diet-induced obesity (DIO). The energy-dense, highly palatable WD is shown to reflect the biochemical parameters of today's Western diet more accurately [44, 45]. The main energy source of WD is carbohydrates (~50%) such as refined sugar with lower protein and fat content (~20-33%) than the HFD [46, 47]. Although the fat content of WD is relatively lower compared to HFD, saturated fat levels are profoundly higher such as cholesterol is ~6-10 times higher in the WD compared to HFD [48]. The key characteristics of human WD are listed in **Table 1**, according to US Department of Agriculture reports in 2013-2018 [49, 50]. Although both obesogenic diets are shown to promote hyperphagia leading to increased weight gain, hyperlipidemia, glucose and insulin intolerance [44, 45], it is shown that the fat content, class of fat (saturated vs. unsaturated) critically affect the development of DIO and associated diseases [46, 47]. More specifically, bioactive saturated fatty acids (SFA) such as palmitate and stearic acid are shown to induce various hallmarks of obesity [51-53].

Contrastingly, the chow diet (CD) is the most common control diet group used in scientific experiments which models a healthy balanced diet. The CD mainly consists of a well-balanced distribution of carbohydrates and fats with high fibre content [43]. The CD mainly consists of agricultural by-products such as corn, oats, wheat and soybean [43].

Table 1.3.1) Macronutrient composition of Western diet (WD), High fat diet (HFD) and Mediterranean diet (MD)*

Diet composition	***WD***	***HFD***	***MD***
% of Calories			
Protein	15	15	17
Carbohydrates	51	30	51
Fat	33	50-60	32
% of fats			
Saturated	33	45-50	21
Monounsaturated (MUFAs)	36	30	56
Polyunsaturated (PUFAs)	24	8-10	15
ω3: ω6 FAs	15:1	15-20:1	2-3:1
Cholesterol, mg/kcal	0.13	0.3	0.16
Fiber, g/kcal	0.01	0.01	0.03

* It should be noted that the composition of human diets are highly variable which is illustrated here as a representative plot of the percentage obtained from literature [46, 48-50, 54-56].

Although both obesogenic diets (HFD and WD) are known to induce oxidative stress, ROS accumulation [57], interfere with vital signalling pathways (such as insulin & mTOR), trigger DNA damage and epigenetic alterations [58] and contribute to OIIM [59]. Importantly, WD has also been shown to mimic the modern fat-dense diets driving the obesity epidemic [60]. Indeed, Bortolin et al. (2018) illustrated that the WD is the most effective diet to induce obesity and obesity-associated diseases [60].

Various studies illustrated the critical effects of obesogenic diets in inducing and/or escalating various hallmarks of obesity [1]. Obesity-induced low-grade chronic inflammation is a vital hallmark of obesity directly modulated by dietary content which are shown to induce and escalate OIIM, especially in liver, muscle and adipose tissues [44, 45]. Although a few mechanisms identified for DIO-driven innate immunity dysfunction, the complex interrelations between obesogenic diets and dysregulated adaptive immunity remain murky.

1.4. Lipotoxicity: Linking high fat intake to obesity associated pathophysiology

Adipose cells and tissues can enlarge in size to store excessive nutrients and lipids in the body. However, plethora of lipids over the storage capacity circulate around as non-stored free-FAs, accumulating around the body. Accumulation of complex lipids and FAs can reach toxic levels in peripheral organs such as liver, kidney, muscles, heart and pancreas [61]. Lipotoxicity defines the metabolic abnormalities, immune dysfunction, cell death and other deleterious effects of accumulated lipids in non-adipose tissues [62]. The lipotoxicity theory was first proposed by Roger Unger (1990s), as an idea that excessive fatty acids in non-adipose tissues could lead to obesity and obesity-associated diseases [63]. Publications confirmed the toxic roles of FAs in the pathogenesis of obesity and associated diseases including T2D, CVDs, MetS and fatty-liver disease [63, 64].

Recent studies illustrated that alongside 'passive' toxicity capacity, FAs also possess 'bioactive' roles in modulating cellular functions including cellular metabolism, apoptosis, cell-cycle, proliferation, migration and differentiation [65-68]. Importantly, bioactive lipids within obesogenic diets were shown to modulate various cellular processes linked with critical hallmarks of obesity and obesity-associated pathophysiologies. Therefore, it is important to identify the distinct bioactive lipids and their modulatory actions within tissues to understand the complex pathological sequelae of obesity.

1.5. Fatty acids

FAs are hydrocarbon structures, classified into categories based on their length (number of carbon atoms), degree of saturation and percentage of structural double-bonds [69]. FAs with 4-10 carbons classified as short-chain, 12-14 carbons as medium-chain, 16-18 carbons as long-chain and <20 carbons as very long-chain FAs. Additionally, FAs without a double bond are known as saturated FAs (SFA) whereas, FAs containing one or more double bonds are termed monounsaturated (MUFAs) or polyunsaturated FAs (PUFAs) [69, 70]. **Table 1.5.1** illustrates prominent FAs and their isomer formula used in the literature.

FAs are utilised as an energy source and promin prominent components of the cell membrane (e.g. phospholipids and glycolipids). However, recently FAs have been identified as bioactive lipid mediators with various critical roles in modulating cellular functions [69, 71]. For example, oxidative derivatives of FAs have been shown to modulate immunity in both pro-

and anti-inflammatory functions [72]. More specifically, in response to tissue damage or pathogen encounters, the biosynthesis of pro-inflammatory lipid mediators (such as prostaglandins and leukotrienes, collectively known as eicosanoids) is essential to create a beneficial acute inflammatory response [72].

Table 1.5.1) Nomenclature of prominent fatty-acids including their isomer formula as commonly used in the literature.

TYPE	ISOMER FORMULA	NAME
SATURATED FAs	4:0	Butyric acid
	12:0	Lauric acid
	14:0	Myristic acid
	16:0	Palmitic acid (PA)
	18:0	Stearic acid (SA)
MONOUNSATURATED FAs	18:1 (ω9)	Oleic acid (OA)
POLYUNSATURATED FAs	18:2 (ω6)	Linoleic acid
	18:3 (ω3)	Alpha-linoleic acid
	18:3 (ω6)	Gamma-linoleic acid
	20:4 (ω6)	Arachidonic acid
	20:5 (ω3)	Eicosapentaenoic acid (EPA)
	22:5 (ω3)	Docosapentaenoic acid (DPA)
	22:6 (ω3)	Docosahexaenoic acid (DHA)

1.5.1 Saturated fatty-acids

SFAs chemically consist of a carbon chain without double bonds [70]. Although SFAs can be synthesised by humans via *de novo* synthesis pathway, their main source is dietary animal fats (**Figure 2**) [70]. SFAs are linked with various deleterious functions in obesity such as reducing cell-membrane fluidity, altering lipoprotein metabolism, impacting cholesterol levels and inducing peripheral inflammation (especially in adipose tissues) [73-75]. Palmitic acid, lauric acid and stearic acids are the three main SFAs shown to stimulate an inflammatory microenvironment.

1.5.1.1 Palmitic acid (PA)

Palmitic acid (PA), also known as n-hexadecanoic acid, is a long-chain FA with 16 carbons in a linear structure [76]. It is commonly found in palm oil, butter, dairy products and meat. PA is one of the most researched SFAs, this is partly due to PA being the most common SFA found in the human body accounting for 20-30% of total FAs as well as the most abundant SFAs in circulation accounting for 27% of total plasma FAs [77-79]. It is also shown that long-

term PA intake promotes the development of various obesity-linked diseases such as CVDs, T2D, liver diseases and cancer [52, 80, 81].

Obesogenic diets such as HFD and WD are enriched in SFAs such as palmitic acid [80, 82]. It is shown that, obesity induces a significant elevation in palmitate, leading to dysregulated glucose metabolism and inflammation in various tissues [79, 83, 84]. Recent studies showed that PA serves not only as a metabolite for adenosine triphosphate (ATP) synthesis, but also as an intracellular signalling molecule involved in various pathophysiologies [81]. PA-induced lipotoxicity leads to endoplasmic reticulum stress and mitochondrial dysfunction via oxidative stress [81]. Moreover, PA also increases signal transducer and activator of transcription-3 (STAT3) expression via phosphorylation of STAT3-Y705 site [85]. PA-induced STAT3 phosphorylation shown to increase prostate cancer cell proliferation and metastasis [85]. This novel data is highly important to highlight the bioactive modulatory roles of PA in molecular pathways via interfering with transcription factors such as STAT3.

Furthermore, bioactive PA is capable of modulating various critical cellular functions including cellular metabolism, inflammation, apoptosis, senescence and autophagy [79, 86]. Autophagy is also known to be a key mechanism against lipotoxicity in cells whereas, PA is shown to modulate autophagy via mTOR dependent pathway [86]. Furthermore, it has been observed in adipocytes that PA can induce autophagy via eliciting ER stress [87]. Importantly, Yin et al. 2015, also observed an ameliorative effect of PA-induced autophagy on PA-induced inflammation which highlights the critical interlinks between cellular actions [87]. Additionally, PA is also shown to escalate obesity-associated diseases such as T2D via directly altering the DNA methylation and epigenetic structure [88]. Hall et al., critically demonstrated that *in vitro* palmitate treatment of human pancreatic islets leads to epigenetic modifications in various genes linked to glycolysis, FA metabolism and cellular functioning which altogether augments T2D [88]. Additionally, recent publications also revealed the critical role of PA-driven palmitoylation of endothelium in triggering the obesity-associated pathophysiologies including CVDs and T2D [89, 90]. Moreover, PA is also shown to have extensive interactions with pro-inflammatory prostaglandins inducing pro-inflammatory cytokine production such as IL-8, IL-6 and TNF-α and contributing to insulin resistance and OIIM in obese individuals [91, 92].

1.5.1.2 Stearic Acid (STE)

Stearic acid (n-Octadecanoic acid) is a long-chain saturated FA composed of an 18-carbon backbone. It is commonly found in meat, dairy products, cocoa and shea butter [93]. Although it is also present in vegetable fat (typically <5%), it is more abundant in animal fat (up to 30%) [94]. STE is the second most abundant SFA found in obesogenic diets following the palmitate [93, 95]. Following the synthesis of PA from acetyl-CoA in *de novo* pahtway, PA gets further elongated in 7-cycles synthesising the 18-carbon STE structure [93].

Generally, SFAs are known to have deleterious effects on health through hypercholesterolemic, atherogenic and thrombotic effects and increases the risk of obesity-linked disease like T2D and CVDs [93, 95]. However, unlike other deleterious SFAs (such as PA, lauric and myristic acids), STE exhibits neutral or even beneficial effects [93]. Unlike hypercholesterolemic effects of PA, STE-enriched diets were shown to reduce total serum and low-density lipoprotein (LDL) cholesterol levels [93, 96, 97]. Recent studies suggested that the replacement of deleterious SFAs with STEs in diet may exhibit beneficial effects on LDL-cholesterol and CVD risk in humans [98]. Recently, it also has been illustrated that dietary-STE and monounsaturated oleic acid have similar beneficial effects on total and LDL cholesterol levels in randomised human trials [99]. Although it has been documented that STEs exhibit a neutral effect (compared to other SFAs), the mechanism underlying this effect is vague.

1.5.2 Unsaturated fatty-acids

Unsaturated FAs (UFA) containing one double-bond are known as monounsaturated FAs (MUFA) and containing more than one double-bond in the carbon backbone are known as polyunsaturated FAs (PUFA). Similar to SFA, UFAs can also be synthesised via lipogenesis or can be acquired through diet. Compared to SFAs, UFAs are typically liquid at room temperature and mainly found in fish and vegetables. Obesogenic diets (HFD and WD) known to contain low proportion of UFAs (~20-30% of total fat content), whereas the MD is known to be rich in terms of UFAs (~60% of total fat content) [100]. This is mainly accounted for by the high consumption of fish, olive oil, vegetables and whole grains in MD. Oleic acid is one of the main MUFAs found in the MD as well as PUFA such as omega-3 (n-3PUFA) [100]. Traditionally, UFAs are known to be beneficial in terms of cholesterol levels, dampening the OIIM and reducing the risk of obesity-associated diseases [100, 101]. Consistently, MD has been shown

to lower blood pressure, improved glucose, insulin and blood lipid profile in both murine models and human cohorts [100].

1.5.2.1 Monounsaturated FA: Oleic acid (OA-OLE)

Oleic acid (cis-9-octadecenoic acid;18-1) is also referred to as monosaturated omega-9 lipid, due to a single double-bond positioned at the ninth carbon. Oleic acid (OA) is a major FA nearly found in every lipid source, including soybean, palm and corn oil [102, 103]. However, olive oil is the main natural source of OA (~56-84% of total FAs)[103]. Similar to SFAs, OA can be acquired from diet or endogenously synthesised by stearoyl-CoA desaturase which converts STE (C18:0) to OA (C18:1 n-9) (**Figure 1.2**) [104].

Similar to other MUFAs, OA is shown to exert various beneficial effects in terms of metabolism, insulin signalling and inflammation. Consistently, MD is highly associated with improved cardiovascular health with lower blood pressure, reduced risk of thrombosis and atherosclerosis [105, 106]. Overall, MD with a high OA content have been shown to reduce the risk of various obesity-associated diseases, such as CVDs, T2D, MetS and neurological diseases [100, 101, 104].

Considering its regulatory effects on cholesterol and FA synthesis, OA has been speculated to be the main bioactive FA responsible for the beneficial effects of olive oil-enriched MD [107]. OA concentration is also shown to be important in modulating the phospholipid composition, affecting the fluidity of biological membranes and mediating a homeostatic balance between SFA and MUFA/PUFA ratio [104]. OA also has been shown to inhibit FA synthesis and also exert hypocholesterolemic effects on both *in vivo* and *in vitro* studies [93, 99, 104]. OA can directly upregulate AMP-activated protein kinase (AMPK) to inhibit the acetyl-CoA carboxylase (ACC) via phosphorylation [104]. Inhibition of ACC directly reduces the available substrate (malonyl-CoA) required for the biosynthesis of FA [104]. OA is also able to indirectly downregulate the lipogenic and cholesterogenic gene expression via modulating the transcription factor called sterol regulatory element-binding protein-1 (SREBP-1). Recently, studies have illustrated that the substitution of SFAs with OA in diet ameliorates obesity and may help to reverse the detrimental effects of SFAs [99, 104].

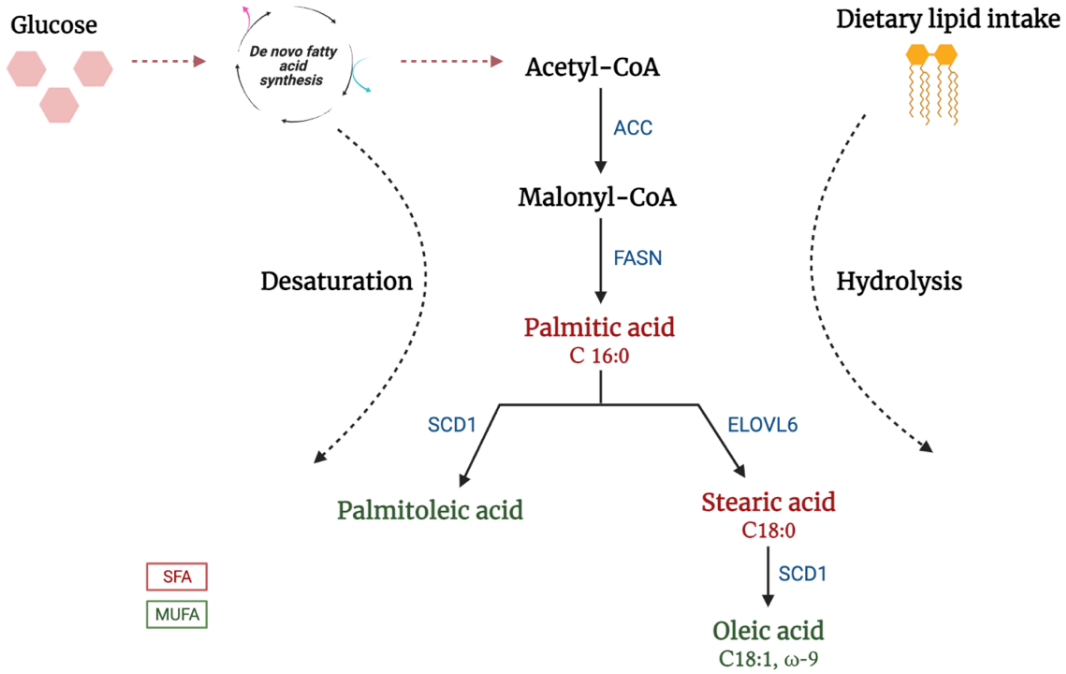


Figure 1.2) Biosynthesis of MUFAs from *De novo* synthesis of FAs
Representative figure of excess glucose molecules converted into SFAs via *de novo* FA synthesis pathway which then condensates into MUFAs such as oleic and palmitoleic acid in animals. The ω represents the chemical location of the double-bond on the carbon molecule. ACC—acetyl CoA carboxylase, FASN—fatty acid synthase, ELOVL6—fatty acid elongases 6, Stearoyl CoA Desaturase 1 (SCD1). Adapted from Piccinin et al 2019 [104]

1.5.2.2 Polyunsaturated FAs: Omega-3 (ω−3) & Omega-6 (ω−6)

Omega FA group belongs to polyunsaturated FAs (PUFA) consisting of multiple double-bonds in their acyl chain. There are two main PUFA families; omega-6 (n-6/ω6) and omega-3 (n-3/ω3)[108]. Importantly, two specific omega FAs cannot be synthesised in mammals; linoleic acid (18:2n-6; LA) from ω6 and α-linolenic acid (18:3n-3: ALA) from ω3 group [108]. Both, linoleic and α-linolenic FAs are obtained from diet and metabolised via multiple catalytic enzymes leading to various bioactive precursor FAs. **Figure 1.3** illustrates the main omega FA metabolism including desaturation and elongation activities mainly occurring in the liver as dietary omega FAs metabolised into active forms [109]. Generally, omega FAs are not available as free-FAs. Initially, they are incorporated into chylomicron triglycerides in intestines and transported to the liver where they attached to albumin protein (produced by the liver) [109].

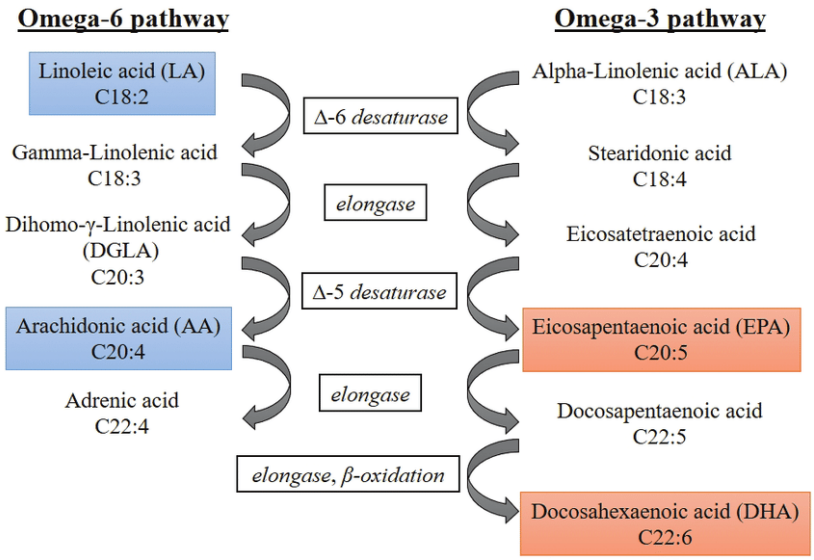


Figure 1.3) Metabolism of Omega fatty acids
To metabolise linoleic and α-linolenic FAs additional double-bonds are added to elongate the acyl chain of FAs which chemically converts them to other key PUFAs named γ-linolenic acid- (18:3n-6) and dihomo-γ-linolenic acid (20:3n-6) [110]. Finally, linoleic acid (ω6) converts to arachidonic acid while α-linolenic acid (ω3) is converted to eicosapentaenoic acid (20:5n-3; EPA) [108, 110]. Furthermore, both arachidonic acid and EPA are further digested where EPA could be converted to docosapentaenoic acid (22:5n-3; DPA) and docosahexaenoic acid (22:6n-3; DHA) [108, 110]. Figure taken from Nagy and Tiuca, 2017 [111].

Omega-3-based FA groups, such as EPA, DHA and ALA, are commonly found in fish oils, seafood, soybean, rapeseed and flaxseed. Whereas, omega-6 groups such as ALA and arachidonic acid (AA) are found in sunflower oil, corn oil, cereals and animal fats [108, 110]. Although both ω3 and ω6 FAs are essential for homeostatic functioning of the body, the ratio between them in the diet is critical where healthy medical practice suggests 4:1 ratio between ω6 and ω3. However, this ratio is highly disrupted in the WD such as 15-20:1, due to the higher consumption of ω6-enriched oils [56, 110]

Generally, ω3 is known to reduce the cardiovascular risk factor whereas, ω6 is shown to have an opposite effect [112-114]. Various studies illustrated that ω3 can reduce triglyceride, low-density cholesterol levels as well as improve vascular functions, heart rate and blood pressure in humans [112-114]. Omega-3 is also expressed beneficial effects on the T2D via restoring homeostatic conditions of insulin signalling and glucose metabolism [115, 116]. Although the exact mechanism remain unclear, it is illustrated that ω3 exerts their effects via recreating a homeostatic microcellular environment. Additionally, it is argued that dietary ω3 supplementation can suppress the synthesis of critical pro-inflammatory lipid groups such as diacylglycerol and ceramides [117-120]. Recently, ω3 FAs were also shown to attenuate the

detrimental effects of HFD via ameliorating mitochondrial functioning in obesity [121]. Contrarily, HFD is shown to reduce the ω3 (EPA) levels in murine models alongside increasing deleterious FAs (SFA and sphingolipids) [122-124]. Although the efficacy and the underlying mechanisms are debated, it is suggested that ω3 FAs exert its main beneficial effect via ameliorating OIIM and also by preventing the accumulation of detrimental bioactive lipids associated with obesity pathophysiology [110, 125-127].

1.6. Complex bioactive lipids- Sphingolipids

Sphingolipids are one of the main complex eukaryotic lipid groups. All sphingolipids consist of a sphingosine (long-chain amino alcohol) backbone attached to a fatty acid with an amide bond [128, 129]. Sphingolipids are known for their role in plasma membrane alongside being an important bioactive signalling molecule. Sphingolipids have crucial roles in various cellular functions including proliferation, migration, apoptosis, senescence and inflammation [128, 129]. Consequently, dysregulation of sphingolipid metabolism is associated with various obesity-linked diseases including cancer, CVDs and inflammatory conditions [128, 129]. Although sphingolipids are highly diverse with 4,000 distinct sphingolipids identified, ceramides are the central element [66, 129, 130].

1.6.1. Ceramides

Ceramides are the main bioactive sphingolipid metabolite composed of sphingosine and amine-linked fatty acid that can vary in length. Although ceramides are known for more than two decades, their bioactive functions have been revealed relatively recently. Initially, Unger's lipotoxicity model (1990s) associated ceramides with various detrimental diseases including T2D, CVDs, cancer, obesity and fatty-liver disease [63, 64, 66]. Ceramides were later described as "the most important deleterious route of lipotoxicity" by the Unger group in 2002 [131].

Recent publication has shown that ceramides do not only induce a passive lipotoxicity but also to be the main bioactive sphingolipid metabolite that mediates various cellular functions including proliferation, apoptosis, migration, senescence, cellular signalling, autophagy and inflammation [1, 127, 132, 133]. Corresponding to crucial bioactive effects, ceramides are highly associated with various obesity-linked pathophysiologies as detailed above [66, 132, 134, 135]. These complex biological mechanisms between ceramide and cellular components are not fully understood yet. However, it has been identified that ceramides

alters these complex processes by interfering with signalling pathways, transcription and by modifying the epigenetic structure of specific cell types [66, 132, 134].

1.6.1.1 Ceramide biosynthesis and metabolism

Although the direct dietary intake is possible, ceramides are known to be mainly synthesised by the *de novo* pathway which is highly preserved across mammals [66, 132, 134]. The *de novo* pathway, starts in the endoplasmic reticulum (ER) and continues in Golgi apparatus for structural modifications [1, 66, 136]. Although palmitoyl-CoA and serine are the main substrates of the biosynthesis pathway, alanine, glycine or stearate can also be used. Importantly, PA is to directly elevate ceramide biosynthesis and induce ceramide accumulation, especially in obese tissue microenvironment [81, 137].

These main substrates condensates by the enzyme serine palmitoyltransferase (SPT) creating a short-lived intermediate called 3-ketosphinganine to initiate the synthesis process (**Figure 1.4**). Following the further condensation process involving various other enzymes, sphinganine is synthesised. In mammals there are 6 different CerS enzymes (CerS1-6) that converts sphinganine into dihydroceramides (via N-acylation modification) with various acyl-chain lengths from 14 to 26 carbons [66, 134]. Finally, dihydroceramide desaturases (DES1 and 2) are enzymes that create a 4-5 trans double bond forming the final main bioactive metabolic signalling lipid of sphingolipids known as ceramides [66, 134]. Similar to CerS enzymes, DES1&2 tissue and cell distribution varies, whereas DES1 is generally accepted as the superior enzyme in most tissues and DES2 is more abundant in skin and gut tissues [66]. Once the ceramide synthesis is completed in ER, ceramides are transported to Golgi via ceramide transfer protein (CERT) or by vesicular transport [132].

In addition to the main biosynthesis de novo pathway, there are two more ceramide synthesis pathways; sphingomyelin hydrolysis and the salvage pathway (also known as the recycling pathway) [1, 66, 136]. **Figure 1.4** illustrates the main substrates and enzymes involved in ceramide biosynthesis pathways.

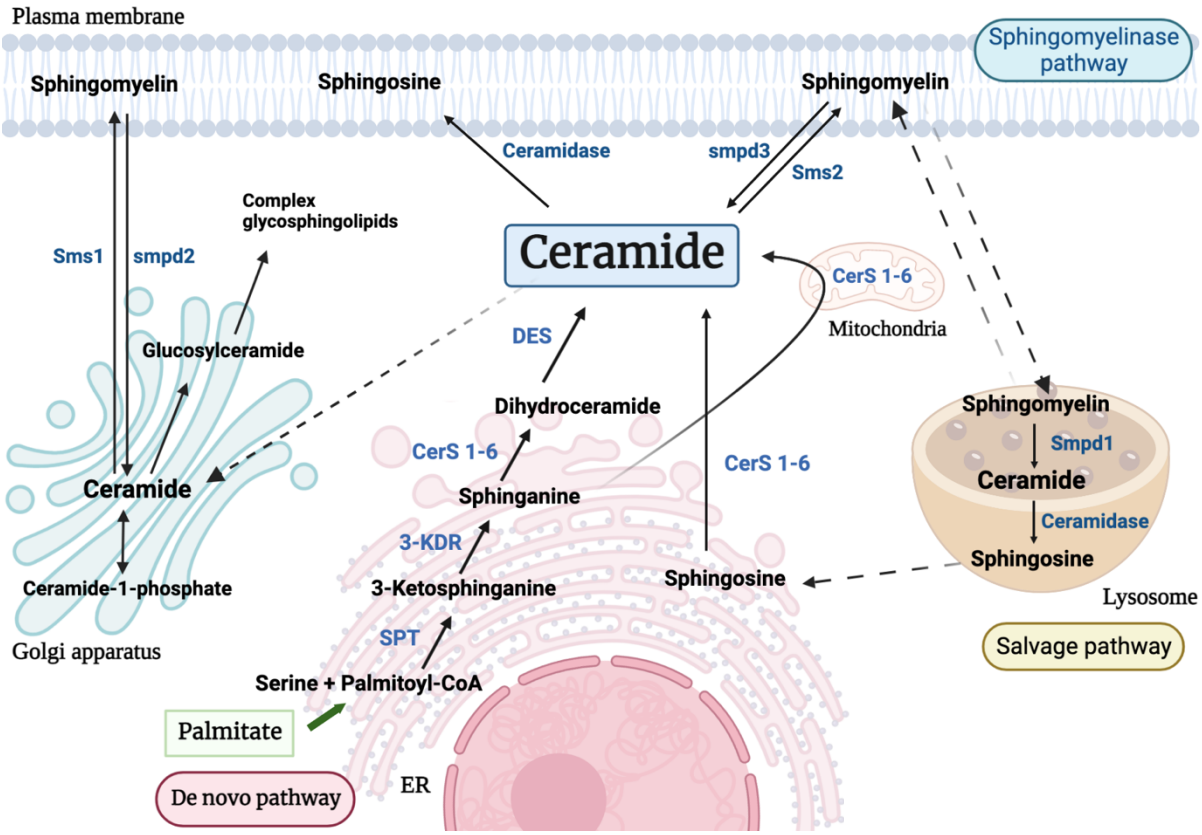


Figure 1.4) Sphingolipid metabolism and ceramide biosynthesis pathways.
Three main ceramide synthesis pathways; **(1)** *De novo* synthesis pathway mainly occurs in ER starting with condensation of palmityl-CoA and serine forming 3-Ketosphinganine. The main substrates condensate together by the enzyme serine palmitoyltransferase (SPT), this forms a short-lived intermediate called 3-ketosphinganine [66, 132, 134]. This intermediate form is directly converted to sphinganine via 3-ketosphinganine reductase (3KSN) [1, 136]. Subsequently, dihydroceramide synthase (CerS) enzymes convert sphinganine into dihydroceramide form via N-acylation modification [66, 134]. In mammals there are 6 different CerS enzymes (CerS1-6), with each enzyme generating a dihydroceramide form with various acyl-chain lengths from 14 to 26 carbons [66, 134]. Each of the Cers1-6 enzymes also has specific substrate specificity and various tissue distribution leading to the generation of distinct sphingolipid classes in different tissues. Finally, dihydroceramide desaturases (DES1 and 2) are enzymes that create a 4-5 trans double bond forming the final main bioactive metabolic signalling lipid of sphingolipids known as ceramides [66, 134]. **(2)** Sphingomyelin hydrolysis pathway synthesises ceramides via the hydrolysis of the sphingomyelin lipid (commonly found in mammalian cellular membranes). Sphingomyelinase (SMase-Sms) is the main catalytic enzyme converting sphingomyelins into ceramides and free choline [1, 66, 136]. **(3)** The salvage (or recycling) pathway synthesise ceramides by the breakdown of surplus complex sphingolipids in acidic lysosomes. The SMase and β-glucosidase-1 degrades sphingomyelin and glucosylceramides, respectively, into ceramides. The ceramides synthesised in lysosomes converted to sphingosine via acid ceramidase before being transferred to cytosol where all sphingosines re-join the de novo synthesis pathway via recycling back to ceramide via CerS enzymes [1, 66, 136]. ER: Endoplasmic reticulum; SPT: Serine palmitoyl transferase; 3-KDR: 3-ketodihydrosphingosine reductase; CerS: Ceramides synthases; DES: Dihydroceramide Δ4-desaturase, SMS: sphingomyelin synthase, smpd1: Acid Sphingomyelinase,

smpd2: Neutral sphingomyelinase1, smpd3: Neutral sphingomyelinase 2. Adapted from Green et al. 2021, and Custodia et al. 2021 [132, 138].

1.6.1.2. Interventions to ceramide biosynthesis

Dysregulation in sphingolipid metabolism and ceramide accumulation in various tissues has been shown to contribute to various obesity-associated pathophysiologies [1, 66, 136]. Consequently, numerous studies targeting ceramide biosynthesis investigated the ameliorative potential of the associated diseases. Recently, therapeutic targeting of sphingolipids via pharmacological inhibitors gained a high interest in the clinical field for treating metabolic and immune diseases [1, 66]. Various *de novo* ceramide synthesis pathway enzymes have been inhibited via different pharmacological inhibitors including SPT, CerS1-6 and DES (**Figure 1.5**) [1, 128]. **Table 1.6.1** represents the direct effects of ceramide biosynthesis inhibition in the context of OIIM as well detailed in our previous review publication [1]. Generally, inhibition of ceramide biosynthesis leads to beneficial effects such as improved glucose tolerance, prevents lipid accumulation and subsequently prevents further weight gain associated with obesogenic diets [1, 139, 140].

Importantly, ceramide biosynthesis pathways are highly interconnected and crucial for cell functioning. Therefore, inhibition of a specific CerS enzyme (or ceramide species) potentially leads to an increase in other ceramide groups as a compensatory effect [141]. This compensatory effect could trigger overload of distinct ceramide groups leading to lipotoxicity in various tissues (such as muscle and liver) [141].

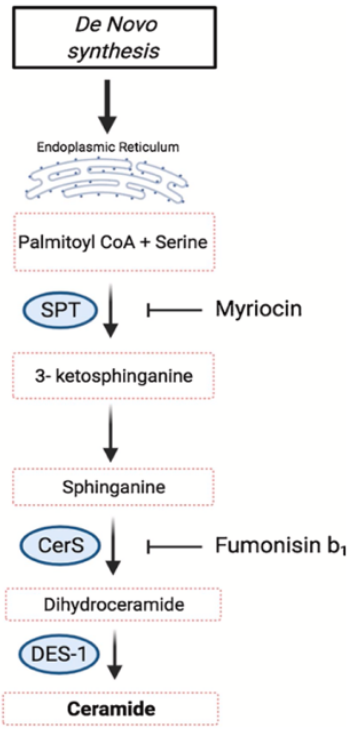


Figure 1.5) Conventional inhibitors used to inhibit the *de novo* ceramide biosynthesis pathway. Myriocin and Fumonisin B_1 (FB_1) are the two main pharmacological inhibitors traditionally used to intervene on ceramide biosynthesis. Myriocin is shown to target SPT, the very first enzyme of *de novo* pathway whereas FB_1 selectively inhibits CerS enzymes. Taken from Kucuk et al 2021 [1].

1.6.1.2.1. Myriocin

Myriocin is a pharmacological inhibitors isolated from *Mycelia sterilia* fungi and used to block PA-driven ceramide synthesis. Myriocin is a natural structural analogue of sphinganine (sphingosine) with a high affinity for SPT enzyme, competitively inhibiting the ceramide biosynthesis via *de novo* pathway [141]. Similar to other ceramide inhibitors, myriocin has been shown to ameliorate CVDs via reducing atherosclerotic plaques [142-145], hypertension [146], insulin resistance, T2D via ameliorating insulin signalling [147-150] and hepatic steatosis via reducing hepatic fibrosis [141, 148, 149, 151]. It should be noted that myriocin beneficial effects are shown even under high-fat feeding conditions[151-153]. This highlights the unique potential of ceramides as a bioactive lipid mediator involved in the pathophysiology of various diseases and the therapeutic potential of intervening with ceramide biosynthesis [141, 142, 148, 149, 151, 154].

1.6.1.2.2. Fingolimod (FTY720)

Fingolimod (FTY720) is a synthetic analogue of myriocin, developed for clinical therapeutic uses [155]. As a myriocin-based derivative, FTY720 is structurally a sphingosine-1-phosphate (S1P) analogue acting as a competitive agonist of 4 main S1P receptors (S1PR1,3-5) [139, 156]. Fingolimod has been shown to have a similar inhibitory effect on ceramide syntheses with a higher efficacy for inhibiting long-chain ceramides [157, 158]. Studies

illustrated the inhibitory effect of fingolimod on ceramide synthesis 2 enzyme (CerS2) [157, 158].

Clinically in 2010, FTY720 (Gilenya;Novartis) was approved by the US Food and Drug Administration for the treatment of relapsing multiple sclerosis (MS) due to its immunosuppressive effects [156]. Fingolimod requires phosphorylation by sphingosine kinase 2 (SK2) *in vivo* to be therapeutically active. Fingolimod phosphate has been shown to directly bind to all of the S1P receptors (excluding $S1P_2$) and leads to internalisation followed by degradation of the receptor [156]. The inhibition of S1P and S1P receptors limits the egress of memory T lymphocytes from lymph nodes and inhibits pro-inflammatory phenotype [156, 159, 160]. Importantly, FTY720 is able to block the egress of central memory T cells but not the effector memory [160]. This was highly important as the FTY720 was shown to save the effector phenotype intact [160]. More recently, it is identified that FTY720 also modulates the function and phenotype of both T and B-cell subsets [160-162]. Initially, Serpero *et al.,* observed that FTY720 treatment in MS patients leads to a significant increase in $CD4^+$ $CD25^{high}$ $CD127^{low}$ regulatory T cell (Treg) populations as well as a significant reduction in interferon γ (IFNγ) and IL-17 levels [162].

FTY720 is shown to bias T cell differentiation towards Treg and Th2 fate whilst downregulating Th1 and Th17 [160-162]. T cell *in vitro* studies illustrated that FTY720-driven downregulation of S1PR1 can modulate GATA3 transcription factor, leading to T cell differentiation bias [160, 163]. Additionally, FTY720 treatment of *ex vivo* T cells diminished pro-inflammatory IL-17 and increased anti-inflammatory IL-10 secretion [161].

Although the exact mechanism of FTY720's biasing effects is still unclear, it is proposed that PI3K/AKT signalling pathway may play a role in its actions. PI3K/AKT signalling pathway is known to be augmented in Tregs in obesity-associated pathological conditions associated with defects in suppressive function and bias toward a pro-inflammatory (Th1/Th17 phenotype) [161, 164-167]. Inhibition of PI3K/AKT pathway by FTY720 was speculated to restore the suppressive Treg phenotype [161, 164, 165]. Based on the current literature, it is suggested that ceramides could be a crucial link between PI3K/AKT pathway that can lead bias in T cell differentiation as observed in obesity-associated pathologies.

1.6.1.2.3. Fumonisin b_1 (FB_1)

Fumonisins was identified with inhibitory functions on CerS due to their structural analogy [168]. There are two major fumonisins, FB_1 and hydrolysed FB1 (HFB_1). Both fumonisins are shown to competitively inhibit ceramide synthesis by binding to the active site of mammalian CerS1-6 [168-170]. Inhibition of CerS leads to the accumulation of sphinganine and sphingosine [169, 170]. Furthermore, genetic CerS knockout models also resembled the physiological characteristics of fumonisins inhibitor, confirming the inhibitory action on both *de novo* and salvage biosynthesis pathways [169-171]. Similar to other inhibitors of ceramide biosynthesis, fumonisins are also well-shown to ameliorate obesity-associated pathologies including T2D, hepatic steatosis, CVDs, autoimmune diseases [132, 151].

Table 1.6.1) Intervention methods to target the *de novo* ceramide biosynthesis pathways. Taken from Kucuk et al. 2021 [1].

Tissue	Experimental model (*in vivo/ in vitro*)	Ceramide species & Tissues	Intervention	Ceramide concentratior	Change in OIIM	Change in pathology	Ref.
SPT (serine palmitoyltransferase)	C57BL/6J mice on HFD 12-20 weeks	Total ceramide including C24:0,C24:1, C22:0 in Adipose tissue, liver, muscle and serum	Pharmacological inhibition via Myriocin and Sptlc knockout model	Reduced	Reduced pro-inflammatory cytokines IL-6, MCP-1, and TNFα with increased anti-inflammatory cytokines (IL-10) More anti-inflammatory M2 macrophages Less macrophage infiltration to periphery	Improvemened insulin sensitivity and glucose homeostasis	Chaurasia et al. 2016
	In Vitro- Human 3T3-L1 adipocytes and RAW264.7 macrophages	Total ceramide and C2:0	Genetic Knockdown of SPT	Reduced	Reduced pro-inflammatory cytokines; IL-6, IFN- γ,TNFα and MCP-1	Restoring the homeostasis of the OIIM	Hamada et al. 2014
Ceramide synthases (CerS 1-6)	C57BL/6 mice on 55.2% HFD for 17 weeks	C16:0, C18:0- adipose tissue, liver	Cers6 genetic knockout	Reduced	No macrophage inflatration and reduced pro-inflammatory cytokines IL-6 and IL-1b	Protected from diet-induced obesity, glucose intolerance and type II diabetes	Turpin et al. 2014
	C57BL/6J mice on 60% HFD for 18 weeks	C16:0- liver and plasma	Cers6 knockdown via antisense oligonucleotides	Reduced (50%)	NA	Improved insulin sensitivity, glucose tolerance with reduced body fat content	Raichur et al. 2019
	In Vitro- Human 3T3-L1 adipocytes and RAW264.7 macrophages	Total ceramide and C2:0	Pharmacological inhibitior of CERs via Fumonisin B1	Reduced	Reduced pro-inflammatory cytokines; IL-6, IFN- γ,TNFα and MCP-1	Restoring the homeostasis of the OIIM	Hamada et al. 2014
	C57BL/6JCrl Cers5 KO mice on 60% HFD for 24	C16:0 and C18:0- lung, spleen, muscle, liver and white adipose tissue	CerS5 genetic knockout	Reduced	Reduction in pro-inflammatory gene expression such as NF-kB, TNFα and IL-1β	Reduced weight gain, ameliorate OIIM	Gosejacob et al. (2016)
	Global knockdown of Cers1 in C57BL/6 mice on 55.2% HFD for 17 weeks	C18:0	Cers1 genetic knockout	Reduced (95%)	NA	Decreased body weight and fat content with improved insulin sensitivity and glucose tolerance	Turpin et al. 2019
Dihydroceramide Desaturase (DES)	C57BL/6 mice on 60% HFD for 12 weeks	Total ceramide- Serum, liver, white adipose tissue	Genetic Degs1 knockout	Reduced	Reduced pro-inflammatory cytokines; IL-1 and TNFα	Reduced fat density and improved insulin sensitivity	Chaurasia et al. 2019

1.6.1.3. Molecular actions of bioactive ceramides

Ceramides were shown to accumulate in multiple tissues around the body during obesity which is shown to induce, escalate or be associated with obesity-linked pathologies [1, 39, 66, 123-125, 145, 151, 172, 173]. Investigations on murine models, primates and human cohorts illustrated a significant elevation of total ceramide levels due to obesogenic diets [66, 125, 172]. This elevation is mainly attributed to the excessive availability of SFAs substrates (PA) within the obesogenic diets [66, 128, 137]. This correlative effect of obesogenic diets on ceramide synthesis and accumulation is elegantly illustrated in non-human primates [135]. Non-human primates fed with WD were shown to gain weight and body fat alongside elevated the plasma ceramide levels which altogether were directly correlated with the progression into diabetic conditions [135]. The direct correlative relationship between PA as a substrate for ceramide biosynthesis was also observed in various *in vitro* studies [81, 174].

Ceramides were suggested as 'universal drivers' of various obesity-associated diseases due to their bioactive modulatory potential on apoptosis, necrosis, cell differentiation, cell migration, proliferation, senescence, ageing, autophagy, mitophagy, cellular metabolism [66, 151, 152, 175]. Ceramides can modulate the fluidity of biological membranes, insulin signalling, glucose metabolism, lipid homeostasis, mitochondrial functioning, ER stress and inflammation (**Figure 1.6**) [1, 81, 134, 176].

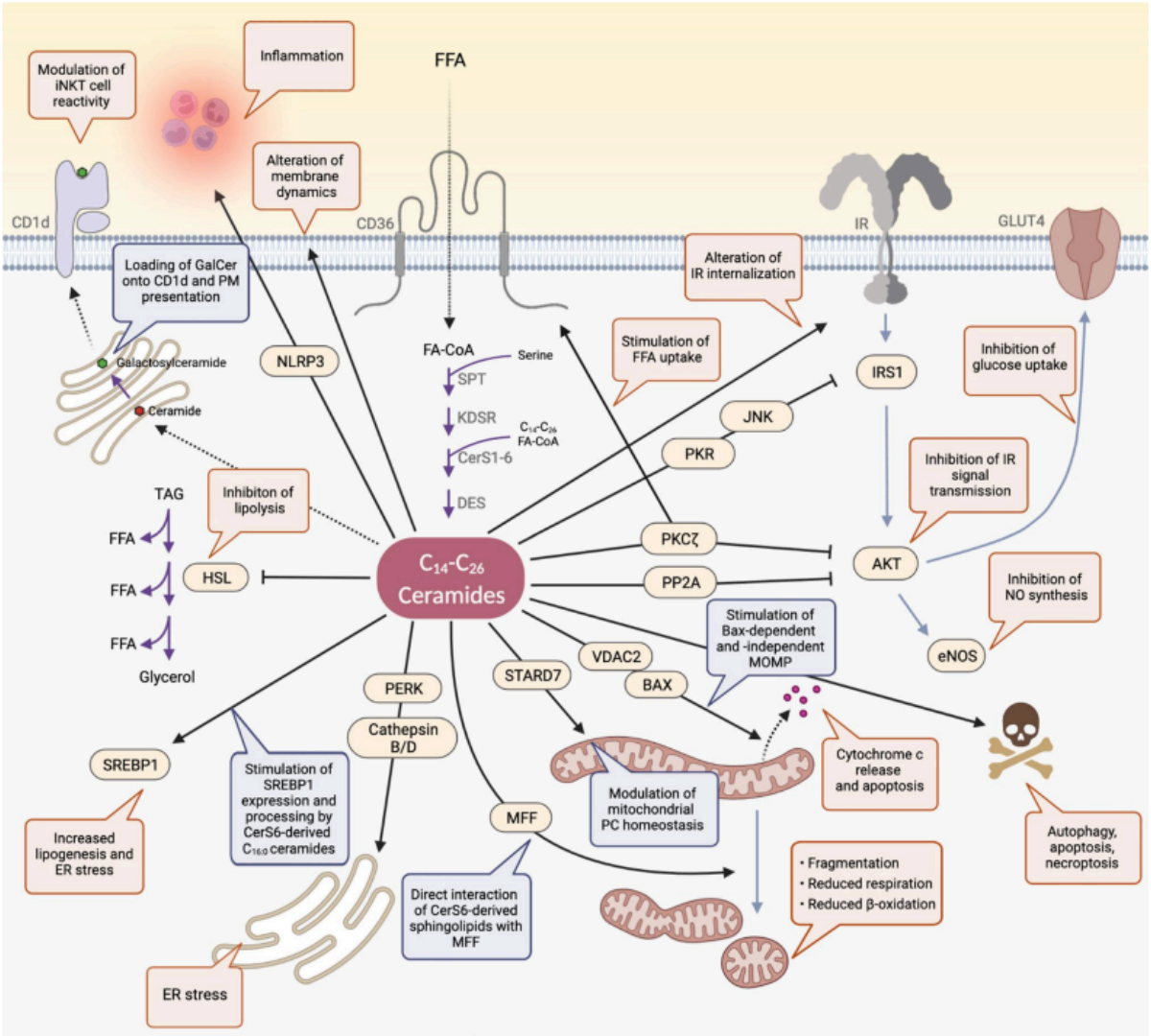


Figure 1.6) Cellular and molecular mechanisms of bioactive ceramides [137]. Ceramides are known to modulate various critical cellular functions including apoptosis, necrosis, cell differentiation, cell migration, proliferation, senescence, ageing, autophagy, mitophagy, cellular metabolism [66, 151, 152, 175]. Ceramides can modulate the fluidity of biological membranes, insulin signalling, glucose metabolism, lipid homeostasis, mitochondrial functioning, ER stress and inflammation [1, 81, 134, 176]. Hammerschmidt and Brüning, 2022, illustrated a comprehensive schematics for the intracellular functions known to be driven or modulated by long-chain bioactive ceramides as illustrated in black arrows. The modulated biological function is shown in red and the underlying mechanisms are shown in blue. Figure taken from Hammerschmidt and Brüning, 2022 [137].

AKT protein kinase B, BAX Bcl-2-associated X protein, CD1d cluster of differentiation 1d, CD36 cluster of differentiation 36 (fatty acid transporter), CerS ceramide synthase, DES dihydroceramide desaturase, eNOS endothelial NO synthase, ER endoplasmic reticulum, FA-CoA fatty acyl-coenzyme A, FFA free fatty acid, GalCer galactosylceramide, GLUT4 glucose transporter 4, HSL hormone-sensitive lipase, iNKT invariant natural killer T cell, IR insulin receptor, JNK c-Jun-N-terminal kinase, KDSR 3-ketodihydrosphingosine reductase, MFF mitochondrial fission factor, MOMP mitochondrial outer membrane permeabilization, NLRP3 NLR family pyrin domain-containing 3, NO nitric oxide, PC phosphatidylcholine, PERK protein kinase RNA-like ER kinase, PKCζ protein kinase C zeta, PKR protein kinase R, PM plasma membrane, PP2A protein phosphatase 2A, SPT serine palmitoyltransferase, SREBP1 sterol regulatory element-binding protein 1, STARD7 StAR-related lipid transfer protein 7, TAG triacylglycerol, VDAC2 voltage-dependent anion channel 2.

Distinct bioactive ceramides are known to alter cellular membranes and impair membrane dynamics, leading to reduced membrane fluidity and trafficking [177-179]. Interestingly, murine models also confirmed that different CerS knockouts can lead to organ-specific and cell compartment-specific changes in membrane morphology associated with disease pathophysiologies [179, 180].

Furthermore, ceramides acts as secondary messengers in controlling lipid metabolism via modulating the uptake and oxidation of FAs [137]. C16 ceramides, increase lipogenesis and ER stress in liver tissue via regulating the activity of sterol regulatory element-binding protein-1 (SREBP1) protein [181]. This modulation by C16 is also speculated to be one of the main mechanisms in the aetiology of T2D and hepatic steatosis [181, 182]. Ceramides are also shown to increase FA uptake via modulating protein kinase-C (PKCζ). PKCζ mediates CD36 FA-receptor in hepatocytes, myocytes and adipocytes inducing FA upregulation that creates a positive loop for ceramide synthesis as it increases the availability of FA substrates for the *de novo* synthesis pathway [181, 182].

Mitochondria is a vital element of cellular energy which illustrates various defects in morphology and functioning during obesity. Ceramides are known to be present in both inner and outer mitochondrial membranes and are able to interfere with mitochondrial functioning via modulating respiratory capacity and ROS production [137, 183, 184]. Obese CerS6-knockdown murine model (with reduced C16 levels) expressed a upregulation in mitochondrial β-oxidation and ADP-based mitochondrial respiration [185, 186].

Ceramides are known to modulate mitochondrial actions by directly interfering with electron transport chain. For example, CerS2 knockout murine model illustrated a reduction in activity of complex IV and II in liver leading to increased ROS generation [141, 187]. More recently, it has been proposed that ceramides may also modulate mitochondria by changing the morphology [185, 188]. As such, accumulation of C16 was shown to comprimise the mitochondrial membranes dynamics and leading to defective respiratory capacity and glucose metabolism in hepatocytes during obesity [185].

The ER is a crucial cellular structure facilitating vital cellular processes including ceramide biogenesis, lipid biosynthesis, protein folding and other metabolic activities. Murine models, illustrated that ceramides can induce ER stress and insulin resistance in fatty-liver

diseases [189, 190] and obesity [191]. There are a few mechanical pathways that illustrate the bioactivity of ceramides on ER stress during obesity. C16 induces ER stress and lipogenesis via SREBP1 as previously mentioned. Furthermore, C16 is also shown to activate CD95-pERK and cathepsin B/D pathway which interrupts autophagy and leads to ER stress [192, 193]. Additionally, inhibition of ceramide synthesis in both pancreatic β-cells [194] and intestinal-epithelial cells [195] ameliorated the myristate and palmitate-induced ER stress in murine models.

Ceramides are also known to act as secondary messengers in pro-apoptotic pathways in hepatocytes, cardiomyocytes and β-cells [137, 145, 196]. This was shown to increase the apoptotic potential in obesity which is associated with the pathogenesis of various diseases such as T2D, fatty-liver diseases, CVDs and autoimmune diseases. Ceramides are implicated in various pro-apoptotic processes such as Fas-capping [197], kinase suppressor of Ras [137] and cathepsin D signalling [198]. Moreover, ceramides also induce apoptosis via BAX-dependent release of cytochrome c leading to mitophagy [137, 199].

Distinct ceramides illustrate different molecular pathways for impairing insulin signalling including direct alteration in internalisation of insulin receptor [137, 200, 201]. Ceramides directly interrupt the insulin receptor (IR) signalling cascade in adipocytes, myocytes, cardiomyocytes and hepatocytes [137, 200, 201]. AKT is the main downstream signalling protein of insulin signalling which leads to pro-survival signals, anabolic metabolism, muscle hypertrophy and nutrient intake [202]. Ceramides are known to inhibit the insulin-stimulated phosphorylation of AKT (pAKT) via both serine/threonine protein phosphatase 2A (PP2A) or the PKCζ [203-205]. Dephosphorylation of AKT by ceramides indirectly modulates the insulin-dependent glucose uptake in adipocytes and myocytes [206, 207].

It is revealed that ceramides can disturb the fusion and translocation of glucose transporter such as GLUT4 [206]. Ceramide-induced inhibition of glucose uptake and insulin signalling are directly linked with obesity-associated pathophysiologies such as insulin resistance, T2D and metabolic conditions [137]. Consistently, inhibiting ceramide synthesis ameliorated the insulin signalling and obesity-associated pathophysiologies [186, 208].

These observations highlighted the complex interplay between bioactive ceramides and their modulatory capabilities on cellular functions and systemic phenotypes [137].

1.7. Immune cells involved in obesity-induced inflammatory microenvironment (OIIM)

Low-grade chronic inflammation is one of the main hallmarks of obesity. Obesity-induced inflammatory microenvironment (OIIM) has been shown to induce and escalate various obesity-linked pathologies including CVDs, T2D, cancer, osteoarthritis, fatty liver disease, metabolic syndrome, depression and autoimmune diseases [2, 7, 19]. In 1990's Hotamisligil et al. first illustrated that inflammatory cytokines produced in OIIM can directly trigger insulin resistance via altering insulin signalling [23]. Importantly, OIIM shown to be established prior to diagnosis of obesity-linked diseases such as T2D [209, 210], suggesting that OIIM is not just a manifestation but also critical driver of obesity-associated pathologies [1, 211].

In oversimplified terms, obesity leads to complex immune dysregulation in various immune cells creating the OIIM. Specifically, infiltration of activated T cells and macrophages have been shown to play crucial roles in the establishment of OIIM [7, 8]. Recent studies illustrated that OIIM can be established in other critical tissues such as the liver [212], pancreas [213], hypothalamus [214, 215], skeletal muscle and fat tissues creating the obesity-induced chronic meta-inflammation [216].

OIIM is a central hallmark of obesity due to is complex interrelations with other obesity hallmarks as previously discussed [7]. Therefore, a better understanding of OIIM and the biological mechanisms inducing the OIIM is required for better therapeutic strategies against obesity-linked pathologies [101].

To understand the complexity of the OIIM, I shall dissect the immune cells involved in maintaining and establishing the OIIM. The immune system itself is composed of two interrelated arms: innate and adaptive immunity. Innate immunity is the first-line defence which recognises common hallmarks of pathogens and initiates inflammatory responses [217]. Contrastingly, adaptive immunity is the second line of defence consisting of highly specialised responses against distinct pathogens [217]. The cross-talk between innate and adaptive immune cells is highly important in the OIIM - dysregulation of one arm can influence the other arm.

However, for purposes of this thesis, I shall be investigating on the adaptive immunity with specific analysis on obesity-induced pro-inflammatory effects on $CD4^+$ T cells.

1.7.1. Adaptive immune system

Adaptive immunity is composed of bone marrow-derived (B cells), thymus-derived (T cells) and natural-killer cells [218]. Alongside innate immunity, adaptive immunity consists of T cells mediating cellular immunity whereas B cells mediating humoral immunity [218]. The adaptive immune response is highly specialised- immune cells specifically form responses against antigens and also orchestrate other immune cells to neutralise pathogens. Unlike innate immunity, adaptive immunity has the capacity for immunological memory where upon future exposure immediate immune responses neutralise pathogens [218]. This specificity is possible through the antigen-specific receptors upon T cells (TCRs) and B cells (BCRs) which recognise antigens and activate the cell [218, 219]. Upon TCR/BCR activation, the cells can differentiate into specific subsets (e.g. T cells can differentiate towards T helper ($CD4^+$), cytotoxic ($CD8^+$), regulatory and memory subtypes [218-220].

1.7.1.1. T cells

T lymphocytes are the primary effectors of adaptive immunity. T lymphocytes are specialised in cytokine secretion, direct cytotoxicity, immune regulation and immune memory functions [218]. Although T cells originate from bone marrow, they are differentiated in the thymus and secondary lymphoid organs [218]. This complex differentiation process creates diversity and heterogeneity within T cells, allowing their action against various immune stimuli. In order to activate an efficient T cell response, antigens are presented to them by antigen presenting cells (APCs) including DCs, macrophages or B cells [218, 221].

In obesity context, T lymphocytes were shown to be elevated in various tissues including adipocytes, myocytes and hepatocytes [222, 223]. This accumulation of tissue-specific T lymphocytes is also associated with obesity-linked diseases including T2D, CVDs, fatty-liver diseases, cancer and autoimmune conditions [222]. Nishimura et al. illustrated that cytotoxic $CD8^+$ T cell populations elevated and induced the migration of macrophages into adipose tissues OIIM [224]. Furthermore, pro-inflammatory cytokines and chemokines released by T cells have been documented to increase the recruitment of other pro-inflammatory immune cells to OIIM [222, 224].

Alternatively, $CD4^+$ T cells are shown to have subset-specific modulations in OIIM including an increase in pro-inflammatory lineages (Th1 and Th17) and a reduction in regulatory T cell lineages (Tregs) [222, 223, 225, 226]. The critical alterations in T cell profile

is shown to be crucial characteristics and mediator of the pathological shift to OIIM [222, 223, 225].

1.7.1.1.1. $CD4^+$ T cell origins and development

T cells originate from lymphoid hematopoietic stem cells found in the bone marrow. Unlike B cells, T cells migrate to the thymus for maturation where T cell receptor (TCR) recombination and $CD4^+$ and $CD8^+$ differentiation occurs [218]. The thymus consists of a complex microcellular environment with a combination of stromal cells, chemokines and cytokines necessary for T-cell maturation [218, 227]. Additionally, within the thymus, T lymphocyte precursors (thymocytes) undergo negative selection where cells with very high and very low affinity MHCs undergo apoptosis and thymocytes with intermediate affinity gets selected [218, 227]. Furthermore, the ability of the TCR to recognise antigens presented by MHC class-I or MHC class-II defines the differentiation into $CD8^+$ or $CD4^+$ respectively [218, 221, 228]. Once the core CD4 T cell receptor forms, thymocytes which become functional naïve $CD4^+$ T cells migrate to secondary lymphoid organs such as spleen, lymph nodes and other lymphoid tissues [227, 229].

The naïve $CD4^+$ T cell population leaving the thymus is highly heterogenous and dynamic in terms of functionality and phenotype, their subsequent travel to the secondary lymphoid organs supports their further differentiation [227, 230, 231]. Interestingly, the $CD4^+$ natural T regulatory cells (nTregs-$Foxp3^+$,$CD25^+$), which have a distinct role of immune regulation, are the only subset fully differentiate in thymus [227, 230, 231]. In the periphery, the naïve $CD4^+$ T cells constantly recirculate between blood, lymph nodes and peripheral tissues searching for antigen recognition [229]. They express two main surface markers of naïve $CD4^+$ T cells; CD62L and CC-chemokine receptor 7 (CCR7), that facilitate the recirculation between tissues [232, 233]. Additionally, human naïve $CD4^+$ remain in G_0 phase of cell cycle which is characterised by high expression of CD45RA and CD27 and low expression of CD44 and CD45RO [234, 235].

Recognition of a specific antigen by TCR and ligation of costimulatory molecules induce the activation of T cells including downstream signalling pathways leading to autocrine secretion of growth factors, cytokines (IL-2 and IL-7) and differential gene expression [227, 234]. Activation-linked changes induces survival, proliferation and further effector differentiation of $CD4^+$ T cells [218, 221]. $CD4^+$ T cells have highly diverse functionality that

requires further specificity and differentiation of naïve T cells according to strength and type of activation and costimulatory molecules. Based on these factors, naïve cells further differentiates into distinct $CD4^+$ effector T cell subtypes such as T-helper 1 (Th1) and Th2, Th17, Th 9, Th 22, follicular-helper T-cell (Tfh) and induced T-regulatory cells (iTregs) [218]. Each T-cell lineage also requires the presence of different cytokines and leads to the expression of distinct transcription factors associated with distinct effector T cell phenotypes [218, 221].

1.7.1.1.2. $CD4^+$ T cell activation

Activation of $CD4^+$ T cells by a cognate antigen presented by MHC-II, is highly important for the further differentiation of naïve $CD4^+$ T cells into distinct effector phenotypes. Although various immune cells are capable of presenting antigens to $CD4^+$ T cells, DCs have been shown to have the highest ability to activate naïve $CD4^+$ T cells [227, 236].

$CD4^+$ T cells require three signals for successful stimulation; "signal-1" through TCR and "signal-2" through co-stimulation molecules and "signal-3" through cytokines (**Figure 1.7**). Following the TCR-MHC-II engagement, co-stimulatory receptors such as CD28, lymphocyte function-associated antigen-1 (LFA-1), cytotoxic T-lymphocyte-associated protein-4 (CTLA-4/CD152) or inducible co-stimulator (ICOS) needs to be activated [227, 237]. Consistently, APCs express the ligands for these co-stimulatory receptors such as CD80, CD86 (for CD28 receptor) and intracellular-adhesion molecule-1 (ICAM1/CD54) for LFA-1 [227, 237]. Co-stimulatory signals are required to augment TCR signalling, promote proliferation, cytokine production and differentiation whereas the absence of co-stimulatory signals leads to anergy (hyporesponsiveness), inhibition of proliferation and differentiation [238]. Contrastingly, dysregulation of TCR signalling can lead to hyperactivation of $CD4^+$ T cells leading to various autoimmune conditions [237].

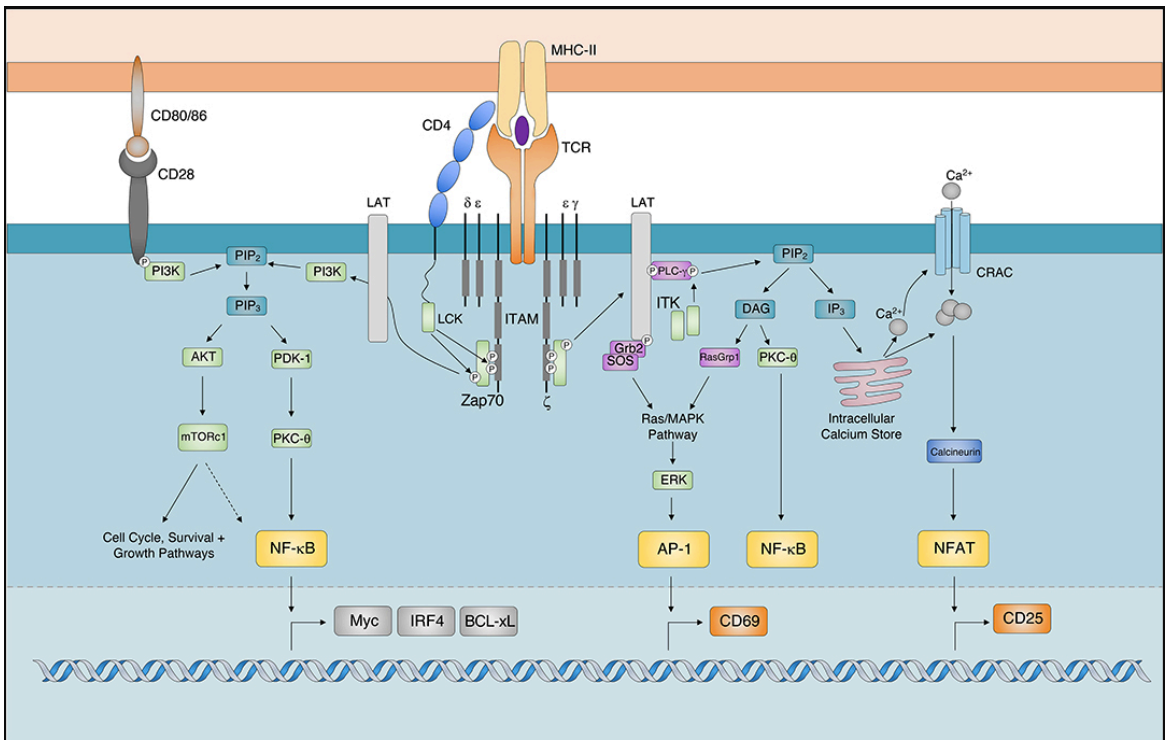


Figure 1.7) Schematic representation of T cell activation signalling pathways. Three crucial activation signals were represented; signal-1" through TCR following the recognition of MHC-II and "signal-2" through co-stimulation molecules (CD28) and "signal-3" through cytokines. Following the phosphorylation of LCK and Zap70, activated Zap70 phosphorylates the scaffold adaptor proteins, Linker for Activated T cells (LAT). Activation of LAT induces a series of downstream phosphorylation events including the activation of PI3K/AKT/mTOR and RAS/MAPK/ERK pathways. Figure taken from Bhattacharyya and Feng, 2020 [239].

Following the activation, the cytokine milieu of the microenvironment is also highly critical in mediating downstream signal transductions and transcription factors for effector $CD4^+$ T cell lineage differentiation [227, 239, 240]. Based on the immune challenge, APCs secrete distinct cytokine and chemokine that recruit $CD4^+$ T cells to the site of inflammation and drive the effector differentiation. During the differentiation process, naïve $CD4^+$ T cell also secretes cytokines associated with the lineage, creating a 'positive feedback loop' to marginally enhance both differentiation and effector response [227, 234, 241].

1.7.1.1.3. $CD4^+$ TCR signalling pathways

Activation of the $CD4^+$ TCR and co-stimulatory receptors induce a series of signalling pathways. The three major pathways shown to play a crucial role in inducing effector T cell phenotype; calcium flux, RAS/MAPK/ERK pathways and PI3K/AKT/mTOR [240, 242, 243].

Lymphocyte-specific protein tyrosine kinase (LCK) and zeta-chain-associated protein kinase-70 (Zap-70) are the two main protein tyrosine kinases (PTKs) that initiates the activation of TCR signalling cascade [239, 244]. Activation of LCK effectively phosphorylates both immunoreceptor Tyrosine-based Activation Motifs (ITAMs) which facilitates the docking and activation of Zap-70 and also directly phosphorylate Zap-70. Additionally, activated LCK contributes to the recruitment of Ras proteins for activating RAS/MAPK/ERK pathways [245]. Activation of Ras induces a sequential activation of the kinases Raf, MAP kinase/ERK kinase 1/2 (MEK 1/2) and ERK 1/2 respectively. Extracellular signal-regulated kinases (ERK 1/2) are critical mediator of TCR signalling and T cell differentiation [246].

Importantly, TCR signalling with contributions of certain cytokines can also stimulate the PI3K-AKT-mTOR pathway [240, 247, 248]. Mechanistically, phosphorylation of CD28 shown to activate p85 subunit of phosphoinositide 3-kinase (PI3K) stimulating the downstream molecules including phosphoinositide-dependent kinase 1 (PDK1) and AKT. Activation of AKT by phosphorylation from two residues; serine 473 (Ser473) and threonine 308 (Thr308) is also shown to be critical for the T cell differentiation and activation alongside cell metabolism, survival and cell-cycle control [240, 249]. Furthermore, AKT also activates mammalian target of rapamycin (mTOR) which induces transcriptional activation of NF-κB.

Activation of the T cells leads to rapid phosphorylation of the kinases inducing the transcription of c-Fos, JunB, mTOR and NF-κB resulting in production of various cytokines to mediate cell differentiation, proliferation and cell metabolism [244, 245, 250]

1.7.1.1.4 Differentiation of $CD4^+$ T cell into effector lineages

1.7.1.1.4.1. Th1

Th1 cells are one of the first identified 'inflammatory' effector $CD4^+$ T cell phenotype [251]. Th1 cells orchestrate inflammatory response by increasing the phagocytotic capacity of macrophages, inducing antibody production by B-cells and secreting further pro-inflammatory mediators including IFN-γ and TNF-α [227, 252]. IL-12 and IFNγ are the two main cytokines inducing expression of the T-box expressed in T cells (T-bet) TF, leading to Th1 differentiation [227, 252-254]. Alongside activating Th-1 differentiation gene network, T-bet is also shown to

suppress Th2 and Th17 cell lineages [227, 255, 256]. In addition to the T-bet master regulator, STAT-1 and STAT-4 TFs were also shown to induce Th1 differentiation [227, 252].

Although both STAT-4 and T-bet can directly induce transcription of IFNγ locus, they do not function linearly, as the pathway of Th1 differentiation is defined by the cytokine milieu in the cellular microenvironment [257, 258]. IFNγ has been shown to activate STAT-1 that directly activates T-bet expression and Th1 differentiation [257, 258]. Additionally, IL-12 secreted by APCs is also shown to activate STAT-4 via the JAK/STAT pathway, inducing IFNγ production and Th1 differentiation [254, 257, 259]. Importantly, both signalling pathways work cooperatively leading to a positive feedback loop that amplifies the expression of T-bet, IFNγ and other Th1-associated genes [227, 258].

Importantly, dysregulation of Th1 population is known to be associated with various inflammatory pathologies. Interestingly, T-bet is also shown to act as a transcriptional regulator by recruiting Bcl-6 to limit the IFNγ expression and Th1 differentiation as a control mechanism [227, 260]. However certain pathological microenvironments, like OIIM, can escape this regulation and trigger an excessive Th1 and Th17 response. It is well known that diet-induced obese mice have higher IFNγ producing Th1 $CD4^+$ T-cells [261, 262]. Accumulation of IFNγ producing Th1 T cells induces the activation and infiltration of pro-inflammatory macrophages to peripheral tissues leading to HFD-induced OIIM in murine models [222, 224, 263-265]. Importantly, it has been recorded that obese visceral and subcutaneous adipose tissue contain 10-20 fold higher Th1 and Th17 population compared to Th2 and Treg populations [222, 266]. Although the exact mechanism of this pathophysiological process is not fully understood yet, it is clear that the Th1 $CD4^+$ T-cell population plays a key role in establishing and propagating the OIIM [224, 263, 264].

1.7.1.1.4.2. Th2

Th2 $CD4^+$ T cell lineage is highly important in B cell humoral immunity and innate immunity [263]. Th2 cells have been shown to modulate various immune cells via secreting IL-4, IL-5 and IL-13 cytokines which inhibit macrophage activation, augment 'anti-inflammatory' M2-macrophage differentiation and induce antibody secretion (e.g. IgA and IgE) [263, 267, 268].

IL-4 is the main cytokine driver of Th2 differentiation that activates the STAT-6 TF and leads to upregulation of GATA Binding Protein 3 (GATA-3) [227, 269, 270]. The GATA-3 TF is the master regulator of Th2 differentiation that enhances Th2 differentiation both directly via growth factor independent 1 transcriptional repressor (Gfi-1) and indirectly via inhibiting T-bet, STAT4 and Th1 differentiation [227, 271]. The balance of the Th1 and Th2 scale is highly interrelated and TFs of each lineage forms a regulatory feedback loop to control the immune response. In addition to GATA-3 master TF, IL-2 induced STAT-5 [272] and IL-4-independent STAT6 TFs are also shown to be essential for a successful Th2 differentiation [227, 271, 273].

Th2 cells are conventionally considered as 'anti-inflammatory' due their alleviating effects on OIIM [227, 262, 266]. Consistently, murine studies illustrated the inverse correlation between Th2 and OIIM where loss of $GATA3^+$ Th2 $CD4^+$ T cells in DIO models exacerbated the OIIM [222, 262]. Importantly, adoptive transfer of $GATA3^+$ Th2 $CD4^+$ T cells into Rag-1-deficient murine models proved the anti-inflammatory and anti-obesity effects of Th2 cells as the DIO mice prevented further weight gain and ameliorated insulin signalling [262]. Additionally, clinical studies on humans illustrated a small but significant decrease in Th2 frequencies within the adipose tissue of obese patients compared to lean [266, 274].

1.7.1.1.4.3. Th17

Th17 $CD4^+$ T helper cells were discovered relatively recently based on the IL-17 cytokine secretion which is shown to be critical T cell phenotype in the pathogenesis of obesity-associated diseases autoimmune diseases including MS, RA, psoriasis and inflammatory-bowel diseases and cancer [275-278]. Th17 cells are capable of producing the three isoforms of 'pro-inflammatory' IL-17 cytokine; IL-17F, IL-17A and IL-17AF [278, 279]. All three isoforms have a similar inflammatory potential, due to their biochemical homology [279, 280]. Crawford et al. 2020, illustrated that alongside pro-inflammatory effects, IL-17 can also trigger a resistance against immune regulation of $CD4^+$ T cells [281]. Additionally, Th17 T cells are also known to secrete other cytokines such as TNF-α, IL-22 and IL-26 which can act as both pro- or anti-inflammatory in a context-dependent manner [278, 282, 283].

Th17 differentiation is relatively more complex compared to other $CD4^+$ T cell lineages. This is because the differentiation consists of 3 stages: (1) initiation of differentiation by TGF-β and IL-6, (2) self-amplification by IL-21 and (3) maintenance/stabilisation via IL-23 [227,

284, 285]. Retinoic-acid receptor-related orphan receptor gamma-T (RORγt) is accepted as the master regulator that works co-operatively with STAT-3 TF in Th17 differentiation [227]. Low concentrations of TGF-β with IL-6 activate RORγt and IL-21 whereas TGF-β-independent signalling pathway (activated via IL-6, IL-21 and IL-23) can also induce STAT-3 activation [227, 284, 286]. Activation of RORγt and STAT-3, activate IL-17 promoters which are further detailed in **Chapter 4.1** [287]

Various murine and human studies illustrated that Th17 $CD4^+$ T-cell frequencies significantly increase with obesity [288-291]. Th17-secreted excessive IL-17 is shown to disrupt to exacerbate the OIIM in adipose, liver and muscle tissues [227, 288]. Importantly, various DIO murine models reported an obese bias in $CD4^+$ T differentiation towards pro-inflammatory Th17 lineage (with a higher IL-17-producing potential), while reciprocally reducing the Treg frequencies within the OIIM [290, 291]. Consistently, clinical data obtained from obesity-linked T2D patients illustrated an increased in Th17 population and IL-17 levels with a significant loss in Treg frequencies [291]. The importance of this delicate balance between Th17 and Treg populations will be further detailed in **Chapter 4.1**.

Although it is not fully understood how obesity can induce this pro-inflammatory Th17 bias, it is speculated that distinct FA metabolites with immunomodulatory potentials and other pro-inflammatory cytokines within obese microenvironments could be definitive [227, 292]. Nicholas et al. 2019, illustrated a 'biasing' effect of long-chain FAs via mitochondrial changes in $CD4^+$ T cells promoting Th17 differentiation within obesity-linked T2D [292]. Additionally, excessive IL-1β presence (secreted by APCs) within the OIIM is also shown to promote Th17 differentiation alongside IL-17 and IL-22 secretion in obese T2 diabetic patients [289].

1.7.1.1.4.4. Regulatory T cells (Tregs)

Regulatory T cells are the main immune cell lineage that controls immune responses and prevents any dysfunction of the immune system [293]. Although Treg lineage accounts for only 10% of $CD4^+$ T cells, they are vital in regulating the balance between the pro- and anti-inflammatory functions [230]. $CD4^+$ T cells can fully differentiate into the natural Tregs (nTregs) phenotype in the thymus or can differentiate from naïve Th0 T cells in periphery known as inducible Tregs (iTregs) [217]. Although Tregs are considered as $CD4^+$ T cell lineage, studies also identified $CD8^+$ T cell lineage with regulatory suppressor functions [293].

Traditionally, Tregs are characterised by two cellular markers; IL-2 receptor-α (CD25) and forkhead box P3 (Foxp3) TF [217, 293]. Treg differentiation depends on various factors such as strong TCR stimulation (most potentially to 'self-antigen'), IL-2 cytokine/signalling and TGF-β leading to induction of Foxp3 [217]. Additionally, there are a few small $Foxp3^-$ Treg subsets identified with regulatory functions [231, 293, 294].

Importantly, TGF-β is shown to be a crucial cytokine for both iTreg and pro-inflammatory Th17 differentiation [227, 293]. Interestingly, TGF-β is shown to be produced by $Foxp3^+$ iTregs (as a paracrine-feedback loop), nTregs and other immune cells including DCs, macrophages and B cells [231, 293]. This illustrates the pluripotent actions of TGF-β, in driving two distinct T cell lineages with opposite inflammatory actions in a context-dependent way which will be detailed in **Chapter 4.1** [227].

Although Foxp3 is the master Treg-defining TF, other TFs including Smad3 and STAT-5 are also shown to play a crucial role in iTreg differentiation via both Foxp3-dependent and Foxp3-independent pathways [227]. Importantly, TGF-β-induced Smad3 is shown to augment Foxp3-expression alongside inhibiting RORγt and Th17 differentiation [227, 295]. Similarly, IL-2 is shown to induce STAT-5 TF that further enhances the Foxp3 expression and iTreg differentiation [227, 296, 297]. Additionally, STAT-5 can inhibit STAT-3 expression impairing Th17 differentiation [227, 296, 297].

Tregs can exhibit their immunosuppressive/regulatory functions via various mechanisms including secretion of anti-inflammatory cytokines (such as IL-10, TGF-β), expression of inhibitory receptors and deprivation of other cells from pro-inflammatory cytokines [223, 293]. The main immunosuppressive cytokine IL-10 is shown to exerts its anti-inflammatory potential by downregulating the expression of MHC-II and co-stimulatory molecules (CD28 and CD80/CD86) on APCs [293, 298]. Additionally, IL-10 can also decrease the secretion of pro-inflammatory cytokines (IL-6) by macrophages and other immune cells [298, 299].

Both human and murine DIO studies illustrated that, $Foxp3^+CD4^+$ Treg population frequencies significantly reduce within the OIIM [222, 223, 225, 226, 262]. The deficiency of Tregs is proven to be a pivotal characteristic that can induce and escalate the OIIM leading to obesity-associated pathologies including T2D, CVDs and autoimmune diseases [223, 225,

300]. Consistently, selective boosting of Treg frequencies in HFD-fed murine model ameliorated insulin sensitivity [226].

1.8. Immunomodulatory actions of bioactive lipids on $CD4^+$ T cells

As previously detailed, $CD4^+$ T cells play a pivotal role in OIIM by secreting pro-inflammatory cytokines and chemokines and recruiting other pro-inflammatory immune cells into the critical tissues of DIO models including adipose, muscle and pancreatic tissue [225, 227, 288]. Zou et al. has highlighted the importance of pro-inflammatory Th1 and Th17 $CD4^+$ T cell biasing with obesity in the establishment of OIIM [301]. Considering the critical pro-inflammatory effects of obesogenic diets as detailed in **Section 1.3**, it is suggested that distinct bioactive immunomodulatory metabolites can play a critical role in driving this obesity-linked pro-inflammatory memory. Consistently, obesogenic diets are also shown to bias the human $CD4^+$ T cell differentiation where increased FA concentration is shown to modulate the RORγt binding to DNA that directly promotes Th17 differentiation [302]

There are various bioactive lipid groups shown to induce this obesity-linked pro-inflammatory memory within different immune cells including macrophages and B-cells [18, 91, 101, 154, 303, 304]. Therefore, it is crucial to identify these bioactive mediators and the mechanisms that allows the immunomodulation of $CD4^+$ T cells.

1.8.1. Palmitic (PA) and Stearic (STE) SFAs

It is known that obesogenic diets are highly enriched with palmitic and stearic SFAs which altogether has critical impacts on obesity and associated diseases as previously discussed [46, 52]. Various studies suggested the immunomodulatory potential of SFAs towards a pro-inflammatory fate inducing the OIIM in various tissues and eventually leading to obesity-associated pathophysiologies [52, 91, 92, 305]. Whereas replacement of SFAs (with unsaturated olive oil) within WD shown to lower plasma cholesterol, lipid accumulation alongside of ameliorating the OIIM which shown to reduce obesity-associated atherosclerosis formation in murine models [305].

The pro-inflammatory effects of SFAs are well shown in macrophages where PA is shown to directly induce activation and dimerization of TLR1, TLR2, TLR4 and TLR6 [83, 84, 86]. Activation TLRs are shown to activate PI3K/AKT and NF-κB pathways leading to production of pro-inflammatory cytokines such as IL-8, IL-6 and TNF-α [86, 304, 306-308].

Recent publications illustrated similar PA-driven pro-inflammatory modulations in DIO adaptive immune cells [101]. Importantly, PA has also been shown to modulate $CD4^+$ T cells and augment the establishment of OIIM. Mauro *et al*. 2017, illustrated that PA can activate the PI3K/p110δ-Akt pathway leading to biased $CD4^+$ T cell differentiation towards a pro-inflammatory $CD44^{hi}$-$CCR7^{lo}$-$CD62L^{lo}$-$CXCR3^+$-$LFA1^+$ effector memory (EM) phenotype in HFD-fed murine models [18]. This priming effect of PA was shown to be independent of alterations in DC antigen presentation process. Similarly, PA also illustrated similar pro-inflammatory EM phenotype in $CD8^+$ T cells trough PA-driven metabolic reprogramming [309, 310]. Recently, PA is also shown to induce obesity-linked hypermetabolic alterations and execrated pro-inflammatory function in B-cells [311]. It is important to highlight hat the same pathways are also detected in both adaptive and innate immune cells, confirming the extensive effect of PA over various immune cell types.

As previously discussed in **Section 1.5** bioactive PA is also well known to modulate various critical cellular functions such as cellular metabolism, apoptosis, senescence, autophagy and epigenetic alterations. It is suggested that PA can also augment inflammatory response through modulating these cellular functions of immune cells. Consistently, bioactive PA-driven alterations in epigenetic structure have been associated with obesity and obesity-associated diseases [88, 312]. Although it is clear that obesity-induced DNA methylation and epigenetic changes play a major role in the establishment of OIIM, immune dysfunction and associated pathologies such as T2D [313-316], the effect of specific bioactive SFAs on epigenetic modifications is not well understood yet [211]. More recently, preliminary data suggested that bioactive SFA palmitate can directly modulate the gene expression profile of human $CD4^+$ T cells [317]. RNA-seq analysis on PA-treated human $CD4^+$ T cells demonstrated 989 upregulated and 1462 downregulated genes that were associated with various obesity-linked pathologies such as T2D and CVDs [317]. Consistent with Mauro et al., RNA-seq data of Zhou et al. (2019) also identified significant increase in gene expression of various PI3K/Akt signalling pathway genes following the *ex vivo* PA-treatment of $CD4^+$ T cells [317].

Although SFAs are known to have pro-inflammatory effects contributing to OIIM, the inflammatory potential of STE is controversial and unclear. There is no exact reason for this disparity yet, but it is speculated that the source of STE could play an important role [95].

Furthermore, some literature suggests an increase in inflammatory markers within the murine and human studies [303, 318], whereas various other studies suggest vice versa [95, 99].

Similar to PA, STE-treated macrophages induce the pro-inflammatory cytokines (TNF-α, IL-1β and IL-6) via inducing NF-κB and cyclooxygenase (COX-2) in a TLR4-dependent manner [303, 318]. Anderson et al., also illustrated that STE accumulation in macrophages can lead to ER stress-mediated apoptosis and induce inflammation in a TLR4/2-independent manner [319]. Furthermore, TLR4/2 independent pro-inflammatory action of STE is also confirmed in chondrocytes where STE was shown to induce pro-inflammatory cytokine synthesis via lactate-hypoxia-inducible factor-1α (HIF1α) pathway [320]. This was important, to confirm the pro-inflammatory effects of STE similar to other SFAs.

1.8.2. Oleic acid (OA) MUFA

Contrarily with deleterious SFAs, MUFAs (OA) are known to express ameliorative effects on the OIIM. Bioactive OA is capable of modulating membrane fluidity, intracellular signalling pathways, cellular metabolism and gene expression of immune cells [321]. Consistently, OA supplemented murine diet shown to elevate anti-inflammatory M2 macrophages and reduce the pro-inflammatory cytokine levels such as IL-1, IL-6 and TNFα [154, 322]. Furthermore, OA has also been shown to exert a regulatory effect on the biosynthesis of detrimental lipid groups (such as ceramides and diacylglycerol) that can potentially ameliorate the SFA-induced inflammation trend in obesity [323]. However, the exact scope of the ameliorative effect of OA on the OIIM is not fully understood yet.

1.8.3. Omega-3 (ω−3) PUFA

Omega-3 PUFAs are known for their anti-inflammatory nature as illustrated in various model organisms and humans. It is well shown that n-3PUFA can systemically improve the cardiovascular functioning [112, 114, 324] and also ameliorate T2D and insulin resistance [110, 116]. It is also suggested by the literature that n-3PUFA have a systemic effect that acts on various tissues at multiple levels [108, 110, 115].

Although the efficacy and complex immunomodulatory mechanisms of n-3PUFA (ω-3) are debatable, it is well known that n-3PUFAs exert their main beneficial effects by inhibiting the chronic OIIM [110, 125, 126]. Recent Meta-analysis highlighted the anti-inflammatory

therapeutic potential of ω-3 on various human autoimmune diseases including RA, MS and systemic lupus [325]. Specifically, a human cohort illustrated a negative association between n-3PUFA concentrations and pro-inflammatory markers such as IL-6, TNF-α, IL-1β alongside a positive association with anti-inflammatory markers such as IL-10 and TGF-β [326]. Furthermore, n-3PUFA is also shown to inhibit the synthesis of various critical pro-inflammatory lipid groups such as ceramides and diacylglycerol which indirectly alleviate the OIIM [117-120].

Literature suggests 3 main anti-inflammatory mechanisms of n-3PUFA in ameliorating the OIIM. Firstly, n-3PUFA are shown to be directly recognised by distinct receptors such as TLR4, NLR pyrin domain containing receptor 3 (Nlrp3) and G-protein-coupled receptors (mainly GPR120) expressed by immune cells (such as macrophages), leading to reduced inflammatory cytokine and chemokine responses [1, 327, 328]. Secondly, n-3PUFA can modulate the activation, differentiation and motility of T-lymphocytes [1, 126, 329, 330]. Thirdly, n-3PUFA can divert the availability of the substrates, such as PA, and inhibit the synthesis of various critical pro-inflammatory lipid groups like ceramides and ω−6 PUFAs [119, 331, 332].

It was initially identified by Oh et al. (2010) that GPR120 can function as n-3PUFA receptor which in turn mediates the anti-inflammatory potential of n-3PUFA in macrophages and adipocytes [327]. Activation of GPR120 by n-3PUFA inhibits both TLR2/3/4 and TNF-α inflammatory signalling pathways [327]. Consistently, n-3PUFA also reduce inflammatory M1 macrophages by inhibiting the M1 pro-inflammatory gene expression and boosting the M2 anti-inflammatory gene expression- including IL-10 production in adipose tissues [327, 333].

Importantly, n-3PUFA signalling through GPR120 impedes the NF-κB-driven pro-inflammatory gene expression of IL-6, TNF-α, IL-1β, iNOS and CD11c [110, 327]. Additionally, n-3PUFA is shown to suppresses the activation of TLR4 receptors (via GPR120) leading to various anti-inflammatory actions and ameliorating the OIIM in obesity-lined diseases such as T2D and CVDs in both murine and humans [334, 335]. Consistently, a randomised double-blind clinical trial on obese pregnant women illustrated that n-3PUFA supplementation to diet significantly reduced TLR4 expression and corresponding pro-inflammatory cytokine expression such as IL-6, IL-8, and TNF-α in both adipose and placental tissues [336]. Furthermore, n-3PUFA is shown to act as a broad inhibitor of NLRP3 inflammasome and inhibits the activation and subsequent pro-inflammatory cytokine

expression of IL-1b, TNFα, MCP-1 [337-339]. Importantly, n-3PUFA-dependent inhibition of Nlrp3 activation has been shown to exert beneficial effects on HFD-induced T2D murine models via alleviation of OIIM [337, 338].

Interestingly, both beneficial n-3PUFA and deleterious pro-inflammatory bioactive SFAs and ceramides were shown to act on the same molecular receptors and pathways such as TLR4 and NLRP3 [1, 120, 339]. Although the full-scale anti-inflammatory mechanism of n-3PUFA's is not fully understood, these unveiled mechanisms indicate potential molecular links among bioactive lipid groups. Recent evidence illustrates that n-3PUFAs can also directly limit the biosynthesis of pro-inflammatory lipid groups, such as ceramides [119, 120, 340].

Recent publications on $CD4^+$ T cells and n-3PUFAs illustrated the anti-inflammatory actions such as reduction in pro-inflammatory T cell fates and cytokines and upregulation of anti-inflammatory T cell fates [126, 341, 342]. It is suggested that, bioactive n-3PUFAs (EPA), can upregulate immune tolerance by directly inducing $Foxp3^+$ Treg differentiation and anti-inflammatory IL-10 cytokine secretion in murine models [126, 341, 343]. Interestingly, an *in vitro* macrophage and naïve $CD4^+$ T cell co-culture model identified the critical role of GPR120 in adipose tissue macrophage-mediated Treg induction via n-3PUFA supplementation [344]. Consistently, GPR120 receptor knockout $CD4^+$ T cells illustrated the importance of GPR120 in n-3PUFA-driven upregulation of IL-10 mTOR and Stat5 [345]. Although these investigations does not provide direct evidence in terms of n-3PUFAs complex mechanism on $CD4^+$ T cells, it highlights the critical interplays between other cell [345, 346].

1.8.4. Ceramides

SFA-enriched obesogenic diets lead to the accumulation of long-chain ceramides (including C16, C18, C22 and C24) in both murine and human models [123, 124, 135, 173, 347]. PA is the main substrate of *de novo* ceramide biosynthesis pathway. Consistently, direct oral gavage of palmitate-rich HDF leads to an immediate significant increase in total ceramide levels in murine models, which is further validated with both murine and human *in vitro* models [174]. Both human and non-human primates, aged individuals had elevated serum C24:1 levels; which is also associated with a higher risk of CVDs and memory impairment [176]. Moreover, the obesogenic diet-induced increase in ceramide levels was highly associated with various obesity-linked diseases including CVDs [173, 348, 349], T2D, insulin resistance [123, 135,

186, 350-352], body weight gain [135, 186, 351], hepatic steatosis [353, 354] and metabolic syndrome [355, 356].

Ceramides have been recognised as a new class of second messengers leading pro-inflammatory modulation of various immune cells in critical tissues associated with obesity-linked pathophysiologies [151]. Distinct bioactive ceramides can directly increase the secretion of pro-inflammatory cytokines like IL-1β, TNF-α, IL-6 and IL-17, in both *in vivo* and *in vitro* models [357-359]. The first pro-inflammatory mechanism of ceramides is identifien on macrophages via TLR4 receptor and downstream activation of the PI3K-AKT pathway and NF-κB TF [148, 360]. It is known that PA-induced ceramide accumulation leads to a dose-dependent expression of pro-inflammatory cytokines like IL-6 via TLR4 in murines [360]. Importantly, it is also observed that PA or ceramide-induced activation of TLR4 leads to an upregulation of ceramide synthesis pathways via activating various ceramide biosynthesis enzyme genes such as Sptlc2 and CerS in NF-κB-dependent manner [132, 148, 361, 362].

Importantly, this highlights the pro-inflammatory modulatory potential of ceramides that can directly and indirectly induce OIIM and also upregulate its biosynthesis creating an inflammatory feed forward loop. Additionally, Vandanmagsar et al. (2011), also identified a critical link of obesity-induced ceramide accumulation leading to OIIM via activating macrophages and T lymphocytes through NLRP3. The NLRP3 inflammasomes were shown to sense ceramides and activate pro-inflammatory cytokine secretion [363, 364]. Overall, the current literature suggests that activation of PI3K p110d-AKT, NF-κB and mTOR signalling pathways via TLR4 and NLRP3 are involved in the ceramide-induced immune modulation. However, considering the extensive modulatory effects of the diverse ceramides acting on various cells in a tissue-specific manner, it is suggested that there are many more mechanistic interactions waiting to be uncovered [1].

We have previously published a comprehensive literature review on the pro-inflammatory effect of ceramides observed on distinct immune cells within obesity-linked pathologies. This review also documented the ameliorative effects observed once the ceramide levels returned to basal levels [1]. Therefore, I will mainly focus on the immunomodulatory actions of ceramides on $CD4^+$ T cell differentiation and functionality that potentially drives the OIIM.

1.8.4.1 Immunomodulatory actions of ceramides on $CD4^+$ T cell differentiation

Three main immunomodulatory actions of ceramides have been observed on $CD4^+$ T cells: (1) motility and homing (2) activation of antigen-recognition receptors (TCR, CD3, CD28) and (3) differentiation to effector phenotype and functions [359, 365]. It should be noted that with all three immunomodulatory actions, there are controversial literature reported, leading to high discrepancies in the field.

The importance of the ceramide modulated biasing effects on $CD4^+$ T cell differentiation and the corresponding impact on the obesity-linked pathophysiologies were noticed relatively recently [359, 366-368]. Bai et al. (2015) reported one of the first direct modulatory effect of ceramides on $CD4^+$ T cell differentiation where inhibition of ceramide synthesis also downregulated the pro-inflammatory Th1, Th2 and Th17 $CD4^+$ T cell phenotypes [369]. Importantly Bai et al reported that ASM enzyme-driven ceramide synthesis can directly mediate $CD4^+$ T cell effector differentiation via altering the T cell activation [369]. The ASM is shown to modulate the intracellular downstream signalling components of both CD3-ZAP70-MAPK/JNK and CD28-PI3K-Akt-mTOR pathways, consequently leading to pro-inflammatory Th1 and Th17 differentiation and upregulated the biosynthesis of ceramides further [368, 369].

Furthermore, Sofi et al. (2016), investigated the immunomodulatory actions of C16 synthesised by CerS6 in a murine knockout model, where C16 directly contributed to inflammation by promoting IFNγ secretion and Th1 differentiation [367]. Differently from Bai et al. (2015), Sofi et al. (2016) illustrated that C16 modulate TCR responsiveness via modulating the TCR affinity and signal transduction [367]. The CerS6 knockout model illustrated a significant reduction in TCR activation and tyrosine phosphorylation including ZAP-70 [367]. Importantly, as previously observed in innate immunity, Sofi et al. (2017), also highlighted the inflammatory feed-forward loop between TCR activation and upregulation of CerS6-induced C16, where both processes modulate functionality of the effector $CD4^+$ T cell to a pro-inflammatory context [367]. Consistently clinical studies also reported an elevation in CerS6 mRNA expression and C16 ceramide concentrations in obese human adipose tissue [186].

Considering the critical role of T cell activation and PI3K-AKT pathway in Treg differentiation, it has been long speculated that ceramides could be directly modulating Treg differentiation. This speculation was further supported by the observation that Tregs gradually deplete and ceramides accumulate during obesity as a result of excessive SFA substrates. Zhou et al. (2016) elegantly illustrated that ASM enzyme of salvage ceramide biosynthesis pathway plays a crucial role in negative regulation of Treg development. The knockout of ASM directly shown to increase Foxp3$^+$ Treg population in both *in vivo* and *in vitro* assays [357]. It is shown that ASM-knockout model with lower ceramide concentration impaired the activation of PI3K-AKT and mTOR pathways, resulting in higher Foxp3 expression and Treg differentiation [357, 368].

Additionally, Hollmann et al. (2016) illustrated consistent data with Zhou et al. (2016) where ASM inhibition either via genetic knockout or pharmacological inhibitors directly elevated the Foxp3$^+$ Treg populations and suppressive actions [370]. However, differently from Zhou et al., they suggested that ceramides modulate T-cell activation by altering the membrane lipid order as the ASM knockout murine model had a higher membrane order potentially facilitating the TCR activation and more suppressive Tregs in the knockout group [370].

It is important to note that different ceramides with different doses are shown to express their immunomodulatory effects in a highly-context dependent manner. In line with Zhou et al. 2016, there are other controversial publications illustrating ceramide-induced modulations in T cell differentiation independent of TCR signalling cascade [365, 371, 372]. Altogether current literature highlights the critical immunomodulation of bioactive ceramides in T cell differentiation however, there are many more mechanistic interactions waiting to be uncovered.

Chapter 2) MATERIALS AND METHODS

Materials

2.1 In vivo murine diet experiments

Table 2.1.1) DIO *in vivo* murine model

Reagents	**Supplier**	**Cat #**
Basal Chow diet (5755)	Test diet, USA	T-5755-1817109
Western rodent Diet (AIN-76A)	Test diet, USA	T-5342-1810060
Western rodent diet with 5% menhaden fish (AIN-76A+ω3)	Test diet, USA	T-5BBQ-1816188-200
HFD rodent diet w/60% energy from fat (58Y1)	Test diet, USA	T-58Y1-58126
FTY720 (SML0700) inhibitor	Sigma-Aldrich	SML0700-5MG

2.2 In vitro cell culturing

Table 2.2.1) General *in vitro* and *ex vivo* cell culture reagents

Reagents	**Supplier**	**Cat #**
Phosphate buffered saline (PBS) tablets 1 tablet per 500ml distilled water	Gibco (ThermoFisher)	18912014
RPMI1640 Med 1X w/L-Glutamine (with phenol red)	Gibco (ThermoFisher)	21875034
Penicillin. Streptomycin solution. 5000 U/ml	Gibco (ThermoFisher)	15070063
Fetal bovine serum (FBS) Referred also as Fetal calf serum (FCS)	Gibco (ThermoFisher)	16000044
L-Glutamine solution (200 mM)	Sigma Aldrich	G7513
2-Mercaptoethanol solution (β-mercaptoethanol)	Gibco (ThermoFisher)	21985023
Minimum Essential Medium (MEM) Non-Essential Amino Acids Solution	Gibco (ThermoFisher)	11140050

Trypan blue solution (0.4%)	Gibco (ThermoFisher)	15250061
Costar multiple well cell culture flat bottom plates Flat bottom, non-pyrogenic, polystyrene (6-well, 12-well, 24-well, 48-well, 96-well)	Corning	3335; 3336; 3337; 3338
Falcon multiple well cell culture plates Flat bottom, non-pyrogenic, polystyrene (6-well, 12-well, 24-well, 48-well, 96-well)	Falcon (ThermoFisher)	351146; 351143; 351147; 351178;
Falcon easy-grip tissue culture dishes (6-well, 12-well, 24-well, 48-well, 96-well)	Falcon (ThermoFisher)	353001
70 µm Cell Strainer, Sterile	Falcon (ThermoFisher)	352350
Falcon™ Round-Bottom Polystyrene Test Tubes	Falcon (ThermoFisher)	10579511

Table 2.2.2) $CD4^+$ T cell isolation and activation

Reagents	**Supplier**	**Cat #**
Red Blood Cell Lysing Buffer Hybri-Max (1X)	Sigma Aldrich	R7757
Ficoll-Paque Plus	Sigma Aldrich	GE17-1440-02
EasySep™ Mouse CD4+ T Cell Isolation Kit	Stemcell Technologies	19852
EasySep™ Mouse Naïve CD4+ T Cell Isolation Kit	Stemcell Technologies	19765
EasySep™ Human CD4+ T Cell Isolation Kit	Stemcell Technologies	17952
EasySep™ Human Naïve CD4+ T Cell Isolation Kit	Stemcell Technologies	19555
Ethylenediaminetetraacetic acid disodium salt solution (EDTA)	Sigma Aldrich	E7889
Dulbecco's phosphate-buffered saline (DPBS) free of calcium and magnesium	Gibco (ThermoFisher)	14190144
EasyEights™ EasySep™ Magnet	Stemcell Technologies	18103
Countess Cell Counting Chamber Slides	Invitrogen (ThermoFisher)	C10228

Table 2.2.3) Cytokines and stimulants

Reagents	**Supplier**	**Cat #**	**Clone**	**Stock concentration**	**Final concentration**
Anti-mouse CD3 Monoclonal Antibody, Functional Grade	eBioscience (ThermoFisher)	14-0032-82	17A2	0.5mg/ml	1µg/ml
Anti-mouse CD28 Monoclonal Antibody, Functional Grade	eBioscience (ThermoFisher)	16-0289-81	CD28.2	1mg/ml	1µg/ml
Anti-human CD3 Monoclonal Antibody, Functional Grade	eBioscience (ThermoFisher)	16-0037-81	OKT3	1mg/ml	2.5µg/ml
Anti-human CD28 Monoclonal Antibody, Functional Grade	eBioscience (ThermoFisher)	16-0289-85	CD28.2	1mg/ml	1.5µg/ml
Dynabeads Human T-Activator CD3/CD28	Gibco (ThermoFisher)	11131D	N/A	4×10^7 Dyna beads/ml	Bead-to-cell ratio 1:1
Recombinant Human IL-2	Peprotech	200-02	E.coli derived	50µg/ml	*23ng/ml (50IU/ml)
Recombinant Human TGF-β1	Peprotech	100-21C	CHO derived	10µg/ml	*10ng/ml
Recombinant IL-12 p70	Peprotech	210-12	CHO derived	10µg/ml	
Recombinant Murine IL-4	Peprotech	214-14	E.coli derived	5µg/ml	
Cell Activation Cocktail 500X	Biolegend	423303	N/A	N/A	1.5µl/ml
GolgiStop Protein Transport Inhibitor (Containing Monensin)	BD Biosciences	554724	N/A	N/A	1µl in 1.5 mL of sample
Phorbol 12-myristate 13-acetate (PMA)	Sigma Aldrich	P1585	N/A	5µg/ml	0.05µg/ml
Ionomycin	Stemcell Technologies	73722	N/A	10 mg/mL	0.5µg/ml
Chloroquine	Cell signaling	14774	N/A	50mM	50µM
Rapamycin	Cell signaling	9904	N/A		

Table 2.2.4) Bioactive lipid groups

Reagent	**Supplier**	**Cat #**	**Stock concentration**	**Final concentration**
C2 Ceramide (d18:1/2:0)	Avanti Polar lipids, US	860502P	3.75mM	0.01µM - 10µM
C6 Ceramide (d18:1/6:0)	Avanti Polar lipids, US	860506P	3.75mM	0.01µM - 10µM
C24 Ceramide (d18:1/24:0)	Avanti Polar lipids, US	860524P	3.75mM	0.01µM - 10µM
Oleic acid	Cayman Chemical	90260	4 & 10mM	50 µM
Sodium palmitate	Sigma Aldrich	P9767	4 mM	50 µM
Stearic acid	Cayman Chemical	10011298	4 & 10mM	50 µM
Bovine Serum Albumin (Fatty-acid free)	Sigma Aldrich	A8806	N/A	4mg/ml

2.3 Flow cytometry

Table 2.3.1) Flow cytometry antibodies used for both *in vivo* and *in vitro* assays

Reagents	**Fluorochrome**	**Supplier**	**Clone**	**Cat #**	**Dilution**
CD4 (anti-mouse)	BV785	Biolegend	GK1.5	100453	1/200
	FITC	Biolegend	RM4-5	100510	1/200
	FITC	eBioscience (ThermoFisher)	GK1.5	11-0041-85	1/200
CD4 (anti-human)	Brilliant Violet 711	Biolegend	OKT4	317440	1/200
CD44 (anti-mouse/human)	BV605	Biolegend	IM7	103047	1/200
CD183 (CXCR3) (anti-mouse)	BV421	Biolegend	CXCR3-173	126529	1/200
CD183 (CXCR3) (anti-human)	BV785	Biolegend	G025H7	353737	1/200
CD11α/CD18 (LFA-1α) (anti-mouse)	FITC	eBioscience (ThermoFisher)	M17/4	11-0111-85	1/200
	APC	Biolegend	H155-78	141009	1/200

CD8 (anti-mouse)	PerCP	Biolegend	53-6.7	100732	1/200
CD8 (anti-human)	PE/Dazzle 594	Biolegend	RPA-T8	301058	1/200
CD45 (anti-mouse)	PE/Dazzle 594	Biolegend	30-F11	103146	1/200
	FITC	Biolegend	30-F11	103108	1/200
CD62L (L-selectin) (anti-mouse)	PE-Cyanine7	eBioscience (ThermoFisher)	MEL-14	25-0621-82	1/200
CD25 (anti-mouse)	APC	Biolegend	PC61	102012	1/200
CD25 (anti-human)	BV605	Biolegend	BC96	302632	1/200
	BV650	Biolegend	BC96	302633	1/200
CD185 (CXCR5) (anti-mouse)	BV605	Biolegend	L138D7	145513	1/200
CD279 (PD-1) (anti-mouse)	BV785	Biolegend	29F.1A12	135225	1/200
CD279 (PD-1) (anti-human)	Brilliant Violet 421	Biolegend	EH12.2H7	329919	1/200
	APC	Biolegend	A17188A	379208	1/200
H-2K^{b} (MHC class-I) (anti-mouse)	Pacific Blue	Biolegend	AF6-88.5	116513	1/100
KLRG-1 (MAFA) (anti-mouse)	eFluor 450	Invitrogen (ThermoFisher)	2F1	48-5893-82	1/100
KLRG-1 (MAFA) (anti-mouse/human)	BV510	Biolegend	2F1/KLRG1	138421	1/100
CD153 (anti-mouse)	APC	Biolegend	RM153	106409	1/100
CD45RO (anti-human)	Pacific Blue	Biolegend	UCHL1	304216	1/200
CD197 (CCR7) (anti-human)	BV605	Biolegend	G043H7	353224	1/100
CD36 (anti-human)	FITC	Biolegend	5-271	336204	1/100
CD57 (anti-human)	PerCP-Cyanine5.5	Biolegend	QA17A04	393312	1/200
CD39 (anti-human)	FITC	Biolegend	A1	328205	1/200
Annexin V	FITC	Biolegend	N/A	640906	1/100
Intracellular staining (ICS)					
BCL-2 (anti-mouse)	eFluor 450	Invitrogen (ThermoFisher)	10C4	48-6992-42	1/100
Foxp3 (anti-mouse/human/rat)	PE	Biolegend	150D	320008	1/100
Foxp3 (anti-human)	PE	Biolegend	206D	320107	1/100
	BV421	Biolegend	206D	320123	1/100
Foxp3 (anti-mouse)	PE	Invitrogen (ThermoFisher)	FJK-16s	12-5773-82	1/100

T-bet (anti-mouse)	PE-Cyanine7	Biolegend	4B10	644824	1/100
RORγt (anti-mouse)	APC	Invitrogen (ThermoFisher)	AFKJS-9	17-6988-82	1/200
RORγt (anti-human)	PE	eBioscience (ThermoFisher)	AFKJS-9	12-6988-80	1/100
Gata3 (anti-mouse/human)	BV421	Biolegend	16E10A23	653814	1/100
H2A.X-Phosphorylated (Ser139) (anti-mouse/human)	PerCP/Cyanine5.5	Biolegend	2F3	613414	1/100
H2A.X-Phosphorylated (Ser139) (anti-mouse/human)	PE	Invitrogen (ThermoFisher)	CR55T33	12-9865-42	1/100
Ki-67 (anti-human)	Alexa Fluor 488	Biolegend	Ki-67	350532	1/200
STAT3 Phospho (Ser727) (anti-human)	PE/Cyanine 7	Biolegend	A16089B	698907	1/200
HIF1α (anti-human)	Alexa Fluor 647	Biolegend	546-16	359705	1/100
Intracellular cytokine staining (ICCS)					
IL-17A (anti-mouse)	PE-Cyanine7	Biolegend	TC11-18H10.1	506922	1/100
	Pacific Blue	Biolegend	TC11-18H10.1	506918	1/100
IL-17A (anti-human)	BV421	Biolegend	BL168	512322	1/100
IFNγ (anti-mouse)	APC	Invitrogen (ThermoFisher)	XMG1.2	17-7311-82	1/100
IL-13 (anti-mouse)	PE-Cyanine7	eBioscience (ThermoFisher)	eBio13A	25-7133-80	1/100
IL-10 (anti-mouse)	PE	Biolegend	JES5-16E3	505007	1/50
IL-10 (anti-human)	PE	Biolegend	JES3-9D7	501404	1/100
IL-4 (anti-human)	FITC	Biolegend	MP4-25D2	500806	1/100
	APC	Biolegend	8D4-8	500714	1/100
IL-6 (anti-human)	PE	Biolegend	MQ2-13A5	501107	1/100
TNF-α (anti-human)	FITC	Biolegend	MAb11	502906	1/200
LC3-II (anti-human)	FITC	Guava	4E12	CS208214	1/20
Flow cytometry kits					
UltraComp eBeads Compensation Beads	N/A	Invitrogen (ThermoFisher)	N/A	01-2222-42	N/A

CountBright™ Absolute Counting Beads	635/385 to 800 nm excitation	Invitrogen (ThermoFisher)		C36950	$0.5x10^5$ beads/50 µl
LIVE/DEAD Fixable Near-IR Dead Cell Stain Kit	APC-CY7 (633/635nm excitation)	Invitrogen (ThermoFisher)	N/A	L10119	1/1000
LIVE/DEAD Fixable Aqua Dead Cell Stain Kit	Alexa Fluor 405 (405 nm excitation)	Invitrogen (ThermoFisher)	N/A	L34957	1/500
Propidium Iodide Solution (PI)	488nm excitation/ (PE-Texas Red)	Biolegend	N/A	421301	0.5 mg/ml
Foxp3/Transcription Factor Fixation/Permeabilization Staining Buffer Set	N/A	eBioscience (ThermoFisher)	N/A	00-5523-00	N/A
Annexin V Binding Buffer	N/A	Biolegend	N/A	422201	N/A
Guava autophagy LC3 antibody-based detection kit	FITC	Luminex Coorporation, USA	4E12	FCCH100 171	1/25

2.4 RNA isolation and RT-qPCR

Table 2.4.1) RNA isolation and cDNA synthesis reagents

Reagent	**Supplier**	**Cat #**
RNeasy Mini Kit	Qiagen	74106
High-Capacity cDNA Reverse Transcription Kit	ThermoFisher, UK	4368814
SYBR TB Green Premix Ex Taq	Takara	RR820W

2.5 Western blotting

Table 2.5.1) Western blotting reagents

Reagent	**Supplier**	**Cat #**
RIPA buffer	Sigma-Aldrich	R0278
Protein Assay Dye Reagent Concentrate (4x)	Bio-Rad, UK	5000006
Protease/phosphatase inhibitor cocktail tablets	Sigma-Aldrich	PPC1010
4x Laemmli protein sample buffer	Bio-Rad, UK	1610747
β-mercaptoethanol	Sigma-Aldrich	M6250
Page Ruler Pre-Stained Protein Ladder (10 to 180 kDa)	ThermoFisher, UK	26616

Precast midi protein gel	Bio-Rad, UK	5671084
Trans-Blot Turbo Midi PVDF transfer packs	Bio-Rad, UK	1704157EDU
ReBlot Plus 10X mild Antibody stripping solution	Sigma Aldrich	2502
ECL Western Blotting Reagent	GE Healthcare	RPN2106
Anti-rabbit IgG, HRP- linked antibody	Cell signalling, USA	7074
Anti-mouse IgG, HRP- linked antibody	Cell signalling, USA	7076

Table 2.5.2) Western blotting antibodies

Reagent	Supplier	Cat #	Host species	Target species	Dilution factor
Anti-human Lck	Cell signalling, USA	2752	Rabbit	Human	1:1000
Anti-human pLck (Tyr 505)	Cell signalling, USA	2751	Rabbit	Human	1:1000
Zap-70 (99F2)	Cell signalling, USA	2705	Rabbit	Human	1:1000
Anti-human ZAP70 (Tyr 319)	Cell signalling, USA	2701	Rabbit	Human	1:1000
phospho-Akt (Ser473) (D9E)	Cell signalling, USA	4060	Rabbit	Human	1:1000
Akt (C67E7)	Cell signalling, USA	4691	Rabbit	Human	1:1000
β-Actin (8H10D10)	Cell signalling, USA	3700	Mouse	Human	1:2000- 1:5000

2.6 ELISA

Table 2.6.1) ELISA reagents

Reagent	Supplier	# Cat
IL-6 Mouse Uncoated ELISA Kit with Plates	Thermo Fisher	88-7064-22
IL-10 Human Uncoated ELISA Kit	Invitrogen (ThermoFisher)	88-7106-88
IL-10 Mouse Uncoated ELISA Kit	Invitrogen (ThermoFisher)	88-7105-88
IFNγ Mouse Uncoated ELISA Kit	Invitrogen (ThermoFisher)	88-7314-88
IL-17A (homodimer) Mouse Uncoated ELISA Kit	Invitrogen (ThermoFisher)	88-7371-88
IL-17A (homodimer) Human Uncoated ELISA Kit	Invitrogen (ThermoFisher)	88-7176-22
Tween-20	Thermo Fisher	10113103

Methods

2. 7 *In vivo* diet experiments

All animal studies were conducted under the UK Home Office regulation (PPL: PDA36EFFD9). All mice used in experiments were wild-type (WT) C57BL/6 female mice (4 weeks old) were purchased from Charles River (UK). All animals were sacrificed with humane schedule 1 procedure involving euthanasia by exposure to rising concentration of CO2, apart from 14-week DIO model where cardiac puncture was utilised to collect blood.

2.7.1 3-week early DIO omega-3 supplementation murine models

To investigate the immunomodulatory alterations within the 3-week early DIO murine models and the specific effects of distinct bioactive lipids such as n-3PUFA, three different diet groups were allocated. Mice were then allocated to a specific diet group (n= 6 animals per group), where they were fed on either western diet (WD) or WD supplemented with 5% menhaden fish (WD+ w3) or chow diet (CD) [Test diet, USA]. **Table 2.7.1** demonstrates the nutritional composition and fatty acid profile of all three diets used for the early DIO murine model experiment. All mice were maintained in a pathogen-free animal unit with 12/12-hour light/dark cycle. Throughout the course of the experiment, mice were carefully monitored and weighed weekly. Each mouse group was fed ad libitum with respective diet for total of 21 days (3-weeks). At day 14, to elicit an immune response and generate memory $CD4^+$ T cells, mice were subjected to allogeneic immunisation as previously described [18, 126, 127]. The allogeneic immunisation was induced by intraperitoneal (i.p) injection of a mixture (1:1 ratio, 1.5 $x10^6$ cell) of splenocytes isolated from WT BALB/c and CBA male mice, following an red blood cell lysis protocol. At day 21 all animals were sacrificed, SLOs (spleen, mesenteric lymph nodes-mLN, peripheral lymph nodes-pLN), and adipose tissue from lower peritoneum (peri-gonadal fat, p.fat) and subcutaneous fat (s.fat) was collected Flow cytometry was conducted on freshly isolated cells whereas samples for lipidomics and qPCR snap frozen and stored at -80°C.

Table 2.7.1) Nutritional composition of experimental diets

A. Composition of experimental diets

Nutrients	CD	WD	WD +ω3	HFD
Energy (Kcal/g)	3.59	4.49	4.50	5.10
- Protein (%)	22.0	15.5	15.5	18.1
- Fat (%)	9.08	40.1	40.0	61.6
- Carbohydrates (%)	68.9	44.4	44.5	20.3
Sucrose (%)	3.90	34.0	34.3	8.85
Cholesterol (%)	-	0.15	0.15	301 (ppm)
Milk fat (%)	-	20.0	15.0	-
Corn oil (%)	-	1.00	0.70	3.23
Crude oil (%)	3.36	-	-	-
Menhaden oil (%)	-	-	5.00	-
Fatty Acid Composition (%)				
Linoleic acid (C18:2n-6)	0.96	1.07	0.84	4.70
α-Linolenic acid (C18:3n-3)	0.11	0.10	0.14	0.39
Arachidonic acid (C20:4n-6)	0.11	0.03	0.07	0.06
Total SFA	0.56	12.1	10.4	13.68
Total MUFA	0.99	4.61	4.48	14.00
Total n-3PUFA	0.11	0.21	1.51	0.39
Total PUFA	1.18	0.58	1.91	-

B. Fatty acid profile of menhaden fish oil (%)

Myristic Acid (C14:0)	6.85	Hexadecadienoic Acid (C16:2n-9)	1.61
Pentadecanoic Acid (C15:0)	0.46	Hexadecatrienoic Acid (C16:3n-6)	1.51
Palmitic Acid (C16:0)	14.8	Hexadecatetrienoic Acid (C16:4n-3)	1.53
Heptadecanoic Acid (C17:0)	0.38	Linoleic Acid (C18:2n-6)	1.93
Stearic Acid (C18:0)	2.55	α-Linolenic acid (C18:3n-3)	1.48
Arachidic Acid (C20:0)	0.17	Stearidonic Acid (C18:4n-3)	3.09
Behenic Acid (C22:0)	0.10	Auricolic Acid (C20:2n-3)	0.18
Lignoceric Acid (C24:0)	0.60	Bishomopinolenic Acid (C20:3n-6)	0.37
Total SFA	25.9	Arachidonic Acid (C20:4n-6)	2.09
Palmitoleic acid (C16:1)	9.74	Eicosapentaenoic Acid (C20:5n-3)	14.2
Oleic Acid (C18:1)	9.58	Heneicosapentaenoic Acid (C21:5n-3)	0.76
Gadoleic Acid (C20:1)	1.48	Adrenic Acid (C22:4n-6)	0.24
Erucic Acid (C22:1)	0.33	Docosapentaenoic Acid (C22:5n-3)	2.82
Selacholeic Acid (c24:1)	0.22	Docosahexaenoic Acid (C22:6n-3)	12.2
Total MUFA	21.4	Total n-3 PUFA	36.3
		Total n-6 PUFA	6.14
		Total PUFA	44.0

2.7.2 FTY720 inhibitor on 3-week early DIO murine model

To test CerS2 inhibition *in vivo* we utilised the pharmacological inhibitor: FTY720. The experimental conditions were kept consistent with the 3-week early-DIO murine model, as detailed in **Section 2.7.1**. However, these animals were either treated with the FTY720 inhibitor (Merck, UK) or vehicle control (saline) whilst WD fed for 21 days. **Figure 4.1** represents the *in vivo* experimental design where each group was given 3 i.p injections of either FTY720 (1mg/kg) or saline on day 11, 16 and 18. On day 14, each group received WT BALB/c and CBA male mice splenocyte injection to induce an allogeneic immune response. Animals were sacrificed on day 21 and tissues of interest were collected for flow cytometry and lipidomics.

2.7.3 14-week DIO weight-gain weight-loss (WGWL) murine model

To investigate the effect of HFD-induced DIO and the weight-gain weight-loss (WGWL), mice were allocated into three groups: CD (10% lipid), HFD (60% lipid content) and HFD-RE (8-weeks HFD + 6-weeks CD) groups. **Table 2.7.1**, illustrates the nutritional contents of the CD and HFD diets. Each mouse group was fed ad libitum with respective diet for total of 98 days (14-weeks). At day 91 , to elicit an immune response and generate memory $CD4^+$ T cells, mice were subjected to allogeneic immunisation as previously described [18, 126, 127]. Animals were sacrificed at day 98 (14-weeks); SLOs and adipose tissue from lower peritoneum (peri-gonadal fat, p.fat) and subcutaneous fat (s.fat) were collected for downstream analysis (flow cytometry, protein and gene expression).

2.7.4 Murine tissue collection and processing

2.7.4.1 Murine fat tissue digestion and lymphocyte isolation

Perigonadal and subcutaneous fat tissues were cut into small pieces and suspended in a solution of PBS+5% BSA containing Collagenase Type II (200mg/ml-Sigma,UK) and calcium chloride (500 mM- Sigma,UK) for digestion. Samples were incubated for 20 min at 37^oC in a shaking incubator and passed through 70µm cell strainer. Following filtering cells were washed twice with PBS+5% BSA before flow cytometry staining.

2.7.4.2 Murine secondary lymphoid organ tissue digestion and lymphocyte isolation

Spleen and lymph nodes (mesenteric, inguinal and popliteal) were collected from WT C57BL/6J female mice following the *in vivo* protocols as detailed in **Section 2.1.** Tissues were disassociated through a 70μM cell strainer and washed with 2% of BSA PBS solution. This cell suspension was centrifuged at 1500 RPM for 5 minutes, and the cell pellet resuspended in red blood cell lysis buffer Hybri-Max (Sigma-Aldrich) according to manufacturer's instructions. Following the red blood cell removal, cell numbers were quantified via trypan blue staining (1:10 dilution) and microscopy with a haemocytometer .

2.8 Isolation of *ex vivo* CD4$^+$ T cells from murine and human samples

2.8.1 Isolation of mouse CD4$^+$ T cells from the SLO lymphocytes

Following the isolation of lymphocytes from spleen and LNs, cells were resuspended in the Easysep CD4$^+$ isolation buffer (DPBS without calcium and magnesium added 2% FCS and 1mM EDTA) to obtain 1x10^8 cells/ml cell suspension. CD4$^+$ T cells were then isolated by using Stemcell EasySep mouse CD4$^+$ T cell isolation kit (Stemcell technologies, UK). The manufacturer's instructions were followed for isolating the murine CD4$^+$ T cells with immunomagnetic negative selection process.

We assessed the purity before and after CD4$^+$ T cells isolated by the Stemcell EasySep kit by the flow cytometry-after isolation ~92% of cells were CD4$^+$ (**Figure 2.1**). We also isolated naïve CD4$^+$ T cells following the manufacter's protocol of the Stemcell EasySep mouse naïve CD4$^+$ T cell isolation kit (Stemcell technologies, UK).

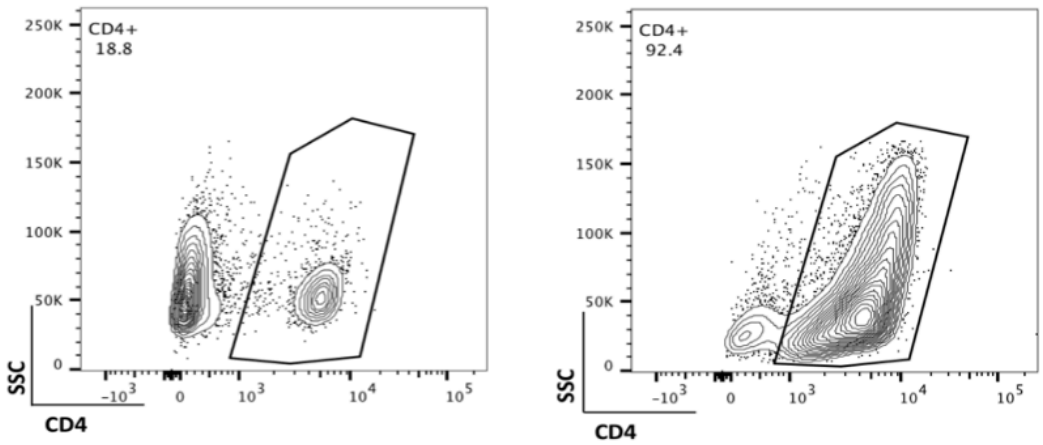


Figure 2.1) Murine splenocyte population CD4% prior to isolation isolated from spleen and LNs and following the CD4$^+$ T cell isolation via Stemcell EasySep kit.

According to the protocol of EasySep Stemcell murine $CD4^+$ T cell isolation kit: 50µl of rat serum was added per ml of sample. Samples were then transferred into 15ml sterile polystyrene round-bottom falcon tube and 50µl of isolation cocktail was added per ml of sample and incubated for 10 mins at room temperature (15- 25ºC). Following the incubation 75µl of Rapidspheres were added per ml of sample and incubated further for 2.5 minutes. Finally, each falcon tube topped up accordingly, before placing the tubes with sample into an appropriate Easysep magnet. As a result of immunomagnetic negative selection, all the non-CD4 cells attached to Rapidsphere beads were pulled by the magnet to the edge of the falcon tube where the ~ 92-96% purity murine $CD4^+$ T cells were carefully collected.

2.8.2 Isolation of human $CD4^+$ T cells from human PBMCs

Human peripheral blood mononuclear cells (PBMCs) were isolated from fresh leukapheresis blood cones from the Birmingham Blood Donor and Transfusion Centre under ethical approval from the NHS West Midlands Research Ethics Committee (REC 20/WA/0092). The leukapheresis blood cones were enriched in leukocytes obtained from blood donation of healthy donors. Blood was diluted with PBS and carefully layered ontop of an equal volume of Ficoll-Paque plus density gradient media. Tubes were then centrifuged at 1200xg for 30 minutes with speed acceleration at 1 and brake at 0. Following the density gradient separation, PBMCs were carefully collected from the interface layer and washed three times with PBS to clear any residual of Ficoll-Paque. PBMCs were then resuspended in PBS and cell numbers were quantified using trypan blue and microscopy with a haemocytometer.

For human $CD4^+$ T cell isolation, we used the Stemcell EasySep human $CD4^+$ T cell isolation kit (EasySep, Stemcell technologies, UK) according to the manufacturer's protocol - the kit demonstrated 94-96% CD4+ purity (*data not shown)*.

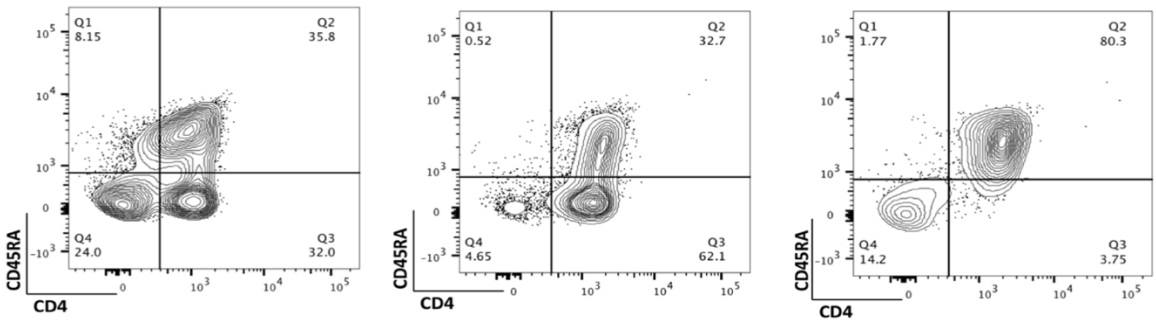


Figure 2.2) Isolation of human naïve $CD4^+$ T cells from fresh human blood cones.
(A) Starting human PBMC population CD4 and CD45RA% prior to isolation **(B)** Cell surface staining of $CD4^+$ T lymphocytes content following the human $CD4^+$ T cell isolation via Stemcell EasySep kit. **(C)** $CD45RA^+CD4^+$ naïve T cell content following the human naïve $CD4^+$ T cell isolation. According to the protocol of Stemcell EasySep human $CD4^+$ T cell isolation kit: human PBMCs were in $5x10^7$ cells/ml in a 15ml sterile polystyrene round-bottom falcon tube and 50µl of isolation cocktail was added per ml of sample followed by incubation for 5 minutes at room temperature (15- 25ºC). Following the incubation 50µl of Rapidspheres were added per ml of sample and topped up with the recommended

medium to the indicated volume while gently pipetting the samples up and down for 2-3 times. Tubes were then placed to the appropriate Easysep separation magnet and incubated at room temperature for 3 minutes. As a result of immunomagnetic negative selection, all the non-CD4 cells attached to Rapidsphere beads were pulled by the magnet to the edge of the falcon tube and human $CD4^+$ T cells were carefully collected from the bottom.

It should be noted that also human naïve $CD4^+$ T cells were isolated according to Stemcell EasySep naïve $CD4^+$ protocol. The purity of human naïve $CD4^+$ T cells was assessed with CD45RA/CD45RO marker expression, purification was ~80-90% (**Figure 2.2C**).

2. 9 *In vitro* experimental protocols

2.9.1 Primary cell culture conditions

Unless otherwise stated, all PBMCs and $CD4^+$ T cells were cultured at 37°C, 5% CO_2 with a complete cell media composed of RPMI-1640 (Sigma- Aldrich), 10% foetal calf serum-FCS (Sigma-Aldrich), 1% non-essential amino acids (Sigma-Aldrich), 2mM L-glutamine (ThermoFisher Scientific), 0.1% β-mercaptoethanol and 1% penicillin and streptomycin (100U/ml penicillin and 100μg/ml streptomycin) (Sigma-Aldrich). Cell culture seeding densities are displayed in **Table 2.9.1**. Additionally, activation methods for $CD4^+$ T cell activation are displayed in **Table 2.9.2**.

Table 2.9.1) Cell culture seeding densities

Cell culture plate size	**Seeding Density (cells/well)**
12 well	$1.0 – 2.0 \times 10^6$
48 well	$0.5 – 1.0 \times 10^6$
96 well	$0.2 - 0.025 \times 10^6$

Table 2.9.2) $CD4^+$ T cell activation reagents

Murine $CD4^+$ T cell activation	
Plate bound anti-CD3 (eBioscience)	1μg/mL
Soluble anti-CD28 (eBioscience)	1μg/mL
Human $CD4^+$ T cell activation	
Plate bound anti-CD3 (eBioscience)	2.5μg/mL
Soluble anti-CD28 (eBioscience)	1.5μg/mL
or	
Human T-Activator CD3/CD28 Dynabeads (Gibco, ThermoFisher UK)	Bead-to-cell ratio 1:1

Experiments which required further activation to analyse the secretory capacity and alternative activation pathways, $CD4^+$ T cells were further activated with PMA (0.05µg/ml) and ionomycin (0.5µg/ml) alongside GolgiStop (1µl per 1.5mL) or with Cell activation cocktail with brefeldin A (500X, 2µl per 1mL) for 4-6 hours. Considering various technical and experimental approaches the cell activation cocktail (500x) was used throughout the experiments unless otherwise stated.

2.9.2 *In vitro* ceramide treatment of murine and human $CD4^+$ T cells

2.9.2.1 Solubilisation of ceramides

Three specific ceramides: C2 Ceramide (d18:1/2:0), C24 Ceramide (d18:1/24:0) and C6 Ceramide (d18:1/6:0) were obtained from Avanti Polar Lipids, US. The low solubility and hydrophobic chemical structure of ceramides required optimisation for solubilisation (*data not shown*). Resultingly, all ceramides were solubilised in a 1:4 ratio of methanol and fatty acid-free BSA (1:4 ratio). The fatty acid-free BSA. AnnexinV/PI analysis illustrated that addition of BSA increased the cell viability and reduced ceramide induced lipotoxicity (*data not shown*). After solubilisation, ach ceramide (C2, C6 and C24), required volume of ceramide/methanol:BSA (<0.05% of medium) solution were added to get final concentration of 3.75mM and were shaken whilst being heated (50^{o}C) for 5 minutes. Finally, the ceramide vials sonicated for 10 minutes in an ultrasound sonicator, aliquoted into 1.5ml glass vials (Cronus, UK) and stored at -20^{o}C. All untreated control groups were treated with the vehicle: methanol:BSA solution as vehicle control. Considering the toxicity effect of organic solvents, the methanol concentration were always kept below 0.05% in the cell culture medium and annexin V/PI flow cytometry analysis was utilised to quantify cell viability in the cell culture (**Supplementary-Figure S4 & 5**)[373].

2.9.2.2 Ceramide treatment during *in vitro* $CD4^+$ T cell differentiation

Isolated $CD4^+$ T cells were cultured with specific cytokines to drive T cell differentiation towards: Th0, Th1 and Treg fates. Initially, a comprehensive literature research was conducted to optimise the concentrations of cytokines, activation signals and blocking antibodies to test in the experiment [374-376]. **Table 2.9.2** represents the reagent concentrations of three optimisation experiments to find appropriate polarisation conditions.

Considering the preliminary data and phenotype detailed in **Chapter 3-4**, we specifically focused on optimising the differentiation Treg fate *in vitro*. The *in vitro* Foxp3$^+$ Treg differentiation was optimised to ~50-60% Foxp3 expression in murine CD4$^+$ T cells by using IL-2: 23ng/ml (50 IU/ml), TGFβ: 10ng/ml 3 days. Th0 groups were not polarised towards any effector fate but instead treated with 23ng/ml (50 IU/ml) IL-2 - they were therefore used as a background expression control for fate-specific transcription factors (**Table 2.9.3**). **Figure 2.3** illustrates the representative flow cytometry plots and the gating strategy used for the assessment of murine CD4$^+$ T cell differentiation towards Treg fate as well as control gating for live/dead and naïve CD4$^+$ T cell isolation. All the mouse naïve CD4$^+$ T cells were simultaneously activated with plate bound anti-CD3 (1µg/mL,eBioscience) and soluble anti-CD28 (1µg/mL,eBioscience)

Table 2.9.3) Cytokines used for the *in vitro* differentiation optimisation experiments

T-cell fate	Cytokines & Antibodies	Exp. 1		Exp. 2		Exp. 3
Th0	IL-2	10 ng/ml		10 ng/ml		23 ng/ml
Th1	IL-2	10 ng/ml		10 ng/ml		23 ng/ml
	IL-12	5 ng/ml		10 ng/ml		10 ng/ml
	Anti-IL4	2 µg/ml		10 µg/ml		-
Th2	IL-2	10 ng/ml		10 ng/ml		-
	IL-4	10 ng/ml		20 ng/ml		-
	Anti- IFN	2 µg/ml		10 µg/ml		-
Th17	IL-6	20 ng/ml		50 ng/ml		-
	TGFß	5 ng/ml		2 ng/ml		-
	Anti-IL4	2 µg/ml		10 µg/ml		-
	Anti- IFN	2 µg/ml		10 µg/ml		-
Treg	IL-2	50 ng/ml		10 ng/ml		23 ng/ml
	TGFß	5 ng/ml		5 ng/ml		10 ng/ml
Stimulation condition	Anti-CD3	2 µg/ml	1 µg/ml	1 µg/ml	5 µg/ml	1 µg/ml
	Anti-CD28	2 µg/ml	1 µg/ml	1 µg/ml	2.5 µg/ml	1 µg/ml

Furthermore, human naïve CD4$^+$ T cells were also optimised for the differentiation towards Foxp3$^+$ Treg fate *in vitro* conditions. Based on the background literature, human naïve CD4$^+$ T cells were differentiated towards Treg *in vitro* under IL-2: 46ng/ml (100 IU/ml), TGFβ: 10ng/ml supplementation and IL-2: 46ng/ml (100 IU/ml) for Th0 for 5 days [377, 378]. All cells were resupplied with fresh media/cytokine cocktails on day 3 according to the group of treatment and cell fate. All the human naïve CD4$^+$ T cells were simultaneously activated with plate bound anti-CD3 (2.5µg/mL,eBioscience) and soluble anti-CD28 (1.5µg/mL,eBioscience)

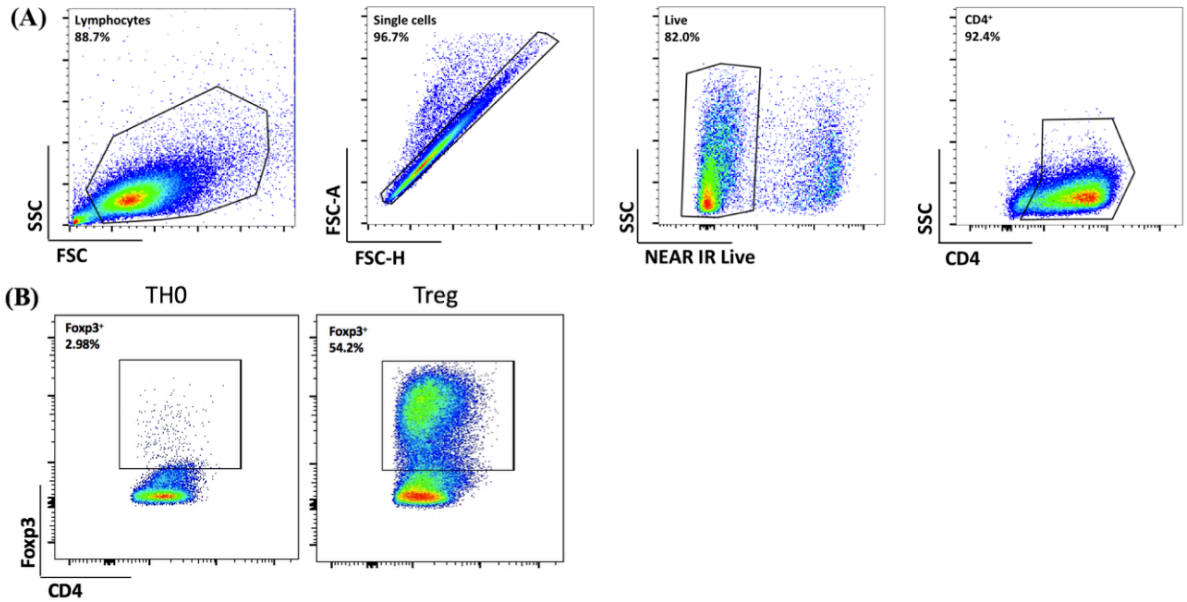


Figure 2.3) Representative flow cytometry gating strategy used for *in vitro* murine CD4$^+$ T cell polarisation analysis. (A) Lymphocytes were gated according to their typical location on forward and side scatter followed by Live cells gated according to near IR$^-$ as dead cells known to be positive where near IR dye react with intracellular amines due to compromised cell membrane. **(B)** Following the CD4$^+$ gating Foxp3$^+$ Tregs gated where Th0 used as a control group.

In both human and mouse T cell conditions, cells were simultaneously treated with the candidate ceramides (0.01μM - 10μM). Following the 3-day culture for mouse and 5-day culture for human, CD4$^+$ T cells were harvested and freshly analysed by flow cytometry and cell culture supernatants were collected and stored at -80 ^{o}C for ELISA.

2.9.3 In vitro time-course activation of human CD4$^+$ T cells pre-treated with ceramides

Following the isolation of human naïve CD4$^+$ T cells from fresh PBMCs of healthy donors, all the cells were seeded and treated with C24 (0.1μM) or vehicle control solution, overnight for 12 hours. Cells were activated by Human T-Activator CD3/CD28 Dynabeads for 5, 10 and 15 min, 30 min or not activated before cell harvest by centrifugation (4000rpm,10 mins,4^{o}C). The supernatant was discarded and the cell pellets were directly stored in -80^{o}C for western blot analysis.

2.9.4 Overnight lipid pre-treatment of human CD4$^+$ T cells *in vitro* with palmitic, stearic and oleic acid

2.9.4.1 Solubilisation and optimisation of lipotoxicity of palmitic, stearic and oleic acid lipids

Both oleic and stearic acids were purchased from Cayman Chemicals, UK whereas, sodium palmitate was purchased from Sigma-Aldrich, UK. Lipids were solubilised in pre-warmed (37-45^{o}C) ethanol: BSA (1:4) solution, added as drop-by-drop followed by a rigorous mix and heated up to 65 ^{o}C for 20 minutes. Constant shaking and heating of the solution aided lipid solubilisation of 10mM and 4mM stock solutions which were stored in -20^{o}C [18].

Following the optimisation of the solubility of lipids with the method detailed above, different solubilisation protocols were also tested to confirm the bioactivity of the candidate lipids. We also tested lipids directly solubilised in the ethanol mixed with different ratios of media and did not observe any notable difference in the viability of the cells with the candidate lipid treatment (*data not shown*). Additionally, the solubilisation method described by Pascual et al. 2021, was also tested where lipid were dissolved in 0.1 M NaOH and warmed at 80 °C until solution appeared clear. This solution was then mixed with a fatty acid-free BSA (dissolved in 0.9% NaCl) in 5:1 ratio of FA/BSA and heated to 45°C [379]. Importantly, there was no observable difference in all protocols tested (*data not shown*) and therefore, the initial method of solubilisation was kept same for consistency.

2.9.4.2 Overnight lipid pre-treatment of human CD4^{+} T cells *in vitro*

As detailed in **Section 2.2**, both murine and human CD4^{+} T cells were isolated by following the Stemcell Easysep protocol. Differently from other *in vitro* assays, cells in this assay were plated in complete media supplemented with 50µM of the candidate lipid groups and vehicle control group. All cells were then incubated for overnight (12hrs) before the activation with plate bound anti-CD3 and soluble anti-CD28. Following activation, cells were further incubated for either 3, 24 or 48 hours before harvest. Based on the preliminary data obtained from the optimisation experiments, 48hrs activation was selected as the optimal time point (*data not shown*)- 3hrs was inadequate to induce an observable difference and 96hrs were also shown to increase the toxicity within the CD4^{+} T cell culture.

It should be noted that, murine $CD4^+$ T cells were pre-treated with lipid overnight without any T cell activation signal presence expressed a high lipotoxicity and cell death, potentially due to the fragile nature of *ex vivo* murine $CD4^+$ T cells (**Figure 2.4)**. The annexinV/PI analysis illustrated around 50-60% of apoptosis with the lipid pre-treatment of murine $CD4^+$ T cells at 48-hour pre-treatment timepoints. Considering this, we have utilised the human $CD4^+$ T cells for the overnight (12hrs) lipid pre-treatment protocol followed by T-cell activation. Finally, following the 3-day (overnight lipid pre-treatment and 48hrs activation), cells were collected and washed with PBS. All conditions were analysed by flow cytometry with 2-3 panels including a PMA stimulation panel for ICCS, qPCR analysis for gene expression and western blotting for the protein quantification.

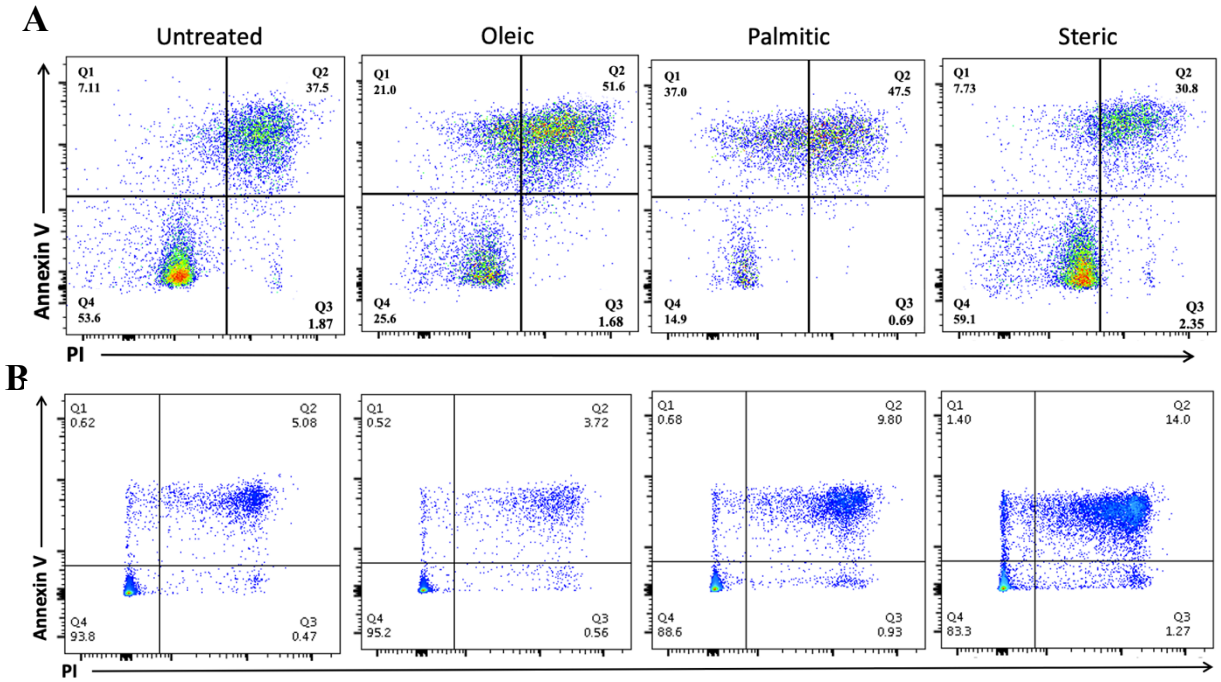


Figure 2.4) Optimisation of cell viability of (A) mouse and **(B)** human $CD4^+$ T cells within the *in* vitro overnight (12hrs) lipid pre-treatment followed by 48hrs of CD3/CD28 T cell activation.

2.10 RNA isolation and cDNA synthesis

Total RNA extraction was carried out using QIAGEN RNeasy Mini kit (Germany) following the manufacturer's protocol. Following the harvest, $CD4^+$ T cells were lysed in 350µL RLT buffer and pipetted up and down elucidating the RNA and DNA. Cell lysates were then centrifugation at 12,000 RCF for 3 minutes, supernatants were removed carefully. Before transferring to an RNeasy Mini spin column placed in a 2 ml collection tube, cells lysates were washed once with 70% ethanol. Samples were then washed with RW1 and RPE buffers respectively and centrifuged in between washes at ≥8000xg for 15 seconds while the flow-

through was discarded. Following the RPE wash, RNeasy spin column with cell lysate was transferred into a new 1.5ml collection tubes where 30-50µL RNase-free water was directly added into the column and centrifuged for 1 minute at ≥8000xg eluting the RNA. RNA concentrations were quantified using a Nanodrop 2000 spectrophotometer (Life technologies, Paisley, UK) and purity was checked by 260/280 and 260/230 ratios. Ratio values >1.5 were considered adequate for cDNA synthesis.

Following total RNA extraction, cDNA was synthesised starting from 1µg of total RNA using the high-capacity cDNA reverse transcription kit according to manufacturer's instruction (Thermo Fisher Scientific, UK) as demonstrated in **Table 2.10.1**. Following the addition of RNA samples, the cDNA synthesis reaction was ran in thermocycler (BioRad,UK) under the specified protocol of the manufacturer. The conditions used for the thermocycler is illustrated in the **Table 2.10.2.** Finally, all resulting cDNA samples were diluted 1/10 with nuclease free water and stored in -20ºC.

Table 2.10.1) cDNA synthesis reaction cocktail content

Component	**Volume**
10x RT buffer	2.0µL
25x dNTP Mix (100 mM)	0.8µL
10x RT random primers	2.0µL
MultiScribe Reverse Transcriptase	1.0µL
Nuclease-free H_2O	4.2µL
RNA sample	10µL
Total per reaction	20µL

Table 2.10.2) cDNA synthesis reaction thermocycler settings

Settings	**Step 1**	**Step 2**	**Step 3**	**Step 4**
Temperature	25ºC	37ºC	85ºC	4ºC
Time	10 minutes	120 minutes	5 minutes	Infinite Hold

2.11 Real time quantitative PCR (RT-qPCR)

Real-time qPCR was performed on a CFX384 Touch Deep Well Real-Time PCR System (Biorad, Hertfordshire, UK) using Takara SYBR TB Green. Each reaction contained 1µl

cDNA, 2.5µl SYBR Green master mix, 0.1µl each of forward and reverse primers and 1.3 µl RNase free water. Polymerase chain reaction was run on parameters 95°C 30sec (95°C 10sec; 59°C 30sec; 78°C 20sec)x40. The threshold cycle (Ct) values were normalized to the house-keeping gene β-actin, and normalised relative to the vehicle control group as indicated in the figure legends. All primers were specifically designed using Roche Life Sciences Universal Probe Library for candidate genes CDKN1C, IDH3G, STK26 and IL2RA (shown in **Table 2.11.1**).

Table 2.11.1) Specific primers designed for the candidate genes identified in the preliminary data.

Gene	**Forward Sequence (3'-5')**	**Reverse Sequence (5'-3')**	**Melting Temperature (Tm)**	**G-C percentage (GC%)**
CDKN1C	ACCAGAACCGCTGGGATT	CACCGTCTCGCGGTAGAA	F: 63.0 R: 64.2	F:50.0 R:50.0
Stk26	GAAAGTACAGAATGGGGCAGA	CTGATTCCTGCTAGCGTTATTCT	F: 62.1 R: 62.9	F:37.0 R:50.0
Idh3g	CCCTCAGATCACCTTCGAGA	GGCATCACCATGACATCAAA	F: 63.9 R:63.3	F:44.4 R:40.9
IL2RA	ACGGGAAGACAAGGTGGAC	TGCCTGAGGCTTCTCTTCA	F: 64.0 R: 64.0	F:57.8 R:52.6

2.12 Western blotting

Cell pellets were lysed with RIPA lysis buffer and protease and phosphatase inhibitors (1:1000). Protein content was quantified by Bradford assay (Biorad, UK). A seven serial dilution of BSA solution was prepared starting from 2mg/ml to 0.015mg/ml by using water. Samples and Protein Assay Dye Reagent Concentrate (1X) were diluted 1:10 with distilled water. Then both standards and samples were loaded into a 96-well flat bottom plate in triplicate and topped up with 200µl/well of protein assay dye reagent. The plate was then incubated at

RT for 5-10 minutes at dark. Average absorbance was measured by BioTek EL808 microtiter plate reader (BioTek, Swindon, UK) at 595nm wavelength– from this absorbance value protein quantification was calculated by utilising the absorbance of standards with the known protein concentration.

Following protein quantification, an equal amount of protein (20-30µg) was mixed with loading buffer (1:4) and heated to 95°C for 5 minutes. Samples were then loaded into a Mini-PROTEAN TGX precast gel and run at 100V for 1 hour 20 minutes. The gel was then transferred onto a Trans-Blot Turbo Transfer nitrocellulose membrane by the transblot machine for 7 minutes. In order to avoid any potential non-specific binding membrane was blocked with 5% Milk in 1X tris buffered saline with 0.1% Tween®20(TBS-T) for 1 hour at room temperature on a rocker. Following the blocking process, the membrane was washed three times with TBS-T solution and incubated overnight at 4°C with the designated primary antibodies.

Subsequently, the membrane was washed three times for 15 minutes with TBS-T and then incubated with the designated HRP-linked secondary antibody (1:2000 dilution either in 5% milk or BSA in TBS-T) and incubated for 1 hour at RT. The membrane was rewashed for three times with TBS-T and ECL western blotting detection reagent was directly added to the membrane for 1-2 minutes. Immediately band densities was measured with ChemiDoc MP imaging system – the resulting image was quantified by ImageJ software and band densities were normalised against β-actin.

2.13 Lipidomics analysis

Following the collection of *in vivo* samples, all the lipidomics experimental procedures and analysis of were carried out by Dr. Dolores Camacho-Munoz with the supervision of Professor Anna Nicolaou at University of Manchester as a collaboration. In brief, the experimental protocol was followed as published in Munoz et al. 2022 [127]. Both p. and s.fat tissues (30–40 mg) were homogenised in ice-cold chloroform/methanol (2:1 v/v, Thermofisher) and spiked with deuterated internal standards; 0 ng each of ceramide N(16)DS (18)-d9, ceramide N(18)S(18)-d3 and ceramide A(16)S(18)-d9 and 50 pmol of Cer/Sph Mixture I (Avanti Polar Lipids, USA). Samples were then centrifuged and the organic later was separated and evaporated for dryness and reconstituted in ethanol. Finally, lipid extracts run on ultrahigh performance liquid chromatography tandem mass spectrometry with an electrospray source (UPLC/ESI-MS/MS) using a Xevo-TQS mass spectrometer (Waters, Milford, Massachusetts,

USA). Adipose tissue lipid extracts were cleaned by solid-phase extraction using a 100 mg Silica-Si cartridge (Strata SI-1-Silica; Phenomenex, UK) before analysed by UPLC/ESI-MS/MS. Ceramides were separated on a C8 column (Acquity UPLC BEH C8; 100 × 2.1 mm; 1.7 μm; Waters, USA) using a gradient elution with water and methanol, both modified with 0.1% formic acid (Fisher Scientific, UK). Relative quantification of ceramides was calculated by using the concentrations the class specific internal standards [127].

2.14 Flow cytometry

2.14.1 Extracellular staining

Cells were harvested and counted with trypan blue as described above and for the *in vivo* murine experiments were adjusted to contain 1-2x10^6 cells per condition whereas, *in vitro* experiments were adjusted to contain 0.5-1x10^6 cells per condition in each flow cytometry panel. All samples were transferred into V-shaped 96-well plate and washed with FACS buffer (PBS + 2% FCS) and stained with the distinct fluorochrome conjugated antibody cocktails based on the panel. All the panels included one live and dead marker either fixable Near IR Live/Dead or fixable aqua dead cell stain. Extracellular staining antibody cocktail including the Live/Dead marker was prepared in PBS and added on samples as 50μl/well and incubated in the dark for 30mins at 4°C. Cells were then centrifuged at 1500rpm, 5 mins and washed at least twice with FACS buffer. Based on the assay requirements, cells were either directly transferred into 5ml falcon (12x75mm) polystyrene tubes for analysis or fixed and further stained with intracellular markers (ICS).

2.14.2 Intracellular staining (ICS)

Following the extracellular staining, cells were centrifuged at 1500rpm, 5 mins and supernatant was discarded. Samples were then mixed and completely resuspended by pipetting up and down in 100μl/well of fixation cocktail (mixture of fixation concentrate with fixation diluent 1:4) and incubated in the dark for 30mins,4°C. Following the fixation, cells were permeabilised by washing twice with the 1X permeabilization buffer (1:10 distilled water) and pelleted by centrifugation at 1500rpm, 5 mins. Intracellular fluorochrome conjugated antibody cocktails were prepared in 1X permeabilization buffer and directly resuspended as 50μl/well to the cell pellets. Cells were then incubated in the dark for 30mins, 4°C for ICS. Following the ICS, cells were further washed with permeabilization buffer at least twice and then transferred

into 5ml falcon (12x75mm) polystyrene tubes and run on BD LSRFortessa X-20. All flow cytometry analysis was conducted using FlowJo v10.

2.14.3 Annexin and PI staining

Following the harvest of the cells and the initial wash with PBS, cells were washed twice with Annexin V binding buffer. Cells were then centrifuged at 1500rpm, 5 mins and resuspended in 100 µL of FITC-conjugated annexin V antibody cocktail (1:40 in annexin V Staining Buffer). Following the incubation in the dark for 15 minutes at RT, cells were then washed with annexin V binding buffer. Finally, Propidium iodide (0.001 mg/ml) (PI) stain was added immediately to samples prior to running on the BD LSRFortessa X-20.

2.14.4 Autophagy LC3-II detection by flow cytometry

In order to specifically quantify LC3-II and autophagy flux levels within specific T cell subsets following the *in vitro* lipid pre-treatment, the Luminex Guava® Autophagy LC3 Antibody-based flow cytometry kit was utilised. The Luminex Guava® Autophagy detection kit provides disruption of the cell plasma membrane using a proprietary selective permeabilization solution where the cytosolic LC3-I gets washed away during washing steps and the LC3-II translocated into the autophagosome kept intact, allowing the quantification of the fluorescence by flow cytometry (**Figure 2.5**). The detection was enabled by the anti-LC3 mouse monoclonal antibody conjugated to FITC, which was also used to quantify and track the levels of LC3 within the cell. The staining protocol suggested by the manufacturer was followed with the modifications mentioned in **Section 5.8.2**.

All the cells were harvested on day 3 as previously detailed in **Section 2.3.4** and resuspended in a RPMI media without FCS and with 50µM of CQ concentration for 4 hrs. Following the incubation, cells were washed with PBS and transferred to V-shaped 96-well plate for the extracellular surface staining with CD4, CD44, CD62L, PD1, CD57 and Near IR live and dead markers as detailed above. Cells were then washed with 1X PBS and then washed once with the supplied 1X assay buffer. Based on the mannufacturer's protocol, cells were resuspended in 50µl/well of 1X Reagent B to enable selective permeabilisation and immediately centrifuged at 1500rpm, 5 mins, 4°C. Cell pellets were then resuspended in 1:20 LC3-II FITC monoclonal antibody cocktail diluted in 1X assay buffer and incubated at RT in

the dark for 30mins. Finally, cells were centrifuged and washed once with 1X assay buffer as detailed above and transferred to into 5ml falcon (12x75mm) polystyrene tubes to be run on BD LSRFortessa X-20.

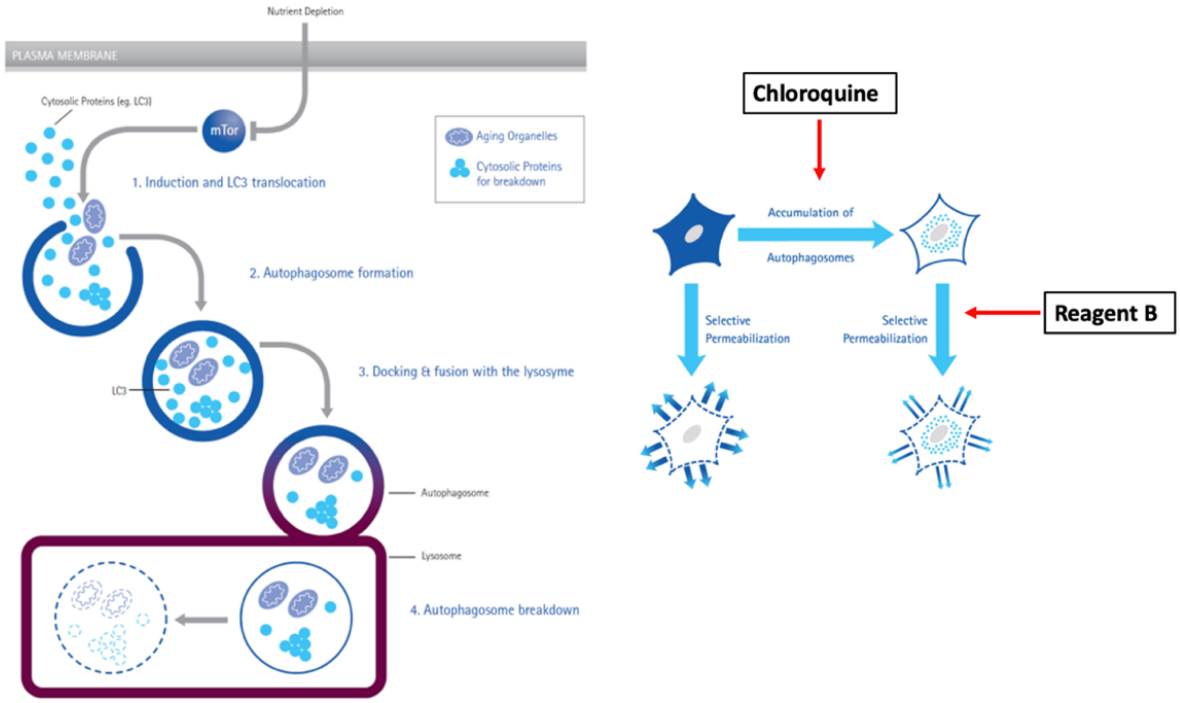


Figure 2.5) Working principles of Guava LC3-II autophagy detection kit. (A) Stages of autophagy induction by nutrient depletion or inhibition of mTOR by certain pharmacological inhibitors. Initial stage consists of sequestration of cytosolic proteins such as LC3 by a membrane vesicle forming an autophagosome. Autophagosomes then fused with lysosome leading to the degradation of autophagosomes. Both the translocation of cytoplasmic LC3 into an autophagosome and the degradation of an autophagosome are two hallmark processes of the autophagy. **(B)** Pharmacological inhibitors like CQ blocks the degradation of autophagosomes and induces the accumulation of autophagosomes for the quantification by the selective LC3-II antibody. Additionally, selective permeabilization of cellular membrane leads to the release of cytosolic LC3-I that discarded by the washing step and enables the Guava kit to selectively detect the autophagosome-linked LC3-II. Figure taken from Guava LC3-II autophagy detection kit manufacturer's information sheet (Luminex Coorporation, USA).

2.14.5 Flow cytometry controls

In order to precisely gate and accurately discriminate between positive and negative cell populations, each flow cytometry marker was run along fluorescence minus one controls (FMO) control. The FMO control contained every other marker used in the panel excluding the marker itself in order to determine the background autofluorescence signal and place the gating for the positive staining. Although for each experiment an unstained control was also run along the samples, FMOs were also utilised to obtain more accurate gating controls as they act as an internal control for potential spillover spread from the other markers or negative populations.

Additionally, in order to precisely control the potential spectral overlap between the fluorochromes used in a panel, single-stain controls were utilised for compensation calculations. UltraComp compensation beads were used for single-stain controls which were stained individually with each antibody and used to test potential spectral overlap between the fluorochromes. **Figure 2.6** illustrates potential spectral overlap between the fluorochromes used within panels run on the BD LSR Fortessa X-20 (4-lasers). Single stained controls were prepared freshly and run along the samples on the BD LSR Fortessa X-20 - compensation was calculated by Diva software which is further validated on FlowJo software. All the absolute cell counts were calculated according to the formula below:

$$[cells/\mu L] = \frac{N\ of\ cell\ events}{N\ of\ bead\ events} \times \frac{Beads\ in\ 50\mu L}{Vol.of\ the\ sample} \times Sample\ dilution$$

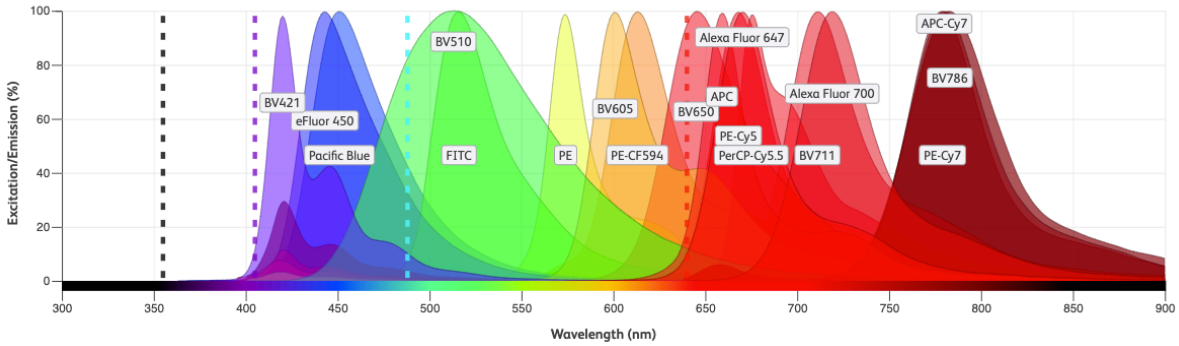


Figure 2.6) Full spectrum of BD LSR Fortessa X-20 flow cytometry with 4-laser setup. Representation of the main flow cytometry channels used throughout the *in vivo* and *in vitro* flow cytometry experiments including the potential spill over between different channels. Specific single stain controls were utilised for each experiment to calculate the required compensation between channels. Figure created with BD panel designing tool.

2.15 Enzyme-Linked Immunosorbent Assays (ELISA)

Cytokine levels were quantification within samples by ELISA using the $CD4^+$ T cell monoculture medium collected from the *in vitro* experiments and stored in -80°C until analysis. Both human and murine IL-10, IL-17 and murine IL-6 and IFN-γ ELISAs were performed according to commercially available manufacturer's protocols (Invitrogen-ThermoFisher). Based on the detection range determined by standard curve of supplied with the ELISA kits, samples were tested with various dilutions and optimised in dilution factor, illustrated in **Table 2.15.1**.

Table 2.15.1) ELISA dilution factors of the samples

Cytokine	Dilution factor	
	Mouse	Human
IL-10	5	2
IL-17a	10	10
IL-6	-	-
IFN-γ	5	-

Initially capture antibody was diluted (1:250) in 1x coating buffer (PBS) and coated a 96-well plate ELISA plate (50µl/well) overnight at 4°C. Wells were then aspirated and washed three times with ELISA wash buffer (1X PBS, 0.05% Tween-20) and then blocked with the ELISA diluent (1X) as 100µl/well for an hour at RT. Plates were then aspirated and washed three times with wash buffer, followed by addition of 50µl/well of standard or sample or ELISA diluent for blank wells in triplicate conditions, plate was incubated at RT for 2hrs or 4°C overnight. The plate was washed at least three times with wash buffer and then the detection antibody (1:250 diluted in ELISA diluent) was added 50µl/well and incubated in RT for 1hr. Following the incubation plate was washed at least three times with wash buffer and 50µl/well of Avidin-HRP enzyme was added before 30 minutes of incubation at RT. Finally, plate was washed 5-7 times with ELISA wash buffer with 1 minute incubation time at each wash. The TMB (1X) solution supplied by the manufacturer was directly added as 50µl/well and incubated in the dark for 15 minutes. The reaction was then stopped by adding 50µl/well of stop solution 2N H_2SO_4. Optical density was directly measured at wavelength 450 nm by BioTek EL808 microtiter plate reader (BioTek, Swindon, UK) and measurement at wavelength 570 nm was used to eliminate any optical imperfections by using the formula $Absorbance = Abs450 - Abs540 - Absblank$. The samples were then quantified according to the standard curve generated from the average absorbance for each standard by using nonlinear regression interpolation of GraphPad Prism v9.

2.16 Epigenetic analysis on differential methylation

Following the collection of the 14-week *in vivo* samples, both naïve and memory $CD4^+$ T cells were isolated using magnetic bead selection from spleen of murine models fed with different diets (CD, HFD and HFD-RE).

The RRBS is an efficient method to investigate genome-wide scale DNA methylation profiles at the single nucleotide level. The incorporation of restriction enzymes and bisulfite sequencing focuses on regions of the genome containing cytosine and guanine (CpG)

dinucleotides (primary sites of DNA methylation) [380]. The CpG islands (GpGI) are genomic regions that contain a high frequency of CpG dinucleotides, as the CpG are well known targets of methylation, they have critical roles in regulating the transcription of various genes [380, 381]. Additionally, around 70% of promoters are known to contain CGIs which are highly exposed to the methylation process leading to direct alterations in gene expression levels [380, 381]. Following the methylation results samples were compared to CpG sites (8-50 reads) of reference genome, creating the differential methylation analysis of CpG sites and the respective genes (**Figure 2.7**).

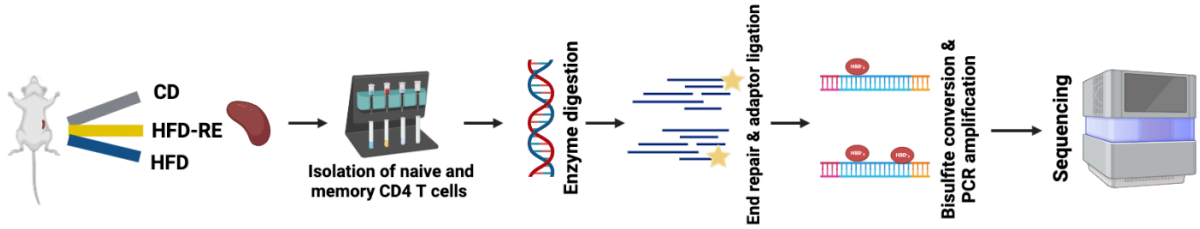


Figure 2.7) Experimental schematic of the RRBS sequencing of CD4$^+$ T cells isolated from 14-week DIO murine models
(A) Experimental schematic of the RRBS sequencing of murine CD4$^+$ T cells obtained from the spleen of female C57BL/6J mice fed on CD, HFD, and HFD-RE (8-wk HFD and 6-wk CD) for 14-weeks and were subjected to an allogeneic immunisation at 13.week. Both naïve and memory CD4$^+$ T cells were isolated by Stemcell isolation kits and used for RRBS analysis in **Nedjai's** laboratory QMUL.

2.17 Data handling and statistics

All the statistical analyses were performed by using GraphPad Prism v9 and in all statistical tests p values: *p<0.05; **p<0.01; ***p<0.001; ****p<0.0001, were considered as statistically significant.

All the *in vivo* experiments and sample size were calculated by using the experimental design tool supported by NC3Rs. A power calculation (p<0.05, power 0.85, two-sided test, mean =5 and SD=3) was utilised to determine that 8 mice are required per group.

The Shapiro-Wilk normality test was performed in all the dataset and p value >0.05 was considered normally distributed and performed a parametric tests. Statistical analysis between normally distributed data with more than two independent groups were conducted by one-way ANOVA test. If necessary, in order to compare among all groups Tukey's multiple comparisons and to compare all the groups to a control group, Dunnett's multiple comparisons corrections were utilised. When applicable for non-normally distributed data, non-parametric tests were performed as such between two independent groups Mann-Whitney test and between more than two independent groups, Kruskal-Wallis analysis was performed. If necessary, the multiple comparisons among groups were checked by using Dunn's multiple comparisons.

Chapter 3) Omega 3 supplementation can ameliorate the OIIM in an early-DIO murine model

3.1. Introduction

The crucial role of T lymphocytes in obesity and associated pathologies, through their contribution to OIIM, is well discussed in **Chapter 1** [1, 18, 127, 301]. Furthermore, obesogenic diets have also been shown to induce distinct 'pro-inflammatory' immunomodulation leading to OIIM and obesity-associated low-grade chronic inflammation. As discussed in **Section 1.8**, distinct bioactive lipid groups are critical immunomodulatory agents found within fat-dense obesogenic diets. Notably, SFAs are recognised by their ability to induce 'pro-inflammatory' modulations whereas, unsaturated or specifically n-3PUFAs are known for their 'anti-inflammatory' immunomodulations.

A previous publication by our group (Cucchi et al., 2019) illustrated the anti-inflammatory modulatory actions of n-3PUFA on $CD4^+$ T cell motility and migration within a CD-fed *in vivo* model [126]. In this *in vivo* study, WT C57BL/6J female mice were fed on CD as health balanced diet control, along with a CD supplemented with 5% menhaden fish oil over a three-week period. Following Cucchi et al., to investigate the DIO, we modified our experimental plan to reflect the obesogenic diet conditions. This consisted of feeding mice with a WD supplemented with 5% menhaden fish oil (source of n-3PUFA). Normally within DIO models mice are fed with obesogenic diets over a long-time course (10-20 weeks), leading to a fully established obesity model [290, 382, 383]. However, here we specifically utilised a 3-week early-DIO model to investigate the early pro-inflammatory modulations and potential ameliorative effect of short-term n-3PUFA supplementation on T-lymphocytes.

During DIO conditions, both $CD4^+$ helper (Th) [384] and $CD8^+$ cytotoxic (Tc), [224] T cells were shown to migrate and infiltrate to critical peripheral tissues, such as fat tissues and SLOs, where they recruit various pro-inflammatory immune cells such as M1 macrophages and promote the OIIM [224, 385-389]. Consistently, an αβ-T cell-deficient DIO murine model showed a significant reduction in obesity-induced inflammation in both adipose and skeletal tissues, highlighting the crucial contributions of T lymphocytes to the OIIM [388].

Literature has shown that DIO (and specifically various bioactive FAs) can bias the obese $CD4^+$ and $CD8^+$ T lymphocytes towards an EM phenotype [18, 390, 391]. Additionally, DIO models fed with obesogenic diets have demonstrated a reduction in naïve T cell frequencies [392]. This effector memory-like phenotype was also shown to contribute to OIIM via an excessive T cell response, migratory modulations, pro-inflammatory effector functions and by promoting the accumulation of other pro-inflammatory immune cells to the periphery [18, 393-395]. Importantly, expression of both chemokine (C-X-C-motif) receptor 3 (CXCR3) and lymphocyte function antigen-1 (LFA-1) on T cells have been demonstrated to be two critical markers for this EM pro-inflammatory phenotype.

The CXCR3 is a critical chemokine receptor known to be highly expressed on effector T cells; including pro-inflammatory Th1 [396], Th17 $CD4^+$ [397] and cytotoxic $CD8^+$ T cells [395, 398]. Importantly, CXCR3 is crucial in T cell trafficking to the periphery and Th1-like pro-inflammatory functions which are mainly mediated by IFNγ-inducible CXCR3-ligands [398]. CXCR3 expression on T cells is also associated with various diseases including RA, CVDs, diabetes and obesity [398-400]. Furthermore, CXCR3 is shown to be crucial in controlling T cell accumulation in obese fat tissue and peripheral OIIM [389, 395]. In DIO models, activation of naïve T cells under the obesogenic diet conditions promoted CXCR3 expression and IFNγ mediated pro-inflammatory effector and cytotoxic T cell subsets [401]. Obesogenic diet-induced expression of CXCR3 is also shown to induce the recruitment of pro-inflammatory M1 macrophages leading to the establishment and maintenance of adipose tissue inflammation. [389, 394, 398, 402]. Similar to $CXCR3^+$ $CD4^+$ T cell pro-inflammatory EM phenotype, CXCR3 expression also biased $CD8^+$ T cells towards a pro-inflammatory 'effector-cytotoxic' phenotype which was increased in frequency within SLOs in DIO and directly contribute to OIIM [389, 394, 402].

Lymphocyte function antigen-1 (LFA-1 or CD11a), is expressed on T cells and plays a crucial role in T cell trafficking to peripheral lymph nodes, migration and infiltration to peripheral tissues [403, 404]. Additionally, LFA-1 is a key integrin (heterodimeric adhesion molecule) during T cell activation, effector functions and lymphocyte memory formation in both $CD4^+$ and $CD8^+$ T cells [18, 403-406]. Additionally, LFA-1 expression on other hemopoietic cells crucially affects $CD4^+$ T cell priming via T cell:APC interactions [403]. Furthermore, as shown by Mauro et al., 2017, the expression of LFA-1 plays a critical role in the infiltration, activation, priming, effector functions and memory formation within $CD4^+$ T

cells during DIO [18]. LFA-1 has been also shown to play a crucial role in $CD8^+$ T cell-related adipose tissue inflammation in DIO conditions. LFA-1^+ $CD8^+$ T cells induce T cell activation in OIIM and contribute to neutrophil-related adipose tissue OIIM in DIO models [387]. A LFA-1 $CD8^+$ T cell knockout DIO murine model, illustrated a significant reduction in T-cell activation and accumulation within the adipose tissue, confirming the important role of LFA-1^+ T lymphocytes in OIIM [383].

Interestingly, there are not many publications on the effect of n-3PUFA supplementation on memory T lymphocytes and expression of the critical EM markers (CXCR3 and LFA-1). Despite this, our group's previous publication illustrated the immunomodulatory potential of n-3PUFA supplementation in CD group, altering the ratio between naïve, central and effector memory $CD4^+$ T cells including CXCR3 and LFA-1 [126].

3.1.1. Effector T cell populations in OIIM

Similar to the increasing trend observed in the EM T lymphocyte populations, obesogenic diets were shown to increase the Th1 and Th17 pro-inflammatory T cell populations leading to OIIM. As previously highlighted, n-3PUFA can directly inhibit the main transcription factors of various pro-inflammatory effector T cell fates (Th1 and Th17) but also suggested that it can induce the differentiation of T cells towards an anti-inflammatory regulatory fate [407]. This will be further investigated in **Chapter 4**.

The immunomodulatory potential of n-3PUFA in diverting both $CD4^+$ and $CD8^+$ T cells towards $Foxp3^+$, $CD25^+$ Treg fate is highly documented throughout various murine models and *in vitro* studies [126, 127, 407, 408]. Although traditionally Tregs were considered as mainly $CD4^+$ T cells, recent studies illustrated the importance of $Foxp3^+$ $CD8^+$ Tregs [409]. This population of Tregs are much smaller and limited compared to $CD4^+$ Tregs. For example, only 0.1-1% of $CD8^+$ T cells were detected to be $Foxp3^+$ in blood, p.LN and spleen whereas, mLN $CD8^+$ Treg frequencies were much higher [410]. Agle et al. 2018, illustrated that $CD8^+$ T cells share a very high homology with $CD4^+$ Tregs in terms of gene expression profile which is very distinct from cytotoxic $CD8^+$ T cells [411]. $Foxp3^+$ $CD8^+$ T can also express other common $CD4^+$ Tregs markers such as CD25 and GITR however, since they are shown to lack some of these surface markers they are mainly defined based on $FOXP3^+$ expression in both murine and human [409].

Similarly, FOXP3$^+$ CD8$^+$ Tregs were also shown to secrete anti-inflammatory cytokines (IL-10 and TGF-β) and downregulate costimulatory molecules on APCs [409, 412-415]. Additionally, Foxp3$^+$ CD8$^+$ Tregs are also capable of inducing the expansion of Foxp3$^+$ CD4$^+$ Tregs- giving rise to further suppression potential for preserving the homeostatic microenvironment [412, 416]. The reduction of these Foxp3$^+$ CD8$^+$ Treg populations is associated with various inflammatory pathologies including obesity [417] and obesity-associated diseases like diabetes [418], cancer, autoimmune diseases, RA and MS [409, 419].

In addition to the effector, cytotoxic and regulatory phenotypes of T lymphocytes, T follicular helper (Tfh) cells are highly specialised and responsible for key interactions with B cells. Tfh cells play a crucial role in the germinal centre formation, cell survival, affinity maturation and class switch recombination of B cells in secondary lymphoid organs (SLOs) including spleen and LNs [420, 421]. Although B cell lymphoma 6 (BCL6) is the main transcription factor of the Tfh cells, they are also characterised by PD1, ICOS and CXCR5 expression [420, 421]. High expression of CXCR5 is a crucial element in the development, migration and localisation at B cell-rich areas in SLOs [420, 421]. Consequently, due to the vital roles of Tfh CD4$^+$ lymphocytes, they are implicated in various obesity-associated diseases such as autoimmune diseases, cancer, MS, systemic lupus and RA [421-425]. Although Tfh cells are highly limited in both number and location, they are shown to be significantly increased with RA [421, 422]. Moreover, obesogenic diets have been found to disturb the balance between CD4$^+$ Tfh and Tregs, with HFD leading to a significant increase in CD4$^+$ Tfh in a lupus murine model [426].

Both CD8$^+$ and CD4$^+$ Tfh cells share homology in gene expression and function in regulating B-cell response and controlling antibody secretion in germinal centres [427, 428]. Similarly, CD8$^+$ Tfh counterparts have also been shown to contribute to CVDs via secreting pro-inflammatory and angiogenic factors [428, 429]. Importantly, the ratio between CD8$^+$ Tfh and CD8$^+$ Tregs has been also shown to be pivotal in controlling the B-cell functioning and the formation of atherosclerosis in a STAT4-dependent manner within SLOs [428, 429].

3.1.2. Obesity-associated T cell exhaustion and senescence

Obesogenic diets are known to induce T-cell immunosenescence and exhaustion independent of chronological ageing [430-433]. Both murine and human exhausted T

lymphocytes are characterised by the expression of programmed cell death-1 (PD-1). PD-1 is an inhibitory receptor of the T cell activation and TCR signalling, regulating effector functions of both $CD4^+$ and $CD8^+$ lymphocytes [434]. DIO was shown to induce PD-1 expression and T-cell exhaustion via various independent pathways including leptin-induced upregulation [430, 431, 433, 435]. The PD-1^+ $CD4^+$ T are known to exhibit features of ageing-associated senescence T cells that are known to accumulate in SLOs with ageing [430, 435]. Importantly, PD-1 expression and T cell exhaustion in association with obesity is also observed in human cohorts with both $CD4^+$ and $CD8^+$ populations [433, 436].

In addition to T cell exhaustion and impairment in functionality leads to cellular anergy and accumulation of senescent T cells within the obese cellular microenvironment [430, 435]. Accumulation of immunosenescent cells in various tissues, especially in visceral adipose tissue is well shown to augment the OIIM and aggravate obesity-associated pathologies like CVDs [430, 433, 435]. The killer cell lectin-like receptor subfamily-G member-1 (KLRG1) is one of the commonly used markers of pre-senescent & senescent T-cells in murine models [437-440]. Importantly, KLRG1 is shown to be highly expressed by terminally differentiated effector T cells with low proliferative potential, functional exhaustion and a short-life span [438, 439, 441]. KLRG1^+ T cells were also shown to exhibit an increased secretion of pro-inflammatory cytokines associated with obesity-associated pathologies [442]. Previous publications on HFD-fed DIO murine models have illustrated that obesity elevates the frequency of KLRG1^+ $CD8^+$ T cells [389].

3.1.3. Aims and hypotheses

Following the Cucchi et al. 2019 paper and the modifications of the experimental plan, this chapter aims to investigate the following hypotheses and questions:

- To dissect the pro-inflammatory modulations of obesogenic diets (WD and HFD) on T lymphocytes in establishing the OIIM in a 3-week early-DIO murine model.
- Investigating the anti-inflammatory potential of dietary n-3PUFA supplementation into obesogenic WD and potential ameliorate effects on WD-driven pro-inflammatory profiles of T cells.
- Identifying the direct immunomodulatory effects of dietary n-3PUFA on Foxp3^+ Treg populations.

Results

3.2. Optimisation of the alloimmunisation protocol for the in vivo diet experiments

One of the main experimental procedures in our *in vivo* experiments is the induction of polyclonal T-cell response via an allogenic immunisation protocol as previously detailed by Prof. Mauro's publications [18, 126, 127]. By definition, allogeneic immunisation is the injection of cells obtained from a genetically dissimilar donor into a recipient which induces an immune response due to immunological incompatibility [393]. In murine models, cells obtained from a different strain of mouse are injected into the recipient to induce an allogeneic immune response [18, 126, 127, 443, 444]. The main purpose of allogeneic immunisation via intraperitoneal (i.p) injection of splenocytes from a different mouse strain is to induce a polyclonal T-cell response in the recipient. This polyclonal activation of T lymphocytes to prompt the creation of memory T cells is well documented within the literature [18, 445-448]. Previous publications and preliminary data by Mauro's group have shown the importance of this polyclonal T cell response and induction of the memory T cells in investigating the immunomodulatory biasing effect of different diets on T-cell populations and functions [18, 126].

Following last publications, Mauro's lab moved to the University of Birmingham (UoB) [18, 126] where the following optimisation experiments were carried out to ensure the consistency of allogeneic immunisation via i.p injection of WT Balb/c and CBA (1:1 ratio) male splenocytes into C57BL/6 recipients.

Initially, we tested the potential polyclonal T cell activation and effector memory response in a small trial with 3 mice; mouse 1 (M1) injected with $7.5x10^4$ splenocytes, M2 injected with $1.5x10^6$ splenocytes and PBS injected for the vehicle control mouse (all 3 mice were fed with CD for 3 weeks). The flow cytometry data obtained from SLOs including the spleen, mLN and pLN were analysed with the same main gating strategy as the actual 3-week DIO experiment (**Figure 3.4**). Importantly, we investigated the main $CD4^+$ T cell subsets including naïve, EM and CM (**Figure 3.1A)** and the key effector memory markers such as LFA-1 and CXCR3 (**Figure 3.1B**) associated with obesogenic diets and DIO [18, 126].

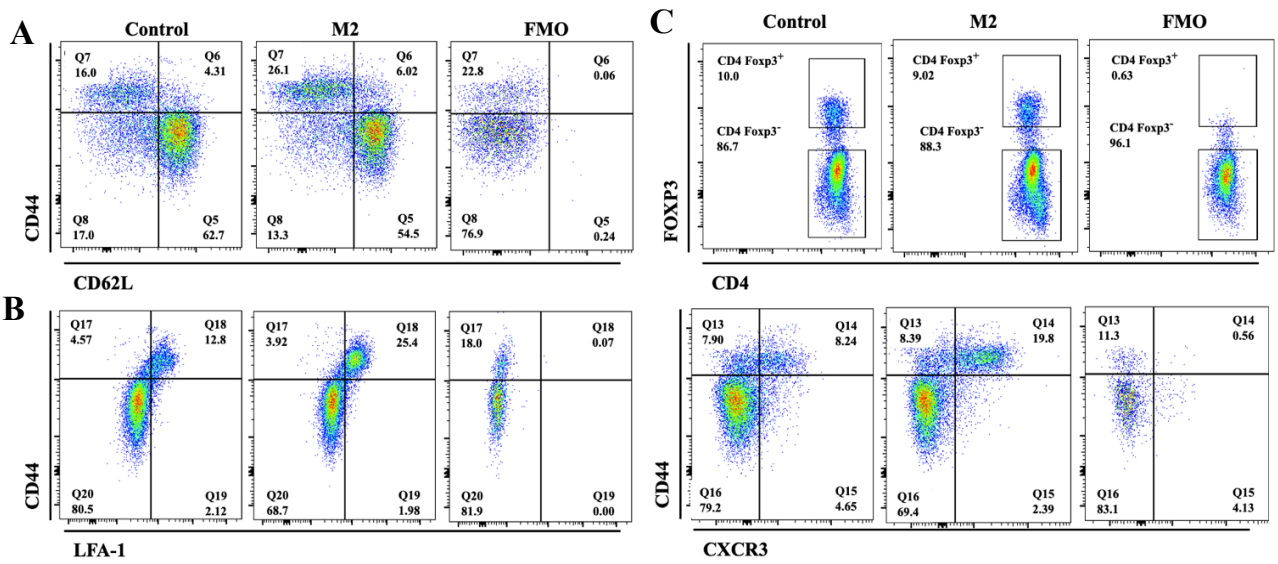


Figure 3.1) Representative flow cytometry plots of main gating strategy for population of interests in the optimisation trial for the allogeneic injection via i.p (A) CD44, CD62L differentiating; naïve ($CD62L^+$, $CD44^-$), CM ($CD62L^+$, $CD44^+$), EM ($CD62L^-$, $CD44^+$) and $CD62L^-$, $CD44^-$. **(B)** Pro-inflammatory effector memory-like T cell markers; $CD44^+$, LFA-1^+ and $CD44^+$, $CXCR3^+$ **(C)** $Foxp3^+$ Tregs. All the flow cytometry plots were obtained spleen tissue of vehicle control mice injected with saline solution and M2 mouse injected with $1.5x10^6$ allogeneic splenocytes.

Importantly, the $CD4^+$ T cell EM ($CD44^+$, $CD62L^-$) population was increased within all SLOs obtained from both M1 (*data not shown*) and M2 compared to the control mice (**Figure 3.1A**). As expected, the mice showed a dose-dependent response in $CD44^+$,$CD62L^-$ populations based on the number of splenocytes injected. Consistently, M2 mouse which received the highest number of splenocytes ($1.5x10^6$), induced a higher EM population of around ~30% in the spleen and ~12% in LNs. This dose-dependent trend was also illustrated with a consistent gradual increase in memory T cell populations of interest such as $CD44^+$, LFA-1^+ and $CD44^+$, $CXCR3^+$ (**Figure 3.2A**). On contrary, unlike EM populations, regulatory $CD4^+$ T cell populations ($CD4^+$, $Foxp3^+$ and $CD4^+$, $Foxp3^+$, $CD25^+$) did not show any observable trend and were not affected by the allogeneic immunisation (**Figure 3.2A**).

Finally, we wanted to ensure that the difference we observed in recipient T lymphocytes was due to the allogeneic immune response given by the recipient's immune response and not by a direct residual effect of the allogeneic splenocytes injected. To investigate this, we utilised information on general mouse haplotype differences between the donor and recipient mouse strains [449]. Both donor strains (Balb/c and CBA) splenocytes are characterised by MHC-I H-$2Kb^-$, whereas the recipient mouse (C57BL/6) T lymphocytes express H-$2Kb^+$. This difference enabled us to differentiate the cells injected (H-$2Kb^-$) and created by the recipient (H-$2Kb^+$).

As expected, flow cytometry analysis on H-2Kb MHC class-I antigen confirmed that around ~97-100% of the cells isolated from the spleen and LNs were H-2Kb$^+$ (**Figure 3.2B)**. Overall, this observation has eliminated the potential risk of detecting any background signal from the injected allogeneic splenocytes and confirmed that the recipient organism managed to clear the allogeneic cells via required immune responses including a polyclonal T cell response and creating an effector memory T cell populations as desired.

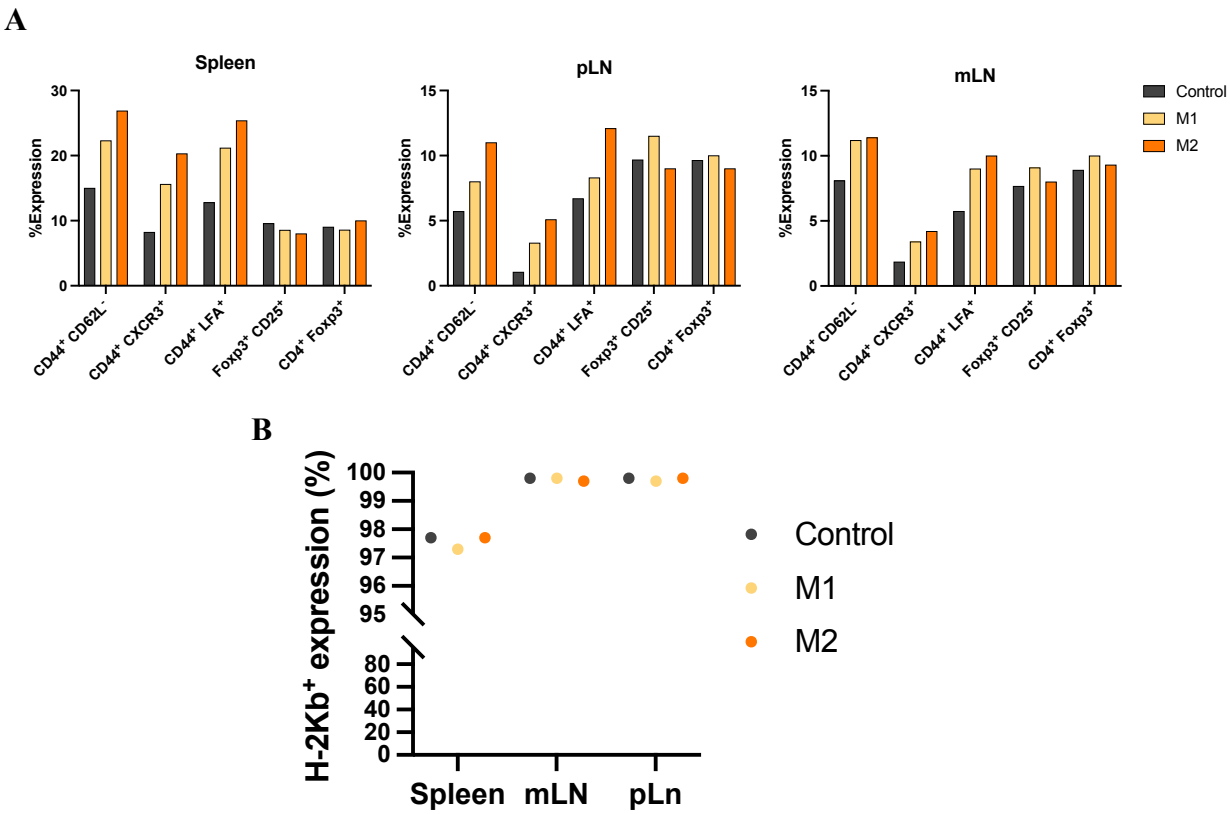


Figure 3.2) Allogeneic splenocyte injection via i.p induced polyclonal T cell response and established T cell memory in a dose-dependent manner
WT C57BL/6 recipient mouse (M1 and M2) received 7.5x10^4 and 1.5x10^6 allogeneic (Balb/c and CBA) splenocytes respectively. Control mice reived a saline vehicle control. **(A)** Flow cytometry staining of key memory and Treg CD4$^+$ T cell populations within SLOs (spleen, mLN and pLN) following a week after the allogeneic injection. **(B)** H-2Kb$^+$ staining of the T cells obtained from SLOs of the recipient mice.

3.3. Characterising the effects of different obesogenic diets and n-3PUFA supplementation on the CD4$^+$ T lymphocyte populations

The effect of different obesogenic diets and n-3PUFA supplementation on the T lymphocytes was investigated in a 3-week experimental setup as previously stated. Following the 3-week diet and allogeneic immunisation, SLOs and fat tissues were collected and general

T lymphocyte populations were investigated using flow cytometry. Additionally, the body weight and parameters of all mice groups were monitored during the experiment. An overall increase in weight change percentage within 3-weeks of ad libitum feeding has been observed in all groups (**Figure 3.3**). In line with Cucchi et al., 2020, there was no significant difference in both overall and final body weight (at d.21) among different groups (**Figure 3.3**) [126].

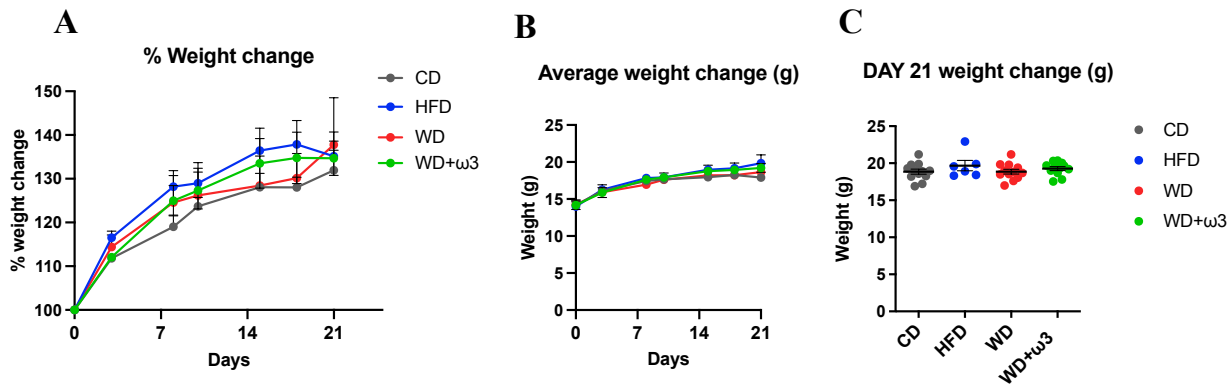


Figure 3.3) Different diets tested did not alter body weight of mice groups throughout the extent of the experiment

(A) Body weight change as percentage between diet groups over the course of 21 days. **(B)** Actual body weight change in grams between diet groups. **(C)** Actual body weight in grams of each individual mice in 4 different diet groups at the final (d.21) of the experiment. Each diet group; n=6. Data presented as mean ± SEM.

Previous publications and the preliminary data obtained by Mauro lab illustrated that the 3-weeks is the minimum time point to observe the effect of the obesogenic diets (specifically WD) and n-3PUFA supplementation on T lymphocytes.

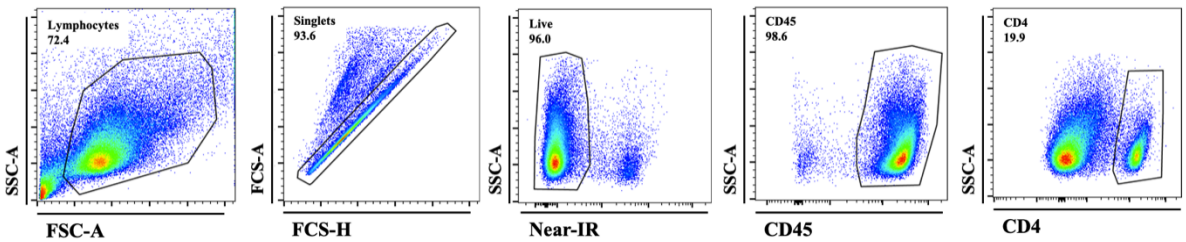


Figure 3.4) Representative flow cytometry gating strategy used as the main gating throughout the experiment.

Lymphocytes were gated based on their location in the forward (FCS) and side scatter (SSC). Doublets and dead cells were gated out. Live $CD45^{high}$, $CD4^{+}$ and $CD8^{+}$ T cells were gated as shown in the final representative flow cytometry gating.

Figure 3.4 illustrates the central gating strategy consistently applied across all experiments to mitigate the risk of any duplicate, dead or non-leukocyte cell contamination. All the markers were gated on the live cell population in order to eliminate any potential background signal. This approach also allowed the detection of any potential live/dead differences associated with different diet groups or cell isolation procedures across different tissues. Importantly, there was no significant difference among diet groups within each tissue tested where the majority of the cells isolated from SLOs were alive (**Figure 3.5A)**. Consistent with the literature digestion processes of the fat tissues were shown to consistently reduce the cell viability in all groups [450, 451]. Consistent with the previous publications, no significant difference was observed in total percentage of $CD4^+$ T cell populations among diet groups in all the tissues investigated (**Figure 3.5B)** [126, 127]. Interestingly, $CD8^+$ T cell frequencies were significantly reduced within the WD+n-3PUFA group compared to the CD group in all of the SLOs and p.fat tissues (**Figure 3.5C**). This observation was consistent with the literature [452].

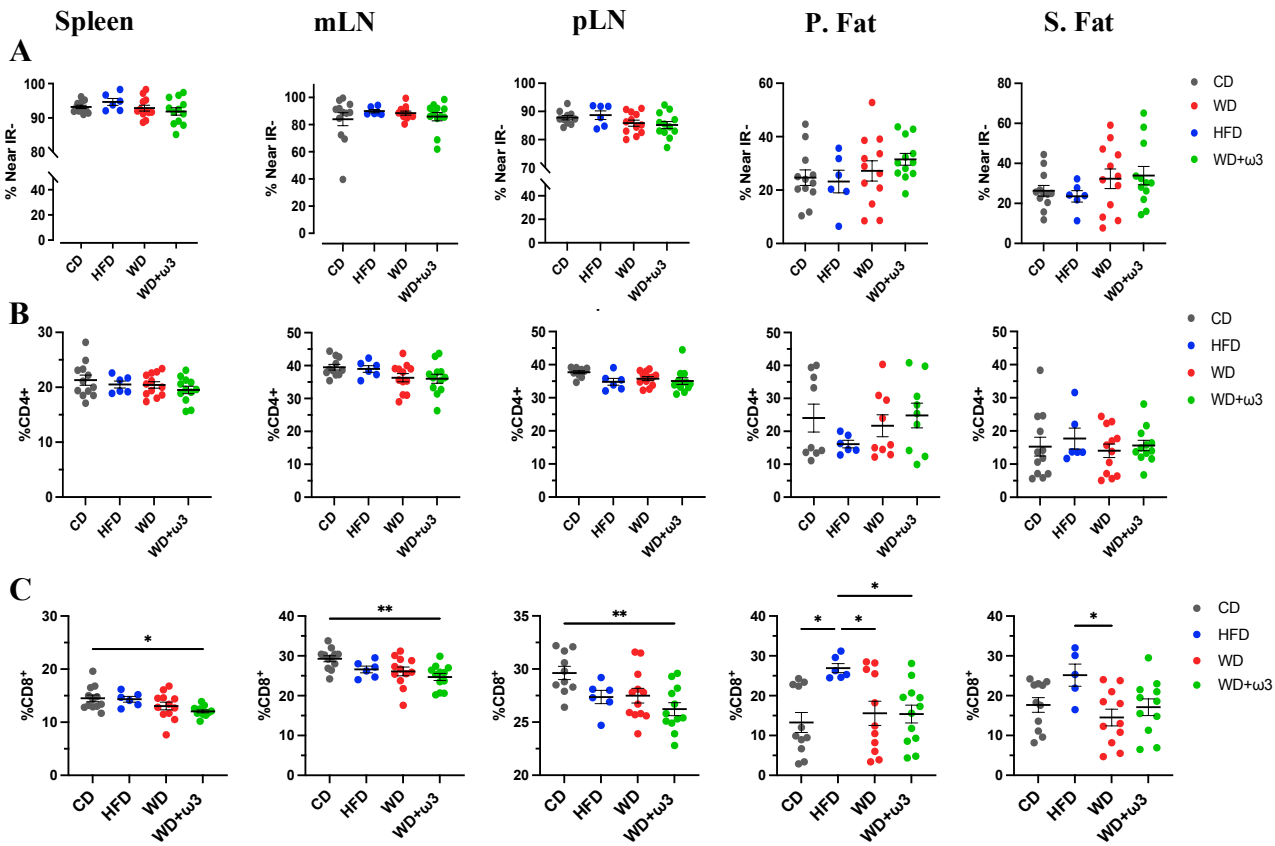


Figure 3.5) Effect of different diets on total live $CD4^+$ and $CD8^+$ T cell populations within SLOs and fat tissues

(A) Quantification of total live lymphocyte as percentage isolated from SLOs (spleen, mLNs, pLNs) and fat tissues (p.fat and s.fat) tissues of female C57BL/6J mice fed on CD, HFD, WD and WD+ n-

3PUFA for 21 days and were subjected to an allogeneic immunisation at d14. **(B)** Quantification of total live $CD4^+$ T cell percentage isolated from SLOs and fat tissues. **(C)** Quantification of total live $CD8^+$ T cell percentage isolated from SLOs and fat tissues. Each point represents an individual mouse in allocated diet groups (two *in vivo* experimental dataset with 6 mice per group pulled together, n=12 in total). One-way ANOVA with Tukey's correction; Data presented as mean ± SEM, *p<0.05; ** p<0.01.

3.4. WD induced pro-inflammatory alterations in the memory $CD4^+$ T lymphocyte populations

Consequently, we wanted to examine the specific subsets of $CD4^+$ T cells among different diet groups starting with the profiling of naïve, central (CM) and effector (EM) memory subsets (**Figure 3.6A**). Based on the literature and Mauro group's previous publications we hypothesised that, obesogenic diets bias the differentiation of EM populations and lead to an altered balance between naïve and memory $CD4^+$ T cell populations [18, 126, 127]. Obesogenic diets did not have a profound effect on naïve $CD4^+$ T cell populations ($CD62L^+$,$CD44^-$) in all tissues, except the spleen (**Figure 3.6B**). Interestingly, naïve $CD4^+$ T cell populations were significantly reduced in WD-fed group which shown to be reversed back to CD (control) levels by n-3PUFA supplementation (**Figure 3.6B**). Interestingly, HFD-fed group did not show any alteration in terms of naïve $CD4^+$ T cell population in all tissues tested.

The central memory (CM) $CD62L^+$,$CD44^+$ $CD4^+$ T cells were significantly increased in WD group compared to CD control in spleen, mLN and pLN. Importantly, n-3PUFA supplementation to WD significantly reduced the CM $CD4^+$ T cell population back to the control levels in all SLOs (**Figure 3.6C**). Although the HFD group did not alter the CM population in the spleen, in a manner similar to WD group, HFD led to a statistically significant increase within LNs. Contrarily to SLOs, both obesogenic diets showed no significant difference in CM $CD4^+$ T populations compared to the CD control in both fat tissues.

Similar to CM populations, EM ($CD44^+$, $CD62L^-$) $CD4^+$ T cells within the spleen of WD group exhibited a statistically significant increase in frequency (**Figure 3.6D**). Interestingly, this upward trend in the EM population in the WD group was not observed in any other lymphatic and fat tissues tested. Additionally, n-3PUFA+WD significantly reduced the EM populations back to CD levels (**Figure 3.6D**).

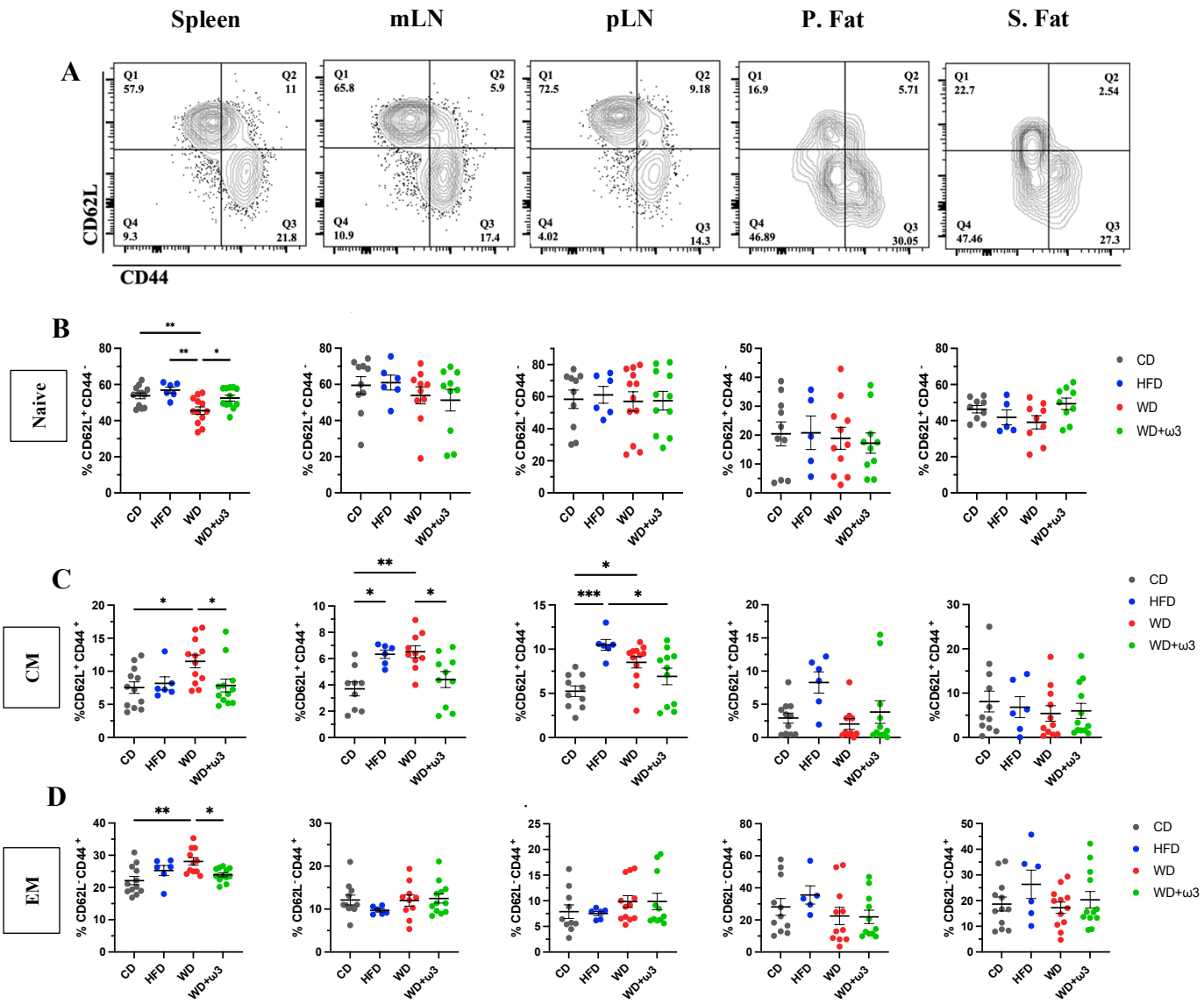


Figure 3.6) WD and n-3PUFA supplementation alters the distribution of main T cell subsets including naïve, CM and EM populations

(A) Representative flow cytometry plots of CD44 and CD62L extracellular staining on $CD4^+$ T cells isolated from SLOs and fat tissues of female C57BL/6J mice fed on CD, HFD, WD and WD+ n-3PUFA and were subjected to an allogeneic immunisation at d14. Quantification of flow cytometry data on **(B)** naïve ($CD44^-$ and $CD62L^+$), **(C)** CM ($CD44^+$ and $CD62L^+$) and **(D)** EM ($CD44^+$ and $CD62L^-$) $CD4^+$ T cell populations within three different SLOs and fat tissues obtained from different diet groups. Each point represents an individual mouse in allocated diet groups (two *in vivo* experimental dataset with 6 mice per group pulled together, n=12 in total). One-way ANOVA with Tukey's correction; Data presented as mean ± SEM, *p<0.05; ** p<0.01, *** p<0.001.

Considering the upward trend observed in memory $CD4^+$ T cell populations with WD, we wanted to investigate the critical pro-inflammatory functional memory T cell markers including LFA-1 and CXCR3 considering their crucial roles in OIIM [18, 395, 401]. **Figure 3.7** illustrates

the representative flow cytometry plots of both CD44$^+$, LFA-1$^+$ and CD44$^+$, CXCR3$^+$ populations gated on total CD4$^+$ T cell populations obtained from pLN tissues.

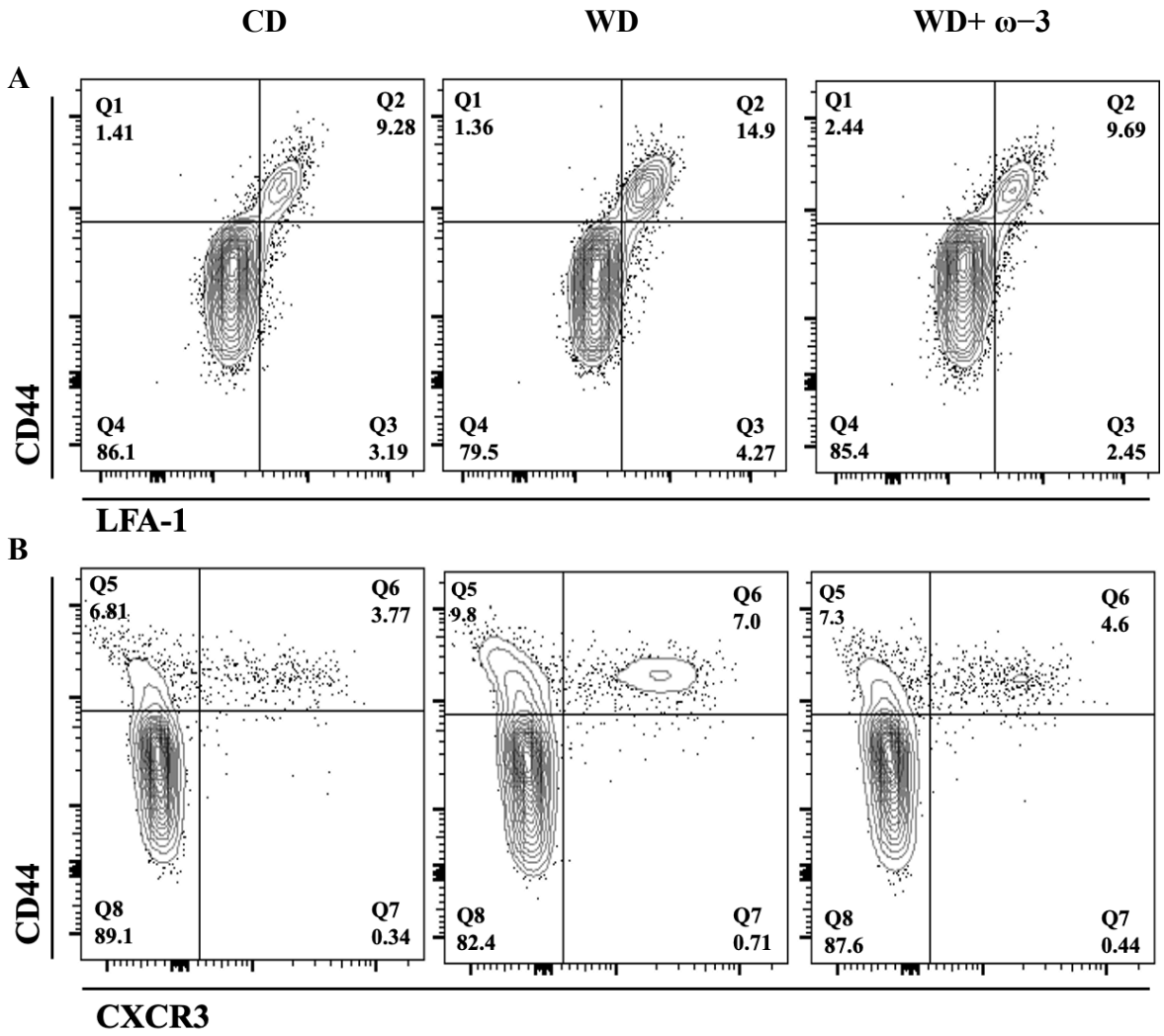


Figure 3.7) n-3PUFA supplementation into WD reduces the CD44$^+$, LFA-1$^+$ and CD44$^+$, CXCR3$^+$ frequencies in pLN

Representative flow cytometry figures of **(A)** CD44$^+$, LFA-1$^+$ and **(B)** CD44$^+$, CXCR3$^+$ populations in pLN tissues obtained from CD control, WD and WD+n-3PUFA mice groups. Representative flow figures and gating strategy used in all tissues as quantified in Figure 3.8.

The WD group illustrated a statistically significant increase in CD44$^+$,LFA-1$^+$ CD4$^+$ T cell population in all the tissues except s.fat compared to the CD (**Figure 3.8A**). Similarly, the HFD group also illustrated a significant increase in CD44$^+$,LFA-1$^+$ population in mLN, pLN and p.fat tissues. Interestingly, n-3PUFA+WD group exhibited a significant decrease in CD44$^+$,LFA-1$^+$ CD4$^+$ T cell frequencies in pLN tissues compared to the WD group (**Figure 3.7-3.8A**). A slight reduction was also observed in both spleen and p.fat tissues, however this reduction was not statistically significant. Interestingly, n-3PUFA supplementation into WD

did not rescue the increased pro-inflammatory CD44^{+},LFA-1^{+} CD4^{+} T cell phenotype in both mLN and s.fat (**Figure 3.8A**).

Interestingly, although the CD44^{+}, LFA-1^{+} population was still significantly higher in WD+n-3PUFA group compared to CD control group, this population was significantly reduced compared to both obesogenic diet (HFD and WD) fed groups within pLN tissue. This 'rescue' trend of WD+n-3PUFA group was also observed in p.fat tissue whereas, the reduction in CD44^{+},LFA-1^{+} CD4^{+} T cell population did not reach the statistical significance compared to WD group (**Figure 3.8A**). However, it was significantly reduced compared to other obesogenic diet (HFD) group.

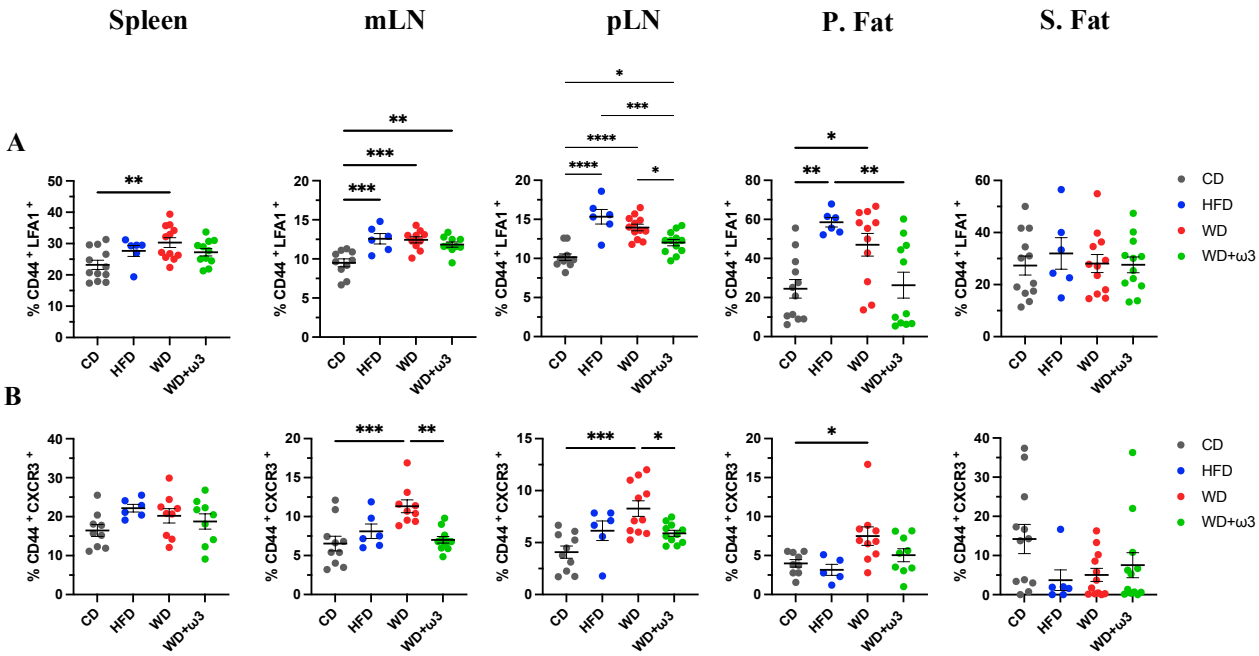


Figure 3.8) n-3PUFA supplementation into WD reduces the pro-inflammatory effector memory phenotype observed in 3-week early DIO murine model
Quantification of flow cytometry data of **(A)** CD44^{+} and LFA-1^{+} and **(B)** CD44^{+} and CXCR3^{+} obesity-associated pro-inflammatory effector memory CD4^{+} T cell populations in three main SLOs and two fat tissues obtained from female C57BL/6J mice fed on CD, HFD, WD and WD+ n-3PUFA. Each point represents an individual mouse in allocated diet groups (two *in vivo* experimental dataset with 6 mice per group pulled together, n=12 in total). One-way ANOVA with Tukey's correction; Data presented as mean ± SEM, *p<0.05; ** p<0.01, *** p<0.001.

Furthermore, similar to the LFA-1^{+} memory population, WD expressed a significant increase CXCR3^{+} memory cells within mLN, pLN and p.fat tissues compared to the CD group (**Figure 3.8B**). Although a similar increasing trend was observed in the spleen, this did not

reach statistical significance. Consistently, n-3PUFA+WD group was shown to significantly reduce the $CD44^+$,$CXCR3^+$ populations in mLN and pLN (**Figure 3.8B**). The 'rescue' trend was also noticed in spleen and p.fat tissues however, this reduction did not reach significance. Additionally, HFD group also showed an increasing trend in terms of $CD44^+$,$CXCR3^+$ populations in SLOs however, the difference was not significantly different from CD group (**Figure 3.8B**).

Overall, specifically pLN and the p.fat tissues were shown to be critical tissues that obesogenic diets directly alter the $CD4^+$ T memory populations towards a pro-inflammatory EM fate, which could be potentially driving and contributing to the OIIM. On contrary, n-3PUFA supplemented WD was shown to 'rescue' this pro-inflammatory EM $CD4^+$ T cell bias towards homeostatic control diet conditions by 're-creating' the balance within $CD4^+$ T cell populations.

3.5. Dissecting the alterations in specific effector $CD4^+$ T helper cell subsets induced by WD and ω−3 supplementation

Following observations on the alterations of the main $CD4^+$ T cell subsets with 3-week of WD and WD+ω−3, we further dissected the effector $CD4^+$ T subsets. To achieve this, we investigated the distinct intracellular TFs-linked with each effector $CD4^+$ T helper cell subsets including T-bet (Th1), Gata3 (Th2), RORγt (Th17) and Foxp3 (Tregs) (**Figure 3.9A**) [218]. It should be noted that due to experimental and technical issues, we could not obtain data from HFD group with some markers.

Consistent with the data on pro-inflammatory EM $CD4^+$ T cells, the WD group was shown to have significantly higher T-bet^+ $CD4^+$ Th1 population in both spleen and LNs (**Figure 3.9B**). Consistently, the association between obesogenic diets and increase in Th1 pro-inflammatory $CD4^+$ T cell frequencies are well shown in the literature [265, 301, 453-455]. Interestingly, we did not observe any significant changes in the $CD4^+$ Th1 cell population within both spleen and mLN of HFD-fed group (**Figure 3.9B**). This response could be potentially due to the short time-course (3-wk) of the experiment where HFD is known to exert obesogenic effects in a longer time frame [44, 45]. Contrarily, n-3PUFA+WD group had significantly reduced T-bet^+ Th1 $CD4^+$ T cell population compared to WD group in both spleen and mLN (**Figure 3.9B**). Additionally, no significant difference was observed between WD+ω−3 group and the CD control group which confirmed that n-3PUFA supplementation rescued the pro-inflammatory

Th1 'bias' and reduced the Th1 percentage back to CD control level. This 'rescue' trend of n-3PUFA was not observed in the pLN tissue where T-bet$^+$ Th1 populations of both WD and WD+ω−3 groups were significantly higher compared to CD control (**Figure 3.9B**).

Furthermore, we have investigated RORγt Th17 subset as one of the main pro-inflammatory effector CD4$^+$ T subsets. Consistent with the literature, RORγt$^+$ Th17 CD4$^+$ T cells were significantly increased in the spleen with the WD compared to CD control (**Figure 3.9C**). Although HFD also illustrated an upward trend with RORγt$^+$ Th17 CD4$^+$ cells, it did not reach statistical significance (**Figure 3.9C**). Importantly, n-3PUFA+WD resulted in a significant reduction in RORγt$^+$Th17 CD4$^+$ population in the spleen compared to WD group. Interestingly, Th17 levels in spleen tissue were shown to recapitulate the data on Th1 pro-inflammatory CD4$^+$ T subset in spleen. However, neither obesogenic diets, nor the n-3PUFA supplemented diet, had any effect on the RORγt$^+$ Th17 CD4$^+$ population within mLN and pLNs (**Figure 3.9C**).

We also analysed Th2 CD4$^+$ T cell populations which are known to be dramatically reduced in peripheral tissues during obesity [383, 453, 456]. Based on the 'anti-inflammatory' actions of Th2 cells such as secreting IL-10 and contributing to M2 macrophage polarisation, Th2 frequencies are negatively correlated with OIIM [385]. Therefore, we investigated the Gata3$^+$ CD4$^+$ Th2 lymphocytes in SLOs (**Figure 3.9D**). Interestingly with 'anti-inflammatory' Th2 levels, we observed a reducing trend in obesogenic diet groups which was mirroring the pro-inflammatory Th1 and Th17 CD4$^+$ T-cell dataset (**Figure 3.9A,B,C**). Even though both HFD and WD spleen and mLN tissues had a reducing trend, only HFD group was statistically significantly reduced in mLN compared to CD control (**Figure 3.9D**). On the other hand, WD+n-3PUFA group was shown to increase the Gata3$^+$ CD4$^+$ Th2 frequencies (**Figure 3.9D**).

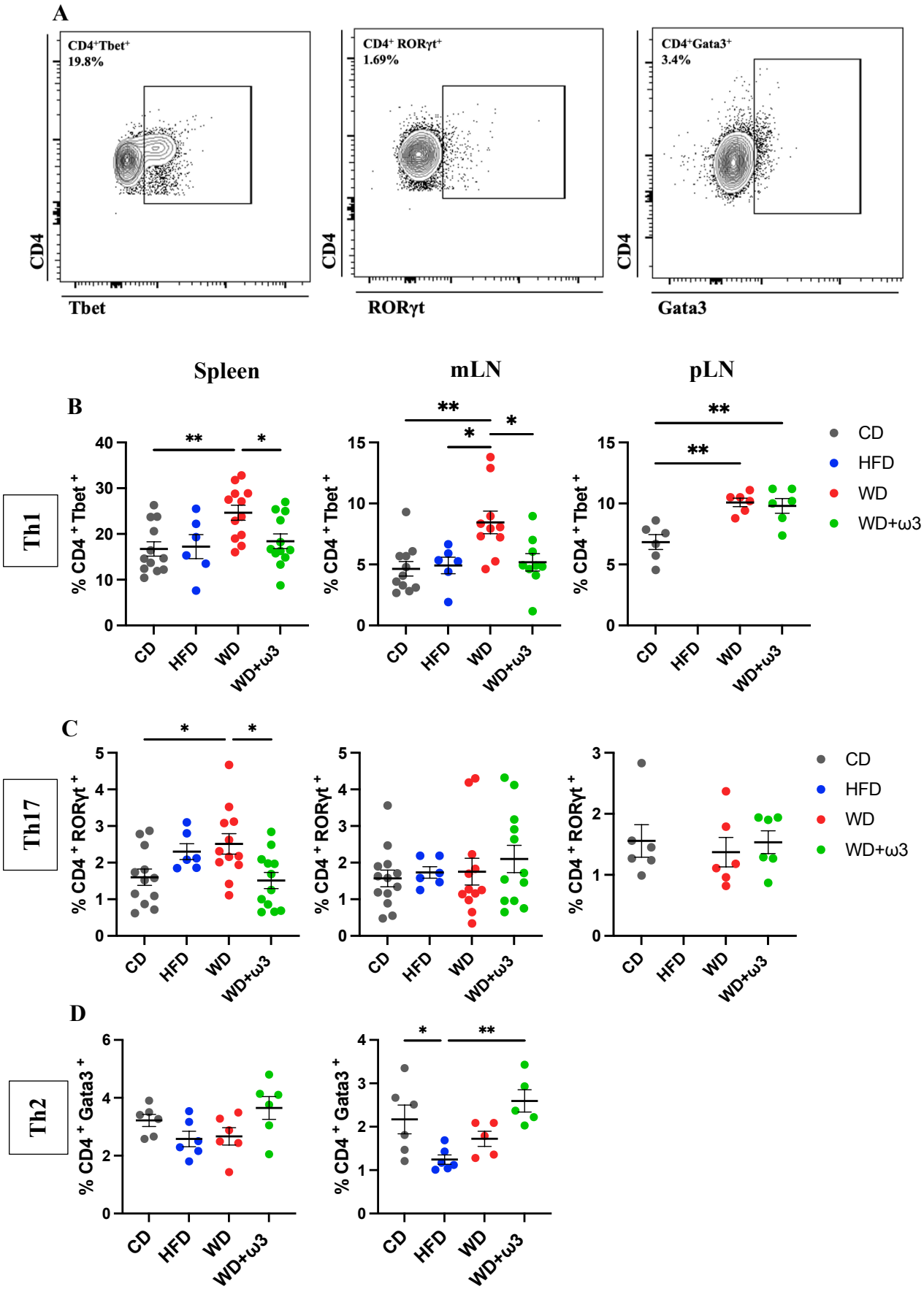


Figure 3.9) WD-induced elevation in pro-inflammatory CD4$^+$ effector T cell subsets can be

abrogated via dietary n-3PUFA supplementation

(A) Representative flow figures of the key intracellular transcription markers for distinct $CD4^+$ effector T cell subsets; $Tbet^+$, $ROR\gamma t^+$, $Gata3^+$ on spleen tissue of female C57BL/6J mice fed on CD control group, subjected to an allogeneic immunisation at d14. Quantification of flow cytometry data of **(B)** $Tbet^+$ for Th1 **(C)** $ROR\gamma t^+$ for Th17 and **(D)** $Gata3^+$ for Th2 effector $CD4^+$ T cell populations within SLO tissues obtained from female C57BL/6J mice fed on CD, HFD, WD and WD+ n-3PUFA. Each point represents an individual mouse in allocated diet groups (two *in vivo* experimental dataset with 6 mice per group pulled together, n=12 in total). One-way ANOVA with Tukey's correction; Data presented as mean ± SEM, *p<0.05; ** p<0.01, *** p<0.001.

Note) Due to a laser failure in first *in vivo* experiment Gata3 staining had only n=6 per diet group obtained from the second *in vivo* experiment.

Additionally, next we sought to investigate the senescence profiles of the early-DIO murine model as suggested by the literature. Consistently, $PD1^+$,$CD4^+$ T 'exhausted' T-lymphocytes were significantly increased in the spleen and mLN of the WD-fed group (**Figure 3.10A**). Similarly, HFD group also illustrated a statistically significant increase in $PD1^+$ $CD4^+$ T cells in the spleen but not in mLN. Interestingly, WD+n-3PUFA had no effect on the exhaustion cells as the $PD1^+$ $CD4^+$ exhausted T-cell frequencies were still elaved in both spleen and mLN (**Figure 3.10A**).

Additionally, we investigated the background senescence marker (KLRG1) expression in main SLOs. In spleen, WD caused a significant increase in $KLRG1^+CD4^+$ T cell population whereas, n-3PUFA supplementation to the diet significantly reduced the senescent $CD4^+$ T cell population, back to CD control levels (**Figure 3.10B**). However, there was no observable trend in both LN tissues. It should be noted that the low level of KLRG1 expression in the samples maybe be due to direct staining following the tissue isolation, without *ex vivo* PMA/Ionomycin stimulation (**Figure 3.10B**).

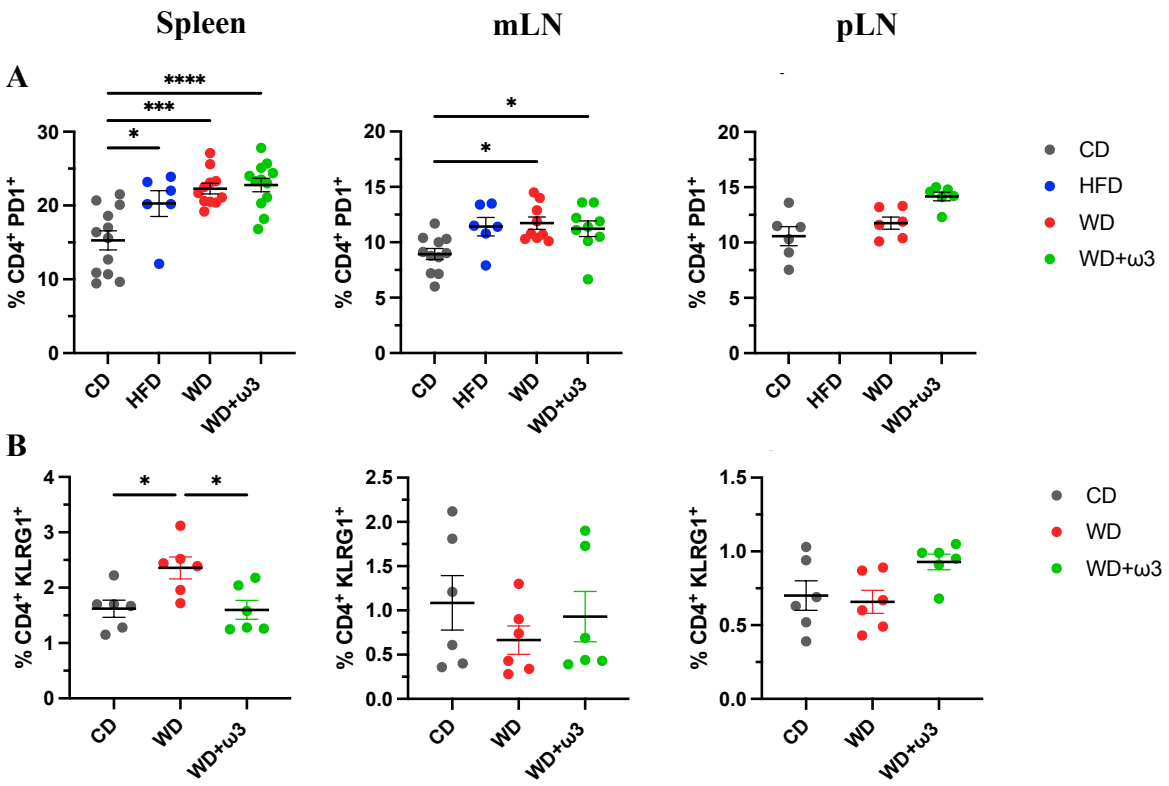


Figure 3.10) WD induces CD4$^+$ T cell exhaustion and senescence in SLOs
Quantification of flow cytometry data of **(A)** PD1$^+$ and **(B)** KLRG1$^+$ CD4$^+$ T cell isolated from SLO tissues obtained from female C57BL/6J mice fed on CD, HFD, WD and WD+ n-3PUFA and were subjected to an allogeneic immunisation at d14. Each point represents an individual mouse in allocated diet groups (two *in vivo* experimental dataset with 6 mice per group pulled together, n=12 in total). One-way ANOVA with Tukey's correction; Data presented as mean ± SEM, *p<0.05; ** p<0.01, *** p<0.001.
Note) Due to a laser failure in first *in vivo* experiment Gata3 staining had only n=6 per diet group obtained from the second *in vivo* experiment.

Finally, based on the crucial pro-inflammatory effect of Tfh CD4$^+$ T cells in RA [422] and diabetes [457] and other obesity-associated diseases, we investigated any potential alterations in the Tfh frequencies within SLOs. Consistent with the limited background literature, in **Figure 3.11**, we did not observe a significant difference with HFD group in both spleen and mLN [456]. Interestingly, we observed a significant increase in the Tfh population with the WD group in both spleen and pLN. Supplementation of n-3PUFA into WD lead to a significant decrease in CXCR5$^+$,PD1$^+$ Tfh populations in both spleen and pLN (**Figure 3.11**). Furthermore, consistent with Esteves de Oliveira et al. 2019, no significant difference was observed among different diet groups in mLN tissue.

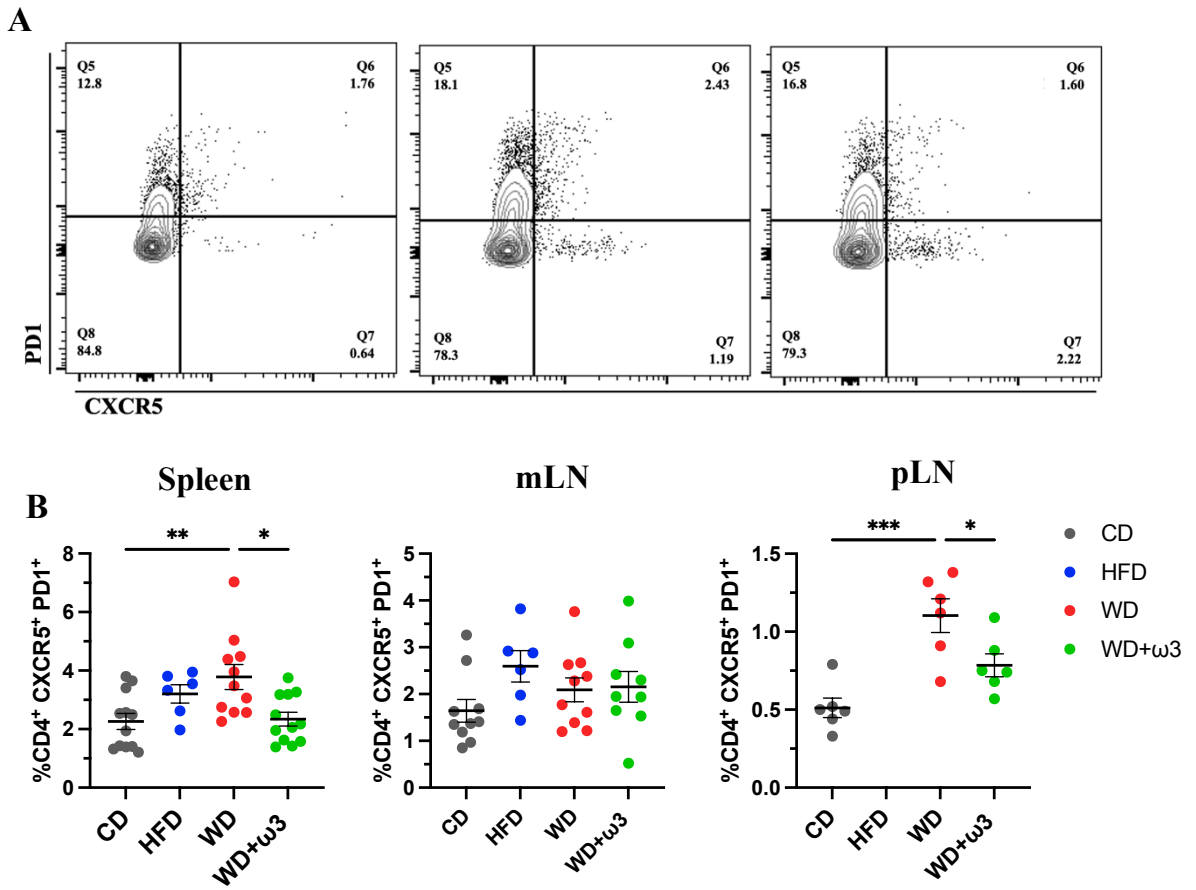


Figure 3.11) Dietary n-3PUFA supplementation into WD alleviates the pro-inflammatory T follicular helper populations

(A) Representative flow figures of Tfh ($CXCR5^+$ $PD1^+$) $CD4^+$ T cell population located in germinal centre of SLOs obtained from female C57BL/6J mice fed on CD, WD and WD+ n-3PUFA and were subjected to an allogeneic immunisation at d14. **(B)** Quantification of flow cytometry data of Tfh cell populations within 3 main SLOs obtained from different diet groups. Each point represents an individual mouse in allocated diet groups (two *in vivo* experimental dataset with 6 mice per group pulled together, n=12 in total). One-way ANOVA with Tukey's correction; Data presented as mean ± SEM, *p<0.05; ** p<0.01, *** p<0.001.

Note) Due to technical issues encountered in the first *in vivo* experiment, pLN tissues only had only n=6 per diet group acquired from the second *in vivo* experiment.

3.6. Investigating the pro-inflammatory effects of WD and homeostatic effects of n-3PUFA on $CD8^+$ T lymphocytes in OIIM

Furthermore, we also investigated any potential modulations within main $CD8^+$ T cell subsets. Similar to the $CD4^+$ T-cell dataset, both HFD and WD did not show a significant alteration in naïve ($CD62L^+$,$CD44^-$) $CD8^+$ T cell populations in both SLOs and fat tissues (**Figure 3.12B**). Interestingly, WD+ n-3PUFA group significantly increased the naïve $CD8^+$ T

cells in s.fat compared to the CD control group. This significant increase was in line with the upward trend observed in naïve $CD4^+$ T cell frequency shown within the s.fat (**Figure 3.6B**).

The CM ($CD62L^+$,$CD44^+$) $CD8^+$ T cell frequencies illustrated an increasing trend within the WD group however, this upward trend only reached statistical significance in mLN and pLN tissues (**Figure 3.12C**). This significant increase in $CD8^+$ CM T cell frequencies recapitulates $CD4^+$ T cell data on LNs (**Figure 3.6C**), but differently from the $CD4^+$ T cell population, no significant difference was detected in spleen harvested from different diet groups (**Figure 3.12C**). Interestingly, n-3PUFA supplementation had no observable effect on $CD8^+$ CM T cell frequencies in all the SLOs and fat tissues tested (**Figure 3.12C**). Contrarily, in pLN WD+ω−3 group illustrated the same significant increase in $CD8^+$ CM T cell frequency compared to CD as WD group (**Figure 3.12C**).

Interestingly, the EM $CD8^+$ ($CD62L^-$,$CD44^+$) T cells, expressed the same elevation trend in the WD group similar to $CD4^+$ T cell dataset. Importantly $CD8^+$ EM T cell frequencies were statistically significantly elevated in both spleen and pLN tissues of WD group compared to CD control (**Figure 3.12D**). **Figure 3.12D** recapitulates the $CD4^+$ EM T cell data of **Figure 3.6D,** where WD+n3-PUFA led to a significant reduction of the $CD8^+$ EM T cell in both spleen and pLN tissues. Similar to the $CD4^+$ T cell dataset, there was no significant difference in $CD8^+$ EM T cell frequencies among different diet groups in both p.fat and s.fat tissues.

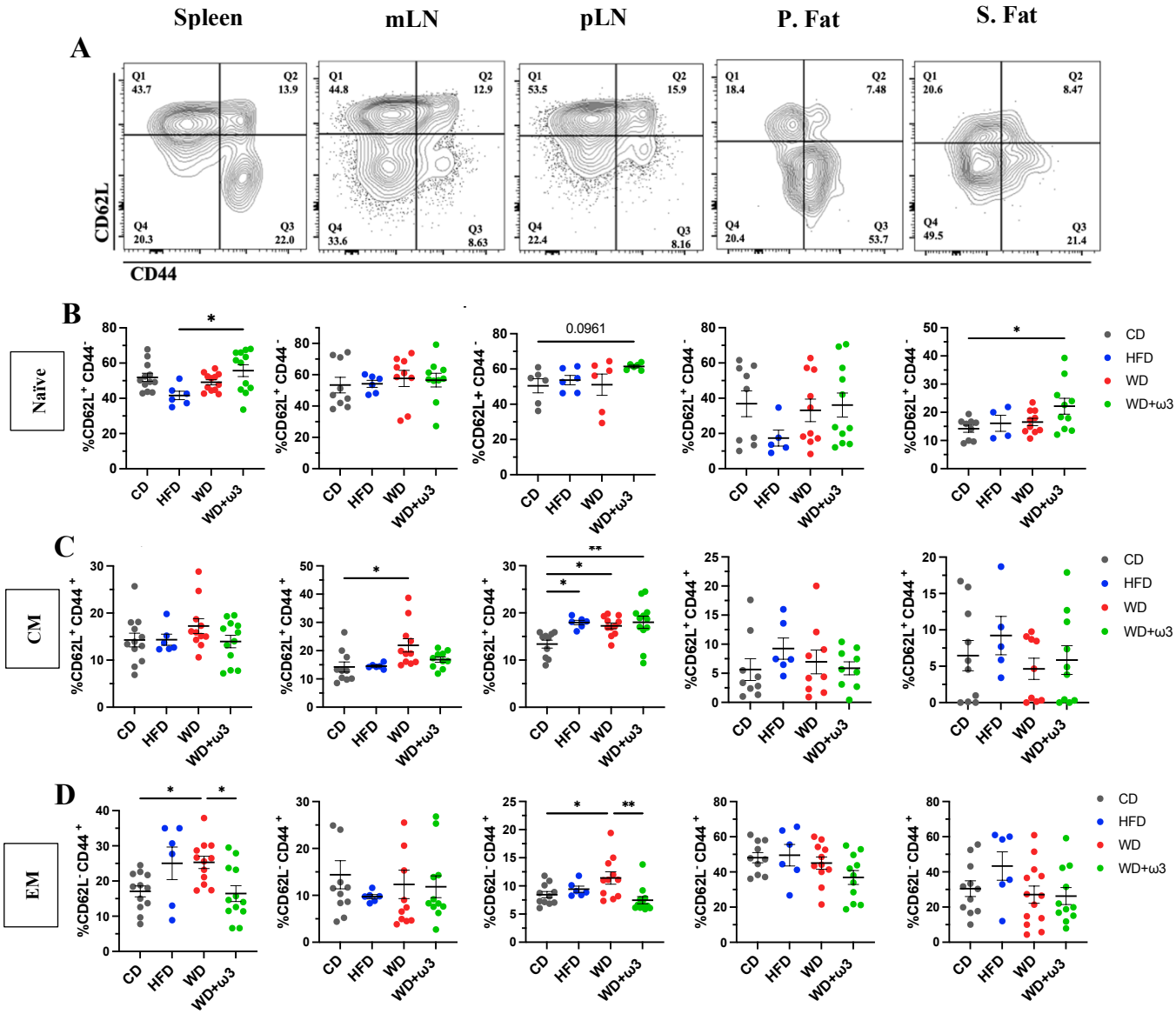


Figure 3.12) WD and n-3PUFA supplementation alters the distribution of main T cell subsets including naïve, CM and EM populations in SLOs and fat tissues

(A) Representative flow figures of the key extracellular markers CD44 and CD62L to distinguish main $CD8^+$ T cell subsets isolated from SLOs and fat tissues of female C57BL/6J mice fed on CD control group, subjected to an allogeneic immunisation at d14. Quantification of flow cytometry data on **(B)** naïve ($CD44^-$ and $CD62L^+$), **(C)** CM ($CD44^+$ and $CD62L^+$) and **(D)** EM ($CD44^+$ and $CD62L^-$) $CD8^+$ T cell populations within three different SLOs and fat tissues obtained from CD, HFD, WD and WD+ n-3PUFA diet groups. Each point represents an individual mouse in allocated diet groups (two *in vivo* experimental dataset with 6 mice per group pulled together, n=12 in total). One-way ANOVA with Tukey's correction; Data presented as mean ± SEM, *p<0.05; ** p<0.01, *** p<0.001.

Similar to $CD4^+$ T cells, CXCR3 expression has been documented to induce a pro-inflammatory effector phenotype in $CD8^+$ T cell populations confirmed by the increase in the frequency of $CXCR3^+$ $CD8^+$ T in SLOs via DIO and directly contributing to OIIM [389, 394].

Similar to $CD4^+$ T cells, LFA-1 also plays a crucial role in $CD8^+$ T cell–related adipose tissue inflammation in DIO conditions. LFA-1^+ $CD8^+$ T cells were shown to induce T cell activation in OIIM and contribute to neutrophil-related adipose tissue OIIM in DIO models [387].

Considering the background literature, we also investigated the expression of CXCR3 and LFA-1 on $CD8^+$ T cell populations isolated from SLOs and fat tissues. Consistent with $CD4^+$ dataset, both obesogenic diets (WD and HFD) illustrated a significant increase in LFA-1^+ $CD8^+$ T in pLN and p.fat tissues compared to CD group (**Figure 3.13A**). Although both obesogenic diets showed an upward trend in both spleen ($p=0.098$) and s.fat ($p=0.073$) tissues, the difference did not reach statistical significance (**Figure 3.13A**). Interestingly, n-3PUFA supplementation lead to a statistically significant reduction in the pro-inflammatory LFA-1^+ $CD8^+$ T cell population in both pLN and p.fat tissues (**Figure 3.13A**), consistent with the LFA-1^+ $CD4^+$ T cell dataset (**Figure 3.8A)**. Differently from $CD4^+$ T cells, LFA-1^+ $CD8^+$ T cell population were significantly reduced in s.fat tissue of WD+n3-PUFA compared to both obesogenic diet groups. Although a similar reduction trend was observed in the spleen, this did not reach statistical significance compared to WD (**Figure 3.13A**).

Furthermore, WD lead to a significant increase in $CXCR3^+CD8^+$ T cell frequencies in all SLOs tested compared to CD control group, similar to the $CD4^+$ T cell dataset (**Figure 3.13B**). However, different from the $CD4^+$ T cell dataset, no difference was observed in $CXCR3^+$ $CD8^+$ T cell frequencies in the fat tissues. Interestingly, n-3PUFA supplementation into WD significantly downregulated the $CXCR3^+$ $CD8^+$ T cell frequencies in all three SLOs and s.fat compared to WD group (**Figure 3.13B**). This was highly critical that only 5% n-3PUFA supplementation to the WD was able to significantly abrogated the upward effect of WD on the distinct pro-inflammatory $CD8^+$ T phenotypes.

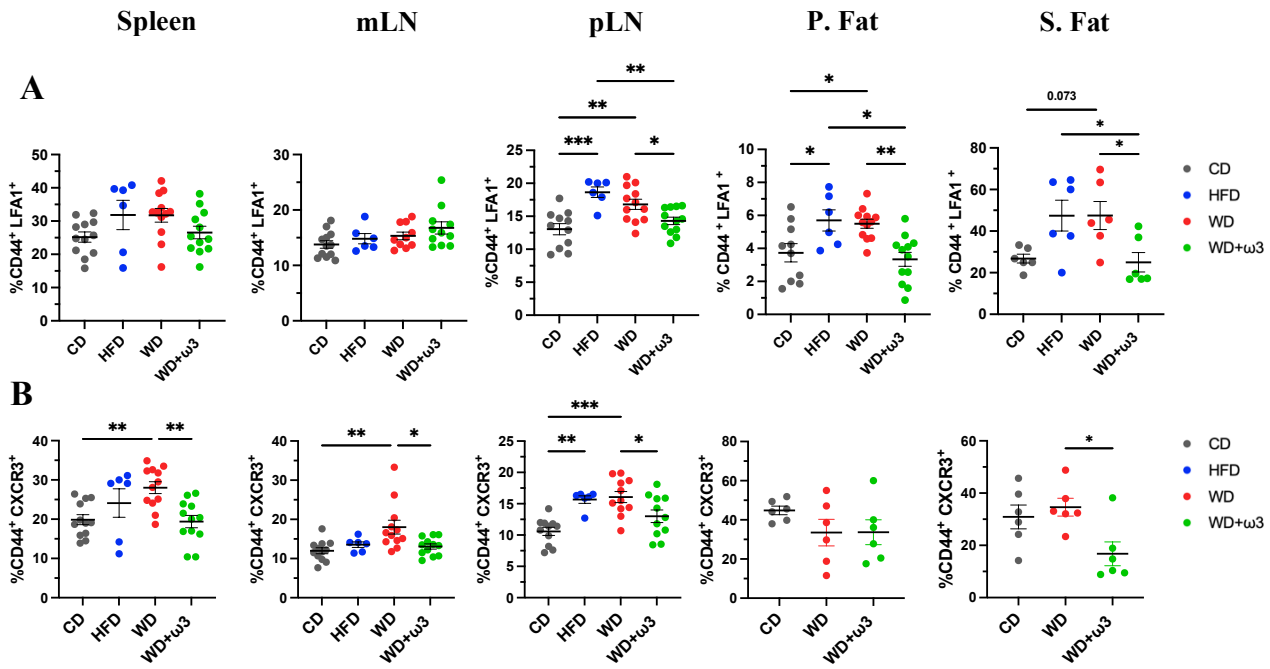


Figure 3.13) n-3PUFA supplementation into WD reduces the pro-inflammatory cytotoxic memory CD8$^+$ T cell population frequencies in 3-week early DIO murine model
Quantification of flow cytometry data of **(A)** CD44$^+$ and LFA-1$^+$ and **(B)** CD44$^+$ and CXCR3$^+$ obesity-associated pro-inflammatory cytotoxic memory CD8$^+$ T cell populations in three main SLOs and two fat tissues obtained from female C57BL/6J mice fed on CD, HFD, WD and WD+ n-3PUFA and were subjected to an allogeneic immunisation via i.p injections at day 14. Each point represents an individual mouse in allocated diet groups (two *in vivo* experimental dataset with 6 mice per group pulled together, n=12 in total). One-way ANOVA with Tukey's correction; Data presented as mean ± SEM, *p<0.05; ** p<0.01, *** p<0.001.

3.7. Dissecting the alterations in specific cytotoxic CD8$^+$ T lymphocyte subsets induced via WD and ω−3 supplementation

Following the CD4$^+$ effector T lymphocytes, CD8$^+$ cytotoxic T cells are the second major T lymphocytes that function in the immune system known to play various critical roles in OIIM during obesity and associated pathologies. Similar to CD4$^+$ T cells, CD8$^+$ cytotoxic T cells are also divided into various subsets such as Tc1, Tc2, Tc17 and Tc22 [217, 458]. In general, the classification of Tc CD8$^+$ T cells mirrors the CD4$^+$ effector T cell subsets including the cytokine secretion profile and their lineage-determining master transcription factors; T-bet for Tc1, Gata3 for Tc2, RORγt for Tc17 and Foxp3 for Treg [217, 458]. Based on the modulations we have observed in the CD4$^+$ effector T cell populations in SLO tissues of obesogenic diets and n-3PUFA supplemented diet, we wanted to examine any potential modulations in CD8$^+$ cytotoxic T cell subset frequencies.

Although not reaching statistical significance, T-bet$^+$ Tc1 CD8$^+$ populations exhibited an increasing trend in both WD and HFD in spleen and mLN tissues, similar to the CD4$^+$ dataset. However, unlike CD4$^+$ T cells, n-3PUFA supplementation to the WD had no ameliorative effect on Tc1 CD8$^+$ T cell populations where T-bet$^+$ Tc1 CD8$^+$ T cell frequencies were still high nearly at the same level as the WD group (**Figure 3.14B**).

Additionally, we also tested RORγt$^+$ CD8$^+$ Tc17 subsets in spleen and mLN tissues. Importantly, similar to the significant changes observed in CD4$^+$ T cell populations in spleen (**Figure 3.9C**), CD8$^+$ Tc17 frequencies showed a similar increasing trend with WD but did not reach statistical significance (**Figure 3.14C**). However, different from the CD4$^+$ dataset, n-3PUFA supplemented WD did not show an observable reduction in the RORγt$^+$ CD8$^+$ Tc17 frequencies, especially in spleen tissue. In terms of the Tc17 population in mLN, there was no observable trend among different diet groups.

When analysing the 'Gata3$^+$ CD8$^+$ Tc2 frequencies, there was no trend observed in the spleen tissue of the obesogenic diets. However in the mLN tissue, the HFD group exhibited a reducing trend whereas, the WD+ω−3 group illustrated a significant increase compared to HFD group. Additionally, despite Gata3$^+$ CD8$^+$ Tc2 levels illustrating an increasing trend within the WD+ω−3 compared to CD and WD groups, this trend did not reach statistical significance. However, this could be potentially due to a technical issue experienced during the second *in vivo* experiment. Technical issues such as loss of CD8 staining and laser failure on the Fortessa, led to the loss of the CD8 dataset in the second in *in vivo* experimental repeat. Based on the CD4$^+$ dataset and considering the reduction in the biological replicates some of the trends observed in the first experiment may potentially reach statistical significance if the experiment would be repeated again.

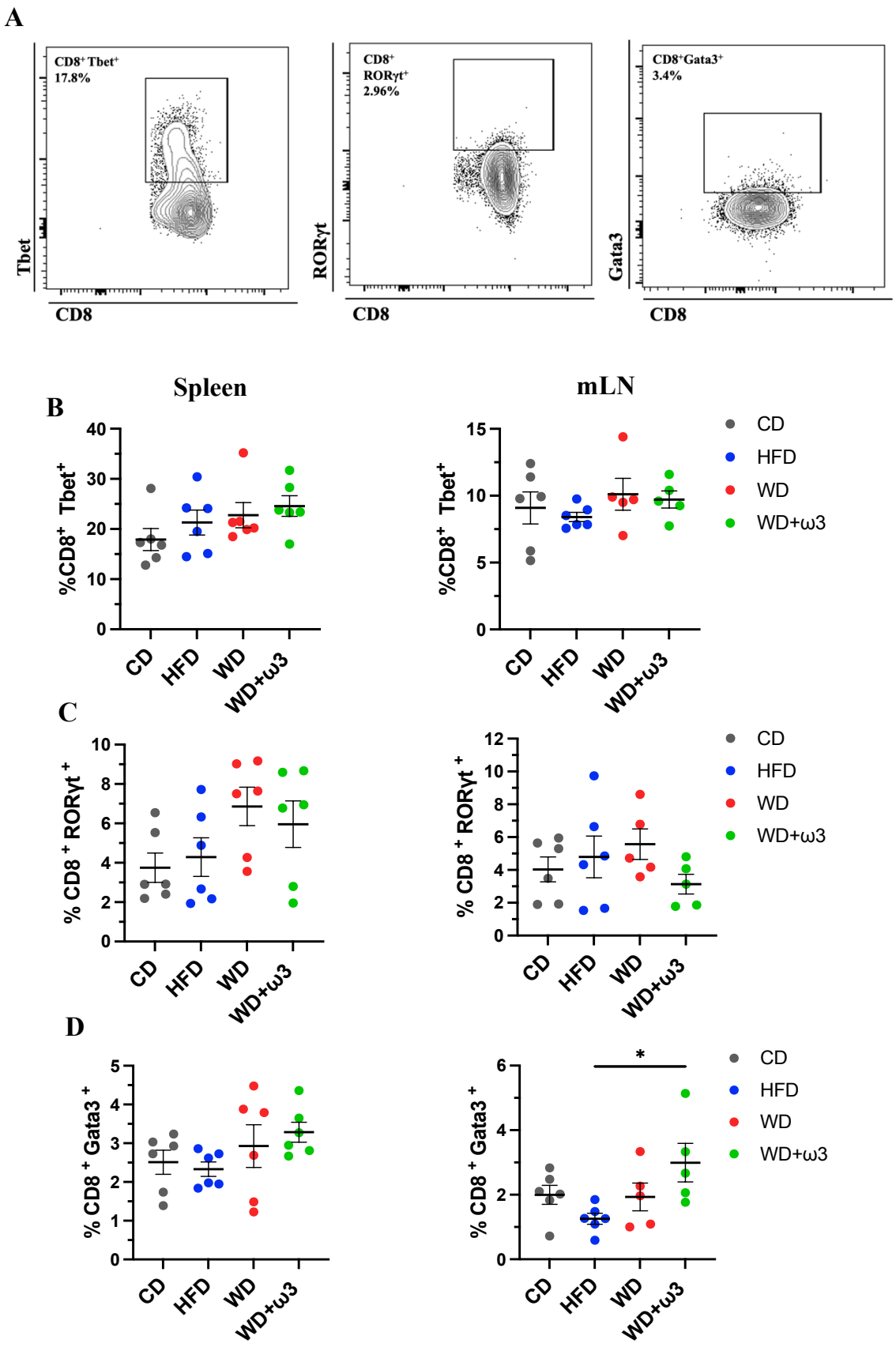


Figure 3.14) Obesogenic diets and n-3PUFA supplementation did not altered cytotoxic CD8$^+$ T cell subsets in 3-week early DIO murine model

(A) Representative flow figures of the key intracellular transcription markers for distinct $CD8^+$ cytotoxic T cell subsets; $Tbet^+$, $ROR\gamma t^+$, $Gata3^+$ on spleen tissue of female C57BL/6J mice fed on CD control group, subjected to an allogeneic immunisation at d14. Quantification of flow cytometry data of **(B)** $Tbet^+$ for Th1 **(C)** $ROR\gamma t^+$ for Th17 and **(D)** $Gata3^+$ for Th2 effector $CD8^+$ T cell populations within spleen and mLN tissues obtained from female C57BL/6J mice fed on CD, HFD, WD and WD+ n-3PUFA. Each point represents an individual mouse in allocated diet groups (two *in vivo* experimental dataset with 6 mice per group pulled together, n=12 in total). One-way ANOVA with Tukey's correction; Data presented as mean ± SEM, *p<0.05; ** p<0.01, *** p<0.001.
Note) Due to a laser failure in first *in vivo* experiment CD8 staining had only n=6 per diet group obtained from the second *in vivo* experiment.

Following the modulations observed in $CD8^+$ cytotoxic T cell subsets with the obesogenic diets and WD+ω−3 groups, we wanted to investigate the DIO-associated $CD8^+$ T cell exhaustion and senescence. However, as mentioned above, we also lost the senescence (KLRG1) in the $CD8^+$ T lymphocyte dataset due to a failure on the acquisition day. However, flow cytometry analysis of exhaustion marker PD1, illustrated a statistically significant increase in $PD1^+$ $CD8^+$ T lymphocytes of the WD-fed group compared to the CD group in spleen tissue, similar to what was observed in the $CD4^+$ T cells (**Figure 3.15A**). Interestingly, contrasting the $CD4^+$ dataset, WD+ω−3 group illustrated a reducing trend in the exhausted $PD1^+$ $CD8^+$ T cells compared to WD. However, this reduction did not reach statistical significance. Both trends observed with WD and WD+ω−3 were shown to be consistent in mLN but in a lower magnitude due to none of the differences were found to be statistically significant (**Figure 3.15A**). Differently from $CD4^+$ T cell's static response to the n-3PUFA supplementation, the $PD1^+$ $CD8^+$ T cell population illustrated a reducing trend within WD+ω−3. These suggest that n3-PUFA can have an ameliorative effect on $CD8^+$ T cell populations in terms of T cell exhaustion induced by obesogenic diets.

Following the modulations observed in $CD4^+$ Tfh ($CXCR5^+$, $PD1^+$) subset between WD and WD+n-3PUFA diet groups (**Figure 3.11)**, we investigated the $CD8^+$ Tfh counterparts as well. Consistently, a significant increase was observed in the spleen of WD group compared to CD control (**Figure 3.15B)**. As previously reported by the literature, the frequency of $CD8^+$ Tfh populations is highly limited (0.5-1%) which is shown to be nearly doubled by WD (~1.5-2%). Importantly, n-3PUFA supplemented group significantly reduced the $CD8^+$ Tfh frequencies back to CD control levels in the spleen. Similar to the $CD4^+$ Tfh dataset, no significant trend was observed between different diet groups in terms of mLN tissue (**Figure 3.15B)**.

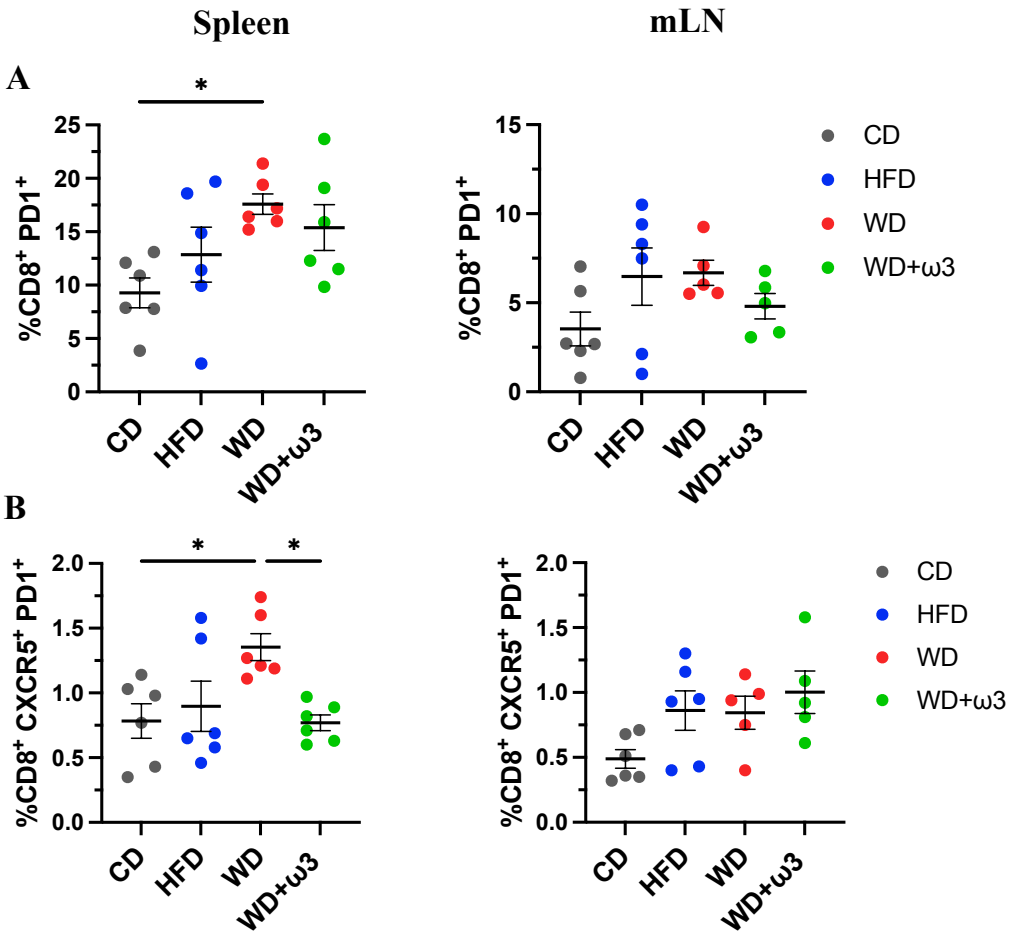


Figure 3.15) n-3PUFA supplementation into WD ameliorated the WD-induced elevation CD8$^+$ Tfh population

Quantification of flow cytometry data of **(A)** PD1$^+$ and **(B)** Tfh (CXCR5$^+$ PD1$^+$) CD8$^+$ T cell population frequencies in spleen and mLN tissues isolated from female C57BL/6J mice fed on CD, HFD, WD and WD+ n-3PUFA and were subjected to an allogeneic immunisation at d14. Each point represents an individual mouse in allocated diet groups (two *in vivo* experimental dataset with 6 mice per group pulled together, n=12 in total). One-way ANOVA with Tukey's correction; Data presented as mean ± SEM, *p<0.05.

3.8. n-3PUFA supplementation to the WD 'boosts' the anti-inflammatory CD4$^+$ and CD8$^+$ Foxp3$^+$ Treg population frequencies *in vivo*

n-3PUFA is known to induce proliferation and accumulation of CD25$^+$,Foxp3$^+$ CD4$^+$ Tregs in tissues such as the liver [459], spleen [460] and adipose tissue [344] of murine models fed with n-3PUFA supplemented CD[408]. Previous publications by our group illustrated the direct effect of short-term n-3PUFA enrichment on CD4$^+$ T cell subsets including effector and central memory and Tregs alongside the modulations on cell polarisation, cytoskeleton dynamics and migratory capacity in both *in vivo* and *in vitro* [126, 127]. Following this we

wanted to further investigate the anti-inflammatory potential of short-term n-3PUFA supplementation specifically in Foxp3$^+$,CD25$^+$ CD4$^+$ and CD8$^+$ Treg subsets fed on obesogenic WD in early-DIO murine model (**Figure 3.16)**.

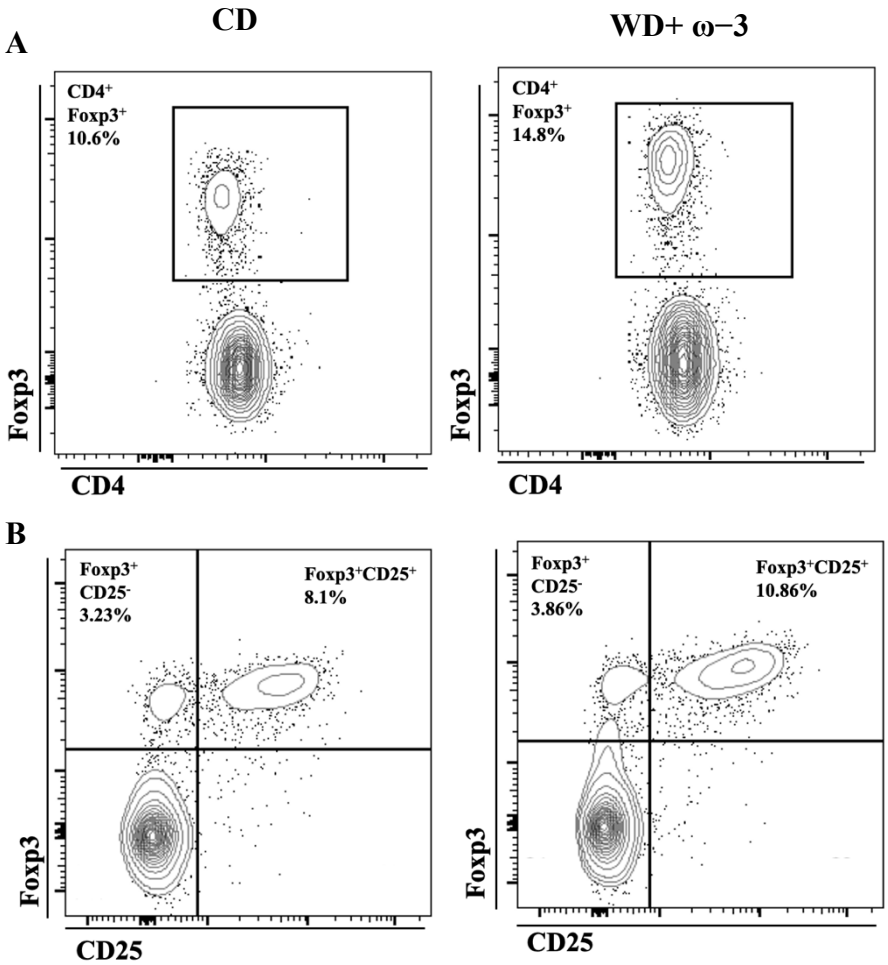


Figure 3.16) Representative flow cytometry plots showing the gating and modulation on Treg population between CD and WD+n-3PUFA groups.
Representative flow figures of the key intracellular transcription marker of CD4$^+$ Treg cell population; Foxp3$^+$ **(A)** and Foxp3$^+$, CD25$^+$ (double positive population) **(B)** stained on SLOs and fat tissues of female C57BL/6J mice fed on CD and WD+n-3PUFA groups, subjected to an allogeneic immunisation at d14.

Figure 3.17, demonstrated no significant difference within Foxp3$^+$ CD4$^+$ Treg frequencies with both obesogenic diets (HFD and WD) compared to CD group in all five tissues tested. Although WD illustrated a reduction in Foxp3$^+$ CD4$^+$ Treg populations compared to CD group, it did not reach statistical significance. Interestingly, the WD+n-3PUFA group induced a significant increase in Foxp3$^+$ CD4$^+$ Treg frequencies in both spleen, mLN and s.fat tissues compared to WD group (**Figure 3.17A**). Interestingly, n-3PUFA supplementation to the WD was significantly higher in terms of Foxp3$^+$ CD4$^+$ Treg frequencies compared to CD control

and HFD in the spleen and mLN. This illustrated that re-boosting the n-3:n-6 PUFAs in WD content improves Treg frequencies compared to even healthy CD, highlighting the direct effect of n-3PUFA in the diet.

Figure 3.17B, illustrates $CD25^+$ $Foxp3^+$ $CD4^+$ as conventional Treg-specific markers to verify $Foxp3^+$ $CD4^+$ frequencies previously observed. Similar to $Foxp3^+$ $CD4^+$ levels, there was no significant reduction in $CD25^+$,$Foxp3^+$ $CD4^+$ Treg frequencies with both of the obesogenic diets compared to CD group. Alongside the $Foxp3^+$ $CD4^+$ Treg levels, the WD+ω−3 group had significantly higher $CD25^+$ $Foxp3^+$ $CD4^+$ Treg levels compared to both WD and CD control in spleen, mLN and both fat tissues (**Figure 3.17B**). Interestingly, different to bulk $Foxp3^+$ $CD4^+$ Treg levels, WD+ω−3 led to a significant elevation in $CD25^+$ $Foxp3^+$ $CD4^+$ Tregs in p.fat tissue compared to CD, HFD and WD groups (**Figure 3.17B**). The increasing trends observed in Treg levels with n-3PUFA supplementation illustrate the crucial capability of n-3PUFA at boosting the Treg levels in various tissues.

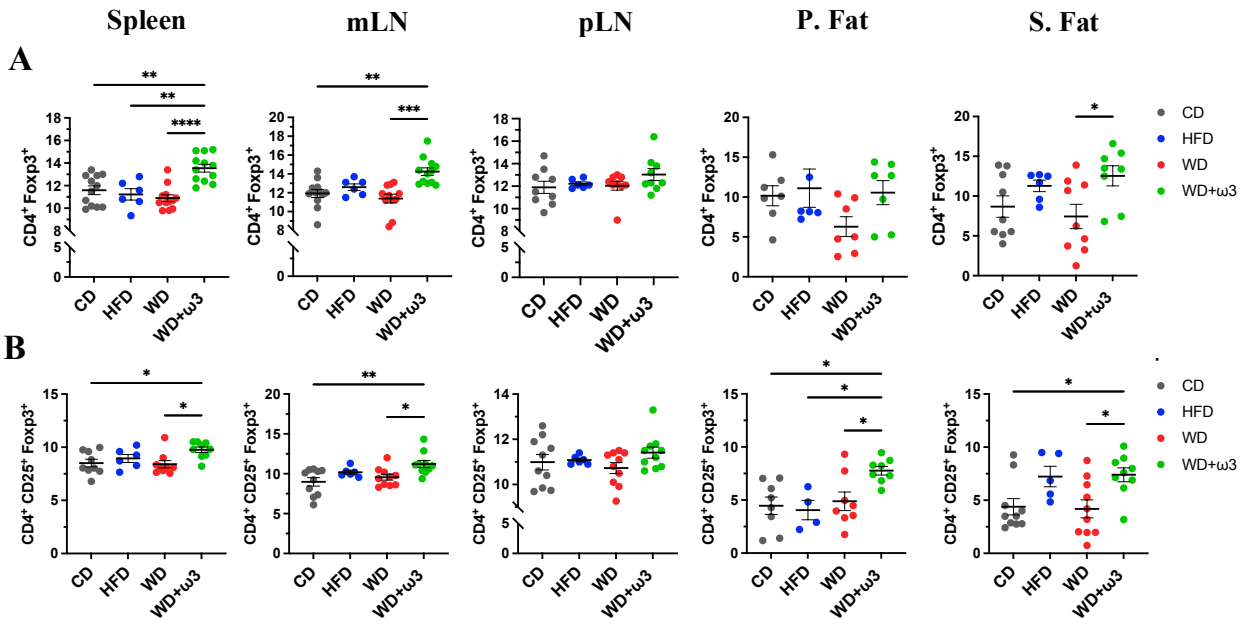


Figure 3.17) n-3PUFA supplementation boosts the $Foxp3^+$ $CD4^+$ Treg populations within SLOs and fat tissue
Quantification of flow cytometry data of **(A)** $Foxp3^+$ and **(B)** $CD25^+$ $Foxp3^+$ $CD4^+$ T cell frequencies within SLOs and fat tissues of mice groups fed on CD, HFD, WD and WD+ n-3PUFA diets. Each point represents an individual mouse in allocated diet groups (two *in vivo* experimental dataset with 6 mice per group pulled together, n=12 in total). One-way ANOVA with Tukey's correction; Data presented as mean ± SEM, *p<0.05; ** p<0.01, *** p<0.001.

Alongside conventional Foxp3^{+}CD4^{+} Tregs, we investigated CD8^{+} counterparts which are also known to express immunosuppressive and regulatory functions similar to CD4^{+} Tregs [409, 461, 462]. Consistently, we detected a very small population of Foxp3^{+} CD8^{+} Treg population [463] **(Figure 3.18)**. However, the WD+ω−3 group had a small but statistically significant rise in Foxp3^{+} CD8^{+} Treg frequencies in both spleen and mLN tissues compared to both HFD and CD control levels. Consistent with the literature although both obesogenic diets illustrated a reducing trend in Foxp3^{+} CD8^{+} Tregs in spleen, only HFD reached statistical significance compared to the CD group [464]. This suggests that n-3PUFA supplementation to the diet can also boost CD8^{+} Foxp3^{+} Treg frequencies even within a short-term of time.

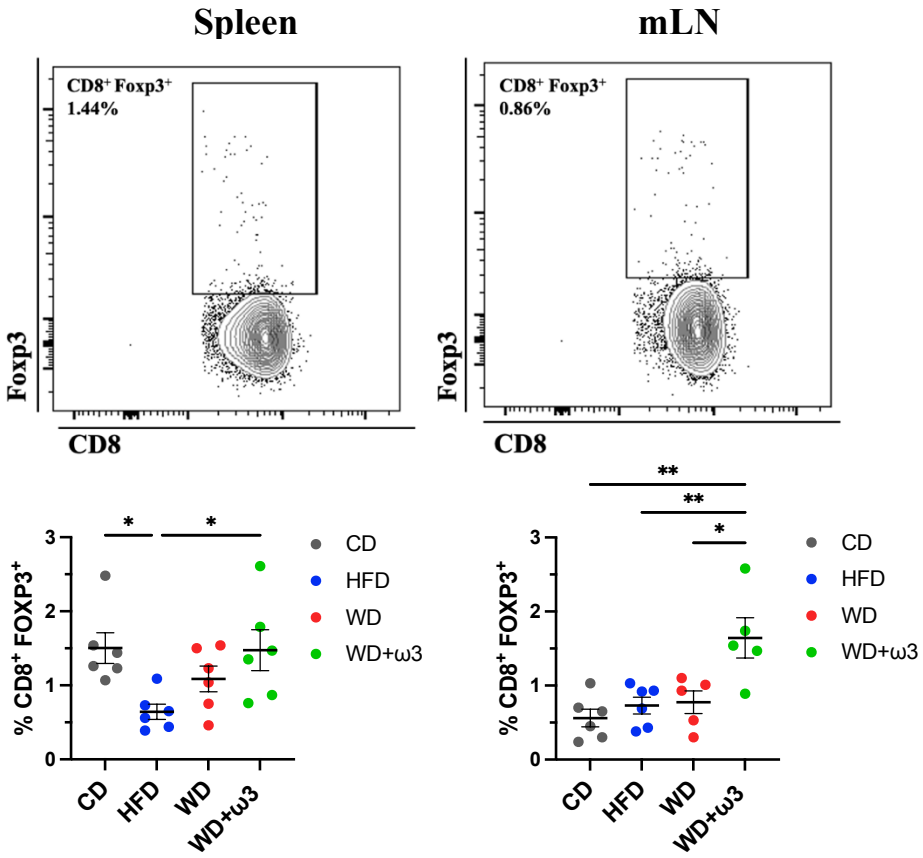


Figure 3.18 n-3PUFA supplementation into WD increases Foxp3^{+} CD8^{+} Treg populations within spleen and mLN tissues
(A) Representative flow figures of the key intracellular transcription marker of CD8^{+} Treg cell population; Foxp3 stained on spleen and mLN tissues of female C57BL/6J mice fed on CD control group, subjected to an allogeneic immunisation at d14. **(B)** Quantification of flow cytometry data of Foxp3^{+} CD8^{+} T cell frequencies within spleen and mLN tissues of mice groups fed on CD, HFD, WD and WD+ n-3PUFA diets. Each point represents an individual mouse in allocated diet groups (two *in vivo* experimental dataset with 6 mice per group pulled together, n=12 in total). One-way ANOVA with Tukey's correction; Data presented as mean ± SEM, *p<0.05; ** p<0.01.

3.9. Discussion

In this chapter, we have begun to phenotype our 3-week early-DIO murine model by characterising the main $CD4^+$ and $CD8^+$ T lymphocyte populations isolated from various fat and SLOs. Additionally, we have also investigated the systemic anti-inflammatory potential of n-3PUFA as dietary supplementation to the obesogenic WD. Following Cucchi et al. 2019, our study investigated the early pro-inflammatory immunomodulations on T cells induced by obesogenic diets and the potent anti-inflammatory impact of dietary n-3PUFA supplementation into the WD. Published as the first co-author in Biochemical Pharmacology (Camacho-Munoz et al., 2022) [127], our work demonstrated that 3-week obesogenic WD increases pro-inflammatory $CD4^+$ and $CD8^+$ T lymphocyte subsets, particularly pro-inflammatory EM subsets ($CXCR3^+$ and $LFA1^+$) and Th1/Th17 effector populations, across certain SLOs and adipose tissues. Notably, n-3PUFA supplementation counteracts this WD-induced pro-inflammatory trend by reducing EM populations in pLNs and dampening Th1/Th17 levels in spleen and pLNs. Most importantly, n-3PUFA supplementation was shown to have a crucial homeostatic effect by boosting the anti-inflammatory Treg cells in SLOs .

It was highly important to optimise the allogeneic immunisation and confirm polyclonal response induced by i.p injection of allogeneic splenocytes. Following the optimisation, two experimental repeats with a total of 12 mice per group confirmed that there was no significant difference in body weight, live cell percentage and bulk $CD4^+$ T lymphocyte populations among different diet groups. This alignment with literature increased our confidence in the specific observations made on distinct T cell populations. Notably, n-3PUFA supplementation significantly reduced total $CD8^+$ T cell frequencies across all SLOs and p.fat. This finding aligns with Xia et al. 2014 study, highlighting fish oil's anti-inflammatory, immunosuppressive effects on $CD8^+$ T cell activation and proliferation [452].

It is generally suggested that obesogenic diet induced immune microenvironment leads to a reduction in naïve T cells by potentially biasing their differentiation towards pro-inflammatory phenotypes in OIIM [18, 126, 465]. This negative association between obesity and the number of naïve T cells was also reported in human cohorts with obesity-linked diseases such CVDs [392, 466]. More recently, it was illustrated that lipids (cholesterol and palmitate) enriched in WD can directly reduce naïve $CD4^+$ T cells and impair the naïve cell response via disrupting glycolytic metabolism [466].

Consistent with the literature, WD was shown to significantly increase the CM ($CD44^+$,$CD62L^+$) $CD4^+$ T cell population within SLOs (**Figure 3.6**) [392]. This may be potentially due to the activated and augmented immunity which contributes to low-grade chronic inflammation in OIIM. However, differently from CD+ω−3 data observed by Cucchi et al. 2019, ω−3 supplementation to WD in our experiments significantly reduced the CM population in SLOs. It is well known that CM T cells are a good source of iTregs where in certain conditions $CD62L^+$ memory T cells gets converted to $Foxp3^+$ Tregs via changes in DNA methylation as shown in both human and murine T-cells [467]. Interestingly, n-3PUFA treatment can directly affect the DNA methylation status of blood leukocytes, pushing them towards an anti-inflammatory status [468-470]. Therefore, based on the mirror motifs between CM and $Foxp3^+$ Treg populations in SLOs of WD+ω−3 group within our experiments (**Figure 3.17**), n-3PUFA altered methylation status may be a key mechanism which leads to conversion of CM T cells to $Foxp3^+$ Treg populations.

Obesogenic diets and DIO are well shown to increase the Th1 $CD4^+$ T cell population as demonstrated in various DIO animal models and human cohorts [265, 301, 383, 453-455]. Specifically, obese adipose tissue shows elevated infiltration of Th1 $CD4^+$ T cells, significantly correlated with body-mass index [385, 453]. In murine models, deficiency of Th1 and IFNγ led to ameliorated OIIM and reduced pro-inflammatory adipose tissue macrophage accumulation [385, 388, 453]. Highlighting their significance, adoptive transfer of obese Th1 effector $CD4^+$ T cells into control mice exacerbated OIIM and obesity-linked pathologies [383, 388, 453]. Consistent with the literature, our 3-week early-DIO murine model illustrated a significant increase in pro-inflammatory Th1 effector $CD4^+$ T cell populations within SLOs tested (**Figure 3.9A**).

Importantly, literature has also demonstrated that n-3PUFA significantly suppresses the Th1 and Th17 pro-inflammatory subsets and associated cytokines- IFN-γ and IL-17, in both human and murine [325, 346, 471, 472]. Notably, dietary n-3PUFA supplementation is known to rebalance pro-inflammatory Th1/Th17 and anti-inflammatory Th2/Tregs ratios, particularly observed in Th1-mediated autoimmune diseases like RA [325, 473, 474]. Our data on early-DIO murine models, in **Figure 3.9**, aligned consistently with conventional literature within the spleen where WD-fed mice induced a significant increase followed by a significant reduction via n-3PUFA supplementation. However, no difference was observed in $ROR\gamma t^+$ Th17 subsets within LNs of different diet groups. Consistently, some publications also suggested no

difference in the percentage of Th17 and Th1 levels in the LNs with the n-3PUFA-supplemented diet groups [408, 475].

Furthermore, in humans, Th2 frequencies in the periphery are inversely correlated with OIIM and insulin resistance where, Th2 fate contributes to the differentiation of 'anti-inflammatory' M2 macrophages, inflammation resolution and reformation of homeostasis [385]. Although we did not detect a significant reduction in Th2 levels with obesogenic diets, there was a mirroring effect between pro-inflammatory Th1 and anti-inflammatory Th2 cell subsets (**Figure 3.9**). Also, despite there being not many publications on the effect of n-3PUFA on Th2 differentiation, we observed an increasing trend with n-3PUFA supplemented- especially compared to obesogenic HFD group.

Interestingly, **Figure 3.14** illustrated a lack of significant alteration in Tc1, Tc17 and Tc2 cytotoxic $CD8^+$ T cell phenotypes across different diet groups- diverging from our observations with $CD4^+$ T cells. Although there are not many publications on direct effect of obesity on specific $CD8^+$ cytotoxic T cell subset, it was suggested that IFNγ producing Tc1 $CD8^+$ T cell frequencies rise in DIO models [383]. However, we did not detect a significant increase in Tc1 $CD8^+$ T cells which could be potentially due to the 3-week course of the obesogenic diet.

Critically our study has a tailored experimental design and the timeframe for implementing obesogenic diets. Unlike the extended 10-20 week duration in typical literature models (with fully established DIO), our 3-week early-DIO model aimed to investigate early pro-inflammatory alterations in T-cells induced by distinct bioactive, immunomodulatory lipid groups prevalent in obesogenic diets [290, 382, 383]. Consistent with our data, Garidou et al. 2015 also reported an increase in Th1 and a reduction trend in Th17 populations of mice fed with an obesogenic diet for a short-term (30 days) [476, 477]. Although the exact reason for the discrepancies in the literature on the effector and cytotoxic T cell subsets (especially such as Th17) modulation by DIO is not fully understood, however it could arise from differential composition and the duration of obesogenic diets, resident microbiota and differences in animal models like age [477]. Another crucial factor that stays unnoticed is the lineage plasticity and the immunomodulatory effects of distinct bioactive, obesogenic diet-linked lipids on lineage plasticity which can 'bias' effector T cell frequencies towards pro- or anti-inflammatory fate. Specifically, Th17 and Treg cell lineage differentiation are shown to be highly variable based on microenvironmental influences such as cytokines and FAs, a subject explored further in **Chapter 4** [478, 479].

The most striking observation of our project was the anti-inflammatory effect of short-term n-3PUFA supplementation in an obesogenic diet which significantly increased Treg population frequencies in both $CD4^+$ and $CD8^+$ T lymphocytes. Following the Cucchi et al. 2019, publication on CD supplemented with n-3PUFA, our model has illustrated the direct effect and the high anti-inflammatory potential of n-3PUFA on WD-induced DIO murine model. The consistent elevation of $Foxp3^+$ and $CD25^+$ Treg populations that we observed in various SLOs and fat tissues has intrigued us to pursue this anti-inflammatory *in vivo* phenotype in more detail via utilising *in vitro* models. This phenotype and the potential mechanisms driving this anti-inflammatory modulation will be further investigated and discussed in **Chapter 4.**

Furthermore, our data on early-DIO-linked T cell exhaustion phenotype was also shown to be consistent with the previous publications - highlighting the effect of obesogenic diets on T cell exhaustion and immunosenescence in both $CD4^+$ and $CD8^+$ T lymphocytes [430, 433, 435, 480]. Although n-3PUFA supplementation was shown to have an ameliorate trend in $CD8^+$ T-cell exhaustion (**Figure 3.15**). Interestingly, we observed no observable effect of n3-PUFA supplementation into WD in terms of $CD4^+$ T cell exhaustion and senescence (**Figure 3.10**). Our data suggest that although n3-PUFA can alleviate OIIM via modulating T cell phenotypes, it does not have an ameliorative effect on the exhaustion and immunosenescence phenotype of $CD4^+$ T cells following DIO.

Furthermore, we noted a small yet significant rise in $CXCR5^+$,$PD1^+$ $CD4^+$ Tfh population within the WD group, which then reverted to control (CD) levels upon n-3PUFA supplementation into WD (**Figure 3.10**). Although Tfh is very limited in number and location wise, they are highly specialised T cell subsets which are well associated with various obesity-linked diseases such as RA [420-422]. Background literature on DIO and Tfh populations is extremely limited, with most available research focused on HFD-induced obesity [456]. Esteves de Oliveira et al. 2019, used a HFD group as a control in an obese asthma model, revealing that HFD alone did not elevate Tfh populations in spleen and mLN unless immune challenge was introduced. Consistent with Esteves de Oliveira et al. data, our DIO model with an allogeneic immune challenge shown to significantly increase the $CXCR5^+$, $PD1^+$ Tfh population.

There is no literature available on this distinct modulation of Tfh cells by n-3PUFA. However, considering that n-3PUFA can interfere with antigen presentation and modulate T:B cell interactions in follicular and marginal zones, it can be hypothesised that n-3PUFA can have potential immunomodulatory effects on Tfh populations. Nevertheless, further investigation is needed to validate this hypothesis.

Furthermore knowing the pro-inflammatory and pro-angiogenic effects of $CD8^+$ Tfh cells [428, 429], our study revealed a noteworthy rise in their frequencies within the WD group, which significantly decreased following n-3PUFA supplementation. Notably, the absence of STAT5 has been linked to elevated $CD8^+$ Tfh percentages in the spleen [481, 482]. In contrast, a STAT4-knockout model fed on a cholesterol-dense obesogenic diet, reported a significant reduction in Tfh populations and a significant increase in $CD8^+$ Treg populations [428]. Similarly, various STAT4-knockout DIO murine models, while exhibiting no weight variation, demonstrated significant reductions in obesity-triggered insulin resistance and adipose inflammation, linked to decreased pro-inflammatory T cells and inflammatory cytokines [483, 484]. It becomes crucial here to highlight that n-3PUFA was shown to inhibit STAT4 expression via modulating mTOR signalling pathway leading to suppression Th1 differentiation [325, 485]. Based on this critical background and our phenotype observed in this 3-week DIO model, it can be hypothesised that n-3PUFA can potentially inhibit STAT4 expression via modulating mTOR signalling pathway leading to the observed decrease in $CD8^+$ Tfh cell frequencies and increase in $CD8^+$ Tregs.

Furthermore, although the group fed with HFD for 3-week has shown to induce an increasing trend in various pro-inflammatory markers and EM T cell fates in general this increasing trend was never reached the statistical significancy in the tissues tested. Similar trends observed in the HFD group, suggests a pro-inflammatory effect as previously shown by the literature. However, the delayed pro-inflammatory effect compared to the WD group aligns with literature findings, where WD induces obesity and comorbidities more swiftly in murine models than HFD [44, 45]. Given these observations, we chose not to further explore the 3-week HFD effect and omitted this group from the second *in vivo* experimental repeat

Chapter 4) Bioactive C24 biases Foxp3$^+$ Treg differentiation towards pro-inflammatory RORγt$^+$ Th17 fate in both *in vivo* and *in vitro* models

4.1. Introduction

After phenotyping the main T lymphocyte subsets of the 3-week WD-fed early-DIO murine model and the ameliorative effect of n-3PUFA in **Chapter 3**, we aimed to identify key changes within the WD driving the pro-inflammatory phenotype. Based on the prominent alterations within immune phenotypes of different diet-fed groups, we wanted to dissect the immunomodulatory link between bioactive lipid groups and DIO-linked pro-inflammatory modulations on T lymphocytes.

4.1.1 The delicate balance between Treg/Th17 CD4$^+$ T cell differentiation

Chapter 1 detailed Treg and Th17 differentiation being driven by lineage-defining TFs: Foxp3 and RORγt. These lineage-defining TFs are activated by cytokines in the extracellular microenvironment and cellular metabolism [227, 486]. For instance, Foxp3$^+$ Treg differentiation relies on TGF-β and IL-2, while RORγt$^+$ Th17 requires TGF-β and IL-6 [227, 486, 487]. Interestingly, in addition to the cytokine TGF-β being commonly required for Treg and Th17 differentiation, these subtypes also share PI3K/AKT, AMPK and mTOR signalling pathways [227, 486, 487]. However, one key difference is STAT3 activation by IL-6, IL-21, and IL-23, inducing RORγt in Th17 cells. Contrastingly, Treg differentiation lacks STAT3, activating Foxp3 via smad3 and/or STAT5 [227, 486, 487]. More detail of this differing mechanism can be found in **Figure 4.1**.

Mechanistically in Th17 cells, mild TCR and CD28 activation triggers PI3K/AKT signalling pathway. This pathway in turn activates mTOR and hypoxia-induced factor 1α (HIF-1α) leading to further activation of RORγt and a switch to glycolysis [227, 486, 487]. The activation of mTOR and HIF-1α has shown to be a critical pathway in inducing Th17-linked gene expression and Th17 phenotype. Conversely, Treg differentiation involves strong TCR activation without pro-inflammatory cytokines (IL-6, IL-21, IL-23), recruiting AMPK to inhibit mTOR and HIF-1α, favouring Foxp3 expression [486].

Considering the homology between the differentiation processes, it is not surprising that Treg and Th17 cells can regulate each other's differentiation. For example, Treg-linked Foxp3 and smad3 can inhibit Th17 differentiation by inhibiting RORγt binding to DNA [486]. On the other hand, Th17-linked mTOR-induced HIF-1α can directly activate the RORγt alongside inhibiting the Treg differentiation by targeting Foxp3 (via ubiquitination and proteasomal degradation) [488-490]. Furthermore, other T effector lineage-associated cytokines and TFs are also known to regulate Treg/Th17 differentiation like Th1-linked IFN-γ promotes Th17 whereas, Th2-linked IL-4 cytokine inhibits Th17 and promotes Treg differentiation [257, 486].

Additionally, lipid biosynthesis and metabolism are known to play critical roles in regulating the differentiation Treg/Th17 balance [491, 492]. Importantly, exacerbated *de novo* FA synthesis and surplus of distinct bioactive lipids are shown to alter Treg/Th17 differentiation in obesity and autoimmune diseases [302, 486, 493]. Interestingly, Bai et al. 2014, reported a novel pathway involving CD39 (ENTPD1) and CD161 activating the ASM-induced ceramide synthesis which activates the Th17 lineage-defining STAT3 and mTOR signalling pathways in Th17-driven Crohn's disease [494]. Particularly, ceramides have been identified as central 'lipid messenger' in mediating Th17 expansion via directly activating mTOR/STAT3 signalling pathway [494-496]. Not only has inhibition of ceramide synthesis been shown to downregulate the Th1 and Th17 pro-inflammatory differentiation *in vitro* [494-496], but this inhibition is also used for the treatment of various Th17-driven inflammatory diseases such as colitis [497, 498] and lung inflammation [499].

Based on the literature, the balance between Treg/Th17 differentiation is highly fragile and susceptible to the immunomodulations from the bioactive lipids available in the cellular microenvironment. Importantly, this potential for immunomodulation is exploited in obesity and OIIM favouring a Th17 bias [288, 290, 291]. Differentiation of this Th17 phenotype is not only important for establishing the OIIM in adipose tissues, but also contributing to other obesity-associated pathologies such as T2D, autoimmune diseases, MS and CVDs [288, 290, 291, 500].

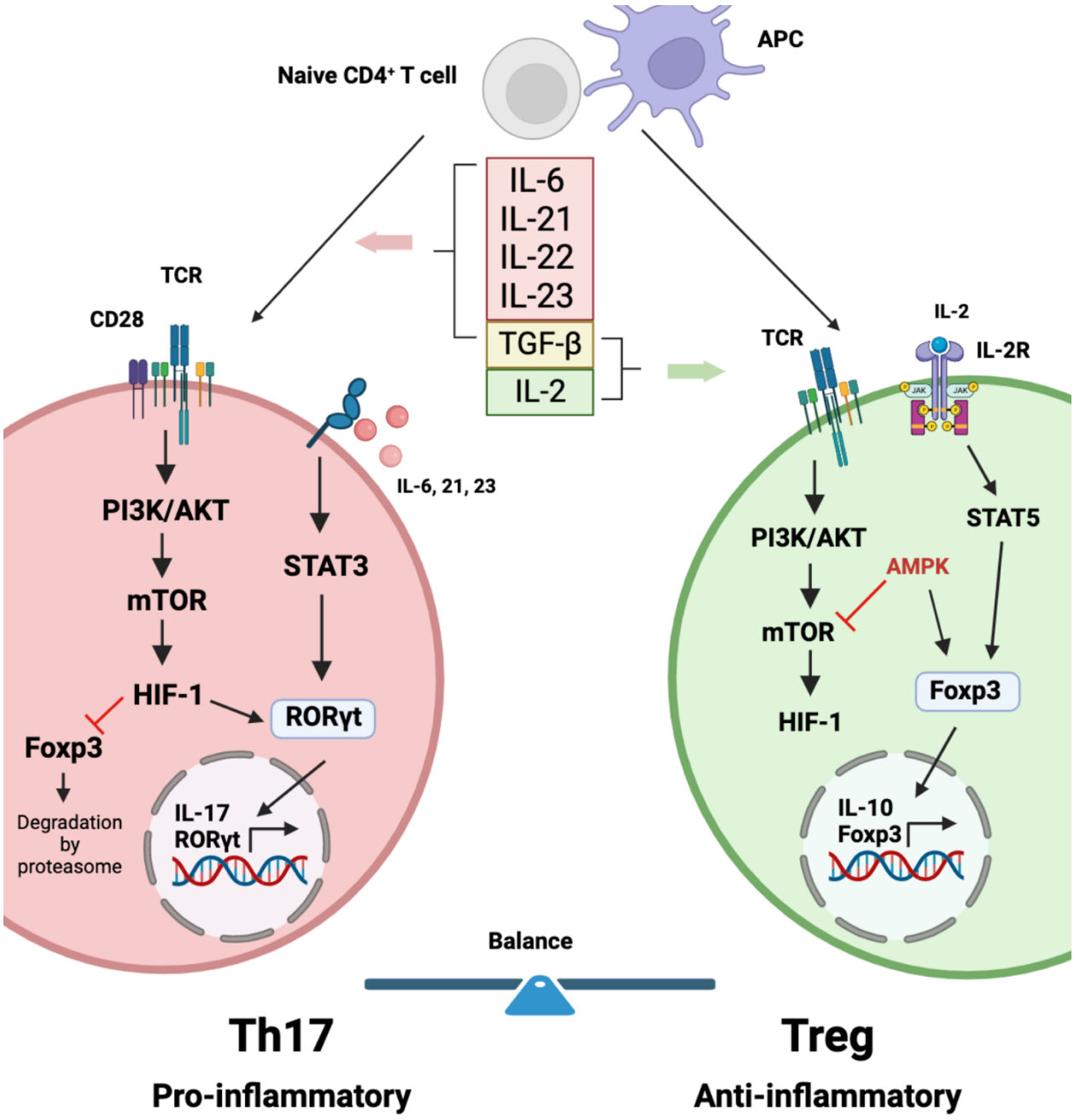


Figure 4.1) Representation of the classical molecular pathways regulating the fragile balance of Th17 and Treg differentiation.

Differentiation of naïve $CD4^+$ T cells towards other effector T cell fates such as Th17 or Treg is regulated by cytokines and cellular metabolism that activates certain critical signalling pathways. **(A)** Th17 differentiation induced by mild T cell activation and pro-inflammatory cytokines (IL-6, IL-21 and IL-23). The ligation of these pro-inflammatory cytokines to their respective receptors activates STAT3. This activation induces the expression of RORγt and IL-17 polarising the cell towards Th17 fate. Additionally, this mild activation of TCR and co-stimulatory molecules induces the activation of the PI3K/AKT pathway which stimulates mTOR and HIF-1α . Activation of HIF-1α directly activates RORγt and other Th17-linked gene expressions while inhibiting the Foxp3 expression. **(B)** On the other hand, a similar but backwards mechanism is used for the $Foxp3^+$ Treg differentiation. A strong TCR and co-stimulatory activation coupled with IL-2 direct binding enhances the Treg-inducing STAT5

activation. As the Foxp3 activity is indispensable for the Treg differentiation, AMP-activated protein kinase (AMPK) and other Treg-linked TFs are known to inhibit the expression of critical Th17-linked TFs including HIF-1α, STAT3 and RORγt. Adapted from Zhang et al. 2021 [486]

4.1.2 Pro-inflammatory immunomodulatory potentials of ceramides on $CD4^+$ T cells

As discussed in **Chapter 1**, ceramides can modulate immune cell functions such as the motility/homing, activation of antigen recognition receptors and the effector phenotype differentiation of $CD4^+$ T cells both *in vivo* and *in vitro* [359, 365, 366, 368]. These bioactive ceramides were shown to induce the production of pro-inflammatory cytokines like IL-1β, TNF-α, IL-6, and IL-17, both in vivo and in vitro, ultimately influencing $CD4^+$ T cell frequencies and functions as well [357-359]. Various bioactive ceramides such as C16 have been shown to induce pro-inflammatory Th1 and Th17 differentiation at distinct concentrations whereas, other ceramides such as C6 induce Treg differentiation at specific concentrations [351, 367, 368, 501].

The literature highlights the discrepancies in the immunomodulatory effects of bioactive ceramides on $CD4^+$ T cells where the distinct bioactive ceramides can express different functions depending on their concentration and the microenvironment. Kue et al., 2012 & 2013 illustrated this discrepancy by demonstrating that the bioactive C6 can induce both Th1 and Treg differentiation under different conditions via stabilising master transcription factors; T-bet and Foxp3, respectively [372, 501]. The C6 ceremide was shown to induce Treg differentiation at high concentrations (5-10μM) in combination with TGF-β cytokine. Whereas lower doses of C6 (1-2.5uM) were shown to bias the $CD4^+$ T cell differentiation towards IFNg-producing Th1 phenotype alongside IL-12 [372, 501]. Additionally, Zhou et al. 2016 also reported a negative association between C6 and Treg differentiation [357]. Despite inconsistent findings, these examples underscore C6's direct impact on $CD4^+$ T cell differentiation *in vitro*.

Kue et al., 2023 & 2013 also investigated the immunomodulatory effects of the highly soluble, short-chain ceramide: C2. Their investigations reported that C2 ceramide itself did not significantly alter $CD4^+$ T cell differentiation [372, 501], despite being reported to inhibit antigen presentation in DCs [502]. High solubility and no known effect on $CD4^+$ T cells made the C2 a logical negative control group in various *in vitro* models [372, 501]. Considering the

background literature, we utilised the C6 and C2 as potential positive and negative controls for our *in vitro* $CD4^+$ T cell differentiation assay.

Ceramide-induced pro-inflammatory immunomodulation has been demonstrated to contribute to various diseases associated with ceramide accumulation. For examples this can be seen in obesity-associated diseases such as colitis, Alzheimer diseases, Parkinson's diseases, diabetes, CVDs [359, 367, 368]. In the context of obesity itself, there is evidence of elevated CerS6 mRNA expression and increased C16 ceramide concentrations in obese human adipose tissue [186]. Furthermore, CerS6 knockout mice models experienced alleviated weight gain due to obesogenic diets and ameliorated glucose intolerance [186]. While the connection between ceramide accumulation in obesity and its immunomodulatory effects is established, the precise contribution of specific ceramides to the OIIM is not yet fully elucidated.

4.1.3 Aims and hypotheses

Following **Chapter 3** early-DIO murine model immune phenotype this chapter aims to investigate the following hypotheses and questions:

- Characterise the lipidomic profiles of different diet groups to identify the critical bioactive lipid groups with the ability to modulate the phenotype of obese $CD4^+$ T cells towards a pro-inflammatory state.
- To identify the immunomodulatory capability of candidate bioactive lipids on pro-inflammatory immunomodulation observed during the establishment of early-DIO OIIM
- Based on the alterations observed in Treg/Th17 $CD4^+$ T cell frequencies in WD fed *in vivo* model, we hypothesised that distinct candidate bioactive ceramides can influence $CD4^+$ T cell differentiation, favouring a pro-inflammatory Th17 differentiation
- Validation of the hypothesis between candidate lipid groups and $CD4^+$ T cell Treg fate by utilising both *in vitro* and *in vivo* models
- Investigating the molecular mechanism underpinning the pro-inflammatory Th17/Treg immunomodulation of bioactive C24 on $CD4^+$ T cell

Results

4.2. N-3PUFA supplementation to diet reduces the WD-induced ceramide synthesis and concentration in 3-week early DIO murine model

As published our collaboration with Nicolaou's group (UoM) demonstrated the effect of n-3PUFA supplementation on the lipidomics profile of various SLOs and fat tissues [126]. This research, utilised a wide-range lipidomics analysis where eicosanoids, docosanoids, octadecanoids, endocannabinoids, sphingolipids and ceramides were investigated between CD and CD+n-3PUFA murine groups. Following the Cucchi et al. 2020 observations on specific ceramides, we sought to investigate potential modulations in ceramide species and concentrations following the WD and WD+n3PUFA diets as previously stated in **Chapter 3**. Although different sphingolipid and ceramide species were detected throughout all the tissues tested, the most abundant concentrations were detected in perigonadal, subcutaneous fat tissues and plasma (systemic) as expected based on the literature [126, 127, 503]. Considering the preliminary data, we investigated the specific ceramide species in the most abundant tissues.

Ceramide nomenclature was investigated based on the classification system reported by Masukawa et al. 2008 where CER [NS] represents ceramide groups with a non-hydroxy fatty acid [N] and a sphingosine [S] base, CER[NDS] is a ceramide with a non-hydroxy fatty acid [N] and a dihydro-sphingosine base [DS] and same ceramide groups starting with [A] represents the α-hydroxy fatty acid linked sphingolipids (**Figure 4.2A**) [504, 505]. Additionally, we have also investigated an important metabolite of ceramides (phosphorylated ceramides), ceramide-1-phosphate (C1P) which is shown to be an important mediator of inflammatory response [506, 507].

Figure 4.2B shows the heatmap of all the ceramide species tested within the perigonadal, subcutaneous fat tissues and systemic plasma obtained from female C57BL/6J WT mice fed on CD, WD and WD+n3-PUFA groups. All ceramides were further differentiated based on their acyl chain and sphingoid base carbon numbers which are shown in the brackets e.g. N(24)S(18) (**Figure 4.2B**). Consistent with the literature, ceramides were most abundantly found in systemic plasma ranging between 40000-500ng/ml. Consistent with the literature the quantification of the distinct ceramide species strikingly illustrated that CER[NS] was the most abundant ceramide species in all three tissues tested [126, 127, 503]. Importantly, CER[NS] species were suggested to be critical secondary metabolic messengers in various signalling pathways regulating lipid and glucose homeostasis, mitochondrial plasticity, and inflammatory

actions [508-510]. Distinct bioactive CER[NS] species have been also suggested as potential predictive biomarkers for various obesity-linked diseases such as CVDs and diabetes due to their critical modulatory [508-510].

A

Fatty acid / Sphingoid	Non-hydroxy fatty acid [N]	α-hydroxy fatty acid [A]
Dihydrosphingosine [DS]	CER[NDS]	CER[ADS]
Sphingosine [S]	CER[NS]	CER[AS]
Phytosphingosine [P]	CER[NP]	CER[AP]

B

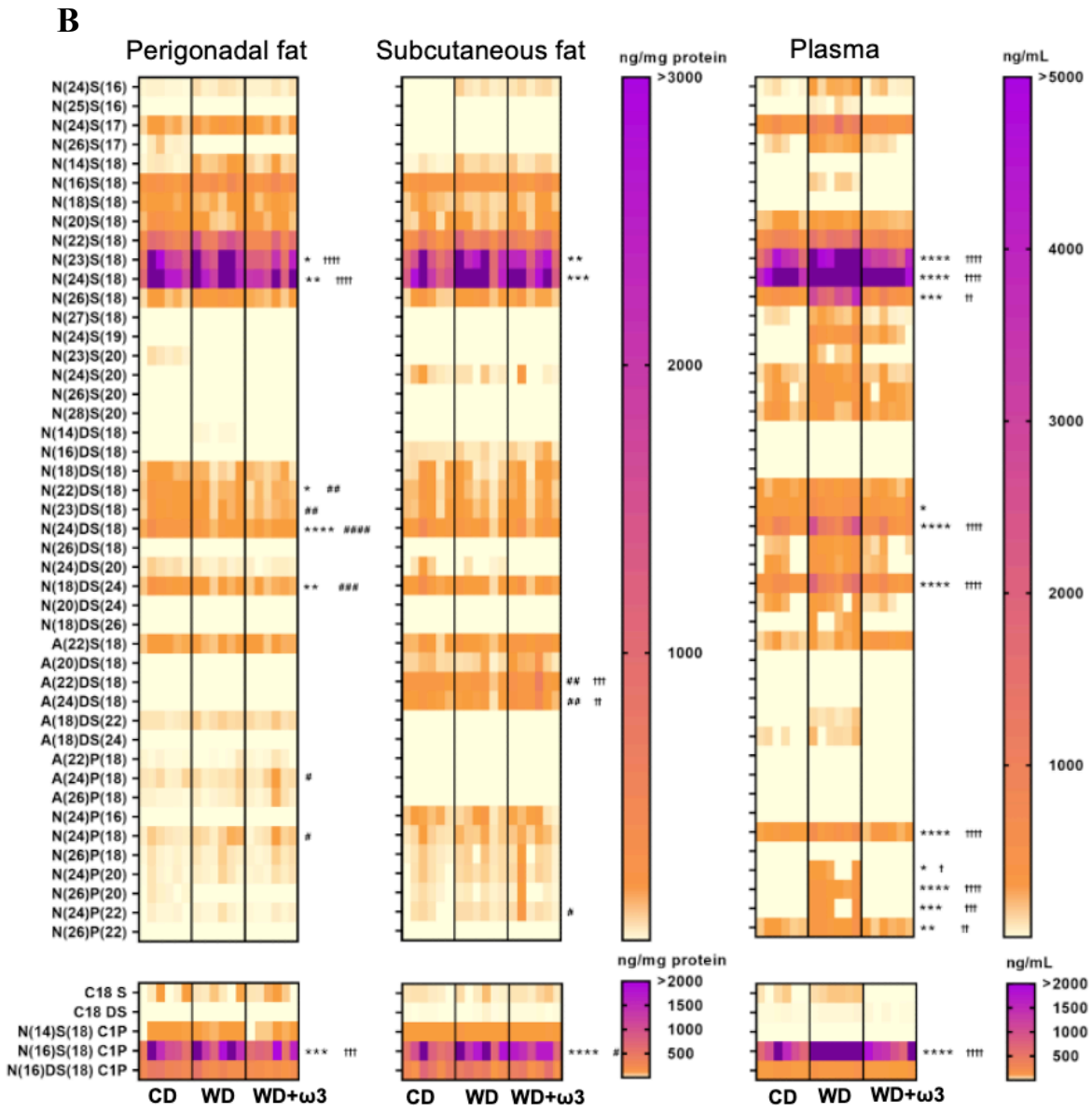


Figure 4.2) n-3PUFA supplementation attenuate the WD-induced elevation thein pro-inflammatory associated ceramides

(A) The main ceramide nomenclature classification system reported by Masukawa et al. 2008[504] **(B)** Heatmap representation of the ceramides, sphingoid bases, phosphorylated ceramides found in fat tissues and plasma including distinct ceramide species. All tissues were obtained from female C57BL/6J mice fed on CD, WD and WD+ n-3PUFA (5% menhaden oil). (n = 6 mice per diet group). Data are expressed as ng/mg protein in solid tissues and ng/ml in plasma. *p < 0.05, **p < 0.01, ***p < 0.001, ****p<0.0001 comparing CD vs WD; #p<0.05,##p<0.01, ###p<0.001, ####p<0.0001 comparing CD vs WD+ω3; †p<0.05, †† p<0.01, ††† p<0.001, †††† p<0.0001 comparing WD vs WD + ω3 (one-way ANOVA; uncorrected Fisher's LSD). *Lipidomics experiments and analysis were carried out by Dr Dolores Camocho-Munoz with the supervision of Prof Anna Nicolaou (University of Manchester)*.

WD group illustrated an increasing trend and contrarily n-3PUFA+WD group illustrated a downward trend in both total ceramide levels and the most abundant CER[NS] species within all three tissues tested (**Figure 4.3A**). The majority of ceramides affected were derivatives of C18 sphingosine, with acyl-chain lengths spanning from C14 to C28 were shown to be significantly elevated with the WD (**Figure 4.2B & 4.3A**). Importantly, C23 and C24 (N(24)S(18)) concentrations were significantly elevated with WD in both adipose tissues and plasma compared to the CD control group. On the contrary, the WD+n-3PUFA group attenuated this increasing effect of WD and significantly reduced C23 and C24 levels in plasma and perigonadal fat but not in subcutaneous fat (**Figure 4.3B**).

Importantly, these long-chain ceramides are generally associated with cellular dysfunction, ROS production, mitochondrial damage, autophagy and inflammation [137, 175]. Finally, it is also worth noting that C26 ceramide illustrated a significant rise with WD as well as a significant attenuation with n-3PUFA supplementation however, these trends were only observed in plasma in a much lower magnitude compared to C23 and C24 (**Figure 4.3B**). Pro-inflammatory N(16)S(18) C1P also illustrated the same trends with the WD and WD+n3-PUFA groups in all three tissues tested (**Figure 4.2B**).

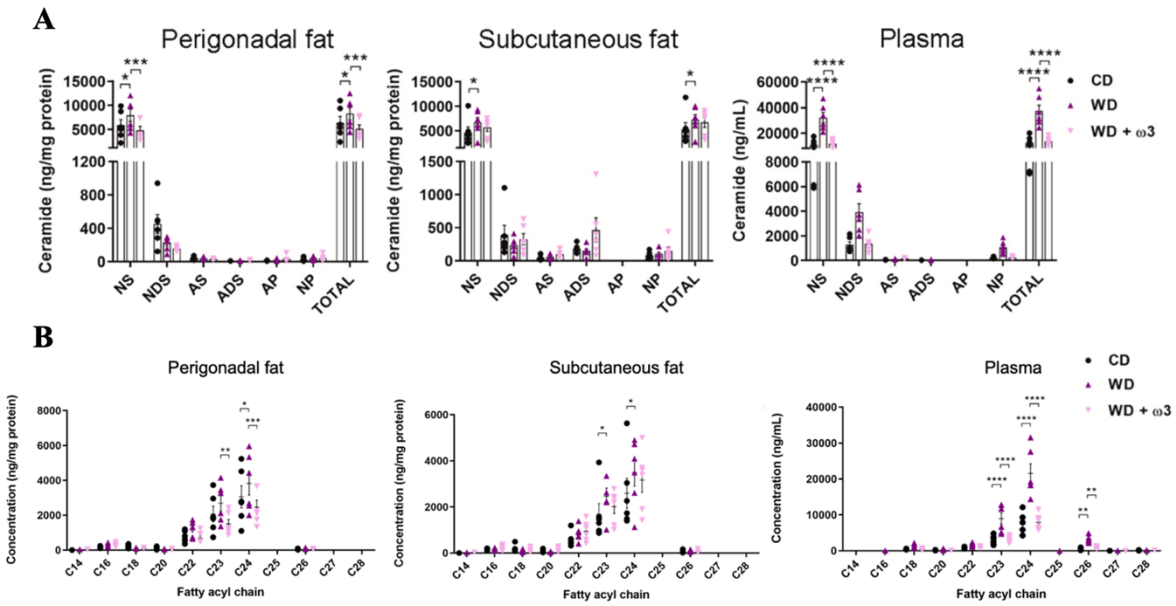


Figure 4.3) Effect of WD and n-3PUFA+WD diets on distinct ceramide species detected in fat tissues and plasma

Quantification of ultrahigh performance liquid chromatography tandem mass spectrometry lipidomics data illustrating the **(A)** total ceramide levels and **(B)** individual CER[NS] species as detected within the fat tissues and plasma obtained from female C57BL/6J mice fed on CD, WD and WD+ n-3PUFA (5% menhaden oil). (n= 6 mice per diet group). The values denote mean ± SEM (A-C). Data is expressed as ng/mg protein in solid tissues and ng/ml in plasma; *$p < 0.05$, **$p < 0.01$, ***$p < 0.001$, **** $p < 0.0001$ (one-way ANOVA; uncorrected Fisher's LSD). †*Lipidomics experiments and analysis were carried out by Dr Dolores Camocho-Munoz with the supervision of Prof Anna Nicolaou (University of Manchester)*.

It should be noted that all the lipidomics experiments and analyses were carried out by Dr Dolores Camacho-Munoz at the University of Manchester with the supervision and guidance of Professor Anna Nicolaou, a lab that specialises in mass spectrometry lipidomics and lipids biology.

4.3. Pharmacological inhibition of CerS2 reduced the C24 synthesis without alleviating the WD-induced effector memory phenotype

As demonstrated in **Chapter 3**, we have characterised the main $CD4^+$ and $CD8^+$ T cell populations in our 3-week early-DIO murine model. Lipidomic analysis in **Section 4.2**, has identified bioactive lipid counterparts altered within the early-DIO pro-inflammatory phenotype. Based on the most profound changes detected in bioactive C24, it was selected as a promising candidate. Considering the background literature on the critical immunomodulatory actions of distinct long-chain bioactive ceramides, we have hypothesised that C24 can directly induce various pro-inflammatory alterations on $CD4^+$ T cell effector fate. To investigate this

potential mechanism further and validate the role of C24, we attempted to inhibit the main C24 synthesising enzyme CerS2.

In line with our previous 3-week (21-day) early DIO *in vivo* murine model, we have fed both groups of wild-type (WT) C57BL/6J female mice with WD for 21 days where, one group was given ceramide synthase inhibitor FTY720 (1mg/kg) via 3 i.p injections on day 11, 16 and 18. Animals were given allogeneic immunisation of WT Balb/C and CBA male splenocytes on day 14. Experimental timeline detailed in **Figure 4.4A**.

To confirm the reduction of long-chain ceramides due to the inhibition of CerS2 via FTY720, we analysed total and specific ceramide levels in the plasma. **Figure 4.4B** illustrated a significant reduction in total plasma ceramide concentration within the FTY720 group compared to the PBS-injected WD-fed control group. Importantly, the FTY720 inhibited the synthesis of long-chain ceramide species including C22, C23 and C24, synthesised by CerS2 enzyme (**Figure 4.4C**) [1, 350]. However, FTY720 also significantly reduced C16, C18, C22 and C23 levels in plasma, suggesting potential non-specific, off-target effects on other enzymes such as CerS1 which was also suggested by the literature [139, 156, 157] (**Figure 4.4C**).

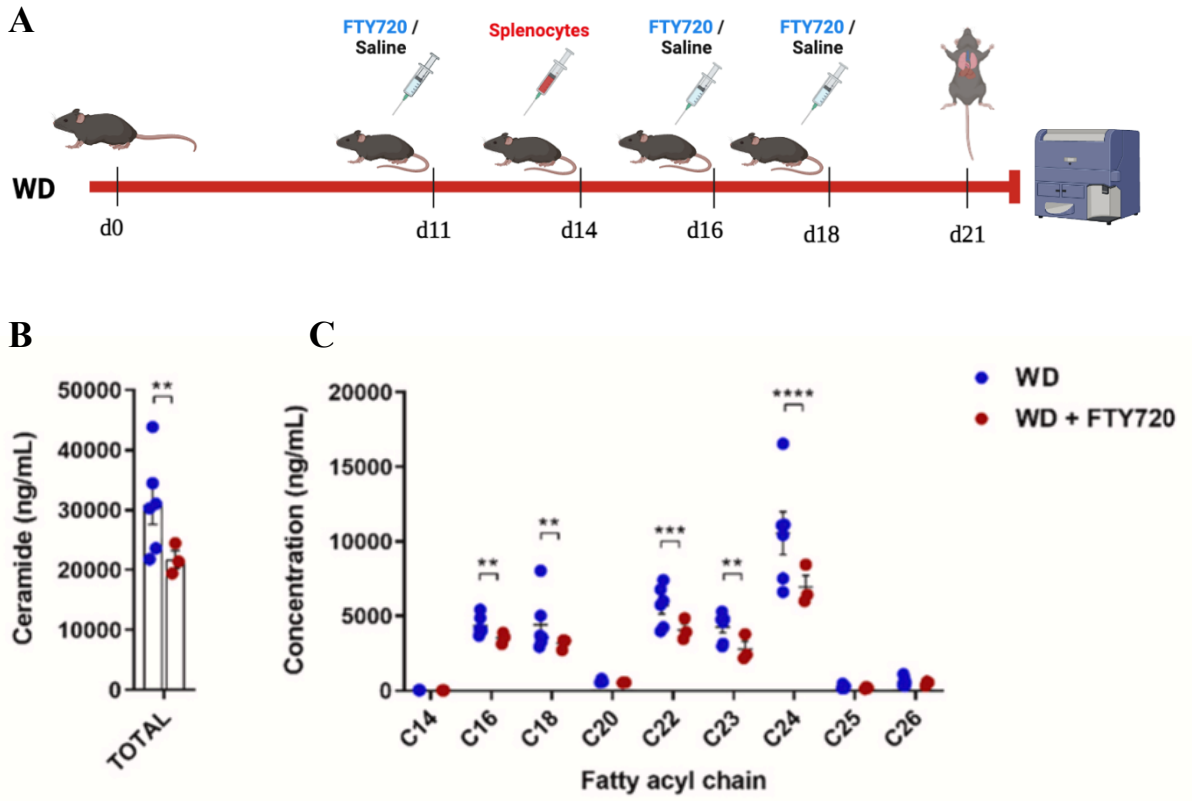


Figure 4.4) The ceramide synthase 2 (CerS2) inhibitor FTY720 reduces plasma ceramide concentration in plasma

(A) Representative schematic of the experimental procedure and the timeline. Quantification of ultrahigh performance liquid chromatography tandem mass spectrometry lipidomics data illustrating the **(B)** total ceramide levels and **(C)** individual CER[NS] species within plasma of female C57BL/6J mice (n = 6) fed western diet (WD) for 21 days and were subjected to an allogenic immunization via intraperitoneal injections at day 14. Inhibition group mice were given intraperitoneal injections of FTY720 (1 mg/ kg) or vehicle control three times (days 11, 14 and 18) (WD + FTY720). Ceramide data expressed as ng/ml in plasma, mean ± SEM; $^{**}p < 0.01$, $^{***}p < 0.001$, $^{****}p < 0.0001$ (one-way ANOVA; uncorrected Fisher's LSD).

Next, we sought to compare the effect of CerS2 inhibition specifically on T lymphocytes following 3 weeks of WD. Similar to 3-week early DIO *in vivo* experiment, we examined the total $CD4^+$ and $CD8^+$ T lymphocytes within the SLOs and fat tissues isolated. **Figure 4.5A** illustrated no significant difference in live cells between vehicle control and FTY720-inhibitor in all tissues except spleen. Splenocytes isolated from the FTY720 group illustrated a small (~3%) but statistically significant reduction (**Figure 4.5A**).

Consistent with the background literature FTY720-treatment statistically significantly reduced $CD4^+$ T cells within spleen and pLNs (**Figure 4.5B**) [156, 159, 160]. A reduction trend was also conserved in mLNs, p.fat and s.fat, however this did not reach statistical significance (**Figure 4.5B**). Similarly, the total $CD8^+$ T cell population percentage in the spleen was also significantly reduced with FTY720 treatment (**Figure 4.5C**). Furthermore, there was no observable trend in the rest of the tissues including pLNs, mLNs, p.fat and s.fat tissues between the control and inhibitor groups (**Figure 4.5C**).

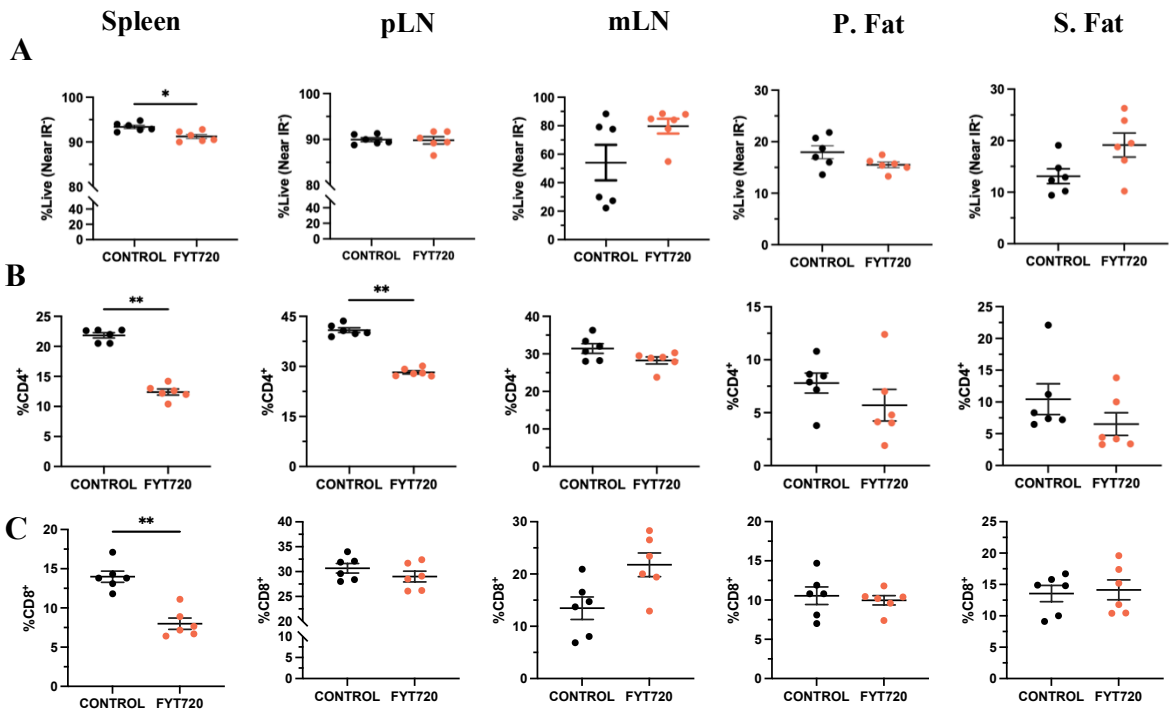


Figure 4.5) Effect FTY720 inhibitor on total live CD4$^+$ and CD8$^+$ T cell populations within SLOs and fat tissues

(A) Quantification of total live lymphocyte **(B)** total CD4$^+$ T lymphocytes and **(C)** total CD8$^+$ T lymphocytes as percentage isolated from SLOs (spleen, mLNs, pLNs) and fat tissues (p.fat and s.fat) tissues of female C57BL/6J mice fed on WD for 21 days. FTY720 inhibitor group mice were given intraperitoneal injections of FTY720 (1 mg/ kg) three times (days 11, 14 and 18) (WD + FTY720) and vehicle control group received 3 PBS injections on respective time points. Both murine groups were also subjected to an allogenic immunization via intraperitoneal injections at day 14. Each point represents an individual mouse in allocated diet groups (n=6). One-way ANOVA with Tukey's correction; Data presented as mean ± SEM, *p<0.05; ** p<0.01.

Consequently, we investigated any potential ameliorative effect of C24 inhibition on the WD-induced pro-inflammatory EM CD4$^+$ T cell phenotype as detected in **Figure 3.6**. Interestingly, the FTY720-inhibitor group illustrated a significant reduction in naïve CD4$^+$ T cells (CD44$^-$,CD62L$^+$) alongside a concomitant increase in EM (CD44$^+$,CD62L$^-$) populations within the spleen tissue compared to the PBS-injected control group (**Figure 4.6C**). Similarly, the inhibitor group illustrated a reduction trend in naïve CD4$^+$ T cell populations with a significant upregulation EM populations within the pLN and p.fat tissues compared to the control group. Furthermore, there was no significant trends observed in the CM populations and other tissues tested (**Figure 4.6C**).

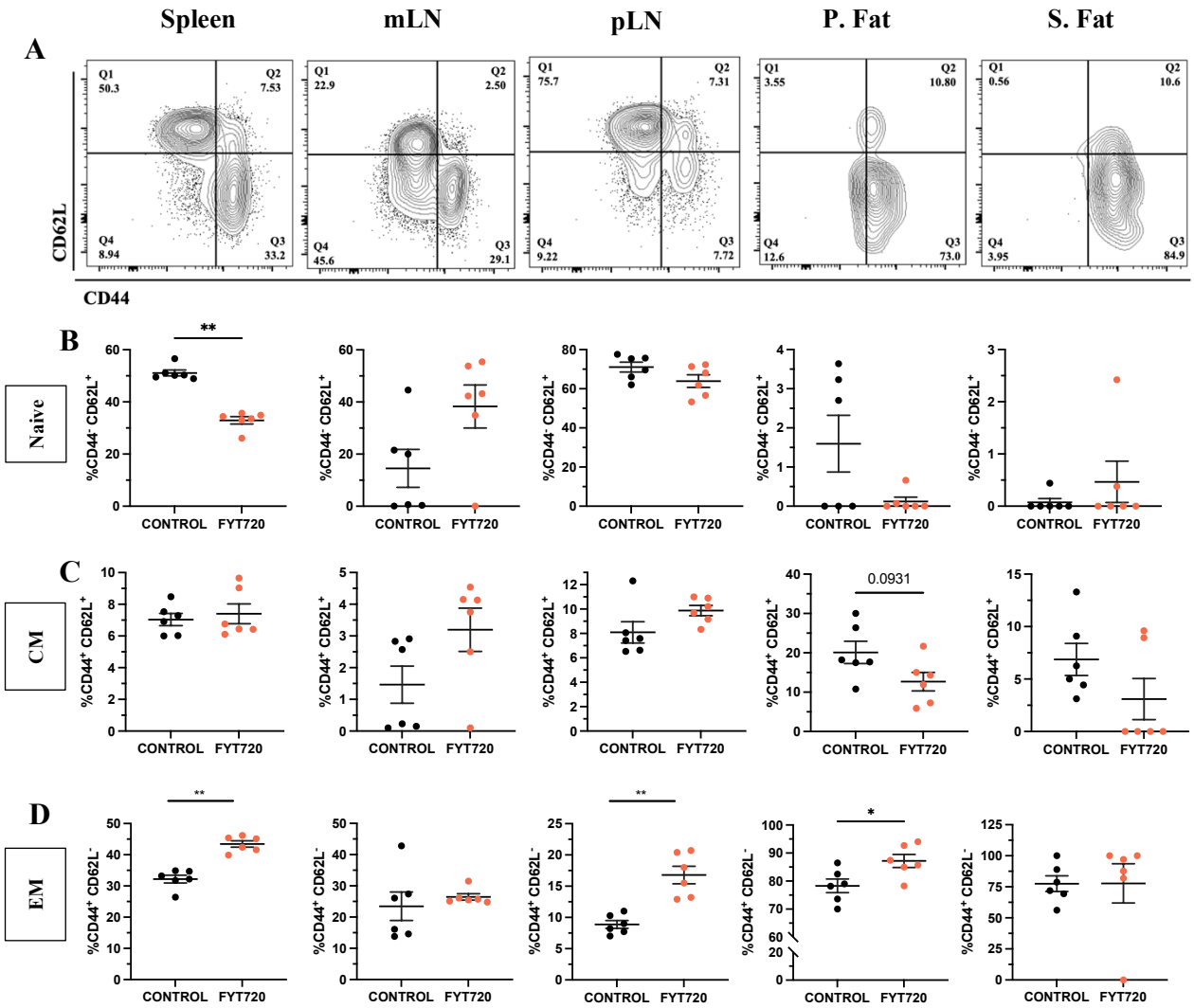


Figure 4.6) Pharmacological inhibition of CerS2 via FTY720 did not attenuate the WD-induced distribution of memory CD4$^+$ T cell subsets

(A) Representative flow cytometry plots of CD44 and CD62L extracellular staining on CD4$^+$ T cells isolated from SLOs and fat tissues of female C57BL/6J mice fed on WD for 21 days and were given intraperitoneal injections of FTY720 (1 mg/ kg) three times (days 11, 14 and 18) (WD+FTY720) or three times PBS injections on respective time points (v.control). Both murine groups were also subjected to an allogenic immunization via intraperitoneal injections at day 14. Quantification of flow cytometry data on **(B)** naïve (CD44$^-$ and CD62L$^+$), **(C)** CM (CD44$^+$ and CD62L$^+$) and **(D)** EM (CD44$^+$ and CD62L$^-$) CD4$^+$ T cell populations within three different SLOs and fat tissues obtained from both groups. Each point represents an individual mouse in allocated diet groups (n=6). One-way ANOVA with Tukey's correction; Data presented as mean ± SEM, *p<0.05; ** p<0.01.

Similar to CD4$^+$ T cell dataset, FTY720 group illustrated an reducing trend in naïve with a concomitant increase in EM CD8$^+$ T cell groups within the spleen and pLN tissues compared to control group. However, no other observable trend was recorded within the other tissues and CD8$^+$ T cell subsets tested (**Supplementary-Figure 1**).

Furthermore, we further investigated the distinct pro-inflammatory functional effector memory T cell markers such as LFA-1 and CXCR3 considering their associations observed with the WD and their pivotal roles in OIIM as detailed in **Chapter 3**. Interestingly, FTY720-inhibitor group did not attenuate the WD-driven increase in LFA-1$^+$,CD44$^+$ CD4$^+$ T cell populations in both SLOs and fat tissues tested. Contrarily, FTY720-inhibitor group significantly elevated the LFA-1$^+$,CD44$^+$ CD4$^+$ T cell populations within the spleen, pLN and p.fat tissues compared PBS-injected control group (**Figure 4.7A**). Similarly, FTY720-inhibitor group illustrated no ameliorative effect on the CXCR3$^+$,CD44$^+$ CD4$^+$ T cell frequencies compared to PBS-injected control group (**Figure 4.7B**).

Furthermore, similar to pro-inflammatory EM CD4$^+$ T populations, CD8$^+$ T cell counterparts illustrated no prominent difference between the FTY720-inhibitor and PBS-injected control groups within the SLOs and p.fat. Interestingly, FTY720-inhibitor illustrated a significant reduction in both LFA-1$^+$,CD44$^+$ and CXCR3$^+$,CD44$^+$ CD8$^+$ T cell populations only in s.fat tissue (**Supplementary-Figure 2**). Additionally, FTY720-inhibitor expressed no alleviating effect on the CXCR5$^+$,PD1$^+$ Tfh CD4$^+$ T cells compared to PBS-injected control group (*data not shown*).

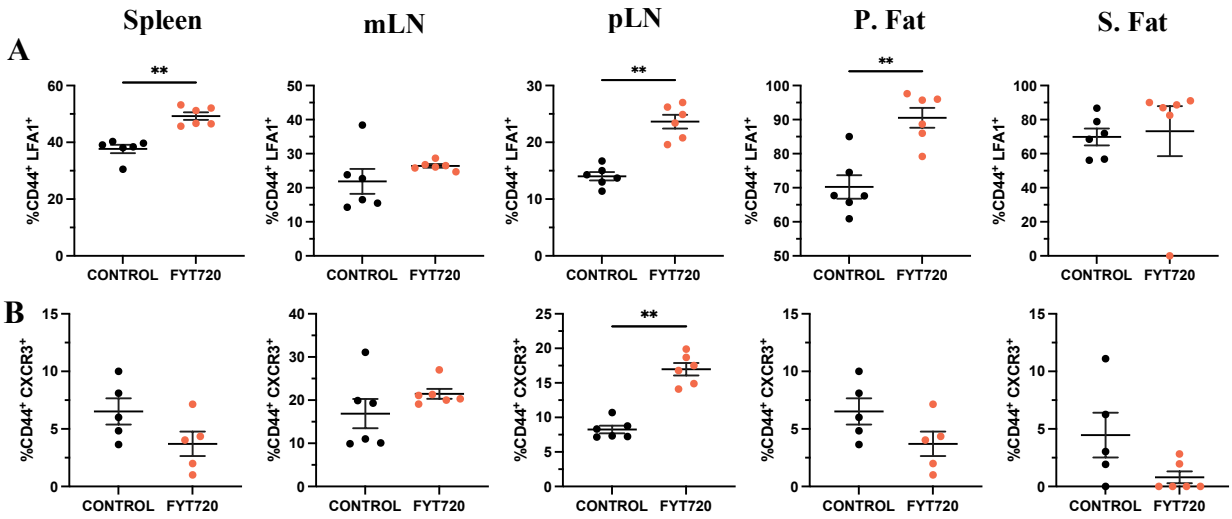


Figure 4.7) Pharmacological inhibition of CerS2 via FTY720 did not attenuate the pro-inflammatory effector memory CD4$^+$ T cell phenotype induced by WD

Quantification of flow cytometry data of **(A)** CD44$^+$ and LFA-1$^+$ and **(B)** CD44$^+$ and CXCR3$^+$ obesity-associated pro-inflammatory effector memory CD4$^+$ T cell populations in three main SLOs and two fat tissues obtained from female C57BL/6J mice fed on WD for 21 days and were given intraperitoneal injections of FTY720 (1 mg/ kg) three times (days 11, 14 and 18) (WD+FTY720) or three times PBS injections on respective time points (v.control). Both murine groups were also subjected to an allogenic

immunization via intraperitoneal injections at day 14. Each point represents an individual mouse in allocated diet groups (n=6). One-way ANOVA with Tukey's correction; Data presented as mean ± SEM, *p<0.05; ** p<0.01.

Altogether these data illustrated that inhibition of bioactive C24 was not capable of reversing the pro-inflammatory alterations in the EM $CD4^+$ T cell populations of the WD-fed murine model. Importantly this suggest that bioactive C24 per se is not responsible for all pro-inflammatory alterations as observed in the WD-fed early DIO murine model whereas, other bioactive lipid components of the WD may also play pivotal roles in modulating the T lymphocytes towards OIIM as further investigated in **Chapter 5**.

4.4. Pharmacological inhibition of C24 synthesis boosted $Foxp3^+$ Treg populations in SLOs

The 3-week early-DIO murine model illustrated a profound alteration between pro-inflammatory subsets including Th1, Th17 and anti-inflammatory Treg subsets as demonstrated in **Section 3.5**. Considering this DIO-associated pro-inflammatory phenotype, we investigated the potential direct effect inhibiting bioactive C24 synthesis on specific effector $CD4^+$ T helper cell subsets *in vivo* murine model.

Figure 4.8A, illustrates representative flow cytometry plots of $Tbet^+$ (Th1) and $ROR\gamma t^+$ (Th17) effector population percentages gated on total live $CD4^+$ T cells including FMO controls. Interestingly, no significant difference was observed in $Tbet^+$ Th1 $CD4^+$ T cells between the PBS-injected WD-fed control group and FTY720-inhibitor WD-fed control group within the SLOs (**Figure 4.8B**).

Importantly, FTY720-inhibitor group illustrated a significant reduction of the $ROR\gamma t^+$ Th17 effector $CD4^+$ T cell population within the pLN tissue and illustrated a notable reduction trend (p=0.06) in both spleen and mLN tissues compared to PBS-injected control (**Figure 4.8C**). These results suggested that bioactive C24 does not directly modulate the Th1 but potentially modulate the Th17 differentiation. Importantly, as even though both groups were fed on WD, inhibition of C24 synthesis was shown to restore the $ROR\gamma t^+$ Th17 effector $CD4^+$ T cell populations (**Figure 4.8C**) back to the CD-fed control mice levels as previously demonstrated in **Figure 3.9C**.

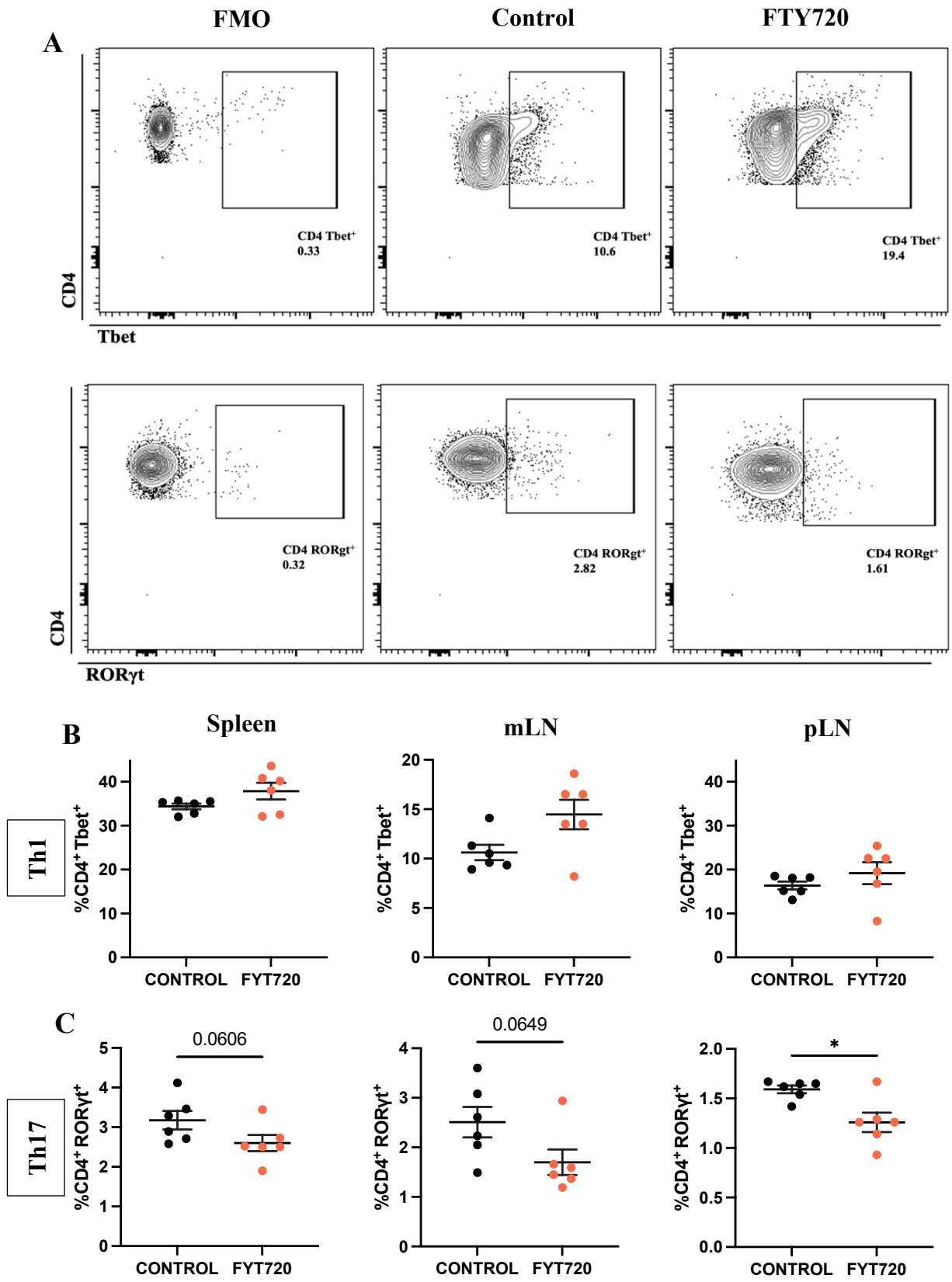


Figure 4.8) CerS2 inhibitor FTY720 attenuates the pro-inflammatory RORγt$^+$ Th17 CD4$^+$ effector T cell subset in SLOs

(A) Representative flow figures of the key intracellular transcription markers for distinct CD4$^+$ effector T cell subsets; Tbet$^+$ and RORγt$^+$ effector populations gated on total live CD4$^+$ T cells. Quantification of

flow cytometry data of **(B)** Tbet^{+} for Th1 and **(C)** RORγt^{+} for Th17 for Th2 effector CD4^{+} T cell populations within SLO tissues obtained from female C57BL/6J mice fed on WD for 21 days and were given intraperitoneal injections of FTY720 (1 mg/ kg) three times (days 11, 14 and 18) (WD+FTY720) or three times PBS injections on respective time points (v.control). Both murine groups were also subjected to an allogenic immunization via intraperitoneal injections at day 14. Each point represents an individual mouse in allocated diet groups (n=6). One-way ANOVA with Tukey's correction; Data presented as mean ± SEM, *p<0.05; ** p<0.01.

Considering the modulation of the Treg populations within the WD-fed early-DIO model and significant ameliorative effect of n-3PUFA supplementation (**Figure 3.17**), we further investigated the direct effect of C24 inhibition on the Treg populations. **Figure 4.9A** representative flow cytometry plots of Foxp3^{+} and CD25^{+},Foxp3^{+} CD4^{+} Treg populations illustrating a drastic increase in Treg subsets with FTY720-inhibitor. Strikingly inhibitor group had significantly higher Foxp3^{+} CD4^{+} Treg populations in all three SLOs compared to the PBS-injected WD-fed control group (**Figure 4.9B**). Consistently, this elevation was accompanied by a concomitant reduction in CD4^{+} Foxp3^{-} T cells within the SLOs (**Figure 4.9C**). Interestingly, there was no significant difference in both fat tissues between groups (**Figure 4.9**). Additionally, consistent with the Foxp3^{+} Treg populations, CD25^{+} Foxp3^{+} CD4^{+} Treg populations were also significantly elevated within the SLOs of FTY720-inhibitor group compared to the control group (**Figure 4.9D**).

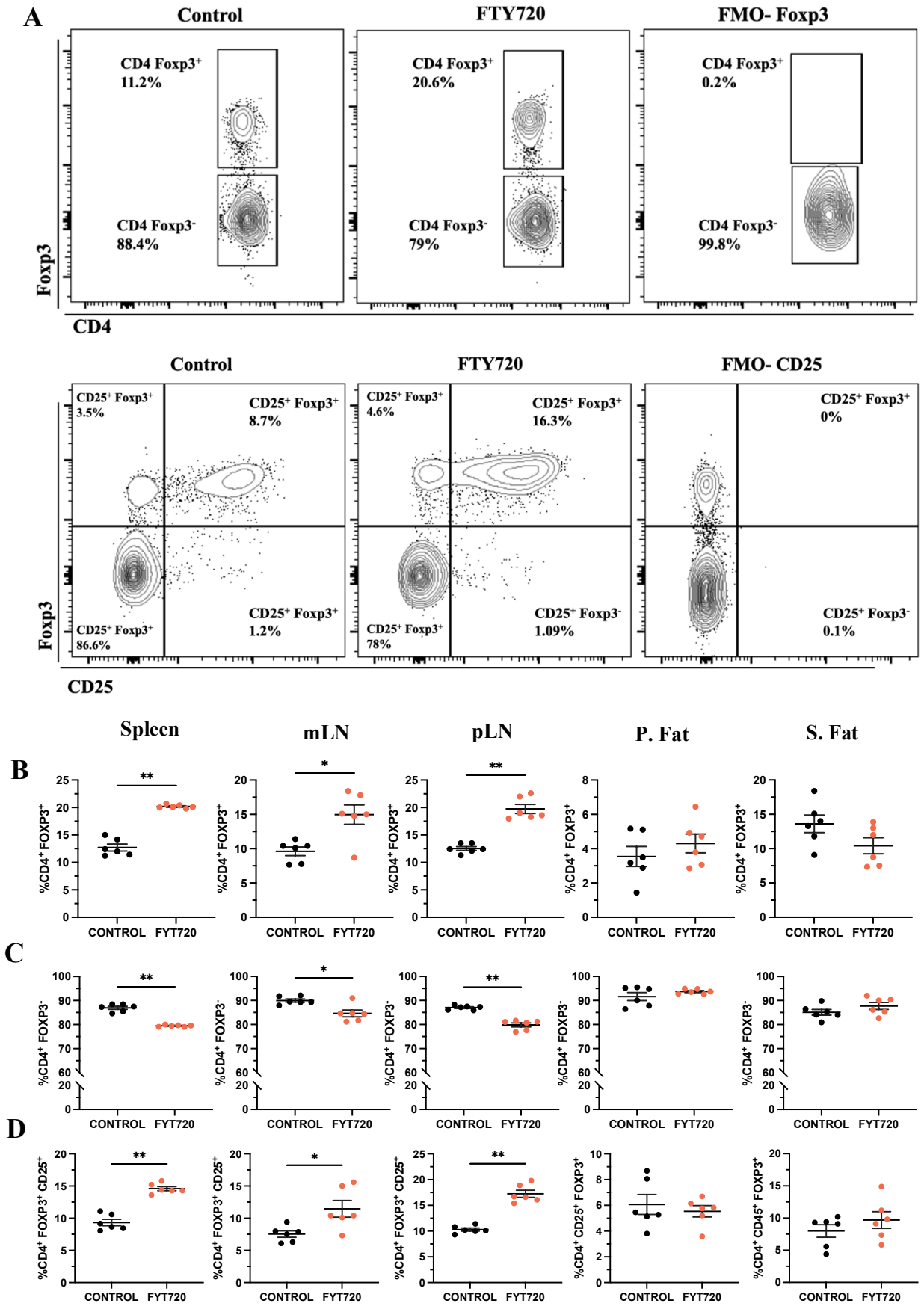


Figure 4.9) CerS2 inhibitor FTY720 increases the Foxp3$^+$ and CD25$^+$ Foxp3$^+$ CD4$^+$ Treg populations within the SLOs of WD-fed murine groups

(A) Representative flow cytometry plots showing the gating and modulation on $Foxp3^+$, $CD25^+$ Treg population between FTY720 inhibitor and PBS-injected vehicle control mice groups. Quantification of flow cytometry data of **(B)** $Foxp3^+$ and **(C)** $Foxp3^-$ and **(D)** $Foxp3^+$, $CD25^+$ $CD4^+$ Treg populations within SLO and fat tissues obtained from female C57BL/6J mice fed on WD for 21 days and were given intraperitoneal injections of FTY720 (1 mg/ kg) three times (days 11, 14 and 18) (WD+FTY720) or three times PBS injections on respective time points (v.control). Both murine groups were also subjected to an allogenic immunization via intraperitoneal injections at day 14. Each point represents an individual mouse in allocated diet groups (n=6). One-way ANOVA with Tukey's correction; Data presented as mean ± SEM, *$p<0.05$; ** $p<0.01$.

Furthermore, we investigated the expression of B-cell lymphoma-2 (BCL-2) intracellular anti-apoptotic marker which is known to play a crucial role in cell survival and inhibition of pro-apoptotic proteins [511]. BCL-2 is shown to be induced by IL-2 and promote immunosuppression via promoting Treg differentiation [512, 513]. Consistently, **Figure 4.10B** demonstrated that CerS2 inhibition by FTY720 leads to a significant increase in $BCL2^+$,$Foxp3^+$ $CD4^+$ T cell percentage within the SLO tissues compared to PBS-injected WD-fed control group (**Figure 4.10A**). This significant increase is further validated by the associated decrease in $BCL2^+$, $Foxp3^-$ $CD4^+$ T cell population within the spleen and pLN tissues (**Figure 4.10C**). Additionally, FTY720-inhibitor group also illustrated a significant increase in $BCL2^+$,$CD25^+$ $CD4^+$ T cell population within the SLOs similar to the $BCL2^+$,$Foxp3^+$ $CD4^+$ T cell dataset (**Figure 4.10D**). Contrarily, CerS2 inhibition via FTY720-inhibitor did not induce an upregulation in Treg differentiation in fat tissues.

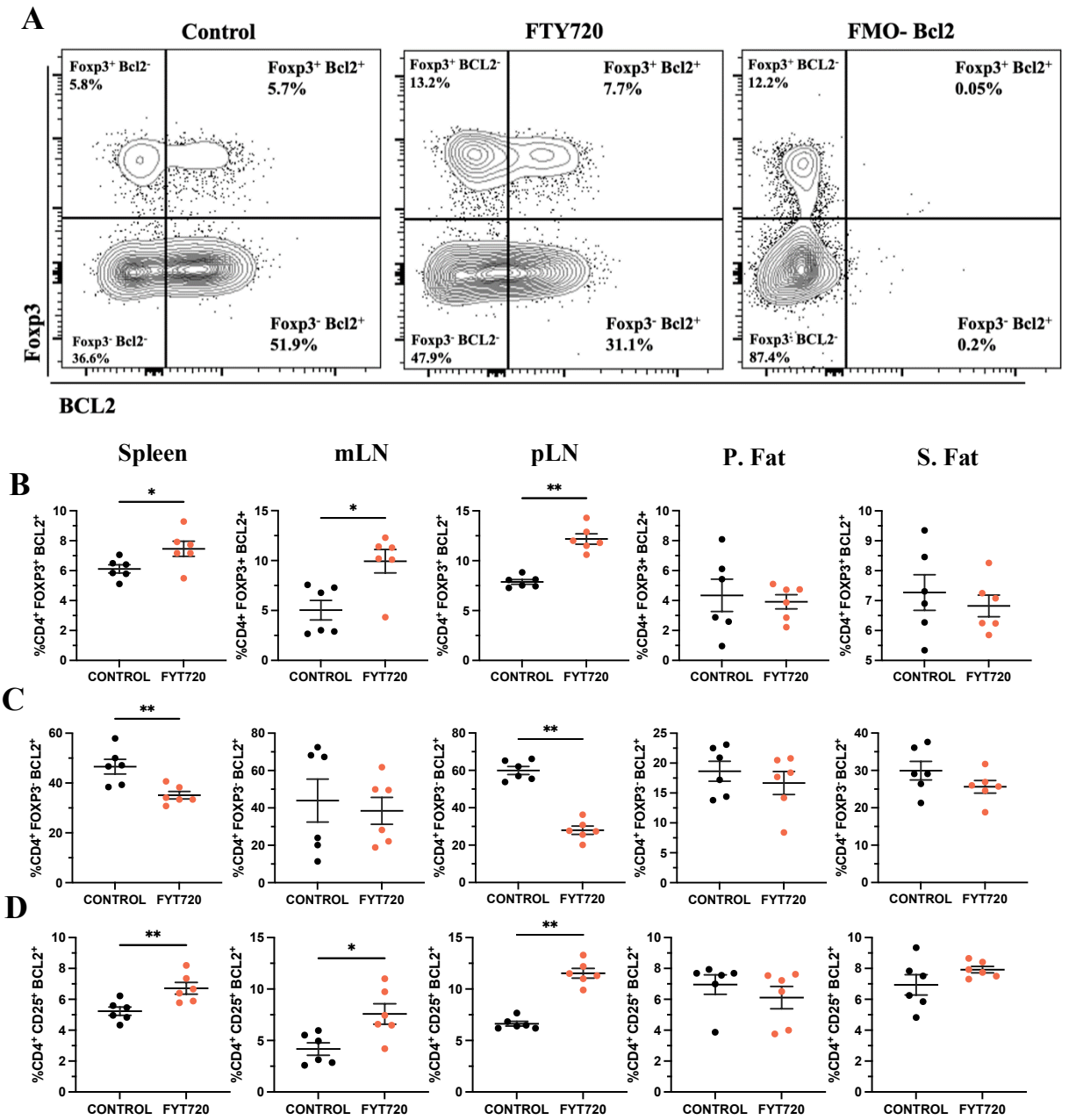


Figure 4.10) CerS2 inhibitor FTY720 increases the BCL-2 expression on the Foxp3$^+$ and CD25$^+$ Foxp3$^+$ CD4$^+$ Treg populations within the SLOs

(A) Representative flow cytometry plots showing the gating and modulation on BCL-2$^+$ Foxp3$^+$ Treg population between FTY720 inhibitor and PBS-injected vehicle control mice groups. Quantification of flow cytometry data of **(B)** Foxp3$^+$ BCL-2$^+$ and **(C)** Foxp3$^-$ BCL-2$^+$ and CD25$^+$, BCL-2$^+$ CD4$^+$ Treg populations within SLO and fat tissues obtained from female C57BL/6J mice fed on WD for 21 days and were given intraperitoneal injections of FTY720 (1 mg/ kg) three times (days 11, 14 and 18) (WD+FTY720) or three times PBS injections on respective time points (v.control). Both murine groups were also subjected to an allogenic immunization via intraperitoneal injections at day 14. Each point represents an individual mouse in allocated diet groups (n=6). One-way ANOVA with Tukey's correction; Data presented as mean ± SEM, *p<0.05; ** p<0.01.

Based on the modulations observed in the PD1-exhaustion and KLRG1-senescence-associated markers within the previous WD *in vivo* experiment in the SLOs (**Figure 3.10**), we investigated the potential effect of CerS2 inhibition on Foxp3$^+$ Treg exhaustion and senescence. However, inhibition of CerS2 by FTY720-inhibitor did not expressed any ameliorative effect on both T-cell exhaustion and senescence profiles of Tregs (**Supplementary-Figure 3**). These data suggests that the WD-induced T-cell exhaustion and senescence profile are not solely induced by bioactive C24, highlighting the importance of other bioactive lipids and metabolites in the immunomodulation of CD4$^+$ T cells.

Altogether, inhibition of C24 synthesis via pharmacological CerS2 inhibitor (FTY720) illustrated no significant effect on the WD-induced pro-inflammatory alterations in the naïve/memory CD4$^+$ T lymphocyte subsets as well as the pro-inflammatory LFA-1$^+$ and CXCR3$^+$ EM CD4$^+$ and CD8$^+$ T cells. These observations suggest that bioactive C24 does not directly and solely modulate the entire pro-inflammatory phenotype observed with the 3-week early-DIO murine model and there are other potential pro-inflammatory immunomodulatory mediators within the obesogenic WD may be leading to the systemic OIIM observed. However, importantly inhibition of C24 synthesis illustrated a significant ameliorative effect specifically in Th17/Treg balance (**Figure 4.11 & 4.12**). FTY720 CerS2 inhibitor was shown to 're-create' the balance between Th17/Treg CD4$^+$ T cells via suppressing the RORγt$^+$ Th17 population and boosting the Foxp3$^+$ and CD25$^+$ Treg populations within the SLOs. This observation was highly important as the C24 inhibition illustrated a similar anti-inflammatory effect as n-3PUFA and recapitulated the effect of WD+n-3PUFA murine group as detailed in **Sections 3.5 and 3.8**. This data suggests that C24 could play a critical role in effector T cell differentiation specifically modulating the Th17/Treg differentiation process which will be further investigated in **Section 4.4**.

It should be noted that similar to most of the pharmacological inhibitors, FTY720 has also been shown to have various off-target effects. Considering the available background literature, we have analysed and interpreted the data very cautiously to avoid any over-interpretation of the data obtained from *in vivo* murine model injected with FTY720-inhibitor.

4.5. Optimisation of ceramide lipotoxicity on murine and human CD4$^+$ Treg polarisation *in vitro* models

Considering the associations observed between WD-induced C24 levels and Foxp3$^+$ Treg depletion as well as the concomitant rise in RORγt$^+$ Th17 populations, we hypothesised that bioactive C24 plays a critical role in modulating Th17/Treg differentiation. To investigate the molecular mechanism underpinning the pro-inflammatory modulatory effects of bioactive C24 on Th17/Treg differentiation, we have directly treated CD4$^+$ T cell with ceramides under *in vitro* Treg differentiation conditions

It is known that high doses of ceramide induce cell death via apoptosis [514] however, various publications have shown to use non-physiological, high ceramide doses (2-10μM) without controlling the viability of CD4$^+$ T cells. Considering the disparities in the field first, we have optimised the lipotoxicity of candidate ceramides with dose-response (0.1μM-10μM) experiment in both human and murine *in vitro* naïve CD4$^+$ T cells under Treg differentiating conditions as detailed in **Section 2** (**Supplementary-Figure S4&5**). Additionally, we have selected the concentrations to be tested based on the average plasma ceramide concentrations detected in the lipidomics dataset (WD-fed group), 0.01- 0.1μM (20,000-30,000 ng/ml) [372, 501].

Following the optimisation of cell viability and ceramide concentrations, we tested the efficacy of our *in vitro* CD4$^+$ T cell differentiation model. It was crucial to be able to induce the Treg differentiation *in vitro* in a similar scale between biological repeats and treatment conditions to obtain a reliable potential difference between treatments. The detection of potential background differences in Foxp3$^+$ Treg levels was also important, considering the high human variability.

In order to check any potential difference between donors and treatments, the basal Foxp3$^+$ Treg levels were recorded from Th0 CD4$^+$ T cells which were not polarised towards any subset but activated and treated with ceramides in the same conditions as Treg polarised groups. **Figure 4.11A** representative flow cytometry plots illustrates the profound induction in Foxp3 expression under Treg differentiation *in vitro* human CD4$^+$ T cells conditions. All of the Treg polarised treatment groups expressed the Foxp3 Treg transcription factor (~55-65%) significantly higher compared to the Th0 control groups in both human (**Figure 4.11B**) and murine model (*data not shown*). Th0 control CD4$^+$ T cell subset groups expressed ~2-5% Foxp3 positivity, illustrating the background Treg levels differentiated naturally following the 3-5 days of cell culturing of the naïve CD4$^+$ T cells. No significant difference was observed among any of the Th0 treatment groups compared to Th0 vehicle control group (**Figure 4.11B**).

These optimisation experiments aimed to reduce the risk of being biased by potential cell death, polarisation difference and background Foxp3 expression differences within our *in vitro* ceramide-treated $CD4^+$ T cell Treg differentiation model.

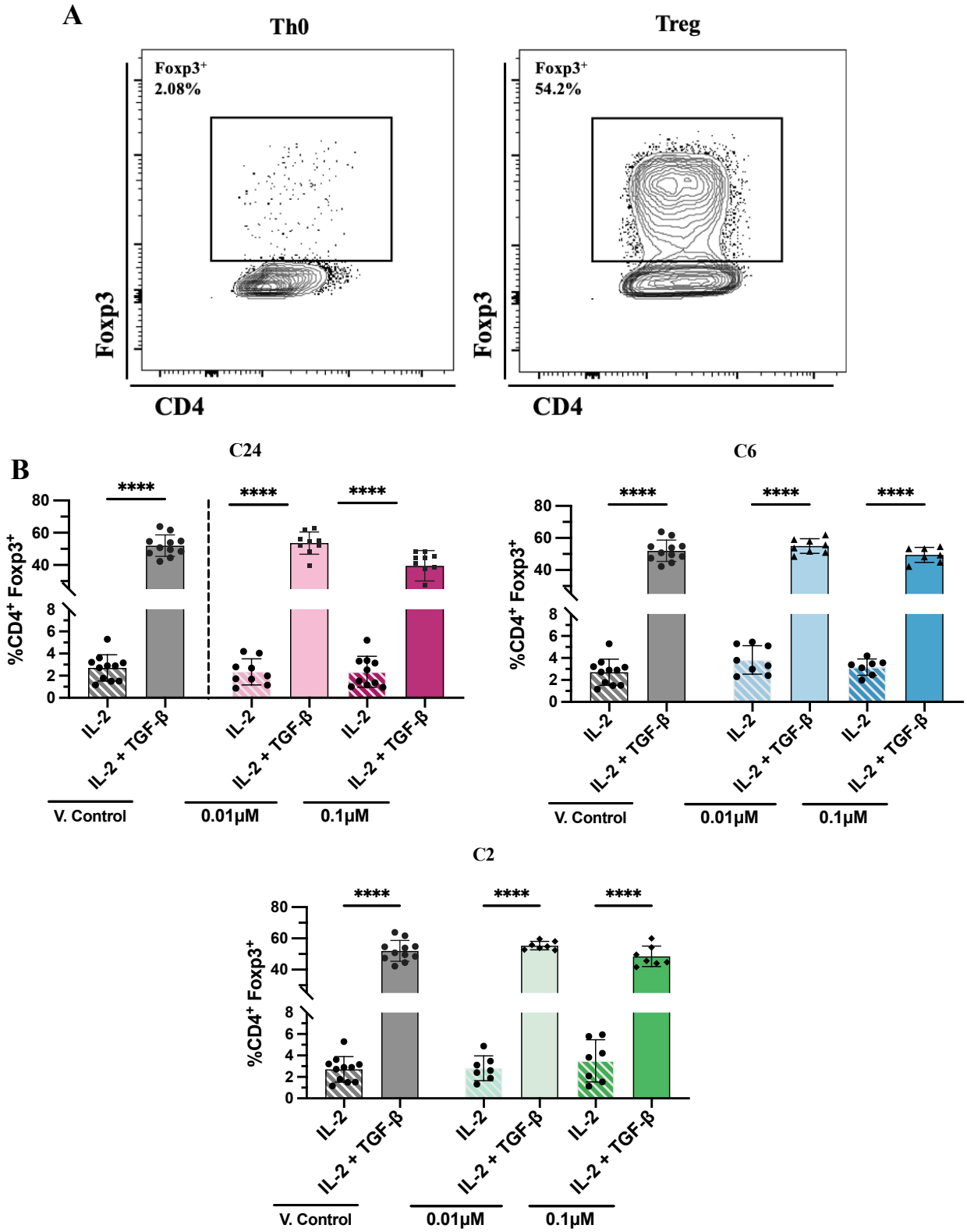


Figure 4.11) Foxp3 expression of *in vitro* iTreg differentiated human $CD4^+$ T cells.

(A) Representative flow cytometry plots illustrating the gating strategy and expression of main Treg-linked intracellular transcription factor; Foxp3 percentage, between IL-2 treated (Th0- undifferentiated) and IL-2 + TGF-β treated (Treg-differentiated) human $CD4^+$ T cells *in vitro* culture conditions. **(B)** Quantification of Foxp3 expression in human *in vitro* Treg differentiated (IL-2: 46ng/ml, TGFβ: 10ng/ml) and Th0 (undifferentiated-(IL-2: 46ng/ml) $CD4^+$ T cells following 5 days of ceramide treatment (C24, C6 and C2). All cell conditions were activated *in vitro* by CD3/CD28 (1.5:2.5µg/mL) plate bound activation. One-way ANOVA with Tukey's correction; Data presented as mean ± SEM (n=3), *p<0.05; ** p<0.01, ***p < 0.001, ****p<0.0001

4.6. C24 ceramide directly interferes with $Foxp3^+$ Treg differentiation of both murine and human $CD4^+$ T cells

Following the optimisation of the *in vitro* Treg differentiation model, we investigated the direct immunomodulatory effect of bioactive C24 (as identified by lipidomics assay) as well as C6 and C2 controls (based on the literature) on $CD4^+$ T cell differentiation. To further ensure the cell viability and to exclude any potential cellular debris, we included Near IR live/dead marker and gated all the markers on live $CD4^+$ T cell populations in all biological repeats. Consistent with the AnnexinV/PI staining data, both murine and human $CD4^+$ T cell *in vitro* models there were no statistically significant differences in live percentage among different ceramide treatment and vehicle control groups (**Supplementary-Figure S6**).

Based on our hypothesised, next we investigated the direct effect of bioactive C24 treatment on $CD4^+$ Treg differentiation *in vitro* through quantifying the latent $Foxp3^+$ Tregs by flow cytometry. **Figure 4.12** illustrates the representative flow cytometry plots of the key lineage-defining TF staining of murine $CD4^+$ T cells following the ceramide treatment under Treg differentiation conditions.

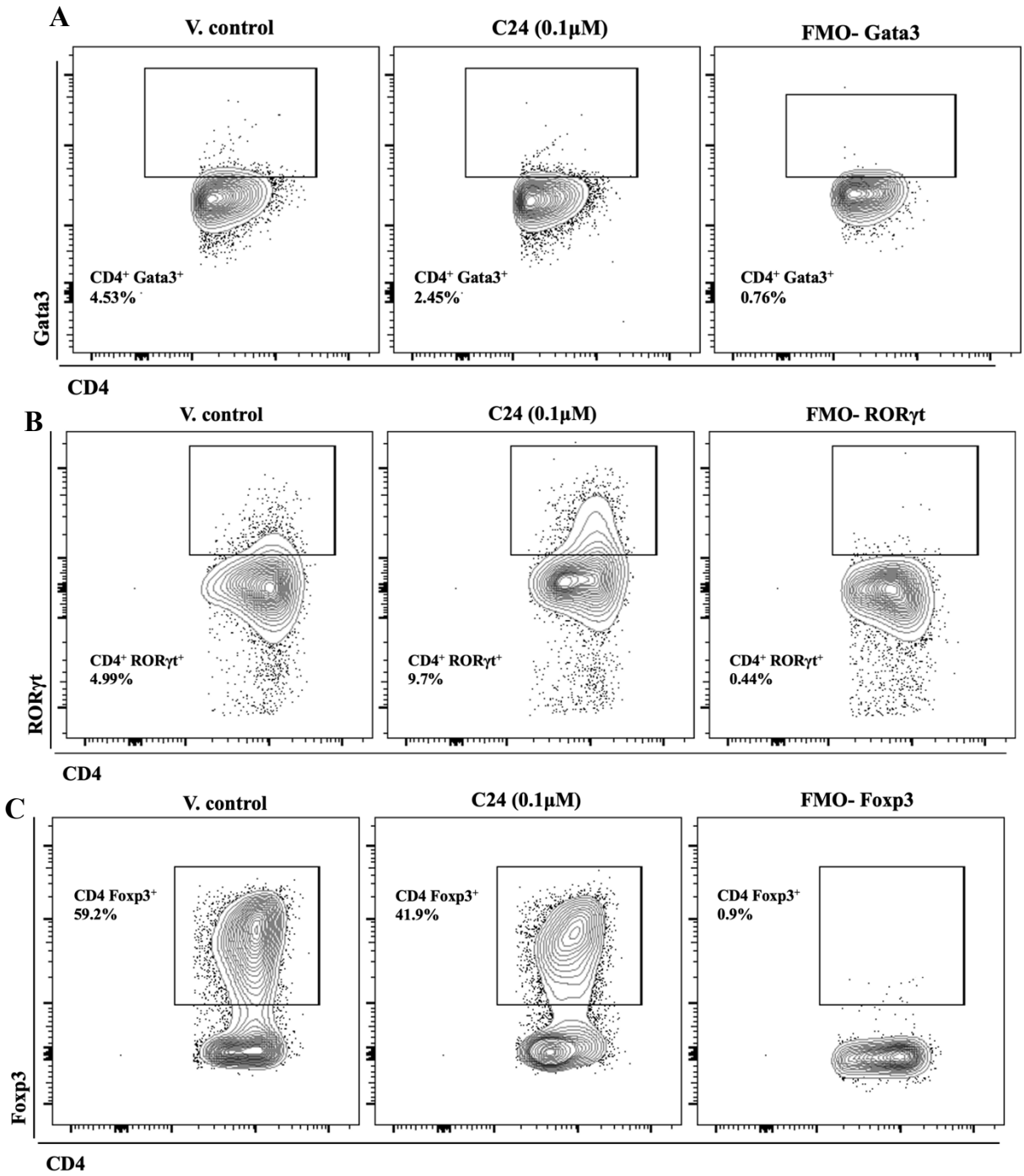


Figure 4.12) Representative flow cytometry plots of key effector CD4$^+$ T cell lineage-defining transcription factors

Representative flow cytometry plots illustrating the gating strategy and expression of main effector murine CD4$^+$ T cell lineage-defining transcription factors **(A)** Gata3 for Th2 **(B)** RORγt for Th17 and **(C)** Foxp3 for Tregs including FMO controls for each markers, respectively. All intracellular markers gated on live total CD4$^+$ T singlets obtained from vehicle control and C24 0.1µM groups, all conditions were activated by CD3/CD28 (1µg/mL) plate bound activation over 3 days of culture. Both vehicle control and C24 treated samples were kept under Treg differentiation conditions; Treg IL-2: 46ng/ml and TGFβ: 10ng/ml over 5 days *in vitro* ceramide treatment.

In the murine differentiation model, neither C6 or C2 significantly were shown to affect the Foxp3$^+$ Treg differentiation (**Figure 4.13A**). Interestingly, only 0.1µM of C24 significantly inhibited the Foxp3$^+$ Treg differentiation compared to the vehicle control following the activation (**Figure 4.13A**). This distinct reduction observed only in C24 ceramide at 0.1µM concentrations suggests a specific inhibitory effect of C24 on Foxp3$^+$ Treg murine CD4$^+$ T cell differentiation. Consistent with the murine dataset, C24 0.1µM group also showed a significant reduction in Foxp3$^+$ human Treg CD4$^+$ T cell differentiation compared to vehicle control (**Figure 4.13B**).

This observation was highly notable as the significant reduction trends observed in Foxp3$^+$ Treg differentiation of both murine and human *in vitro* models (**Figure 4.13**), were recapitulating the reduction observed in Treg frequencies with WD in murine *in vivo* models (**Figure 3.17**). Importantly, the significant inhibitory effect has only been observed at a distinct concentration which was consistently also detected in WD-fed murine group tissues (**Figure 3.17**). Although both C2 and C6 0.01µM treatment groups illustrated no significant changes in the murine dataset, within humans 0.1µM of C6 significantly reduced the Foxp3$^+$ Treg differentiation compared to vehicle control (**Figure 4.13B**). These *in vitro* observations demonstrate that within both mouse and humans the direct immunomodulation of WD-derived C24 that can bias CD4$^+$ T cells away from Treg fate as observed in DIO-linked pro-inflammatory phenotype.

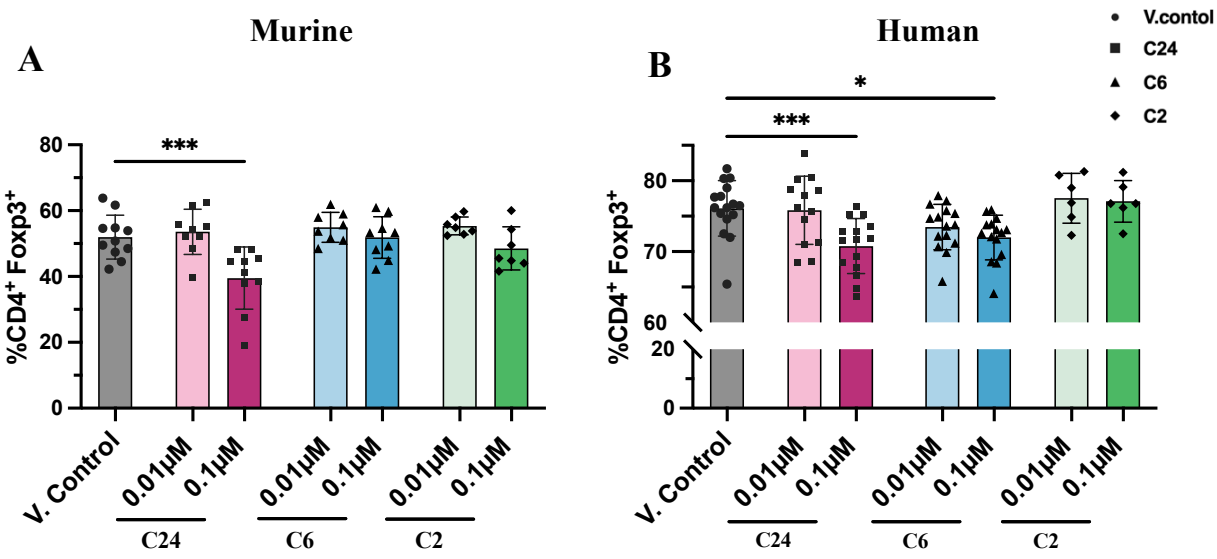


Figure 4.13) C24 0.1µM reduces the Foxp3$^+$ Treg differentiation in both murine and human *in vitro* CD4$^+$ T cell Treg differentiation models

Quantification of Foxp3 expression within the single live total murine CD4$^+$ T cells treated with C24, C6 and C2 (0.01µM and 0.1µM) or left untreated for 3 days, followed by CD3/CD28 (1 µg/mL) plate

bound activation under *in vitro* Treg differentiation conditions (n=5-6 mice pooled together as naïve $CD4^+$ cells isolated from murine spleen and LNs). **(B)** Quantification of Foxp3 expression within the single live total human $CD4^+$ cells treated with C24, C6 and C2 (.01μM and 0.1μM) or left untreated for 5 days, followed by CD3/CD28 (1.5/2.5μg/mL) plate bound activation under *in vitro* Treg differentiation conditions (n=4, naïve $CD4^+$ cells isolated from human PBMCs). Both vehicle control and C24 treated samples were kept under Treg differentiation conditions; IL-2: 46ng/ml and TGFβ: 10ng/ml over 5 days *in vitro* ceramide treatment. One-way ANOVA with Tukey's correction; Data presented as mean ± SEM, *p<0.05; ** p<0.01, *** p<0.001.

Considering the inhibitory effect of C24 at 0.1μM on Treg differentiation, we investigated if bioactive C24 was biasing the differentiation towards another effector $CD4^+$ T cell phenotype which were tested by main TF markers including T-bet for Th1, Gata3 for Th2 and RORγt for Th17.

Interestingly, C24 treatment at 0.1μM on Treg differentiating conditions resulted in a significant increase in RORγt expression in both murine and human $CD4^+$ T cells (**Figure 4.14A**). Consistent with the Foxp3 dataset, no other ceramides (C2 and C6) or concentrations were shown to modulate the RORγt expression in both murine and human $CD4^+$ T cells (**Figure 4.14A**).

Furthermore, we also analysed the main Th2 lineage-determining TF GATA3 which is generally known to have ameliorative effects in OIIM [383, 453]. Importantly, C24 0.1μM treatment on Treg differentiating $CD4^+$ T cells were shown to reduce the Gata3 expression in both murine and human *in vitro* models (**Figure 4.14B**).There was no statistically significant modulation observed in the C2 and C6 treatment groups of both species.

It should be noted that C2 ceramide treatment at both concentrations illustrated no modulatory effect on either Foxp3, RORγt and Gata3 expression in the murine system. Based on this consistent non-effective feature of C2 at both concentrations, we eliminated the C2 control group from the human $CD4^+$ T cells *in vitro* system. Additionally, we have experienced some issues with the intracellular staining of the Tbet transcription factor representing the Th1 effector $CD4^+$ T cell phenotype. However we tried to overcome this issue by measuring the Th-1 signature cytokine levels (IFNγ) (**Figure 4.19**).

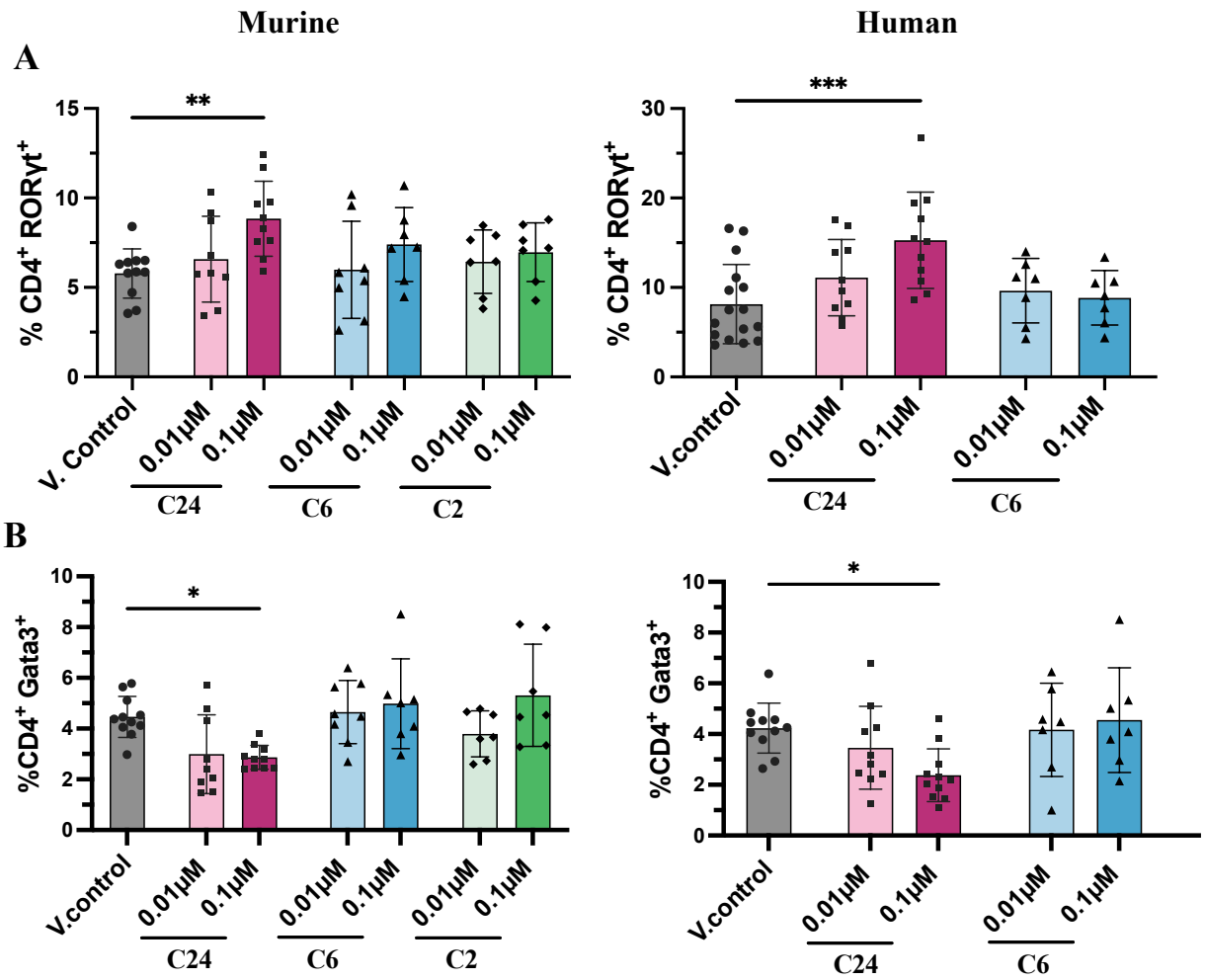


Figure 4.14) C24 0.1μM increases the RORγt$^+$ Th17 differentiation in both murine and human *in vitro* CD4$^+$ T cell Treg differentiation models

Quantification of **(A)** RORγt and **(B)** Gata3 expression within the single live total murine CD4$^+$ T cells treated with C24, C6 and C2 (0.01 and 0.1 μM) or left untreated for 3-5 days. All murine cells were activated by CD3/CD28 (1μg/mL) plate bound activation under *in vitro* Treg differentiation conditions for 3 days (n=5-6 mice pooled together as naïve CD4$^+$ cells isolated from murine spleen and LNs). All human were activated by CD3/CD28 (1.5/2.5μg/mL) plate bound activation under *in vitro* Treg differentiation conditions (IL-2: 46ng/ml and TGFβ: 10ng/ml) (n=4, naïve CD4$^+$ cells isolated from human PBMCs).One-way ANOVA with Tukey's correction; Data presented as mean ± SEM, *p<0.05; ** p<0.01, *** p<0.001.

Strikingly, bioactive C24 ceramide at physiological concentrations (0.1μM) as detected in WD-fed murine model, was shown to directly modulate the differentiation of CD4$^+$ T cell towards a pro-inflammatory RORγt$^+$ Th17 effector phenotype even under Treg differentiating *in vitro* conditions. It is also worth noting from these *in vitro* datasets that, Gata3 expression was mirroring the Foxp3 expression profile of C24 0.1μM treatment group in both human and murine models. This is particularly important considering the essential role of Gata3 in

regulating Foxp3 expression and Treg cell functions as previously reported in the literature [515-517].

4.7. C24 ceramide induces the secretion of Th17 effector CD4$^+$ T cell fate specific IL-17 and reduces IL-10 cytokine secretion

As previously detailed, the secretory profile and capacity of the CD4$^+$ T cells play a critical role in the establishment of OIIM [383, 453]. Following the lineage-defining TFs, to further dissect the immunomodulatory effects of bioactive C24, we also investigated the cytokine expression profile of the C24 treated CD4$^+$ T cells. All the cell culture media obtained from the corresponding *in vitro* samples as analysed by flow cytometry in **Figure 4.13 & 4.14** where both murine and human CD4$^+$ T cell monocultures were treated with C24, C6 and C2 *in vitro* under Treg differentiating conditions.

Consistent with the significant reduction in Foxp3$^+$ Treg levels, a concomitant decrease was observed in Treg-linked IL-10 levels in murine CD4$^+$ T cells treated with C24 0.1μM (**Figure 4.15**). Although the murine C6 0.1μM group also showed a decreasing trend compared to vehicle control, it did not reach statistical significance ($p=0.69$). Consistent with the Foxp3$^+$ Treg levels, C2 treatment was also ineffective in modulating the IL-10 levels.

Human CD4$^+$ T cells treated with C24 0.1μM *in vitro* also illustrated a reducing trend however, however differently from the murine CD4$^+$ T cells, this reduction was not statistically significant from the vehicle control group ($p=0.42$) (**Figure 4.15B)**. The high donor-to-donor variation observed in the human IL-10 levels may be the potential reason for why statistical significance was not achieved (**Figure 4.15B**). Consistently, C6 treatment showed no modulation on IL-10 levels (**Figure 4.15B**).

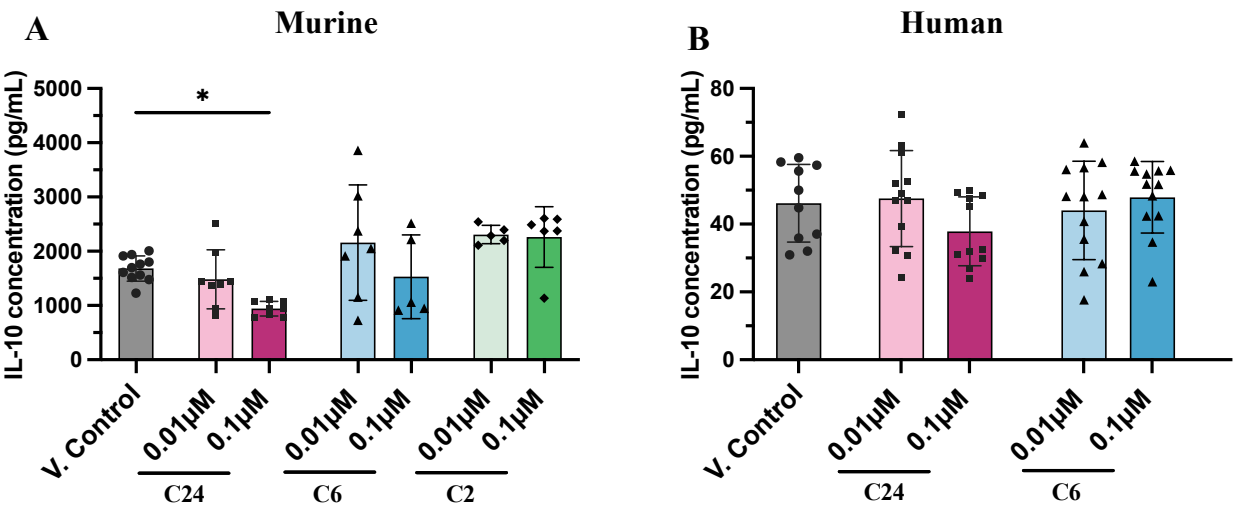


Figure 4.15) C24 0.1µM treatment reduces the IL-10 cytokine levels in both murine and human *in vitro* CD4$^+$ Treg differentiation models

IL-10 cytokine concentration (pg/ml) within the *in vitro* **(A)** murine (pooled naive CD4$^+$ T cells from n=5-6 mice) and **(B)** human (n=4-5 with 2 technical replicated per donor, naïve CD4$^+$ T cells isolated from human PBMCs) monoculture media measured by ELISA. Cell culture media obtained from the corresponding *in vitro* samples as analysed by flow cytometry in **Figure 4.13-4.14**. One-way ANOVA with Tukey's correction; Data presented as mean ± SEM, *p<0.05; ** p<0.01, *** p<0.001.

Considering the significant reduction observed with human Foxp3$^+$ Treg differentiation with C24 0.1µM group, but did not lead to a concomitant significant reduction in IL-10 levels within media, we tested the IL-10 production capacity of C24 0.1µM-treated human CD4$^+$ T cells. In order to compare the ability of the cells to produce IL-10, cells were treated with PMA/INO stimulation to induce cytokine production following the *in vitro* ceramide treatment protocol. The intracellular detection of cytokines within the cells was detected by flow cytometry through utilising Golgi stop solution to prevent the release of cytokines.

Importantly, C24 0.1µM treatment significantly reduced the total IL-10$^+$ CD4$^+$ T cell percentage compared to vehicle control (**Figure 4.16A**). The mean fluorescence intensity (MFI) is commonly used as the premier method for detecting intracellular cytokine staining by flow cytometry detection of average relative amount of a molecule detected by the fluorescence in a distinct channel [518]. Consistently, IL-10 MFI levels also illustrated a significant reduction with C24 0.1µM group compared to vehicle control (**Figure 4.16B**). Similar to the Foxp3$^+$ Treg percentages, C6 treatment was ineffective in modulating the IL-10 expression by the human CD4$^+$ T cell (**Figure 4.16**).

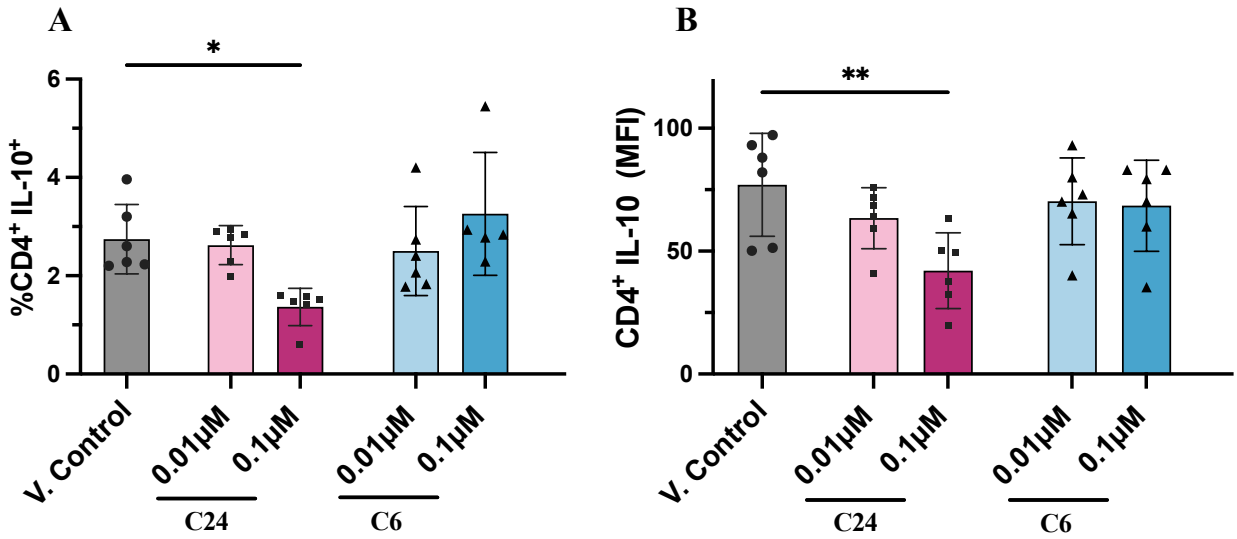


Figure 4.16) C24 0.1µM downregulated the IL-10$^+$ Treg population in human *in vitro* CD4$^+$ T cell Treg differentiation model

Quantification of the intracellular cytokine staining (ICCS) illustrates **(A)** frequencies of IL-10$^+$ CD4$^+$ T cells and **(B)** average mean fluorescence intensity (MFI) of IL-10 expression within the live CD4$^+$ T cell population within the human CD4$^+$ T cell monoculture treated with C24, C6 (0.01 and 0.1 µM) or left untreated for 5 days (n=3 with 2 technical replicated per donor, naïve CD4$^+$ cells isolated from human PBMCs). All human were activated by CD3/CD28 (1.5/2.5µg/mL) plate bound activation under *in vitro* Treg differentiation conditions (IL-2: 46ng/ml and TGFβ: 10ng/ml). Cell culture media obtained from the corresponding *in vitro* samples as analysed by flow cytometry in **Figure 4.20**. One-way ANOVA with Tukey's correction; Data presented as mean ± SEM, *p<0.05; ** p<0.01.

Although the reducing trend did not reach statistical significance in terms of IL-10 levels measured by ELISA within the human CD4$^+$ T cells treated with C24 0.1µM, this data illustrated a significant reduction in IL-10 production capacity when the cells were further activated via PMA and INO even under the Treg differentiating conditions.

Furthermore, considering the mirror image observed between the Foxp3$^+$ Tregs and RORγt$^+$ Th17 CD4$^+$ T cell populations following the C24 treatment, we measured the IL-17 levels by ELISA within the cell culture media of both murine and human CD4$^+$ T cells treated with ceramides under Treg differentiating conditions. Importantly, treatment of murine CD4$^+$ T cell monoculture with C24 at 0.1µM induced a statistically significant elevation in IL-17 cytokine levels (**Figure 4.17A**). Similar to the RORγt levels, IL-17 levels were not significantly different in any other ceramide group or doses tested.

In terms of the human CD4$^+$ T cell *in vitro* model, the total IL-17 levels were below the detectable limit of the IL-17 ELISA. However, some of the values were possible to interpolate via second-order polynomial-quadratic test based on the standard curve. **Figure 4.17B** shows

all the interpolated values, from these values C24 0.1µM treatment expressed a notable increasing trend compared to the vehicle control where the majority of the samples were below the standard curve and not been able to interpolated. Similarly, all the C6 and C24 at 0.01µM samples were also below the detectable limit. Although the IL-17 levels were significantly higher in C24 at 0.1µM group, this was not statistically significant due to the vehicle control values being below the detectable limit of the human IL-17 ELISA (**Figure 4.17A**).

It is also worth noting that although we have tried to analyse IL-17 via intracellular flow cytometry staining, we could obtain a consistent stain. This may be been due to technical issues with the staining protocol or antibody. Considering the shift observed in the expression of RORγt (Th-17-master TF), it would have been very interesting to analyse the capacity of IL-17 secretion with the intracellular cytokine staining especially in the human *in vitro* conditions.

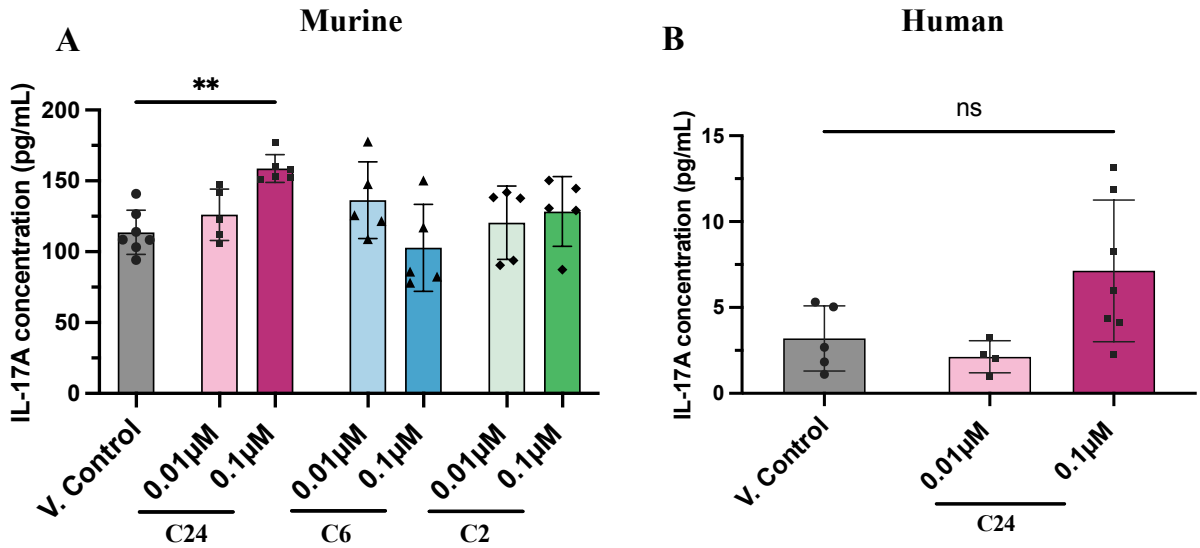


Figure 4.17) C24 0.1µM treatment increases the IL-17A cytokine levels in both murine and human *in vitro* CD4$^+$ Treg differentiation models

IL-17A cytokine concentration (pg/ml) from the *in vitro* **(A)** murine (pooled naive CD4$^+$ T cells from n=5-6 mice) and **(B)** human (n=4, naïve CD4$^+$ T cells isolated from human PBMCs) monoculture supernatant measured by ELISA. Cell culture media obtained from the corresponding *in vitro* samples as analysed by flow cytometry in **Figure 4.20**. Multiple human cell culture samples were below the detectable limit of human IL-17A ELISA. One-way ANOVA with Tukey's correction; Data presented as mean ± SEM, *p<0.05; ** p<0.01, *** p<0.001.

Following the significant reduction observed in Gata3 TF (Th2) and the known essential role of Th2 cells in regulating the Treg differentiation and functioning [515-517], we investigated the IL-13 levels of both murine and human CD4$^+$ T *in vitro* ceramide treatment under Treg differentiating conditions. Consistent with the significant reduction observed in the Gata3 (**Figure 4.14B**), mouse *in vitro* CD4$^+$ T cells both the MFI and percentage of IL-13$^+$

$CD4^+$ T cell frequency demonstrated a statistically significant decrease upon C24 0.1uM treatment comparing to the vehicle control (**Figure 4.18A**). However in humans, only the MFI levels exhibited a statistically significant reduction, the reduction trend observed in the percentage of cells did not reach statistical significance (p-value=0.0565) (**Figure 4.18B**).

Consistent with the Gata3 dataset (**Figure 4.14B**), both murine and human $CD4^+$ T cells showed no modulation in IL-13 with C6 treatment (**Figure 4.18**). These results were important in highlighting the association between the $Foxp3^+$, IL-10 producing $CD4^+$ Treg populations and $Gata3^+$, IL-13 producing Th2 effector $CD4^+$ T cell phenotypes as suggested by the literature [515-517].

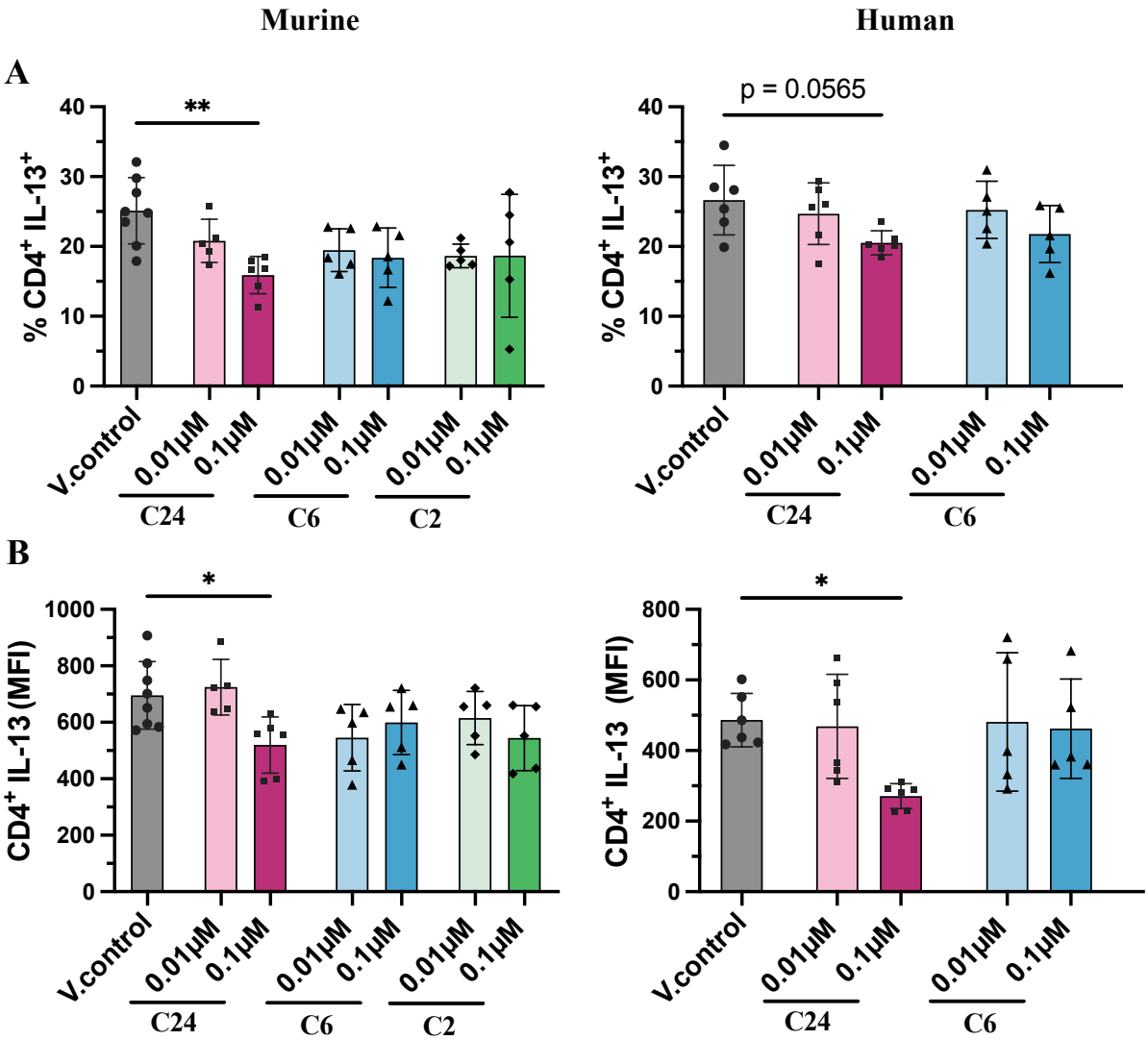


Figure 4.18) C24 0.1μM reduces the IL-13$^+$ Th2 population in human *in vitro* CD4$^+$ T cell Treg differentiation model

Quantification of the intracellular cytokine staining (ICCS) illustrates **(A)** frequencies of murine and human IL-13$^+$ CD4$^+$ T cells and **(B)** average mean fluorescence intensity (MFI) of IL-13 expression

within the murine and human live $CD4^+$ T cell population treated with C24, C6, C2 (0.01 and 0.1 μM) or left untreated. All murine cells were activated by CD3/CD28 (1μg/mL) plate bound activation under *in vitro* Treg differentiation conditions (IL-2: 46ng/ml and TGFβ: 10ng/ml) for 3 days (n=5-6 mice pooled together as naïve $CD4^+$ cells isolated from murine spleen and LNs). All human $CD4^+$ T cells were activated by CD3/CD28 (1.5/2.5μg/mL) plate bound activation under *in vitro* Treg differentiation conditions (IL-2: 46ng/ml and TGFβ: 10ng/ml) (n=3, naïve $CD4^+$ cells isolated from human PBMCs).One-way ANOVA with Tukey's correction. Data presented as mean ± SEM, *p<0.05; ** p<0.01, *** p<0.001.

Furthermore, we investigated the IFNγ as the signature cytokine of the Th1 effector $CD4^+$ T cell subset. The $Tbet^+$ Th1 effector $CD4^+$ T cells are known to predominantly secrete IFN, a pro-inflammatory cytokine which shown to elevate with DIO obesity [224, 263, 264]. Consistent with the literature, we have observed a significant increase in $Tbet^+$ Th1 $CD4^+$ T cell subsets within the SLOs of the WD-fed group (**Figure 3.9**). Interestingly, we did not observe any significant difference with the IFNγ levels of murine $CD4^+$ T cells treated with C24 under Treg differentiating *in vitro* conditions (**Figure 4.19A**). However, it should be noted that C24 0.01μM illustrated an increasing trend in $IFN\gamma^+$ MFI levels compared to vehicle control (p=0.06) (**Figure 4.19B**).

Additionally *in vitro* cytokine secretion from the ceramide-treated murine $CD4^+$ T cells under Treg differentiating conditions over 3 days, were also quantified by murine IFNγ ELISA. Confirming the increasing trend observed in the murine C24 0.01μM group via flow cytometry, IFNγ levels were statistically significantly elevated in the murine C24 0.01μM group compared to vehicle control (**Figure 4.19C**). Importantly, these results suggest that C24, C6 and C2 ceramides do not profoundly modulate the Th1 and Th1-associated cytokine expression and secretion of murine $CD4^+$ T cells *in vitro*.

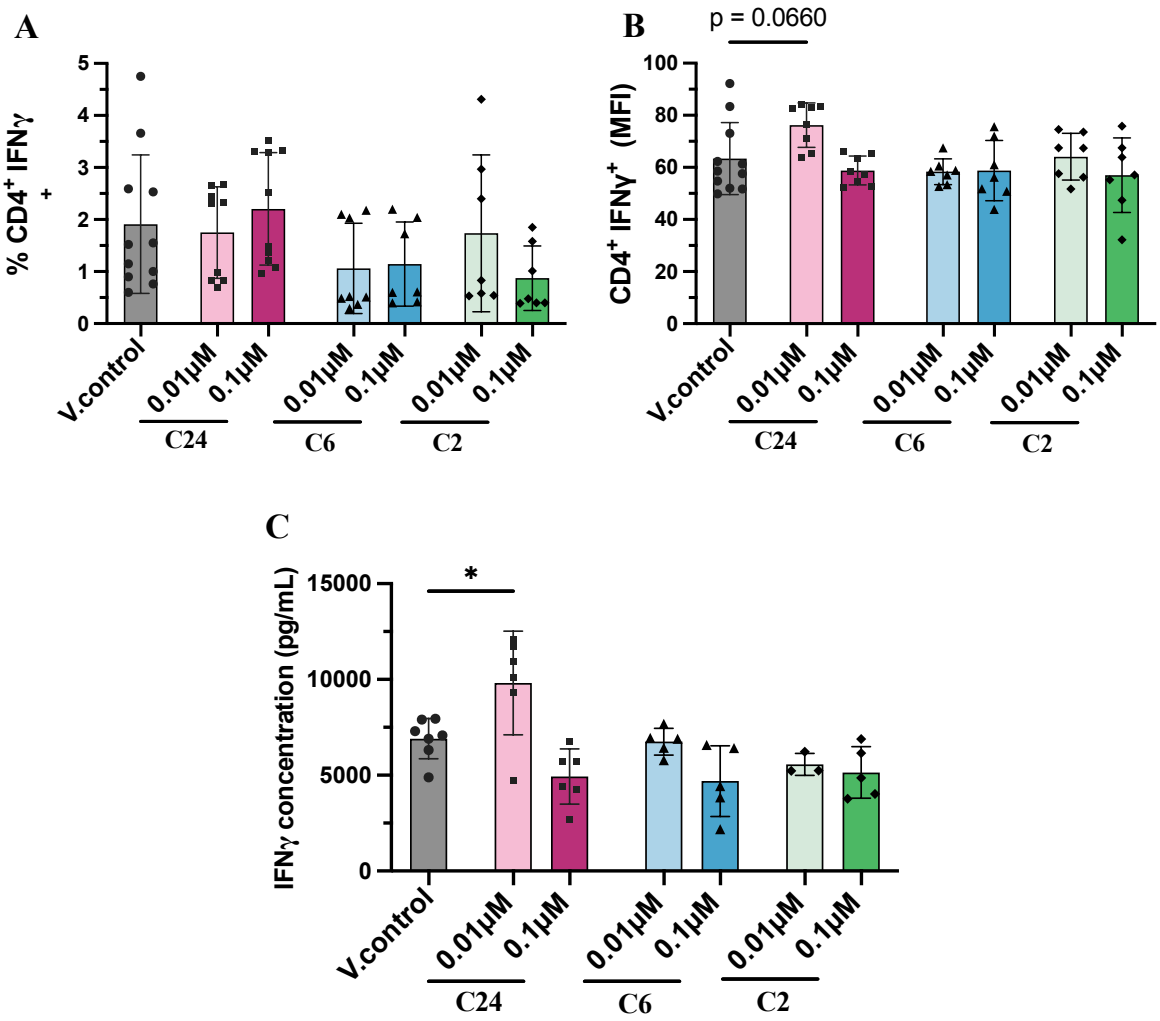


Figure 4.19) Exogenous ceramide treatment illustrated no modulatory effect on IFNγ expression within murine CD4$^+$ T cell Treg differentiation model

Quantification of the intracellular cytokine staining (ICCS) illustrates **(A)** frequencies of murine IFNγ$^+$ CD4$^+$ T cells and **(B)** average mean fluorescence intensity (MFI) of IFNγ expression within the murine and human live CD4$^+$ T cell population treated with C24, C6, C2 (0.01 and 0.1 μM) or with vehicle control. **(C)** IFNγ cytokine concentration within the *in vitro* murine CD4$^+$ T cell monoculture media measured by ELISA and shown as pg/ml. All murine cells were activated by CD3/CD28 (1μg/mL) plate bound activation under *in vitro* Treg differentiation conditions (IL-2: 46ng/ml and TGFβ: 10ng/ml) for 3 days (n=5-6 mice pooled together as naïve CD4$^+$ cells isolated from murine spleen and LNs). One-way ANOVA with Tukey's correction. Data presented as mean ± SEM, *p<0.05; ** p<0.01, *** p<0.001

Note) Considering little-to-no modulatory effects observed in the murine *in vitro* C24 treatment under Treg differentiation conditions, we did not follow up this in human *in vitro* system.

4.8 *In vitro* supplementation of omega-3 to the ceramide treated $CD4^+$ T cells did not ameliorate the pro-inflammatory effect of C24

The n-3PUFA supplementation into WD was shown to induce significant anti-inflammatory effects in DIO murine model by reducing the pro-inflammatory $CD4^+$ T cell markers and increasing the $Foxp3^+$ Treg populations within SLOs (**Figure 3.9 & 3.17**). Consistent with the literature these anti-inflammatory effects can contribute to resolving the OIIM and re-establish a homeostatic immune environment. Considering our previous publication and the literature, we investigated the anti-inflammatory potential of n-3PUFA supplementation on $CD4^+$ T treated with C24 under Treg differentiation conditions and if n-3PUFA can potentially revert the pro-inflammatory Th17-biasing of C24 *in vitro* [126].

Interestingly, simultaneous supplementation of 50μM EPA along C24 0.1μM treatment did not demonstrate any alleviating effect on human $CD4^+$ T cells where C24 0.1μM+EPA group still had significantly lower $Foxp3^+$ Treg differentiation similar to C24 0.1μM treatment group (**Figure 4.20A**). Consistent with the previous dataset, none of the other treatment groups expressed a difference compared to vehicle control group, suggesting that EPA supplementation does not alleviate the C24-driven pro-inflammatory immunomodulation in $CD4^+$ Treg differentiation.

Furthermore, we have also investigated the $ROR\gamma t^+$ $CD4^+$ T cell percentage from the same human $CD4^+$ T cell monoculture treated within C24, C6 and EPA-supplemented (50μM) groups (**Figure 4.20B**). Consistent with **Figure 4.14**, C24 0.1μM induced a significant increase in $ROR\gamma t^+$ $CD4^+$ T cell percentage even under Treg differentiating *in vitro* conditions whereas, EPA supplementation was able to significantly downregulate this increase in $ROR\gamma t^+$ $CD4^+$ T cell percentage back to vehicle control levels (**Figure 4.20B**). Although C6 treatment groups also illustrated a reducing trend, none of these reductions reached statistical significance (**Figure 4.20B**).

Similar to previous in experiments, the cell viability under EPA and C24 conditions were also controlled, especially considering the consistent downregulation observed in both TF expression. Consistently, no difference was observed in cell viability between treatment and vehicle control groups, eliminating the risk of EPA-induced lipotoxicity and cell death within the culture (**Supplementary-Figure S7**).

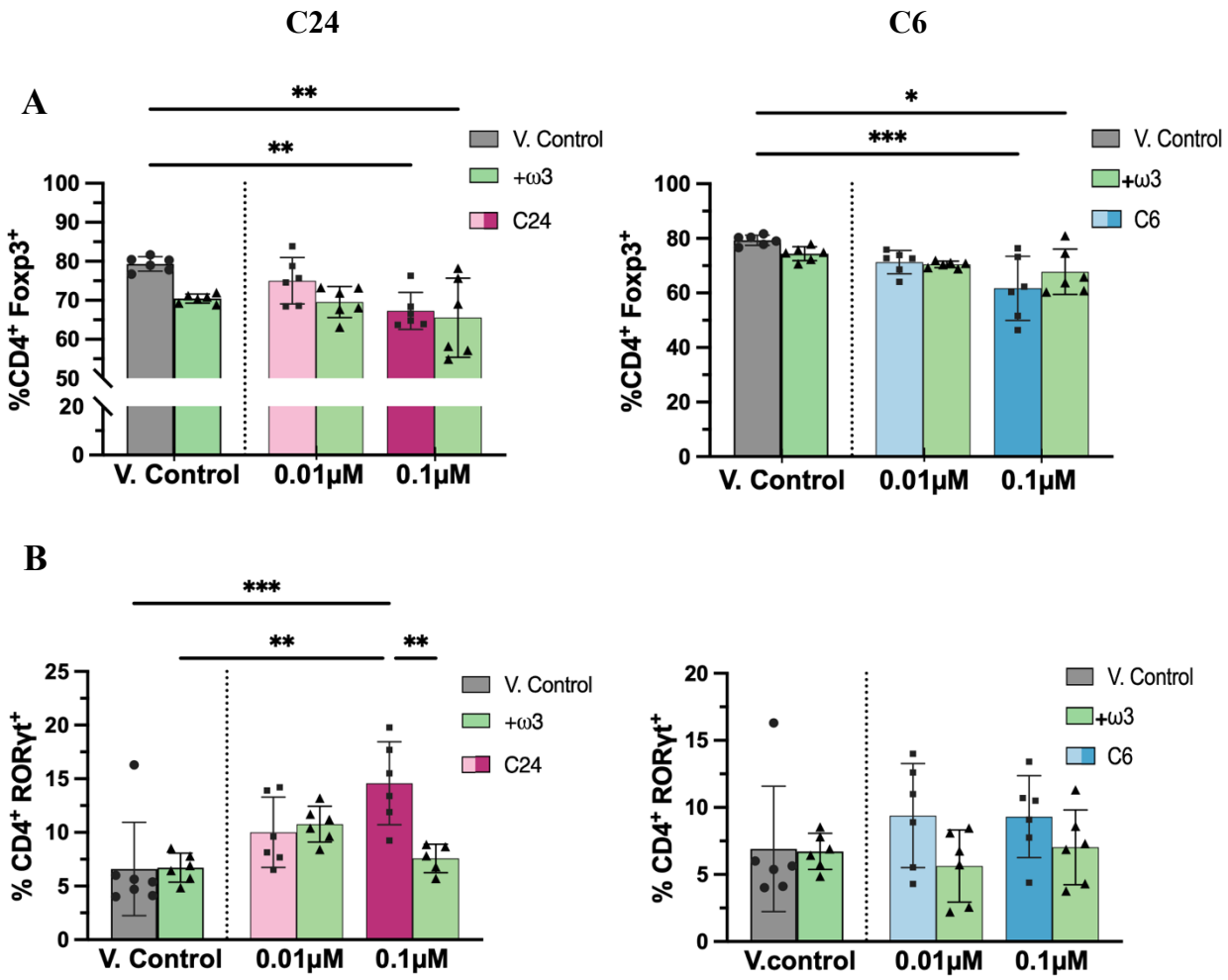


Figure 4.20) EPA supplementation down regulates the C24-induced RORγt expression in human CD4+ T cells under in vitro Treg differentiation conditions

Quantification of **(A)** Foxp3 **(B)** RORγt expression within the single live total human $CD4^+$ T cells treated with C24 or C6 ceramides (0.01 and 0.1µM) or candidate ceramides supplemented with EPA (50µM) as well as the untreated vehicle controls. All the cells were activated by CD3(1.5µg/mL) and CD28 (2.5µg/mL) plate bound activation under *in vitro* Treg differentiation conditions (IL-2: 46ng/ml and TGFβ: 10ng/ml) for 5 days. (n=3 with 2 technical replicated per donor, naïve $CD4^+$ cells isolated from human PBMCs). One-way ANOVA; Data presented as mean ± SEM, *p<0.05; ** p<0.01, *** p<0.001.

Altogether, n-3PUFA (EPA) supplementation was shown to inhibit the RORγt$^+$ T cell differentiation however, not induce the expression of Foxp3$^+$ Treg differentiation as observed in the murine *in vivo* models (**Figure 4.20**).

Considering the recent literature suggesting that n-3PUFA can exert its anti-inflammatory functions indirectly via modulating the biosynthesis of other deleterious lipid groups and metabolites in systemic levels [325, 519]. Considering the significant reduction in deleterious long-chain ceramides within the n-3PUFA supplemented WD group as recorded by lipidomics dataset (**Figure 3.17**), we hypothesised that n-3PUFA can indirectly upregulate the $Foxp3^{+}$ Treg expression via inhibiting the synthesis of pro-inflammatory ceramide synthesis.

Based on literature and our lipidomics data, ceramide synthesis mainly occurs in fat, liver and muscle tissues around the body [1, 127, 137, 151, 503]. Considering this we have analysed the expression of the main ceramide synthesis enzymes (CerS and DES) only within the perigonadal and subcutaneous fat tissues. The CerS5 and CerS6 known to synthesise C12, C14, C16 and C18 ceramides and CerS2 synthesise C22, C24 and C26.

Importantly, consistent with the ceramide levels detected (**Figure 4.3**) and the pro-inflammatory phenotype observed (**Figure 3.8**) in the WD murine group, the expression of CerS2, CerS5 and CerS6 enzyme genes were significantly upregulated in perigonadal fat tissue of WD group compared to the CD control group (**Figure 4.21A**). Furthermore, the WD+n-3PUFA group illustrated a significant reduction in the expression of CerS2, CerS5 and CerS6 enzymes compared to WD, which recapitulates the significant reduction in total ceramide levels as well as the attenuating effect observed in the WD-induced pro-inflammatory phenotype (**Figure 4.21A**). This data illustrated that n-3PUFA supplementation into WD was able to reduce the ceramide synthesis back to CD control group levels as well as ceramide concentrations (**Figure 4.3**). Similarly, DES1 expression was also significantly elevated in the WD group compared to CD whereas although WD+n3-PUFA group illustrated a reducing trend, this was not found to be statistically significant (**Figure 4.21B**). On the other hand, the consistent absence of pro-inflammatory phenotype reported in **Figure 3.8**, subcutaneous fat tissue of WD and the WD+n-3PUFA groups showed no effect in terms of CerS and DES gene expression levels either (**Figure 4.21B**).

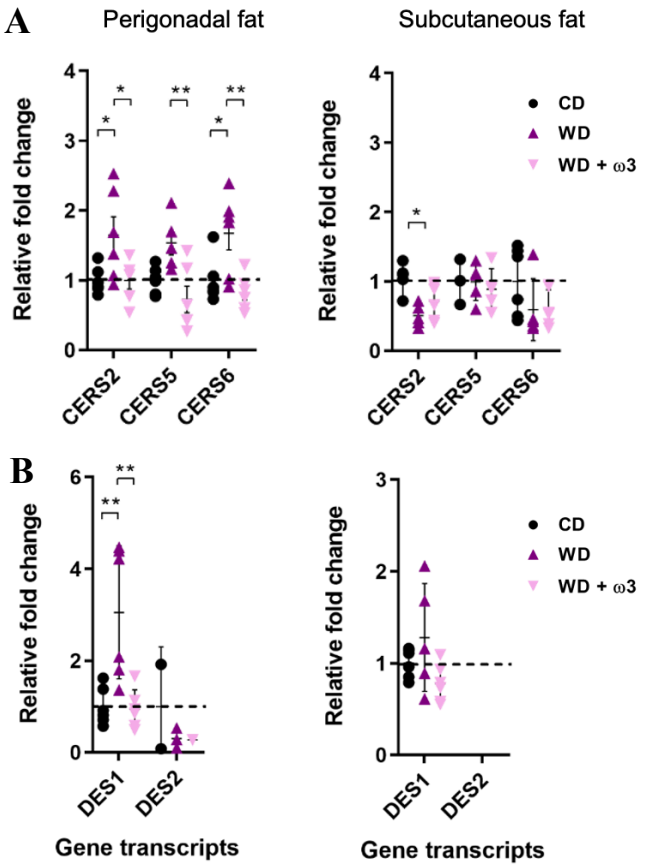


Figure 4.21) Effect of 3-week WD and n-3PUFA supplementation on the gene expression of ceramide biosynthesis enzymes, CerS2, 5 and 6 in murine fat tissue
Relative gene expression of **(A)** CerS2, 5 and 6 enzymes and **(B)** DES1 and 2 within the peripheral and subcutaneous fat tissues obtained from female C57BL/6J mice fed on CD, WD and WD+ n-3PUFA (5% menhaden oil). (n = 6 mice per diet group). Total RNA was extracted using the TRIzol method, purified using a mirVana kit and quantified using RT-qPCR; expressed as fold change (2^-ΔΔCt). Gene expression was normalized against β-actin, relative to CD group and data were expressed as mean ± SEM relative to CD; *p < 0.05, **p < 0.01 (one-way ANOVA with Tukey's post-hoc adjustment).
§*This experiment and analysis was carried out by Dr Dolores Camacho-Munoz at the University of Manchester with the supervision and guidance of Professor Anna Nicolaou.*

4.9 Bioactive C24 alone is not responsible for the WD-induced cellular senescence on CD4$^+$ T cells

Various publications reported a significant increase in ceramide levels in senescent cells where ceramide levels were shown to be associated with key cellular senescence factors such as inhibition of DNA synthesis, cell growth and proliferation [520]. More recently, it has been shown that long-chain C24 ceramide can induce cellular senescence in bone-derived mesenchymal stem cells *in vivo* and *in vitro* suggesting that bioactive ceramides can directly contribute to senescence [176]. Consistent with the literature, our 3-week early-DIO murine

model also illustrated a significant elevation in PD1 (exhaustion marker) and senescence-associated KLRG1 marker within WD group (**Figure 3.10**). To test the direct potential of C24 in inducing T cell exhaustion and senescence, we investigated various key senescence markers within our *in vitro* C24 treatment of human $CD4^+$ T cells under Treg differentiation conditions.

Figure 4.22A illustrated no observable difference in the main human cellular senescence-associated marker (CD57) and exhaustion marker (PD1) between C24 treated groups and the vehicle control (**Figure 4.22A**). Similarly, both γH2AX DNA damage marker and Ki67 proliferative capacity markers illustrated no significant difference between C24 and the control groups (**Figure 4.22B**). Altogether, these data illustrated that C24 had no effect on the induction of cellular senescence on human $CD4^+$ T cells under Treg differentiating conditions *in vitro*.

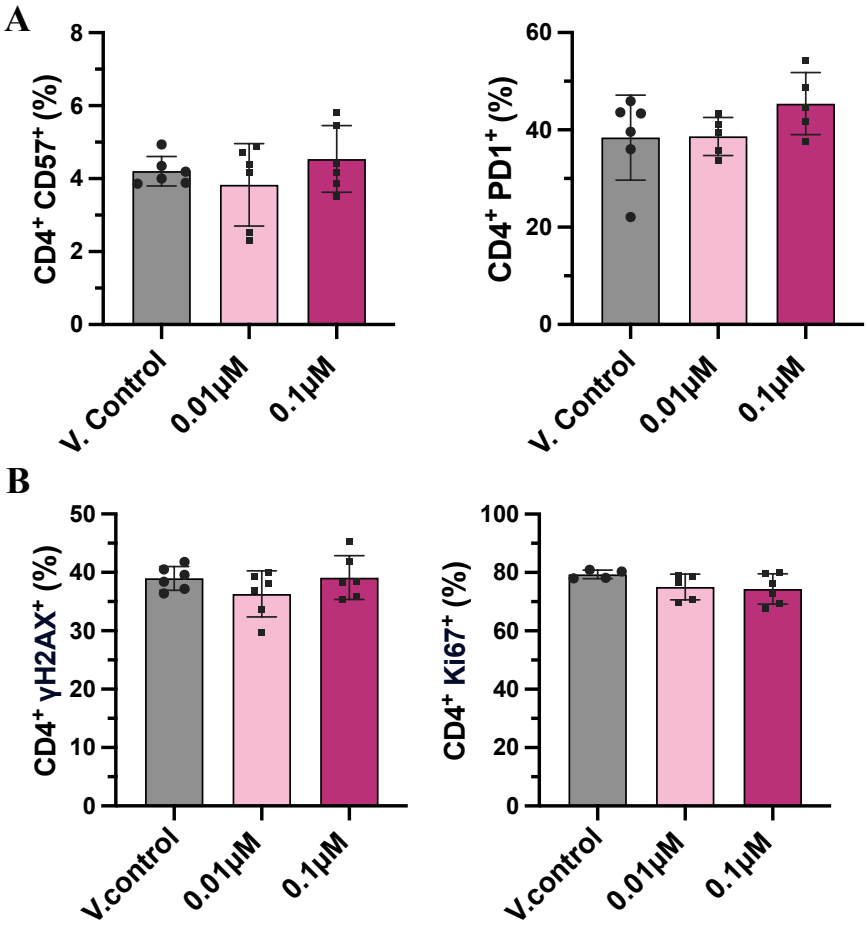


Figure 4.22) Exogenous *in vitro* C24 treatment shows no effect on cellular senescence of human $CD4^+$ T cells under Treg differentiation conditions

Quantification of **(A)** CD57, PD1 **(B)** γH2AX, Ki67 and **(C)** TNF-α expression within the single live total human $CD4^+$ T cells treated with 0.01µM and 0.1µM C24 or left untreated as vehicle control. All the cells were activated by CD3/CD28 (1.5/2.5µg/mL) plate bound activation under *in vitro* Treg

differentiation conditions (IL-2: 46ng/ml and TGFβ: 10ng/ml) for 5 days. (n=3 with 2 technical replicated per donor, naïve $CD4^+$ cells isolated from human PBMCs). Data presented as mean ± SEM.

Additionally, $Foxp3^+$ $CD4^+$ Tregs subsets did not express any observable difference of T-cell exhaustion and senescence markers between C24-treated and vehicle controls (*data not shown*). Altogether this data illustrated that specifically, C24 does not directly induce cellular senescence on both $Foxp3^+$ Tregs and total $CD4^+$ T cells in our *in vitro* model. However, there are various other potential bioactive metabolites derived from the WD that can directly induce the cellular senescence profile observed within the 3-week early DIO *in vivo* model.

4.10 Potential molecular mechanisms underpinning the pro-inflammatory immunomodulation of C24 against CD4+ Treg fate and biasing towards RORγt+ Th17

We have illustrated the pro-inflammatory immunomodulatory effect of bioactive C24, biasing the $CD4^+$ T differentiation towards $ROR\gamma t^+$ Th17 phenotype and inhibiting the $Foxp3^+$ Treg differentiation both *in vivo* and *in vitro*. Based on this immunomodulatory effect of C24, we aimed to dissect potential molecular mechanisms underpinning this pro-inflammatory modulation. As IL-6 is known to be the main lineage-determining cytokine in Th17 differentiation, we initially checked the IL-6 cytokine levels in the *in vitro* murine $CD4^+$ T cell differentiation model [227, 486, 487]. Consistent with the literature, we did not detect prominent IL-6 levels within the murine *in vitro* $CD4^+$ T cell culture as most of the conditions were below the detectable limit of murine IL-6 ELISA (<3pg/mL) (**Supplementary-Fig. S8**). These results confirmed that, C24-driven Treg/Th17 differentiation bias, was not driven by modulations in IL-6 levels within cell culture. This observation suggested another critical Th17/Treg differentiation mechanism modulated by ceramides.

Considering the previously detailed literature reporting a critical modulation of ceramides on TCR signalling in T lymphocytes [367, 521], we investigated ant potential modulation of C24 on human $CD4^+$ T cell TCR activation that could lead to Th17/Treg differentiation modulations. Various publications illustrated that distinct ceramides lead to an increase in TCR activation [367, 522, 523] whereas other publications demonstrated opposite, inhibitory effects on TCR activation and signalling [366, 524]. As an example, Sofi et al. 2017 illustrated the long-chain ceramides synthesised by CerS6 (C16) play a critical role in the TCR activation by ZAP-70 phosphorylation and cytokine production in an alloantigen response situation [367].

Considering LCK as the first kinase transducing TCR signalling and Zap-70 is one of the first downstream early-proximal signalling components which gets phosphorylated during the TCR activation, we initially investigated the early proximal signalling components [525]. Quantification of p-LCK/total LCK protein levels in C24 0.1µM treated human naïve $CD4^+$ T cells, revealed no significant difference compared to vehicle control in a time-course tested (5-30 mins) (**Figure 4.23A**). Similarly, phosphorylation ZAP-70 in C24 treated cells illustrated no observable difference in terms of relative fold change compared to vehicle control over the time-course (**Figure 4.23B**). These results suggested that the difference we have observed with Foxp3/RORγt transcription factor expressions and Treg/Th17 differentiation were not induced by the C24-induced modulation in TCR strength or activation.

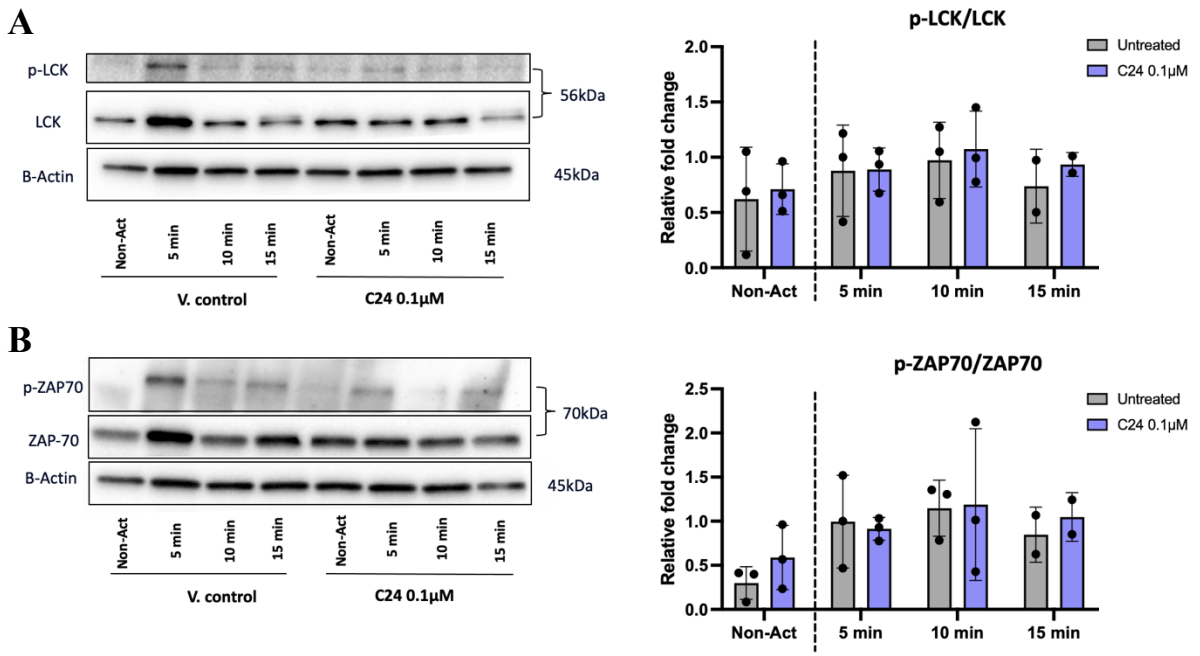


Figure 4.23) ***In vitro*** **C24 treatment does not affect the early proximal signalling components of TCR signalling**

Representative western blots (left) and densitometric quantification (right, n=3) of **(A)** pLCK, LCK and **(B)** pZap70, Zap70 of human $CD4^+$ T cells isolated from human PBMCs which were treated with C24 ceramide with 0.1µM or left untreated overnight (12 hours). Following the treatment all cells were activated by human dynabeads T cell activator (CD3/CD28) kit (bead-to-cell ratio of 1:1) for the indicated time points; non-activated, 5, 10 and 15 minutes. Data expressed as mean ± SEM.

Considering no significant modulation recorded in LCK and Zap-70 upper TCR activation level, we examined potential modulations within the downstream components (Akt and Erk) of TCR activation-linked signalling pathways including PI3K/AKT and Ras/MAPK.

Differently from the upper signalling components, both pAkt/Akt and pErk/Erk levels were significantly reduced with C24 0.1μM treatment groups specifically at 10 minutes timepoint following the CD3/CD28 activation stimulation (**Figure 4.24**). It should be noted that pErk/Erk levels were also significantly reduced in C24 0.1μM treatment, at 5 minutes following the activation stimulation where this reduction trend was preserved until 15 minutes following the activation (**Figure 4.24B**). Consistent with the literature no difference was observed with the 30 minutes of activation as potentially all the TCR activation pathway gets fully saturated [366].

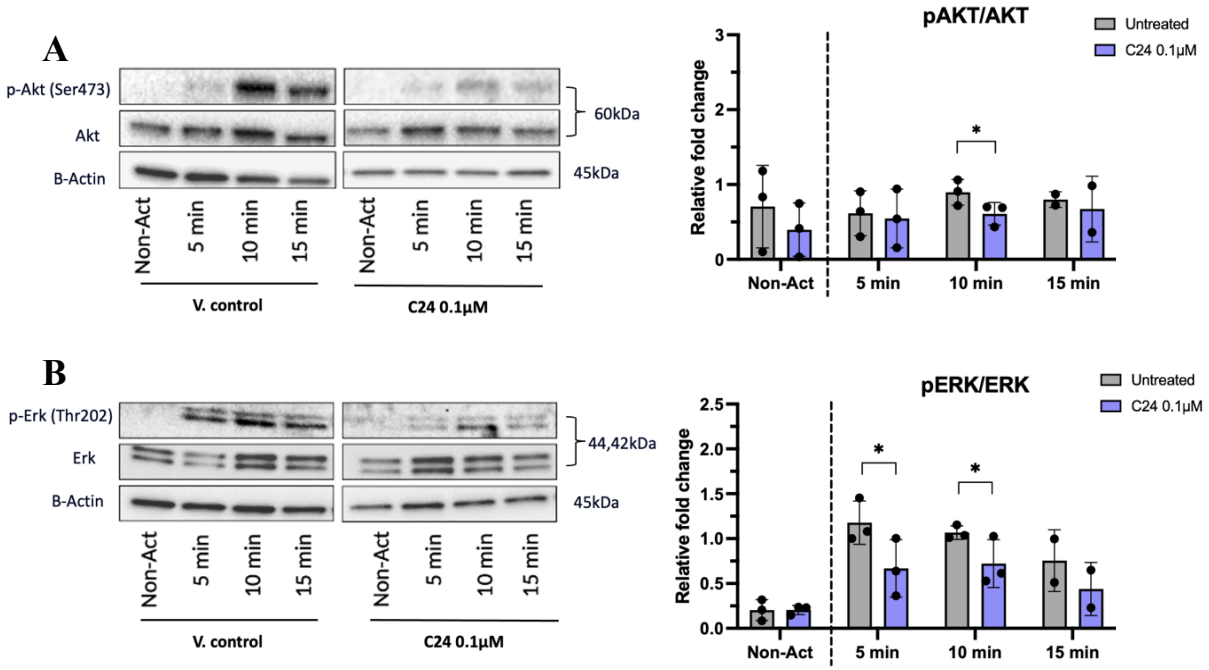


Figure 4.24) ***In vitro*** **C24 treatment reduces the downstream components of TCR signalling in human CD4$^+$ T cells**

Representative blots (left) and densitometric quantification (right, n=3) of **(A)** pAkt, Akt and **(B)** pErk, Erk of human CD4$^+$ T cells isolated from human PBMCs which were treated with C24 ceramide with 0.1μM or left untreated overnight (12 hours). Following the treatment all cells were activated by human dynabeads T cell activator (CD3/CD28) kit (bead-to-cell ratio of 1:1) for the indicated time points (5-15 minutes). Data normalised to β-actin and expressed as mean ± SEM relative to Akt and Erk, *$p <$ 0.05 (one-tailed Student's *t*-test).

As previously detailed in **Section 4.1.1**, Bai et al. demonstrated the critical role of CD39 transmembrane proteins in amplifying ceramide synthesis by augmenting the ASM activity, mediating STAT-3 and mTOR signalling cascades and eventually driving the Th17 differentiation [368, 494, 495]. Considering this background literature, we investigated the role of CD39-driven secondary signalling cascade that can potentially bias the differentiation towards RORγt$^+$ Th17 phenotype and inhibit Foxp3$^+$ Treg differentiation.

Initially, we examined the expression of CD39, STAT-3 and HIF-1α, on human $CD4^+$ T cells *in vitro* Treg differentiation model where cells were treated only with C24 0.1μM or vehicle control under 5-day *in vitro* Treg differentiation conditions (**Figure 4.25A**). Interestingly, all three markers illustrated an increasing trend compared to the vehicle control conditions (**Figure 4.25B**). Furthermore, $STAT\text{-}3^+$ $CD4^+$ T cells were also shown to express the CD39 and HIF-1α much higher in C24 0.1μM group compared to the vehicle control (**Figure 4.25C**). This data suggests that C24 at 0.1μM treatment was able to induce higher expression of CD39 and HIF-1α in $STAT\text{-}3^+$ $CD4^+$ T cells.

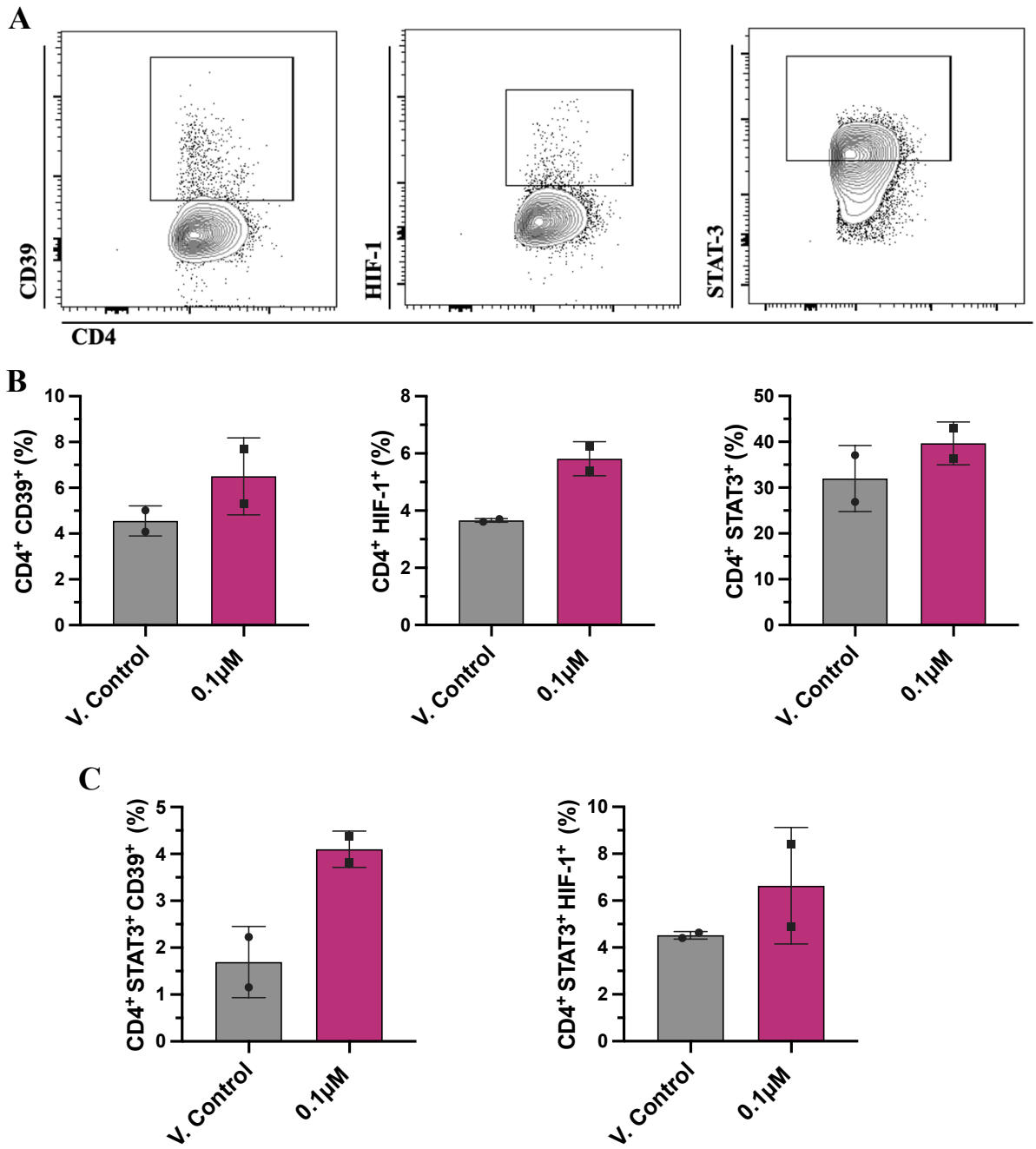


Figure 4.25) Exogenous C24 0.1μM increases the CD39, STAT-3 and HIF-1α expression within the human *in vitro* CD4$^+$ T cell Treg differentiation models

Representative flow cytometry plots illustrating the gating strategy and expression of main effector human CD4$^+$ T cell markers **(A)** CD39, HIF-1 and STAT-3 within the live total human CD4$^+$ T cells vehicle control samples. Quantification of **(B)** CD39, HIF-1α and STAT-3 markers gated within the total human CD4$^+$ T cells treated with treated with C24 (0.1μM) and **(C)** frequencies of CD39$^+$ and HIF-1α$^+$ CD4$^+$ T cells gated on live STAT-3$^+$ CD4$^+$ T cells treated with C24 (0.1μM) or left untreated for 5days under Treg differentiation conditions (IL-2: 46ng/ml and TGFβ: 10ng/ml). All human were activated by CD3/CD28 (1.5/2.5μg/mL) plate bound activation (n=2 with 2-3 technical replicates per individual experiment, naïve CD4$^+$ cells isolated from human PBMCs).

Furthermore, we have further investigated the role of CD39/STAT-3/HIF-1α within the Foxp3$^+$ Treg and RORγt$^+$ Th17 subsets. Consistently **Figure 4.26A** recapitulated **Figure 4.13-14** illustrating a reduction in Foxp3 and elevation of RORγt levels with 0.1μM C24 treatment. Importantly, C24 induced increase in CD39, HIF-1 and STAT-3 expression shown to be associated with lower Foxp3$^+$ Treg and a higher RORγt$^+$ Th17 frequencies. The full gating strategy used to analyse these samples was represented by the vehicle control group (**Supplementary-Figure S9**).

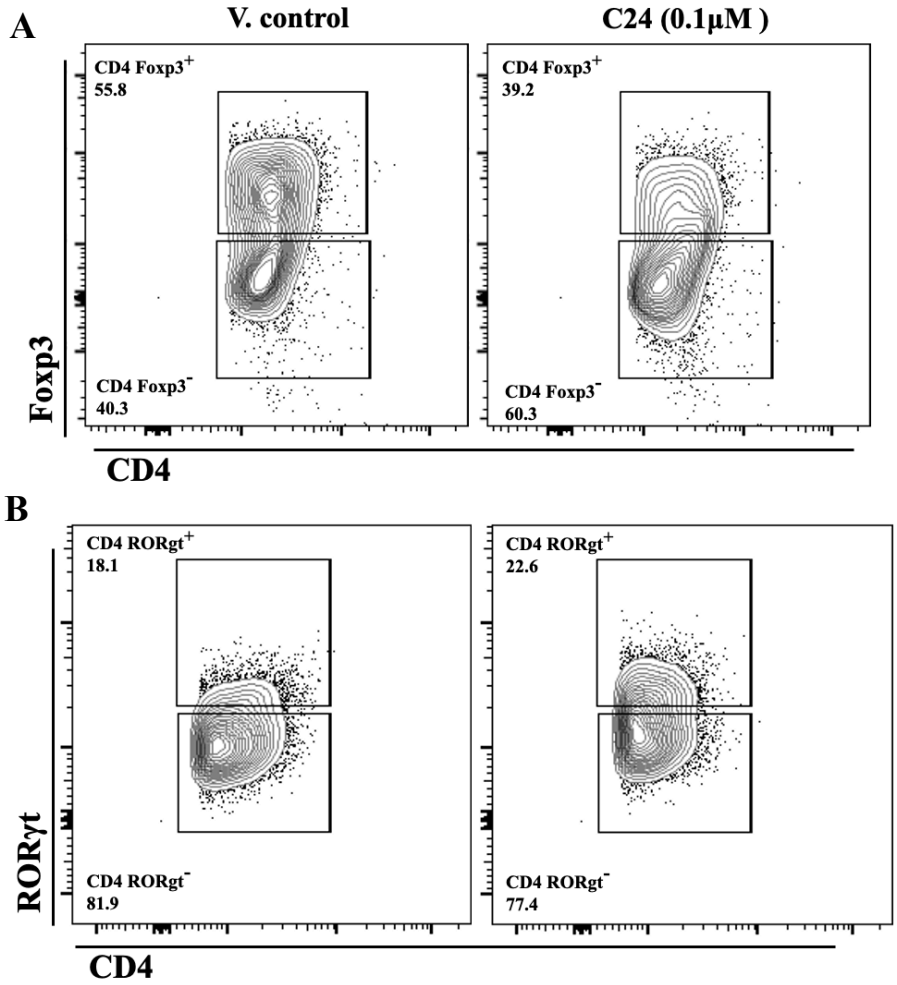


Figure 4.26) Representative flow cytometry plots of key effector CD4$^+$ T cell lineage-defining transcription factors in human CD4$^+$ T cells under Treg differentiation conditions
Representative flow cytometry plots illustrating the gating strategy and expression of main effector murine CD4$^+$ T cell lineage-defining transcription factors **(A)** Foxp3 for Treg and **(B)** RORγt for Th17. All intracellular markers gated on live total CD4$^+$ T singlets obtained from vehicle control and C24 0.1μM groups, all conditions were activated by CD3/CD28 (1.5/2.5μg/mL) plate bound activation. Both vehicle control and C24 treated samples were kept under Treg differentiation conditions; Treg IL-2: 46ng/ml and TGFβ: 10ng/ml over 5 days *in vitro* ceramide treatment.

Importantly, **Figure 4.27A** illustrates the positive correlation observed between HIF-1α and RORγt where, bioactive C24 0.1μM treatment shown to profoundly increase the HIF-1α^{+},RORγt^{+} double-positive Th17 CD4^{+} T cell populations even under *in vitro* Treg differentiation conditions. Additionally, C24 0.1μM treatment group also induced an elevation of CD39 and HIF-1 expression specifically within the RORγt^{+} Th17 population. (**Figure 4.28B**). Consistently, RORγt^{-} CD4^{+} T cell populations within both groups illustrated no observable modulation, suggesting a specific modulation within RORγt^{+} Th17 populations. Contrarily, C24 0.1μM illustrated no observable modulatory effect in terms of CD39 and HIF-1α within the Foxp3^{+} CD4^{+} Treg populations (**Figure 4.28A**).

Finally, we analysed STAT-3 expression within the Foxp3^{+} Treg and RORγt^{+} Th17 populations treated with C24 0.1μM. STAT-3 is known to be one of the main Th17 lineage-defining TFs and consistent with the literature, RORγt^{+} Th17 populations had higher STAT-3 levels (20-40%) compared to Foxp3^{+} Treg population (5-10%) (**Figure 4.28C**). Importantly, C24 0.1μM treatment was shown to increase the STAT-3 levels in Foxp3^{+} Tregs but to a higher extent within RORγt^{+} Th17 CD4^{+} T cells compared to vehicle control group (**Figure 4.28C**). Consistent with our hypothesis, STAT-3^{+} Treg and Th17 cells also had elevated CD39 and HIF-1α expression with the C24 0.1μM treatment compared to vehicle control (**Figure 4.28C**). Importantly, CD39, HIF-1α and STAT-3 expressions were consistently lower in Foxp3^{+} Treg population compared to RORγt^{+} Th17 CD4^{+} T cells in both C24 0.1μM and vehicle control. Although C24 predominantly biases the differentiation towards RORγt^{+} Th17 effector fate, it can also have a potentially small but detectable effect on Foxp3^{+} Treg CD4^{+} T cells as well.

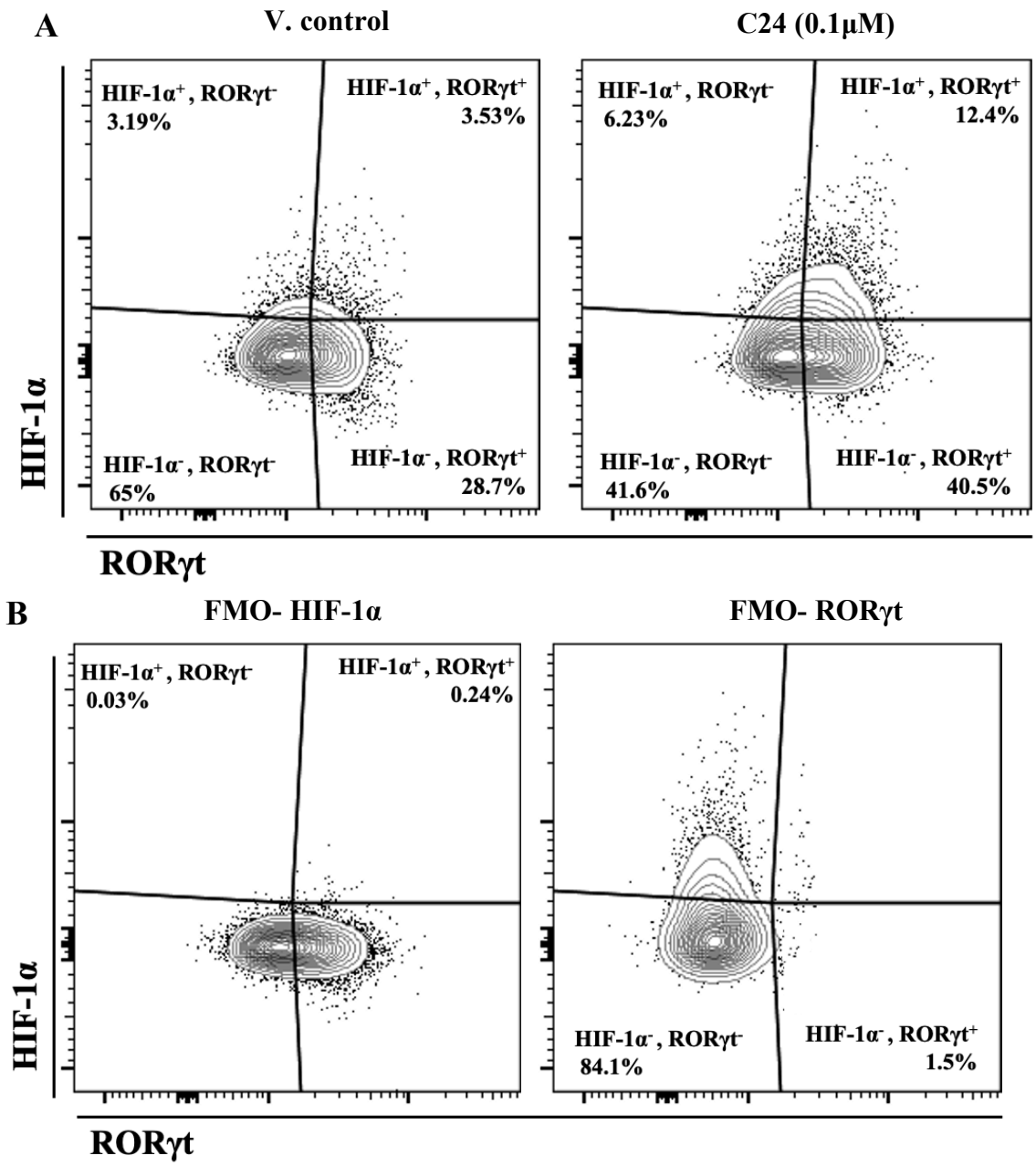


Figure 4.27) Representative flow cytometry plots of HIF-1α and RORγt human CD4$^+$ T cell populations CD4$^+$ T cells under *in vitro* Treg differentiation conditions

Representative flow cytometry plots illustrating the gating strategy and expression of **(A)** HIF-1α and RORγt within human CD4$^+$ T cell populations including the representation of **(B)** FMO HIF-1α and FMO RORγt samples used to decide the gating strategy, respectively. All intracellular markers gated on live total CD4$^+$ T singlets obtained from vehicle control and C24 0.1μM groups, all conditions were activated by CD3/CD28 (1.5/2.5μg/mL) plate bound activation. Both vehicle control and C24 treated samples were kept under Treg differentiation conditions; Treg IL-2: 46ng/ml and TGFβ: 10ng/ml over 5 days *in vitro* ceramide treatment.

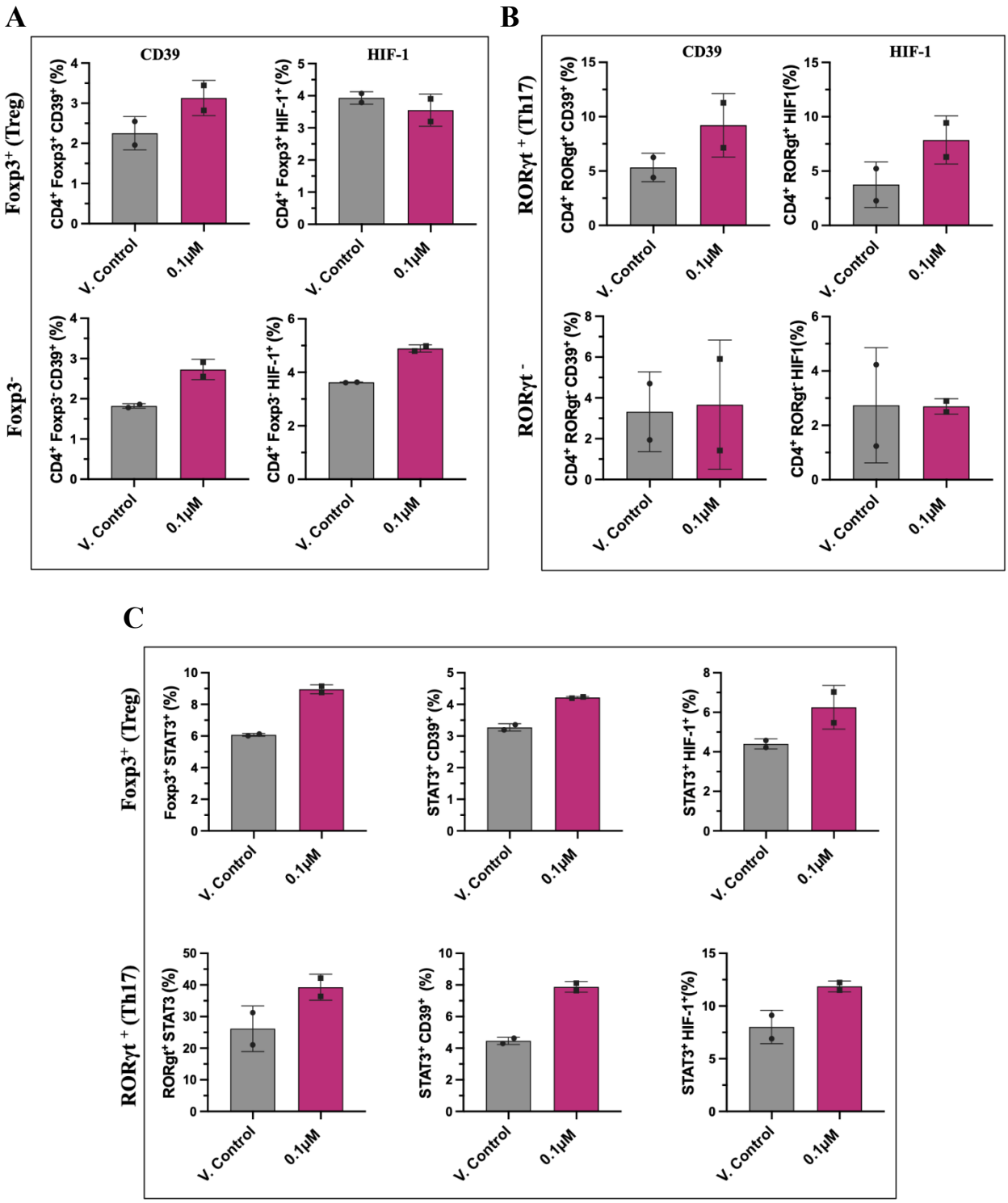


Figure 4.28) Exogenous C24 0.1μM increases the CD39, STAT-3 and HIF-1 expression specifically within RORγt$^+$ Th17 CD4$^+$ T cells even under Treg differentiation conditions

Quantification of **(A)** CD39, HIF-1α within the human Foxp3$^+$ Tregs and **(B)** RORγt$^+$ Th17 CD4$^+$ T cells populations and **(C)** frequencies of CD39$^+$, HIF-1α$^+$ and STAT-3$^+$ cells, gated within the human Foxp3$^+$ Tregs and RORγt$^+$ Th17 CD4$^+$ T cells populations. Both C24 (0.1μM) treated and untreated vehicle control groups were activated by CD3/CD28 (1.5/2.5μg/mL) plate bound activation and kept under *in vitro* Treg differentiation conditions (IL-2: 46ng/ml and TGFβ: 10ng/ml). (n=2 with 2-3 technical replicates per individual experiment, naïve CD4$^+$ cells isolated from human PBMCs).

Although this data is limited with only two biological replicates, it suggests a promising upward trend in CD39/STAT-3/ HIF-1α with C24 treatment specifically observed with RORγt$^+$ Th17 populations. The positive association observed between RORγt$^+$ Th17 and CD39/STAT-3/HIF-1α linked secondary Th17 differentiation mechanism appears highly interesting.

4.11 Discussion

In this chapter, we have investigated WD-derived bioactive lipid species as potential key drivers of the pro-inflammatory immunomodulations observed within 3-week early-DIO murine model in **Chapter 3**. A comprehensive lipidomic profiling analysis on murine models fed with CD, WD and WD+n-3PUFA diets, identified key lipid mediators of the immune profiles reported.

It is known that ceramides accumulate within various peripheral tissues due to excessive availability of SFAs (such as palmitate) within the obesogenic diets, oxidative stress, hypoxia and inflammation linked with DIO [81, 135, 137, 174]. Consistently, WD was shown to significantly increase the total ceramide concentrations specifically in peripheral fat tissues and systemic plasma of the early DIO murine model (**Figures 4.2 & 4.3**). More importantly, distinct long-chain ceramides (C23 and C24) were elevated with the WD whereas, supplementation of n-3PUFA reduced these bioactive ceramides back to CD control levels. This was highly important as the long-chain ceramide species (C16-C26) was shown to accumulate in various cell types and compartments leading to various detrimental effects linked with obesity and associated diseases [137, 356]. In a clinical study on non-diabetic obese women with hepatic steatosis, C24:1 levels were detected to be significantly elevated in inflamed subcutaneous adipose tissue [137, 526]. Another obese cohort also identified a significant upregulation of total ceramides and long-chain ceramides within the subcutaneous adipose tissues, suggesting adverse effects of C24 obesity-associated chronic inflammation [355].

4.11.1 *In vivo* inhibition of C24 alleviated the Th17/Treg CD4$^+$ T cell balance

To validate the critical role of long-chain bioactive C24 as the key immunomodulator of the pro-inflammatory immune phenotype observed in our 3-week early DIO murine model, we utilised FTY720 pharmacological inhibitor of the CerS2 enzyme. Consistently, we inhibition of long-chain ceramides including C23 and C24 by CerS2 inhibition (**Figure 4.4**) [139, 157,

158, 527]. Although compensatory effects between different CerS enzymes and ceramides (C16) was previously recorded in the literature, we did not detect any compensatory increase in the plasma ceramide levels [137, 141]. However as previously highlighted, similar to other pharmacological inhibitors available, FTY720 illustrated various unintentional off-target effects, especially on adaptive immune cells. Importantly, a few non-target long-chain ceramide species (C26 and C18) were also reduced as a potential off-target effect of FTY720 by inhibiting the CerS1 as suggested by the literature [139, 156, 157].

Following the confirmation of C24 inhibition in the WD-fed FTY720 inhibitor group, we investigated any alterations in the immune phenotype and specifically alterations in the effector $CD4^+$ T cell populations compared to the WD-fed PBS injected control group. FTY720 is known to be an immunosuppressive drug used to treat inflammatory diseases due to its ability to limit the egress of T lymphocytes from lymph nodes by inhibiting the homing receptors (CCR7 or CD62L) [156, 159, 160]. The FTY720 treated group illustrated a significant reduction in total $CD4^+$ and $CD8^+$ T cells in SLOs (**Figure 4.5**) alongside a specific depletion in naïve and CM T lymphocytes within the SLOs (**Figure 4.6**). Consistently, FTY720 is known to specifically deplete the naïve and CM T lymphocytes in peripheral SLOs due to the inhibitory effect of FTY720 on homing receptors [160, 163, 528-530]. Previous publications illustrated no significant effect of FTY720 on EM populations whereas, various publications also recorded a relative increase of EM and TEMRA in peripheral tissues and SLOs considering the reduction in naïve and CM frequencies [528, 530, 531]. Consistently, our 3-week WD-fed FTY720 injected murine model expressed an increasing trend of EM T cell populations in some SLOs and fat tissues (**Figures 4.6**). Altogether, our results support the literature and illustrated consistent trends with the FTY720 injected models in the literature, considering the ratios between naïve, CM and EM $CD4^+$ T cell populations [163, 528-530].

Importantly, we have illustrated that 'selective' inhibition of CerS2 and C24 synthesis failed to reduce the pro-inflammatory functional EM T cell markers (CXCR3 and LFA-1) in both $CD4^+$ and $CD8^+$ T cells within the tissues tested (**Figure 4.7**). However, this data also suggested that the inhibition of C24 does not account for the WD-induced upregulation in pro-inflammatory functional EM T cell populations as previously observed in **Figure 3.11**.

It has been recently suggested that inhibition of the S1P-ceramide synthesis pathway can modulate the differentiation of Th17/Treg $CD4^+$ T cell fates [532, 533]. Consistently, FTY720

CerS2 inhibitor model illustrated a significant reduction motif recorded in RORγt$^+$ Th17 and a concomitant increase in Foxp3$^+$ Treg populations within the SLOs of the FTY720 inhibitor group. Interestingly, a S1P-knockout murine model was also shown to reduce the Th17 CD4$^+$ T cell frequencies in lung, colon and LN tissues and significantly increased the Treg populations [534]. Consistently Liao et al., also illustrated the enhancing effect of S1P in the genesis of Th17 population [532]. This publication also suggested that the immunosuppressive effect of FTY720 is not only related to the egress of CD4$^+$ T cells but also the direct inhibition of Th17-mediated inflammation [532]. Consistently, human MS patients received FTY720 inhibitor were shown to significantly elevate the Foxp3$^+$ Treg populations within the plasma [534] and a significantly reduce RORγt$^+$ Th17 CD4$^+$ T cell frequencies [533]. It is also suggested that FTY720 can potentially affect the differential retention of specific effector T cell subsets such as Treg, Th2 and Th17 [537].

However, the exact mechanism of how S1P inhibition by FTY720 can modulate the Th17/Treg differentiation is still unclear. Interestingly, Eken et al. 2017 illustrated that specific deletion of S1P from murine naïve CD4$^+$ T cells did not affect the differentiation of the cells towards Foxp3$^+$ Treg fate *in vitro*, which highlighted that the immunomodulatory effect is not driven by S1P per se [534]. This observation was important as it suggested that there are other systemic effects of FTY720 such as inhibiting the bioactive ceramide synthesis pathways alongside inhibiting the S1P-linked ceramide synthesis pathway.

Importantly, consistent with our dataset, recent publications also illustrated the profound anti-inflammatory effect of FTY720 via inhibiting the pro-inflammatory ceramide synthesis [535, 536]. Recently, Rivas et al. illustrated FTY720 alleviating the inflammatory effects of palmitate in skeletal muscle tissues by inhibiting the accumulation of ceramides [536]. Additionally, various other publications also recorded a similar reduction in Th17 and elevation in Treg CD4$^+$ T cell populations by using other ceramide synthesis inhibitors targeting different enzymes on different ceramide biosynthesis pathways [366, 367, 524, 537]. Zhang et al. 2013, reported that inhibition of the ASM via desipramine lead to a significant increase in Foxp3$^+$ Treg and a concomitant decrease in Th17 CD4$^+$ T cells in alleviating the allergic rhinitis murine model [537]. Additionally, inhibition of ASM and ceramide biosynthesis (salvage pathway) shown to significantly increase the Foxp3$^+$ Treg frequencies in a human cohort going through an antidepressant treatment [524].

4.11.2 *In vitro* C24 treatment enhanced the RORγt$^+$ Th17 differentiation with concomitant inhibition of Foxp3$^+$ Treg differentiation of naïve human and murine CD4$^+$ T cells

Following one of the open questions in the literature, we investigated the direct immunomodulatory effect of the C24 specifically in the differentiation process of CD4$^+$ T cells *in vitro* monoculture tested on both murine and human naïve CD4$^+$ T cells.

Importantly, we conducted an extensive literature research to select and optimise the concentrations of bioactive ceramides and cytokines (IL-2 and TGF-β) used for the *in vitro* CD4$^+$ T cell differentiation protocol (**Table 2.9.3**) [351, 357, 368, 372, 377, 378, 501, 538, 539].

Our dataset illustrated that the *in vitro* treatment of bioactive C24 at physiological concentrations (0.1μM) as detected in the WD-fed murine model, leads to a significant reduction in Foxp3$^+$ Treg differentiation (**Figure 4.13**). Simultaneously, treatment with 0.1μM of C24 induced a concomitant increase in the differentiation of pro-inflammatory RORγt$^+$ Th17 effector CD4$^+$ T cell phenotype even under Treg differentiating *in vitro* conditions (**Figure 4.14**). This observation was highly important as it recapitulated the same pro-inflammatory immune phenotype that has been observed within the WD-fed murine *in vivo* dataset (**Figures 3.9 & 3.17**). Importantly, following the isolation of naïve cells a group of cells were left undifferentiated for the duration of the cell culture in order to obtain the background Foxp3$^+$ Treg percentage due to any undesirable biological variance.

4.11.3 Secretory profile and capacity of *in vitro* C24 treated CD4$^+$ T cells

We have also investigated the secretory capacity and profile of the *in vitro* ceramide-treated CD4$^+$ T cells under the Treg differentiation protocol. Importantly, the reduction trend in IL-10 production and IL-10-producing CD4$^+$ T cell frequencies following the PMA/INO stimulation also revealed the modulatory effect of C24 (0.1μM) on cytokine production capacity and cytokine secretion profile of the CD4$^+$ T cell, consistent with Foxp3 expression and total IL-10 cytokine level within the cell culture.

Importantly, we have utilised both ELISA and flow cytometry methods for quantifying the secreted cytokines and to detect the production of the given cytokine within the cell respectively [540, 541]. According to the literature, both methods have different advantages and technical limitations which were taken into consideration [518, 540, 541].

ELISA quantified the total cytokine concentration secreted by the $CD4^+$ T cells into *in vitro* cell culture. Considering that our experimental protocol consisted of differentiating $CD4^+$ T cell monoculture, it can be rightfully assumed that any detected cytokine is secreted by the $CD4^+$ T cells, eliminating any potential background signals.

However, quantifying the cytokine concentration in the cell culture does not provide detailed information on the single-cell level and the secretory capacity of cells [540, 541]. This was also crucial for our experimental setup, as the residual reduction in IL-10 concentration within media of the C24 0.1μM group could have been due to the total reduction in total $Foxp3^+$ Treg differentiation cells as detected. To evaluate further, we have utilised intracellular cytokine staining (ICCS) by flow cytometry which is a premier technique for investigating the cytokine profile and the secretory capacity at the single-cell level [540, 541]. As previously mentioned, PMA/INO activation is shown to be the most efficient stimulus to induce cytokine secretion of *in vitro* $CD4^+$ T cells before ICCS. It should be noted that ICCS can detect intracellular cytokine production at a specific time point based on the stimulation with PMA/INO. Therefore, we have analysed the intracellular cytokine accumulation following 4hrs of PMA/INO stimulation [540]. The ICCS enabled us to detect the intracellular cytokine production before secreted into the media following the PMA/INO stimulation demonstrating the cytokine expression capacity at single-cell level. We have analysed the data to demonstrate both the percentage of the cells producing the given cytokine and the average relative amount of cytokine produced by population (MFI). Altogether, these factors illustrate the importance to perform at least two different cytokine detection assays to validate the observations.

4.11.4 Molecular mechanism of bioactive C24 inducing Th17 differentiation

Consistent with our hypothesis and preliminary *in vivo* datasets (3-week DIO and FT720-inhibitor murine models), various recent publications also suggested potential links between long-chain bioactive ceramides and Th17/Treg differentiation. These publications showed the importance of ceramide synthesis and ceramide levels in the differentiation Th17 $CD4^+$ T cell fate [366, 367, 524, 537, 542]. The common observation between the publications was the profound reduction in $ROR\gamma t^+$, IL-17 and Th17 frequencies with the inhibition of ceramide synthesis observed at multiple levels [366, 367, 524, 537, 542]. Recently, a comprehensive quantitative genome-scale metabolic modelling coupled with multiomics dataset on human $CD4^+$ T cell demonstrated the crucial role of ceramide synthesis pathways in modulating the

Th17 differentiation and IL-17 expression [543]. In line with our publication, Sen at al. 2021 elegantly illustrated the dynamic regulation of distinct bioactive long-chain ceramides (C18-24) in early stages of human $CD4^+$ T cell differentiation where lipidome and metabolome dataset highlighted the ceramides as the key 'indicator and modulator' of the human Th17/Treg differentiation process [543].

However the exact immunomodulatory mechanisms or molecular pathways are still vague. Although a few potential mechanisms has been suggested in the literature, the most commonly suggested one is ceramides modulating T cell differentiation through the modulation of T-cell activation [357, 366, 495, 544]. However, the background literature involved various disparities like Shin et al. 2021, suggested a downregulation of TCR activation whereas various publication suggested an upregulation of T-cell activation with ceramide accumulation [357, 366, 369, 495, 522, 544]. Interestingly, we did not observe any significant difference with the C24 treatment in the activation of central core TCR molecular components; Zap-70 and LCK (**Figure 4.23**). However, we have observed a significant reduction in the activation of key downstream components of activation pathways (Akt and Erk) (**Figure 4.24**). Importantly, this data illustrated the C24 does not induce a direct modulation of the core, early proximal signalling TCR components but modulate the downstream signalling pathways.

It is recently shown that besides main Th17 differentiation pathways; IL-6/IL-6R pathway, the CD39/ceramides/STAT3/mTOR signalling cascade are critical in defining $ROR\gamma t^+$Th17 differentiation [494-496]. In line with our i*n vivo* and *in vitro* observations on the Th17/Treg balance, Bai et al. illustrated the critical STAT3/mTOR pathway that is mainly driven by bioactive ceramides in inducing Th17 differentiation [494-496].

Recent publications on the critical contribution of CD39, inducing the STAT-3 and mTOR signalling cascades to drive $ROR\gamma t^+$ Th17 differentiation and inhibit $Foxp3^+$ Treg differentiation [368, 494-496]. Consistent with this literature and our hypothesis, we demonstrated that 0.1µM C24 treatment directly enhances the Th17 differentiation and inhibits $Foxp3^+$ Treg fate via potentially upregulating the CD39, mTOR/STAT-3 and HIF-1α signalling pathway [494-496]. Consistently, bioactive ceramides are known to directly activate the STAT-3, mTOR and HIF-1α TFs via inducing the phosphorylation and inducing the binding of these TFs to the target promoter regions in various cell types [368, 369, 494, 496, 545, 546]. Importantly as previously detailed, HIF-1α is a key metabolic sensor that regulates various critical pro-inflammatory pathways including Th17 $CD4^+$ T cell differentiation [490, 547-549].

It is also shown that HIF-1α can transcriptionally activate the RORγt^{+} leading to Th17 differentiation and simultaneously inhibit the Treg differentiation by causing the proteasomal degradation of Foxp3 [490].

Importantly, STAT3 and HIF-1α are key TFs that are known to induce the expression of each other, also known as the "Warburg's vicious circle" [550]. The constitutive activation between STAT3 and HIF-1α shown to drive a chronical Th17 phenotype with exaggerated IL-17 secretion and metabolic switch of aerobic glycolysis [550-552]. Importantly, observation of no modulation in IL-6 levels and the downregulation of Akt and Erk activation suggested that the C24-induced Th17 differentiation is not raised directly from TCR-induced 'classical' Th17 differentiation pathway but induced mainly by the secondary CD39/STAT3/HIF-1α pathway. There are two known regulatory pathways that ceramides can inhibit the activation of Akt and Erk; (1) via the recruitment of protein kinase C, inhibiting the activation and translocation of Akt and (2) via the activation of protein phosphatase 2A, known to dephosphorylate Akt [553, 554]. Based on our *in vitro* dataset, C24 potentially overrides the 'classical' pathway by inhibiting the strong TCR signalling of PI3K/Akt and preventing the potential induction of Foxp3 while driving the cell towards RORγt expression via directly enhancing the STAT3 and HIF-1α activation. Considering this background literature, it was highly important to detect a upregulation of HIF-1 with C24 treatment specifically in RORγt^{+} Th17 alongside the elevation of CD39 and STAT-3 (**Figure 4.28**). Therefore, our data illustrates the potential molecular mechanism of CD39, mTOR/STAT3 and HIF-1α driven by C24, leading to the expansion of Th17 alongside attenuating the Treg differentiation. **Figure 6.2** illustrates the summary of main findings of our dataset and the proposed immunomodulatory molecular mechanism of the bioactive C24 on Th17/Treg differentiation.

4.10.5 Systemic effect of n-3PUFA supplementation

The direct supplementation of n-3PUFA into WD leads to a significant alleviation of the WD-induced pro-inflammatory phenotype specifically shown to re-establish the depleted Foxp3^{+} Treg population as well as a concomitant reduction in pro-inflammatory RORγt^{+} Th17 T cell populations detected within specific SLOs (**Figures 3.9, 3.14, 3.17-3.18**). The anti-inflammatory potential of n-3PUFA with inhibition of pro-inflammatory (Th1 and Th17) and boosting the anti-inflammatory (Treg) CD4^{+} T cells were previously discussed in **Chapter1** [341, 407, 475, 555, 556]. This chapter suggested two anti-inflammatory actions of n-3PUFA

in alleviating the OIIM, (1) by direct inhibition of RORγt^{+} Th17 differentiation and (2) by indirect inhibition of deleterious pro-inflammatory ceramide synthesis.

In line with our dataset, n-3PUFA species were shown to blunt the Th17 differentiation of both human *ex vivo* and murine *in vivo* CD4^{+} T cells as illustrated by the literature [408, 557, 558]. Although the exact mechanism is not fully understood yet, it has been suggested that n-3PUFA can downregulate Th17 differentiation by inhibiting the critical components of T cell differentiation pathways including mTOR, STAT3 and NF-κB [325, 559-561]. Consistent with Kong et al. we did not observe any significant elevation in Foxp3 expression in n-3PUFA treated CD4^{+} T cell monoculture whereas, this publication reported a significant increase in Foxp3 with the n3-PUFA treated cells only within a DC coculture [562].

Furthermore, consistent with the literature, we have observed a systemic effect of n-3PUFA by inhibiting pro-inflammatory ceramides via downregulating *de novo* pathway enzymes (CerS and DES) within the key hotspots of ceramide synthesis like fat tissues (**Figures 4.2-4.3**) [119, 126, 408, 563]. Background literature on human cohorts, suggested that the replacement of palmitate or high-fat within the diet with PUFAs can reduce the circulating ceramide levels [564-566]. More recently, n-3PUFA has been suggested to ameliorate the ceramide-induced lipotoxicity in metabolic syndrome [567]. Additionally, a few publications suggested that n-3PUFA can directly inhibit the synthesis of distinct ceramide species where this inhibition in pro-inflammatory ceramide groups alleviates the obesity-linked pathologies associated with ceramide accumulation [119, 568]. Dong et al. 2017, illustrated that n-3PUFA supplementation to the diet was able to significantly reduce the ceramide synthesis via the inhibition of the gene expression of sptlc3 and Degs2 enzymes in a hepatic steatosis murine model [119]. This limited background literature has is further supported our observations suggesting that n-3PUFA can potentially induce an anti-inflammatory effect via regulating the deleterious ceramide levels. Altogether, these ameliorative effect of n-3PUFA on Th17/Treg populations illustrated a critical therapeutic potential in obesity-linked inflammatory diseases like arthritis [325, 341, 407, 408, 569].

4.11.6 Limitations and additional experimental plans

Background literature highlighted the multifactorial bioactivity of ceramides on various biological factors. Considering our dataset, it should be noted that the analysis and the

interpretation of the data were handled very cautiously and examined within the literature to avoid any over-interpretation. Considering the challenges and the technical limitations during the project there are a few factors that would be interesting to further evaluate.

Although an extensive literature research was undertaken to select the most suitable commercially available CerS inhibitor, our *in vivo* lipidomic assay suggested potential off-targets effect of the FTY720. Considering this, it would also be pertinent to measure the gene expression levels of other CerS enzymes within tissues (liver) obtained from the FT720 group. Furthermore, considering the modulations observed in $CD8^+$ T cell populations within the previous 3-week early DIO murine model we aimed to investigate the same markers within the FTY720-inhibitor *in vivo* experiment however, due to technical issues, we did not obtain any staining of $CD8^+$ T cells. Additionally, considering the modulations observed in cytokine levels and cytokine secretion capacity within the *in vitro* $CD4^+$ T cells, it would be interesting to evaluate the cytokine secretion capacity *ex vivo*.

Additionally, it would be very interesting to test this pro-inflammatory immunomodulatory action of bioactive C24 on different differentiation conditions such as the Th17 differentiation *in vitro* model. Considering the background literature, we could investigate cell-cell interactions in co-culture experiments with key cell types like APCs. These experiments will enable us to investigate other potential indirect immunomodulatory actions of C24 on $CD4^+$ T cell differentiation and activation.

It should be noted that the dataset on the CD39, HIF-1α and STAT3 molecular mechanism of C24 is created with only 2 biological replicates (n=2), we need to increase the n number to be able to conduct statistical analysis. It would be very interesting to further investigate this mechanism, at gene expression (qPCR) and protein (western blot) levels.

Following the immunomodulations observed on Th17/Treg fates, it would be interesting to test the immunosuppressive capacity and the metabolic changes of $CD4^+$ T cells following the bioactive C24 treatment *in vitro* and *in vivo*. Background literature suggests that long-chain ceramides can induce the cellular metabolism towards glycolysis and lipogenesis (required for Th17 differentiation) [486]. Contrarily, Treg differentiating $CD4^+$ T cell metabolism has shown to upregulate oxidative phosphorylation [486]. It would be pertinent to measure various key markers associated with the immune suppressive capacity of Tregs like Tim-3 and CTLA-4.

Chapter 5) HFD-induced long-lasting epigenetic changes alters the autophagy and senescence in EM T cells of formerly obese mouse model

5.1. Introduction

The importance of T cells in obesity and OIIM has been well shown in the literature and detailed within the previous chapters of this thesis [18, 301, 383, 385, 386, 435, 570]. Previous publications from our group have reported that HFD-feeding biases the T cells by expanding pro-inflammatory EM $CD4^+$ T cells ($CD44^+CD62L^-$, $CXCR3^+$ or $LFA1^+$) when challenged by an allogeneic immunisation [18]. The importance of $CD44^+$ $CXCR3^+$ and $LFA1^+$ EM populations in murine and human OIIMs were previously detailed in **Chapter 3.1** [18].

Recent background literature has suggested that immune cells can undergo 'obesogenic memory or reprogramming' where cells retain the HFD-induced pro-inflammatory phenotype and promote OIIM and weight regain even after the weight loss [262, 301, 571-574]. Initially, this obesogenic reprogramming has been suggested to be present within adipose tissues and adipose tissue-resident innate immune cells [571, 574]. For example Schmitz et al. 2016, demonstrated that weight loss can induce an ameliorative effect on liver tissue homeostasis but, DIO-linked inflammation is retained in adipose tissues [571, 575]. Consistently, Zou et al. 2018 demonstrated that, this 'obesogenic reprogramming' is not dependent on hyperphagia, physiological or metabolic changes but considerably mediated by $CD4^+$T cells [301]. Although there are various discrepancies in the field, it is well shown that the 'obesogenic memory/reprogramming' can occur in various tissues and the weight loss can only provide a partial amelioration of OIIM certain tissues [571, 576, 577]. Therefore it is crucial to investigate the molecular mechanisms underpinning this long-lasting, persistent 'obesogenic reprogramming' phenotype specifically in T-cells [571-574].

Specifically, Sougiannis et al. utilised a WGWG murine model that demonstrated a significant elevation in pro-inflammatory "M1" macrophages and cytotoxic $CD8^+$ T cell populations within the fat tissue of formerly-obese mice [578]. Additionally, pro-inflammatory CD8-associated cytokines like TNFα and IFN-γ, were significantly elevated within the formerly-obese group [578]. Along with few other publications, Sougiannis et al. 2020, have suggested HFD-induced obesity promotes the imprinting of 'obesogenic

memory/reprogramming' within the T cells towards a pro-inflammatory state which is retained even after the weight loss [301, 570, 579]. Interestingly, it is also suggested that the obesity-driven 'obesogenic reprogramming' of $CD4^+$ T cells can directly promote the OIIM and mediate weight regain in murine models following a weight loss[301]. This $CD4^+$ T cell-mediated obesogenic memory is also suggested to play a critical role in human obesity and associated pathologies considering that majority of the formerly obese patients are shown to regain the weight within 2 years post weight loss [571, 575, 580-582]. Moreover, this retention of HFD-induced obesogenic priming effect within immune cells may potentially increase the risk of obesity-associated inflammatory diseases later in life even after weight loss [583-586]. Therefore, it is critical to understand the molecular mechanisms leading to this HFD-induced long-lasting obesogenic memory/reprogramming and its subsequent implications.

It has been suggested that the content of HFD enriched with deleterious lipid groups can lead to metabolic and epigenetic alterations of immune cells, leading to the dysregulated, pro-inflammatory immune response in OIIM [430, 570, 575]. On the other hand, weight loss can ameliorate the metabolic profile of immune cells, the obesogenic reprogramming of the immune cell functionally persists and can directly induce pro-inflammatory modulations even after the weight loss [301, 432, 571, 575, 585]. Consistently, long-term adoptive persistency of the obesogenic reprogram on T cells induced by past-HFD exposure, provided further evidence for the involvement of epigenetic modifications like DNA methylation [432, 585, 587-590]. Although the exact mechanism of how HFD can directly induce a long-term, persistent epigenetic modification, especially in the pro-inflammatory obesity-linked T cell phenotype is still unclear, bioactive lipid groups are suggested as key mediators. In line with our dataset, recent publications demonstrated novel observations on direct epigenetic alterations induced by bioactive lipid groups within the HFD, altering the transcription profile of the immune cells and leading to long-term functional alterations [379, 432, 570, 579, 585, 589].

5.1.1 Bioactive lipid groups

Previous publications suggests PA is an effective bioactive driver of the HFD-induced pro-inflammatory EM phenotype observed in $CD4^+$ T cells. Mauro et al. 2017, identified bioactive PA as the key modulator where direct *in vitro* PA exposure to $CD4^+$ T cells induced the activation of PI3K p110d-Akt-dependent pathway and led to the HFD-induced EM priming effect [18]. As previously detailed in **Chapter 1**, PA is the most common SFA in the body

accounting for more than 30% of the total FAs in the blood [76]. But more importantly, PA accumulation within the blood alongside increasing lipolysis has been observed in both ageing and obesity [311]. Interestingly, recent publications have illustrated a direct, deleterious memory/reprogramming of various cell types via direct epigenetic modifications driven by PA and other bioactive SFAs [88, 591]. Publication by Hall et al. 2014, firstly suggested a long-lasting epigenetic modification driven by PA. *In vitro* exposure of healthy human pancreatic β-cells to PA (48-hrs) induced a significant and persistent modulations in DNA methylation of critical genomic regions (promoters and CpG islands) [88]. These regions were then shown to alter the genome-wide mRNA expression of 290 genes [88, 592]. More recently, direct *in vitro* exposure of human Schwann cells to bioactive PA (50 μM) caused a long-term stable transcriptional alteration via direct alteration of DNA methylation profiles, promoting metastasis and inducing a 'metastatic memory' [379]. Consistently Pascual et al. 2021 also illustrated that the lipid metabolism and metabolic changes per se did not completely elucidate the metastatic aggressiveness of the PA-treated cells [379]. Moreover, the epigenetic alterations on the DNA methylation profile directly mediated by PA were also shown to regulate macrophage polarisation towards a pro-inflammatory M1 phenotype within OIIM [593]. *In vitro,* exposure of bone-marrow-derived macrophages to PA and STE were shown to directly elevate the DNA methylation of CpGs, leading to polarisation bias towards the pro-inflammatory M1 phenotype [593].

Importantly, Wang et al. 2016 also suggested deleterious effects of STE SFAs similar to PA. More specifically, the STE was shown to directly induce pro-inflammatory reprogramming of macrophages via directly altering the DNA methylation configuration [593]. Consistently Sehgal et al. 2023 further confirmed the critical mediator roles of both PA and STE SFAs in DNA methylation of the CpGs where they also reported an association between the SFA contents of the liver and the hepatic DNA methylation in obese individuals [594]. In line with this, a recent publication by Hata et al. 2023, identified STE as a critically bioactive deleterious-mediator that can directly induce long-lasting alterations in DNA methylation profiles of macrophages [585]. STE-induced methylation configurations were shown to drive macrophages towards an inflammatory phenotype as in obese conditions, even after weight loss [585].

Contrary to the bioactive deleterious SFAs, OA is shown to exert beneficial effects including altering membrane fluidity, intracellular signalling pathways and gene expression as previously discussed in **Chapter 1**. Altogether, these beneficial physiological effects of OA induce an ameliorative effects on the OIIM [321]. Although the exact mechanism of OA in

alleviating the OIIM is not fully defined yet, various mechanisms are suggested including the induction of anti-inflammatory Treg subsets and enhancement of antioxidants and anti-inflammatory cytokines [321, 595]. Importantly, bioactive OA is also suggested to induce these anti-inflammatory immunomodulatory effects inducing anti-inflammatory epigenetic modulations on immune cells [321, 595-598]. Pompura et al. 2020, demonstrated the capability of bioactive OA in inducing direct alterations in the DNA methylation status of thymic T-cells, leading them towards $FOXP3^+$ Treg fate [596, 597]. OA-induced modulations in methylation structure prompted an elevation of the Foxp3 expression which elevated the Treg population and enhanced the suppressive capacity of Tregs within the MS patients [595, 597].
Considering the recent literature developing around the idea of 'obesogenic immune memory/reprogramming' we have hypothesised that HFD-derived distinct bioactive lipids can induce epigenetic imprinting during obesity which then can persist even long-after the weight loss and lead to long-lasting functional pro-inflammatory predispositions of T cells.

5.1.2 Autophagy in T cells under obese conditions

Autophagy is one of the main evolutionarily conserved cellular catabolic functions that maintain cellular homeostasis by mediating the 'degradation and recycling' of the damaged intracellular molecules and organelles [599, 600]. Dysfunction of autophagy has been long associated with age- and obesity-related diseases such as cancer, T2D and CVDs [599, 601]. Although autophagy is a highly dynamic and complex process, the core pathway involves the formation of double membrane vesicles called autophagosomes which engulf cytosolic content and fuse with lysosomes for the degradation, releasing ATP and other macromolecules [599, 600, 602] (**Figure 5.1**). Autophagy is known to be mediated by two upstream nutrient-sensing pathways; mTOR and AMPK alongside other fundamentally important intracellular mediators such as autophagy-related (ATG) proteins and microtubule-associated protein light chain 3 (LC3) proteins.

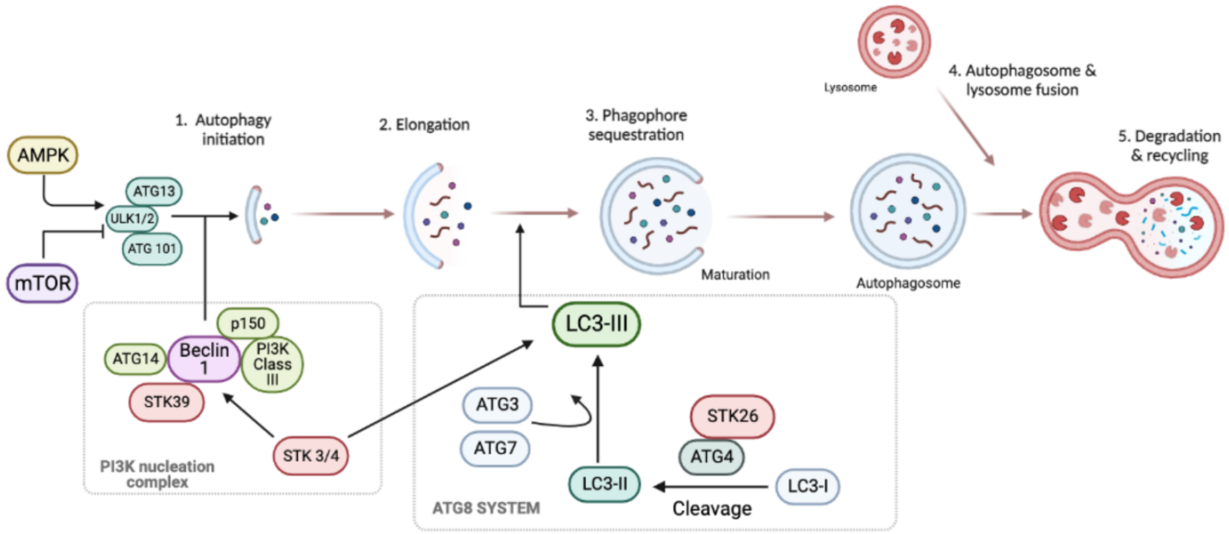


Figure 5.1) A schematic of the main canonical autophagy pathway. Autophagy signal is generally induced by cellular or metabolic stress such as starvation, hypoxia, ROS, DNA and organelle damage which induces the activation of AMPK and/or mTOR metabolic sensors. Activation of AMPK acts as an activator whereas activated mTOR acts as a negative regulator of the autophagy activation. Once the autophagy is activated various autophagy-related proteins gets activated initiating from the Unc-51-like kinase 1/2 (ULK1/2) initiation complex including ATG13 and ATG101. Simultaneously, activation of PI3K nucleation complex compromised of Beclin-1, p150, ATG14 and STK39 is required to induce the formation of cup-shaped structure known as phagophore[603]. Importantly, STK3/4 kinases also shown to play a crucial role in inducing autophagy by both directly phosphorylates LC3 at threonine 50 (Thr50) and also activating the Beclin-1 complex. In the elongation process the formation of LC3-I initiates with the cleavage of LC3 by Atg4 protease, creating the cytosolic LC3-1 form. The STK26 (MST4) protein kinase is shown to be crucial in upstream activation of Atg4 [604]. LC3-I is then conjugated to phosphatidylethanolamine (PE) by Atg7 and Atg3, creating the LC-III form. On the PE conjugated into the LC3-III complex can directly incorporated into the autophagosomal membrane before the phagophore sequestration and formation of mature autophagosome. Following the formation of mature autophagosome with the cytosolic cargo, it fuses with lysosome for the total degradation and recycling process. Figure structure adapted from Hansen et al. 2018 [600].

Autophagy is generally induced by cellular and metabolic stress including starvation, hypoxia, ROS, DNA and organelle damage. The type, dose and duration of the inducer stress is shown to be critical in defining the functionality of the autophagy which is highly complicated and not fully understood considering the dynamic nature of autophagy [599]. Autophagy is suggested to play a critical role in obesogenesis and obesity-linked diseases by modulating cellular metabolism including lipid metabolism, cell survival, differentiation and cellular senescence [599]. Although literature demonstrated strong links between autophagy and obesity, the field is highly controversial and contains various inconsistencies, illustrating the complexity of molecular mechanisms linking autophagy and obesity which are not fully understood. Although it is still not clear if autophagy is enhanced or suppressed in obesity, it is

well shown that autophagy is highly dysregulated in obesity potentially due to dyslipidaemia, overnutrition and bioactive effects of lipids [599, 605, 606].

Various background publications reported elevated autophagy levels in adipose tissues and downregulation in the liver, heart and pancreas of both obese humans and murine models [599, 607-612]. However it should be noted that the high discrepancies in the field of autophagy in obesity prevent any reasonable conclusion and emphasise a few points including;

- Autophagy is highly variable between models of obesity,
- Autophagy is highly mediated by genetic predisposition and other environmental factors such as diet
- Autophagy exhibits organ and tissue specificity, illustrating a high variance between tissues of the same obese model
- Autophagy exhibits a high variance with the level of obesity and biological age

Altogether, it is still not fully understood whether the changes in autophagy modulate the progress of obesogenesis (and associated diseases) or whether alterations in autophagy functioning are consequences of obesity [599].

Furthermore, autophagy is known to shape immune profiles under both homeostasis and obesity pathophysiology conditions. Autophagy can facilitate immune activation [613, 614], differentiation [615, 616], immunosenescence [617] and immunometabolism of immune cells including T-cells [599, 618, 619]. Obesogenic-diet-derived bioactive lipids were also suggested to modulate autophagy flux within the immune cells. For example, obesogenic diets and distinct bioactive SFAs (PA) were shown to upregulate autophagy levels in adipose tissue which lead to a significant elevation of pro-inflammatory cytokine expression such as IL-1β, IL-6, and IL-8 within obese individuals and murine models [607, 620]. Contrarily, various publications illustrated a down-regulation of autophagy with lipid overload within T lymphocytes [599, 621, 622]. Guerrero-Ros et al. 2020 illustrated that OA lipid overload inhibits autophagy and leads to a defective T cell response both *in vivo* and *in vitro* models [621].

Therefore, it is highly interesting to investigate immunomodulatory roles of bioactive lipids in mediating autophagy which may also shape various aspects of T cells including activation, differentiation and functioning in the context of obesity [599, 621, 622]

5.1.3 Senescence in obesity pathophysiology

Cellular senescence is another evolutionary conserved phenomenon induced by endogenous and exogenous stresses such as DNA damage, telomere dysfunction, inflammation, and metabolic dysfunctions which leads the cell to an irreversible cell-cycle arrest and acquisition of senescence-associated secretory phenotype (SASP) [435, 570]. One of the main features of senescent cells is the elevated expression of cyclin-dependent kinase inhibitors that play critical roles in senescence accumulation [623]. Senescent cells in general are known to promote degeneration, ageing, chronic systemic inflammation, also known as inflammaging, as well as age-associated pathologies such as CVDs, cancer and autoimmune diseases [623, 624]. This systemic deleterious effects of senescent cells are mainly attributed to the release of pro-inflammatory SASP factors and the dispersion of senescence to non-senescent cells [625, 626].

Importantly, immune cell exhaustion and senescence induced by obesogenic diets and obesity are two critical dysfunctional states that coexist in an OIIM where senescent cells were shown to be highly inflammatory and execrated secretion of SASPs [430, 435, 570, 579, 627]. Senescent immune cells are known to acquire a pro-inflammatory SASPs phenotype mainly consisting of elevated IL-2, IL-4, IL-6, IL-8, TNF, and IFN-γ cytokines [430, 570, 628]. A senescent immune cell is mainly defined with a non-proliferative capacity but excessive pro-inflammatory SASP phenotype leading to immune dysfunction [628, 629]. For example, in human blood terminally differentiated memory also known as Temra ($CD45RO^-$,$CCR7^-$) cell population is the main T cell subset expressesing the characteristics of cellular senescence such as loss of extracellular receptors such as CD28, CD27, CD45RO and re-expression CD45RA alongside the upregulation of PD1 (exhaustion marker) and CD57 (senescence marker) [630, 631]. It is well shown that the Temra cell population accumulates with age as well as chronic inflammatory diseases that makes Temra population pivotal for investigating senescence in T lymphocytes [630, 631].

Although this complex relationship between obesity and immune senescence is documented, the exact drivers of this mechanism are not understood. Background literature suggested that constant oxidative stress (ROS), repeated antigenic stimulation, hypoxia and DNA-damage induced by long-term FA exposure can directly trigger the exhaustion and senescence in immune cells [430, 433, 435, 570, 579, 632] (**Figure 5.2**). More interestingly, similar to the HFD-driven long-term obesogenic memory/reprogramming on pro-inflammatory

EM CD4$^+$ T cell phenotype, HFD-exposure in earlier life was also shown to induce a senescence-associated phenotype on CD4$^+$ T cells of the formerly obese mice.

Interestingly, recent publications suggested that distinct bioactive SFA's are potential drivers of this long-lasting immune senescence phenotype in obesity. For example lIshaq et al. 2022 identified the bioactive PA as one of the main deleterious mediators of the process where direct *in vitro* PA-exposure was shown to induce DNA damage and senescence phenotype in human adipocytes [633].

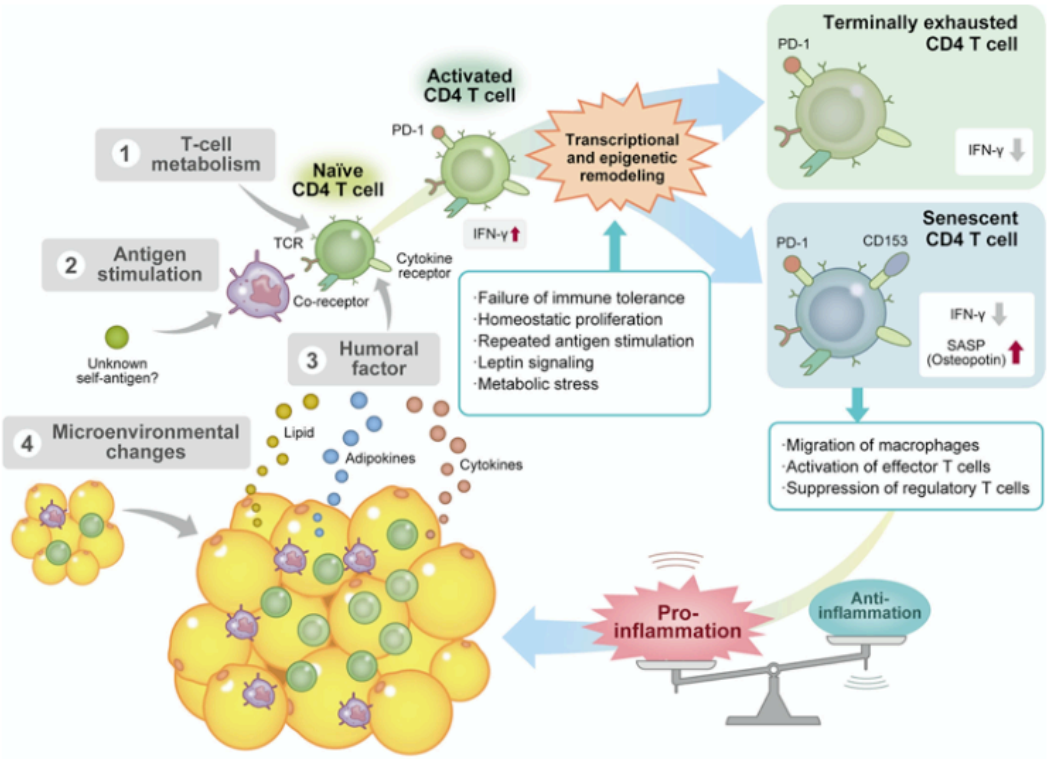


Figure 5.2) Obesity-driven senescence profile on CD4$^+$ T cells
There are various factors known to modulate the differentiation of CD4$^+$ T cells under obese conditions such as 1) modulations in T cell metabolism potentially induced by plethora of lipids in the obese microenvironment 2) constant antigen stimulation triggered by pro-inflammatory APC migrated into the periphery 3) other humoral factors including other pro-inflammatory cytokines and lipids available in the obese microenvironment 4) Overall alterations in the cellular microenvironment. Altogether these factors known to trigger various transcriptional and epigenetic alterations that prompts the differentiation of pro-inflammatory phenotypes and establish the OIIM. This exacerbated OIIM also known to induce immune exhaustion and senescence that also drives the senescence-associated secretory phenotype (SASP). Figure taken from **Shirakawa and Sano, 2023** [570].

5.1.4 Aims and hypothesis

As detailed previously, Mauro et al. 2017 publication on the biasing effect of HFD (8 weeks) on T cells inducing an excessive expansion of pro-inflammatory EM CD4$^+$ T cells

($CD44^+$,$CD62L^-$, $CXCR3^+$ or $LFA1^+$) when challenged by an allogeneic immunisation, formed the basis of this chapter [18]. Following this previous publication, we wanted to further investigate the functionality and impact of these HFD-induced pro-inflammatory EM $CD4^+$ T cell populations specifically after weight-loss. Based on this, we have utilised a **weight gain-weight loss (WGWL)** *in vivo* model where C57BL/6J (4-week old) female mice placed on HFD (60% lipid) for 8-weeks and switched back to CD (standard diet) for 6-weeks to induce a weight loss by diet regime, defined as HFD-Recovery (HFD-RE) (WGWL) model group (**Figure 5.3A**). The other two control groups received a continuous HFD or CD for 14-weeks. Similar to the early-DIO (3-week) murine model and 8-week HFD model, an allogeneic immunisation by i.p injection of allogeneic splenocyte was utilised to induce a polyclonal T cell response and establish T cell memory on week 13. Based on this model, this chapter aims to investigate the following open questions and hypotheses:

- Further investigate the molecular drivers of the pro-inflammatory EM $CD4^+$ T cell phenotype observed in the HFD group.
- Investigate the long-term effects of past obesity and weight loss on the DIO model by phenotyping the weight-gain-weight-loss model, particularly focusing on the pro-inflammatory EM $CD4^+$ T phenotype in different SLOs and fat tissues.
- Based on the preliminary dataset, dissect the underlying mechanism potentially driving the long-term reprogramming/bias in $CD4^+$ T cell EM populations as observed 14-week *in vivo* murine model.
- Identify distinct bioactive drivers of the long-term epigenetic reprogramming on $CD4^+$ T cells inducing an execrated EM phenotype in both *in vivo* and *in vitro* models.
- Identify any functional changes linked with the persistent epigenetic reprogramming of $CD4^+$ T cells that can potentially drive the pro-inflammatory EM T cell phenotype.

Results

5.2. Establishment and characterisation of the *in vivo* 14-week HFD fed DIO murine model T lymphocytes

Conventionally, DIO models are established by feeding the animals with an energy-dense obesogenic diet (HFD or WD) for 4-30 weeks [634-638]. These energy-dense obesogenic diets composed of a high SFA and sugar-content, supply 60% of calorie intake from the fat content- as detailed in **Section 1.3**. Importantly, there are a few common parameters to observe on the DIO murine models including; weight gain, hyperlipidemia (total body fat), visceral adiposity

index, blood pressure, glucose and insulin intolerance [634-637]. Following the background literature, we have investigated the body weight gain index as well as the adiposity index over the 14-week course of the experiment (**Figure 5.3A**) [18, 634-637]. Although all three mice groups progressively gained weight, ad libitum feeding of HFD was observed to significantly increase the total body weight gain percentage (**Figure 5.3B**). Similarly, the HFD-RE group gained weight in line with the HFD until the diet reversal to CD at week 8. The HFD-RE group was shown to significantly lose weight compared to HFD and return to the control (CD) group range (**Figure 5.3B**). Additionally, the 14-week HFD group was also shown to have a significantly elevated weight gain index compared to HFD-RE and CD group on the final body weight measurement (98.day) (**Figure 5.3B**).

It should be noted that, female C57BL/6J mice are known to be more resistant to the obesogenic physiological effects of fat-dense diets potentially as a result of oestrogen [639, 640]. It is shown in the literature that although both male and female mice had a similar elevation in total body weight gain percentage, males tend to gain weight faster than females. Importantly, although the magnitude of weight gain, hyperlipidemia and visceral adiposity index are shown to be different between male and female models, females were shown to wane the earlier difference in expressing DIO-parameters, especially after 11-15 weeks obesogenic diets [639-643]. Consistent with the literature, the HFD group illustrated a significant increase in the visceral adiposity index within both p.fat and s.fat tissues compared to CD at week 14 (**Figure 5.3C**). In line with the literature, the HFD-RE group illustrated a significant reduction in total body weight and visceral fat (p.fat and s.fat tissues), illustrating re-establish of the homeostatic visceral fat index comparable to the CD control group (**Figure 5.3C**). Consistently, it has been demonstrated that reintroduction of CD following HFD leads to weight loss, visceral fat loss and normalisation of other metabolic parameters within a week as recorded in both sexes of DIO murine models [585, 641].

Following the establishment of the 14-week DIO and WGWL models, we phenotyped the different T cell immune subsets within main SLOs (spleen, pLN and mLN) and two fat tissues (s.fat and p.fat). Similar to other *in vivo* experiments presented, we have checked the live/dead, $CD8^+$ and $CD4^+$ T cell subsets and observed no significant difference between different diet groups in all the tissues tested (**Supplementary-Figure S10**).

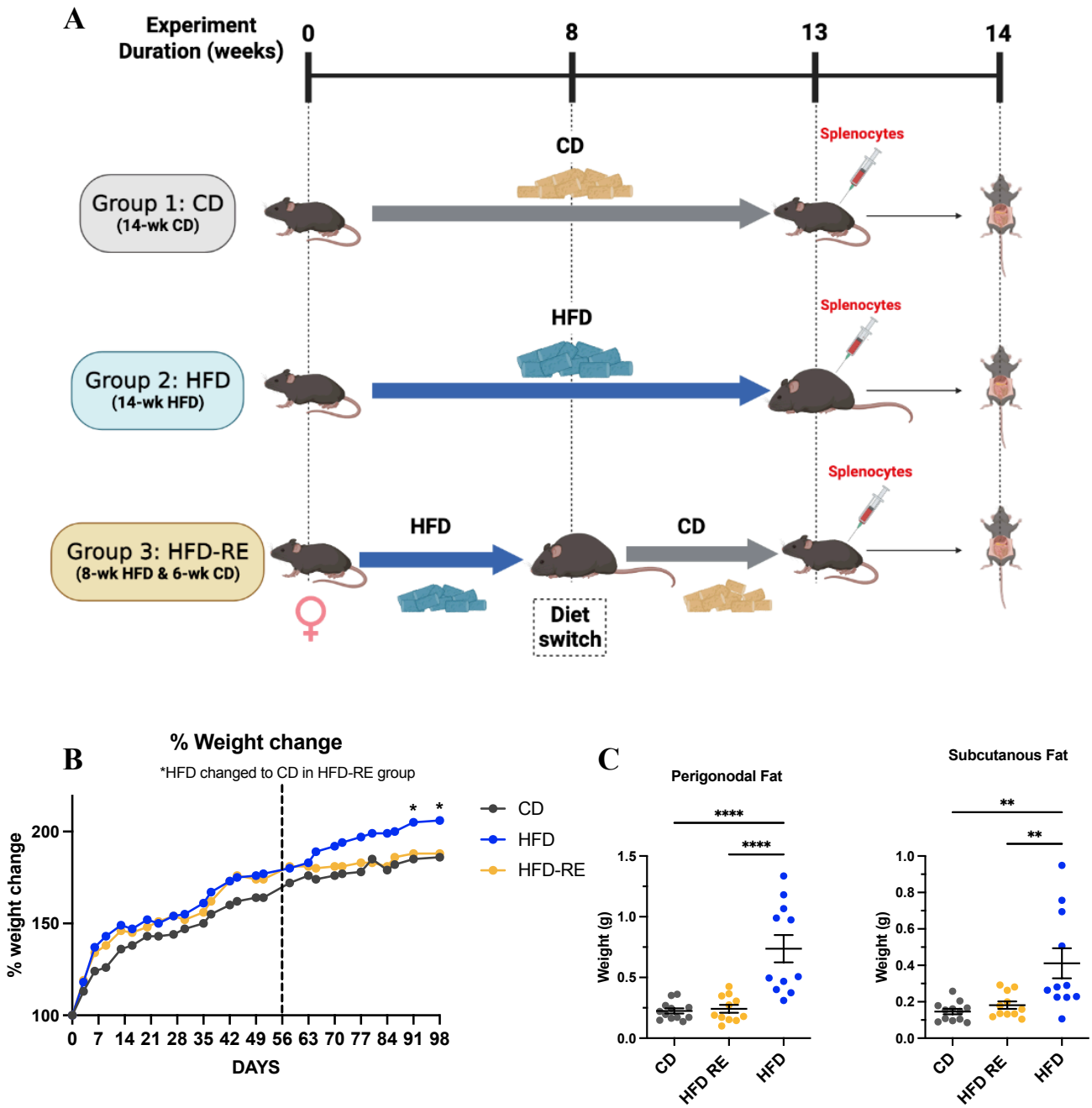


Figure 5.3) 14-week HFD feeding increased the total body weight and fat content in murine model

(A) Experimental schematic illustrating the WGWL *in vivo* experimental protocol on female C57BL/6J mice at age 4-week old. Control group (1) were fed on CD for 14-weeks and group (2) HFD group were fed on HFD for 14-weeks throughout the experiment. The HFD-RE Group (3) were fed on HFD for 8-weeks and switched to CD diet at week 8 for another 6 weeks to induce weight loss. All mice groups were subjected to an allogeneic immunisation at 13.week with CBA and BALB/C splenocyte i.p injection and went through an allogeneic immune challenge for inducing an memory response. **(B)** Body weight change percentage of female WT C57BL/6 mice groups fed with the CD (control), HFD and HFD-RE diet groups over the course of 14-weeks (98days). **(C)** Fat weight in grams as harvested from all three diet groups on the cull days. Two *in vivo* experimental repeats, each diet group; n=12. Data presented as mean ± SEM. Ordinary one-way Anova *P < 0.05, **P < 0.01, ***P < 0.001, ****P < 0.0001.

5.3. HFD induces a persistent bias in CD4$^+$ T cell differentiation towards pro-inflammatory effector memory subset

Mauro et al. 2017 publication illustrated that HFD-induced obesity induces a bias towards pro-inflammatory EM T cell subsets (CD44$^+$,LFA-1$^+$ and CD44$^+$,CXCR3$^+$)[18]. Following this, we sought to investigate this pro-inflammatory EM T cell phenotype further in an WGWL murine model (HFD-RE).

Figure 5.4A illustrated the representative flow cytometry plots of CD44 and CD62L gating strategy used to investigate the main CD4$^+$ T cell subsets: naïve (Q1), central (CM-Q2) and effector (EM-Q3) memory subsets; amongst the different diet groups.

Consistent with the literature, 14-week HFD-fed murine group illustrated a slight reduction trend in naïve CD4$^+$ T cell (CD62L$^+$, CD44$^-$) frequencies within the spleen and pLN tissues. Importantly, HDF group naïve CD4$^+$ T cell absolute counts within pLNs illustrated a statistically significant reduction compared to CD control. Furthermore, naïve CD4$^+$ T cell frequencies of HFD-RE and CD groups were highly comparable, suggesting a recovery of naïve CD4$^+$ T cell populations from the effects of 8-week HFD feeding.

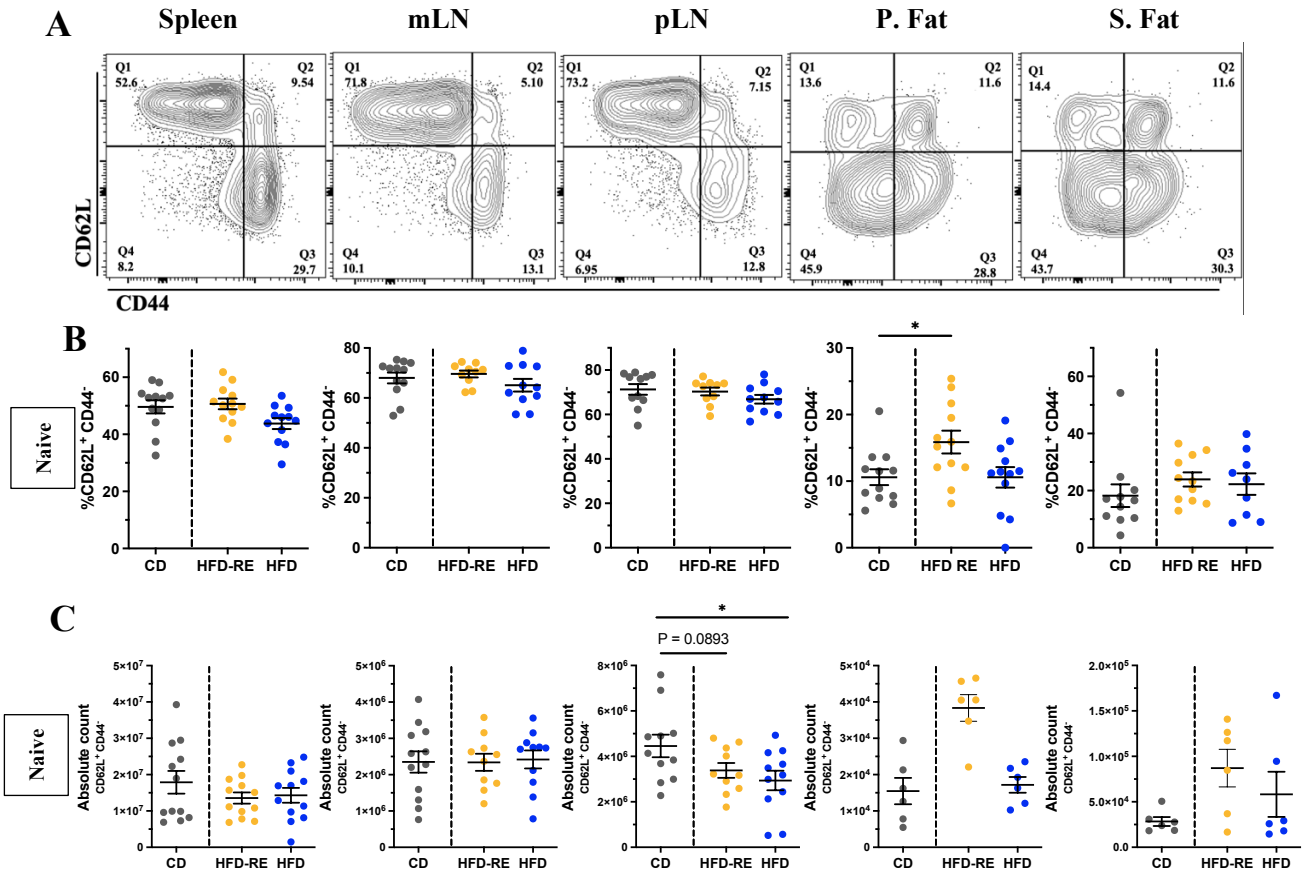


Figure 5.4) Effects of HFD and HFD-RE (WGWL) on naive CD4$^+$ T cell populations within SLOs and fat tissues

(A) Representative flow cytometry plots of CD44 and CD62L extracellular staining on $CD4^+$ T cells isolated from SLOs and fat tissues of female C57BL/6J mice fed on CD, HFD, and HFD-RE (8-wk HFD and 6-wk CD) for 14-weeks and were subjected to an allogeneic immunisation at 13.week with CBA and BALB/B splenocyte injection. Quantification of flow cytometry data on **(B)** naïve ($CD44^-$ and $CD62L^+$) frequencies and **(C)** absolute cell counts of naïve ($CD44^-$ and $CD62L^+$) $CD4^+$ T cells populations within three different SLOs and fat tissues obtained from different diet groups. Each point represents an individual mouse in allocated diet groups (two *in vivo* experimental dataset with 6 mice per group shown together, n=12 in total). One-way ANOVA with Dunnett's correction; Data presented as mean ± SEM, *p<0.05; ** p<0.01, *** p<0.001.

Furthermore, consistent with the Mauro et al. 2017 dataset, the CM ($CD62L^+$,$CD44^+$) $CD4^+$ T cell frequencies were generally not modulated between the diet groups in SLOs and fat tissues. Interestingly, only HFD group CM $CD4^+$ T cell percentages were significantly elevated within mLN and pLNs tissues compared to CD control. However, the absolute CM $CD4^+$ T cell counts did not validate these increase within the LNs where all three diet groups were comparable (**Figure 5.5A**). Additionally, consistent with the previous publication and preliminary data of Mauro et al. 2017, the HFD-RE group did not affect the $CD4^+$ $CD4^+$ T cell CM frequencies or CM absolute cell counts in both SLOs and fat tissues tested (**Figure 5.5B**).

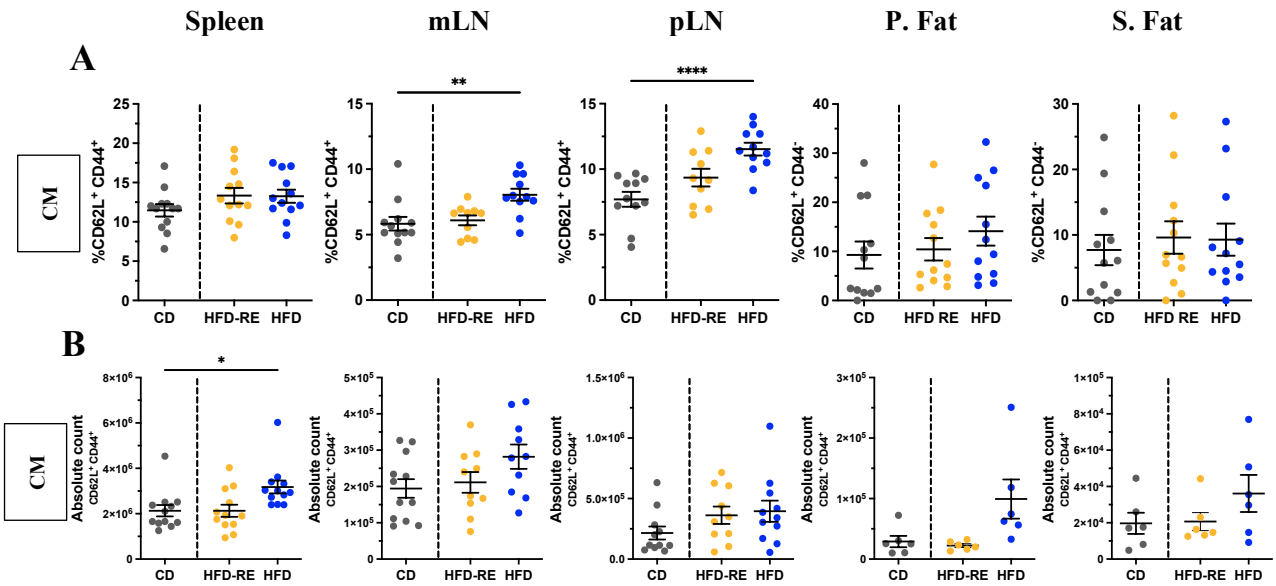


Figure 5.5) Effects of HFD and HFD-RE (WGWL) on CM $CD4^+$ T cell populations within SLOs and fat tissues

Quantification of flow cytometry data on **(A)** CM ($CD44^+$ and $CD62L^+$) frequencies and **(B)** Absolute cell counts of CM ($CD44^+$ and $CD62L^+$) $CD4^+$ T cells within three different SLOs and fat tissues obtained from different diet groups. Each point represents an individual mouse in allocated diet groups (two *in vivo* experimental dataset with 6 mice per group shown together, n=12 in total). One-way ANOVA with Dunnett's correction; Data presented as mean ± SEM, *p<0.05; ** p<0.01, *** p<0.001.§

Second *in vivo* dataset (n=6) of the fat tissues was not been able to analyse due to technical limitations experienced with the counting beads on the day.

Importantly, consistent with the Mauro et al. 2017, HFD-fed group illustrated a significant increase (~10%) in EM ($CD44^+$,$CD62L^-$) $CD4^+$ T cell population frequencies within the spleen, pLNs and s.fat tissues compared to the CD control (**Figure 5.6A**). Although absolute cell counts of EM $CD4^+$ T cells were significantly elevated in the HFD group within the spleen, pLN, the slight increase observed in s.fat tissues did not reach statistical significance (**Figure 5.6B**). Interestingly, the EM $CD4^+$ T cell populations were also significantly elevated within the pLNs and s.fat tissues of the HFD-RE group compared to CD control (**Figure 5.6A**). This was highly striking as both HFD (14-week) group and HFD-RE (8-week HFD + 6-week CD) groups were able to induce a comparable expansion of EM $CD4^+$ T cell populations within the pLNs and s.fat tissues (**Figure 5.6A**). Consistent with the elevated EM $CD4^+$ T cell frequencies (**Figure 5.6A**), the absolute count of EM cells also illustrated a significant elevation in both HFD and HFD-RE groups compared to CD control within the pLNs tissue (**Figure 5.6B**). This data suggests that, formerly obese mice (previously fed with HFD), can still induce an excessive expansion of deleterious pro-inflammatory effector memory T cell when challenged by allogeneic immunisation even after they have lost the weight they gained.

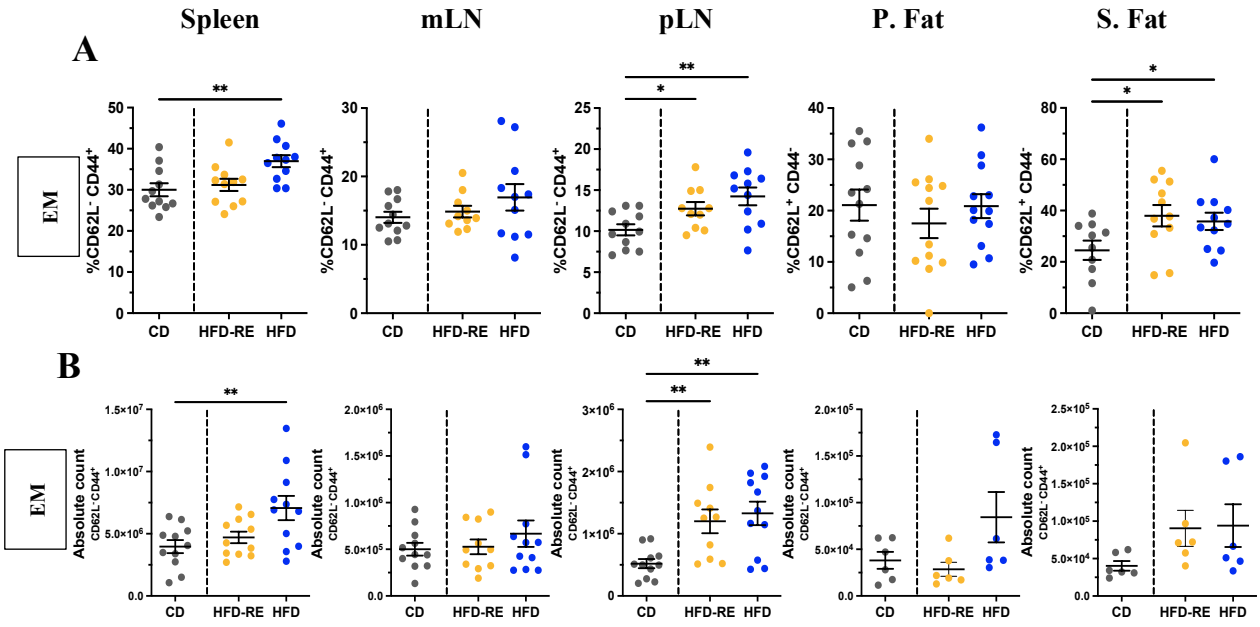


Figure 5.6) Exposure to HFD induces a long-term increase in the $CD4^+$ T cell EM population frequencies

Quantification of flow cytometry data on **(A)** EM ($CD44^+$ and $CD62L^-$) frequencies and **(B)** Absolute cell counts of EM ($CD44^+$ and $CD62L^-$) $CD4^+$ T cells within three different SLOs and fat tissues obtained from different diet groups. Each point represents an individual mouse in allocated diet groups

(two *in vivo* experimental dataset with 6 mice per group shown together, n=12 in total). One-way ANOVA with Dunnett's correction; Data presented as mean ± SEM, *p<0.05; ** p<0.01, *** p<0.001.§ Second *in vivo* dataset (n=6) of the fat tissues was not been able to analyse due to technical limitations experienced with the counting beads on the day.

Following the alterations observed in $CD4^+$ T cell subsets, we sought to investigate any potential modulations on main $CD8^+$ T cell subsets as represented by flow cytometry plots in **Figure 5.7A**.

The naïve ($CD62L^+$, $CD44^-$) $CD8^+$ T cell populations did not express any prominent modulation within SLOs and fat tissues of different diet groups, except spleen tissue. Interestingly, naïve $CD8^+$ T cell frequencies were significantly reduced in the HFD group compared to the CD whereas, absolute cell counts of naïve $CD8^+$ T cells also demonstrated a prominent reduction with both HFD and HFD-RE groups (**Supplementary-Figure S11**).

Furthermore, both diet groups illustrated no modulation in the central memory ($CD62L^+$, $CD44^+$) $CD8^+$ T cell frequencies and absolute cell counts compared to CD control group within both SLOs and fat tissues, except pLN tissue. Interestingly, the CM $CD8^+$ T cell populations were significantly upregulated within pLN of both HFD and HFD-RE groups compared to the CD control which was further confirmed by the absolute cell counts from the pLN tissue (**Figure 5.7**).

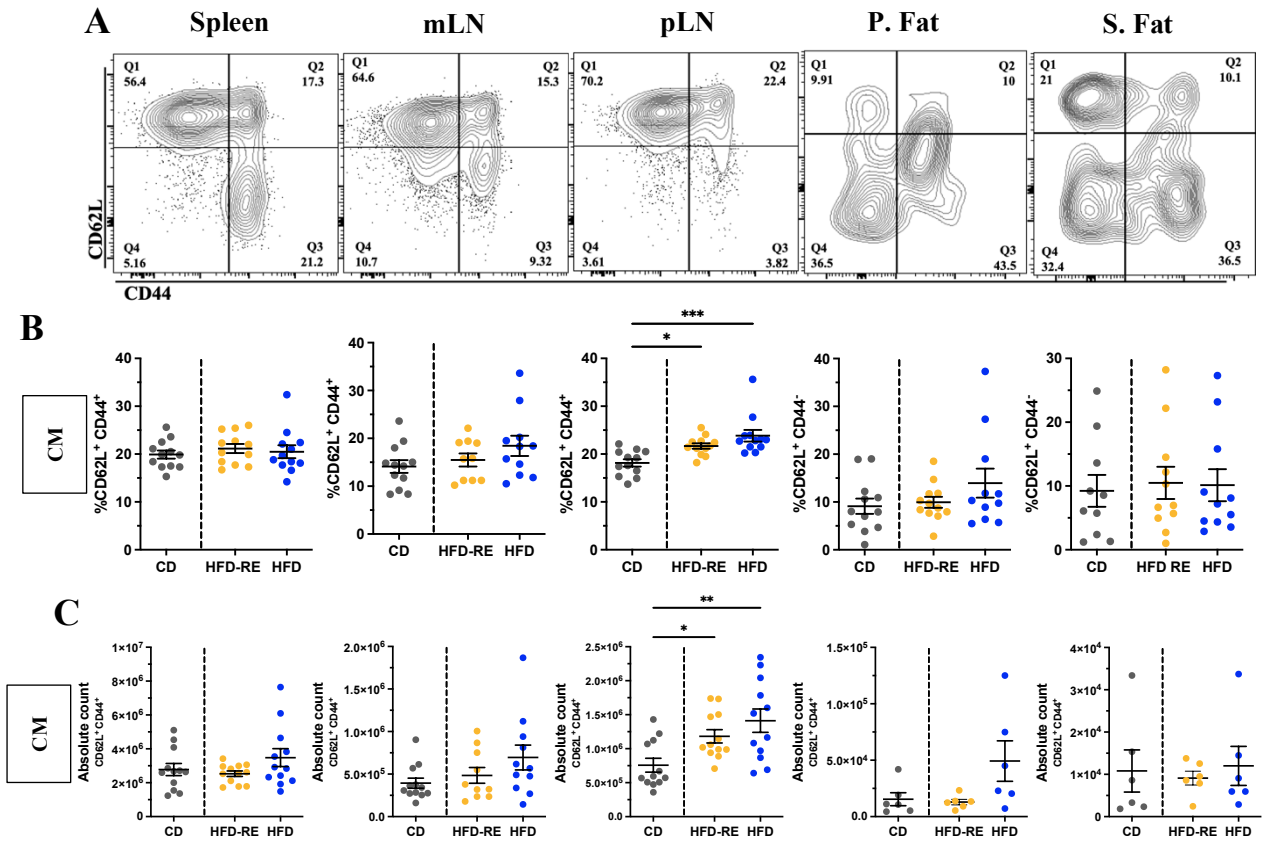


Figure 5.7) Exposure to HFD induces a long-term increase in the CD8$^+$ T cell CM population in pLN of HFD-RE (WGWL) group

Quantification of flow cytometry data on **(A)** CM (CD44$^+$ and CD62L$^+$) frequencies and **(B)** absolute cell counts of CM (CD44$^+$ and CD62L$^+$) CD8$^+$ T cells within three different SLOs and fat tissues obtained from different diet groups. Each point represents an individual mouse in allocated diet groups (two *in vivo* experimental dataset with 6 mice per group shown together, n=12 in total). One-way ANOVA with Dunnett's correction; Data presented as mean ± SEM, *p<0.05; ** p<0.01, *** p<0.001.§ Second *in vivo* dataset (n=6) of the fat tissues was not been able to analyse due to technical limitations experienced with the counting beads on the day.

Moreover, we have also investigated the CD8$^+$ EM (CD62L$^-$, CD44$^+$) T cell populations within SLOs and fat tissues. Like CD4$^+$ EM dataset, the HFD group illustrated a significant elevation of the CD8$^+$ EM T cell frequencies within the spleen and pLN as well as a slight increasing trend of s.fat tissue compared to CD control (**Figure 5.8A**). Consistent with the CD8$^+$ EM T cell percentages, absolute CD8$^+$ EM T cell counts also validated these significant increases within the spleen and pLN of the HFD group (**Figure 5.8B**). Importantly, differently from percentages, absolute cell counts of CD8$^+$ EM T populations were found to be significantly elevated within the mLN tissue (**Figure 5.8B**). In contrast to the CD4$^+$ EM T cell dataset, the HFD-RE group demonstrated no observable change in both CD8$^+$ EM T cell percentage and absolute cell counts compared to CD control within all the tissues tested.

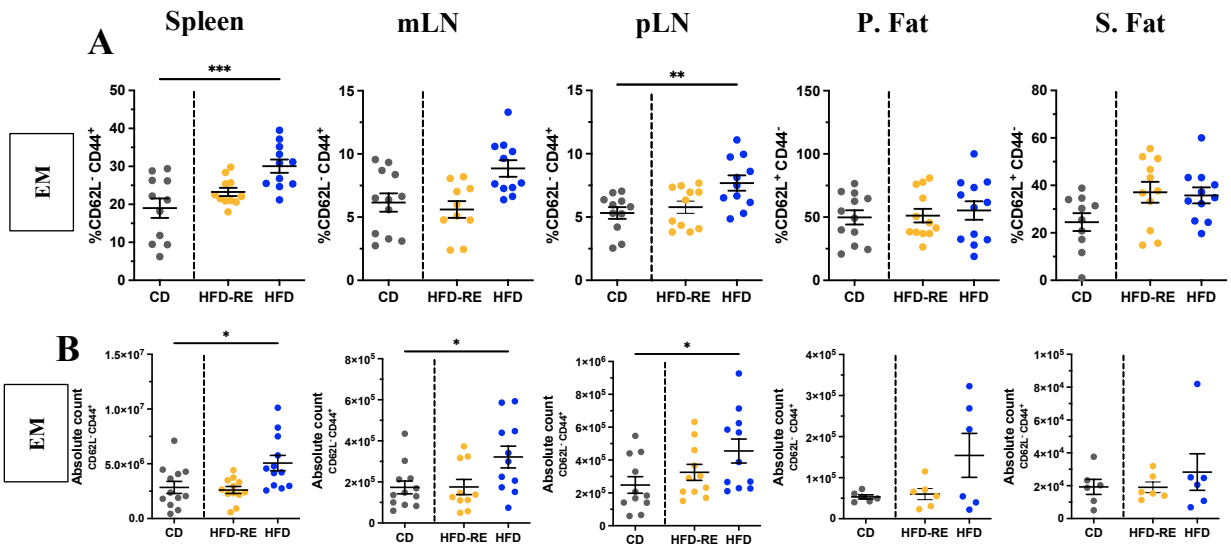


Figure 5.8) Exposure to HFD induces an increase in the CD8$^+$ T cell EM population in pLN
Quantification of flow cytometry data on **(A)** EM (CD44$^+$ and CD62L$^-$) frequencies and **(B)** absolute cell counts of EM (CD44$^+$ and CD62L$^-$) CD8$^+$ T cells within three different SLOs and fat tissues obtained from different diet groups. Each point represents an individual mouse in allocated diet groups (two *in vivo* experimental dataset with 6 mice per group shown together, n=12 in total). One-way ANOVA with Dunnett's correction; Data presented as mean ± SEM, *p<0.05; ** p<0.01, *** p<0.001.§ Second *in vivo* dataset (n=6) of the fat tissues was not been able to analyse due to technical limitations experienced with the counting beads on the day.

Taken together, HFD induced a significant increase specifically in CD4$^+$ T cell EM populations within SLOs and s.fat tissues. However more interestingly, this HFD-induced upregulation trend was shown to prime the distribution of CD4$^+$ T cells in the HFD-RE group towards an EM phenotype in certain SLOs even after the weight loss whereas, this profound bias was not observed in CD8$^+$ T cell lineage.

5.4. HFD-induced past history of obesity primes the differentiation of CD4$^+$ T cells towards CXCR3$^+$- LFA-1$^+$ pro-inflammatory effector memory phenotype

Following the elevations in CD4$^+$ T cell EM populations in both HFD and HFD-RE groups (**Figure 5.6**), we further investigated the HFD-biased distribution of CD4$^+$ T EM subsets with pro-inflammatory, tissue-infiltrating T-cell markers; CXCR3$^+$ and LFA-1$^+$ populations specifically after the weight loss in the HFD-RE group. The critical roles of CXCR3 and LFA-1 pro-inflammatory markers within the OIIM in obesity and obesity-associated pathophysiologies are previously detailed in **Chapter 3** [18, 389, 395, 398, 400].

Consistent with the Mauro et al. 2017, HFD group illustrated a statistically significant increase in $CD44^+$,LFA-1^+ $CD4^+$ T cell population compared to the CD in all three SLOs, but not in the fat tissues (**Figure 5.10A**). Importantly, although the $CD44^+$,LFA-1^+ $CD4^+$ T cell absolute cell counts illustrated a notable increasing trend in SLOs of the HFD group, only the pLN tissue reached the statistical significance compared to CD control (**Figure 5.10B**).

Interestingly, the $CD44^+$, LFA-1^+ $CD4^+$ T cell frequencies were significantly elevated within the pLN tissue of the HFD-RE group compared to CD control where this significant elevation was further validated by the absolute cell counts within pLN. Furthermore, no difference was observed in $CD44^+$,LFA-1^+ $CD4^+$ T cell frequencies or absolute counts within the spleen, mLN and fat tissues of the HFD-RE group compared to CD control.

Similar with the LFA-1^+ memory population, the HFD-fed group was also shown to significantly increase the $CD44^+$,$CXCR3^+$ population frequencies in the spleen, mLN, pLN and the p.fat tissue compared to CD control (**Figure 5.10C**). Consistently, absolute cell counts of $CD44^+$,$CXCR3^+$ $CD4^+$ T cells illustrated significant increase within the SLOs and an increasing trend in fat tissues (**Figure 5.10D**). Interestingly, the $CD44^+$,$CXCR3^+$ population frequencies and absolute cell counts of the HFD-RE group were highly comparable to the CD control in all of the tissues, except pLN. Similar to LFA-1^+ memory population, the HFD-RE group was also shown to induce the expansion of $CD44^+$,$CXCR3^+$ $CD4^+$ T cell populations significantly higher than the CD control group within the pLN tissue.

Figure 5.9 illustrates the representative flow cytometry plots of $CD44^+$, LFA-1^+ - $CXCR3^+$ $CD4^+$ T populations, demonstrating the preservation of the HFD-induced elevation in the population even after the weight loss of the HFD-RE group compared to the CD control group within pLN. Taken together, both HFD and HFD-RE groups expressed the increased potential of inducing an exacerbated $CD4^+$ EM T cell response via elevating the expansion of deleterious, pro-inflammatory LFA-1^+ and $CXCR3^+$ memory T cell populations specifically in the pLN tissue as well as certain fat tissues.

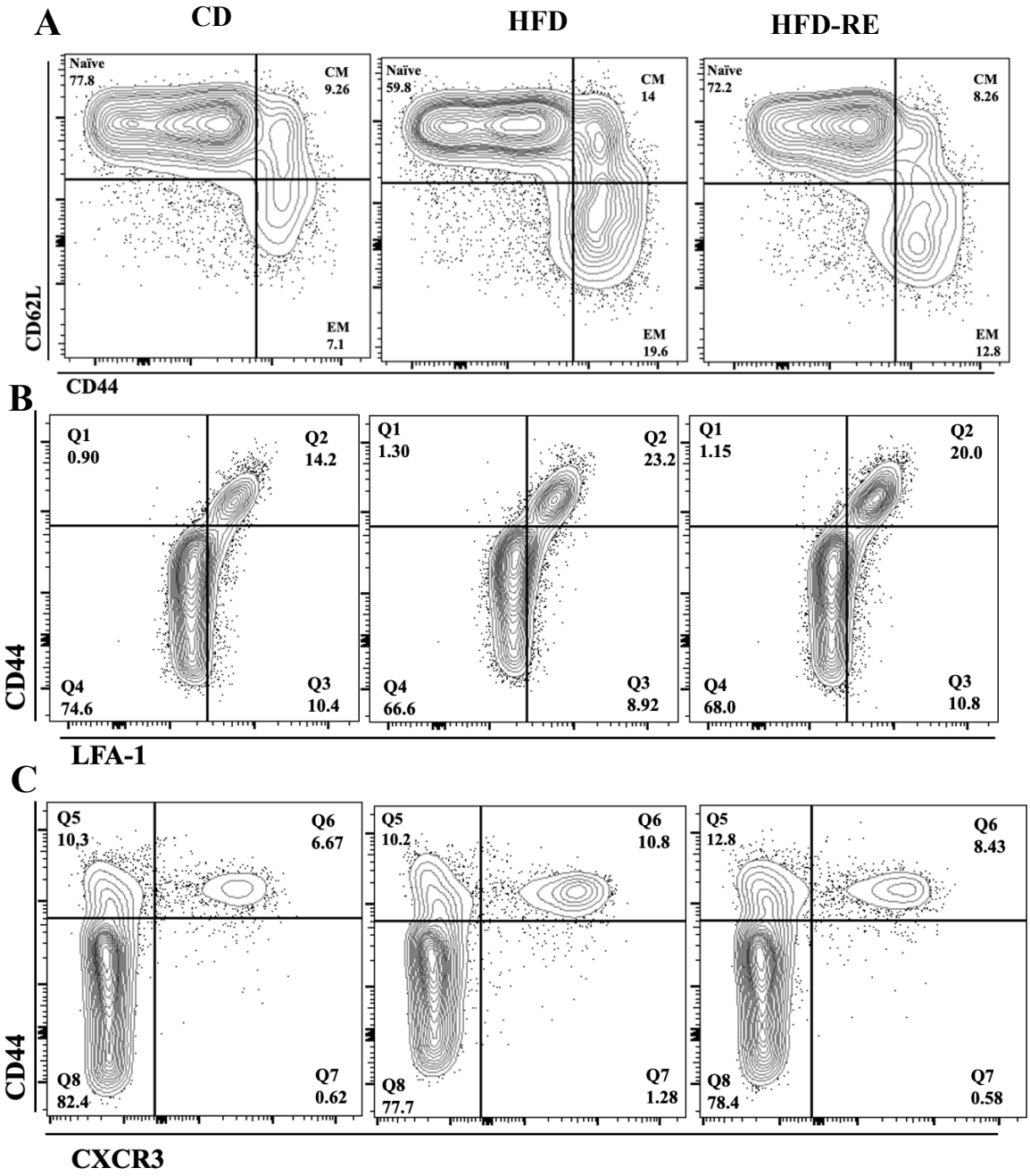


Figure 5.9) Representative flow cytometry plots of pLN tissues obtained CD, HFD and HDF-RE groups

Representative flow cytometry figures of **(A)** $CD44^+$, $CD62L^-$ (EM) **(B)** $CD44^+$, $LFA\text{-}1^+$ (Q2) and **(C)** $CD44^+$, $CXCR3^+$ (Q6) populations obtained from the pLN tissues of CD, HFD and HFD-RE (8-wk HFD and 6-wk CD) for 14-weeks and were subjected to an allogeneic immunisation at 13.week with CBA and BALB/C i.p injection. Representative flow figures and gating strategy used in all tissues as quantified in **Figure 5.4 - 5.6**

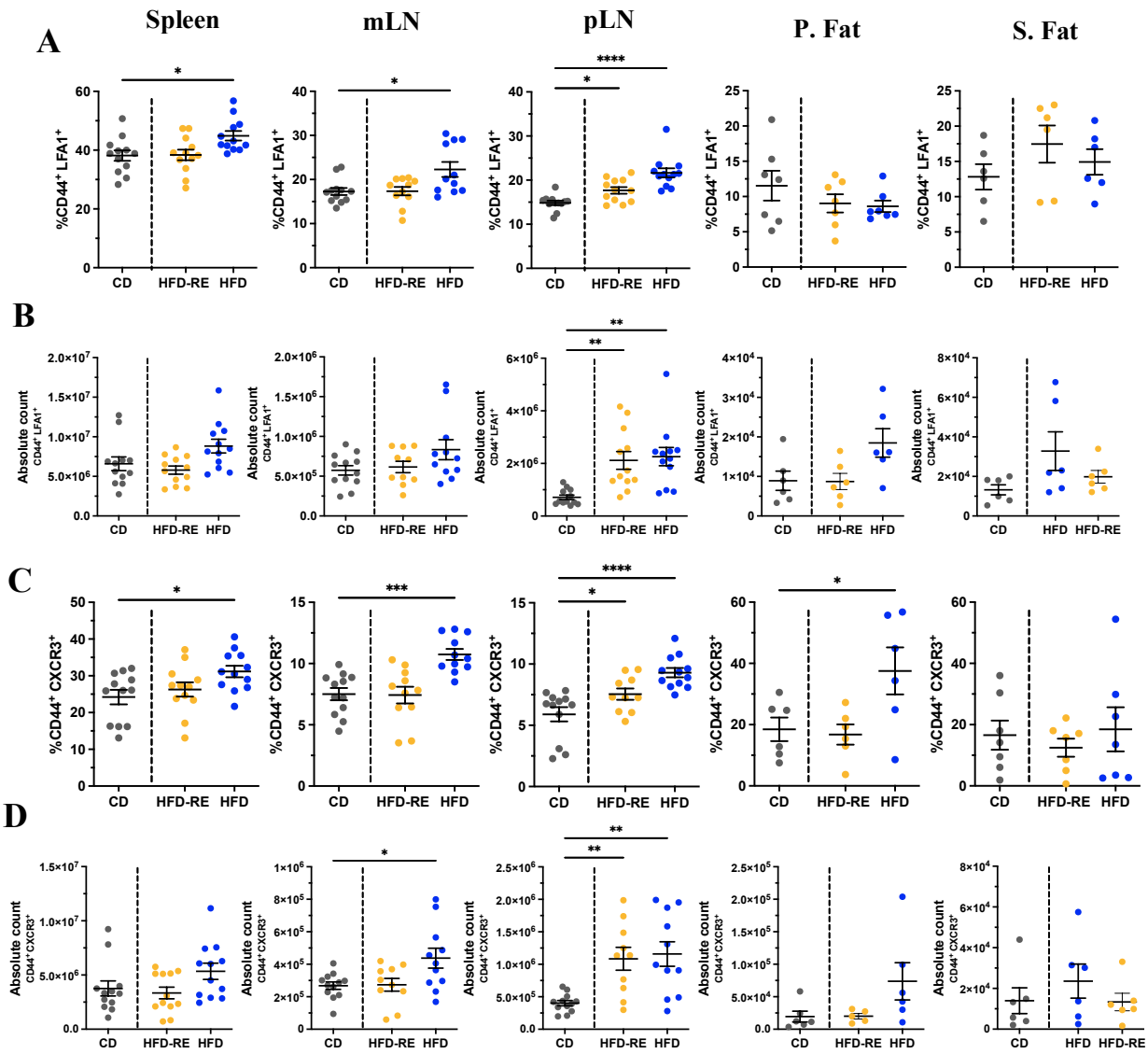


Figure 5.10) Exposure to HFD induces a long-term increase in the pro-inflammatory CXCR3$^+$ and LFA-1$^+$ CD44$^+$ CD4$^+$ T cell EM populations

Quantification of **(A)** CD44$^+$ and LFA-1$^+$ pro-inflammatory effector memory CD4$^+$ T cell population frequencies **(B)** Absolute cell counts of CD44$^+$ and LFA-1$^+$ CD4$^+$ T cells **(C)** CD44$^+$ and CXCR3$^+$ pro-inflammatory EM CD4$^+$ T cell population frequencies and **(D)** Absolute cell counts of CD44$^+$ and CXCR3$^+$ CD4$^+$ T cells obtained from the three main SLOs and two fat tissues obtained from female C57BL/6J mice fed on CD, HFD, and HFD-RE (8-wk HFD and 6-wk CD) for 14-weeks and were subjected to an allogeneic immunisation at 13.week. Each point represents an individual mouse in allocated diet groups (two *in vivo* experimental dataset with 6 mice per group shown together, n=12 in total). One-way ANOVA with Dunnett's correction; Data presented as mean ± SEM, *p<0.05; ** p<0.01, *** p<0.001. § Second *in vivo* dataset (n=6) of the fat tissues was not been able to analyse due to technical limitations experienced with the counting beads on the day.

Following the $CD4^+$ T cells, we investigated the pro-inflammatory EM markers in $CD8^+$ T lineage. Similar to the $CD4^+$ T cell dataset, LFA-1^+ memory $CD8^+$ T cell populations were significantly elevated within all three SLOs and p.fat tissues of the HFD-fed group compared to CD control (**Figure 5.11A**). Although the absolute counts of $CD44^+$,LFA-1^+ $CD8^+$ T cells also expressed similar increasing trends within spleen, mLN, pLN and fat tissues, only the spleen and pLNs were shown to be statistically significant compared to CD control (**Figure 5.11B**). Interestingly, like $CD4^+$ T cell dataset, the HFD-RE group $CD44^+$, LFA-1^+ $CD8^+$ T cell frequencies were significantly elevated within the pLN but not in other tissues tested. However, unlike the $CD4^+$ T cell dataset, this elevation in $CD44^+$, LFA-1^+ $CD8^+$ T cell percentage was not validated by the absolute cell counts obtained from pLN of the HFD-RE group (**Figure 5.11**).

Furthermore, the HFD group also expressed a significant elevation in the $CD44^+$,$CXCR3^+$ $CD8^+$ T cell frequencies and the absolute cell counts within all three SLOs (spleen, mLNs and pLNs) tissues compared to the CD control group (**Figure 5.11C&D**). Similar to the LFA-1^+ memory $CD8^+$ T cell populations, HFD-RE group also expressed significantly higher $CXCR3^+$ memory $CD8^+$ T cell population frequencies within the pLN compared to CD control group, which was not observed in any other tissue tested (**Figure 5.11C**). The absolute cell counts of the $CXCR3^+$ memory $CD8^+$ T cell populations were also profoundly increased compared to the CD group however, did not reach the statistical significance ($p=0.0569$) (**Figure 5.11D**).

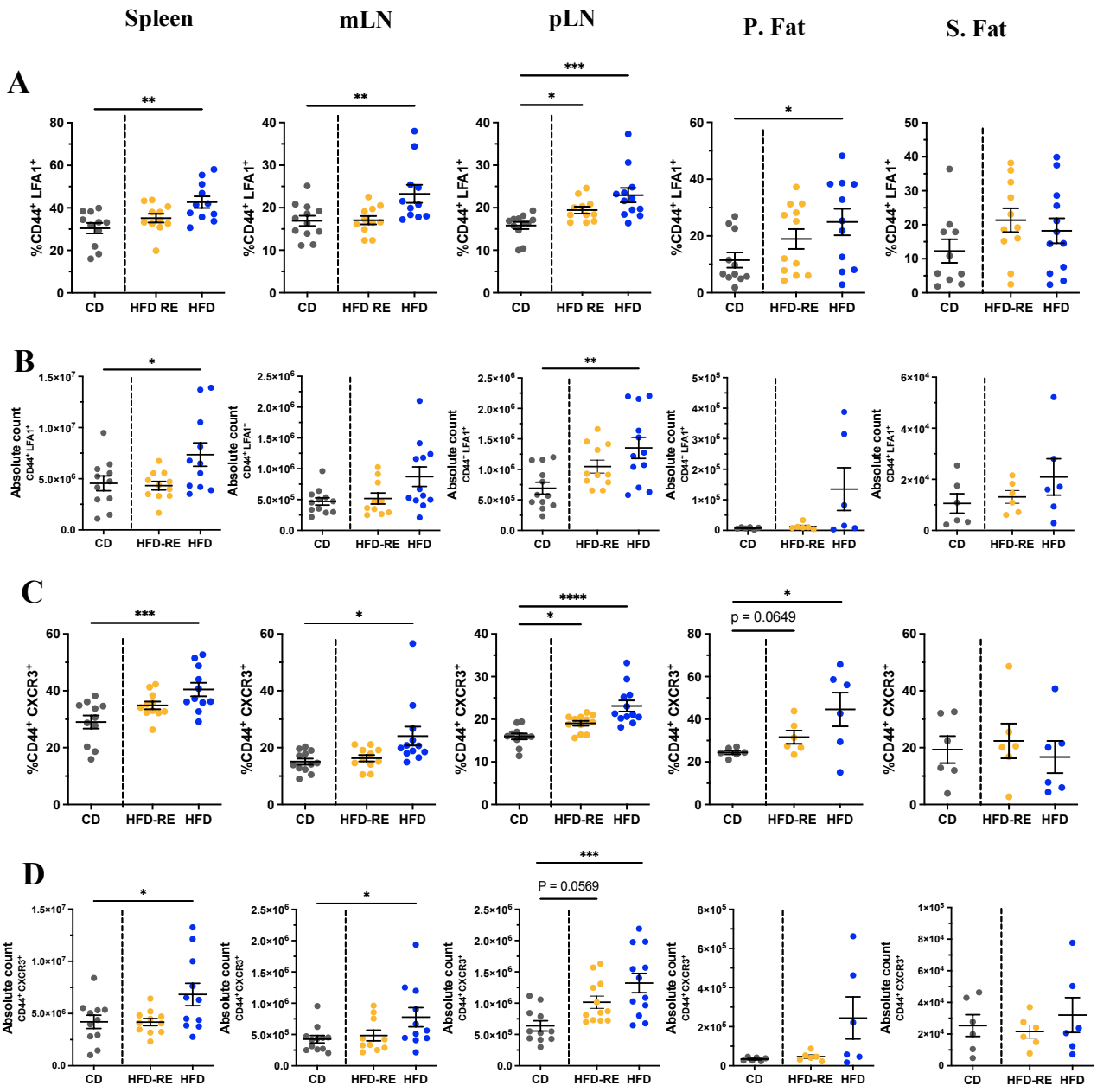


Figure 5.11) Exposure to HFD induces a long-term increase in the pro-inflammatory CXCR3$^+$ and LFA-1$^+$ CD44$^+$ CD8$^+$ T cell EM populations

Quantification of **(A)** CD44$^+$ and LFA-1$^+$ pro-inflammatory memory CD8$^+$ T cell population frequencies **(B)** Absolute cell counts of CD44$^+$ and LFA-1$^+$ CD8$^+$ T cells **(C)** CD44$^+$ and CXCR3$^+$ pro-inflammatory memory CD8$^+$ T cell population frequencies and **(D)** Absolute cell counts of CD44$^+$ and CXCR3$^+$ CD8$^+$ T cells obtained from the three main SLOs and two fat tissues obtained from female C57BL/6J mice fed on CD, HFD, and HFD-RE (8-wk HFD and 6-wk CD) for 14-weeks and were subjected to an allogeneic immunisation at 13.week with CBA and BALB/C i.p injections. Each point represents an individual mouse in allocated diet groups (two *in vivo* experimental dataset with 6 mice per group shown together, n=12 in total). One-way ANOVA with Dunnett's correction; Data presented as mean ± SEM, *p<0.05; ** p<0.01, *** p<0.001. § Second *in vivo* dataset (n=6) of the fat tissues was not been able to analyse due to technical limitations experienced with the counting beads on the day.

Collectively, these data suggest a novel 'obesogenic memory' in $CD4^+$ T cells where HFD-feeding in the earlier life of a formerly obese model can induce a long-lasting bias on $CD4^+$ T cells that induces an exacerbated pro-inflammatory LFA-1^+-$CXCR3^+$ EM phenotype against polyclonal T cell challenges well after weight has been lost. Considering the importance of the exacerbated T cell responses in obesity and obesity-linked pathophysiologies, we sought to determine and dissect the factors leading to this long-term immunomodulatory biasing effect of HFD within HFD-RE WGWL model.

5.5 HFD-induced alterations in distinct effector $CD4^+$ and cytotoxic $CD8^+$ T cell subsets

Following the alterations observed in main naïve and memory $CD4^+$ T cell populations following the 14-week HFD-induced obesity conditions, we wanted to further investigate the effector $CD4^+$ T helper subsets by using main intracellular lineage-defining TFs of each effector $CD4^+$ T cell subsets.

In addition to the elevation observed in the EM $CD4^+$ T cell populations, HFD group was also shown to have significantly higher T-bet^+,$CD4^+$ Th1 cell subsets within the spleen compared to CD group. Similarly, HFD pLN tissue also illustrated a similar elevation trend with T-bet^+, $CD4^+$ Th1 cells in addition to significant elevation of RORγt^+ Th17 $CD4^+$ T population compared to CD control (**Supplementary-Figure S12**). Consistent with the literature, HFD-fed 14-week DIO model was shown to induce elevation trends in pro-inflammatory Th1 and Th17 $CD4^+$ T cell subsets which was recovered with the weight loss in HFD-RE group [265, 301, 453-455] (**Supplementary-Figure S12**).

Furthermore, we have also investigated the cytotoxic $CD8^+$ T cell subsets within the SLOs of 14-week DIO and WGWL murine groups. Consistent with the background literature, pro-inflammatory Tc1 $CD8^+$ T cell frequencies were significantly elevated within the spleen and pLN tissues of the HFD-fed DIO group compared to the CD control (**Figure 5.12**). Interestingly, HFD-RE group was shown to retain the significantly elevated Tc1 $CD8^+$ T cell frequencies within the spleen tissue, even after the weight loss. Additionally, there was no observable difference in RORγt^+-Tc17 and Gata-3^+-Tc2 $CD8^+$ T cell subsets between different diet groups (*data not shown*).

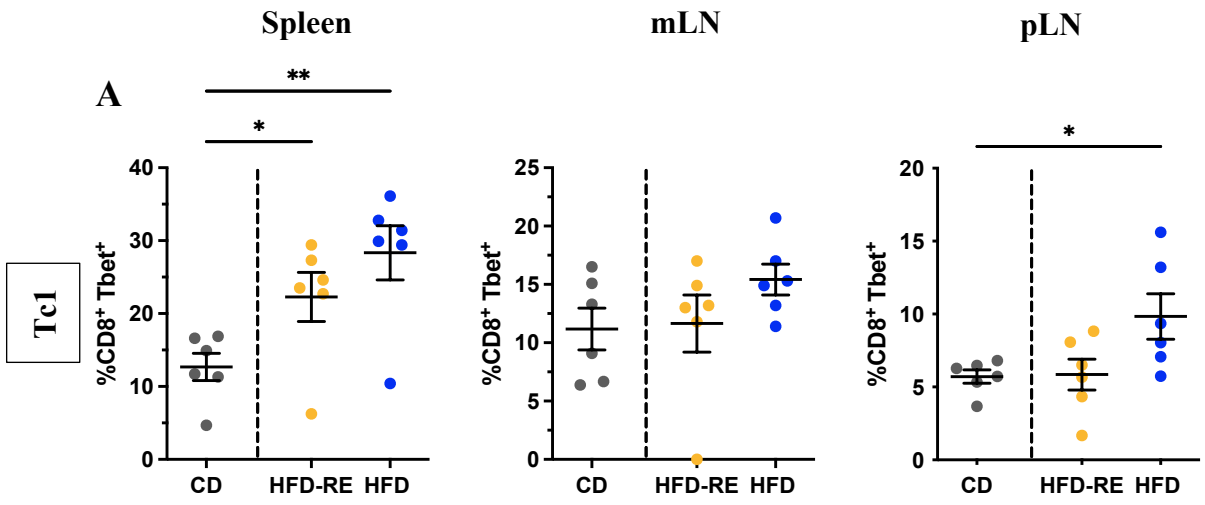


Figure 5.12) HFD feeding induced elevation of Tbet$^+$ Tc1 cytotoxic CD8$^+$ T cell subsets
(A) Quantification of flow cytometry data of Tbet$^+$ for Tc1 cytotoxic CD8$^+$ T cell population within SLO tissues obtained from female C57BL/6J mice fed on CD, HFD, and HFD-RE (8-wk HFD and 6-wk CD) for 14-weeks and were subjected to an allogeneic immunisation with CBA and BALB/C splenocyte i.p injection at 13.week. Each point represents an individual mouse in allocated diet groups (one *in vivo* experimental dataset with 6 mice). One-way ANOVA with Dunnett's correction; Data presented as mean ± SEM, *p<0.05; ** p<0.01, *** p<0.001

Additionally, consistently with the 3-week early-DIO *in vivo* murine model, no significant reduction in Foxp3$^+$ CD4$^+$ frequencies was observed within SLOs. Interestingly, in line with the literature HFD was shown to negatively affect the Foxp3$^+$,CD25$^+$ CD4$^+$ Treg populations in p.fat tissue, where weight loss of HFD-RE group was shown to recover Treg populations comparable to CD control [401, 644, 645] (*data not shown*).

5.6. Exogenous *in vitro* exposure of bioactive saturated fatty acids recapitulates the HFD-induced pro-inflammatory effector memory bias in human CD4$^+$ T cells

Based on the previous dataset published by Mauro et al. 2017, we wanted to utilise a reductionist approach and design a CD4$^+$ T cell monoculture lipid treatment protocol in order to 'mimic' the *in vivo* HFD-induced plethora of distinct bioactive lipid groups *in vitro*. We sought to investigate if distinct bioactive FAs can directly induce the pro-inflammatory EM phenotype, which would also elucidate potential drivers of the observed phenotype. Therefore, we pre-treated the CD4$^+$ T cells with exogenous supplementation of distinct bioactive lipids

followed by 3 day activation and cell culturing. The bioactive lipid groups investigated were saturated (Palmitate-PA and Stearic acid-STE) and mono-unsaturated (Oleic acid-OA) FAs.

We have optimised the *in vitro* treatment time and toxicity of lipids on human $CD4^+$ T cells where human $CD4^+$ T cells were pre-treated with lipids overnight before the activation for 48hrs (**Section 2.9.4**). Additionally, in order to examine any potential background difference between donors we have included the same set of lipid treatment groups on non-activated $CD4^+$ T cells following the 3 days cell culture. We have also controlled for cell viability (Near IR) and activation status of each experiment (**Supplementary-Figure S13-14**).

Following this, we investigated any potential direct 'biasing' effect of distinct bioactive FAs on main naïve and memory $CD4^+$ T cell subsets as observed within the HFD-fed DIO murine groups. **Figure 5.13A**, demonstrates representative flow cytometry plots of the untreated vehicle control group samples stained for CD45RO and CCR7 markers for defining the naïve and memory $CD4^+$ T cell using FMO for gating strategy.

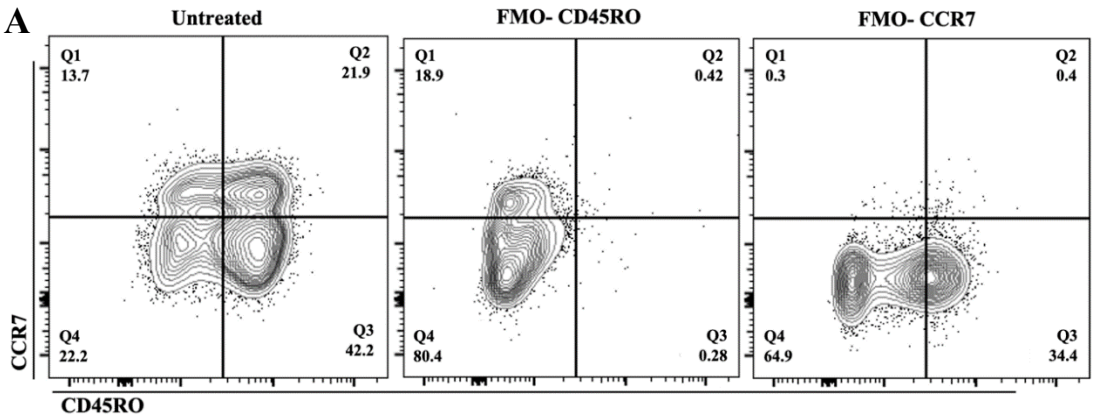
Pre-treatment of human $CD4^+$ T cells with individual SFA group: PA and STE, led to a significant reduction in activated, naïve ($CD45RO^-$, $CCR7^+$) $CD4^+$ T cell frequencies compared to untreated vehicle control (**Figure 5.13B**). Importantly, no observable change was recorded among non-activated treatment groups, suggesting a constant background naïve frequencies obtained from different donors (**Figure 5.13B**).

Interestingly, overnight PA and STE pre-treatment of human $CD4^+$ T cells were shown to induce a statistically significant concomitant upregulation of EM ($CD45RO^+$, $CCR7^-$) $CD4^+$ T cell subsets compared to the untreated-vehicle control (**Figure 5.13C**). It should be noted that this SFA-induced 'biasing' effect towards EM fate was only observed within the activated groups whereas, non-activated $CD4^+$ T cells illustrated no observable change (**Figure 5.13C**). This observation suggests that there was no prominent difference within the background $CD4^+$ T cell subset distribution of the human donors (n=4). Similar to the naïve population, both bioactive SFAs: PA and STE pre-treated groups illustrated a significant elevation in $CD45RO^+$,$CCR7^-$ EM $CD4^+$ T cells following the T-cell activation (**Figure 5.13C**).

Furthermore, consistent with the HFD-fed *in vivo* model, none of the lipid groups illustrated any significant modulation within the $CD45RO^+$, $CCR7^+$ CM $CD4^+$ T cell subsets, except the STE treatment group (**Figure 5.13D**). Interestingly, STE-treated $CD4^+$ T cells

illustrated a significant reduction in CM $CD4^+$ T cell frequencies compared to the untreated control group.

It should be noted that, no modulation was observed in any $CD4^+$ T cell subsets within the non-activated treatment groups suggesting that bioactive FAs expressed their 'priming' effect following an activation stimulus which is in line with the *in vivo* murine model dataset. Importantly, *in vitro* SFA pre-treatment of human $CD4^+$ T cells were also shown to recapitulate the significant increase in EM frequencies with a concomitant decrease in naïve $CD4^+$ T cells as previously reported in an obese cohort by Mauro et al [18].


A
Untreated
FMO- CD45RO
FMO- CCR7
Q1
13.7
Q2
21.9
Q4
22.2
Q3
42.2
Q1
18.9
Q2
0.42
Q4
80.4
Q3
0.28
Q1
0.3
Q2
0.4
Q4
64.9
Q3
34.4
CCR7
CD45RO

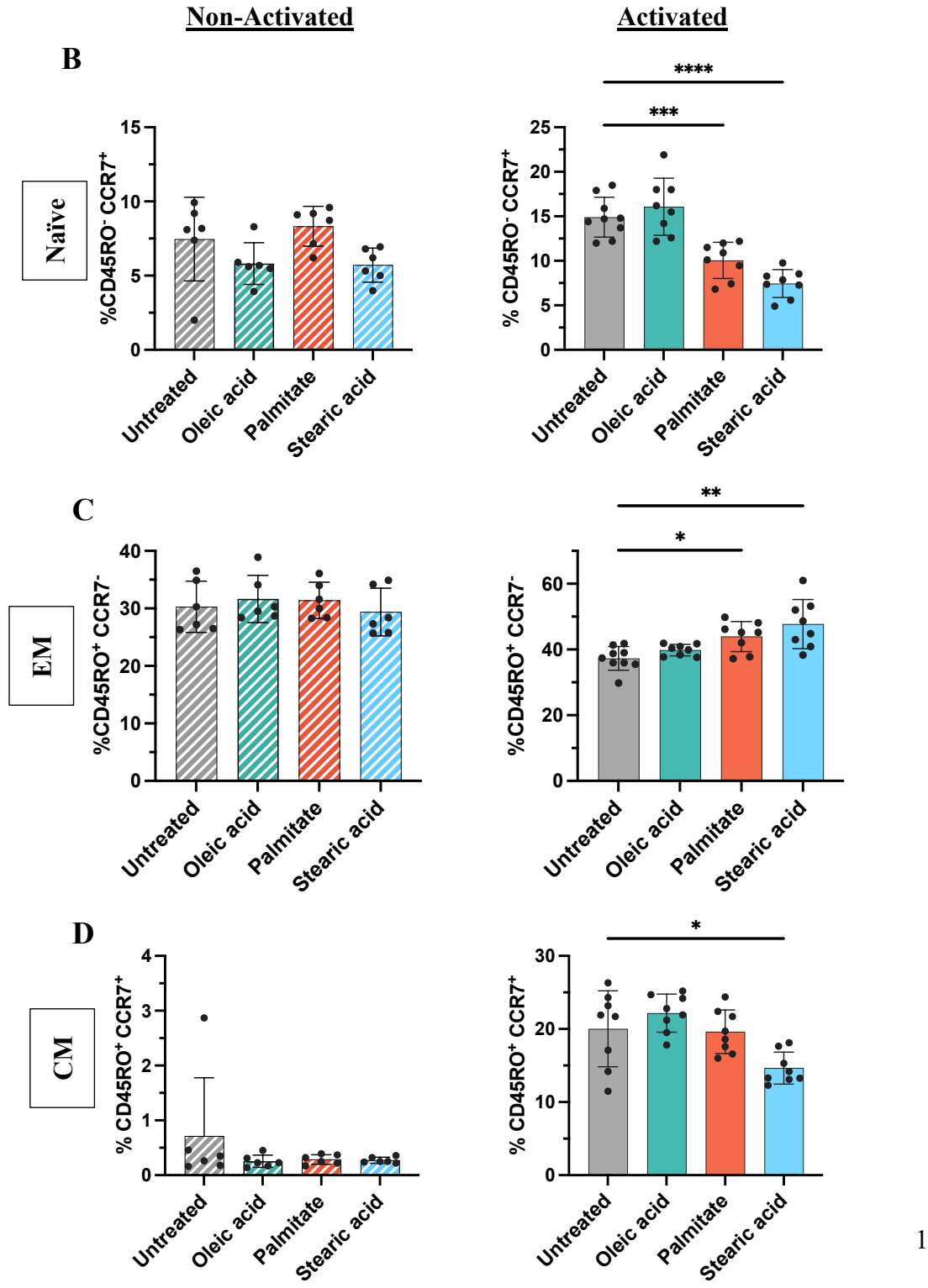

Non-Activated
Activated
B
Naïve
%CD45RO- CCR7+
% CD45RO- CCR7+
****
***
C
EM
%CD45RO+ CCR7-
%CD45RO+ CCR7-
**
*
D
CM
% CD45RO+ CCR7+
% CD45RO+ CCR7+
*
Untreated
Oleic acid
Palmitate
Stearic acid

Figure 5.13) Exogenous SFA (PA and STE) pre-treatment induces elevation of human EM CD4$^+$ T cell population *in vitro*

(A) Representative flow cytometry plots of CD45RO and CCR7 expression within the human CD4$^+$ T cell untreated vehicle control group and the FMO CD54RO and FMO CCR7 gating strategy controls used to place the gate. Quantification of **(B)** naïve (CD45RO$^-$ and CCR7$^+$), **(C)** EM (CD45RO$^+$ and CCR7$^-$) and **(D)** EM (CD45RO$^+$ and CCR7$^+$) CD4$^+$ T cell population frequencies within human CD4$^+$ T cells pre-treated with 50µM of Oleic acid, Palmitate, stearic acid overnight without any activation signal. Cells were then either left non-activated or activated with plate bound CD3 (2.5µg/mL) and CD28 (1.5µg/mL) for 48 hours following the overnight lipid pre-treatment. The untreated control group represents the vehicle control group and received the ethanol: BSA (1:4) solution used for the solubilisation of lipid groups. Each point represents an individual technical replicate of the treatment group (n=4). Kruskal-Wallis with Dunnett's correction; Data presented as mean ± SEM, *p<0.05, ** p<0.01, *** p<0.001.

Additionally, we also investigated the Treg frequencies within the lipid pre-treated *in vitro* CD4$^+$ T cell model. Consistent with the other main CD4$^+$ T cell subset distribution, Foxp3$^+$ Treg population did not illustrate any observable variance within the non-activated CD4$^+$ T cell groups (**Figure 5.14A**).

Following the activation CD4$^+$ T cells OA pre-treated group induced a significant elevation in Foxp3$^+$ Treg population compared to the vehicle control (**Figure 5.14B**). Contrarily, the Foxp3$^+$Treg frequencies were significantly reduced following the STE pre-treatment compared to control group (**Figure 5.14B**). Consistently, the elevation observed in Foxp3$^+$ Treg population within the OA-treated group was also confirmed by the significant elevation observed in the main Treg-associated cytokine, IL-10 secretion (**Figure 5.14C**).

Altogether, *in vitro* lipid pre-treatment of CD4$^+$ T cells were shown to recapitulate the deleterious 'priming' effect of bioactive SFAs (PA and STE) on human CD4$^+$ T cells and induce them towards a pro-inflammatory EM phenotype as observed in the 14-week HFD-fed DIO murine model. These observations were important to for the identification of main bioactive lipid drivers and the validation of a reliable *in vitro* assay that recapitulates the DIO-linked pro-inflammatory EM bias in human CD4$^+$ T cells.

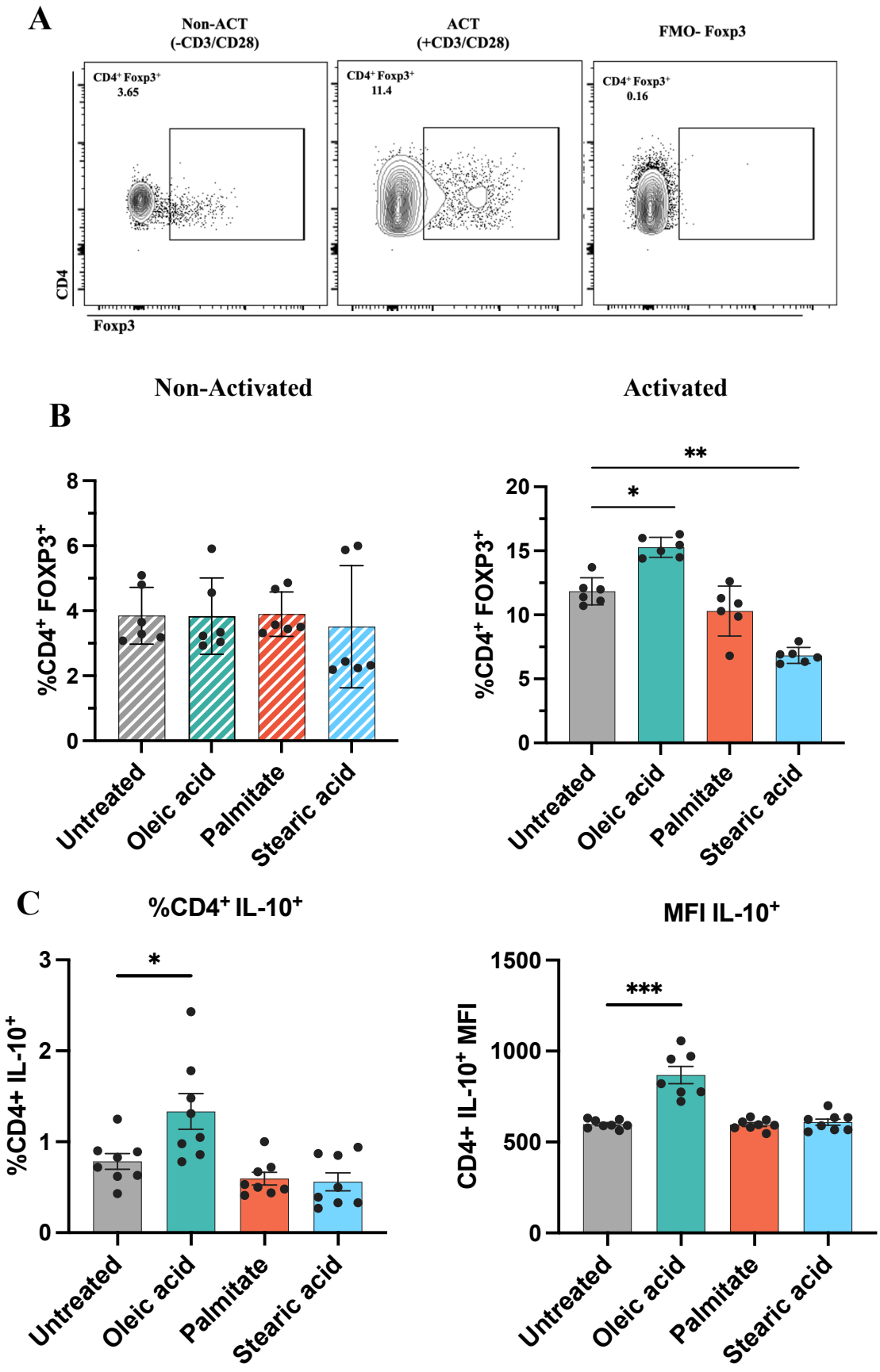


Figure 5.14) Foxp3$^+$ Treg population within human CD4$^+$ T cells on 3-day *in vitro* lipid treatment assay

(A) Representative flow cytometry plots of main Treg defining transcription factor Foxp3 expression on non-activated, activated and the FMO control (used to place the gating) in the untreated human $CD4^+$ T cell (vehicle control group). **(B)** Quantification of Foxp3 expression and **(C)** IL-10 expression within non-activated and activated human $CD4^+$ T cells pre-treated with 50μM of Oleic acid, palmitate, stearic acid overnight without any activation signal. Cells were then either left non-activated or activated with plate bound CD3 (2.5μg/mL) and CD28 (1.5μg/mL) for 48 hours following the overnight lipid pre-treatment. The untreated control group represents the vehicle control group and received the ethanol: BSA (1:4) solution used for the solubilisation of lipid groups. Each point represents an individual technical replicate of the treatment group (n=3). Kruskal-Wallis with Dunnett's correction; Data presented as mean ± SEM, *p<0.05, ** p<0.01, *** p<0.001.

5.7. HFD promotes epigenetic modification of critical genes that may underpin the long-lasting bias in pro-inflammatory effector memory phenotype

Following the observation that the WGWL group (HFD-RE), still expresses the HFD-induced exacerbated pro-inflammatory $CD44^+$ LFA-1^+- $CXCR3^+$ EM $CD4^+$ T cell phenotype when challenged by an allogeneic immunisation, we sought to investigate the potential mechanism driving the HFD-induced long-term 'priming/reprogramming' effect. This observation was highly intriguing as the formerly obese HFD-RE group were shown to retain this exacerbated pro-inflammatory EM 'priming' effect despite they returned to a body weight, body fat tissue content.

Following the recent publications suggesting a novel concept of 'obesogenic diet-driven immune memory/reprogramming' via epigenetic and metabolic reprogramming of immune cells, we investigated any potential direct epigenetic modifications on the DNA methylation profile of $CD4^+$ T cells [25, 379, 585, 589, 590]. We have investigated the DNA methylation profile of our 14-week DIO *in vivo* model by utilising an unbiased, high-throughput reduced-representation bisulfide sequencing (RRBS) on naïve and memory ($CD44^+$) $CD4^+$ T lymphocytes isolated from the spleens of all three diet group mice (CD, HFD, HFD-RE). The RRBS and the subsequent bioinformatic analysis were carried out in collaboration with **Dr Belinda Nedjai's** laboratory at QMUL as detailed in **Section 2.16** (**Figure 5.15**).

Bioinformatic analysis on the RRBS dataset identified total of 991 unique differentially methylated genes (DMG) defined using adjusted P<0.05 and |log2(fold-change)|>2.0. As expected the highest number of differentially methylated genes were identified between CD and HFD group (442 DMGs); 299 hypermethylated and 143 hypomethylated (**Table 5.1**). On the other hand, 8 weeks of HFD in the HFD-RE group were shown to induce hypomethylation

of 177 genes which could potentially suggest a higher transcriptional activity based on the methylation gene area (**Table 5.1**). Additionally, following the weight-loss of the HFD-RE group most of the DMG were shown to be re-hypermethylated compared to higher accessibility (down-methylation) in HFD group (**Table 5.1**). This suggests an ameliorative effect of weight loss at the epigenetic level by reverting the methylation status of various genes back to the CD control configuration. **Table 5.2** illustrates the comparison between two DMG datasets between HFD-RE vs. CD compared to HFD vs. CD group. This comparative analysis between datasets identified the candidate genes uniquely differentially methylated in HFD vs CD and RE vs CD memory datasets (**Table 5.2 & Figure 5.15**). Interestingly, 70 unique genes were commonly differentially methylated between HFD and HFD-RE groups compared to CD whereas, 22 genes were hypermethylated and 48 genes were hypomethylated (**Table 5.2 & Figure 5.16A**).

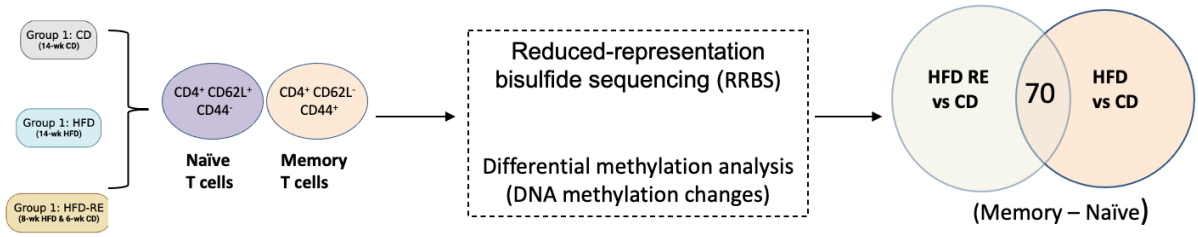


Figure 5.15) Past DIO by 8-weeks of HFD exposure induces a persistent epigenetic alteration in methylation structure of murine CD4$^+$ T cells inducing a long-term reprogramming
Experimental schematic of the RRBS sequencing data analysis of murine CD4$^+$ T cells obtained from the spleen of female C57BL/6J mice fed on CD, HFD, and HFD-RE (8-wk HFD and 6-wk CD) for 14-weeks and were subjected to an allogeneic immunisation at 13.week. Both naïve and memory CD4$^+$ T cells were isolated by Stemcell isolation kits and used for RRBS analysis in **Nedjai's** laboratory QMUL.

Table 5.1) Differentially methylated genes in spleen memory CD4$^+$ T cells of the diet groups

	HFD vs. CD	**HFD-RE vs. CD**	**HFD-RE vs. HFD**
	Unique genes from experiment in memory samples		
Up methylated	299	87	232
Down methylated	143	177	53

Table 5.2) Differentially methylated genes uniquely appear in memory cells between HFD-RE vs. CD compared to HFD vs. CD group

	(HFD vs. CD) compared to (HFD-RE vs. CD)
Up methylated	22
Down methylated	48

This data suggests that HFD feeding for a given period of time induced a persistent reduction in the methylation status of these 48 genes which remained in similar methylation conformation to the HFD group even well after the weight loss (**Figure 5.16A**).

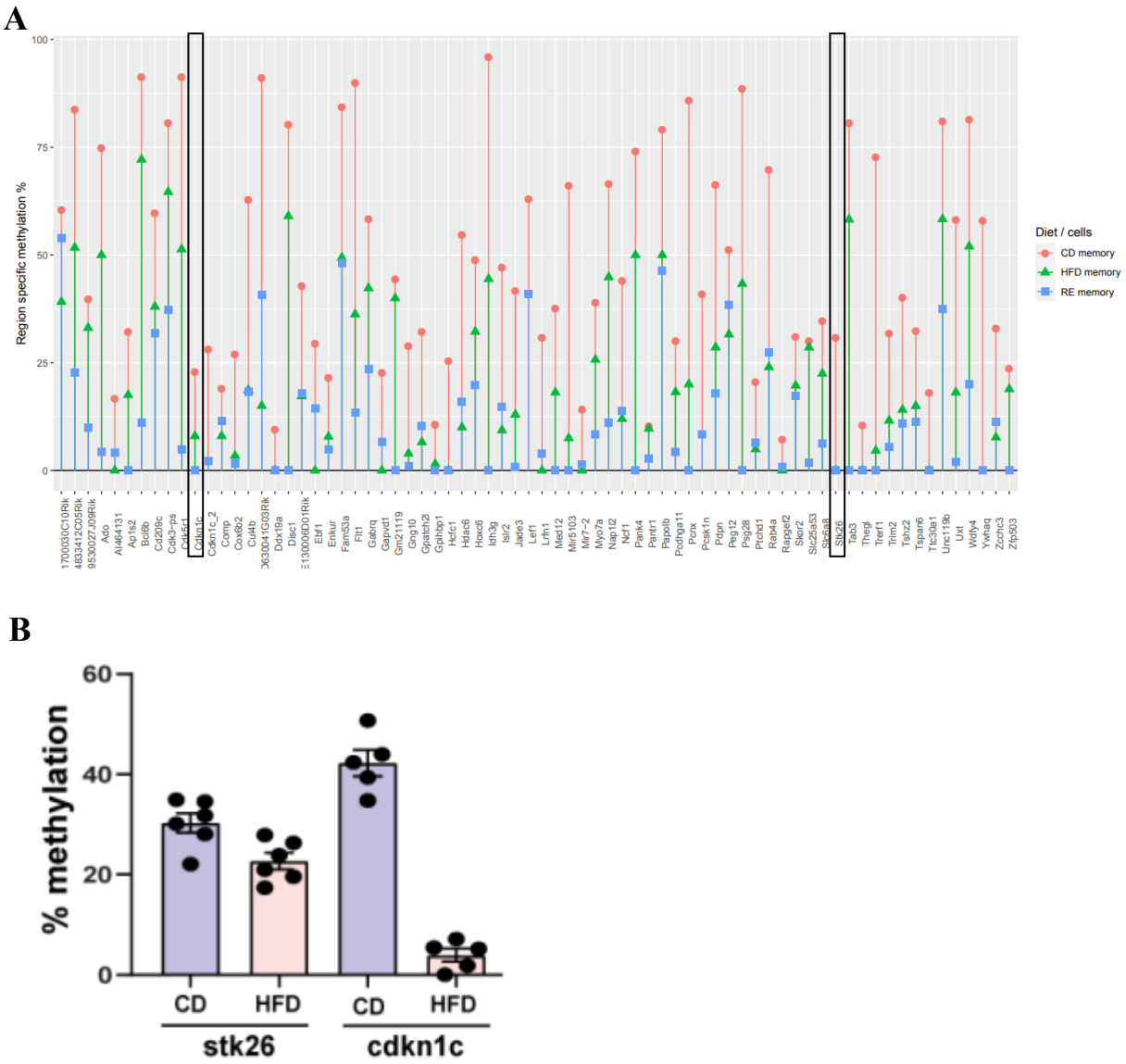


Figure 5.16) Past DIO by 8-weeks of HFD exposure induced a persistent hypomethylation of STK26 and CDKN1C within murine CD4$^+$ T cells

(A) Differential methylation status of DMG identified within the memory CD44$^+$ CD4$^+$ T cells isolated from the spleen of female C57BL/6J mice fed on CD, HFD, and HFD-RE (8-wk HFD and 6-wk CD) for 14-weeks and were subjected to an allogeneic immunisation at 13.week. **(B)** Targetted pyrosequencing analysis illustrating the differential methylation status of STK26 and CDKN1C within the memory CD44$^+$ CD4$^+$ T cells isolated from the spleen of female C57BL/6J mice fed on CD and HFD groups. All RRBS and pyrosequencing experiments and analysis were carried out by **Dr Belinda Nedjai's** laboratory in QMUL as a collaboration.

A deep bioinformatic analysis was carried out for identifying the top hits through extrapolating the genes that appeared differentially methylated between HFD and HFD-RE memory cells compared to CD memory groups.

Following the identification of 70 differentially methylated candidate genes, 9 genes were biologically curated due to the extensive literature research, evaluating any potential links established between each of the 9 genes and obesity, inflammation, diet and effector memory T cell response. We also performed two pathway analyses using DAVID and Enrichr databases. Additionally we extensively reviewed the cell-type gene expression profiles and associated pathways, aiming to identify key genes that may elucidate the underlining molecular mechanism of obesity-driven long-lasting pro-inflammatory EM phenotype.

Two particular genes named serine/threonine kinase 26 (STK26/MST4) and cyclin-dependent kinase inhibitor-1C (CDKN1C) were identified highly prominent within T cells in both murine and human conditions and crucial in biological processes such as cell cycle, apoptosis, autophagy and cellular senescence. Both DAVID and Enrichr pathway analyses and gene ontology analysis, suggested these two promising candidate genes based on their relation with myeloid cells differentiation pathways, inflammatory pathways and TCA cycle pathways.

Following the untargeted genome-wide RRBS sequencing, a targeted pyrosequencing analysis was utilised to specifically investigate the methylation status of the two main candidate genes. The hypomethylation status of STK26 and CDKN1C was further confirmed by pyrosequencing analysis on the memory $CD44^+$ $CD4^+$ T cells obtained from CD control and HFD groups (**Figure 5.16B**). This consistent hypomethylation further confirmed the RRBS data, suggesting HFD-induced potential alterations in the transcriptional profiles of STK26 and CDKN1C genes within the memory $CD4^+$ T cells.

5.8. Hypomethylation of STK26 and CDKN1C by HFD-derived bioactive PA and STE induces elevation of gene expression and protein levels

STK26 is one of the four members of the serine/threonine kinase (STK) family, involved in the regulation of various critical biological processes including proliferation [646], migration [647], apoptosis [648] and inflammation [646, 649, 650]. Importantly, Huang et al. 2017 identified a critical role of STK26 in inducing autophagy via directly phosphorylating the

ATG4B. Although both STK26 and ATG4B enzymes are not in the conventional canonical autophagy pathway, their profound effect in inducing autophagy in a non-canonical pathway has been validated in both murine and human conditions [649, 651, 652]. Inhibition of STK26 via a specific Hesperadin inhibitor, was shown to significantly reduce autophagy within an *in vivo* murine model which further validated the parallel role of STK26 with LC3 in inducing autophagy [653].

The gene expression analysis with the gene expression atlas and human protein atlas databases suggested a high STK26 expression in $CD4^+$ T cells and T cell progenitor hematopoietic stem cells in humans as well murine conditions (**Figure 5.17**) [654, 655].

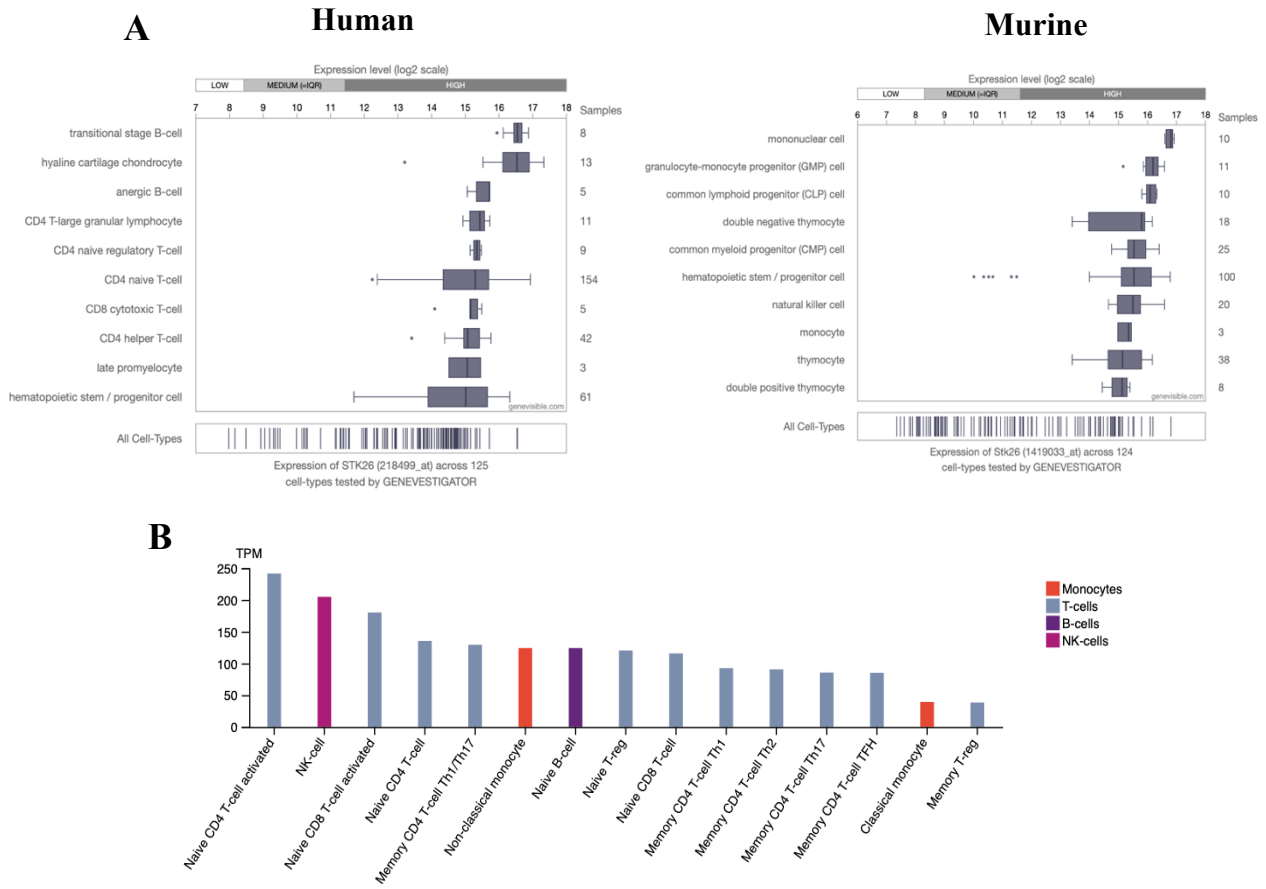


Figure 5.17) STK26 gene expression in human and murine $CD4^+$ T cells
(A) Serine/threonine kinase 26 (SKT26) gene expression profiles of human and murine immune cells analysed across 125 cell-types tested and presented by Genevestigator image credit: Genevestigator (https://genevestigator.com/search/?s=STK26) **(B)** SKT26 protein expression within specific immune cells were visualised by Human protein atlas based on the data set of Schmiedel et al. 2018, (https://www.proteinatlas.org/ENSG00000134602-STK26/immune+cell) [654]. Image credit: Human Protein Atlas proteinatlas.org

Based on the significant hypomethylation observed on STK26 within both HFD and HFD-RE groups of the 14-week DIO experiment, we hypothesised that hypomethylation could modulate the expression of STK26 protein within $CD4^+$ T cells and assessed the STK26 protein levels within cells obtained from the pLN tissues of all three diet groups. The western blot analysis on three mice from each group demonstrated a statistically significant upregulation of STK26 protein within the HFD group compared to CD group (**Figure 5.18**). Although HFD-RE group also illustrated a prominent increase in STK26 protein level, this increase did not reach the statistical significance. Considering the notable increasing trend observed with the HFD-RE group, it is crucial to increase the number of biological replicates for an adequate statistical test.

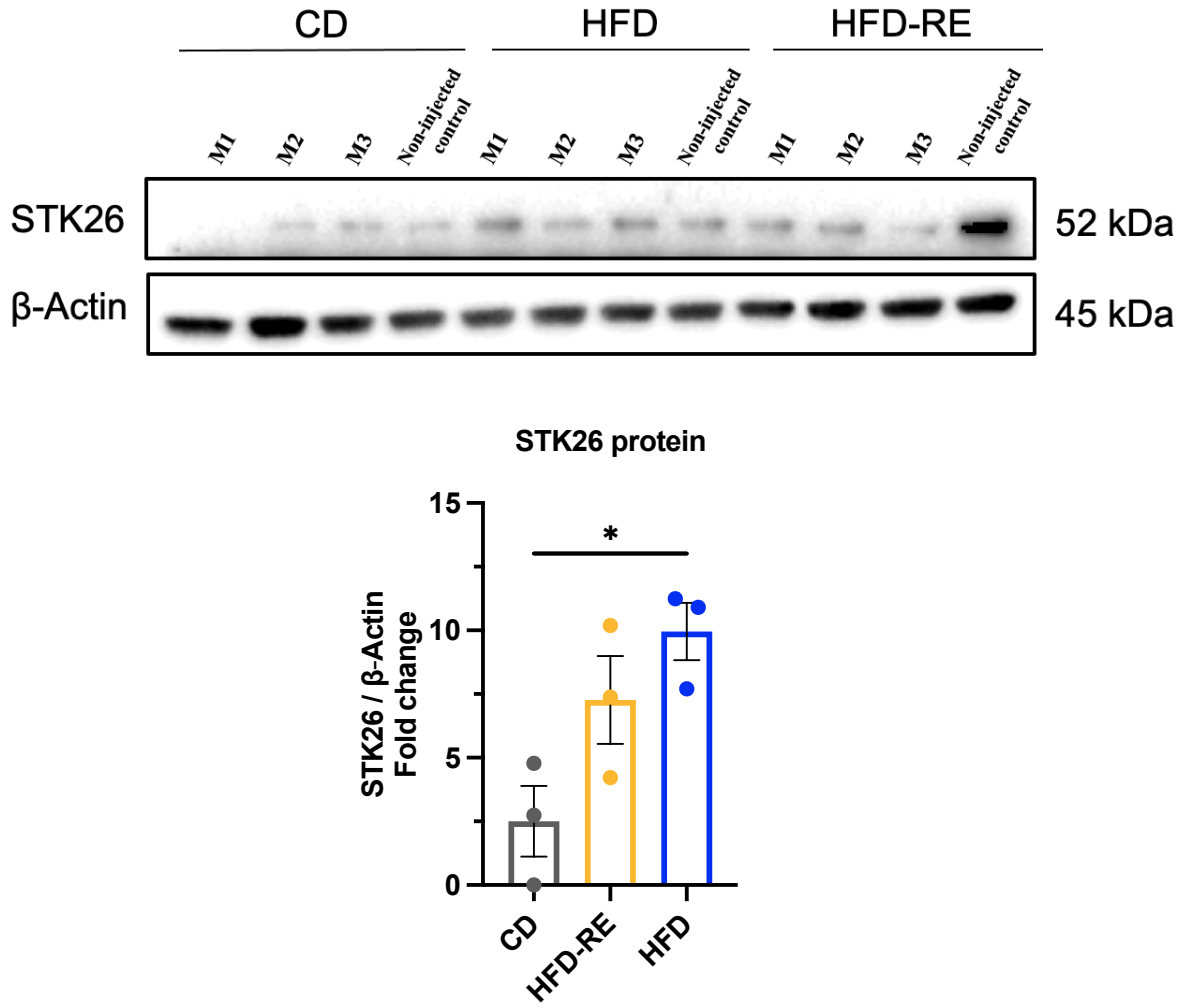


Figure 5.18) HFD-feeding increases the STK26 protein levels within pLN tissues of the 14-wk DIO murine model

(A) STK26 protein was detected by western blotting and expression normalised to β-actin **(B)** Quantification of the STK26 protein within murine cells isolated from pLN issues obtained from female C57BL/6J mice fed on CD, HFD, and HFD-RE (8-wk HFD and 6-wk CD) for 14-weeks and were subjected to an allogeneic immunisation at 13.week. Each point represents an individual mouse (M1-

A

M3) in allocated diet groups (one *in vivo* experimental dataset with 6 mice per group) (n=3). Unpaired two-tailed student t-test; Data presented as mean ± SEM, *p<0.05; ** p<0.01, *** p<0.001. Westerns blots and quantification conducted by **Atrayee Gope** (MRes student).§ It should be noted that although it was planned to analyse the each mouse under each diet groups (n=3), we were unable to carry out this analysis due to technical issue experienced during the cull day.

Additionally, to investigate the potential direct role of HFD-derived bioactive SFAs such as PA and STE on the hypomethylation of STK26 within CD4+ T cell, we have utilised *in* vitro lipid pre-treated human CD4+ T cell samples (as detailed in Section 5.5) to analyse gene expression and protein levels of STK26. Initially, we have tested the gene expression of an known activation marker IL-2Rα (CD25) via qPCR to further confirm the flow cytometry observations on human *in vitro* lipid pre-treated $CD4^+$ T cell (**Supplementary-Figure S14-15**)

Strikingly, both SFA-treated groups: PA and STE induced a significant elevation of STK26 gene expression levels compared to the vehicle control group (**Figure 5.19**). Interestingly, this increase was consistent within both activated and non-activated human $CD4^+$ T cell groups treated with PA and STE (**Figure 5.19**). Importantly, the relative fold change of the elevations observed in non-activated groups we small (~x2) whereas, activation $CD4^+$ T cell following the pre-treatment of PA and STE were shown to increase relative fold change ~4 times compared vehicle control group.

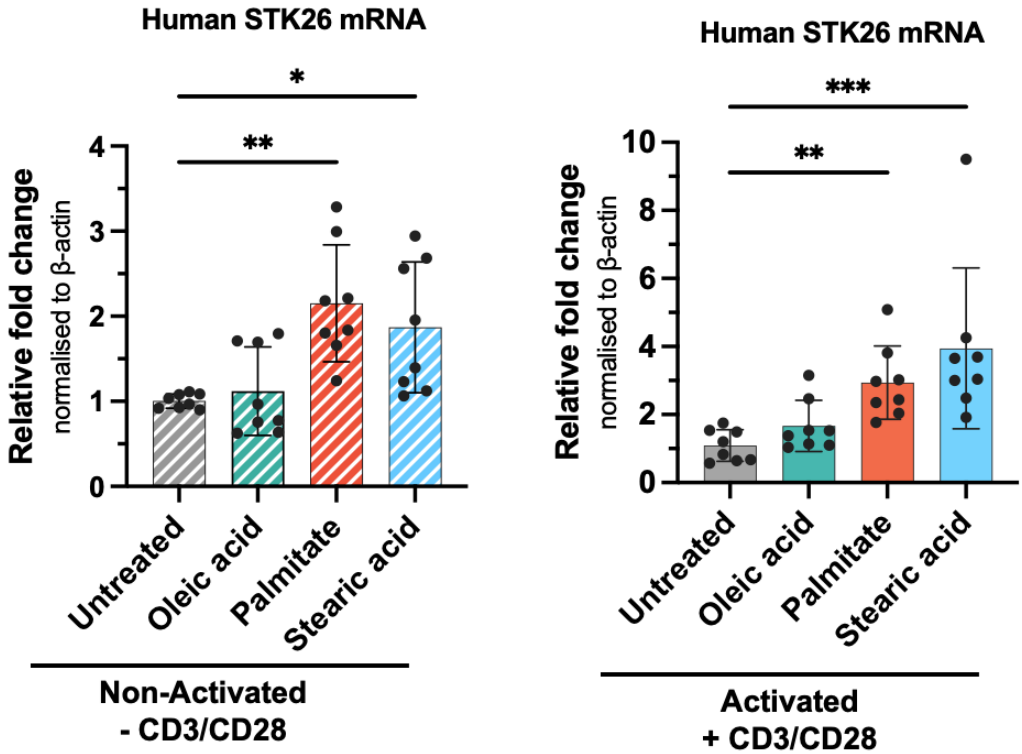


Figure 5.19) STK26 mRNA expression within human $CD4^+$ T cells on 3-day *in vitro* lipid pre-treatment assay

STK26 mRNA expression within the human $CD4^+$ T cells pre-treated with 50μM of Oleic acid, palmitate, stearic acid overnight without any activation signal. Cells were then either left non-activated or activated with plate bound CD3 (2.5μg/mL) and CD28 (1.5μg/mL) for 48 hours following the overnight lipid pre-treatment. The untreated control group represents the vehicle control group and received the ethanol: BSA (1:4) solution used for the solubilisation of lipid groups. Each point represents an individual technical replicate of the treatment group (n=4). Kruskal-Wallis with Dunnett's correction; Data presented as mean ± SEM, *p<0.05, ** p<0.01, *** p<0.001.

In line with the mRNA expression dataset, western blot analysis of *in vitro* PA pre-treated human $CD4^+$ T cells illustrated a significant increase in the STK26 protein compared to the untreated control group (**Figure 5.20B**). However, contrasting the upregulation observed in STK26 gene expression level, STE treatment did not induce any upregulation in the STK26 protein levels compared to vehicle control group (**Figure 5.20B**). It is well known that modulation in mRNA gene expression level does not always necessarily reflect a modulation in protein level. On the hand, consistently with the small modulation observed at the STK26 mRNA levels, no difference was observed in STK26 protein levels between non-activated lipid pre-treatment groups (**Figure 5.20C**).

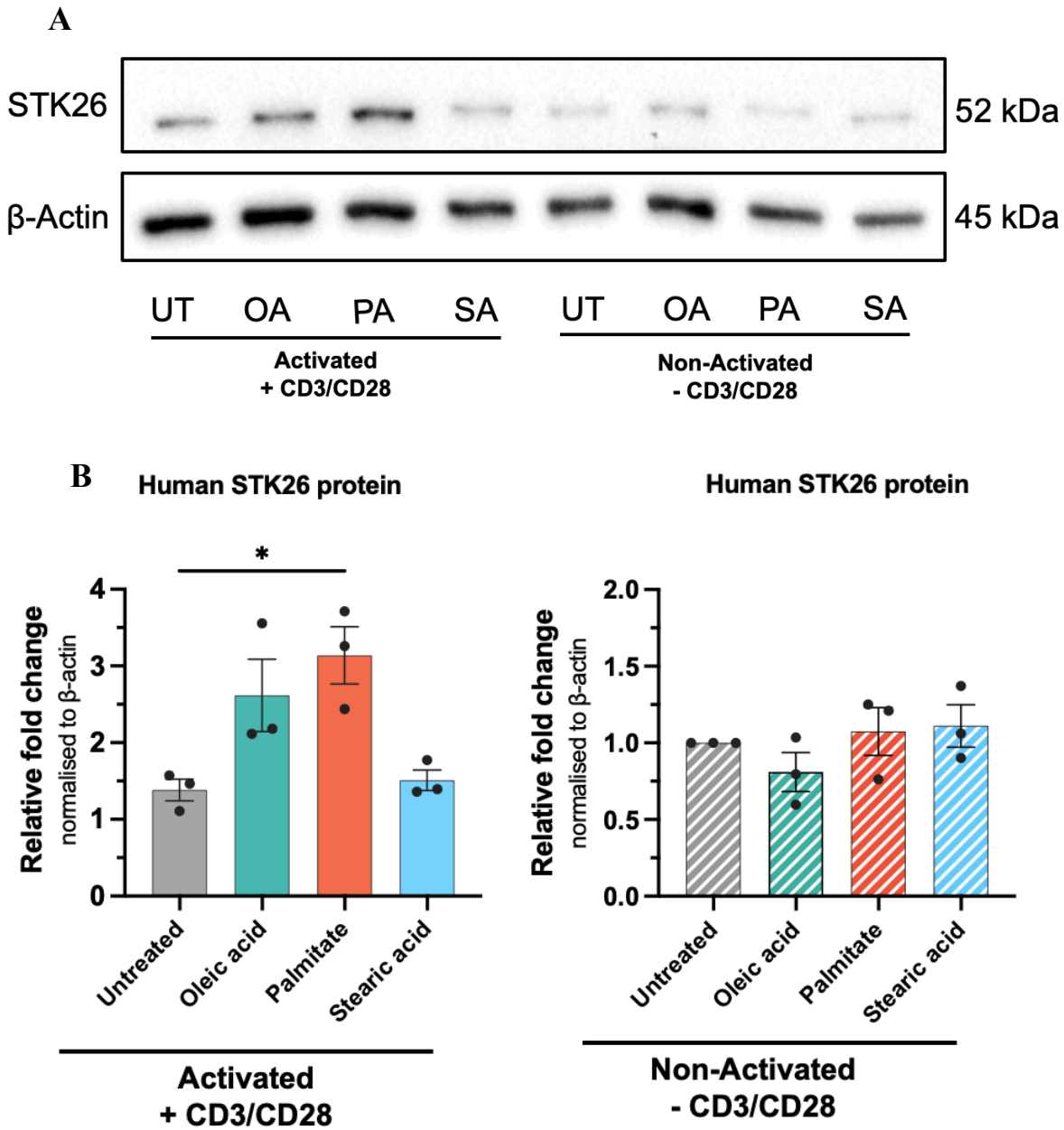


Figure 5.20) Palmitate pre-treatment of human CD4$^+$ T cell *in vitro* induces upregulation of STK26 protein

(A) STK26 protein was detected by western blotting and expression normalised to β-actin, relative to untreated (vehicle control) group **(B)** Quantification of the STK26 protein within human CD4$^+$ T cells pre-treated with 50μM of Oleic acid, palmitate, stearic acid overnight without any activation signal. Cells were then either left non-activated or activated with plate bound CD3 (2.5μg/mL) and CD28 (1.5μg/mL) for 48 hours following the overnight lipid pre-treatment. The untreated control group represents the vehicle control group and received the ethanol: BSA (1:4) solution used for the solubilisation of lipid groups. Each point represents an individual technical replicate of the treatment group (n=3). Unpaired two-tailed student t-test; Data presented as mean ± SEM, *p<0.05; ** p<0.01, *** p<0.001. Carried out by **Atrayee Gope** (MRes student).

Furthermore, CDKN1C ($p57^{KIP2}$) is a well-known inhibitor protein, binding to several cyclin-dependent kinases and G1 cyclin complexes that induce a negative regulation on the cell cycle G1-phase [656, 657]. Consistently, CDKN1C is shown to act as a negative regulator of cell proliferation and plays a critical role in maintaining a nonproliferative cell state such as senescence [656-658]. Alteration in CDKN1C methylation status was shown to trigger dysregulation in CDKN1C expression which has been associated with various cancer types [656-658]. Additionally, CDKN1C has been also shown to be involved in the induction of cellular senescence. The upregulation of CDKN1C expression was suggested to induce a senescent phenotype in various cell types including astrocytes and prostate carcinomas [659-661]. Giovannini et al., illustrated the direct augmenting effect of CDKN1C accumulation in inducing cellular senescence [662]. Despite the publications in carcinomas, the link between CDKN1C and cellular senescence of immune cells is not well understood.

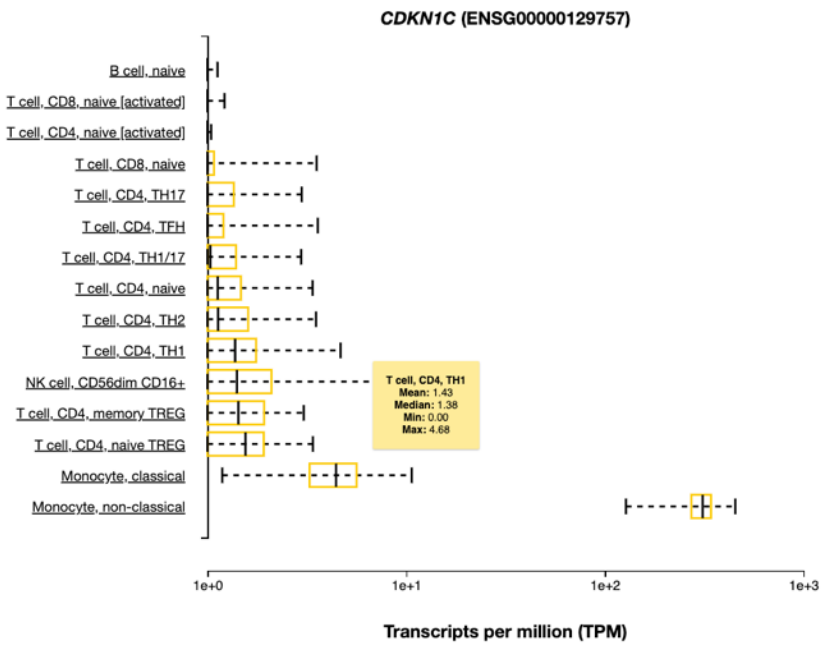


Figure 5.21) CDKN1C ($p57^{KIP2}$) gene expression in human $CD4^+$ T cells
Cyclin-dependent kinase inhibitor 1C- CDKN1C ($p57^{KIP2}$) protein expression within specific immune cells were visualised by Human protein atlas based on the data set of Schmiedel et al. 2018, (https://www.proteinatlas.org/ENSG00000129757-CDKN1C/immune+cell)[654]. Image credit: Human Protein Atlas proteinatlas.org

Importantly, both the immune cell gene expression and human protein atlas databases, illustrated the expression of CDKN1C within the human $CD4^+$ T cells following the highest CDKN1C-expressing cells: monocytes (**Figure 5.21**). Following this, we attempted to investigate the expression of CDKN1C protein within the murine $CD4^+$ T cells isolated from

the splenocytes of all three different *in vivo* diet groups. However due to technical limitations of the CDKN1C antibody in western blotting, we were unable to obtain any reliable image (*data not shown*).

Secondly, we investigated the CDKN1C mRNA expression of human $CD4^+$ T cells pre-treated with candidate lipid groups under both activated and non-activated *in vitro* conditions (**Figure 5.22**). Similar to STK26 mRNA expression profile, both *in vitro* PA and STE treatment groups induced a significant upregulation of CDKN1C mRNA expression within both activated and non-activated human $CD4^+$ T cells compared to untreated vehicle control (**Figure 5.22**). Similar to the STK26 expression, the increasing fold change was greater in the activated cells than nonactivated.

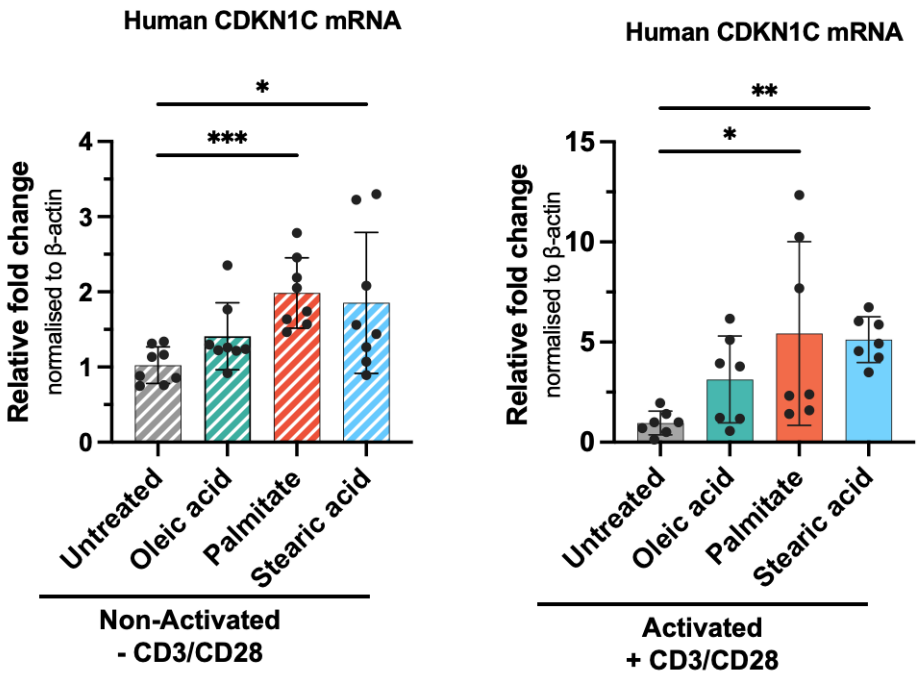


Figure 5.22) CDKN1C mRNA expression within human $CD4^+$ T cells on 3-day *in vitro* lipid pre-treatment assay

CDKN1C mRNA expression within the human $CD4^+$ T cells pre-treated with 50µM of Oleic acid, palmitate, stearic acid overnight without any activation signal. Cells were then either left non-activated or activated with plate bound CD3 (2.5µg/mL) and CD28 (1.5µg/mL) for 48 hours following the overnight lipid pre-treatment. The untreated control group represents the vehicle control group and received the ethanol: BSA (1:4) solution used for the solubilisation of lipid groups. Each point represents an individual technical replicate of the treatment group (n=4). Kruskal-Wallis with Dunnett's correction; Data presented as mean ± SEM, *p<0.05, ** p<0.01, *** p<0.001.

5.9. Potential functional cellular alterations on T lymphocytes associated with HFD-driven hypomethylation-linked upregulation of STK26 and CDKN1C

Importantly, HFD was capable to induce hypomethylation and concomitant elevation in gene expression of two prominent candidate genes (STK26 and CDKN1C) within both HFD and HFD-RE murine groups. Furthermore, *in vitro* PA and STE pre-treatment groups were shown to be capable of generating the HFD-induced pro-inflammatory EM phenotype as well as the concomitant elevation of the STK26 and CDKN1C candidate gene expression in human $CD4^+$ T cells. Considering our hypothesis, we investigated for any potential modulations in the cellular functions (autophagy and senescence) known to be associated with the STK26 and CDKN1C candidate genes identified.

5.9.1. Modulations in autophagy flux capacity within *ex vivo* murine CD4 T cells isolated from SLOs of different diet groups

Following the observations that, both HFD-feeding *in vivo* and SFA-treatment *in vitro* were able to induce the overexpression of STK26 within $CD4^+$ T cells (via hypomethylation), we have investigated for any potential STK26-driven modulation in the autophagic degradation capacity (also known as autophagic flux).

It was highly crucial to measure the real-time autophagy capacity of distinct $CD4^+$ T cell subsets, especially on the EM population of interests such as $CXCR3^+$ and $LFA1^+$ $CD44^+$ $CD4^+$ T cells isolated from *in vivo* murine diet groups. To be able to specifically investigate this we utilised a specific autophagy LC3-II detection kit (Guava) by flow cytometry. As autophagy is a constitutive cycle of degradation it is essential to use certain pharmacological autophagic flux inhibitors such as chloroquine (CQ) to prevent lysosomal degradation and allow the quantification of accumulated cellular LC3. The guava autophagy detection kit protocol was updated and optimised for the staining of extracellular markers and cell viability (CQ-dose) (**Supplementary-Figure S16**) [663].

In line with the hypothesis and STK26 upregulation (**Figure 5.18**), autophagy flux was shown to be significantly elevated within spleen $CD4^+$ T cells of both HFD and HFD-RE groups (**Figure 5.23A**). Importantly, the autophagy flux was also significantly increased within pro-inflammatory EM $CD4^+$ T cell ($LFA\text{-}1^+$ and $CXCR3^+$ $CD44^+$) spleen populations compared to

the CD control (**Figure 5.23**). Although a similar rising trend was observed with total and EM CD4$^+$ T cell populations within the pLN tissue, unlike the spleen this increase did not reach the statistical significance (**Figure 5.23B**).

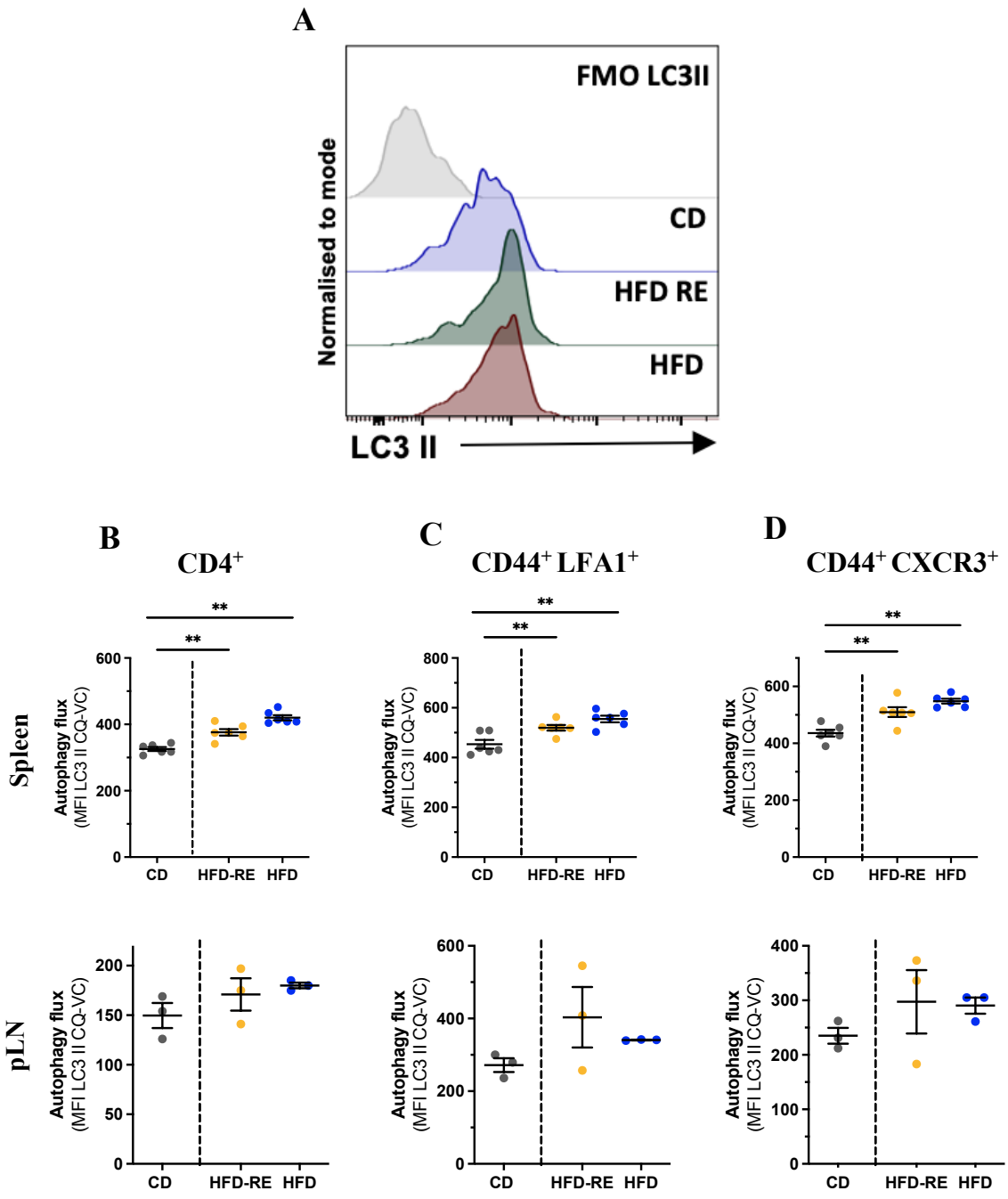


Figure 5.23) Exposure to HFD induces a long-term increase in the autophagy flux within the EM CD4$^+$ T cell populations of formerly obese mice group

(A) Representative flow cytometry histogram showing LC3 expression on CD44$^+$ CXCR3$^+$ gated within live CD4$^+$ T cells from splenocytes isolated from CD, HFD and HFD RE mice. Quantification of LC3-II on **(B)** live CD4$^+$ T cells, **(C)** CD44$^+$ LFA-1$^+$ and **(D)** CD44$^+$ CXCR3$^+$CD4$^+$ T cells isolated from Spleen and pLN tissues were collected and digested from female C57BL/6J mice fed on CD, HFD, and HFD-RE (8-wk HFD and 6-wk CD) for 14-weeks and were subjected to an allogeneic immunisation at

13.week. Both cells from spleen and pLN were incubated *ex vivo* with 100µM of CQ within RPMI for 4 hours. Cells were then stained for extracellular markers and autophagosome -bound intracellular LC3-II via Guava kit as optimised. Each point represents an individual mouse in allocated diet groups (one *in vivo* experimental dataset with 6 mice per group shown together, n=6 in total). One-way ANOVA with Dunnett's correction; Data presented as mean ± SEM, *p<0.05; ** p<0.01, *** p<0.001. **§** Second set of the *in vivo* experiment pLN tissues (n=3) were not been able to analyse due to technical limitations experienced with the counting beads on the day.

Importantly, this data further validated the potential association between the HFD-driven hypomethylation of STK26 and the consecutive STK26 upregulation-driven functional elevation in the autophagy capacity of the $CD4^+$ T cells. Interestingly, consistent with the persistent hypomethylation on STK26 and CDKN1C genes (driven by past HFD-exposure), HFD-RE group was shown to possess a persistently increased autophagy flux within $CD4^+$ T cells, indicating no amelioration on the functional elevation of the autophagy flux even well after the weight loss.

5.9.2 Modulations in autophagy flux capacity within *in vitro* lipid treated human $CD4^+$ T cells

To investigate potential direct mechanistic links between bioactive SFAs and functional alterations observed in autophagy in association with the hypomethylation and overexpression of STK26, we utilised the *in vitro* lipid pre-treatment human $CD4^+$ T cell assay. Similar to the murine *ex vivo* conditions, we optimised the LC3-II detection by Guava autophagy detection kit where following the 3-day *in vitro* lipid pre-treatment protocol human $CD4^+$ T cells were further treated with CQ for 4 hrs (**Supplementary-Figure S17**). The dose of the CQ autophagy flux inhibitor is further optimised to 50µM on human $CD4^+$ T cells based on the dose-response and time-response optimisation experiments (**Supplementary-Figure S18**).

Importantly, the LC3-II levels within the *in vitro* lipid pre-treated human $CD4^+$ T cells expressed a high donor-to-donor variation that prevented any clear conclusion (**Figure 5.24A**). Although the initial analysis with two donors illustrated an increasing trend in both $CD4^+$ $LC3^+$ percentage and MFI levels with PA lipid pre-treatment, donor 3 expressed a completely different response with an oversaturated autophagic flux in all treatment and untreated conditions (**Figure 5.24B**). In addition to the oversaturated shift in LC3-II, donor 3 also illustrated a different motif in the distribution of general $CD4^+$ T cell populations, illustrated with the ancestorial backgatings (**Figure 5.25**).

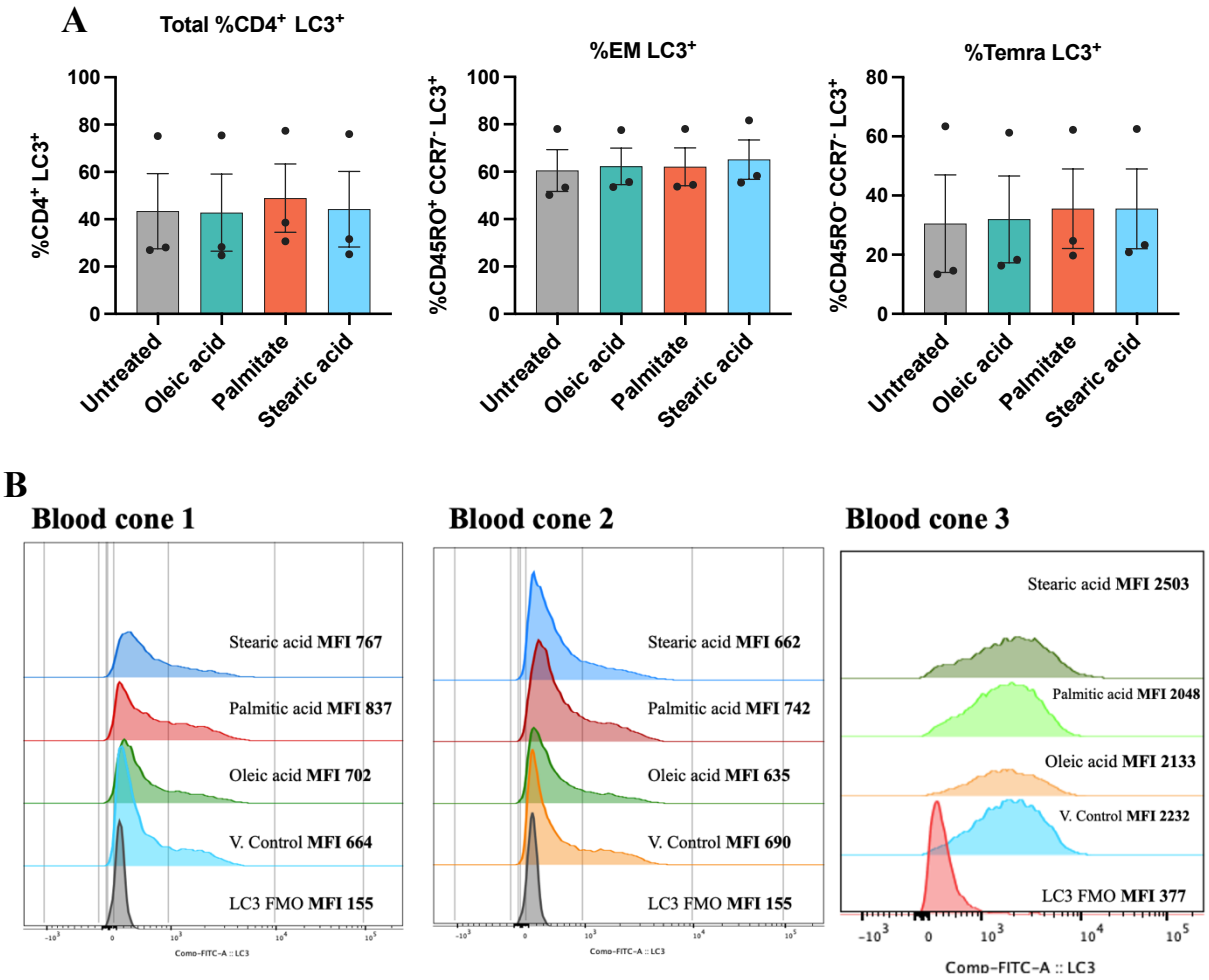


Figure 5.24) Detection of autophagosome-bound intracellular LC3-II within *in vitro* human CD4$^+$ T cells pre-treated with bioactive lipids

(A) Quantification of LC3$^+$ percentage within total human CD4$^+$ T cells, EM CD4$^+$ T cells and Temra (CD45RO$^-$, CCR7$^-$) CD4$^+$ T cells pre-treated with 50µM of Oleic acid, Palmitate, stearic acid overnight without any activation signal. Cells were then either left non-activated or activated with plate bound CD3 (2.5µg/mL) and CD28 (1.5µg/mL) for 48 hours following the overnight lipid pre-treatment. The untreated control group represents the vehicle control group and received the ethanol: BSA (1:4) solution used for the solubilisation of lipid groups. Following the 3-day *in vitro* culture, all cells were treated with 50µM CQ and incubated for 4 hours. Each point represents an individual donor (n=3). **(B)** Representative flow cytometry histogram plots illustrating the shift in LC3-II MFI within FMO gating control (grey), CQ Mock vehicle control (blue), oleic acid (green), palmitate (red) and stearic acid (dark-blue). Highlighting the donor-to-donor variance between the n=3 individual blood cones used each biological replicate.

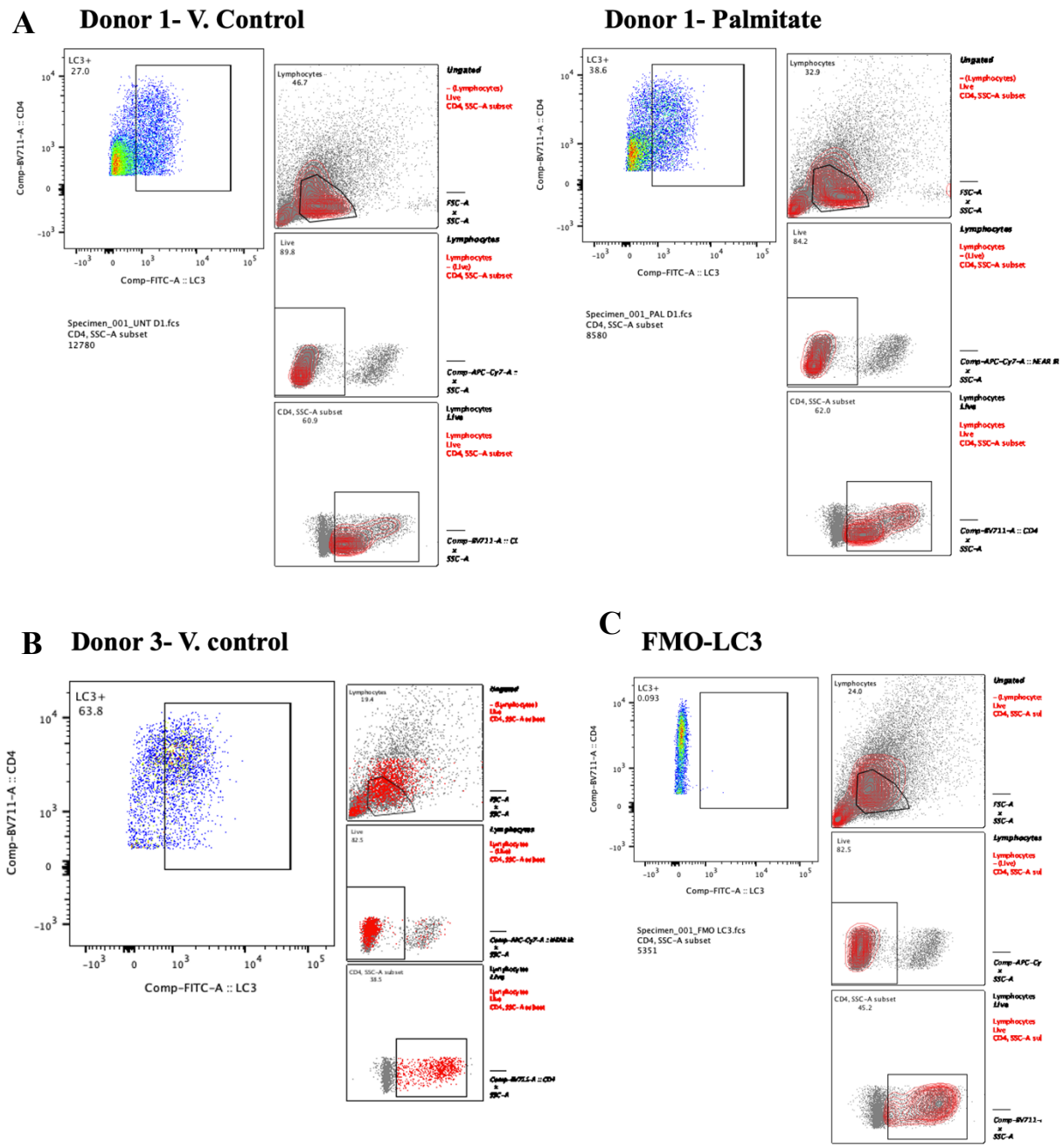


Figure 5.25) Donor to donor variance in LC3-II expression within *in vitro* human CD4$^+$ T cells pre-treated with bioactive lipids

Representative flow cytometry plots including the ancestral gates used for the **(A)** Donor 1 **(B)** Donor 2 and **(C)** LC3 FMO gating control used for the gating strategy of human CD4$^+$ T cells *in vitro* lipid pre-treatment protocol. Freshly isolated human PBMCs were treated with 50µM of Oleic acid, Palmitate, stearic acid overnight without any activation signal. Cells were then either left non-activated or activated with plate bound CD3 (2.5µg/mL) and CD28 (1.5µg/mL) for 48 hours following the overnight lipid pre-treatment.

Importantly, the large variation in autophagy flux levels within human donors is well documented by the various extensive publications where the difference in diurnal rhythm,

exercise, nutrients and daily routines of the donor were suggested as potential factors leading to a high variance in autophagy levels [617, 619, 664].Therefore to validate the initial increasing trend with the PA treatment as demonstrated in **Figure 5.25A**, further donors should be processed.

5.9.3. Modulations in cellular senescence of *ex vivo* murine and *in vitro* human $CD4^+$ T cells

As previously detailed in **Section 5.8**, CDKN1C expression have been associated with cellular senescence [662]. Considering the persistent HFD-driven CDKN1C hypomethylation in both HFD and HFD-RE groups and significant upregulation of CDKN1C gene expression *in vitro* SFA-treated conditions, we sought to investigate any potential changes within senescence profiles of $CD4^+$ T cells obtained *in vivo* murine diet groups and the *in vitro* pre-lipid treated human $CD4^+$ T cells.

Interestingly, both HFD and HFD-RE groups illustrated no significant change within $PD1^+CD4^+$ T cell frequencies in the SLOs tissues compared to the CD control (**Figure 5.26A**). Although HFD groups expressed an increasing trend in the exhausted $PD1^+$ $CD4^+$ T cell population frequencies within all three SLOs tested, none of this elevation was found to be statistically significant. Similarly, murine senescence-linked marker KLRG1 also illustrated no observable difference between the different diet groups (**Figure 5.26B**).

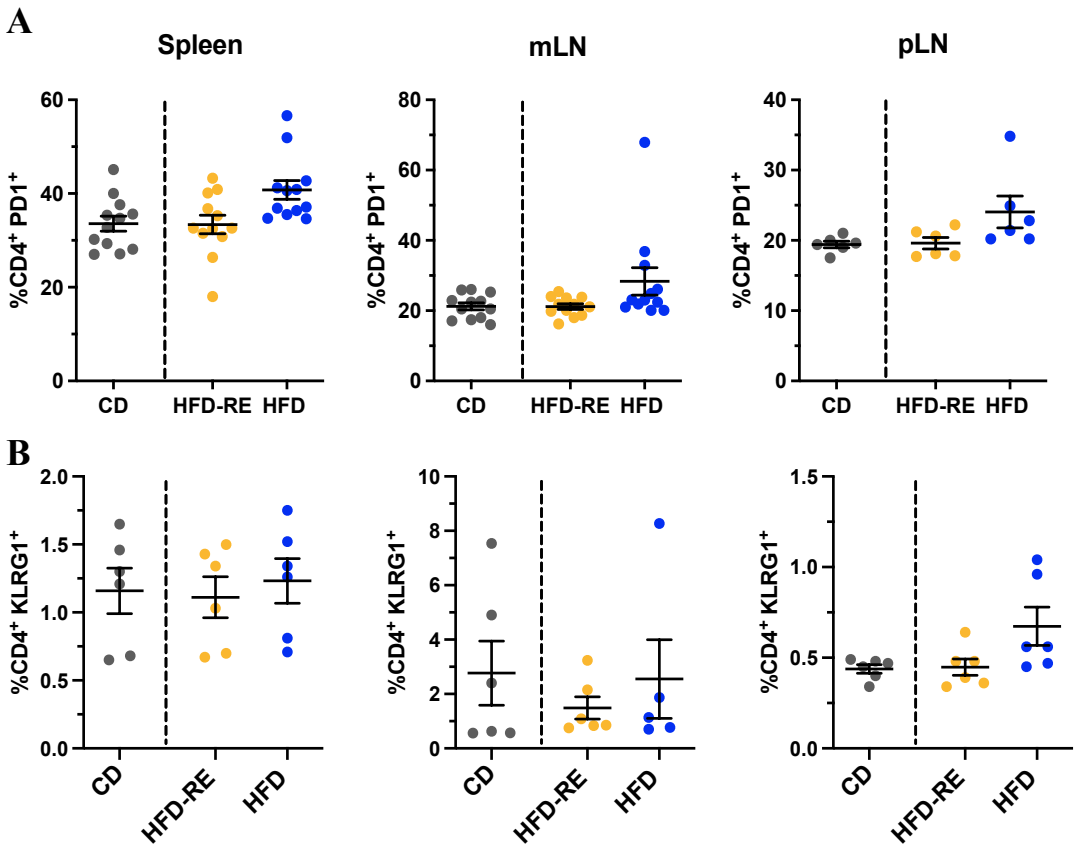


Figure 5.26) Expression of exhaustion and senescence markers on SLO CD4$^+$ T cells of 14-week DIO mouse model

Quantification of flow cytometry data of **(A)** PD1$^+$ for exhaustion and **(B)** KLRG1$^+$ for senescence markers on mouse CD4$^+$ T cell populations within SLO tissues obtained from female C57BL/6J mice fed on CD, HFD, and HFD-RE (8-wk HFD and 6-wk CD) for 14-weeks and were subjected to an allogeneic immunisation at 13.week with CBA and BALB/C splenocyte i.p injection. Each point represents an individual mouse in allocated diet groups (one *in vivo* experimental dataset with 6 mice per group).

Considering the phenotype profoundly observed within pLN EM CD4$^+$ T cell populations (**Figure 5.6**), we further investigated the senescence profile of EM CD4$^+$ T cells. Interestingly, KLRG1$^+$CD44$^+$ T cell populations were significantly elevated within the pLN tissue of both HFD and HFD-RE groups compared to CD control, suggesting a HFD-driven KLRG1$^+$ senescence-linked memory T cell profile (**Figure 5.27A**). More interestingly, this HFD-induced increase in KLRG1$^+$ senescence-linked memory T cell frequencies was found to be persistently elevated within the pLN tissue of the HFD-RE group, even after the weight loss. Additionally, this persistent increase in KLRG1 expression was further detected within the pro-inflammatory LFA1$^+$ CD44$^+$ CD4$^+$ T cell populations isolated from the pLN of both HFD and HFD-RE groups compared to CD control (**Figure 5.27B**). Although the CXCR3$^+$ EM CD4$^+$ T cell populations also illustrated the same increasing trend with the KLRG1 expression in pLN, this increase did not reach statistical significance (**Figure 5.27C**). Altogether this data suggests

that, HFD-driven long-term epigenetic reprogramming can lead to a potential senescence profile on the long-lived memory CD4$^+$ T cell populations in later life which persists even well after the weight loss.

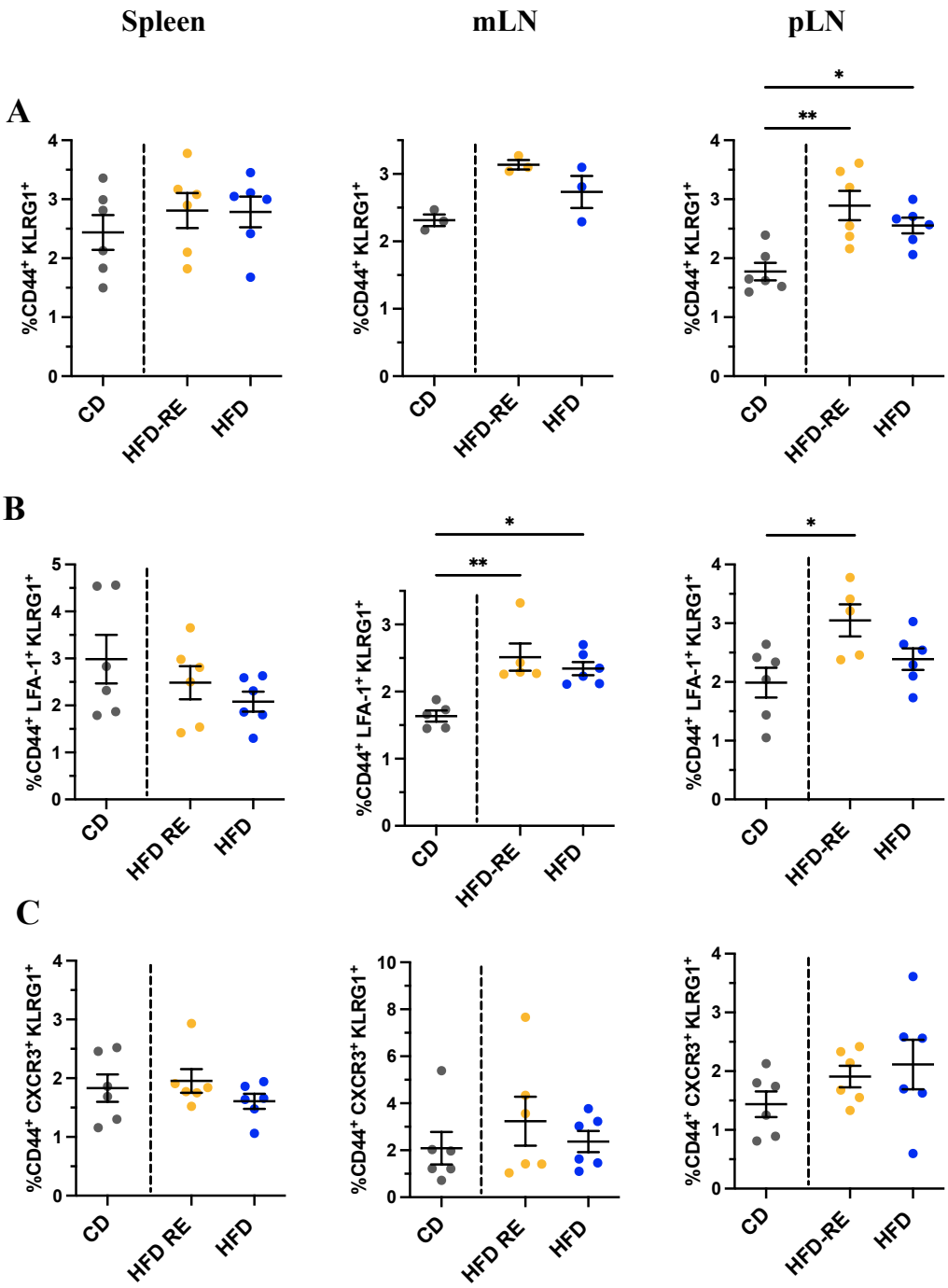


Figure 5.27) HFD feeding induced an elevation in senescence markers of EM CD4$^+$ T cell populations

Quantification of flow cytometry data of KLRG1$^+$ expression on **(A)** CD44$^+$ EM **(B)** CD44$^+$ LFA-1$^+$and **(C)** CD44$^+$ CXCR3$^+$ mouse CD4$^+$ T cell populations within SLO tissues obtained from female C57BL/6J mice fed on CD, HFD, and HFD-RE (8-wk HFD and 6-wk CD) for 14-weeks and were subjected to an

allogeneic immunisation at 13.week with CBA and BALB/C splenocyte i.p injection. Each point represents an individual mouse in allocated diet groups (one *in vivo* experimental dataset with 6 mice per group). One-way ANOVA with Dunnett's correction; Data presented as mean ± SEM, *p<0.05; ** p<0.01, *** p<0.001.

In addition to the *in vivo* 14-week DIO WGWL model, we wanted to further investigate any potential direct effect of bioactive SFAs on the senescence and SASP profiles of the *in vitro* human $CD4^+$ T cells following the lipid pre-treatment assay. Considering the critical role of Temra $CD4^+$ T cells, we have particularly investigated the senescence in Temra populations.

Importantly, we did not observe a significant difference in Temra population frequencies among different lipid treatment groups compared to the vehicle control (**Figure 5.28A**). However it should be noted that, each donor illustrated a high variance in their Temra cell populations potentially due to differences in age, sex, exercise and medical history of each donor. **Figure 5.28B**, illustrates the representative flow cytometry plots of vehicle control group senescence markers investigated on Temra $CD4^+$ T cells. In line with the increasing trend observed in PD1 expression within the HFD-fed group, both PA- and STE-treated human $CD4^+$ T cells were shown to significantly increase the PD1 expression compared to vehicle control (**Figure 5.28C**). Interestingly, within the Temra populations, only STE-treated groups were shown to induce a significantly elevation of PD1 expression (**Figure 5.28D**). Importantly, CD57 human-senescence marker illustrated an increasing trend within Temra populations of the PA and STE-treated groups **(Figure 5.28D**).

Additionally, we also investigated for two senescence-associated intracellular markers for DNA damage (γ-H2AX) and cell proliferation (Ki67). Interestingly, STE treatment expressed a consistent reduction in both γ-H2AX and Ki67 expression within both total $CD4^+$ T and Temra cell populations compared to the vehicle control group **(Figure 5.28C&D**). Contrarily, PA treatment led to a notable increase ($p=0.056$) in γ-H2AX DNA damage marker expression within both total $CD4^+$ T and Temra cell populations (**Figure 5.28C&D**) whereas, no difference was observed in terms of the Ki67 expression compared to the vehicle control group (**Figure 5.28C&D**). Consistently with the literature, OA treatment did not illustrate any observable modulations of the senescence-associated markers [633, 665].

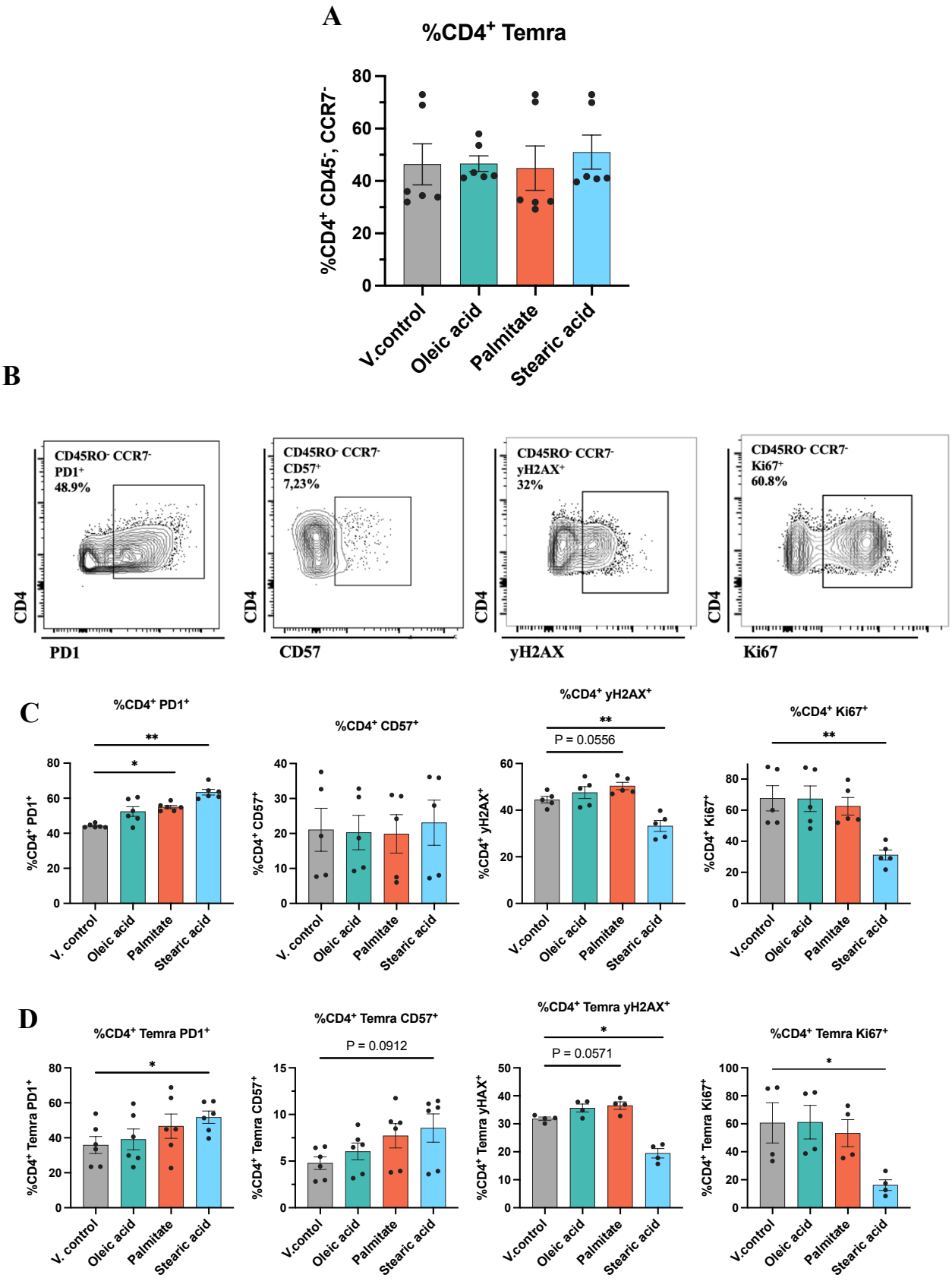


Figure 5.28) In vitro SFA (PA and STE) pre-treatment of human CD4+ T cell phenotype induces an exhaustion and senescence phenotype

(A) Quantification of human Temra ($CD45RO^-$ and $CCR7^-$) population within expressing total human $CD4^+$ T cell within *in vitro* lipid pre-treatment assay. **(B)** Representative flow cytometry plots of $PD1^+$, $CD57^+$, γ-H2AX $^+$ and $Ki\text{-}67^+$ expressing total human $CD4^+$ T cell within *in vitro* lipid pre-treatment assay. **(C)** Quantification of $PD1^+$, $CD57^+$, γ-H2AX $^+$ and $Ki\text{-}67^+$ expression within the total human $CD4^+$ T cell within *in vitro* lipid pre-treatment assay. **(D)** Quantification of $PD1^+$, $CD57^+$, γ-H2AX $^+$ and $Ki\text{-}67^+$ expression within the human Temra ($CD45RO^-$ and $CCR7^-$) $CD4^+$ T cell pre-treated with 50μM of Oleic acid, Palmitate, stearic acid overnight without any activation signal. Cells were then either left non-activated or activated with plate bound CD3 (2.5μg/mL) and CD28 (1.5μg/mL) for 48 hours following the overnight lipid pre-treatment. The untreated control group represents the vehicle control group and received the ethanol: BSA (1:4) solution used for the solubilisation of lipid groups. Each point represents an individual technical replicate of the treatment group (n=3). Kruskal-Wallis with Dunnett's correction; Data presented as mean ± SEM, *$p<0.05$, ** $p<0.01$, *** $p<0.001$.

Next, we investigated the SASP profile of the human $CD4^+$ T cells following the 3-day *in vitro* lipid pre-treatment assay. Interestingly, IL-4^+ $CD4^+$ T cell frequencies were shown to be significantly upregulated with STE treatment compared to vehicle control (**Figure 5.29A**). Additionally, IL-4^+ $CD4^+$ T cell frequencies were also significantly upregulated within Temra populations of both PA and STE treated conditions compared to the control group (**Figure 5.29B**). This suggested that the increase in IL-4^+ $CD4^+$ T cell frequencies are potentially senescence-associated as the IL-4^+ $CD4^+$ T frequencies were detected to be specifically elevated within the senescence-linked Temra population (**Figure 5.29B**).

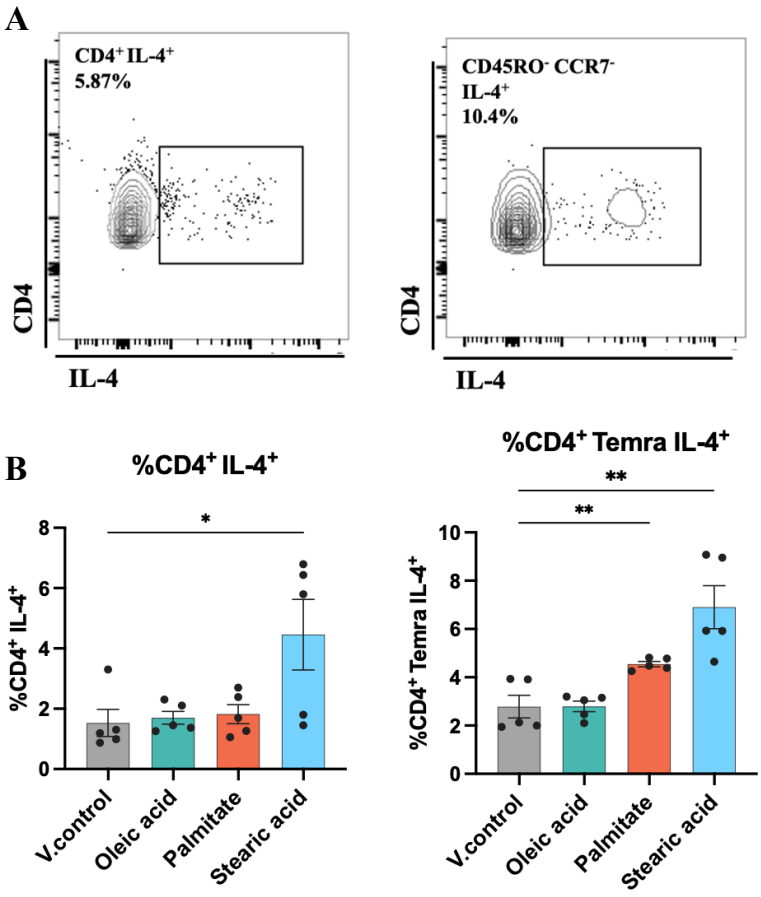


Figure 5.29) Secretory phenotype of human CD4$^+$ T cell pre-treated with bioactive *lipids in vitro*
(A) Quantification of the intracellular cytokine staining (ICCS) illustrates **(A)** frequencies of IL-4$^+$ CD4$^+$ T cells in total CD4$^+$ populations **(B)** frequencies of IL-4$^+$ CD4$^+$ T cells in Temra (CD45RO$^-$ and CCR7$^-$) populations of human CD4$^+$ T cell pre-treated with 50µM of Oleic acid, Palmitate, stearic acid overnight without any activation signal. Cells were then either left non-activated or activated with plate bound CD3 (2.5µg/mL) and CD28 (1.5µg/mL) for 48 hours following the overnight lipid pre-treatment. The untreated control group represents the vehicle control group and received the ethanol: BSA (1:4) solution used for the solubilisation of lipid groups. Each point represents an individual technical replicate of the treatment group (n=3). Kruskal-Wallis with Dunnett's correction; Data presented as mean ± SEM, *p<0.05.

5.10. Discussion

This chapter has investigated the long-term deleterious effects of HFD feeding and the potential effects of weight loss by a WGWL murine model. Importantly, previous identification of the critical immunomodulatory roles of HFD (and bioactive PA) in driving an 'obesogenic bias/reprogramming' towards a pro-inflammatory EM (CXCR3$^+$ and LFA-1$^+$ CD44$^+$) CD4$^+$ T cell phenotype by Mauro et al. 2017, formed the basis of this project[18]. Considering the previously detailed importance of excessive expansion of these deleterious inflammatory

effector memory $CD4^+$ T phenotype, this chapter investigated the effect of weight loss by utilising a WGWL approach.

Previous publications on WGWL experimental models speculated a potential obesogenic reprogramming of innate immune cells following HFD-induced obesity which was retained even after the weight loss [571-574]. Based on the literature, a comprehensive immune phenotyping was carried out focusing on both $CD4^+$ and $CD8^+$ T cell populations isolated from main SLOs and fat tissues to investigate any potential alterations following the weight loss (HFD-RE group).

In line with the background literature and the 8-week DIO model investigated in Mauro et al. 2017, HFD group had significant reduction in naïve subsets along with a concomitant increase in the EM population $CD4^+$ T cells in the pLN tissue (**Figure 5.5 & 5.6**) [18, 126, 392, 466]. Furthermore, HFD group also expressed a significant elevation in EM population $CD8^+$ T cell populations within the SLOs tested (**Figure 5.7 & 5.8**). Consistently, a recent publication by Cottam et al. 2022 speculated a similar bidirectional transition of $CD8^+$ T cell specifically towards $CD8^+$ EM phenotype following the exposure of HFD in adipose tissue of an 18-week DIO murine model [432]. This dataset was detected in a different DIO *in vivo* model with a method called RNA velocity to evaluate the cell progression via splicing of the mRNA sequences [432].

More interestingly, HFD-RE group was also shown to express a significant novel elevation of EM $CD4^+$ T cell population compared to CD. This observation was highly important, suggesting a potential 'obesogenic memory/reprogramming' driven by past HFD-feeding biasing the $CD4^+$ T cell towards and EM lineage even after the weight loss. Interestingly, HFD-RE group did not express a similar obesogenic biasing effects in $CD8^+$ T cell population where EM $CD8^+$ T cells were shown to return to CD control levels following the weight loss.

Consistent with the Mauro et al. 2017, HFD group expressed critical elevations in distinct pro-inflammatory associated EM populations $CXCR3^+$ and LFA-1^+ $CD44^+$ T cell populations (**Figure 5.10 & 5.11**). Strikingly similar to the 14-week HFD-fed DIO murine group, the specific expansion of pro-inflammatory associated $CXCR3^+$-LFA-1^+ $CD44^+$ EM populations were shown to be significantly elevated within the pLN tissues of the HFD-RE group (**Figure 5.10**). Importantly, absolute cell counts of both EM $CD4^+$ and $CXCR3^+$ and LFA-1^+ $CD44^+$ T

cell populations also validated the significant increase observed in frequencies within the pLN. This indicates an actual increase within the cell frequencies and not just an elevation relative to parental cell populations [666]. This dataset demonstrated that the HFD was not just able to bias the expansion of EM $CD4^+$ T cells during the HFD-feeding course but was also capable of persistently retaining the capacity of inducing an exacerbated pro-inflammatory EM phenotype in formerly-obese (HFD-RE) group, even well after the weight loss. This this persistent obesogenic bias was particularly interesting, especially considering the relatively short-term (8-week) exposure to HFD in our model compared to the conventional longer-term (12-32 weeks) exposure prior to weight loss process in the literature.

It should be also noted that this persistent biasing effect was shown to be mainly altering the pro-inflammatory EM T cell subsets whereas the main effector T cell subsets (Th1, Th17 and Th2) were mainly unaffected or shown to return to CD control levels following the weight loss.

Recently, similar observations have been published in the field supporting the hypothesis of long-lasting HFD-driven obesity-induced immune memory resulting from obesogenic reprogramming that persists after the weight loss [432, 578, 585]. Importantly, Hata et al. 2023, demonstrated that HFD-driven DIO in earlier life can directly induce a long-lasting obesogenic reprogramming of macrophages even after weight loss and normalisation of metabolic abnormalities induced by HFD exposure [585]. Additionally, systemic exposure of the HFD and DIO-driven deleterious priming on macrophages were shown to trigger an exacerbated pro-inflammatory and pro-angiogenic functional modulations, aggravating choroidal neovascularization and age-related macular degeneration pathophysiologies [585].

Consistent with our observations, Sougiannis et al. 2020 also reported that the murine group exposed to HFD (21-weeks) and DIO in earlier life were able to significantly elevate the pro-inflammatory M1 macrophages, cytotoxic $CD8^+$ T cells and various inflammatory mediators (TNFα and IFN-γ), in later life even after the weight loss compared to control mice [578]. In line with this publication, we observed a significant increase in total CM $CD8^+$ T cell population in the pLN tissue of the HFD groups which were retained significantly high within the HFD-RE, even after the weight loss (**Figure 5.7B**).

More importantly, following the significant elevation observed in $CD8^+$ T cells within our *in vivo* model and by Sougiannis et al. 2020, we also demonstrated a specific increase in pro-inflammatory associated $CXCR3^+$ - $LFA\text{-}1^+$ $CD44^+$ pro-inflammatory $CD8^+$ T cells within

pLN tissue (**Figure 5.11**). Importantly, following Sougiannis et al. 2020, we have further identified a persistently retained elevation specifically in pro-inflammatory associated Tc1 $CD8^+$ T cell frequencies within the HFD-RE group comparable to HFD group (**Figure 5.13A**) [578]. This data can suggest that the significant elevation observed within cytotoxic $CD8^+$ T cell population could be potentially raised by the particular increase in pro-inflammatory associated Tc1 $CD8^+$ T cells.

Altogether, these data illustrating that HFD-induced past history of obesity in earlier life can persistently prime differentiation of $CD4^+$ T cells towards $CXCR3^+$-$LFA\text{-}1^+$ pro-inflammatory EM phenotype following a polyclonal T cell stimuli experienced well after the weight loss. This striking observation on $CD4^+$ T cell population is novel and has not been reported elsewhere yet.

As previously detailed , the increase in the frequencies of the pro-inflammatory functional EM T cell subsets such as $CXCR3^+$ - $LFA\text{-}1^+$ $CD44^+$ T cells in peripheral tissues are shown to be critically associated with obesity and obesity-linked diseases [18, 127, 222, 225, 266, 288, 570]. Intriguingly, Zou et al. 2018 also illustrated striking characteristics of $CD4^+$ T cells by directly mediating and promoting weight regain by persistently retaining an obesogenic memory-induced OIIM in formerly obese murine models [301]. Adoptive transfer of $CD4^+$ T cells from obese mice were shown to be capable of inducing an OIIM and mediated weight gain within the healthy weight host mouse [301]. Along with the weight re-gain, T lymphocytes have also been speculated to be a critical driving force in human frailty due to the T cell mediated cytokines and adipokines that can resemble chronic inflammation features of aging also known as inflammaging [667].

Considering this functional importance of the T lymphocytes in obesogenic memory where weight loss is mainly shown to alleviate visceral adiposity and metabolic parameters, but not the HDF-driven persistent T cell-mediated obesity-linked inflammation [668]. Consistently, it was highly important to investigate the underlying mechanism of this HFD-induced long-lasting, persistently transferable ‘obesogenic reprogramming’ that triggers an exacerbated pro-inflammatory EM response even after the weight loss is achieved.

5.10.1 Potential molecular mechanisms and drivers of the obesogenic memory phenotype in T lymphocytes

To investigate the observed obesogenic memory phenotype further, we utilised two approaches targeting different aspects. First, an untargeted, broad approach was utilised to investigate genome-wide potential epigenetic alterations that can induce and persistently retain the observed phenotype formerly obese *in vivo* murine model. Secondly, a targeted, reductionist *in vitro* approach, aimed to elucidate the potential molecular mechanism by attempting to recapitulate the *in vivo* phenotype *in vitro.* This targeted *in vitro* approach enabled us to develop a reliable and consistent method for investigating the molecular mechanism further but also aimed to identify the distinct bioactive lipid groups that were hypothesised to be the potential main drivers of the process.

Background literature from various cell types demonstrated that HFDs that alter the lipidome may also have long-lasting epigenetic modifications and persistent transcriptional and functional alterations on immune cells leading to dysfunctional immune responses, even after weight loss [432, 585, 593, 594, 669]. Importantly, both genome-wide unbiased RRBS and targeted pyrosequencing on $CD44^+$ memory $CD4^+$ T cells identified various differentially methylated candidate genes between different diet groups. Critically, HFD exposure in the early life of the HFD-RE group was capable of inducing and persistently retaining the methylation conformation of certain biofunctional genes (STK26 and CDKN1C) similar to the HFD group, even well after the weight loss. This differential modifications on the methylation status of the candidate genes were also shown to induce a significant upregulation of the STK26 protein within pLN tissue, whereas CDKN1C analysis is still in progress (**Figure 5.29**). Additionally, our preliminary data suggests critical functional alterations linked with the candidate genes that may underpin the observed long-lasting exacerbated pro-inflammatory EM phenotype.

In line with our dataset, recent publications illustrated consistent observations and further validated the direct modulatory effects of HFD in inducing epigenetic alterations that can lead to functional changes shaping an exaggerated immune phenotype in macrophages and other immune cells, even after the weight loss [432, 585].

Hata et al. 2023, illustrated that, past HFD-feeding in HFD-RE (WGWL) group fed with HFD for inducing DIO (11-weeks) and followed by a chow diet for weight loss (9-weeks), was able to trigger persistent epigenomic modifications of adipose tissue macrophages (ATMs)

inducing an enhanced angiogenic and inflammatory response [585]. Assay for transposase-accessible chromatin sequencing (ATAC-seq) on ATMs isolated from different diet groups identified various inflammation-associated genes to be persistently altered within the HFD-RE group similar to HFD group methylation conformation. Exposure to the HFD in earlier life was shown to selectively and persistently induce the accessibility of pro-inflammatory associated activator protein-1 (AP-1)- target genes including NF-κB, vascular endothelial growth factor A (Vegfa), angiopoietin 1 (Angpt1) whilst simultaneously inhibiting anti-inflammatory genes such as IL-10 within HFD-RE ATMs [585]. These HFD-induced long-lasting epigenetic modifications were also shown to induce an exacerbated pro-inflammatory IL-1β, IL-2, IL-12, TNF-α and IFN-γ cytokine production within the HFD-RE group [585].

Interestingly, Hata et al. identified STK39 as one of the epigenetically modulated genes between CD and HFD-RE groups which restrain methylation conformation HFD group even after the weight loss [585]. This observation was highly interesting as STK39 was shown to share homology with STK26, as both proteins were shown to be directly activated via STRAD-mouse protein-25 (MO25) protein complex [670]. More importantly, STK39 is another known mediator of autophagy where downregulation of STK39 protein was also shown to induce autophagy through a downstream kinase of the with no K (lysine) protein kinase-1(WNK1) in various mammalian cell lines [671].

Furthermore, Cottam et al. 2022, within the 27-week WGWL (HFD 18-week followed by CD 9-week) experimental plan, reported a distinct HFD-driven obesity-associated T cell exhaustion profile specifically on $CD8^+$ T EM population common in both HFD and HFD-RE groups [432]. Importantly, Cottam et al.2022, also reported various exhaustion/senescence-associated markers such as PD-1, Tox, Entpd1, Tigit, and Lag3 were persistently elevated in both HFD and HFD-RE groups compared to CD [432].

The critical immunomodulatory effects of distinct bioactive lipids and our previous publication identifying bioactive PA as the key mediator of excessive expansion of inflammatory EM $CD4^+$ T cells in both mice and humans, is previously discussed [18]. Consistent with Mauro et al. 2017, it was highly striking to record that *in vitro* SFA lipid pre-treatment prior to T cell activation was able to recapitulate the same HFD-induced obesogenic biasing/priming effect on human $CD4^+$ T cells, driving a profound pro-inflammatory EM phenotype *in vitro* (**Figure 5.19**). Additionally, the *in vitro* overnight pre-treatment of PA and STE was capable of directly elevating gene expression of STK26 and CDKN1C as well the protein level of STK26 *in vitro* in human $CD4^+$ T cell monoculture following T cell activation

(**Figure 5.27 & 5.28**). Interestingly, analysis of non-activated conditions were also consistent with the *in vivo* dataset, illustrating a priming effect of lipid pre-treatment in biasing the expansion of EM $CD4^+$ T cells and the functional changes, only following an activation signal for T cells like CD3/CD28 (**Figure 5.19**).

Additionally, consistent with the beneficial effects recorded in the literature, OA was shown to induce Foxp3 expression and elevating IL-10 expression, without any observable effect on inflammatory markers within *in vitro* human $CD4^+$ T cells pre-treatment conditions (**Figure 5.20**) [321, 595]. importantly this data further validated the bioactivity and functionality of oleic acid *in vitro* conditions and not just an ineffectual FA [321, 595].

As the *in vitro* SFA-treated conditions were shown to recapitulate the HFD-induced relative increase in STK26 and CDKN1C gene expression and the obesogenic biasing pro-inflammatory EM $CD4^+$ T cell phenotype, we hypothesised that bioactive PA and/or STE can directly induce the hypomethylation in the human $CD4^+$ T cell as observed in *in vivo*. A targeted pyrosequencing analysis is still ongoin to investigate the methylation status of the STK26 and CDKN1C within the *in vitro* SFA pre-treated human $CD4^+$ T cells. However importantly, a recent publication by Pascual et al. 2021 demonstrated that PA can directly modulate long-term alterations in methylation profiles of Schwann cells alongside methyltransferase Set1A mediator, driving a pro-metastatic memory in murine models [379].

5.10.2 Bioactive SFAs can recapitulate the HFD-induced alterations in cellular functions linked with STK26 and CDKN1C

Following the pro-inflammatory EM phenotype, the HFD-induced alterations in methylation profiles and respective modulations in STK26 and CDKN1C expression, were also shown to modulate the associated cellular function (autophagy and senescence, respectively) within the *in vivo* HFD-exposed murine groups. Following our *in vitro* dataset illustrating that distinct bioactive lipids per se can also trigger pro-inflammatory EM phenotype in $CD4^+$ T cells, we have also demonstrated that *in vitro* bioactive SFAs pre-treatment can induce a significant elevation in STK26 and CDKN1C gene expression alongside potential direct modulations in associated cellular functions autophagy and senescence respectively (**Figure 5.19, 5.27 & 5.30**).

Although we have shown the detection and optimisation of autophagy flux detection via LC3 flow cytometry kit and elevation in certain senescence/exhaustion-associated markers in both *in vivo* and *in vitro* conditions, there are still certain critical investigations ongoing before drawing a conclusive result (**Section 5.8**). Although the background literature is highly limited on the immune cells, there are certain recent publications illustrating both supportive and contradictory associations between SFAs and functional changes in autophagy and senescence exhibiting inconsistent and controversial effects.

Interestingly, publications suggested inhibition of autophagy with the PA accumulation in macrophages and PBMCs [622, 672]. Interestingly, lipid overload with increasing doses of OA has also recently been shown to inhibit autophagy in $CD4^+$ T cells in both *in vivo* and *in vitro* conditions [621]. However, our preliminary data, did not record any observable reduction in autophagy with the OA treatment of human $CD4^+$ T cells (**Figure 5.35**). On the other hand, consistent with our hypothesis, various publications reported an enhancement in the autophagy flux with SFA supplementation of immune cells [673-678]. It is well shown within the literature with various cell types (adipocytes, hepatocytes, neutrophils) that PA directly enhances the autophagy flux, potentially as a pro-survival mechanism against the PA-induced lipotoxicity and apoptosis [673-678]. More interestingly, recent publications identified autophagy as a crucial mediator of memory $CD8^+$ T cell expansion process where inhibition of autophagy was shown to reduce the formation of the EM $CD8^+$ T cell population against an infection [679, 680]. Additionally, *ex vivo* analysis of $CD8^+$ T cells obtained from human liver illustrated that, autophagy flux was profoundly increased particularly in highly proliferative and cytotoxic functioning resident $CD8^+$ T cells with a high cytokine production capacity as well [680]. Importantly, illustrating the critical role of autophagy in shaping the resident pro-inflammatory EM $CD8^+$ T cell populations, which is highly important considering our preliminary data and the EM $CD4^+$ T phenotype identified alongside the potential functional alterations of autophagy within the DIO pathophysiology. However, our dataset is not conclusive yet and more experiments are in-line to reach a conclusive outcome on whether the autophagy modulation (upregulated/downregulated) is due to the plethora of lipids or if it is a compensatory effect aiming to clear the excessive lipid content (lipophagy).

Furthermore, consistent with our *in vitro* SFA treatment illustrating an increasing senescence markers and the *in vivo* HFD DIO model, recent publications also reported bioactive SFAs as potent mediators of senescence phenotype. Frasca et al. 2022 illustrated that obesity

augments the accumulation of PA and age-associated senescence profile in B cells through a metabolic reprogramming prompted by bioactive PA [311]. *In vitro* PA treatment (50μM) was also shown to induce a long-lasting pro-inflammatory epigenetic reprogramming of B-cells and an immunosenescence phenotype by elevating pro-inflammatory T-bet mRNA expression [311].

Consistently, *in vitro* PA lipid treatment is shown to induce DNA damage, senescence profile and SASP phenotype in human subcutaneous and omental adipocytes. Recently Shirakawa et al., identified a long-lived $CD4^+$ T cell ($CD153^+$,$PD\text{-}1^+$) population that persistently exhibited a cellular senescence profile within the formerly obese mice, even after weight loss [430, 579]. This population was shown to express a pro-inflammatory ($T\text{-}bet^+$-Th1) profile with an elevated senescence-associated beta-galactosidase and DNA-damage marker γ-H2AX within the visceral adipose tissue [430, 579]. Importantly, past HFD exposure in life elevated the $CD153^+$,$PD\text{-}1^+$ $CD4^+$ T cell population which prompted the OIIM within the formerly obese murine group [430, 579]. Altogether a self-sustaining chronic inflammatory loop induced by a priming effect on $CD4^+$ T cells from past HFD exposure [430, 435, 570, 579]. Recently, PA was also identified as a critical mediator of cellular senescence in an *in vitro* human Kawasaki disease model [681]. PA was further validated to directly induce cellular senescence in human endothelial cells by enhancing the accumulation of intracellular ROS production [681]. Interestingly, Ishaq et al. 2022, reported a significant ameliorative effect of OA on the PA-induced DNA damage and senescence profile [633].

Chapter 6) DISCUSSION

This chapter will summarise the main findings of my project, which focused on the distinct immunomodulatory effects of bioactive lipid groups on T-lymphocytes during both early-DIO (3-week), full-established DIO (14-week) and weight loss (WGWL) murine models. Utilisation of different DIO models at different stages of obesity enhanced our understanding of each stage of DIO and the establishment of the DIO-linked OIIM. As such early-DIO at 3-weeks enabled the investigation of the early immunomodulatory effects of obesogenic diets on T cell immunity at early-DIO prior to the physical diagnosis of obesity. 14-week HFD-fed fully established DIO model was utilised to investigate long-term obesity-induced immune alterations specifically on T cells. Whereas, 14-week DIO with a WGWL model investigated the direct effects of HFD on the T cell immune phenotype and any potential ameliorate effects of the weight loss. In addition to the *in vivo* models, for investigating the potential molecular mechanisms of both stages of DIO, we developed pertinent *in vitro* approaches.

6.1. Addressing the hypotheses and overall findings

Chapter 3 and **4** aimed to phenotype the early pro-inflammatory modulations of obesogenic diets on T cells in and the establishment of the OIIM in an early-DIO murine model fed with WD or HFD for 3-weeks. Alongside the other important observations detailed in the **Chapter 3**, the early-DIO phenotype induced a profound elevation in pro-inflammatory Th1 and Th17 effector $CD4^+$ T cell phenotypes and reducing trend in Treg population in various tissues (**Figure 3.9 & 3.16**). Concomitantly, n-3PUFA supplementation significantly increased $Foxp3^+$ Treg T-cell populations whilst reducing the pro-inflammatory Th1 and Th17 populations within various tissues. These pertinent immunomodulations highlighted the high potential ameliorative effect of n-3PUFA supplementation on the OIIM (**Figure 3.9 & 3.16**). Importantly, literature suggests that obesogenic diets like WD can induce alterations in lipidomics profile which shape the immune phenotype [126, 127, 669]. Consistent with the literature, our extensive T-cell phenotyping coupled with unbiased lipidomics analysis on the 3-week early-DIO murine model identified potential WD-induced early alterations in both lipidomics profile and immune phenotype (**Chapter 3). Figure 6.1**, summarises the main outcomes of the project which is published in Biochemical Pharmacology as 'Omega-3 polyunsaturated fatty acids reverse the impact of western diets on regulatory T cell responses through averting ceramide-mediated pathways' [127].

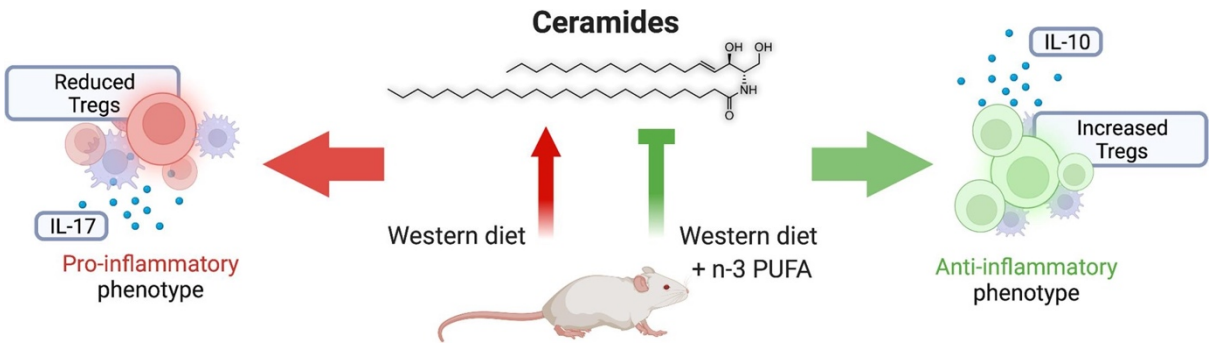


Figure 6.1) A schematic of the main outcomes of the 3-week early DIO model with the critical immunomodulatory effects of bioactive lipids
This project identified the critical bioactive lipid groups that were shown to express an immunomodulatory effect and specifically drive the Th17/Treg differentiation process during the establishment of OIIM in an early DIO murine model. Importantly, western diet-driven C24 induced a biasing effect towards pro-inflammatory Th17 fate whereas n-3PUFA supplementation was shown to ameliorate this pro-inflammatory biasing effect and re-create the fragile Th17/Treg balance of $CD4^+$ T cells in both *in vivo* and *in vitro* models. Illustration by Dr M. Certo as published in Munoz et al. 2022 [127].

As hypothesised based on the lipidomics and immune phenotype datasets, we illustrated the potential of the long-chain C24 ceramide in shaping the early-DIO immune microenvironment by inhibiting the differentiation of $Foxp3^+$ Tregs and inducing an pro-inflammatory $ROR\gamma t^+$ Th17 phenotype. Following the alterations in the T lymphocyte phenotypes *in vivo*, this distinct and direct pro-inflammatory immunomodulatory actions of C24 were further validated on both murine and human $CD4^+$ T cells *in vitro* differentiation models. Consistently, C24 supplementation into both murine and human $CD4^+$ T cell *in vitro* monocultures induced the $ROR\gamma t^+$ Th17 phenotype alongside inhibiting $Foxp3^+$ Tregs (**Figure 4.20 & 4.21**). On the other hand, unlike the observed *in vivo* data, n-3PUFA supplementation into the $CD4^+$ T cell monoculture did not exhibit any direct alleviating effect on $Foxp3^+$ Treg differentiation (**Figure 4.27**). However, n-3PUFA supplementation into the *in vitro* $CD4^+$ T cell differentiation model alleviated the C24-induced elevation in the $ROR\gamma t^+$ Th17 levels (**Figure 4.27**).

In **Chapter 4**, we started to investigate the potential molecular mechanism underpinning the C24-driven pro-inflammatory immunomodulatory effects. Bioactive C24 at 0.1μM was shown to directly activate the CD39, mTOR/STAT-3 and HIF-1α signalling pathway. **Figure 6.2** illustrates the representative proposed model of molecular mechanism triggered by C24 to drive the Th17/Treg differentiation towards pro-inflammatory RORγt^{+} Th17 phenotype whilst inhibiting Foxp3^{+} Treg differentiation.

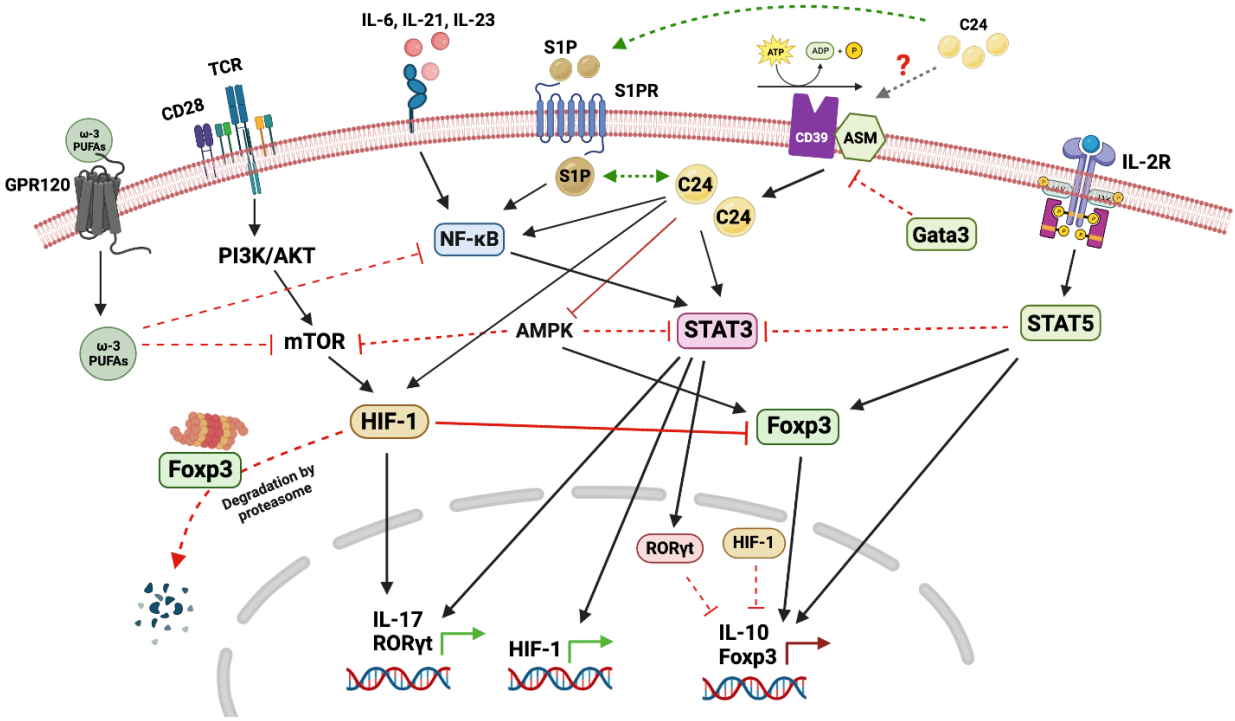


Figure 6.2) A schematic summary of the proposed Th17/Treg differentiation pathways modulated by bioactive C24 in inducing the Th17

ATP accumulates within the extracellular space and upon C24 exposure. C24 activates CD39 (which is responsible for catalysing the conversion of ATP and ADP to AMP). Therefore activation of CD39 initiates a cascade of events which includes the further synthesis of ceramides by ASM within the cell. Alternatively, bioactive ceramides can directly enter the cell cytoplasm through the lipid bilayer or be converted into S1P - another bioactive form. S1P enters the cell via the S1PR receptor. After internalisation the ceramides directly activate key transcription factors such as STAT3, HIF-1α and NF-κB. These critical Th17-lineage defining factors then further activate the transcriptional amplification of more Th17-linked proteins and TFs such as HIF-1α, IL-17a, RORγt. Similar to other lineage defining TFs, Th17-linked factors are also shown to inhibit the expression of other competitor lineage defining factors such as Foxp3 and IL-10.

The final chapter (**Chapter 5**) focused in phenotyping the HFD-induced T cell alterations and the long-term persistent implications of HFD-induced obesity on T cells of 14-week fully-established DIO and WGWL models. Following the Mauro et al. 2017 publication, we have further validated the elevated expansion of pro-inflammatory EM CD4^{+} T cells (CD44^{+} CD62L^{-}, CXCR3^{+} or LFA1^{+}) within the HFD-fed group [18]. Importantly, the WGWL model (HFD-

RE) group also exhibited an exaggerated pro-inflammatory EM $CD4^+$ phenotype ($CD44^+$, $CXCR3^+$ or $LFA1^+$) once challenged by an allogeneic stimuli. Interestingly, only 8-weeks of HFD exposure in early life induced the long-lasting pro-inflammatory EM $CD4^+$ phenotype which was retained after weight loss. Considering the known critical contributions of long-lived EM $CD4^+$ T cell populations to OIIM and disease pathologies, we further investigated both the drivers and molecular mechanisms of this pro-inflammatory reprogramming phenotype [18, 395, 401, 682-684]. Additionally, overnight *in vitro* lipid pre-treatment on human $CD4^+$ T cells recapitulated the HFD-induced pro-inflammatory EM $CD4^+$ T cell phenotype by direct PA and STE exposure. Considering recent publications suggesting obesogenic memory, we hypothesised that distinct bioactive SFAs could potentially drive direct epigenetic modulations, leading to reprogramming of cells and which retain the pro-inflammatory functionality even after weight loss (HFD-RE). To investigate this, an unbiased genome-wide RRBS analysis was utilised on memory $CD4^+$ T cells isolated from 14-week CD-control, HFD and HFD-RE murine groups. This RRBS analysis identified a set of hypomethylated genes, two of which had associations with mediating autophagy (STK26) and senescence (CDKN1C). To investigate any potential long-term alterations driven by HFD or particular bioactive SFAs, we utilised both *in vivo* and *in vitro* models to analyse alterations in autophagy flux and cellular senescence profiles of $CD4^+$ T cells. Despite the preliminary data supporting our hypothesis that SFA driven hypomethylation leads to an upregulation in both autophagy and senescence within the SFA treated memory $CD4^+$ T cells, firm conclusions from our data set are yet to be reached and more experiments needed. Therefore, this chapter seeks to highlight further experiments, open ended questions and limitations of our models.

6.2 Ceramides and n-3PUFA as active mediators of T cell lineage plasticity

A main observation from this thesis was investigating the dynamic plasticity of T cells which is shown to shape the obesity-associated immune phenotype and contribute to OIIM. Additionally, this thesis also demonstrated the profound ability of distinct bioactive lipid groups at modulating immunity in either a deleterious and/or ameliorative manner by exploiting the dynamic potential of T lineage plasticity [453, 685]. Recent literature has highlighted the critical importance of bioactive lipids in potential therapeutic avenues for alleviating the OIIM and the lack of complex understanding in the immunomodulatory mechanism driven by bioactive lipids.

Although the plasticity of T lineages is often overlooked by the literature, recent publications have highlighted the importance of dynamic T cell lineage plasticity within cancer and obesity [453, 685, 686]. For example, key organs such as lymphoid organs and adipose tissues, were shown to be highly plastic in responding to the changing microenvironment by expanding certain cell lineages [632, 686-688]. Interestingly, environmental factors such as nutrition and exercise were shown to be crucial at inducing obesity-linked lineage reprogramming- also known as 'transdifferentiation' - of critical cell types such as adipocytes and immune cells [632, 686-688]. In line with our 3-week early DIO dataset, Treg and Th17 $CD4^+$ T cell subsets were identified as two major modulators tissue plasticity in the SLOs and fat tissues that orchestrate the OIIM in obesity-associated diseases [226, 486, 686].

Chapter 1 detailed characteristics of OIIM where obese conditions predisposed T cells towards a Th17 bias with a loss of Treg populations [226, 290]. Interestingly in the clinic, the Th17-associated cytokine: IL17, is used as an early marker of atherosclerosis and other CVDs associated with obesity [689-691]. Recent publications in obese and early-obese/overweight children cohorts illustrated a systemic elevation in Th17 frequencies as well as other Th17-associated pro-inflammatory markers (RORγt and IL-17a) within the peripheral blood samples, suggesting Th17 phenotype as a systemically observable parameter in obesity [691-693]. Importantly Schindler et al. illustrated that, the profound increase in Th17 levels is not consequence of an obesity-linked inflammatory diseases but, it is an obesogenic diet driven characteristics of obesity [692]. Additionally Schindler et al., also highlighted that the Th17 bias does not only occur in obesity but begins to form in overweight individuals [692]. This suggests that the disruption in Th17/Treg balance is an key early obesity-induced alteration in immune system as we also recorded within our 3-week early-DIO model [692].

Considering the obesity-driven Th17/Treg imbalance, it is crucial to have a better understanding on the plasticity of T cells and the mechanistical drivers of this obesity-induced pro-inflammatory transdifferentiation. Importantly, synthesis of distinct bioactive lipids and metabolites has been shown to be key for Th17 differentiation within obese conditions. Other important immunomodulatory metabolites such as acetyl CoA and lactate have also been able to modulate and elevate Th17 differentiation with via enhance fatty acid synthesis [302, 694]. Considering the suggested critical immunomodulatory roles of bioactive FAs, it was reassuring to report that 0.1μM of C24 was able to induce a significant shift towards $ROR\gamma t^+$ Th17 effector $CD4^+$ T cell phenotype and a significant reduction in Foxp3 expression on the $CD4^+$ T cells. This observation suggested a novel pro-inflammatory modulation of C24 that biases the $CD4^+$

T cells towards inflammatory Th17 phenotype as well as inhibiting the Treg differentiation. Following the publication our publication as Munoz et al., various new publications were also published highlighting the critical role of long-chain bioactive ceramides in Th17 differentiation and effector function by using different experimental approaches [543]. Bioactive ceramides have also been identified as central drivers of the pro-inflammatory Th17 phenotype in other obesity-linked pathologies (such as CVDs), autoimmune diseases and asthma [695-697].

Considering the critical importance of Th17/Treg balance in shaping the obesity-linked inflammatory phenotype, various clinical publications and methods were investigated to therapeutically downregulate Th17 and increase Treg populations within obesity. A recent publication demonstrated a significant ameliorative effect on OIIM by downregulating STAT3-driven Th17 differentiation via overexpression a negative regulator of STAT3 called retinoid-interferon-induced mortality (GRIM)-19 [698]. Importantly, dieting-induced weight loss in overweight and obese children were shown to significantly downregulate the Th17 that ameliorated the obesity-linked chronic inflammation [699]. This study suggested that critical alterations in the diet content can alleviate the Th17-driven obesity-linked chronic inflammation [699]. Consistently, background literature also highlighted the reversibility of the Th17 fate back to Treg fate during the resolution of inflammatory conditions, highlighting the plasticity of transdifferentiation and the therapeutic opportunity for ameliorating the Th17/Treg-mediated chronic obesity-linked inflammation [478]. Considering these relevant literature, we have further demonstrated the ameliorative effect of dietary n-3PUFA supplementation into the WD which was shown to alleviate the obesity-associated Th17 cell-mediated inflammation via re-establishing the Th17/Treg balance. This observation was also supported by the literature illustrating the ameliorative effect of n-3PUFA supplementation specifically on obesity-linked Th17 cell-mediated inflammation pathophysiologies such as colitis and RA [341, 475, 558, 561, 700, 701].

6.3 Potential molecular links between bioactive C24 and n-3PUFA in mediating the Th17/Treg balance

Interestingly utilisation of broad spectrum, unbiased lipidomics analysis to investigate the lipidomic profile changes between WD-fed early-DIO groups with and without n-3PUFA, highlighted the significant alterations in various critical lipid groups (**Figure 4.2**). Alongside

the observed early-DIO Th17/Treg pro-inflammatory phenotype with increasing C24 levels within WD, n-3PUFA supplementation into WD was not just able to ameliorate the Th17/Treg phenotype, but also shown to reduce plasma C24 concentration (**Figure 4.3**).

Following the observation of direct pro-inflammatory biasing effect of C24 towards Th17 and inhibiting the Treg expansion, following our hypothesis we investigated anti-inflammatory actions of n-3PUFA and the potential mechanisms re-balancing Th17/Treg population within OIIM. Interestingly n-3PUFA re-balanced Th17/Treg populations at two differential levels: via active reduction of pro-inflammatory RORγt$^+$ Th17 differentiation potentially through direct inhibition of mTOR, STAT3 and NF-κB pathways; and via an indirect mechanism that inhibits the synthesis of pro-inflammatory C24, inducing an homeostatic balance in Th17/Treg populations by diminishing the main deleterious driver (Th17).

As the literature suggested, n-3PUFAs directly inhibits RORγt$^+$ Th17 expansion by inhibiting the critical components of T cell differentiation pathways including mTOR, STAT3 and NF-κB (**Figure 4.20B**) [325, 408, 557, 558, 702, 703]. Although *in vitro* supplementation of n-3PUFA into the C24-treated CD4$^+$ T cell monoculture illustrated this direct downregulation in RORγt$^+$ Th17 differentiation, further investigation of gene expression of mTOR, STAT3 and NF-κB in n-3PUFA treated CD4$^+$ T cells would validate this observation [325, 408, 557, 558, 702, 703]. On the other hand, in line with Kong et al. and Chiurchiu et al, n-3PUFA supplementation into CD4$^+$ T cell monoculture did not augment Foxp3$^+$ Treg differentiation, suggesting an indirect secondary anti-inflammatory mechanism of n-3PUFA on CD4$^+$ T cells at inducing the elevation in the Treg differentiation as observed *in vivo* [557, 562]. Interestingly, lipidomics analysis illustrated that n-3PUFA supplementation into WD diminished the WD-induced elevation of pro-inflammatory C24 levels and recovering the disturbed Th17/Treg balance in murine models (**Figure 4.3**). Furthermore, dietary n-3PUFA supplementation also inhibited the systemic ceramide synthesis enzymes like C24-producing CerS2 enzyme (**Figure 4.29**). Consistently, Balogun et al. also reported a significant reduction in long-chain ceramide levels with n-3PUFA supplemented diet, by using a different lipidomic approach [118, 704]. This data suggested an indirect anti-inflammatory effect of n-3PUFA on balancing the Th17/Treg distribution via inhibiting the synthesis of pro-inflammatory deleterious ceramides and ameliorating the OIIM. Consistently, various recent publications also started to suggest a critical link between n-3PUFA and bioactive deleterious ceramide groups

in mediating and/or ameliorating various obesity-linked inflammatory pathologies including CVDs, T2D, hepatic steatosis [118, 119, 125, 408, 705].

Importantly, our *in vitro* data is limited by the focus solely on the immunomodulatory effects of bioactive lipids on $CD4^+$ T cells. However, there could be other indirect immunomodulatory actions mediated by other immune cells like DCs [562, 706].

6.4 Proposed model of C24-driven Th17 differentiation under DIO conditions and outstanding questions

The importance of bioactive long-chain ceramides has been discussed previously within **Chapter 4** and above. Following our publication, Sen at al. 2021 demonstrated the key modulatory roles of bioactive long-chain ceramides (C18-24) on Th17 differentiation and the expression of IL-17A and IL-17F [543]. Importantly, ceramide synthesis have been shown to play a critical role in inducing Th17 differentiation via a distinct non-classical pathway as demonstrated by Bai et al. Differently from the IL-6 dependent pathway, this non-classical pathway is driven by CD39/CD161/ceramides/STAT3/mTOR signalling cascade which directly drives $ROR\gamma t^+$ Th17 differentiation alongside inhibiting $Foxp3^+$ Treg differentiation [368, 369, 494, 496]. Consistent with the publications of Bai et al, our *in vitro* C24-treated human $CD4^+$ T cell conditions were shown to induce a significant elevation along the CD39/STAT3/mTOR pathway as well as significant reduction in the Foxp3 expression.

Considering the critical roles of HIF-1α in STAT3/mTOR-pathway and T cell differentiation process, we have investigated any potential role of HIF-1α in C24-driven Th17 biasing, reported a potential increase in HIF-1α expression within the C24-treated $CD4^+$ T cells undergoing the differentiation process *in vitro* (**Figure 4.37**). This was also supported by recent publications suggesting a potential interaction between bioactive ceramides and HIF-1α [695, 707]. Recently, a C24-associated bioactive ceramide group was identified as a novel non-hypoxic activator of HIF-1α in vascular cells similar to our observations on C24-driven HIF-1α activation[707]. Although preliminary observations were highly promising, more rigorous testing involving further donors are necessary to confirm this mechanism. Additionally, it would be pertinent to investigate the gene expression and protein levels of CD39/ STAT3/mTOR1 and HIF-1α following the bioactive C24 treatment to further validate the observed phenomenon.

Furthermore, there are still outstanding questions of how specifically bioactive C24 can activate the CD39/ STAT3/mTOR1 and HIF-1α pathway and whether there are other potential factors playing a role in this mechanism.

Despite Bai et al suggesting that any antibody or ligand can activate CD39 downstream signalling, which includes activating ceramide synthesis via the ASM enzyme at the cell membrane. Our data has illustrated that direct C24 supplementation into the $CD4^+$ T cell microenvironment can increase CD39/STAT3/mTOR1 and HIF-1α components. These observations are further supported by the ability of ceramides to easily pass through the cellular membrane due to their hydrophobic properties and homology with the lipid bilayer. Once internalised, bioactive ceramides can directly induce the activation of certain TFs such as STAT3, HIF-1α and NF-κB [368, 369, 494, 496, 545, 546, 708, 709]. Another possible mechanism for how CD24 could activate HIF-1α could be through immunometabolic changes resulting from activation of CD39. The CD39 ecto-nucleotidase is responsible for the conversion of adenosine triphosphate (ATP) to adenosine diphosphate (ADP) or adenosine monophosphate (AMP). It is demonstrated that lipid metabolism can directly activate CD39, produce ATP to induce Th17-mediated inflammation within the obese adipose tissue [710, 711]. Additionally, ceramides induce a pseudo-hypoxic state within the obese microenvironment, which could be another important driver for initiating CD39/STAT3/mTOR/HIF-1α signalling [368, 369, 709, 712]. Additionally, ceramides are known to induce ROS accumulation and oxidative stress, which in turn are also key mediators of CD39/STAT3 activation and T cell differentiation [713-715]. Therefore, activation of CD39/STAT3/mTOR/HIF-1α pathway can potentially induced or mediated by the pseudo-hypoxic and high oxidative stress within the obese cellular environment augmented by the bioactive ceramides (**Figure 6.3**).

Additionally, similar to bioactive C24, it is highly probable that other bioactive ceramide groups can directly mediate Th17/Treg differentiation fates. For example, sphingosine 1-phosphate (S1P) is a potent derivative metabolite of ceramides is thought to have immunomodulatory effects. Human and murine models have demonstrated that S1P is highly associated with C24 [716]. Both S1P and C24 were also shown to be working together and mediate deleterious effects on obesity-associated CVDs conditions [716, 717]. A recent publication speculated that S1P modulates the Th17/Treg differentiation process through reducing Th17 frequencies and increasing Treg differentiation of ex vivo human $CD4^+$ T cells

[534, 718]. Interestingly, S1P also inducing the expression of HIF-1α in normoxic conditions [707]. Therefore, considering the background literature, it would be interesting to investigate the potential interactions between bioactive S1P and C24 further in modulating Th17/Treg fates and understanding this under obesity conditions and its associated pathologies. Furthermore, Wang et al. 2022 identified the clinical importance of WD-derived ceramides and HIF-1α co-interactions as a critical driver of atherosclerosis pathophysiology whereas, inhibition of HIF-1α shown to ameliorate atherosclerosis [695].

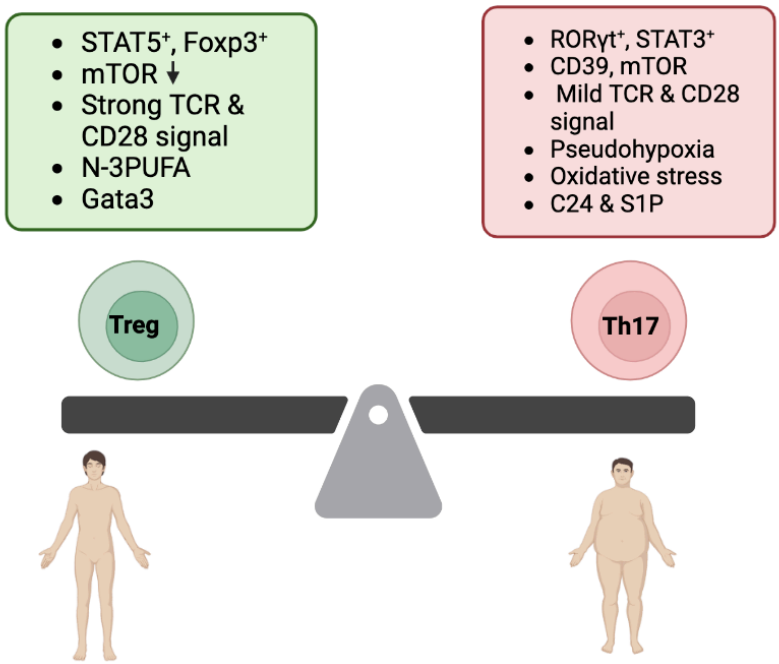


Figure 6.3) Obesity-linked factors mediating the fragile Th17/Treg balance
A summary of the critical factors other than the main cytokine drivers of the Th17/Treg differentiation in obese microcellular environment. Based on the literature Treg differentiation is initiated with a strong potentially self-recognition inducing the activation of STAT5 and Foxp3 transcription factors where mTOR signal is also shown to be generally inhibited via various factors such as AMPK. The n-3PUFA supplementation were shown to ameliorate the obesity-driven Th17 bias by supressing the Th17 differentiation both directly and indirectly. On the other hand, Th17 differentiation is shown to be driven by a milder TCR activation which activates RORγt and STAT3 transcription factors. In line with the literature, in this thesis we have identified the immunomodulatory role of bioactive C24 in inducing oxidative stress and pseudohypoxic microenvironment that augments the Th17 differentiation via CD39/ STAT3/mTOR1 and HIF-1α driven pathway.

6.5 Experimental limitations and future work

Similar to all experimental approaches, our experimental models also has different limitations that should be noted. Throughout our research we have tried to identify these experimental limitations and developed potential solutions to overcome these limitations.

6.5.1 Limitations of *in vivo* DIO murine models

6.5.1.1 Sexual dimorphism in DIO models

Conventionally, DIO murine models were accepted as a representative model for the diet-induced etiology of obesity in humans [719, 720]. DIO murine models resemble various key characteristics of human obesity including increased body fat, body weight, increased leptin, insulin and triglycerides within the blood [719, 721, 722]. Various research illustrated the commonality of global gene-expression pattern and altered biological pathways (including immune response and angiogenesis) between the DIO murine models and humans [719, 721, 722].

However, DIO murine models express various differences based on strain, sex and age of the animal, directly affecting the response of obesogenesis. Irrespective of species, males and younger mice are known to be more sensitive to DIO and DIO-associated pathologies. Predominantly this is mainly due to feeding behaviour, metabolic (energy-expenditure) responses, hormonal and behavioural differences [639, 719]. Despite sexual dimorphism being well documented, conventionally most DIO research has been published on male mice due to their higher magnitude of weight gain, adiposity and other obesity-associated characteristics [639]. Contrasting males, female C57BL/6J mice are more resistant to the obesogenic physiological effects of fat-dense diets- this resistance is thought to be due the hormone, oestrogen. Interestingly mice undergoing an ovariectomy exhibited diminish this protective feature of females against DIO [641, 643, 723]. Although there are some disparities in the field, recent publications also suggested that behavioural differences in exercise, energy-expenditure and fat tissue distribution between sexes enables females to be less affected by DIO [639, 641]. Importantly, although the magnitude of weight gain, hyperlipidemia and visceral adiposity index are shown to be different between male and female mice models, females were shown to wane the earlier difference in expressing DIO parameters, especially after 11-15 weeks obesogenic diets [639-643]. Interestingly, no difference was recorded in the capacity of dieting and weight loss conditions between sexes [641].

The sexual dimorphism observed in DIO-linked physiological characteristics is also suggested to affect the immune response of the different sexes. Although both sexes induce pro-inflammatory alterations in general immune phenotype and establish the chronic OIIM, male mice induce a higher inflammatory gene expression against obesogenic diets [643]. Interestingly in line with our *in vivo* dataset from both 3-week and 14-week female DIO murine models (**Figure 3.17 & 5.15**), female mice were protected against the prominent loss of Treg populations within obesogenic diet-driven OIIM compared to male mice [724, 725].

To limit the DIO-linked sexual dimorphism, we planned to compare the male and female immune response in 14-week DIO and WGWL models of male C57BL/6J mice groups. This experiment was conducted during the thesis write-up period, therefore any conclusions of the data have not been made due to timeframe. Additionally, considering the importance of DIO-linked physiological alterations, we plan to utilise metabolic cages. These metabolic cages will trace the eating behaviours and metabolic changes associated with DIO. However limitations of their use includes: high variance among the individual behaviour of mice, metabolic rate recorded by the analyser could not be instantaneous and accurate and behavioural changes linked with single-housing protocol of the metabolic cages [726].

Furthermore, we would like to further investigate the obesity-related systemic metabolic parameters from the blood samples obtained from mice groups to document the weekly development of obesity-linked physiological changes. This intravenous blood collection of mice per group throughout experiment at critical time points such as before diet switch and after diet switch would enable us to investigate both obesity-related systemic metabolic parameters (insulin and glucose) and HFD-driven pro-inflammatory EM $CD4^+$ T cell phenotype.

6.5.1.3 Time of recovery in the WGWL DIO murine models

Additionally, to fully assess the HFD-driven epigenetic reprogramming in the 14-week WGWL model and EM $CD4^+$ T cell phenotype , the time points used within the experiment could be expanded. Although, translating mouse age into human age is highly controversial, utilising conventional conversion formulas enable the calculation of relative life phase equivalence between humans and mouse [727]. Based on this calculation, within our 14-week WGWL model the exposure of mice to HFD at 4 weeks old is relative to adolescence (13 years old) in human. The weight loss via dieting the mice at 12-week old is equivalent to early

adulthood (20-23 years old) and lost weight at 20-week old accounting for adulthood stage (28 years old) in human terms [727]. Within this experimental plan we aimed to investigate translationally relevant DIO model and the potential effects of weight loss during adolescence (early-adulthood) which has been identified as a critical age group due to social interactions and behavioural changes in early adulthood [728, 729].

To investigate the longevity of this HFD-driven epigenetic reprogramming, we extended the recovery period of the HFD-RE and mice in this group have received the HFD for 8 weeks and then received 12 weeks of CD. In this extended recovery experimental plan the 'recovery' or dieting time for weight loss has been doubled compared to the original experimental plan. Considering the lack of knowledge on the potential long-term effects of HFD and past DIO in earlier life, it is important to identify the duration for this long-lasting pro-inflammatory epigenetic modification following the weight loss. It should be noted that similar to our original experimental plan both Hata et al. 2023 and Cottam et al. 2022 publications included a WGWL model fed with HFD for 11 weeks and CD for 9 weeks as the weight loss period [432, 585]. Considering their observations on past DIO-driven persistent reprogramming on macrophages up to 9 weeks of dieting period, it would be highly pertinent to investigate our newly proposed model with 12 weeks to identify the range modulations [432, 585]. This extended time course experiment has been carried out recently but it has not been possible to analyse and draw conclusions.

6.5.2 Limitations of *in vitro* lipid treatment of $CD4^+$ T cells

Following the observations *in vivo* DIO models, we developed different *in vitro* experiments to investigate these phenotypes further. Although the *in vitro* assays are reductionist approaches, they have advantages including homogeneously controlled microenvironment within cell culture. These advantages are important in molecular mechanistical studies. Therefore *in vitro* models were useful for testing the direct immunomodulatory roles of our candidate bioactive lipids specifically on $CD4^+$ T cells. However it should be noted that this *in vitro* system fails to recapitulate the complex *in vivo* conditions like cell-to-cell interactions.

Analysing the immune and lipidomic profiles of the DIO *in vivo* murine models to identify the distinct candidate lipids and range of physiologically relevant concentrations. As

detailed before, for each *in vitro* assay we have done a reasonable amount of optimisation experiments by testing the dose response in time course assays, toxicity and optimised the other cellular conditions like T-cell activation.

Supporting the literature, our optimised *in vitro* lipid treatment assays were highly effective in identifying the direct immunomodulatory roles of bioactive candidate lipid groups by recapitulating the immune phenotype observed DIO *in vivo* murine models. The *in vitro* lipid pre-treatment protocol was shown to recapitulate the HFD-driven pro-inflammatory EM phenotype observed in the 14 week WGWL experiment on human $CD4^+$ T cells.

Based on our hypothesis: distinct bioactive SFAs (such as PA and STE) can directly trigger long-lasting, persistent epigenetic modifications in the methylation profiles of STK26 and CDKN1C genes specifically within $CD4^+$ T cells. To further validate this hypothesis, we plan to utilise targeted pyrosequencing to investigate the methylation status of these candidate genes within human $CD4^+$ T cells following *in vitro* pre-lipid treatment. Although, this experiment was previously planned and carried out, the pyrosequencing experiment was delayed due to the technical limitations. This dataset will identify the distinct bioactive potential of specific SFAs in inducing the phenotype observed in EM population via directly altering the methylation status of STK26 and CDKN1C genes as previously identified by the RRBS and pyrosequencing of 14-week WGWL *in vivo* murine $CD4^+$ T cells.

6.5.2.1 Human leukocytes cones

All human $CD4^+$ T cells and PBMCs were isolated from the leukapheresis blood cones obtained from healthy (fit-to-donate) donors as collected by National Blood and Transplant Service (NBTC). A key limitation of utilising these donors is the limited information about the donors such as donor age, sex, underlying medical conditions or current medical status. Therefore, often large donor-to-donor variation is observed when using analysing samples.

However, to try and account for any variation between experimental setups, we isolate both naïve and total $CD4^+$ T cells. This process potentially reduced the variance that could have been induced by other cell types. Additionally, we also attempt to compensate for this high human variation by staining for control markers of $CD4^+$ T cells subsets. This phenotyping of each donor identified any prominent background biasing of $CD4^+$ T cells subsets towards a specific fate prior to the *in vitro* lipid treatments. Alongside this we increase the number of

biological replicates within the data sets to account for general human variance between the samples.

6.5.3 Dissecting the functional changes in autophagy and senescence profiles of $CD4^+$ T cells following SFA exposure

6.5.3.1 Investigating the immunometabolism of T cells following the bioactive lipid treatment

Following the alterations in cellular function and immune phenotype, it pertinent to investigate the effect of bioactive lipid on the T-cell metabolism following the different bioactive lipid treatments (C24 and SFAs). Background literature has already illustrated importance of bioactive lipid-driven metabolic alterations that can mediate T-cell differentiation, immune phenotype and cellular functions during obesity. To investigate the effect of long-chain fatty acids on the cellular metabolism a specific Seahorse kit called Seahorse XF Palmitate Oxidation Stress Test Kit could be utilised.

6.5.3.2 Autophagy flux capacity

As previously highlighted, investigating the dynamic process of autophagy within the complex pathophysiology of obesity is highly challenging- we experienced these challenges within both our *in vivo* and *in vitro* models.

Following our preliminary observations, we aim to validate LC3-II modulations further by quantifying LC3-II protein levels via western blotting within the murine $CD4^+$ T cells isolated from the 14-week diet groups. However, using western blot may limiting due to our hypothesis investigating the autophagy capacity on specific EM $CD4^+$ T cell populations ($CXCR3^+$ and LFA-1^+). Therefore we need be able to distinguish between these specific $CD4^+$ T cell subsets to investigate the LC3-II-autophagy levels. To overcome this, we plan to utilise Imagestream technology or cell sorting strategies which would enable us to investigate the autophagy flux capacity within specific subsets of memory $CD4^+$ T cells isolated from 14-week WGWL *in vivo* murine models. Similarly in human $CD4^+$ T cell *in vitro* lipid pre-treatment assays, we are also aiming to utilise LC3-II protein quantification with western blotting alongside another method to investigate the autophagy flux. However, it should be noted that consistent with the literature, we observed high donor-to-donor variance in the autophagy flux

levels between human leukapheresis blood cones. In attempts to reduce this variation between donors we planned to increase the biological replicates and also isolate PBMCs from donors in which we know the health status/age/sex to hold as a comparison.

Additionally following the western blot protein quantification of STK26 protein within pLN tissues of 14-week WGWL *in vivo* murine models, we would like to investigate the relative STK26 gene expression via qPCR. This experiment would further validate our hypothesis that HFD (or bioactive SFA)-driven hypomethylation of STK26 can directly induce an elevation in STK26 expression at both genomic and protein levels as observed in the *in vitro* lipid pre-treated human $CD4^+$ T cell samples.

Furthermore, to investigate the potential critical role of STK26 in mediating autophagy within $CD4^+$ T cells under complex *in vivo* conditions, we plan to utilise a specific STK26-knockout mice model. Use of this knockout model in our CD and HFD diet experiments will examine if the knockout reduces the effect of HFD-driven pro-inflammatory EM $CD4^+$ T cell phenotype within 8 and 14 week DIO models. Currently we have obtained the STK26-knockout mice to our animal facility and are backcrossing to the C57BL/6J mice background. In addition to the *in vivo* STK26 knockout model experiments, we have also planned to utilise distinct STK26 inhibitors such as hesperadin within our *in vitro* human $CD4^+$ T cell lipid pre-treatment assays [604, 730]. It would be important to investigate the SFA-driven pro-inflammatory EM $CD4^+$ T cell phenotype and the autophagy flux capacity of the *in vitro* lipid pre-treated human $CD4^+$ T cells following the pharmacological inhibition of STK26 [604, 730]. Consistently, a recent publication by Wu et al. 2020, demonstrated a significant downregulation of autophagy flux within the *in vitro* cell conditions treated with the STK26 inhibitor hesperidin [653]. Finally, considering the critical interaction of STK26 and ATG4b proteins in mediating the autophagy in a non-canonical pathway, we seek to investigate the ATG4b expression in both gene and protein levels within both 14-week WGWL *in vivo* model and *in vitro* assay [604].

6.5.3.3 Senescence profile

Furthermore, there are further experiments needed to fully assess the HFD-driven senescence phenotype observed *in vivo* with the KLRG1 senescence-associated marker expression as well as the SASP phenotype observed *in vitro* with the lipid pre-treatment of human $CD4^+$ T cells. For example, quantification of CDKN1C protein and gene expression

levels within the pLN tissues of the 14-week WGWL *in vivo* protocol samples would provide further details on the direct alterations induced by hypomethylation. Although it was originally planned to quantify the CDKN1C protein levels from *in vivo* WGWL model, technical difficulties with the antibody prevented this quantification.

Moreover, there are few defined senescence markers for mouse and those which are expressed in human systems are not translatable to mouse (e.g. CD57 or loss of CD28) [731]. Despite designing multiple flow cytometry panels to investigate the senescence profile of $CD4^+$ T cells isolated from the 14-week *in vivo* WGWL murine model, we did not observe a profound senescence profile with the markers tested. However, considering the lack of adequate phenotype observed and the background literature, it would be interesting to incubate the cells *ex vivo* and further activate them PMA/ionomycin stimulation to investigate any additional the difference in the expression potential of senescence-associated markers between the different diet groups. Additionally, it would be interesting to investigate the senescence markers or senescence-associated T cell populations such as $CD153^+$ $PD1^+$ $CD4^+$ T cells in the fat tissues [430, 570]. Finally, it would be pertinent to investigate the senescence profile with other reliable methods such as β-galactosidase histochemical staining [732, 733]. This method may be appropriate because senescent cells are known to increase the expression of β-galactosidase due to the reduction in lysosomal pH [732, 733]. Moreover, cellular senescence is highly complex phenotype which could be driven by various mediators through different pathways and identification of a specific senescence-associated marker would enable us to investigate a potential molecular mechanism driving the senescence profile.

6.6 Investigating the clinical obese human samples

Furthermore, to investigate the relevance of our observed HFD-driven pro-inflammatory EM $CD4^+$ T cell phenotype in a clinical setting, we have planned to utilise samples from obese cohorts. This would also allow the investigation of any functional changes associated with the EM phenotype like autophagy and senescence. Recent collaboration with Dr. Hogan of Maynooth University gave us access of PBMCs and adipose tissue samples from obese patients before and after weight loss. Weight loss in these patients was induced either bariatric surgery or pharmacological treatment (GLP-1). This study will inform us about the impact of weight-loss in adulthood on the $CD4^+$ T cell profile and whether the weight loss will revert the pro-inflammatory biased obese immune system towards to a pre-obese state. Understanding the

molecular mechanism driving this obesity-linked immune reprogramming would also address the clinical, translational potential of this project in a human context.

Additionally, another collaboration with Buchinger Wilhelmi clinic (Switzerland) provided us whole blood samples from obese patients who underwent clinically controlled fasting to induce weight loss. This cohort provides details of patient sex, age and BMI before fasting, as well as samples prior to and after fasting. This cohort resemblances our *in vivo* murine model experimental plan with the DIO with 8-weeks of HFD feeding followed by a recovery/weight loss period for 6 weeks by CD feeding – therefore these samples are pivotal to investigate the obesity-linked pro-inflammatory EM phenotype as well as autophagy and senescence profiles. Therefore, this study will also illustrate the clinical translational potential of the obesity-linked phenotype detailed within this thesis.

6.7 Potential crosstalk between autophagy and senescence

As previously discussed, the plethora of deleterious bioactive lipid groups in obese microenvironment is shown to induce various critical conditions such as hypoxia, excessive ROS generation, oxidative stress, DNA and organelle damage. All these factors are known to be critical in inducing the complex cellular functions such as autophagy and cellular senescence. Consistently, it is well known that DIO induces a senescence profile in various cell types including T cells [430, 435, 570, 579]. On the other hand, although autophagy is traditionally known to be activated by nutrient depletion or starvation, various publications reported an activation of autophagy under obese conditions potentially due to exacerbated cellular stress like ROS production [607-609]. As previously detailed, the role and functions of autophagy in obese cellular environment is still highly controversial and poorly understood.

Our preliminary dataset on 14-week WGWL murine model suggested a persistent elevation in both autophagy flux and senescence profile on $CD4^+$ T cells isolated from HFD and HFD-RE groups. Interestingly consistent with our preliminary data on the bioactive SFA-driven $CD4^+$ T cell functional alterations in autophagy and senescence has recently speculated to be highly interconnected and may have critical roles in DIO immune microenvironment through this crosstalk [633, 734-736].

In line with our observation on WGWL murine model, recently Zhu et al. 2022 identified bioactive PA as a key metabolite that can induce cellular senescence and elevated autophagy flux through excessive ROS generation that leads to a vascular endothelial damage associated with CVDs and Kawasaki disease (KD) [681]. The KD is an inflammatory acute systemic vasculitis that obesity has been shown to affect the outcomes of the disease phenotype due to the obesity-induced pro-inflammatory immunity [737]. Specifically PA was shown to significantly accumulate within the coronary artery lesions of KD patients where particularly PA was shown to induce cellular senescence and autophagy with increased LC3-II protein [681]. Interestingly, it was previously suggested in the literature that PA could induce an indirect enhancement in the autophagy levels as a protective mechanism against the PA-induced ROS production, oxidative stress and apoptosis [675].

On the other hand, Lee et al. 2021 suggested PA-treatment elevates the LC3-I to LC3-II conversion however, also shown to reduce the fusion of autophagosomes and lysosomes, representing a lower autophagic flux [734]. Lee illustrated that in human endothelial cells this PA-driven reduction in autophagic flux was shown to directly induce an senescence profile [734]. This PA-driven reduced autophagic flux and was identified as the key driver of senescence due the crucial roles of autophagy in mediating the anti-senescence functions like recycling the exhausted and damaged organelles and cellular debris [734]. This publication was highly important for various reasons such as highlighting the inconsistencies within the field about the distinct modulatory effects of bioactive SFAs on autophagy and senescence profile but also illustrating that even an significant increase in LC3-II does not necessary lead to an increased autophagy flux capacity and functionality [599, 734]. Considering these recent publications, we have also planned to check for other key autophagy markers of autophagy flux such as p62 protein by western blotting but also to visualise and assess the fusion of autophagosomes and lysosomes process via fluorescence microscopy.

Considering these discrepancies in the field and our dataset, it is highly crucial to understand this complex interplay between autophagy and senescence in driving a pro-inflammatory immune phenotype. This obesity-linked pro-inflammatory immune phenotype with altered autophagy capacity and senescence profile is shown to be a critical clinical factor underlaying various obesity-linked inflammatory diseases as reported in KD. Additionally, identification of the exact molecular mechanism and complex interactions between autophagy and senescence in obesity pathophysiologies would enable us to potentially coordinate the

regulation of senescence state by selective activation or inhibition of autophagy in a tissue-specific context via precise medicine [735].

6.8 Cellular lipid bilayer membrane order

Furthermore, we have begun to analyse the effects of distinct bioactive candidate lipids on cellular lipid bilayer organisation of human $CD4^+$ T cells following the 3-day *in vitro* treatment in collaboration with Dr. Maria Makarova (UoB). Following the *in vitro* treatment, cells were stained with dye di-4-ANEPPDHQ and imaged under 488nm laser confocal microscopy. The images then analysed by Toblerone package (lucapanconi-Luca Panconi) of GitHub, utilised to measure membrane lipid order in live cells. The preliminary data suggests that C24 ceramide induces more ordered lipid bilayer compared to control. Similarly, both SFAs (PA and STE) were also induced an increase in lipid bilayer order whereas contrarily OA treatment of human $CD4^+$ T cells induced a high lipid bilayer disorganisation. Although this dataset is not conclusive as it is not finalised yet, however, initial observations confirmed membrane bilayer alterations induced by bioactive lipid groups as previously suggested by the literature and detailed in **Chapter 1**.

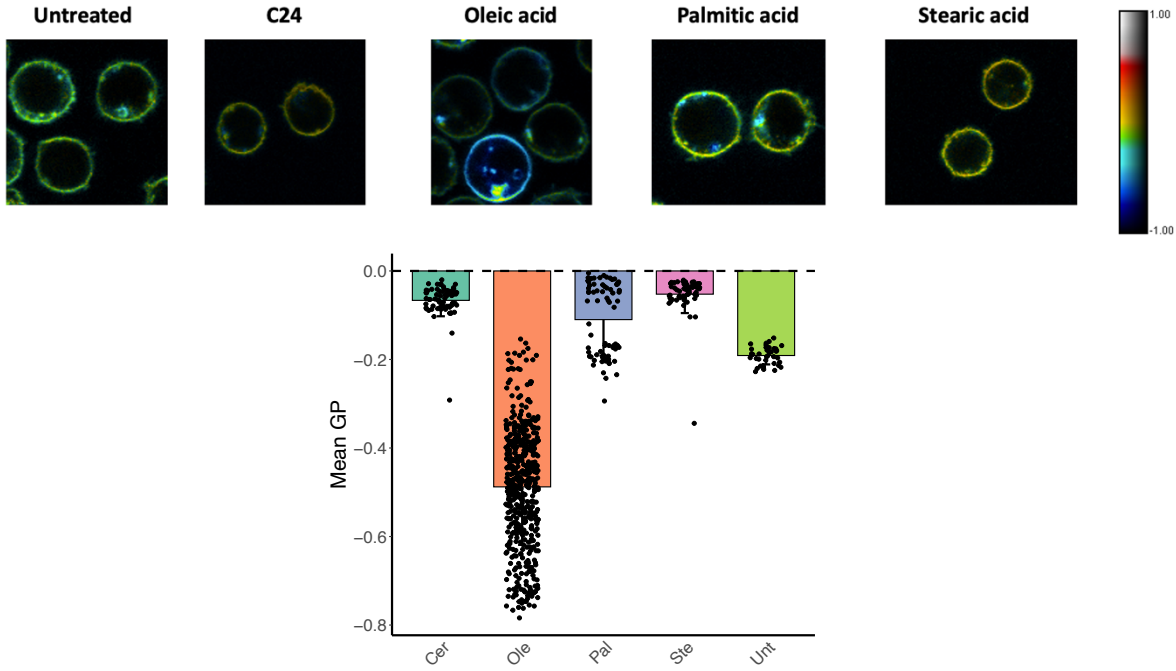


Figure 6.4) Direct alterations of cellular lipid bilayer following the *in vitro* bioactive lipid treatment of human $CD4^+$ T cells
Pseudocoloured generalised polarisation (GP) of images and quantification of human $CD4^+$ T cells following 3-days of in vitro treatment with the candidate bioactive lipid groups. Quantification of mean

GP of the cells following the visualisation via di-4-ANEPPDHQ (5µM, 30mins) dye. The pseudo-colour bar illustrates the generalised polarisation values- high membrane order is represented as red and disordered membrane as blue. § This project is running in a collaboration where all the staining and visualisation is done by **Dr. Maria Makarova** (UoB)

6.9 Conclusions and implications

This thesis has investigated the immunomodulatory capacities of bioactive lipid groups on T cells under obesogenic diet conditions and within the OIIM. Overall, *in vivo* and *in vitro* investigations highlighted the potential clinical implications on T cells within the OIIM, which may widen our knowledge on obese pathophysiology and weight loss (recovery state).

In addition to the weight loss recovery models, this project has also investigated the potential ameliorative effects of bioactive n-3PUFA via investigating its anti-inflammatory capacity through both *in vivo* and *in vitro* models. This work is important considering various clinical studies and trials detailing the beneficial clinical implications of dietary n-3PUFA supplementation within various obesity-associated diseases such as CVDs, RA and other autoimmune diseases. Alongside the previously discussed background literature on the distinct anti-inflammatory, ameliorative effects of n-3PUFA on various immune cells, recent clinical trials utilising dietary n-3PUFA supplementation should also be noted. More specifically, Kris-Etherton et al. 2019, extensively reviewed recent clinical trials of n-3PUFA supplementation in CVDs patients, highlighting that ~1-4g/day of n-PUFA (EPA and DHA) could significantly reduce the risk of CVDs - this suggests that n-3PUFA may be a critical clinical agent in the primary and secondary prevention of CVDs [738]. Recently another nationwide, randomised, double-blind clinical trial demonstrated the clinical beneficial effect of n-3PUFA supplementation coupled with vitamin D against autoimmune diseases (RA, polymyalgia rheumatica, autoimmune thyroid disease, psoriasis) [739, 740]. Hahn et al. 2022, illustrated that 5 years of vitamin D (2000 IU/day) and n-3PUFA dietary supplementation (1000 mg/day) in

older adults significantly reduced autoimmune disease incident and hazard ratio compared to the control group [739]. Furthermore, a recent case-control study with obese and lean female participants illustrated that n-3PUFA supplementation for a month has alleviated the peripheral immune cell mitochondrial dysfunction and inflammation in obese females. Importantly, dietary n-3PUFA supplementation has also been shown to significantly reduce the pro-inflammatory Th1 and Th17 T lymphocytes populations and ameliorate the OIIM by reducing the pro-inflammatory factors within the PBMCs obtained from these obese females [741]. This clinical observation recorded by Borja-Magno et al. 2023, was particularly important considering our *in vivo* and *in vitro* dataset illustrating the direct ameliorative potential of n-3PUFA in reducing the obesity-associated Th17 population as demonstrated in Chapter 3 and 4 [741].

Furthermore, this thesis has illustrated the limitations of conventional weight loss through analysing the T cells in peripheral lymphoid organs - a past history of obesity lead to a persistent long-term biasing effects towards pro-inflammatory EM fate that limits the re-establishment of homeostatic immune microenvironment. It is known that weight loss leads to various beneficial effects in re-establishing the homeostasis in metabolism and functionality of various tissues. Consistently various modern drugs recently approved by FDA such as Zepbound™ (tirzepatide) aims to induce weight loss for treating obesity and potential obesity-associated pathologies. However, our observation was particularly important to indicate that weight loss per se may not be critically effective against obesity-linked pro-inflammatory EM bias of peripheral T cells. Perhaps, a past history of obesity could induce morphological alterations in the peripheral SLOs leading to an EM $CD4^+$ T cell bias that primes immunity towards state of chronic inflammation, which despite weight loss being achieved, may contribute as a risk factor for obesity-linked autoimmune diseases in previously obese individuals.

Overall, this thesis illustrated that, alongside the weight loss approach, supplementation of distinct bioactive lipid groups such as n-3PUFA could be beneficial in ameliorating the obesity-induced pro-inflammatory biasing effect on T cells and establishing a homeostatic immune microenvironment. Furthermore, our data suggests that potential selective dietary restriction of certain deleterious bioactive lipid groups (such as PA and STE) could led to a secondary prevention approach against the obesity-associated pro-inflammatory EM biasing effects of these deleterious bioactive lipids on T cells.

Considering the complex nature of obesity pathophysiology, it is important to understand the different aspects of the pathological sequelae of obesity and to combine different therapeutics approaches to prevent or ameliorate these deleterious processes. Our data suggests that, distinct dietary modifications such as n-3PUFA supplementation and restriction of certain deleterious bioactive lipid groups could be crucial secondary prevention approaches in alleviating the pro-inflammatory effects of obesity.

REFERENCES

1. Kucuk, S., et al., *Unwrapping the mechanisms of ceramide and fatty acid-initiated signals leading to immune-inflammatory responses in obesity.* Int J Biochem Cell Biol, 2021. **135**: p. 105972.
2. Chooi, Y.C., C. Ding, and F. Magkos, *The epidemiology of obesity.* Metabolism, 2019. **92**: p. 6-10.
3. Spinelli, A., et al., *Prevalence of Severe Obesity among Primary School Children in 21 European Countries.* Obes Facts, 2019. **12**(2): p. 244-258.
4. Shah, B., et al., *Sex and gender differences in childhood obesity: contributing to the research agenda.* BMJ Nutr Prev Health, 2020. **3**(2): p. 387-390.
5. Mehrzad, R., R. Mehrzad, and Elsevier, *Inflammation and obesity : a new and novel approach to manage obesity and its consequences*. 2022.
6. Mehrzad, R. and ScienceDirect, *Obesity : global impact and epidemiology*. 2020.
7. Donohoe, C.L., et al., *Emerging Concepts Linking Obesity with the Hallmarks of Cancer.* Trends Endocrinol Metab, 2017. **28**(1): p. 46-62.
8. Salvestrini, V., C. Sell, and A. Lorenzini, *Obesity May Accelerate the Aging Process.* Front Endocrinol (Lausanne), 2019. **10**: p. 266.
9. Setayesh, T., et al., *Impact of obesity and overweight on DNA stability: Few facts and many hypotheses.* Mutat Res Rev Mutat Res, 2018. **777**: p. 64-91.
10. Manna, P. and S.K. Jain, *Obesity, Oxidative Stress, Adipose Tissue Dysfunction, and the Associated Health Risks: Causes and Therapeutic Strategies.* Metab Syndr Relat Disord, 2015. **13**(10): p. 423-44.
11. Ott, C., et al., *Role of advanced glycation end products in cellular signaling.* Redox Biol, 2014. **2**: p. 411-29.
12. Palmai-Pallag, T. and C.Z. Bachrati, *Inflammation-induced DNA damage and damage-induced inflammation: a vicious cycle.* Microbes Infect, 2014. **16**(10): p. 822-32.
13. Hernandez-Aguilera, A., et al., *Mitochondrial dysfunction: a basic mechanism in inflammation-related non-communicable diseases and therapeutic opportunities.* Mediators Inflamm, 2013. **2013**: p. 135698.
14. Heinonen, S., et al., *Impaired Mitochondrial Biogenesis in Adipose Tissue in Acquired Obesity.* Diabetes, 2015. **64**(9): p. 3135-45.
15. Laplante, M. and D.M. Sabatini, *mTOR signaling at a glance.* J Cell Sci, 2009. **122**(Pt 20): p. 3589-94.
16. McArdle, M.A., et al., *Mechanisms of obesity-induced inflammation and insulin resistance: insights into the emerging role of nutritional strategies.* Front Endocrinol (Lausanne), 2013. **4**: p. 52.
17. Saxton, R.A. and D.M. Sabatini, *mTOR Signaling in Growth, Metabolism, and Disease.* Cell, 2017. **168**(6): p. 960-976.
18. Mauro, C., et al., *Obesity-Induced Metabolic Stress Leads to Biased Effector Memory CD4(+) T Cell Differentiation via PI3K p110delta-Akt-Mediated Signals.* Cell Metab, 2017. **25**(3): p. 593-609.
19. Hotamisligil, G.S., *Inflammation, metaflammation and immunometabolic disorders.* Nature, 2017. **542**(7640): p. 177-185.
20. Global, B.M.I.M.C., et al., *Body-mass index and all-cause mortality: individual-participant-data meta-analysis of 239 prospective studies in four continents.* Lancet, 2016. **388**(10046): p. 776-86.
21. Taylor, E.M., A.D. Jones, and T.M. Henagan, *A Review of Mitochondrial-derived Fatty Acids in Epigenetic Regulation of Obesity and Type 2 Diabetes.* J Nutrit Health Food Sci, 2014. **2**(3): p. 1-4.

22. Tubaro, M., et al., *The ESC textbook of intensive and acute cardiovascular care*. 2021, Oxford University Press,: Oxford. p. 1 online resource (1088 pages).
23. Hotamisligil, G.S., et al., *IRS-1-mediated inhibition of insulin receptor tyrosine kinase activity in TNF-alpha- and obesity-induced insulin resistance.* Science, 1996. **271**(5249): p. 665-8.
24. Oh, D.Y. and J.M. Olefsky, *G protein-coupled receptors as targets for anti-diabetic therapeutics.* Nat Rev Drug Discov, 2016. **15**(3): p. 161-72.
25. Xu, X., et al., *A genome-wide methylation study on obesity: differential variability and differential methylation.* Epigenetics, 2013. **8**(5): p. 522-33.
26. Aslibekyan, S., et al., *Epigenome-wide study identifies novel methylation loci associated with body mass index and waist circumference.* Obesity (Silver Spring), 2015. **23**(7): p. 1493-501.
27. Khan, S.S., et al., *Association of Body Mass Index With Lifetime Risk of Cardiovascular Disease and Compression of Morbidity.* JAMA Cardiol, 2018. **3**(4): p. 280-287.
28. Dikaiou, P., et al., *Obesity, overweight and risk for cardiovascular disease and mortality in young women.* Eur J Prev Cardiol, 2021. **28**(12): p. 1351-1359.
29. Elagizi, A., et al., *An Overview and Update on Obesity and the Obesity Paradox in Cardiovascular Diseases.* Prog Cardiovasc Dis, 2018. **61**(2): p. 142-150.
30. Powell-Wiley, T.M., et al., *Obesity and Cardiovascular Disease: A Scientific Statement From the American Heart Association.* Circulation, 2021. **143**(21): p. e984-e1010.
31. Nolan, P.B., et al., *Prevalence of metabolic syndrome and metabolic syndrome components in young adults: A pooled analysis.* Prev Med Rep, 2017. **7**: p. 211-215.
32. Vassallo, P., S.L. Driver, and N.J. Stone, *Metabolic Syndrome: An Evolving Clinical Construct.* Prog Cardiovasc Dis, 2016. **59**(2): p. 172-177.
33. Saklayen, M.G., *The Global Epidemic of the Metabolic Syndrome.* Curr Hypertens Rep, 2018. **20**(2): p. 12.
34. Moore, J.X., N. Chaudhary, and T. Akinyemiju, *Metabolic Syndrome Prevalence by Race/Ethnicity and Sex in the United States, National Health and Nutrition Examination Survey, 1988-2012.* Prev Chronic Dis, 2017. **14**: p. E24.
35. Sjogren, L., et al., *Impact of obesity on intensive care outcomes in patients with COVID-19 in Sweden-A cohort study.* PLoS One, 2021. **16**(10): p. e0257891.
36. Popkin, B.M., et al., *Individuals with obesity and COVID-19: A global perspective on the epidemiology and biological relationships.* Obes Rev, 2020. **21**(11): p. e13128.
37. Port, J.R., et al., *Western diet increases COVID-19 disease severity in the Syrian hamster.* bioRxiv, 2021.
38. Trujillo-Mayol, I., et al., *Western Dietary Pattern Antioxidant Intakes and Oxidative Stress: Importance During the SARS-CoV-2/COVID-19 Pandemic.* Adv Nutr, 2021. **12**(3): p. 670-681.
39. Hruby, A. and F.B. Hu, *The Epidemiology of Obesity: A Big Picture.* Pharmacoeconomics, 2015. **33**(7): p. 673-89.
40. Meldrum, D.R., M.A. Morris, and J.C. Gambone, *Obesity pandemic: causes, consequences, and solutions-but do we have the will?* Fertil Steril, 2017. **107**(4): p. 833-839.
41. Goran, M.I. and T.L. Alderete, *Targeting adipose tissue inflammation to treat the underlying basis of the metabolic complications of obesity.* Nestle Nutr Inst Workshop Ser, 2012. **73**: p. 49-60; discussion p61-6.
42. Freire, R., *Scientific evidence of diets for weight loss: Different macronutrient composition, intermittent fasting, and popular diets.* Nutrition, 2020. **69**: p. 110549.
43. Warden, C.H. and J.S. Fisler, *Comparisons of diets used in animal models of high-fat feeding.* Cell Metab, 2008. **7**(4): p. 277.

44. Sampey, B.P., et al., *Cafeteria diet is a robust model of human metabolic syndrome with liver and adipose inflammation: comparison to high-fat diet.* Obesity (Silver Spring), 2011. **19**(6): p. 1109-17.
45. Higa, T.S., et al., *Comparison between cafeteria and high-fat diets in the induction of metabolic dysfunction in mice.* Int J Physiol Pathophysiol Pharmacol, 2014. **6**(1): p. 47-54.
46. Shively, C.A., et al., *Mediterranean versus Western Diet Effects on Caloric Intake, Obesity, Metabolism, and Hepatosteatosis in Nonhuman Primates.* Obesity (Silver Spring), 2019. **27**(5): p. 777-784.
47. Loh, M.Y., et al., *Dietary fat type and level influence adiposity development in obese but not lean Zucker rats.* Proc Soc Exp Biol Med, 1998. **218**(1): p. 38-44.
48. Almeida-Suhett, C.P., et al., *Control diet in a high-fat diet study in mice: Regular chow and purified low-fat diet have similar effects on phenotypic, metabolic, and behavioral outcomes.* Nutr Neurosci, 2019. **22**(1): p. 19-28.
49. Agriculture, U.S.D.o., *Energy intakes: percentages of energy from protein, carbohydrate, fat, and alcohol, by gender and age. What We Eat in America, NHANES 2013-2014*, in *Agricultural Research Service*. 2016.
50. Agriculture, U.S.D.o., *Nutrient Intakes from Food and Beverages: Mean Amounts Consumed per Individual, by Gender and Age, What We Eat in America, NHANES 2017-2018*. 2020, U.S. Department of Agriculture: Agricultural Research Service.
51. Statovci, D., et al., *The Impact of Western Diet and Nutrients on the Microbiota and Immune Response at Mucosal Interfaces.* Front Immunol, 2017. **8**: p. 838.
52. Kien, C.L., et al., *Dietary intake of palmitate and oleate has broad impact on systemic and tissue lipid profiles in humans.* Am J Clin Nutr, 2014. **99**(3): p. 436-45.
53. Choi, S. and A.J. Snider, *Sphingolipids in High Fat Diet and Obesity-Related Diseases.* Mediators Inflamm, 2015. **2015**: p. 520618.
54. Cordain, L., et al., *Origins and evolution of the Western diet: health implications for the 21st century.* Am J Clin Nutr, 2005. **81**(2): p. 341-54.
55. Cheng, H.S., et al., *Increased susceptibility of post-weaning rats on high-fat diet to metabolic syndrome.* J Adv Res, 2017. **8**(6): p. 743-752.
56. Calder, P.C., *Omega-3 polyunsaturated fatty acids and inflammatory processes: nutrition or pharmacology?* Br J Clin Pharmacol, 2013. **75**(3): p. 645-62.
57. Sparks, L.M., et al., *A high-fat diet coordinately downregulates genes required for mitochondrial oxidative phosphorylation in skeletal muscle.* Diabetes, 2005. **54**(7): p. 1926-33.
58. Remely, M., et al., *Vitamin E Modifies High-Fat Diet-Induced Increase of DNA Strand Breaks, and Changes in Expression and DNA Methylation of Dnmt1 and MLH1 in C57BL/6J Male Mice.* Nutrients, 2017. **9**(6).
59. Song, F., et al., *RAGE regulates the metabolic and inflammatory response to high-fat feeding in mice.* Diabetes, 2014. **63**(6): p. 1948-65.
60. Bortolin, R.C., et al., *A new animal diet based on human Western diet is a robust diet-induced obesity model: comparison to high-fat and cafeteria diets in term of metabolic and gut microbiota disruption.* Int J Obes (Lond), 2018. **42**(3): p. 525-534.
61. Nishi, H., T. Higashihara, and R. Inagi, *Lipotoxicity in Kidney, Heart, and Skeletal Muscle Dysfunction.* Nutrients, 2019. **11**(7).
62. Lee, Y., et al., *Beta-cell lipotoxicity in the pathogenesis of non-insulin-dependent diabetes mellitus of obese rats: impairment in adipocyte-beta-cell relationships.* Proc Natl Acad Sci U S A, 1994. **91**(23): p. 10878-82.
63. Unger, R.H., *Lipotoxicity in the pathogenesis of obesity-dependent NIDDM. Genetic and clinical implications.* Diabetes, 1995. **44**(8): p. 863-70.

64. Yazici, D. and H. Sezer, *Insulin Resistance, Obesity and Lipotoxicity.* Adv Exp Med Biol, 2017. **960**: p. 277-304.
65. Machate, D.J., et al., *Fatty Acid Diets: Regulation of Gut Microbiota Composition and Obesity and Its Related Metabolic Dysbiosis.* Int J Mol Sci, 2020. **21**(11).
66. Chaurasia, B. and S.A. Summers, *Ceramides - Lipotoxic Inducers of Metabolic Disorders.* Trends Endocrinol Metab, 2015. **26**(10): p. 538-550.
67. Chiurchiu, V., A. Leuti, and M. Maccarrone, *Bioactive Lipids and Chronic Inflammation: Managing the Fire Within.* Front Immunol, 2018. **9**: p. 38.
68. Leuti, A., et al., *Bioactive lipids, inflammation and chronic diseases.* Adv Drug Deliv Rev, 2020. **159**: p. 133-169.
69. de Jong, A.J., et al., *Fatty acids, lipid mediators, and T-cell function.* Front Immunol, 2014. **5**: p. 483.
70. Pizzorno, J.E. and M.T. Murray, *Textbook of natural medicine*. 4th ed. 2013, St. Louis, Mo.: Elsevier/Churchill Livingstone. xxv, 1916 p.
71. Calder, P.C., *The relationship between the fatty acid composition of immune cells and their function.* Prostaglandins Leukot Essent Fatty Acids, 2008. **79**(3-5): p. 101-8.
72. Yao, C. and S. Narumiya, *Prostaglandin-cytokine crosstalk in chronic inflammation.* Br J Pharmacol, 2019. **176**(3): p. 337-354.
73. Due, A., et al., *Comparison of the effects on insulin resistance and glucose tolerance of 6-mo high-monounsaturated-fat, low-fat, and control diets.* Am J Clin Nutr, 2008. **87**(4): p. 855-62.
74. de Wit, N., et al., *Saturated fat stimulates obesity and hepatic steatosis and affects gut microbiota composition by an enhanced overflow of dietary fat to the distal intestine.* Am J Physiol Gastrointest Liver Physiol, 2012. **303**(5): p. G589-99.
75. Phillips, C.M., et al., *High dietary saturated fat intake accentuates obesity risk associated with the fat mass and obesity-associated gene in adults.* J Nutr, 2012. **142**(5): p. 824-31.
76. Carta, G., et al., *Palmitic Acid: Physiological Role, Metabolism and Nutritional Implications.* Front Physiol, 2017. **8**: p. 902.
77. Melo, H.M., et al., *Palmitate Is Increased in the Cerebrospinal Fluid of Humans with Obesity and Induces Memory Impairment in Mice via Pro-inflammatory TNF-alpha.* Cell Rep, 2020. **30**(7): p. 2180-2194 e8.
78. Quehenberger, O., et al., *Lipidomics reveals a remarkable diversity of lipids in human plasma.* J Lipid Res, 2010. **51**(11): p. 3299-305.
79. Qiu, T., et al., *Obesity-induced elevated palmitic acid promotes inflammation and glucose metabolism disorders through GPRs/NF-kappaB/KLF7 pathway.* Nutr Diabetes, 2022. **12**(1): p. 23.
80. Chen, B., et al., *Dietary Fatty Acids Alter Lipid Profiles and Induce Myocardial Dysfunction without Causing Metabolic Disorders in Mice.* Nutrients, 2018. **10**(1).
81. Itami, N., et al., *Palmitic acid induces ceramide accumulation, mitochondrial protein hyperacetylation, and mitochondrial dysfunction in porcine oocytes.* Biol Reprod, 2018. **98**(5): p. 644-653.
82. Fatima, S., et al., *High-fat diet feeding and palmitic acid increase CRC growth in beta2AR-dependent manner.* Cell Death Dis, 2019. **10**(10): p. 711.
83. Murru, E., et al., *Impact of Dietary Palmitic Acid on Lipid Metabolism.* Front Nutr, 2022. **9**: p. 861664.
84. Zhou, H., C.J. Urso, and V. Jadeja, *Saturated Fatty Acids in Obesity-Associated Inflammation.* J Inflamm Res, 2020. **13**: p. 1-14.
85. Kwan, H.Y., et al., *Signal transducer and activator of transcription-3 drives the high-fat diet-associated prostate cancer growth.* Cell Death Dis, 2019. **10**(9): p. 637.

86. Korbecki, J. and K. Bajdak-Rusinek, *The effect of palmitic acid on inflammatory response in macrophages: an overview of molecular mechanisms.* Inflamm Res, 2019. **68**(11): p. 915-932.
87. Yin, J., et al., *Palmitate induces endoplasmic reticulum stress and autophagy in mature adipocytes: implications for apoptosis and inflammation.* Int J Mol Med, 2015. **35**(4): p. 932-40.
88. Hall, E., et al., *Effects of palmitate on genome-wide mRNA expression and DNA methylation patterns in human pancreatic islets.* BMC Med, 2014. **12**: p. 103.
89. Wei, X., et al., *Endothelial Palmitoylation Cycling Coordinates Vessel Remodeling in Peripheral Artery Disease.* Circ Res, 2020. **127**(2): p. 249-265.
90. Dong, G., et al., *Palmitoylation couples insulin hypersecretion with beta cell failure in diabetes.* Cell Metab, 2023. **35**(2): p. 332-344 e7.
91. Henkel, J., et al., *Enhanced Palmitate-Induced Interleukin-8 Formation in Human Macrophages by Insulin or Prostaglandin E2.* Biomedicines, 2021. **9**(5).
92. Coll, T., et al., *Cyclooxygenase 2 inhibition exacerbates palmitate-induced inflammation and insulin resistance in skeletal muscle cells.* Endocrinology, 2010. **151**(2): p. 537-48.
93. Crupkin, M. and A. Zambelli, *Detrimental Impact of Trans Fats on Human Health: Stearic Acid-Rich Fats as Possible Substitutes.* Compr Rev Food Sci Food Saf, 2008. **7**(3): p. 271-279.
94. Salas, J.J., et al., *Biochemistry of high stearic sunflower, a new source of saturated fats.* Prog Lipid Res, 2014. **55**: p. 30-42.
95. van Rooijen, M.A. and R.P. Mensink, *Palmitic Acid Versus Stearic Acid: Effects of Interesterification and Intakes on Cardiometabolic Risk Markers - A Systematic Review.* Nutrients, 2020. **12**(3).
96. Fernandez, M.L. and K.L. West, *Mechanisms by which dietary fatty acids modulate plasma lipids.* J Nutr, 2005. **135**(9): p. 2075-8.
97. Dougherty, R.M., M.A. Allman, and J.M. Iacono, *Effects of diets containing high or low amounts of stearic acid on plasma lipoprotein fractions and fecal fatty acid excretion of men.* Am J Clin Nutr, 1995. **61**(5): p. 1120-8.
98. Hunter, J.E., J. Zhang, and P.M. Kris-Etherton, *Cardiovascular disease risk of dietary stearic acid compared with trans, other saturated, and unsaturated fatty acids: a systematic review.* Am J Clin Nutr, 2010. **91**(1): p. 46-63.
99. Meng, H., et al., *Comparison of diets enriched in stearic, oleic, and palmitic acids on inflammation, immune response, cardiometabolic risk factors, and fecal bile acid concentrations in mildly hypercholesterolemic postmenopausal women-randomized crossover trial.* Am J Clin Nutr, 2019. **110**(2): p. 305-315.
100. Ravaut, G., et al., *Monounsaturated Fatty Acids in Obesity-Related Inflammation.* Int J Mol Sci, 2020. **22**(1).
101. Rogero, M.M. and P.C. Calder, *Obesity, Inflammation, Toll-Like Receptor 4 and Fatty Acids.* Nutrients, 2018. **10**(4).
102. Preedy, V.R. and R.R. Watson, *Olives and olive oil in health and disease prevention*. 2021, Academic Press,: Amsterdam. p. 1 online resource.
103. Servili, M., et al., *Biological Activities of Phenolic Compounds of Extra Virgin Olive Oil.* Antioxidants (Basel), 2013. **3**(1): p. 1-23.
104. Piccinin, E., et al., *Role of Oleic Acid in the Gut-Liver Axis: From Diet to the Regulation of Its Synthesis via Stearoyl-CoA Desaturase 1 (SCD1).* Nutrients, 2019. **11**(10).
105. Cesari, F., et al., *Aging process, adherence to Mediterranean diet and nutritional status in a large cohort of nonagenarians: Effects on endothelial progenitor cells.* Nutr Metab Cardiovasc Dis, 2018. **28**(1): p. 84-90.

106. De Filippis, F., et al., *High-level adherence to a Mediterranean diet beneficially impacts the gut microbiota and associated metabolome.* Gut, 2016. **65**(11): p. 1812-1821.
107. Teres, S., et al., *Oleic acid content is responsible for the reduction in blood pressure induced by olive oil.* Proc Natl Acad Sci U S A, 2008. **105**(37): p. 13811-6.
108. Calder, P.C., *Fatty acids and inflammation: the cutting edge between food and pharma.* Eur J Pharmacol, 2011. **668 Suppl 1**: p. S50-8.
109. Watanabe, Y. and I. Tatsuno, *Prevention of Cardiovascular Events with Omega-3 Polyunsaturated Fatty Acids and the Mechanism Involved.* J Atheroscler Thromb, 2020. **27**(3): p. 183-198.
110. Wall, R., et al., *Fatty acids from fish: the anti-inflammatory potential of long-chain omega-3 fatty acids.* Nutr Rev, 2010. **68**(5): p. 280-9.
111. Egalini, F., et al., *The Effects of Omega 3 and Omega 6 Fatty Acids on Glucose Metabolism: An Updated Review.* Nutrients, 2023. **15**(12).
112. Innes, J.K. and P.C. Calder, *The Differential Effects of Eicosapentaenoic Acid and Docosahexaenoic Acid on Cardiometabolic Risk Factors: A Systematic Review.* Int J Mol Sci, 2018. **19**(2).
113. Burke, M.F., F.M. Burke, and D.E. Soffer, *Review of Cardiometabolic Effects of Prescription Omega-3 Fatty Acids.* Curr Atheroscler Rep, 2017. **19**(12): p. 60.
114. Chan, D.C., et al., *Effect of omega-3 fatty acid supplementation on arterial elasticity in patients with familial hypercholesterolaemia on statin therapy.* Nutr Metab Cardiovasc Dis, 2016. **26**(12): p. 1140-1145.
115. Roman, G.C., et al., *Mediterranean diet: The role of long-chain omega-3 fatty acids in fish; polyphenols in fruits, vegetables, cereals, coffee, tea, cacao and wine; probiotics and vitamins in prevention of stroke, age-related cognitive decline, and Alzheimer disease.* Rev Neurol (Paris), 2019. **175**(10): p. 724-741.
116. Tortosa-Caparros, E., et al., *Anti-inflammatory effects of omega 3 and omega 6 polyunsaturated fatty acids in cardiovascular disease and metabolic syndrome.* Crit Rev Food Sci Nutr, 2017. **57**(16): p. 3421-3429.
117. Vesper, H., et al., *Sphingolipids in food and the emerging importance of sphingolipids to nutrition.* J Nutr, 1999. **129**(7): p. 1239-50.
118. Jolly, C.A., et al., *Dietary (n-3) polyunsaturated fatty acids suppress murine lymphoproliferation, interleukin-2 secretion, and the formation of diacylglycerol and ceramide.* J Nutr, 1997. **127**(1): p. 37-43.
119. Dong, Y.Q., et al., *Omega-3 PUFA ameliorates hyperhomocysteinemia-induced hepatic steatosis in mice by inhibiting hepatic ceramide synthesis.* Acta Pharmacol Sin, 2017. **38**(12): p. 1601-1610.
120. Li, J., et al., *Omega-3FAs Can Inhibit the Inflammation and Insulin Resistance of Adipose Tissue Caused by HHcy Induced Lipids Profile Changing in Mice.* Front Physiol, 2021. **12**: p. 628122.
121. Martins, A.R., et al., *Attenuation of obesity and insulin resistance by fish oil supplementation is associated with improved skeletal muscle mitochondrial function in mice fed a high-fat diet.* J Nutr Biochem, 2018. **55**: p. 76-88.
122. Pakiet, A., et al., *The effect of western diet on mice brain lipid composition.* Nutr Metab (Lond), 2019. **16**: p. 81.
123. Zalewska, A., et al., *High-Fat Diet Affects Ceramide Content, Disturbs Mitochondrial Redox Balance, and Induces Apoptosis in the Submandibular Glands of Mice.* Biomolecules, 2019. **9**(12).
124. Sambolin-Escobales, L., et al., *High-Fat Diet and Short-Term Unpredictable Stress Increase Long-Chain Ceramides Without Enhancing Behavioral Despair.* Front Mol Biosci, 2022. **9**: p. 859760.

125. Lanza, I.R., et al., *Influence of fish oil on skeletal muscle mitochondrial energetics and lipid metabolites during high-fat diet.* Am J Physiol Endocrinol Metab, 2013. **304**(12): p. E1391-403.
126. Cucchi, D., et al., *Omega-3 polyunsaturated fatty acids impinge on CD4+ T cell motility and adipose tissue distribution via direct and lipid mediator-dependent effects.* Cardiovasc Res, 2020. **116**(5): p. 1006-1020.
127. Camacho-Munoz, D., et al., *Omega-3 polyunsaturated fatty acids reverse the impact of western diets on regulatory T cell responses through averting ceramide-mediated pathways.* Biochem Pharmacol, 2022. **204**: p. 115211.
128. Hannun, Y.A. and L.M. Obeid, *Sphingolipids and their metabolism in physiology and disease.* Nat Rev Mol Cell Biol, 2018. **19**(3): p. 175-191.
129. Korner, C. and F. Frohlich, *Compartmentation and functions of sphingolipids.* Curr Opin Cell Biol, 2022. **74**: p. 104-111.
130. Sud, M., et al., *LMSD: LIPID MAPS structure database.* Nucleic Acids Res, 2007. **35**(Database issue): p. D527-32.
131. Unger, R.H., *Lipotoxic diseases.* Annu Rev Med, 2002. **53**: p. 319-36.
132. Green, C.D., et al., *Sphingolipids in metabolic disease: The good, the bad, and the unknown.* Cell Metab, 2021. **33**(7): p. 1293-1306.
133. Wang, J., et al., *Functions of Sphingolipids in Pathogenesis During Host-Pathogen Interactions.* Front Microbiol, 2021. **12**: p. 701041.
134. Aburasayn, H., R. Al Batran, and J.R. Ussher, *Targeting ceramide metabolism in obesity.* Am J Physiol Endocrinol Metab, 2016. **311**(2): p. E423-35.
135. Brozinick, J.T., et al., *Plasma sphingolipids are biomarkers of metabolic syndrome in non-human primates maintained on a Western-style diet.* Int J Obes (Lond), 2013. **37**(8): p. 1064-70.
136. Bikman, B.T. and S.A. Summers, *Ceramides as modulators of cellular and whole-body metabolism.* J Clin Invest, 2011. **121**(11): p. 4222-30.
137. Hammerschmidt, P. and J.C. Bruning, *Contribution of specific ceramides to obesity-associated metabolic diseases.* Cell Mol Life Sci, 2022. **79**(8): p. 395.
138. Custodia, A., et al., *Ceramide Metabolism and Parkinson's Disease-Therapeutic Targets.* Biomolecules, 2021. **11**(7).
139. Bruce, C.R., et al., *The sphingosine-1-phosphate analog FTY720 reduces muscle ceramide content and improves glucose tolerance in high fat-fed male mice.* Endocrinology, 2013. **154**(1): p. 65-76.
140. Moon, M.H., et al., *Antiobesity activity of a sphingosine 1-phosphate analogue FTY720 observed in adipocytes and obese mouse model.* Exp Mol Med, 2012. **44**(10): p. 603-14.
141. Raichur, S., et al., *CerS2 haploinsufficiency inhibits beta-oxidation and confers susceptibility to diet-induced steatohepatitis and insulin resistance.* Cell Metab, 2014. **20**(4): p. 687-95.
142. Kasumov, T., et al., *Ceramide as a mediator of non-alcoholic Fatty liver disease and associated atherosclerosis.* PLoS One, 2015. **10**(5): p. e0126910.
143. Chun, L., et al., *Inhibition of ceramide synthesis reverses endothelial dysfunction and atherosclerosis in streptozotocin-induced diabetic rats.* Diabetes Res Clin Pract, 2011. **93**(1): p. 77-85.
144. Glaros, E.N., et al., *Myriocin slows the progression of established atherosclerotic lesions in apolipoprotein E gene knockout mice.* J Lipid Res, 2008. **49**(2): p. 324-31.
145. Choi, R.H., et al., *Ceramides and other sphingolipids as drivers of cardiovascular disease.* Nat Rev Cardiol, 2021. **18**(10): p. 701-711.

146. Zhang, Q.J., et al., *Ceramide mediates vascular dysfunction in diet-induced obesity by PP2A-mediated dephosphorylation of the eNOS-Akt complex.* Diabetes, 2012. **61**(7): p. 1848-59.
147. Holland, W.L., et al., *Inhibition of ceramide synthesis ameliorates glucocorticoid-, saturated-fat-, and obesity-induced insulin resistance.* Cell Metab, 2007. **5**(3): p. 167-79.
148. Holland, W.L., et al., *Lipid-induced insulin resistance mediated by the proinflammatory receptor TLR4 requires saturated fatty acid-induced ceramide biosynthesis in mice.* J Clin Invest, 2011. **121**(5): p. 1858-70.
149. Chaurasia, B., et al., *Adipocyte Ceramides Regulate Subcutaneous Adipose Browning, Inflammation, and Metabolism.* Cell Metab, 2016. **24**(6): p. 820-834.
150. Ussher, J.R., et al., *Inhibition of de novo ceramide synthesis reverses diet-induced insulin resistance and enhances whole-body oxygen consumption.* Diabetes, 2010. **59**(10): p. 2453-64.
151. Varre, J.V., W.L. Holland, and S.A. Summers, *You aren't IMMUNE to the ceramides that accumulate in cardiometabolic disease.* Biochim Biophys Acta Mol Cell Biol Lipids, 2022. **1867**(6): p. 159125.
152. Summers, S.A., B. Chaurasia, and W.L. Holland, *Metabolic Messengers: ceramides.* Nat Metab, 2019. **1**(11): p. 1051-1058.
153. Holland, W.L. and S.A. Summers, *Sphingolipids, insulin resistance, and metabolic disease: new insights from in vivo manipulation of sphingolipid metabolism.* Endocr Rev, 2008. **29**(4): p. 381-402.
154. Holland, W.L., et al., *Receptor-mediated activation of ceramidase activity initiates the pleiotropic actions of adiponectin.* Nat Med, 2011. **17**(1): p. 55-63.
155. Kahan, B.D., *FTY720: from bench to bedside.* Transplant Proc, 2004. **36**(2 Suppl): p. 531S-543S.
156. Brinkmann, V., et al., *Fingolimod (FTY720): discovery and development of an oral drug to treat multiple sclerosis.* Nat Rev Drug Discov, 2010. **9**(11): p. 883-97.
157. Berdyshev, E.V., et al., *FTY720 inhibits ceramide synthases and up-regulates dihydrosphingosine 1-phosphate formation in human lung endothelial cells.* J Biol Chem, 2009. **284**(9): p. 5467-77.
158. Skacel, J., B.S. Slusher, and T. Tsukamoto, *Small Molecule Inhibitors Targeting Biosynthesis of Ceramide, the Central Hub of the Sphingolipid Network.* J Med Chem, 2021. **64**(1): p. 279-297.
159. Payne, S.G., et al., *The immunosuppressant drug FTY720 inhibits cytosolic phospholipase A2 independently of sphingosine-1-phosphate receptors.* Blood, 2007. **109**(3): p. 1077-85.
160. Sica, F., D. Centonze, and F. Buttari, *Fingolimod Immune Effects Beyond Its Sequestration Ability.* Neurol Ther, 2019. **8**(2): p. 231-240.
161. Dominguez-Villar, M., et al., *Fingolimod modulates T cell phenotype and regulatory T cell plasticity in vivo.* J Autoimmun, 2019. **96**: p. 40-49.
162. Serpero, L.D., et al., *Fingolimod modulates peripheral effector and regulatory T cells in MS patients.* J Neuroimmune Pharmacol, 2013. **8**(5): p. 1106-13.
163. Mazzola, M.A., et al., *Identification of a novel mechanism of action of fingolimod (FTY720) on human effector T cell function through TCF-1 upregulation.* J Neuroinflammation, 2015. **12**: p. 245.
164. Hou, H., et al., *Fingolimod ameliorates the development of experimental autoimmune encephalomyelitis by inhibiting Akt-mTOR axis in mice.* Int Immunopharmacol, 2016. **30**: p. 171-178.

165. Matsuoka, Y., et al., *A novel immunosuppressive agent FTY720 induced Akt dephosphorylation in leukemia cells.* Br J Pharmacol, 2003. **138**(7): p. 1303-12.
166. Kitz, A., et al., *AKT isoforms modulate Th1-like Treg generation and function in human autoimmune disease.* EMBO Rep, 2016. **17**(8): p. 1169-83.
167. Kitz, A. and M. Dominguez-Villar, *Molecular mechanisms underlying Th1-like Treg generation and function.* Cell Mol Life Sci, 2017. **74**(22): p. 4059-4075.
168. Gelderblom, W.C., et al., *Fumonisins--novel mycotoxins with cancer-promoting activity produced by Fusarium moniliforme.* Appl Environ Microbiol, 1988. **54**(7): p. 1806-11.
169. Riley, R.T. and A.H. Merrill, Jr., *Ceramide synthase inhibition by fumonisins: a perfect storm of perturbed sphingolipid metabolism, signaling, and disease.* J Lipid Res, 2019. **60**(7): p. 1183-1189.
170. Zitomer, N.C., et al., *Ceramide synthase inhibition by fumonisin B1 causes accumulation of 1-deoxysphinganine: a novel category of bioactive 1-deoxysphingoid bases and 1-deoxydihydroceramides biosynthesized by mammalian cell lines and animals.* J Biol Chem, 2009. **284**(8): p. 4786-95.
171. Pewzner-Jung, Y., et al., *A critical role for ceramide synthase 2 in liver homeostasis: II. insights into molecular changes leading to hepatopathy.* J Biol Chem, 2010. **285**(14): p. 10911-23.
172. Adams, J.M., 2nd, et al., *Ceramide content is increased in skeletal muscle from obese insulin-resistant humans.* Diabetes, 2004. **53**(1): p. 25-31.
173. Butler, T.J., D. Ashford, and A.M. Seymour, *Western diet increases cardiac ceramide content in healthy and hypertrophied hearts.* Nutr Metab Cardiovasc Dis, 2017. **27**(11): p. 991-998.
174. Tran, T.T., et al., *Short Term Palmitate Supply Impairs Intestinal Insulin Signaling via Ceramide Production.* J Biol Chem, 2016. **291**(31): p. 16328-38.
175. Chaurasia, B. and S.A. Summers, *Ceramides in Metabolism: Key Lipotoxic Players.* Annu Rev Physiol, 2021. **83**: p. 303-330.
176. Khayrullin, A., et al., *Very Long-Chain C24:1 Ceramide Is Increased in Serum Extracellular Vesicles with Aging and Can Induce Senescence in Bone-Derived Mesenchymal Stem Cells.* Cells, 2019. **8**(1).
177. Veiga, M.P., et al., *Ceramides in phospholipid membranes: effects on bilayer stability and transition to nonlamellar phases.* Biophys J, 1999. **76**(1 Pt 1): p. 342-50.
178. Hannun, Y.A. and L.M. Obeid, *Principles of bioactive lipid signalling: lessons from sphingolipids.* Nat Rev Mol Cell Biol, 2008. **9**(2): p. 139-50.
179. Silva, L.C., et al., *Ablation of ceramide synthase 2 strongly affects biophysical properties of membranes.* J Lipid Res, 2012. **53**(3): p. 430-436.
180. Pewzner-Jung, Y., et al., *A critical role for ceramide synthase 2 in liver homeostasis: I. alterations in lipid metabolic pathways.* J Biol Chem, 2010. **285**(14): p. 10902-10.
181. Kim, Y.R., et al., *Hepatic triglyceride accumulation via endoplasmic reticulum stress-induced SREBP-1 activation is regulated by ceramide synthases.* Exp Mol Med, 2019. **51**(11): p. 1-16.
182. Vatner, D.F., et al., *Insulin-independent regulation of hepatic triglyceride synthesis by fatty acids.* Proc Natl Acad Sci U S A, 2015. **112**(4): p. 1143-8.
183. Novgorodov, S.A., et al., *Developmentally regulated ceramide synthase 6 increases mitochondrial Ca2+ loading capacity and promotes apoptosis.* J Biol Chem, 2011. **286**(6): p. 4644-58.
184. Roszczyc-Owsiejczuk, K. and P. Zabielski, *Sphingolipids as a Culprit of Mitochondrial Dysfunction in Insulin Resistance and Type 2 Diabetes.* Front Endocrinol (Lausanne), 2021. **12**: p. 635175.

185. Hammerschmidt, P., et al., *CerS6-Derived Sphingolipids Interact with Mff and Promote Mitochondrial Fragmentation in Obesity.* Cell, 2019. **177**(6): p. 1536-1552 e23.
186. Turpin, S.M., et al., *Obesity-induced CerS6-dependent C16:0 ceramide production promotes weight gain and glucose intolerance.* Cell Metab, 2014. **20**(4): p. 678-86.
187. Zigdon, H., et al., *Ablation of ceramide synthase 2 causes chronic oxidative stress due to disruption of the mitochondrial respiratory chain.* J Biol Chem, 2013. **288**(7): p. 4947-56.
188. Smith, M.E., et al., *Mitochondrial fission mediates ceramide-induced metabolic disruption in skeletal muscle.* Biochem J, 2013. **456**(3): p. 427-39.
189. Park, W.J. and J.W. Park, *The role of sphingolipids in endoplasmic reticulum stress.* FEBS Lett, 2020. **594**(22): p. 3632-3651.
190. Correnti, J., et al., *Liver-specific ceramide reduction alleviates steatosis and insulin resistance in alcohol-fed mice.* J Lipid Res, 2020. **61**(7): p. 983-994.
191. Contreras, C., et al., *Central ceramide-induced hypothalamic lipotoxicity and ER stress regulate energy balance.* Cell Rep, 2014. **9**(1): p. 366-377.
192. Park, M.A., et al., *Vorinostat and sorafenib increase ER stress, autophagy and apoptosis via ceramide-dependent CD95 and PERK activation.* Cancer Biol Ther, 2008. **7**(10): p. 1648-62.
193. Liu, F., et al., *Ceramide activates lysosomal cathepsin B and cathepsin D to attenuate autophagy and induces ER stress to suppress myeloid-derived suppressor cells.* Oncotarget, 2016. **7**(51): p. 83907-83925.
194. Boslem, E., et al., *A lipidomic screen of palmitate-treated MIN6 beta-cells links sphingolipid metabolites with endoplasmic reticulum (ER) stress and impaired protein trafficking.* Biochem J, 2011. **435**(1): p. 267-76.
195. Choi, S., et al., *Myristate-induced endoplasmic reticulum stress requires ceramide synthases 5/6 and generation of C14-ceramide in intestinal epithelial cells.* FASEB J, 2018. **32**(10): p. 5724-5736.
196. Boslem, E., P.J. Meikle, and T.J. Biden, *Roles of ceramide and sphingolipids in pancreatic beta-cell function and dysfunction.* Islets, 2012. **4**(3): p. 177-87.
197. Cremesti, A., et al., *Ceramide enables fas to cap and kill.* J Biol Chem, 2001. **276**(26): p. 23954-61.
198. Heinrich, M., et al., *Ceramide as an activator lipid of cathepsin D.* Adv Exp Med Biol, 2000. **477**: p. 305-15.
199. Schull, S., et al., *Cytochrome c oxidase deficiency accelerates mitochondrial apoptosis by activating ceramide synthase 6.* Cell Death Dis, 2015. **6**: p. e1691.
200. Chavez, J.A. and S.A. Summers, *A ceramide-centric view of insulin resistance.* Cell Metab, 2012. **15**(5): p. 585-94.
201. Hage Hassan, R., et al., *Sustained Action of Ceramide on the Insulin Signaling Pathway in Muscle Cells: IMPLICATION OF THE DOUBLE-STRANDED RNA-ACTIVATED PROTEIN KINASE.* J Biol Chem, 2016. **291**(6): p. 3019-29.
202. Saltiel, A.R. and C.R. Kahn, *Insulin signalling and the regulation of glucose and lipid metabolism.* Nature, 2001. **414**(6865): p. 799-806.
203. Mukhopadhyay, A., et al., *Direct interaction between the inhibitor 2 and ceramide via sphingolipid-protein binding is involved in the regulation of protein phosphatase 2A activity and signaling.* FASEB J, 2009. **23**(3): p. 751-63.
204. Fox, T.E., et al., *Ceramide recruits and activates protein kinase C zeta (PKC zeta) within structured membrane microdomains.* J Biol Chem, 2007. **282**(17): p. 12450-7.
205. Apostolidis, S.A., et al., *Phosphatase PP2A is requisite for the function of regulatory T cells.* Nat Immunol, 2016. **17**(5): p. 556-64.

206. Summers, S.A., et al., *Regulation of insulin-stimulated glucose transporter GLUT4 translocation and Akt kinase activity by ceramide.* Mol Cell Biol, 1998. **18**(9): p. 5457-64.
207. JeBailey, L., et al., *Ceramide- and oxidant-induced insulin resistance involve loss of insulin-dependent Rac-activation and actin remodeling in muscle cells.* Diabetes, 2007. **56**(2): p. 394-403.
208. Yang, G., et al., *Central role of ceramide biosynthesis in body weight regulation, energy metabolism, and the metabolic syndrome.* Am J Physiol Endocrinol Metab, 2009. **297**(1): p. E211-24.
209. Vozarova, B., et al., *High white blood cell count is associated with a worsening of insulin sensitivity and predicts the development of type 2 diabetes.* Diabetes, 2002. **51**(2): p. 455-61.
210. Thorand, B., et al., *C-reactive protein as a predictor for incident diabetes mellitus among middle-aged men: results from the MONICA Augsburg cohort study, 1984-1998.* Arch Intern Med, 2003. **163**(1): p. 93-9.
211. Naidoo, V., M. Naidoo, and M. Ghai, *Cell- and tissue-specific epigenetic changes associated with chronic inflammation in insulin resistance and type 2 diabetes mellitus.* Scand J Immunol, 2018. **88**(6): p. e12723.
212. Cai, D., et al., *Local and systemic insulin resistance resulting from hepatic activation of IKK-beta and NF-kappaB.* Nat Med, 2005. **11**(2): p. 183-90.
213. Ehses, J.A., et al., *Increased number of islet-associated macrophages in type 2 diabetes.* Diabetes, 2007. **56**(9): p. 2356-70.
214. Milanski, M., et al., *Inhibition of hypothalamic inflammation reverses diet-induced insulin resistance in the liver.* Diabetes, 2012. **61**(6): p. 1455-62.
215. De Souza, C.T., et al., *Consumption of a fat-rich diet activates a proinflammatory response and induces insulin resistance in the hypothalamus.* Endocrinology, 2005. **146**(10): p. 4192-9.
216. Varma, V., et al., *Muscle inflammatory response and insulin resistance: synergistic interaction between macrophages and fatty acids leads to impaired insulin action.* Am J Physiol Endocrinol Metab, 2009. **296**(6): p. E1300-10.
217. Murphy, K., et al., *Janeway's immunobiology*. 10th edition. / ed. 2022, New York: W.W. Norton and Company. xxii, 800 pages.
218. Murphy, K., et al., *Janeway's immunobiology*. Tenth edition. /
International student edition. ed. 2022, New York: W.W. Norton and Company. xxii, 800, A-47, G-44, C-2, I-43 pages.
219. Flajnik, M.F. and M. Kasahara, *Origin and evolution of the adaptive immune system: genetic events and selective pressures.* Nat Rev Genet, 2010. **11**(1): p. 47-59.
220. Kannan, A., et al., *Signal transduction via the T cell antigen receptor in naive and effector/memory T cells.* Int J Biochem Cell Biol, 2012. **44**(12): p. 2129-34.
221. Larosa, D.F. and J.S. Orange, *1. Lymphocytes.* J Allergy Clin Immunol, 2008. **121**(2 Suppl): p. S364-9; quiz S412.
222. Liu, R. and B.S. Nikolajczyk, *Tissue Immune Cells Fuel Obesity-Associated Inflammation in Adipose Tissue and Beyond.* Front Immunol, 2019. **10**: p. 1587.
223. Osborn, O. and J.M. Olefsky, *The cellular and signaling networks linking the immune system and metabolism in disease.* Nat Med, 2012. **18**(3): p. 363-74.
224. Nishimura, S., et al., *CD8+ effector T cells contribute to macrophage recruitment and adipose tissue inflammation in obesity.* Nat Med, 2009. **15**(8): p. 914-20.
225. Exley, M.A., et al., *Interplay between the immune system and adipose tissue in obesity.* J Endocrinol, 2014. **223**(2): p. R41-8.

226. Feuerer, M., et al., *Lean, but not obese, fat is enriched for a unique population of regulatory T cells that affect metabolic parameters.* Nat Med, 2009. **15**(8): p. 930-9.
227. Luckheeram, R.V., et al., *CD4(+)T cells: differentiation and functions.* Clin Dev Immunol, 2012. **2012**: p. 925135.
228. Marshall, N.B. and S.L. Swain, *Cytotoxic CD4 T cells in antiviral immunity.* J Biomed Biotechnol, 2011. **2011**: p. 954602.
229. Drayton, D.L., et al., *Lymphoid organ development: from ontogeny to neogenesis.* Nat Immunol, 2006. **7**(4): p. 344-53.
230. Schmitt, E.G. and C.B. Williams, *Generation and function of induced regulatory T cells.* Front Immunol, 2013. **4**: p. 152.
231. Kanamori, M., et al., *Induced Regulatory T Cells: Their Development, Stability, and Applications.* Trends Immunol, 2016. **37**(11): p. 803-811.
232. Brenchley, J.M., et al., *Expansion of activated human naive T-cells precedes effector function.* Clin Exp Immunol, 2002. **130**(3): p. 432-40.
233. von Andrian, U.H. and C.R. Mackay, *T-cell function and migration. Two sides of the same coin.* N Engl J Med, 2000. **343**(14): p. 1020-34.
234. Tubo, N.J. and M.K. Jenkins, *CD4+ T Cells: guardians of the phagosome.* Clin Microbiol Rev, 2014. **27**(2): p. 200-13.
235. Hang, J., et al., *The clinical implication of CD45RA(+) naive T cells and CD45RO(+) memory T cells in advanced pancreatic cancer: a proxy for tumor biology and outcome prediction.* Cancer Med, 2019. **8**(3): p. 1326-1335.
236. Jenkins, M.K., et al., *In vivo activation of antigen-specific CD4 T cells.* Annu Rev Immunol, 2001. **19**: p. 23-45.
237. Smith-Garvin, J.E., G.A. Koretzky, and M.S. Jordan, *T cell activation.* Annu Rev Immunol, 2009. **27**: p. 591-619.
238. Yamada, A., A.D. Salama, and M.H. Sayegh, *The role of novel T cell costimulatory pathways in autoimmunity and transplantation.* J Am Soc Nephrol, 2002. **13**(2): p. 559-575.
239. Bhattacharyya, N.D. and C.G. Feng, *Regulation of T Helper Cell Fate by TCR Signal Strength.* Front Immunol, 2020. **11**: p. 624.
240. Shyer, J.A., R.A. Flavell, and W. Bailis, *Metabolic signaling in T cells.* Cell Res, 2020. **30**(8): p. 649-659.
241. Ashkar, S., et al., *Eta-1 (osteopontin): an early component of type-1 (cell-mediated) immunity.* Science, 2000. **287**(5454): p. 860-4.
242. Savignac, M., B. Mellstrom, and J.R. Naranjo, *Calcium-dependent transcription of cytokine genes in T lymphocytes.* Pflugers Arch, 2007. **454**(4): p. 523-33.
243. Takeda, K., et al., *CD28 stimulation triggers NF-kappaB activation through the CARMA1-PKCtheta-Grb2/Gads axis.* Int Immunol, 2008. **20**(12): p. 1507-15.
244. Lovatt, M., et al., *Lck regulates the threshold of activation in primary T cells, while both Lck and Fyn contribute to the magnitude of the extracellular signal-related kinase response.* Mol Cell Biol, 2006. **26**(22): p. 8655-65.
245. Hwang, J.R., et al., *Recent insights of T cell receptor-mediated signaling pathways for T cell activation and development.* Exp Mol Med, 2020. **52**(5): p. 750-761.
246. Bertin, S., et al., *Dual-specificity phosphatase 6 regulates CD4+ T-cell functions and restrains spontaneous colitis in IL-10-deficient mice.* Mucosal Immunol, 2015. **8**(3): p. 505-15.
247. Chen, L. and D.B. Flies, *Molecular mechanisms of T cell co-stimulation and co-inhibition.* Nat Rev Immunol, 2013. **13**(4): p. 227-42.
248. Saveliev, A., et al., *Function of the nucleotide exchange activity of vav1 in T cell development and activation.* Sci Signal, 2009. **2**(101): p. ra83.

249. Sasaki, T., et al., *Function of PI3Kgamma in thymocyte development, T cell activation, and neutrophil migration.* Science, 2000. **287**(5455): p. 1040-6.
250. Samelson, L.E., *Signal transduction mediated by the T cell antigen receptor: the role of adapter proteins.* Annu Rev Immunol, 2002. **20**: p. 371-94.
251. Murphy, K., et al., *Janeway's immunobiology*. 7th ed. 2008, New York ; London: Garland Science. xxi, 887 p.
252. Silva, R., et al., *Influence of pro- and anti-inflammatory cytokines in Th1 polarization after allogeneic stimulation.* Int J Biomed Sci, 2005. **1**(1): p. 46-52.
253. Trinchieri, G., S. Pflanz, and R.A. Kastelein, *The IL-12 family of heterodimeric cytokines: new players in the regulation of T cell responses.* Immunity, 2003. **19**(5): p. 641-4.
254. Thierfelder, W.E., et al., *Requirement for Stat4 in interleukin-12-mediated responses of natural killer and T cells.* Nature, 1996. **382**(6587): p. 171-4.
255. Lugo-Villarino, G., et al., *T-bet is required for optimal production of IFN-gamma and antigen-specific T cell activation by dendritic cells.* Proc Natl Acad Sci U S A, 2003. **100**(13): p. 7749-54.
256. Lazarevic, V., et al., *T-bet represses T(H)17 differentiation by preventing Runx1-mediated activation of the gene encoding RORgammat.* Nat Immunol, 2011. **12**(1): p. 96-104.
257. Zhu, J., H. Yamane, and W.E. Paul, *Differentiation of effector CD4 T cell populations (*).* Annu Rev Immunol, 2010. **28**: p. 445-89.
258. Afkarian, M., et al., *T-bet is a STAT1-induced regulator of IL-12R expression in naive CD4+ T cells.* Nat Immunol, 2002. **3**(6): p. 549-57.
259. Trinchieri, G. and A. Sher, *Cooperation of Toll-like receptor signals in innate immune defence.* Nat Rev Immunol, 2007. **7**(3): p. 179-90.
260. Oestreich, K.J., A.C. Huang, and A.S. Weinmann, *The lineage-defining factors T-bet and Bcl-6 collaborate to regulate Th1 gene expression patterns.* J Exp Med, 2011. **208**(5): p. 1001-13.
261. Winer, D.A., et al., *B cells promote insulin resistance through modulation of T cells and production of pathogenic IgG antibodies.* Nat Med, 2011. **17**(5): p. 610-7.
262. Winer, S., et al., *Normalization of obesity-associated insulin resistance through immunotherapy.* Nat Med, 2009. **15**(8): p. 921-9.
263. Chawla, A., K.D. Nguyen, and Y.P. Goh, *Macrophage-mediated inflammation in metabolic disease.* Nat Rev Immunol, 2011. **11**(11): p. 738-49.
264. Kintscher, U., et al., *T-lymphocyte infiltration in visceral adipose tissue: a primary event in adipose tissue inflammation and the development of obesity-mediated insulin resistance.* Arterioscler Thromb Vasc Biol, 2008. **28**(7): p. 1304-10.
265. Strissel, K.J., et al., *T-cell recruitment and Th1 polarization in adipose tissue during diet-induced obesity in C57BL/6 mice.* Obesity (Silver Spring), 2010. **18**(10): p. 1918-25.
266. McLaughlin, T., et al., *T-cell profile in adipose tissue is associated with insulin resistance and systemic inflammation in humans.* Arterioscler Thromb Vasc Biol, 2014. **34**(12): p. 2637-43.
267. Nakayama, T., et al., *Th2 Cells in Health and Disease.* Annu Rev Immunol, 2017. **35**: p. 53-84.
268. Vergadi, E., et al., *Akt Signaling Pathway in Macrophage Activation and M1/M2 Polarization.* J Immunol, 2017. **198**(3): p. 1006-1014.
269. Zhu, J., et al., *Stat6 is necessary and sufficient for IL-4's role in Th2 differentiation and cell expansion.* J Immunol, 2001. **166**(12): p. 7276-81.

270. Glimcher, L.H. and K.M. Murphy, *Lineage commitment in the immune system: the T helper lymphocyte grows up.* Genes Dev, 2000. **14**(14): p. 1693-711.
271. Zhu, J., et al., *GATA-3 promotes Th2 responses through three different mechanisms: induction of Th2 cytokine production, selective growth of Th2 cells and inhibition of Th1 cell-specific factors.* Cell Res, 2006. **16**(1): p. 3-10.
272. Cote-Sierra, J., et al., *Interleukin 2 plays a central role in Th2 differentiation.* Proc Natl Acad Sci U S A, 2004. **101**(11): p. 3880-5.
273. Horiuchi, S., et al., *Genome-wide analysis reveals unique regulation of transcription of Th2-specific genes by GATA3.* J Immunol, 2011. **186**(11): p. 6378-89.
274. Zeyda, M., et al., *Inflammation correlates with markers of T-cell subsets including regulatory T cells in adipose tissue from obese patients.* Obesity (Silver Spring), 2011. **19**(4): p. 743-8.
275. Luger, D., et al., *Either a Th17 or a Th1 effector response can drive autoimmunity: conditions of disease induction affect dominant effector category.* J Exp Med, 2008. **205**(4): p. 799-810.
276. Patel, D.D. and V.K. Kuchroo, *Th17 Cell Pathway in Human Immunity: Lessons from Genetics and Therapeutic Interventions.* Immunity, 2015. **43**(6): p. 1040-51.
277. Cua, D.J., et al., *Interleukin-23 rather than interleukin-12 is the critical cytokine for autoimmune inflammation of the brain.* Nature, 2003. **421**(6924): p. 744-8.
278. Tesmer, L.A., et al., *Th17 cells in human disease.* Immunol Rev, 2008. **223**: p. 87-113.
279. Kuestner, R.E., et al., *Identification of the IL-17 receptor related molecule IL-17RC as the receptor for IL-17F.* J Immunol, 2007. **179**(8): p. 5462-73.
280. Wright, J.F., et al., *Identification of an interleukin 17F/17A heterodimer in activated human CD4+ T cells.* J Biol Chem, 2007. **282**(18): p. 13447-55.
281. Crawford, M.P., et al., *CD4 T cell-intrinsic role for the T helper 17 signature cytokine IL-17: Effector resistance to immune suppression.* Proc Natl Acad Sci U S A, 2020. **117**(32): p. 19408-19414.
282. Zheng, Y., et al., *Interleukin-22, a T(H)17 cytokine, mediates IL-23-induced dermal inflammation and acanthosis.* Nature, 2007. **445**(7128): p. 648-51.
283. Chung, Y., et al., *Expression and regulation of IL-22 in the IL-17-producing CD4+ T lymphocytes.* Cell Res, 2006. **16**(11): p. 902-7.
284. Veldhoen, M., et al., *TGFbeta in the context of an inflammatory cytokine milieu supports de novo differentiation of IL-17-producing T cells.* Immunity, 2006. **24**(2): p. 179-89.
285. Langrish, C.L., et al., *IL-23 drives a pathogenic T cell population that induces autoimmune inflammation.* J Exp Med, 2005. **201**(2): p. 233-40.
286. Yang, X.O., et al., *T helper 17 lineage differentiation is programmed by orphan nuclear receptors ROR alpha and ROR gamma.* Immunity, 2008. **28**(1): p. 29-39.
287. Chen, Z., et al., *Selective regulatory function of Socs3 in the formation of IL-17-secreting T cells.* Proc Natl Acad Sci U S A, 2006. **103**(21): p. 8137-42.
288. Fabbrini, E., et al., *Association between specific adipose tissue CD4+ T-cell populations and insulin resistance in obese individuals.* Gastroenterology, 2013. **145**(2): p. 366-74 e1-3.
289. Dalmas, E., et al., *T cell-derived IL-22 amplifies IL-1beta-driven inflammation in human adipose tissue: relevance to obesity and type 2 diabetes.* Diabetes, 2014. **63**(6): p. 1966-77.
290. Winer, S., et al., *Obesity predisposes to Th17 bias.* Eur J Immunol, 2009. **39**(9): p. 2629-35.

291. Jagannathan-Bogdan, M., et al., *Elevated proinflammatory cytokine production by a skewed T cell compartment requires monocytes and promotes inflammation in type 2 diabetes.* J Immunol, 2011. **186**(2): p. 1162-72.
292. Nicholas, D.A., et al., *Fatty Acid Metabolites Combine with Reduced beta Oxidation to Activate Th17 Inflammation in Human Type 2 Diabetes.* Cell Metab, 2019. **30**(3): p. 447-461 e5.
293. Raphael, I., et al., *T cell subsets and their signature cytokines in autoimmune and inflammatory diseases.* Cytokine, 2015. **74**(1): p. 5-17.
294. Workman, C.J., et al., *The development and function of regulatory T cells.* Cell Mol Life Sci, 2009. **66**(16): p. 2603-22.
295. Martinez, G.J., et al., *Smad3 differentially regulates the induction of regulatory and inflammatory T cell differentiation.* J Biol Chem, 2009. **284**(51): p. 35283-6.
296. Laurence, A., et al., *Interleukin-2 signaling via STAT5 constrains T helper 17 cell generation.* Immunity, 2007. **26**(3): p. 371-81.
297. Kaplan, M.H., et al., *STAT3-dependent IL-21 production from T helper cells regulates hematopoietic progenitor cell homeostasis.* Blood, 2011. **117**(23): p. 6198-201.
298. Ding, L., et al., *IL-10 inhibits macrophage costimulatory activity by selectively inhibiting the up-regulation of B7 expression.* J Immunol, 1993. **151**(3): p. 1224-34.
299. Williams, L.M., et al., *Interleukin-10 suppression of myeloid cell activation--a continuing puzzle.* Immunology, 2004. **113**(3): p. 281-92.
300. Gavin, M.A., et al., *Foxp3-dependent programme of regulatory T-cell differentiation.* Nature, 2007. **445**(7129): p. 771-5.
301. Zou, J., et al., *CD4+ T cells memorize obesity and promote weight regain.* Cell Mol Immunol, 2018. **15**(6): p. 630-639.
302. Endo, Y., et al., *Obesity Drives Th17 Cell Differentiation by Inducing the Lipid Metabolic Kinase, ACC1.* Cell Rep, 2015. **12**(6): p. 1042-55.
303. Lee, J.Y., et al., *Saturated fatty acids, but not unsaturated fatty acids, induce the expression of cyclooxygenase-2 mediated through Toll-like receptor 4.* J Biol Chem, 2001. **276**(20): p. 16683-9.
304. Eguchi, K., et al., *Saturated fatty acid and TLR signaling link beta cell dysfunction and islet inflammation.* Cell Metab, 2012. **15**(4): p. 518-33.
305. Lian, Z., et al., *Replacing Saturated Fat With Unsaturated Fat in Western Diet Reduces Foamy Monocytes and Atherosclerosis in Male Ldlr(-/-) Mice.* Arterioscler Thromb Vasc Biol, 2020. **40**(1): p. 72-85.
306. Lee, J.Y., et al., *Saturated fatty acid activates but polyunsaturated fatty acid inhibits Toll-like receptor 2 dimerized with Toll-like receptor 6 or 1.* J Biol Chem, 2004. **279**(17): p. 16971-9.
307. Lee, J.Y., et al., *Reciprocal modulation of Toll-like receptor-4 signaling pathways involving MyD88 and phosphatidylinositol 3-kinase/AKT by saturated and polyunsaturated fatty acids.* J Biol Chem, 2003. **278**(39): p. 37041-51.
308. Hwang, D.H., J.A. Kim, and J.Y. Lee, *Mechanisms for the activation of Toll-like receptor 2/4 by saturated fatty acids and inhibition by docosahexaenoic acid.* Eur J Pharmacol, 2016. **785**: p. 24-35.
309. O'Sullivan, D., et al., *Memory CD8(+) T cells use cell-intrinsic lipolysis to support the metabolic programming necessary for development.* Immunity, 2014. **41**(1): p. 75-88.
310. Pearce, E.L., et al., *Enhancing CD8 T-cell memory by modulating fatty acid metabolism.* Nature, 2009. **460**(7251): p. 103-7.
311. Frasca, D., et al., *Obesity Accelerates Age-Associated Defects in Human B Cells Through a Metabolic Reprogramming Induced by the Fatty Acid Palmitate.* Front Aging, 2021. **2**: p. 828697.

312. Igoillo-Esteve, M., et al., *Palmitate induces a pro-inflammatory response in human pancreatic islets that mimics CCL2 expression by beta cells in type 2 diabetes.* Diabetologia, 2010. **53**(7): p. 1395-405.
313. Bruniquel, D. and R.H. Schwartz, *Selective, stable demethylation of the interleukin-2 gene enhances transcription by an active process.* Nat Immunol, 2003. **4**(3): p. 235-40.
314. Kersh, E.N., et al., *Rapid demethylation of the IFN-gamma gene occurs in memory but not naive CD8 T cells.* J Immunol, 2006. **176**(7): p. 4083-93.
315. Gamper, C.J., et al., *Identification of DNA methyltransferase 3a as a T cell receptor-induced regulator of Th1 and Th2 differentiation.* J Immunol, 2009. **183**(4): p. 2267-76.
316. Medzhitov, R. and T. Horng, *Transcriptional control of the inflammatory response.* Nat Rev Immunol, 2009. **9**(10): p. 692-703.
317. Zhou, T., et al., *Upregulation of SLAMF3 on human T cells is induced by palmitic acid through the STAT5-PI3K/Akt pathway and features the chronic inflammatory profiles of type 2 diabetes.* Cell Death Dis, 2019. **10**(8): p. 559.
318. Wang, Z., et al., *Saturated fatty acids activate microglia via Toll-like receptor 4/NF-kappaB signalling.* Br J Nutr, 2012. **107**(2): p. 229-41.
319. Anderson, E.K., A.A. Hill, and A.H. Hasty, *Stearic acid accumulation in macrophages induces toll-like receptor 4/2-independent inflammation leading to endoplasmic reticulum stress-mediated apoptosis.* Arterioscler Thromb Vasc Biol, 2012. **32**(7): p. 1687-95.
320. Miao, H., et al., *Stearic acid induces proinflammatory cytokine production partly through activation of lactate-HIF1alpha pathway in chondrocytes.* Sci Rep, 2015. **5**: p. 13092.
321. Santa-Maria, C., et al., *Update on Anti-Inflammatory Molecular Mechanisms Induced by Oleic Acid.* Nutrients, 2023. **15**(1).
322. Camell, C. and C.W. Smith, *Dietary oleic acid increases m2 macrophages in the mesenteric adipose tissue.* PLoS One, 2013. **8**(9): p. e75147.
323. Ertunc, M.E. and G.S. Hotamisligil, *Lipid signaling and lipotoxicity in metaflammation: indications for metabolic disease pathogenesis and treatment.* J Lipid Res, 2016. **57**(12): p. 2099-2114.
324. Hu, Y., F.B. Hu, and J.E. Manson, *Marine Omega-3 Supplementation and Cardiovascular Disease: An Updated Meta-Analysis of 13 Randomized Controlled Trials Involving 127 477 Participants.* J Am Heart Assoc, 2019. **8**(19): p. e013543.
325. Li, X., et al., *Therapeutic Potential of omega-3 Polyunsaturated Fatty Acids in Human Autoimmune Diseases.* Front Immunol, 2019. **10**: p. 2241.
326. Ferrucci, L., et al., *Relationship of plasma polyunsaturated fatty acids to circulating inflammatory markers.* J Clin Endocrinol Metab, 2006. **91**(2): p. 439-46.
327. Oh, D.Y., et al., *GPR120 is an omega-3 fatty acid receptor mediating potent anti-inflammatory and insulin-sensitizing effects.* Cell, 2010. **142**(5): p. 687-98.
328. Mildenberger, J., et al., *N-3 PUFAs induce inflammatory tolerance by formation of KEAP1-containing SQSTM1/p62-bodies and activation of NFE2L2.* Autophagy, 2017. **13**(10): p. 1664-1678.
329. Petursdottir, D.H. and I. Hardardottir, *Dietary fish oil decreases secretion of T helper (Th) 1-type cytokines by a direct effect on murine splenic T cells but enhances secretion of a Th2-type cytokine by an effect on accessory cells.* Br J Nutr, 2009. **101**(7): p. 1040-6.
330. Kew, S., et al., *Effects of oils rich in eicosapentaenoic and docosahexaenoic acids on immune cell composition and function in healthy humans.* Am J Clin Nutr, 2004. **79**(4): p. 674-81.

331. Kendall, A.C., et al., *Dynamics of the human skin mediator lipidome in response to dietary omega-3 fatty acid supplementation.* FASEB J, 2019. **33**(11): p. 13014-13027.
332. Nicolaou, A., et al., *Polyunsaturated Fatty Acid-derived lipid mediators and T cell function.* Front Immunol, 2014. **5**: p. 75.
333. Lee, K.R., Y. Midgette, and R. Shah, *Fish Oil Derived Omega 3 Fatty Acids Suppress Adipose NLRP3 Inflammasome Signaling in Human Obesity.* J Endocr Soc, 2019. **3**(3): p. 504-515.
334. Liu, H.Q., et al., *A high ratio of dietary n-3/n-6 polyunsaturated fatty acids improves obesity-linked inflammation and insulin resistance through suppressing activation of TLR4 in SD rats.* Nutr Res, 2013. **33**(10): p. 849-58.
335. Eraky, S.M., N. Abdel-Rahman, and L.A. Eissa, *Modulating effects of omega-3 fatty acids and pioglitazone combination on insulin resistance through toll-like receptor 4 in type 2 diabetes mellitus.* Prostaglandins Leukot Essent Fatty Acids, 2018. **136**: p. 123-129.
336. Haghiac, M., et al., *Dietary Omega-3 Fatty Acid Supplementation Reduces Inflammation in Obese Pregnant Women: A Randomized Double-Blind Controlled Clinical Trial.* PLoS One, 2015. **10**(9): p. e0137309.
337. Kumar, N., et al., *15-Lipoxygenase metabolites of alpha-linolenic acid, [13-(S)-HPOTrE and 13-(S)-HOTrE], mediate anti-inflammatory effects by inactivating NLRP3 inflammasome.* Sci Rep, 2016. **6**: p. 31649.
338. Yan, Y., et al., *Omega-3 fatty acids prevent inflammation and metabolic disorder through inhibition of NLRP3 inflammasome activation.* Immunity, 2013. **38**(6): p. 1154-63.
339. Martinez-Micaelo, N., et al., *Dietary fatty acid composition is sensed by the NLRP3 inflammasome: omega-3 fatty acid (DHA) prevents NLRP3 activation in human macrophages.* Food Funct, 2016. **7**(8): p. 3480-7.
340. Tachtsis, B., et al., *Omega-3 Polyunsaturated Fatty Acids Mitigate Palmitate-Induced Impairments in Skeletal Muscle Cell Viability and Differentiation.* Front Physiol, 2020. **11**: p. 563.
341. Kim, J.Y., et al., *N-3 polyunsaturated fatty acids restore Th17 and Treg balance in collagen antibody-induced arthritis.* PLoS One, 2018. **13**(3): p. e0194331.
342. Qin, S., et al., *Endogenous n-3 polyunsaturated fatty acids protect against imiquimod-induced psoriasis-like inflammation via the IL-17/IL-23 axis.* Mol Med Rep, 2014. **9**(6): p. 2097-104.
343. Iwami, D., et al., *Purified eicosapentaenoic acid induces prolonged survival of cardiac allografts and generates regulatory T cells.* Am J Transplant, 2009. **9**(6): p. 1294-307.
344. Onodera, T., et al., *Eicosapentaenoic acid and 5-HEPE enhance macrophage-mediated Treg induction in mice.* Sci Rep, 2017. **7**(1): p. 4560.
345. Yang, W., et al., *GPR120 Inhibits Colitis Through Regulation of CD4(+) T Cell Interleukin 10 Production.* Gastroenterology, 2022. **162**(1): p. 150-165.
346. Liddle, D.M., et al., *Dietary omega-3 polyunsaturated fatty acids modulate CD4(+) T-cell subset markers, adipocyte antigen-presentation potential, and NLRP3 inflammasome activity in a coculture model of obese adipose tissue.* Nutrition, 2021. **91-92**: p. 111388.
347. Watt, M.J., et al., *Regulation of plasma ceramide levels with fatty acid oversupply: evidence that the liver detects and secretes de novo synthesised ceramide.* Diabetologia, 2012. **55**(10): p. 2741-2746.
348. Wang, D.D., et al., *Plasma Ceramides, Mediterranean Diet, and Incident Cardiovascular Disease in the PREDIMED Trial (Prevencion con Dieta Mediterranea).* Circulation, 2017. **135**(21): p. 2028-2040.

349. Poss, A.M., et al., *Machine learning reveals serum sphingolipids as cholesterol-independent biomarkers of coronary artery disease.* J Clin Invest, 2020. **130**(3): p. 1363-1376.
350. Raichur, S., et al., *The role of C16:0 ceramide in the development of obesity and type 2 diabetes: CerS6 inhibition as a novel therapeutic approach.* Mol Metab, 2019. **21**: p. 36-50.
351. Turpin-Nolan, S.M., et al., *CerS1-Derived C18:0 Ceramide in Skeletal Muscle Promotes Obesity-Induced Insulin Resistance.* Cell Rep, 2019. **26**(1): p. 1-10 e7.
352. Broskey, N.T., et al., *Skeletal muscle ceramides and daily fat oxidation in obesity and diabetes.* Metabolism, 2018. **82**: p. 118-123.
353. Apostolopoulou, M., et al., *Specific Hepatic Sphingolipids Relate to Insulin Resistance, Oxidative Stress, and Inflammation in Nonalcoholic Steatohepatitis.* Diabetes Care, 2018. **41**(6): p. 1235-1243.
354. Gorden, D.L., et al., *Biomarkers of NAFLD progression: a lipidomics approach to an epidemic.* J Lipid Res, 2015. **56**(3): p. 722-736.
355. Choromanska, B., et al., *Metabolic Syndrome is Associated with Ceramide Accumulation in Visceral Adipose Tissue of Women with Morbid Obesity.* Obesity (Silver Spring), 2019. **27**(3): p. 444-453.
356. Turpin-Nolan, S.M. and J.C. Bruning, *The role of ceramides in metabolic disorders: when size and localization matters.* Nat Rev Endocrinol, 2020. **16**(4): p. 224-233.
357. Zhou, Y., et al., *Acid Sphingomyelinase (ASM) is a Negative Regulator of Regulatory T Cell (Treg) Development.* Cell Physiol Biochem, 2016. **39**(3): p. 985-95.
358. Kim, M.H., et al., *Hepatic inflammatory cytokine production can be regulated by modulating sphingomyelinase and ceramide synthase 6.* Int J Mol Med, 2017. **39**(2): p. 453-462.
359. Hollmann, C., et al., *Translational Approaches Targeting Ceramide Generation From Sphingomyelin in T Cells to Modulate Immunity in Humans.* Front Immunol, 2019. **10**: p. 2363.
360. Hamada, Y., et al., *Involvement of de novo ceramide synthesis in pro-inflammatory adipokine secretion and adipocyte-macrophage interaction.* J Nutr Biochem, 2014. **25**(12): p. 1309-16.
361. Hu, W., et al., *Palmitate increases sphingosine-1-phosphate in C2C12 myotubes via upregulation of sphingosine kinase message and activity.* J Lipid Res, 2009. **50**(9): p. 1852-62.
362. Hu, W., et al., *Differential regulation of dihydroceramide desaturase by palmitate versus monounsaturated fatty acids: implications for insulin resistance.* J Biol Chem, 2011. **286**(19): p. 16596-605.
363. Vandanmagsar, B., et al., *The NLRP3 inflammasome instigates obesity-induced inflammation and insulin resistance.* Nat Med, 2011. **17**(2): p. 179-88.
364. Camell, C.D., et al., *Macrophage-specific de Novo Synthesis of Ceramide Is Dispensable for Inflammasome-driven Inflammation and Insulin Resistance in Obesity.* J Biol Chem, 2015. **290**(49): p. 29402-13.
365. Avota, E., M.N. de Lira, and S. Schneider-Schaulies, *Sphingomyelin Breakdown in T Cells: Role of Membrane Compartmentalization in T Cell Signaling and Interference by a Pathogen.* Front Cell Dev Biol, 2019. **7**: p. 152.
366. Shin, S.H., et al., *Ceramide Synthase 2 Null Mice Are Protected from Ovalbumin-Induced Asthma with Higher T Cell Receptor Signal Strength in CD4+ T Cells.* Int J Mol Sci, 2021. **22**(5).
367. Sofi, M.H., et al., *Ceramide synthesis regulates T cell activity and GVHD development.* JCI Insight, 2017. **2**(10).

368. Bai, A. and Y. Guo, *Acid sphingomyelinase mediates human CD4(+) T-cell signaling: potential roles in T-cell responses and diseases.* Cell Death Dis, 2017. **8**(7): p. e2963.
369. Bai, A., et al., *Role of acid sphingomyelinase bioactivity in human CD4+ T-cell activation and immune responses.* Cell Death Dis, 2015. **6**: p. e1828.
370. Hollmann, C., et al., *Inhibition of Acid Sphingomyelinase Allows for Selective Targeting of CD4+ Conventional versus Foxp3+ Regulatory T Cells.* J Immunol, 2016. **197**(8): p. 3130-3141.
371. O'Byrne, D. and D. Sansom, *Lack of costimulation by both sphingomyelinase and C2 ceramide in resting human T cells.* Immunology, 2000. **100**(2): p. 225-30.
372. Kue, C.S., et al., *C6-ceramide enhances Interleukin-12-mediated T helper type 1 cell responses through a cyclooxygenase-2-dependent pathway.* Immunobiology, 2012. **217**(6): p. 601-9.
373. Alsabeeh, N., et al., *Cell culture models of fatty acid overload: Problems and solutions.* Biochim Biophys Acta Mol Cell Biol Lipids, 2018. **1863**(2): p. 143-151.
374. Flaherty, S. and J.M. Reynolds, *Mouse Naive CD4+ T Cell Isolation and In vitro Differentiation into T Cell Subsets.* J Vis Exp, 2015(98).
375. Martinez-Sanchez, M.E., et al., *Role of Cytokine Combinations on CD4+ T Cell Differentiation, Partial Polarization, and Plasticity: Continuous Network Modeling Approach.* Front Physiol, 2018. **9**: p. 877.
376. Yang, W., X. Chen, and H. Hu, *CD4(+) T-Cell Differentiation In Vitro.* Methods Mol Biol, 2020. **2111**: p. 91-99.
377. Schmidt, A., et al., *In Vitro Differentiation of Human CD4+FOXP3+ Induced Regulatory T Cells (iTregs) from Naive CD4+ T Cells Using a TGF-beta-containing Protocol.* J Vis Exp, 2016(118).
378. Schmidt, A., et al., *Comparative Analysis of Protocols to Induce Human CD4+Foxp3+ Regulatory T Cells by Combinations of IL-2, TGF-beta, Retinoic Acid, Rapamycin and Butyrate.* PLoS One, 2016. **11**(2): p. e0148474.
379. Pascual, G., et al., *Dietary palmitic acid promotes a prometastatic memory via Schwann cells.* Nature, 2021. **599**(7885): p. 485-490.
380. Meissner, A., et al., *Reduced representation bisulfite sequencing for comparative high-resolution DNA methylation analysis.* Nucleic Acids Res, 2005. **33**(18): p. 5868-77.
381. Deaton, A.M. and A. Bird, *CpG islands and the regulation of transcription.* Genes Dev, 2011. **25**(10): p. 1010-22.
382. Chen, Y., et al., *Adipose tissue dendritic cells enhances inflammation by prompting the generation of Th17 cells.* PLoS One, 2014. **9**(3): p. e92450.
383. Wang, Q., Y. Wang, and D. Xu, *The roles of T cells in obese adipose tissue inflammation.* Adipocyte, 2021. **10**(1): p. 435-445.
384. Zhang, H., et al., *Interferon-gamma induced adipose tissue inflammation is linked to endothelial dysfunction in type 2 diabetic mice.* Basic Res Cardiol, 2011. **106**(6): p. 1135-45.
385. Wang, Q. and H. Wu, *T Cells in Adipose Tissue: Critical Players in Immunometabolism.* Front Immunol, 2018. **9**: p. 2509.
386. Wu, H., et al., *T-cell accumulation and regulated on activation, normal T cell expressed and secreted upregulation in adipose tissue in obesity.* Circulation, 2007. **115**(8): p. 1029-38.
387. Jiang, E., et al., *Essential role of CD11a in CD8+ T-cell accumulation and activation in adipose tissue.* Arterioscler Thromb Vasc Biol, 2014. **34**(1): p. 34-43.
388. Khan, I.M., et al., *Attenuated adipose tissue and skeletal muscle inflammation in obese mice with combined CD4+ and CD8+ T cell deficiency.* Atherosclerosis, 2014. **233**(2): p. 419-428.

389. Kiran, S., et al., *High Fat Diet-Induced CD8(+) T Cells in Adipose Tissue Mediate Macrophages to Sustain Low-Grade Chronic Inflammation.* Front Immunol, 2021. **12**: p. 680944.
390. Macintyre, A.N., et al., *Protein kinase B controls transcriptional programs that direct cytotoxic T cell fate but is dispensable for T cell metabolism.* Immunity, 2011. **34**(2): p. 224-36.
391. Finlay, D.K., et al., *PDK1 regulation of mTOR and hypoxia-inducible factor 1 integrate metabolism and migration of CD8+ T cells.* J Exp Med, 2012. **209**(13): p. 2441-53.
392. Olson, N.C., et al., *Decreased naive and increased memory CD4(+) T cells are associated with subclinical atherosclerosis: the multi-ethnic study of atherosclerosis.* PLoS One, 2013. **8**(8): p. e71498.
393. Lakkis, F.G. and R.I. Lechler, *Origin and biology of the allogeneic response.* Cold Spring Harb Perspect Med, 2013. **3**(8).
394. Hu, J.K., et al., *Expression of chemokine receptor CXCR3 on T cells affects the balance between effector and memory CD8 T-cell generation.* Proc Natl Acad Sci U S A, 2011. **108**(21): p. E118-27.
395. Rocha, V.Z., et al., *CXCR3 controls T-cell accumulation in fat inflammation.* Arterioscler Thromb Vasc Biol, 2014. **34**(7): p. 1374-81.
396. Kim, C.H., et al., *Rules of chemokine receptor association with T cell polarization in vivo.* J Clin Invest, 2001. **108**(9): p. 1331-9.
397. Steinmetz, O.M., et al., *CXCR3 mediates renal Th1 and Th17 immune response in murine lupus nephritis.* J Immunol, 2009. **183**(7): p. 4693-704.
398. Groom, J.R. and A.D. Luster, *CXCR3 in T cell function.* Exp Cell Res, 2011. **317**(5): p. 620-31.
399. Loetscher, P., et al., *CCR5 is characteristic of Th1 lymphocytes.* Nature, 1998. **391**(6665): p. 344-5.
400. Norii, M., et al., *Selective recruitment of CXCR3+ and CCR5+ CCR4+ T cells into synovial tissue in patients with rheumatoid arthritis.* Acta Med Okayama, 2006. **60**(3): p. 149-57.
401. Deiuliis, J.A., et al., *CXCR3 modulates obesity-induced visceral adipose inflammation and systemic insulin resistance.* Obesity (Silver Spring), 2014. **22**(5): p. 1264-74.
402. Kurachi, M., et al., *Chemokine receptor CXCR3 facilitates CD8(+) T cell differentiation into short-lived effector cells leading to memory degeneration.* J Exp Med, 2011. **208**(8): p. 1605-20.
403. Kandula, S. and C. Abraham, *LFA-1 on CD4+ T cells is required for optimal antigen-dependent activation in vivo.* J Immunol, 2004. **173**(7): p. 4443-51.
404. Walling, B.L. and M. Kim, *LFA-1 in T Cell Migration and Differentiation.* Front Immunol, 2018. **9**: p. 952.
405. Bose, T.O., et al., *CD11a regulates effector CD8 T cell differentiation and central memory development in response to infection with Listeria monocytogenes.* Infect Immun, 2013. **81**(4): p. 1140-51.
406. Li, D., J.J. Molldrem, and Q. Ma, *LFA-1 regulates CD8+ T cell activation via T cell receptor-mediated and LFA-1-mediated Erk1/2 signal pathways.* J Biol Chem, 2009. **284**(31): p. 21001-10.
407. Han, S.C., et al., *Fermented fish oil suppresses T helper 1/2 cell response in a mouse model of atopic dermatitis via generation of CD4+CD25+Foxp3+ T cells.* BMC Immunol, 2012. **13**: p. 44.
408. Gutierrez, S., S.L. Svahn, and M.E. Johansson, *Effects of Omega-3 Fatty Acids on Immune Cells.* Int J Mol Sci, 2019. **20**(20).

409. Niederlova, V., et al., *CD8(+) Tregs revisited: A heterogeneous population with different phenotypes and properties.* Eur J Immunol, 2021. **51**(3): p. 512-530.
410. Manavalan, J.S., et al., *Alloantigen specific CD8+CD28- FOXP3+ T suppressor cells induce ILT3+ ILT4+ tolerogenic endothelial cells, inhibiting alloreactivity.* Int Immunol, 2004. **16**(8): p. 1055-68.
411. Agle, K., et al., *Bim regulates the survival and suppressive capability of CD8(+) FOXP3(+) regulatory T cells during murine GVHD.* Blood, 2018. **132**(4): p. 435-447.
412. Sun, J., et al., *Efficient Therapeutic Function and Mechanisms of Human Polyclonal CD8(+)CD103(+)Foxp3(+) Regulatory T Cells on Collagen-Induced Arthritis in Mice.* J Immunol Res, 2019. **2019**: p. 8575407.
413. Beres, A.J., et al., *CD8+ Foxp3+ regulatory T cells are induced during graft-versus-host disease and mitigate disease severity.* J Immunol, 2012. **189**(1): p. 464-74.
414. Iamsawat, S., et al., *Vitamin C stabilizes CD8+ iTregs and enhances their therapeutic potential in controlling murine GVHD and leukemia relapse.* Blood Adv, 2019. **3**(24): p. 4187-4201.
415. Ablamunits, V., B. Bisikirska, and K.C. Herold, *Acquisition of regulatory function by human CD8(+) T cells treated with anti-CD3 antibody requires TNF.* Eur J Immunol, 2010. **40**(10): p. 2891-901.
416. Lerret, N.M., et al., *Donor-specific CD8+ Foxp3+ T cells protect skin allografts and facilitate induction of conventional CD4+ Foxp3+ regulatory T cells.* Am J Transplant, 2012. **12**(9): p. 2335-47.
417. Nunez Ruiz, A., et al., *Diminished levels of regulatory T cell subsets (CD8+Foxp3, CD4+Foxp3 and CD4+CD39+Foxp3) but increased Foxp3 expression in adipose tissue from overweight subjects.* Nutrition, 2016. **32**(9): p. 943-54.
418. Shimokawa, C., et al., *CD8(+) regulatory T cells are critical in prevention of autoimmune-mediated diabetes.* Nat Commun, 2020. **11**(1): p. 1922.
419. Yu, Y., et al., *Recent advances in CD8(+) regulatory T cell research.* Oncol Lett, 2018. **15**(6): p. 8187-8194.
420. Crotty, S., *T follicular helper cell differentiation, function, and roles in disease.* Immunity, 2014. **41**(4): p. 529-42.
421. Krishnaswamy, J.K., et al., *Determination of T Follicular Helper Cell Fate by Dendritic Cells.* Front Immunol, 2018. **9**: p. 2169.
422. Cao, G., et al., *CD4+CXCR5+PD-1+ T Follicular Helper Cells Play a Pivotal Role in the Development of Rheumatoid Arthritis.* Med Sci Monit, 2019. **25**: p. 3032-3040.
423. Lin, J., et al., *PD-1+CXCR5-CD4+T cells are correlated with the severity of systemic lupus erythematosus.* Rheumatology (Oxford), 2019. **58**(12): p. 2188-2192.
424. Shi, W., et al., *PD-1 regulates CXCR5(+) CD4 T cell-mediated proinflammatory functions in non-small cell lung cancer patients.* Int Immunopharmacol, 2020. **82**: p. 106295.
425. Holm Hansen, R., et al., *Increased Intrathecal Activity of Follicular Helper T Cells in Patients With Relapsing-Remitting Multiple Sclerosis.* Neurol Neuroimmunol Neuroinflamm, 2022. **9**(5).
426. Kono, M., et al., *The Impact of Obesity and a High-Fat Diet on Clinical and Immunological Features in Systemic Lupus Erythematosus.* Nutrients, 2021. **13**(2).
427. Chen, Y., et al., *CXCR5(+)PD-1(+) follicular helper CD8 T cells control B cell tolerance.* Nat Commun, 2019. **10**(1): p. 4415.
428. Taghavie-Moghadam, P.L., et al., *STAT4 Regulates the CD8(+) Regulatory T Cell/T Follicular Helper Cell Axis and Promotes Atherogenesis in Insulin-Resistant Ldlr(-/-) Mice.* J Immunol, 2017. **199**(10): p. 3453-3465.

429. Clement, M., et al., *Control of the T follicular helper-germinal center B-cell axis by CD8(+) regulatory T cells limits atherosclerosis and tertiary lymphoid organ development.* Circulation, 2015. **131**(6): p. 560-70.
430. Shirakawa, K., et al., *Obesity accelerates T cell senescence in murine visceral adipose tissue.* J Clin Invest, 2016. **126**(12): p. 4626-4639.
431. Wang, Z., et al., *Paradoxical effects of obesity on T cell function during tumor progression and PD-1 checkpoint blockade.* Nat Med, 2019. **25**(1): p. 141-151.
432. Cottam, M.A., et al., *Multiomics reveals persistence of obesity-associated immune cell phenotypes in adipose tissue during weight loss and weight regain in mice.* Nat Commun, 2022. **13**(1): p. 2950.
433. Porsche, C.E., et al., *Obesity results in adipose tissue T cell exhaustion.* JCI Insight, 2021. **6**(8).
434. Sharpe, A.H. and K.E. Pauken, *The diverse functions of the PD1 inhibitory pathway.* Nat Rev Immunol, 2018. **18**(3): p. 153-167.
435. Shirakawa, K. and M. Sano, *T Cell Immunosenescence in Aging, Obesity, and Cardiovascular Disease.* Cells, 2021. **10**(9).
436. Brunelli, D.T., et al., *Obesity Increases Gene Expression of Markers Associated With Immunosenescence in Obese Middle-Aged Individuals.* Front Immunol, 2021. **12**: p. 806400.
437. Ramello, M.C., et al., *Polyfunctional KLRG-1(+)CD57(+) Senescent CD4(+) T Cells Infiltrate Tumors and Are Expanded in Peripheral Blood From Breast Cancer Patients.* Front Immunol, 2021. **12**: p. 713132.
438. Henson, S.M. and A.N. Akbar, *KLRG1--more than a marker for T cell senescence.* Age (Dordr), 2009. **31**(4): p. 285-91.
439. Beyersdorf, N., et al., *Characterization of mouse CD4 T cell subsets defined by expression of KLRG1.* Eur J Immunol, 2007. **37**(12): p. 3445-54.
440. Voehringer, D., M. Koschella, and H. Pircher, *Lack of proliferative capacity of human effector and memory T cells expressing killer cell lectinlike receptor G1 (KLRG1).* Blood, 2002. **100**(10): p. 3698-702.
441. Reiley, W.W., et al., *Distinct functions of antigen-specific CD4 T cells during murine Mycobacterium tuberculosis infection.* Proc Natl Acad Sci U S A, 2010. **107**(45): p. 19408-13.
442. Li, L., et al., *KLRG1 restricts memory T cell antitumor immunity.* Oncotarget, 2016. **7**(38): p. 61670-61678.
443. Labarthe, M.C., et al., *A novel murine model of allogeneic vaccination against prostate cancer.* Cancer Immunol Immunother, 2008. **57**(4): p. 453-65.
444. Hoffmann, C.C., et al., *Modification of mouse immune responses against allogeneic tumor by pretreatment of antigen with mitomycin C or X-irradiation.* J Immunopharmacol, 1980. **2**(2): p. 213-23.
445. Savir, Y., et al., *Balancing speed and accuracy of polyclonal T cell activation: a role for extracellular feedback.* BMC Syst Biol, 2012. **6**: p. 111.
446. Pennock, N.D., et al., *T cell responses: naive to memory and everything in between.* Adv Physiol Educ, 2013. **37**(4): p. 273-83.
447. Young, B.M., et al., *Polyclonal and antigen-specific responses of T cells and T cell subsets.* Methods Mol Biol, 2008. **447**: p. 277-94.
448. Rezvani, K., et al., *Ex vivo characterization of polyclonal memory CD8+ T-cell responses to PRAME-specific peptides in patients with acute lymphoblastic leukemia and acute and chronic myeloid leukemia.* Blood, 2009. **113**(10): p. 2245-55.
449. Xia, J., et al., *Non-Invasive Monitoring of CNS MHC-I Molecules in Ischemic Stroke Mice.* Theranostics, 2017. **7**(11): p. 2837-2848.

450. Morris, D.L., et al., *Adipose tissue macrophages function as antigen-presenting cells and regulate adipose tissue CD4+ T cells in mice.* Diabetes, 2013. **62**(8): p. 2762-72.
451. Zhou, H., et al., *DsbA-L deficiency in T cells promotes diet-induced thermogenesis through suppressing IFN-gamma production.* Nat Commun, 2021. **12**(1): p. 326.
452. Xia, S., et al., *Chronic intake of high fish oil diet induces myeloid-derived suppressor cells to promote tumor growth.* Cancer Immunol Immunother, 2014. **63**(7): p. 663-73.
453. Park, C.S. and N. Shastri, *The Role of T Cells in Obesity-Associated Inflammation and Metabolic Disease.* Immune Netw, 2022. **22**(1): p. e13.
454. Rocha, V.Z., et al., *Interferon-gamma, a Th1 cytokine, regulates fat inflammation: a role for adaptive immunity in obesity.* Circ Res, 2008. **103**(5): p. 467-76.
455. Cho, K.W., et al., *An MHC II-dependent activation loop between adipose tissue macrophages and CD4+ T cells controls obesity-induced inflammation.* Cell Rep, 2014. **9**(2): p. 605-17.
456. Esteves de Oliveira, E., et al., *Obesity affects peripheral lymphoid organs immune response in murine asthma model.* Immunology, 2019. **157**(3): p. 268-279.
457. Liu, Y., et al., *Bcl-6-directed follicular helper T cells promote vascular inflammatory injury in diabetic retinopathy.* Theranostics, 2020. **10**(9): p. 4250-4264.
458. St Paul, M. and P.S. Ohashi, *The Roles of CD8(+) T Cell Subsets in Antitumor Immunity.* Trends Cell Biol, 2020. **30**(9): p. 695-704.
459. Lian, M., et al., *Dietary n-3 PUFA Protects Mice from Con A Induced Liver Injury by Modulating Regulatory T Cells and PPAR-gamma Expression.* PLoS One, 2015. **10**(7): p. e0132741.
460. Woodworth, H.L., et al., *Dietary fish oil alters T lymphocyte cell populations and exacerbates disease in a mouse model of inflammatory colitis.* Cancer Res, 2010. **70**(20): p. 7960-9.
461. Mishra, S., et al., *CD8(+) Regulatory T Cell - A Mystery to Be Revealed.* Front Immunol, 2021. **12**: p. 708874.
462. Hahn, B.H., et al., *Tolerogenic treatment of lupus mice with consensus peptide induces Foxp3-expressing, apoptosis-resistant, TGFbeta-secreting CD8+ T cell suppressors.* J Immunol, 2005. **175**(11): p. 7728-37.
463. Churlaud, G., et al., *Human and Mouse CD8(+)CD25(+)FOXP3(+) Regulatory T Cells at Steady State and during Interleukin-2 Therapy.* Front Immunol, 2015. **6**: p. 171.
464. Nunez-Ruiz, A., et al., *Obesity modulates the immune macroenvironment associated with breast cancer development.* PLoS One, 2022. **17**(4): p. e0266827.
465. Yang, H., et al., *Obesity accelerates thymic aging.* Blood, 2009. **114**(18): p. 3803-12.
466. Gaddis, D.E., et al., *Atherosclerosis Impairs Naive CD4 T-Cell Responses via Disruption of Glycolysis.* Arterioscler Thromb Vasc Biol, 2021. **41**(9): p. 2387-2398.
467. Zhang, X., et al., *CD4(+)CD62L(+) central memory T cells can be converted to Foxp3(+) T cells.* PLoS One, 2013. **8**(10): p. e77322.
468. Karimi, M., et al., *DHA-rich n-3 fatty acid supplementation decreases DNA methylation in blood leukocytes: the OmegAD study.* Am J Clin Nutr, 2017. **106**(4): p. 1157-1165.
469. Tremblay, B.L., et al., *Epigenetic changes in blood leukocytes following an omega-3 fatty acid supplementation.* Clin Epigenetics, 2017. **9**: p. 43.
470. Huoman, J., et al., *Combined prenatal Lactobacillus reuteri and omega-3 supplementation synergistically modulates DNA methylation in neonatal T helper cells.* Clin Epigenetics, 2021. **13**(1): p. 135.
471. Shoda, H., et al., *Dietary Omega-3 Fatty Acids Suppress Experimental Autoimmune Uveitis in Association with Inhibition of Th1 and Th17 Cell Function.* PLoS One, 2015. **10**(9): p. e0138241.

472. Li, Y., et al., *Endogenous n-3 Polyunsaturated Fatty Acids Attenuate T Cell-Mediated Hepatitis via Autophagy Activation.* Front Immunol, 2016. **7**: p. 350.
473. Mizota, T., et al., *Effect of dietary fatty acid composition on Th1/Th2 polarization in lymphocytes.* JPEN J Parenter Enteral Nutr, 2009. **33**(4): p. 390-6.
474. Suzuki, D., et al., *Effects of perioperative immunonutrition on cell-mediated immunity, T helper type 1 (Th1)/Th2 differentiation, and Th17 response after pancreaticoduodenectomy.* Surgery, 2010. **148**(3): p. 573-81.
475. Huang, C.H., et al., *Dietary omega-6/omega-3 Polyunsaturated Fatty Acid Ratios Affect the Homeostasis of Th/Treg Cells in Mice With Dextran Sulfate Sodium-Induced Colitis.* JPEN J Parenter Enteral Nutr, 2017. **41**(4): p. 647-656.
476. Garidou, L., et al., *The Gut Microbiota Regulates Intestinal CD4 T Cells Expressing RORgammat and Controls Metabolic Disease.* Cell Metab, 2015. **22**(1): p. 100-12.
477. Winer, D.A., et al., *The Intestinal Immune System in Obesity and Insulin Resistance.* Cell Metab, 2016. **23**(3): p. 413-26.
478. Gagliani, N., et al., *Th17 cells transdifferentiate into regulatory T cells during resolution of inflammation.* Nature, 2015. **523**(7559): p. 221-5.
479. Sandner, L., et al., *The Tyrosine Kinase Tec Regulates Effector Th17 Differentiation, Pathogenicity, and Plasticity in T-Cell-Driven Intestinal Inflammation.* Front Immunol, 2021. **12**: p. 750466.
480. Dyck, L., et al., *Suppressive effects of the obese tumor microenvironment on CD8 T cell infiltration and effector function.* J Exp Med, 2022. **219**(3).
481. Beghini, M., et al., *Adipocyte STAT5 deficiency does not affect blood glucose homeostasis in obese mice.* PLoS One, 2021. **16**(11): p. e0260501.
482. Kaltenecker, D., et al., *Adipocyte STAT5 deficiency promotes adiposity and impairs lipid mobilisation in mice.* Diabetologia, 2017. **60**(2): p. 296-305.
483. Dobrian, A.D., et al., *STAT4 contributes to adipose tissue inflammation and atherosclerosis.* J Endocrinol, 2015. **227**(1): p. 13-24.
484. Dobrian, A.D., et al., *STAT4 deficiency reduces obesity-induced insulin resistance and adipose tissue inflammation.* Diabetes, 2013. **62**(12): p. 4109-21.
485. Powell, J.D., et al., *Regulation of immune responses by mTOR.* Annu Rev Immunol, 2012. **30**: p. 39-68.
486. Zhang, S., et al., *The Alterations in and the Role of the Th17/Treg Balance in Metabolic Diseases.* Front Immunol, 2021. **12**: p. 678355.
487. Bettelli, E., et al., *Reciprocal developmental pathways for the generation of pathogenic effector TH17 and regulatory T cells.* Nature, 2006. **441**(7090): p. 235-8.
488. Hot, A. and P. Miossec, *Effects of interleukin (IL)-17A and IL-17F in human rheumatoid arthritis synoviocytes.* Ann Rheum Dis, 2011. **70**(5): p. 727-32.
489. Miossec, P., *Interleukin-17 and Th17 cells: from adult to juvenile arthritis--now it is serious!* Arthritis Rheum, 2011. **63**(8): p. 2168-71.
490. Dang, E.V., et al., *Control of T(H)17/T(reg) balance by hypoxia-inducible factor 1.* Cell, 2011. **146**(5): p. 772-84.
491. Berod, L., et al., *De novo fatty acid synthesis controls the fate between regulatory T and T helper 17 cells.* Nat Med, 2014. **20**(11): p. 1327-33.
492. Barbi, J., D. Pardoll, and F. Pan, *Metabolic control of the Treg/Th17 axis.* Immunol Rev, 2013. **252**(1): p. 52-77.
493. Qin, Y., C. Gao, and J. Luo, *Metabolism Characteristics of Th17 and Regulatory T Cells in Autoimmune Diseases.* Front Immunol, 2022. **13**: p. 828191.
494. Bai, A., et al., *CD39 and CD161 modulate Th17 responses in Crohn's disease.* J Immunol, 2014. **193**(7): p. 3366-77.

495. Bai, A., et al., *Role of acid sphingomyelinase bioactivity in human CD4+ T-cell activation and immune responses.* Cell Death Dis, 2015. **6**(7): p. e1828.
496. Bai, A. and S. Robson, *Beyond ecto-nucleotidase: CD39 defines human Th17 cells with CD161.* Purinergic Signal, 2015. **11**(3): p. 317-9.
497. Sakata, A., et al., *Acid sphingomyelinase inhibition suppresses lipopolysaccharide-mediated release of inflammatory cytokines from macrophages and protects against disease pathology in dextran sulphate sodium-induced colitis in mice.* Immunology, 2007. **122**(1): p. 54-64.
498. Bauer, J., et al., *Lipid alterations in experimental murine colitis: role of ceramide and imipramine for matrix metalloproteinase-1 expression.* PLoS One, 2009. **4**(9): p. e7197.
499. von Bismarck, P., et al., *Improved pulmonary function by acid sphingomyelinase inhibition in a newborn piglet lavage model.* Am J Respir Crit Care Med, 2008. **177**(11): p. 1233-41.
500. Endo, Y., K. Yokote, and T. Nakayama, *The obesity-related pathology and Th17 cells.* Cell Mol Life Sci, 2017. **74**(7): p. 1231-1245.
501. Kue, C.S., et al., *C6-ceramide in combination with transforming growth factor-beta enhances Treg cell differentiation and stable FoxP3 expression in vitro and in vivo.* Immunobiology, 2013. **218**(7): p. 952-9.
502. Sallusto, F., et al., *Ceramide inhibits antigen uptake and presentation by dendritic cells.* J Exp Med, 1996. **184**(6): p. 2411-6.
503. Li, Y., C.L. Talbot, and B. Chaurasia, *Ceramides in Adipose Tissue.* Front Endocrinol (Lausanne), 2020. **11**: p. 407.
504. Masukawa, Y., et al., *Characterization of overall ceramide species in human stratum corneum.* J Lipid Res, 2008. **49**(7): p. 1466-76.
505. Kendall, A.C., et al., *Lipid functions in skin: Differential effects of n-3 polyunsaturated fatty acids on cutaneous ceramides, in a human skin organ culture model.* Biochim Biophys Acta Biomembr, 2017. **1859**(9 Pt B): p. 1679-1689.
506. Arana, L., et al., *Ceramide and ceramide 1-phosphate in health and disease.* Lipids Health Dis, 2010. **9**: p. 15.
507. Gomez-Munoz, A., et al., *Ceramide-1-phosphate in cell survival and inflammatory signaling.* Adv Exp Med Biol, 2010. **688**: p. 118-30.
508. Hilvo, M., et al., *Ceramide stearic to palmitic acid ratio predicts incident diabetes.* Diabetologia, 2018. **61**(6): p. 1424-1434.
509. Laaksonen, R., et al., *Plasma ceramides predict cardiovascular death in patients with stable coronary artery disease and acute coronary syndromes beyond LDL-cholesterol.* Eur Heart J, 2016. **37**(25): p. 1967-76.
510. McGurk, K.A., et al., *Heritability and family-based GWAS analyses of the N-acyl ethanolamine and ceramide plasma lipidome.* Hum Mol Genet, 2021. **30**(6): p. 500-513.
511. Charo, J., et al., *Bcl-2 overexpression enhances tumor-specific T-cell survival.* Cancer Res, 2005. **65**(5): p. 2001-8.
512. Liu, L., et al., *BCL-2 expression promotes immunosuppression in chronic lymphocytic leukemia by enhancing regulatory T cell differentiation and cytotoxic T cell exhaustion.* Mol Cancer, 2022. **21**(1): p. 59.
513. Hirakawa, M., et al., *Low-dose IL-2 selectively activates subsets of CD4(+) Tregs and NK cells.* JCI Insight, 2016. **1**(18): p. e89278.
514. Furlong, S.J., N.D. Ridgway, and D.W. Hoskin, *Modulation of ceramide metabolism in T-leukemia cell lines potentiates apoptosis induced by the cationic antimicrobial peptide bovine lactoferricin.* Int J Oncol, 2008. **32**(3): p. 537-44.

515. Wang, Y., M.A. Su, and Y.Y. Wan, *An essential role of the transcription factor GATA-3 for the function of regulatory T cells.* Immunity, 2011. **35**(3): p. 337-48.
516. Wohlfert, E.A., et al., *GATA3 controls Foxp3(+) regulatory T cell fate during inflammation in mice.* J Clin Invest, 2011. **121**(11): p. 4503-15.
517. Xu, K., et al., *GATA3, HDAC6, and BCL6 Regulate FOXP3+ Treg Plasticity and Determine Treg Conversion into Either Novel Antigen-Presenting Cell-Like Treg or Th1-Treg.* Front Immunol, 2018. **9**: p. 45.
518. Saxena, A., et al., *Ultrasensitive Quantification of Cytokine Proteins in Single Lymphocytes From Human Blood Following ex-vivo Stimulation.* Front Immunol, 2018. **9**: p. 2462.
519. Simonetto, M., et al., *A Novel Anti-Inflammatory Role of Omega-3 PUFAs in Prevention and Treatment of Atherosclerosis and Vascular Cognitive Impairment and Dementia.* Nutrients, 2019. **11**(10).
520. Li, S. and H.E. Kim, *Implications of Sphingolipids on Aging and Age-Related Diseases.* Front Aging, 2021. **2**: p. 797320.
521. Rotolo, J.A., et al., *Cytolytic T cells induce ceramide-rich platforms in target cell membranes to initiate graft-versus-host disease.* Blood, 2009. **114**(17): p. 3693-706.
522. Hose, M., et al., *Cell-intrinsic ceramides determine T cell function during melanoma progression.* Elife, 2022. **11**.
523. Menne, C., et al., *Ceramide-induced TCR up-regulation.* J Immunol, 2000. **165**(6): p. 3065-72.
524. Wiese, T., et al., *Inhibition of acid sphingomyelinase increases regulatory T cells in humans.* Brain Commun, 2021. **3**(2): p. fcab020.
525. Wei, Q., et al., *Lck bound to coreceptor is less active than free Lck.* Proc Natl Acad Sci U S A, 2020. **117**(27): p. 15809-15817.
526. Kolak, M., et al., *Adipose tissue inflammation and increased ceramide content characterize subjects with high liver fat content independent of obesity.* Diabetes, 2007. **56**(8): p. 1960-8.
527. Schiffmann, S., et al., *Inhibitors of specific ceramide synthases.* Biochimie, 2012. **94**(2): p. 558-65.
528. Hofmann, M., V. Brinkmann, and H.G. Zerwes, *FTY720 preferentially depletes naive T cells from peripheral and lymphoid organs.* Int Immunopharmacol, 2006. **6**(13-14): p. 1902-10.
529. Mehling, M., et al., *FTY720 therapy exerts differential effects on T cell subsets in multiple sclerosis.* Neurology, 2008. **71**(16): p. 1261-7.
530. Benechet, A.P., et al., *T cell-intrinsic S1PR1 regulates endogenous effector T-cell egress dynamics from lymph nodes during infection.* Proc Natl Acad Sci U S A, 2016. **113**(8): p. 2182-7.
531. Nakashima, D., et al., *Impaired initiation of contact hypersensitivity by FTY720.* J Invest Dermatol, 2008. **128**(12): p. 2833-41.
532. Liao, J.J., M.C. Huang, and E.J. Goetzl, *Cutting edge: Alternative signaling of Th17 cell development by sphingosine 1-phosphate.* J Immunol, 2007. **178**(9): p. 5425-8.
533. Mehling, M., et al., *Th17 central memory T cells are reduced by FTY720 in patients with multiple sclerosis.* Neurology, 2010. **75**(5): p. 403-10.
534. Eken, A., et al., *S1P(1) deletion differentially affects TH17 and Regulatory T cells.* Sci Rep, 2017. **7**(1): p. 12905.
535. Crivelli, S.M., et al., *FTY720 decreases ceramides levels in the brain and prevents memory impairments in a mouse model of familial Alzheimer's disease expressing APOE4.* Biomed Pharmacother, 2022. **152**: p. 113240.

536. Rivas, D.A., et al., *Sphingosine-1-phosphate analog FTY720 reverses obesity but not age-induced anabolic resistance to muscle contraction.* Am J Physiol Cell Physiol, 2019. **317**(3): p. C502-C512.
537. Zhang, Y., et al., *Antidepressant drug, desipramine, alleviates allergic rhinitis by regulating Treg and Th17 cells.* Int J Immunopathol Pharmacol, 2013. **26**(1): p. 107-15.
538. Gu, J., et al., *Protocol for in vitro isolation, induction, expansion, and determination of human natural regulatory T cells and induced regulatory T cells.* STAR Protoc, 2022. **3**(4): p. 101740.
539. Luo, Y., et al., *Negligible Effect of Sodium Chloride on the Development and Function of TGF-beta-Induced CD4(+) Foxp3(+) Regulatory T Cells.* Cell Rep, 2019. **26**(7): p. 1869-1879 e3.
540. Yin, Y., A. Mitson-Salazar, and C. Prussin, *Detection of Intracellular Cytokines by Flow Cytometry.* Curr Protoc Immunol, 2015. **110**: p. 6 24 1-6 24 18.
541. Shooshtari, P., et al., *Correlation analysis of intracellular and secreted cytokines via the generalized integrated mean fluorescence intensity.* Cytometry A, 2010. **77**(9): p. 873-80.
542. Shin, S.H., et al., *A Novel Selective Sphingosine Kinase 2 Inhibitor, HWG-35D, Ameliorates the Severity of Imiquimod-Induced Psoriasis Model by Blocking Th17 Differentiation of Naive CD4 T Lymphocytes.* Int J Mol Sci, 2020. **21**(21).
543. Sen, P., et al., *Quantitative genome-scale metabolic modeling of human CD4(+) T cell differentiation reveals subset-specific regulation of glycosphingolipid pathways.* Cell Rep, 2021. **37**(6): p. 109973.
544. Pandey, M.K., et al., *Immunological cell type characterization and Th1-Th17 cytokine production in a mouse model of Gaucher disease.* Mol Genet Metab, 2012. **106**(3): p. 310-22.
545. Lu, S., et al., *Ceramide Induces Human Hepcidin Gene Transcription through JAK/STAT3 Pathway.* PLoS One, 2016. **11**(1): p. e0147474.
546. Xuan, L., et al., *Ceramide induces MMP-9 expression through JAK2/STAT3 pathway in airway epithelium.* Lipids Health Dis, 2020. **19**(1): p. 196.
547. Gaffen, S.L., et al., *The IL-23-IL-17 immune axis: from mechanisms to therapeutic testing.* Nat Rev Immunol, 2014. **14**(9): p. 585-600.
548. Ciofani, M., et al., *A validated regulatory network for Th17 cell specification.* Cell, 2012. **151**(2): p. 289-303.
549. Duvel, K., et al., *Activation of a metabolic gene regulatory network downstream of mTOR complex 1.* Mol Cell, 2010. **39**(2): p. 171-83.
550. Demaria, M. and V. Poli, *PKM2, STAT3 and HIF-1alpha: The Warburg's vicious circle.* JAKSTAT, 2012. **1**(3): p. 194-6.
551. Demaria, M. and V. Poli, *From the nucleus to the mitochondria and back: the odyssey of a multitask STAT3.* Cell Cycle, 2011. **10**(19): p. 3221-2.
552. Demaria, M., et al., *A STAT3-mediated metabolic switch is involved in tumour transformation and STAT3 addiction.* Aging (Albany NY), 2010. **2**(11): p. 823-42.
553. Xia, Q.S., et al., *New role for ceramide in hypoxia and insulin resistance.* World J Gastroenterol, 2020. **26**(18): p. 2177-2186.
554. Hsieh, C.T., et al., *Ceramide inhibits insulin-stimulated Akt phosphorylation through activation of Rheb/mTORC1/S6K signaling in skeletal muscle.* Cell Signal, 2014. **26**(7): p. 1400-8.
555. Huang, C.H., et al., *A soybean and fish oil mixture with different n-6/n-3 PUFA ratios modulates the inflammatory reaction in mice with dextran sulfate sodium-induced acute colitis.* Clin Nutr, 2015. **34**(5): p. 1018-24.

556. Mukaro, V.R., et al., *Leukocyte numbers and function in subjects eating n-3 enriched foods: selective depression of natural killer cell levels.* Arthritis Res Ther, 2008. **10**(3): p. R57.
557. Chiurchiu, V., et al., *Proresolving lipid mediators resolvin D1, resolvin D2, and maresin 1 are critical in modulating T cell responses.* Sci Transl Med, 2016. **8**(353): p. 353ra111.
558. Jeffery, L., et al., *Plasma Levels of Eicosapentaenoic Acid Are Associated with Anti-TNF Responsiveness in Rheumatoid Arthritis and Inhibit the Etanercept-driven Rise in Th17 Cell Differentiation in Vitro.* J Rheumatol, 2017. **44**(6): p. 748-756.
559. Bi, X., et al., *omega-3 polyunsaturated fatty acids ameliorate type 1 diabetes and autoimmunity.* J Clin Invest, 2017. **127**(5): p. 1757-1771.
560. Chi, H., *Regulation and function of mTOR signalling in T cell fate decisions.* Nat Rev Immunol, 2012. **12**(5): p. 325-38.
561. Allen, M.J., et al., *n-3 PUFAs reduce T-helper 17 cell differentiation by decreasing responsiveness to interleukin-6 in isolated mouse splenic CD4(+) T cells.* J Nutr, 2014. **144**(8): p. 1306-13.
562. Kong, W., J.H. Yen, and D. Ganea, *Docosahexaenoic acid prevents dendritic cell maturation, inhibits antigen-specific Th1/Th17 differentiation and suppresses experimental autoimmune encephalomyelitis.* Brain Behav Immun, 2011. **25**(5): p. 872-82.
563. Pinel, A., et al., *N-3PUFA differentially modulate palmitate-induced lipotoxicity through alterations of its metabolism in C2C12 muscle cells.* Biochim Biophys Acta, 2016. **1861**(1): p. 12-20.
564. Rosqvist, F., et al., *Overeating Saturated Fat Promotes Fatty Liver and Ceramides Compared With Polyunsaturated Fat: A Randomized Trial.* J Clin Endocrinol Metab, 2019. **104**(12): p. 6207-6219.
565. Kien, C.L., et al., *A lipidomics analysis of the relationship between dietary fatty acid composition and insulin sensitivity in young adults.* Diabetes, 2013. **62**(4): p. 1054-63.
566. Heilbronn, L.K., et al., *The effect of short-term overfeeding on serum lipids in healthy humans.* Obesity (Silver Spring), 2013. **21**(12): p. E649-59.
567. Walchuk, C., Y. Wang, and M. Suh, *The impact of EPA and DHA on ceramide lipotoxicity in the metabolic syndrome.* Br J Nutr, 2021. **125**(8): p. 863-875.
568. Jin, J., et al., *Docosahexaenoic acid antagonizes the boosting effect of palmitic acid on LPS inflammatory signaling by inhibiting gene transcription and ceramide synthesis.* PLoS One, 2018. **13**(2): p. e0193343.
569. Lanchais, K., F. Capel, and A. Tournadre, *Could Omega 3 Fatty Acids Preserve Muscle Health in Rheumatoid Arthritis?* Nutrients, 2020. **12**(1).
570. Shirakawa, K. and M. Sano, *Drastic transformation of visceral adipose tissue and peripheral CD4 T cells in obesity.* Front Immunol, 2022. **13**: p. 1044737.
571. Schmitz, J., et al., *Obesogenic memory can confer long-term increases in adipose tissue but not liver inflammation and insulin resistance after weight loss.* Mol Metab, 2016. **5**(5): p. 328-339.
572. Zamarron, B.F., et al., *Macrophage Proliferation Sustains Adipose Tissue Inflammation in Formerly Obese Mice.* Diabetes, 2017. **66**(2): p. 392-406.
573. Mehta, T., et al., *Impact of weight cycling on risk of morbidity and mortality.* Obes Rev, 2014. **15**(11): p. 870-81.
574. Kosteli, A., et al., *Weight loss and lipolysis promote a dynamic immune response in murine adipose tissue.* J Clin Invest, 2010. **120**(10): p. 3466-79.
575. Surendar, J., et al., *Macrophages Mediate Increased CD8 T Cell Inflammation During Weight Loss in Formerly Obese Mice.* Front Endocrinol (Lausanne), 2020. **11**: p. 257.

576. Trachta, P., et al., *Laparoscopic sleeve gastrectomy ameliorates mRNA expression of inflammation-related genes in subcutaneous adipose tissue but not in peripheral monocytes of obese patients.* Mol Cell Endocrinol, 2014. **383**(1-2): p. 96-102.
577. Pardina, E., et al., *Only C-reactive protein, but not TNF-alpha or IL6, reflects the improvement in inflammation after bariatric surgery.* Obes Surg, 2012. **22**(1): p. 131-9.
578. Sougiannis, A.T., et al., *Impact of weight loss and partial weight regain on immune cell and inflammatory markers in adipose tissue in male mice.* J Appl Physiol (1985), 2020. **129**(4): p. 909-919.
579. Shirakawa, K., et al., *Negative legacy of obesity.* PLoS One, 2017. **12**(10): p. e0186303.
580. Hall, K.D. and S. Kahan, *Maintenance of Lost Weight and Long-Term Management of Obesity.* Med Clin North Am, 2018. **102**(1): p. 183-197.
581. Kraschnewski, J.L., et al., *Long-term weight loss maintenance in the United States.* Int J Obes (Lond), 2010. **34**(11): p. 1644-54.
582. Wadden, T.A., et al., *Four-year weight losses in the Look AHEAD study: factors associated with long-term success.* Obesity (Silver Spring), 2011. **19**(10): p. 1987-98.
583. Forsythe, L.K., J.M. Wallace, and M.B. Livingstone, *Obesity and inflammation: the effects of weight loss.* Nutr Res Rev, 2008. **21**(2): p. 117-33.
584. Khanna, D., et al., *Obesity: A Chronic Low-Grade Inflammation and Its Markers.* Cureus, 2022. **14**(2): p. e22711.
585. Hata, M., et al., *Past history of obesity triggers persistent epigenetic changes in innate immunity and exacerbates neuroinflammation.* Science, 2023. **379**(6627): p. 45-62.
586. Look, A.R.G., et al., *Cardiovascular effects of intensive lifestyle intervention in type 2 diabetes.* N Engl J Med, 2013. **369**(2): p. 145-54.
587. Rossi, E.L., et al., *Obesity-Associated Alterations in Inflammation, Epigenetics, and Mammary Tumor Growth Persist in Formerly Obese Mice.* Cancer Prev Res (Phila), 2016. **9**(5): p. 339-48.
588. Bultman, S.J., *A Reversible Epigenetic Link between Obesity and Cancer Risk.* Trends Endocrinol Metab, 2018. **29**(8): p. 529-531.
589. Wang, X., et al., *Obesity related methylation changes in DNA of peripheral blood leukocytes.* BMC Med, 2010. **8**: p. 87.
590. Mendelson, M.M., et al., *Association of Body Mass Index with DNA Methylation and Gene Expression in Blood Cells and Relations to Cardiometabolic Disease: A Mendelian Randomization Approach.* PLoS Med, 2017. **14**(1): p. e1002215.
591. Hussey, B., et al., *DNA methylation of tumour necrosis factor (TNF) alpha gene is associated with specific blood fatty acid levels in a gender-specific manner.* Mol Genet Genomic Med, 2021. **9**(12): p. e1679.
592. Fradin, D. and P. Bougneres, *beta cells keep bad epigenetic memories of palmitate.* BMC Med, 2014. **12**: p. 104.
593. Wang, X., et al., *Epigenetic regulation of macrophage polarization and inflammation by DNA methylation in obesity.* JCI Insight, 2016. **1**(19): p. e87748.
594. Sehgal, R., et al., *Liver saturated fat content associates with hepatic DNA methylation in obese individuals.* Clin Epigenetics, 2023. **15**(1): p. 21.
595. Pompura, S.L., et al., *Oleic acid restores suppressive defects in tissue-resident FOXP3 Tregs from patients with multiple sclerosis.* J Clin Invest, 2021. **131**(2).
596. Hidalgo, M.A., M.D. Carretta, and R.A. Burgos, *Long Chain Fatty Acids as Modulators of Immune Cells Function: Contribution of FFA1 and FFA4 Receptors.* Front Physiol, 2021. **12**: p. 668330.
597. Pompura, S.L., D.A. Hafler, and M. Dominguez-Villar, *Fatty Acid Metabolism and T Cells in Multiple Sclerosis.* Front Immunol, 2022. **13**: p. 869197.

598. Perez-Mojica, J.E., et al., *Docosahexaenoic acid and oleic acid induce altered DNA methylation of individual CpG loci in Jurkat T cells.* Prostaglandins Leukot Essent Fatty Acids, 2020. **158**: p. 102128.
599. Zhang, Y., J.R. Sowers, and J. Ren, *Targeting autophagy in obesity: from pathophysiology to management.* Nat Rev Endocrinol, 2018. **14**(6): p. 356-376.
600. Hansen, M., D.C. Rubinsztein, and D.W. Walker, *Autophagy as a promoter of longevity: insights from model organisms.* Nat Rev Mol Cell Biol, 2018. **19**(9): p. 579-593.
601. Choi, A.M., S.W. Ryter, and B. Levine, *Autophagy in human health and disease.* N Engl J Med, 2013. **368**(7): p. 651-62.
602. Galluzzi, L., et al., *Metabolic control of autophagy.* Cell, 2014. **159**(6): p. 1263-76.
603. Wang, D., et al., *Emerging role of the Hippo pathway in autophagy.* Cell Death Dis, 2020. **11**(10): p. 880.
604. Huang, T., et al., *MST4 Phosphorylation of ATG4B Regulates Autophagic Activity, Tumorigenicity, and Radioresistance in Glioblastoma.* Cancer Cell, 2017. **32**(6): p. 840-855 e8.
605. Kim, K.H. and M.S. Lee, *Autophagy--a key player in cellular and body metabolism.* Nat Rev Endocrinol, 2014. **10**(6): p. 322-37.
606. Soussi, H., K. Clement, and I. Dugail, *Adipose tissue autophagy status in obesity: Expression and flux--two faces of the picture.* Autophagy, 2016. **12**(3): p. 588-9.
607. Jansen, H.J., et al., *Autophagy activity is up-regulated in adipose tissue of obese individuals and modulates proinflammatory cytokine expression.* Endocrinology, 2012. **153**(12): p. 5866-74.
608. Kovsan, J., et al., *Altered autophagy in human adipose tissues in obesity.* J Clin Endocrinol Metab, 2011. **96**(2): p. E268-77.
609. Kosacka, J., et al., *Autophagy in adipose tissue of patients with obesity and type 2 diabetes.* Mol Cell Endocrinol, 2015. **409**: p. 21-32.
610. Mizunoe, Y., et al., *Involvement of lysosomal dysfunction in autophagosome accumulation and early pathologies in adipose tissue of obese mice.* Autophagy, 2017. **13**(4): p. 642-653.
611. Xu, X., et al., *Akt2 knockout preserves cardiac function in high-fat diet-induced obesity by rescuing cardiac autophagosome maturation.* J Mol Cell Biol, 2013. **5**(1): p. 61-3.
612. Lopez-Vicario, C., et al., *Inhibition of soluble epoxide hydrolase modulates inflammation and autophagy in obese adipose tissue and liver: role for omega-3 epoxides.* Proc Natl Acad Sci U S A, 2015. **112**(2): p. 536-41.
613. Clarke, A.J. and A.K. Simon, *Autophagy in the renewal, differentiation and homeostasis of immune cells.* Nat Rev Immunol, 2019. **19**(3): p. 170-183.
614. Hubbard, V.M., et al., *Macroautophagy regulates energy metabolism during effector T cell activation.* J Immunol, 2010. **185**(12): p. 7349-57.
615. Mortensen, M., et al., *The autophagy protein Atg7 is essential for hematopoietic stem cell maintenance.* J Exp Med, 2011. **208**(3): p. 455-67.
616. Riffelmacher, T., et al., *Autophagy-Dependent Generation of Free Fatty Acids Is Critical for Normal Neutrophil Differentiation.* Immunity, 2017. **47**(3): p. 466-480 e5.
617. Phadwal, K., et al., *A novel method for autophagy detection in primary cells: impaired levels of macroautophagy in immunosenescent T cells.* Autophagy, 2012. **8**(4): p. 677-89.
618. Pua, H.H., et al., *A critical role for the autophagy gene Atg5 in T cell survival and proliferation.* J Exp Med, 2007. **204**(1): p. 25-31.
619. Zinecker, H. and A.K. Simon, *Autophagy takes it all - autophagy inducers target immune aging.* Dis Model Mech, 2022. **15**(1).

620. Ju, L., et al., *Obesity-associated inflammation triggers an autophagy-lysosomal response in adipocytes and causes degradation of perilipin 1.* Cell Death Dis, 2019. **10**(2): p. 121.
621. Guerrero-Ros, I., et al., *The negative effect of lipid challenge on autophagy inhibits T cell responses.* Autophagy, 2020. **16**(2): p. 223-238.
622. RostamiRad, A., et al., *Palmitate-induced impairment of autophagy turnover leads to increased apoptosis and inflammation in peripheral blood mononuclear cells.* Immunobiology, 2018. **223**(3): p. 269-278.
623. Di Micco, R., et al., *Cellular senescence in ageing: from mechanisms to therapeutic opportunities.* Nat Rev Mol Cell Biol, 2021. **22**(2): p. 75-95.
624. Franceschi, C., et al., *Inflamm-aging. An evolutionary perspective on immunosenescence.* Ann N Y Acad Sci, 2000. **908**: p. 244-54.
625. Huang, W., et al., *Cellular senescence: the good, the bad and the unknown.* Nat Rev Nephrol, 2022. **18**(10): p. 611-627.
626. Xu, M., et al., *Senolytics improve physical function and increase lifespan in old age.* Nat Med, 2018. **24**(8): p. 1246-1256.
627. Zhao, Y., Q. Shao, and G. Peng, *Exhaustion and senescence: two crucial dysfunctional states of T cells in the tumor microenvironment.* Cell Mol Immunol, 2020. **17**(1): p. 27-35.
628. Kumari, R. and P. Jat, *Mechanisms of Cellular Senescence: Cell Cycle Arrest and Senescence Associated Secretory Phenotype.* Front Cell Dev Biol, 2021. **9**: p. 645593.
629. Covre, L.P., et al., *The role of senescent T cells in immunopathology.* Aging Cell, 2020. **19**(12): p. e13272.
630. Perl, A. and L. Morel, *Expanding scope of TEMRA in autoimmunity.* EBioMedicine, 2023. **90**: p. 104520.
631. Salumets, A., et al., *Epigenetic quantification of immunosenescent CD8(+) TEMRA cells in human blood.* Aging Cell, 2022. **21**(5): p. e13607.
632. Lu, J., et al., *Adipose Tissue-Resident Immune Cells in Obesity and Type 2 Diabetes.* Front Immunol, 2019. **10**: p. 1173.
633. Ishaq, A., et al., *Palmitate induces DNA damage and senescence in human adipocytes in vitro that can be alleviated by oleic acid but not inorganic nitrate.* Exp Gerontol, 2022. **163**: p. 111798.
634. Della Vedova, M.C., et al., *A Mouse Model of Diet-Induced Obesity Resembling Most Features of Human Metabolic Syndrome.* Nutr Metab Insights, 2016. **9**: p. 93-102.
635. Lozano, I., et al., *High-fructose and high-fat diet-induced disorders in rats: impact on diabetes risk, hepatic and vascular complications.* Nutr Metab (Lond), 2016. **13**: p. 15.
636. Lutz, T.A. and S.C. Woods, *Overview of animal models of obesity.* Curr Protoc Pharmacol, 2012. **Chapter 5**: p. Unit5 61.
637. Zhuhua, Z., et al., *A novel mice model of metabolic syndrome: the high-fat-high-fructose diet-fed ICR mice.* Exp Anim, 2015. **64**(4): p. 435-42.
638. Samuelsson, A.M., et al., *Diet-induced obesity in female mice leads to offspring hyperphagia, adiposity, hypertension, and insulin resistance: a novel murine model of developmental programming.* Hypertension, 2008. **51**(2): p. 383-92.
639. Maric, I., et al., *Sex and Species Differences in the Development of Diet-Induced Obesity and Metabolic Disturbances in Rodents.* Front Nutr, 2022. **9**: p. 828522.
640. Gelineau, R.R., et al., *The behavioral and physiological effects of high-fat diet and alcohol consumption: Sex differences in C57BL6/J mice.* Brain Behav, 2017. **7**(6): p. e00708.

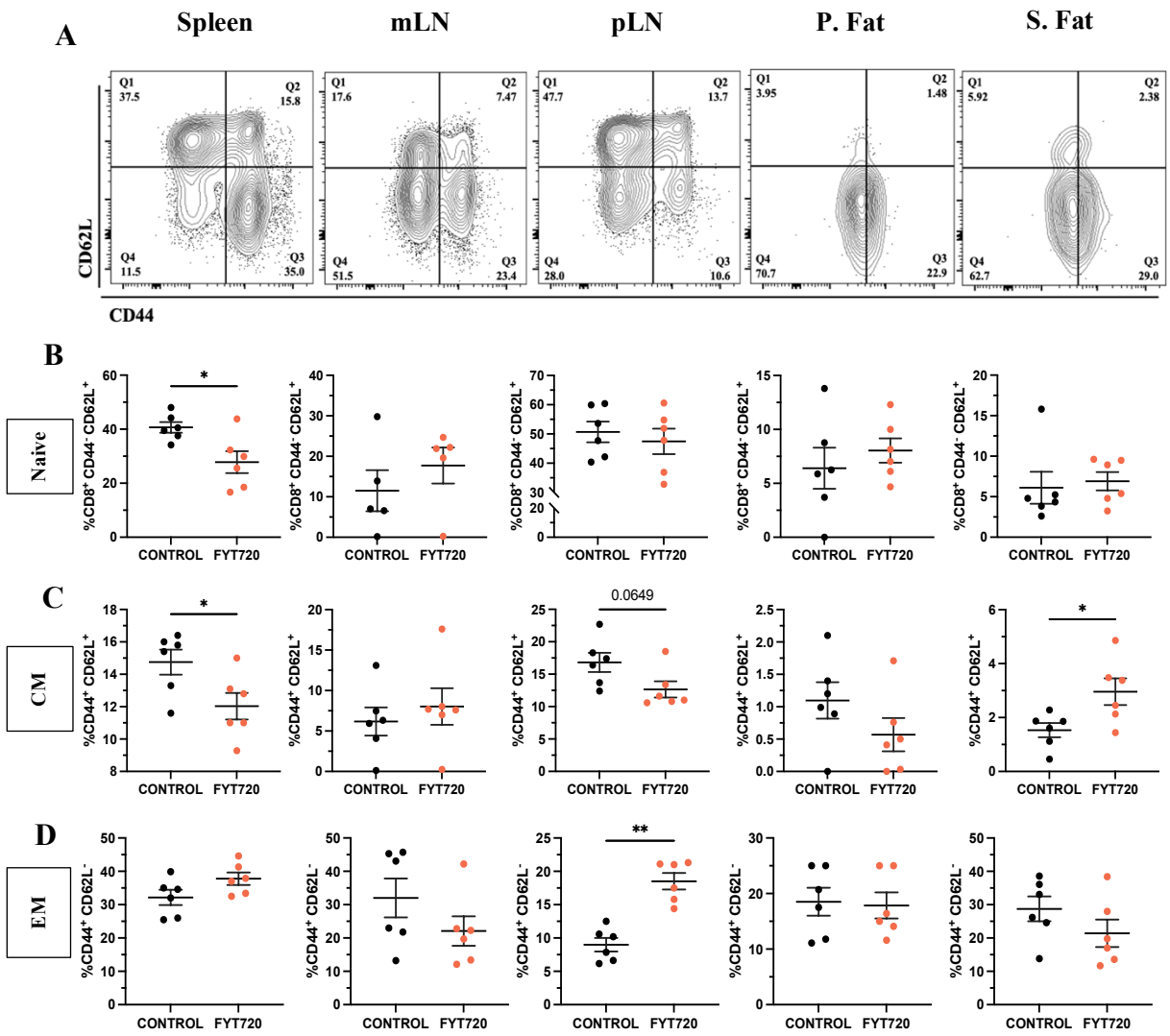
641. Oraha, J., et al., *Sex-specific changes in metabolism during the transition from chow to high-fat diet feeding are abolished in response to dieting in C57BL/6J mice.* Int J Obes (Lond), 2022. **46**(10): p. 1749-1758.
642. Casimiro, I., et al., *Phenotypic sexual dimorphism in response to dietary fat manipulation in C57BL/6J mice.* J Diabetes Complications, 2021. **35**(2): p. 107795.
643. Grove, K.L., et al., *A microarray analysis of sexual dimorphism of adipose tissues in high-fat-diet-induced obese mice.* Int J Obes (Lond), 2010. **34**(6): p. 989-1000.
644. Deiuliis, J., et al., *Visceral adipose inflammation in obesity is associated with critical alterations in tregulatory cell numbers.* PLoS One, 2011. **6**(1): p. e16376.
645. Zeng, Q., et al., *A Unique Population: Adipose-Resident Regulatory T Cells.* Front Immunol, 2018. **9**: p. 2075.
646. Huang, C.Y., et al., *Caspase activation of mammalian sterile 20-like kinase 3 (Mst3). Nuclear translocation and induction of apoptosis.* J Biol Chem, 2002. **277**(37): p. 34367-74.
647. Mardakheh, F.K., A. Self, and C.J. Marshall, *RHO binding to FAM65A regulates Golgi reorientation during cell migration.* J Cell Sci, 2016. **129**(24): p. 4466-4479.
648. Dan, I., et al., *Cloning of MASK, a novel member of the mammalian germinal center kinase III subfamily, with apoptosis-inducing properties.* J Biol Chem, 2002. **277**(8): p. 5929-39.
649. Shi, Z. and Z. Zhou, *MST kinases in innate immune signaling.* Cell Stress, 2017. **2**(1): p. 4-13.
650. Jiao, S., et al., *The kinase MST4 limits inflammatory responses through direct phosphorylation of the adaptor TRAF6.* Nat Immunol, 2015. **16**(3): p. 246-57.
651. Shi, X., et al., *MST4 as a novel therapeutic target for autophagy and radiosensitivity in gastric cancer.* IUBMB Life, 2023. **75**(2): p. 117-136.
652. Liu, P., et al., *MST4 promotes proliferation, invasion, and metastasis of gastric cancer by enhancing autophagy.* Heliyon, 2023. **9**(6): p. e16735.
653. Wu, X., et al., *MST4 Kinase Inhibitor Hesperadin Attenuates Autophagy and Behavioral Disorder via the MST4/AKT Pathway in Intracerebral Hemorrhage Mice.* Behav Neurol, 2020. **2020**: p. 2476861.
654. Schmiedel, B.J., et al., *Impact of Genetic Polymorphisms on Human Immune Cell Gene Expression.* Cell, 2018. **175**(6): p. 1701-1715 e16.
655. Monaco, G., et al., *RNA-Seq Signatures Normalized by mRNA Abundance Allow Absolute Deconvolution of Human Immune Cell Types.* Cell Rep, 2019. **26**(6): p. 1627-1640 e7.
656. Potikha, T., et al., *p57Kip2 (cdkn1c): sequence, splice variants and unique temporal and spatial expression pattern in the rat pancreas.* Lab Invest, 2005. **85**(3): p. 364-75.
657. Mademtzoglou, D., et al., *Cellular localization of the cell cycle inhibitor Cdkn1c controls growth arrest of adult skeletal muscle stem cells.* Elife, 2018. **7**.
658. Larson, P.S., et al., *CDKN1C/p57kip2 is a candidate tumor suppressor gene in human breast cancer.* BMC Cancer, 2008. **8**: p. 68.
659. Tsugu, A., et al., *Expression of p57(KIP2) potently blocks the growth of human astrocytomas and induces cell senescence.* Am J Pathol, 2000. **157**(3): p. 919-32.
660. Schwarze, S.R., et al., *Role of cyclin-dependent kinase inhibitors in the growth arrest at senescence in human prostate epithelial and uroepithelial cells.* Oncogene, 2001. **20**(57): p. 8184-92.
661. Borriello, A., et al., *p57(Kip2) and cancer: time for a critical appraisal.* Mol Cancer Res, 2011. **9**(10): p. 1269-84.

662. Giovannini, C., et al., *CDKN1C/P57 is regulated by the Notch target gene Hes1 and induces senescence in human hepatocellular carcinoma.* Am J Pathol, 2012. **181**(2): p. 413-22.
663. Mauthe, M., et al., *Chloroquine inhibits autophagic flux by decreasing autophagosome-lysosome fusion.* Autophagy, 2018. **14**(8): p. 1435-1455.
664. Alsaleh, G., et al., *Autophagy in T cells from aged donors is maintained by spermidine and correlates with function and vaccine responses.* Elife, 2020. **9**.
665. Schurmanns, L., A. Hamann, and H.D. Osiewacz, *Lifespan Increase of Podospora anserina by Oleic Acid Is Linked to Alterations in Energy Metabolism, Membrane Trafficking and Autophagy.* Cells, 2022. **11**(3).
666. Nicholson, J.K., et al., *Evaluation of a method for counting absolute numbers of cells with a flow cytometer.* Clin Diagn Lab Immunol, 1997. **4**(3): p. 309-13.
667. Desdin-Mico, G., et al., *T cells with dysfunctional mitochondria induce multimorbidity and premature senescence.* Science, 2020. **368**(6497): p. 1371-1376.
668. Rodrigues, M.O.M., et al., *Caloric restriction-induced weight loss with a high-fat diet does not fully recover visceral adipose tissue inflammation in previously obese C57BL/6 mice.* Appl Physiol Nutr Metab, 2020. **45**(12): p. 1353-1359.
669. Christ, A., et al., *Western Diet Triggers NLRP3-Dependent Innate Immune Reprogramming.* Cell, 2018. **172**(1-2): p. 162-175 e14.
670. Filippi, B.M., et al., *MO25 is a master regulator of SPAK/OSR1 and MST3/MST4/YSK1 protein kinases.* EMBO J, 2011. **30**(9): p. 1730-41.
671. Gallolu Kankanamalage, S., et al., *WNK1 is an unexpected autophagy inhibitor.* Autophagy, 2017. **13**(5): p. 969-970.
672. Las, G., et al., *Fatty acids suppress autophagic turnover in beta-cells.* J Biol Chem, 2011. **286**(49): p. 42534-42544.
673. Park, M., et al., *Palmitate induces ER stress and autophagy in H9c2 cells: implications for apoptosis and adiponectin resistance.* J Cell Physiol, 2015. **230**(3): p. 630-9.
674. Martino, L., et al., *Palmitate activates autophagy in INS-1E beta-cells and in isolated rat and human pancreatic islets.* PLoS One, 2012. **7**(5): p. e36188.
675. Jiang, X.S., et al., *Autophagy Protects against Palmitic Acid-Induced Apoptosis in Podocytes in vitro.* Sci Rep, 2017. **7**: p. 42764.
676. Cai, N., et al., *Autophagy protects against palmitate-induced apoptosis in hepatocytes.* Cell Biosci, 2014. **4**: p. 28.
677. Peng, Z., et al., *Autophagy Induced by Palmitic Acid Regulates Neutrophil Adhesion Through the Granule-Dependent Degradation of alphaMbeta2 Integrin in Dairy Cows With Fatty Liver.* Front Immunol, 2021. **12**: p. 726829.
678. Tan, S.H., et al., *Induction of autophagy by palmitic acid via protein kinase C-mediated signaling pathway independent of mTOR (mammalian target of rapamycin).* J Biol Chem, 2012. **287**(18): p. 14364-76.
679. Puleston, D.J., et al., *Autophagy is a critical regulator of memory CD8(+) T cell formation.* Elife, 2014. **3**.
680. Swadling, L., et al., *Human Liver Memory CD8(+) T Cells Use Autophagy for Tissue Residence.* Cell Rep, 2020. **30**(3): p. 687-698 e6.
681. Zhu, Q., et al., *Palmitic Acid, A Critical Metabolite, Aggravates Cellular Senescence Through Reactive Oxygen Species Generation in Kawasaki Disease.* Front Pharmacol, 2022. **13**: p. 809157.
682. O'Boyle, G., et al., *Chemokine receptor CXCR3 agonist prevents human T-cell migration in a humanized model of arthritic inflammation.* Proc Natl Acad Sci U S A, 2012. **109**(12): p. 4598-603.

683. Breser, M.L., et al., *Expression of CXCR3 on specific T cells is essential for homing to the prostate gland in an experimental model of chronic prostatitis/chronic pelvic pain syndrome.* J Immunol, 2013. **190**(7): p. 3121-33.
684. Krinninger, P., et al., *Peripheral monocytes of obese women display increased chemokine receptor expression and migration capacity.* J Clin Endocrinol Metab, 2014. **99**(7): p. 2500-9.
685. O'Shea, J.J. and W.E. Paul, *Mechanisms underlying lineage commitment and plasticity of helper CD4+ T cells.* Science, 2010. **327**(5969): p. 1098-102.
686. Pasquarelli-do-Nascimento, G., et al., *Obesity and adipose tissue impact on T-cell response and cancer immune checkpoint blockade therapy.* Immunother Adv, 2022. **2**(1): p. ltac015.
687. Cinti, S., *Adipose Organ Development and Remodeling.* Compr Physiol, 2018. **8**(4): p. 1357-1431.
688. Corvera, S., *Cellular Heterogeneity in Adipose Tissues.* Annu Rev Physiol, 2021. **83**: p. 257-278.
689. Tarantino, G., et al., *Is serum Interleukin-17 associated with early atherosclerosis in obese patients?* J Transl Med, 2014. **12**: p. 214.
690. Mottaghi, A., et al., *Vitamin A supplementation reduces IL-17 and RORc gene expression in atherosclerotic patients.* Scand J Immunol, 2014. **80**(2): p. 151-7.
691. Croce, S., et al., *Adipose Tissue Immunomodulation and Treg/Th17 Imbalance in the Impaired Glucose Metabolism of Children with Obesity.* Children (Basel), 2021. **8**(7).
692. Schindler, T.I., et al., *T(H)17 Cell Frequency in Peripheral Blood Is Elevated in Overweight Children without Chronic Inflammatory Diseases.* Front Immunol, 2017. **8**: p. 1543.
693. Luczynski, W., et al., *Elevated levels of Th17 cells in children with central obesity.* Scand J Clin Lab Invest, 2015. **75**(7): p. 595-601.
694. Pucino, V., et al., *Lactate Buildup at the Site of Chronic Inflammation Promotes Disease by Inducing CD4(+) T Cell Metabolic Rewiring.* Cell Metab, 2019. **30**(6): p. 1055-1074 e8.
695. Wang, P., et al., *Disruption of adipocyte HIF-1alpha improves atherosclerosis through the inhibition of ceramide generation.* Acta Pharm Sin B, 2022. **12**(4): p. 1899-1912.
696. Zhang, Q., et al., *TH17 cells promote CNS inflammation by sensing danger signals via Mincle.* Nat Commun, 2022. **13**(1): p. 2406.
697. Hartel, J.C., N. Merz, and S. Grosch, *How sphingolipids affect T cells in the resolution of inflammation.* Front Pharmacol, 2022. **13**: p. 1002915.
698. Jhun, J., et al., *GRIM19 Impedes Obesity by Regulating Inflammatory White Fat Browning and Promoting Th17/Treg Balance.* Cells, 2021. **10**(1).
699. Artemniak-Wojtowicz, D., et al., *Changes of Peripheral Th17 Cells Subset in Overweight and Obese Children After Body Weight Reduction.* Front Endocrinol (Lausanne), 2022. **13**: p. 917402.
700. Monk, J.M., et al., *n3 PUFAs reduce mouse CD4+ T-cell ex vivo polarization into Th17 cells.* J Nutr, 2013. **143**(9): p. 1501-8.
701. Monk, J.M., et al., *Dietary n-3 polyunsaturated fatty acids (PUFA) decrease obesity-associated Th17 cell-mediated inflammation during colitis.* PLoS One, 2012. **7**(11): p. e49739.
702. Kagohashi, Y., et al., *Maternal dietary n-6/n-3 fatty acid ratio affects type 1 diabetes development in the offspring of non-obese diabetic mice.* Congenit Anom (Kyoto), 2010. **50**(4): p. 212-20.
703. Oh, D.Y., et al., *A Gpr120-selective agonist improves insulin resistance and chronic inflammation in obese mice.* Nat Med, 2014. **20**(8): p. 942-7.

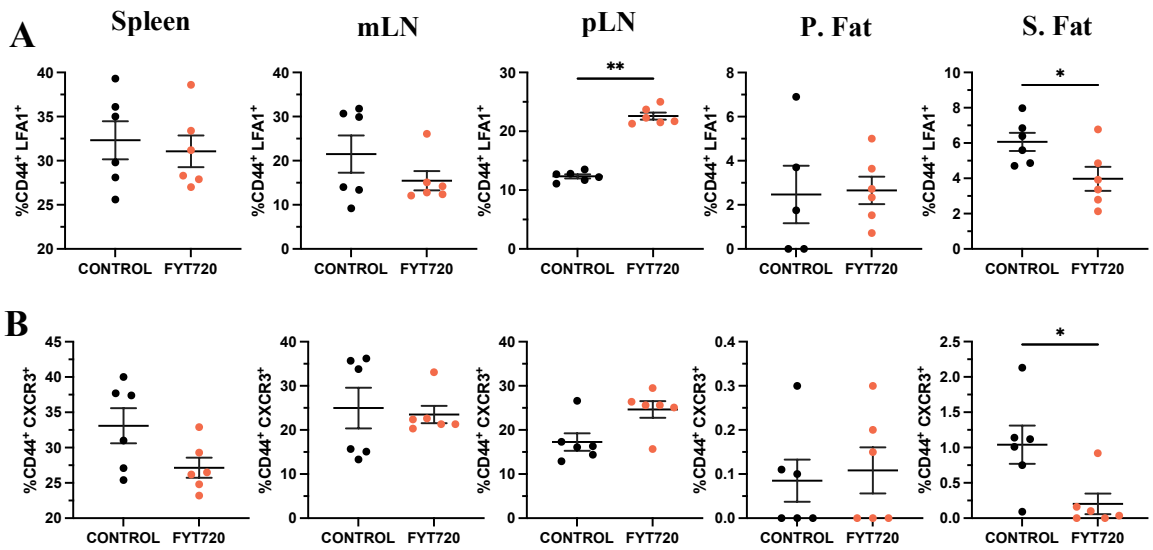
704. Balogun, K.A., et al., *Dietary omega-3 polyunsaturated fatty acids alter the fatty acid composition of hepatic and plasma bioactive lipids in C57BL/6 mice: a lipidomic approach.* PLoS One, 2013. **8**(11): p. e82399.
705. Heras, A., et al., *Dietary long-chain omega 3 fatty acids modify sphingolipid metabolism to facilitate airway hyperreactivity.* Sci Rep, 2022. **12**(1): p. 19735.
706. Stelzner, K., et al., *Free fatty acids sensitize dendritic cells to amplify TH1/TH17-immune responses.* Eur J Immunol, 2016. **46**(8): p. 2043-53.
707. Michaud, M.D., et al., *Sphingosine-1-phosphate: a novel nonhypoxic activator of hypoxia-inducible factor-1 in vascular cells.* Arterioscler Thromb Vasc Biol, 2009. **29**(6): p. 902-8.
708. Gill, J.S. and A.J. Windebank, *Ceramide initiates NFkappaB-mediated caspase activation in neuronal apoptosis.* Neurobiol Dis, 2000. **7**(4): p. 448-61.
709. Gaggini, M., et al., *Ceramides as Mediators of Oxidative Stress and Inflammation in Cardiometabolic Disease.* Int J Mol Sci, 2022. **23**(5).
710. Papanikolaou, A., et al., *Cholesterol-dependent lipid assemblies regulate the activity of the ecto-nucleotidase CD39.* J Biol Chem, 2005. **280**(28): p. 26406-14.
711. Pandolfi, J.B., et al., *ATP-Induced Inflammation Drives Tissue-Resident Th17 Cells in Metabolically Unhealthy Obesity.* J Immunol, 2016. **196**(8): p. 3287-96.
712. Salminen, A., K. Kaarniranta, and A. Kauppinen, *Hypoxia-Inducible Histone Lysine Demethylases: Impact on the Aging Process and Age-Related Diseases.* Aging Dis, 2016. **7**(2): p. 180-200.
713. Rashida Gnanaprakasam, J.N., R. Wu, and R. Wang, *Metabolic Reprogramming in Modulating T Cell Reactive Oxygen Species Generation and Antioxidant Capacity.* Front Immunol, 2018. **9**: p. 1075.
714. Yan, Z., Q. Chen, and Y. Xia, *Oxidative Stress Contributes to Inflammatory and Cellular Damage in Systemic Lupus Erythematosus: Cellular Markers and Molecular Mechanism.* J Inflamm Res, 2023. **16**: p. 453-465.
715. Moesta, A.K., X.Y. Li, and M.J. Smyth, *Targeting CD39 in cancer.* Nat Rev Immunol, 2020. **20**(12): p. 739-755.
716. Argraves, K.M., et al., *S1P, dihydro-S1P and C24:1-ceramide levels in the HDL-containing fraction of serum inversely correlate with occurrence of ischemic heart disease.* Lipids Health Dis, 2011. **10**: p. 70.
717. Cannavo, A., et al., *Sphingosine Kinases and Sphingosine 1-Phosphate Receptors: Signaling and Actions in the Cardiovascular System.* Front Pharmacol, 2017. **8**: p. 556.
718. Zehra Okus, F., et al., *S1P analogues SEW2871, BAF312 and FTY720 affect human Th17 and Treg generation ex vivo.* Int Immunopharmacol, 2022. **107**: p. 108665.
719. Li, S., et al., *Assessment of diet-induced obese rats as an obesity model by comparative functional genomics.* Obesity (Silver Spring), 2008. **16**(4): p. 811-8.
720. Tschop, M. and M.L. Heiman, *Rodent obesity models: an overview.* Exp Clin Endocrinol Diabetes, 2001. **109**(6): p. 307-19.
721. Lopez, I.P., et al., *DNA microarray analysis of genes differentially expressed in diet-induced (cafeteria) obese rats.* Obes Res, 2003. **11**(2): p. 188-94.
722. Moraes, R.C., et al., *Study of the alteration of gene expression in adipose tissue of diet-induced obese mice by microarray and reverse transcription-polymerase chain reaction analyses.* Endocrinology, 2003. **144**(11): p. 4773-82.
723. Hong, J., et al., *Differential susceptibility to obesity between male, female and ovariectomized female mice.* Nutr J, 2009. **8**: p. 11.
724. Pettersson, U.S., et al., *Female mice are protected against high-fat diet induced metabolic syndrome and increase the regulatory T cell population in adipose tissue.* PLoS One, 2012. **7**(9): p. e46057.

725. Ishikawa, A., et al., *Estrogen regulates sex-specific localization of regulatory T cells in adipose tissue of obese female mice.* PLoS One, 2020. **15**(4): p. e0230885.
726. Speakman, J.R., *Measuring energy metabolism in the mouse - theoretical, practical, and analytical considerations.* Front Physiol, 2013. **4**: p. 34.
727. Dutta, S. and P. Sengupta, *Men and mice: Relating their ages.* Life Sci, 2016. **152**: p. 244-8.
728. Nicolucci, A. and C. Maffeis, *The adolescent with obesity: what perspectives for treatment?* Ital J Pediatr, 2022. **48**(1): p. 9.
729. Kansra, A.R., S. Lakkunarajah, and M.S. Jay, *Childhood and Adolescent Obesity: A Review.* Front Pediatr, 2020. **8**: p. 581461.
730. Xiong, W., et al., *Structure-Based Screen Identification of a Mammalian Ste20-like Kinase 4 (MST4) Inhibitor with Therapeutic Potential for Pituitary Tumors.* Mol Cancer Ther, 2016. **15**(3): p. 412-20.
731. Yousefzadeh, M.J., et al., *Mouse Models of Accelerated Cellular Senescence.* Methods Mol Biol, 2019. **1896**: p. 203-230.
732. Gorgoulis, V., et al., *Cellular Senescence: Defining a Path Forward.* Cell, 2019. **179**(4): p. 813-827.
733. Martinez-Zamudio, R.I., et al., *Senescence-associated beta-galactosidase reveals the abundance of senescent CD8+ T cells in aging humans.* Aging Cell, 2021. **20**(5): p. e13344.
734. Lee, J., et al., *C1q/TNF-related protein-9 attenuates palmitic acid-induced endothelial cell senescence via increasing autophagy.* Mol Cell Endocrinol, 2021. **521**: p. 111114.
735. Lee, Y., et al., *Coordinate regulation of the senescent state by selective autophagy.* Dev Cell, 2021. **56**(10): p. 1512-1525 e7.
736. Kwon, Y., et al., *Autophagy Is Pro-Senescence When Seen in Close-Up, but Anti-Senescence in Long-Shot.* Mol Cells, 2017. **40**(9): p. 607-612.
737. Shi, H., et al., *Overweight, obesity and coronary artery lesions among Kawasaki disease patients.* Nutr Metab Cardiovasc Dis, 2021. **31**(5): p. 1604-1612.
738. Kris-Etherton, P.M., et al., *Recent Clinical Trials Shed New Light on the Cardiovascular Benefits of Omega-3 Fatty Acids.* Methodist Debakey Cardiovasc J, 2019. **15**(3): p. 171-178.
739. Hahn, J., et al., *Vitamin D and marine omega 3 fatty acid supplementation and incident autoimmune disease: VITAL randomized controlled trial.* BMJ, 2022. **376**: p. e066452.
740. Clark, C.C.T., et al., *Efficacy of omega-3 supplementation in patients with psoriasis: a meta-analysis of randomized controlled trials.* Clin Rheumatol, 2019. **38**(4): p. 977-988.
741. Borja-Magno, A.I., et al., *Supplementation with EPA and DHA omega-3 fatty acids improves peripheral immune cell mitochondrial dysfunction and inflammation in subjects with obesity.* J Nutr Biochem, 2023. **120**: p. 109415.



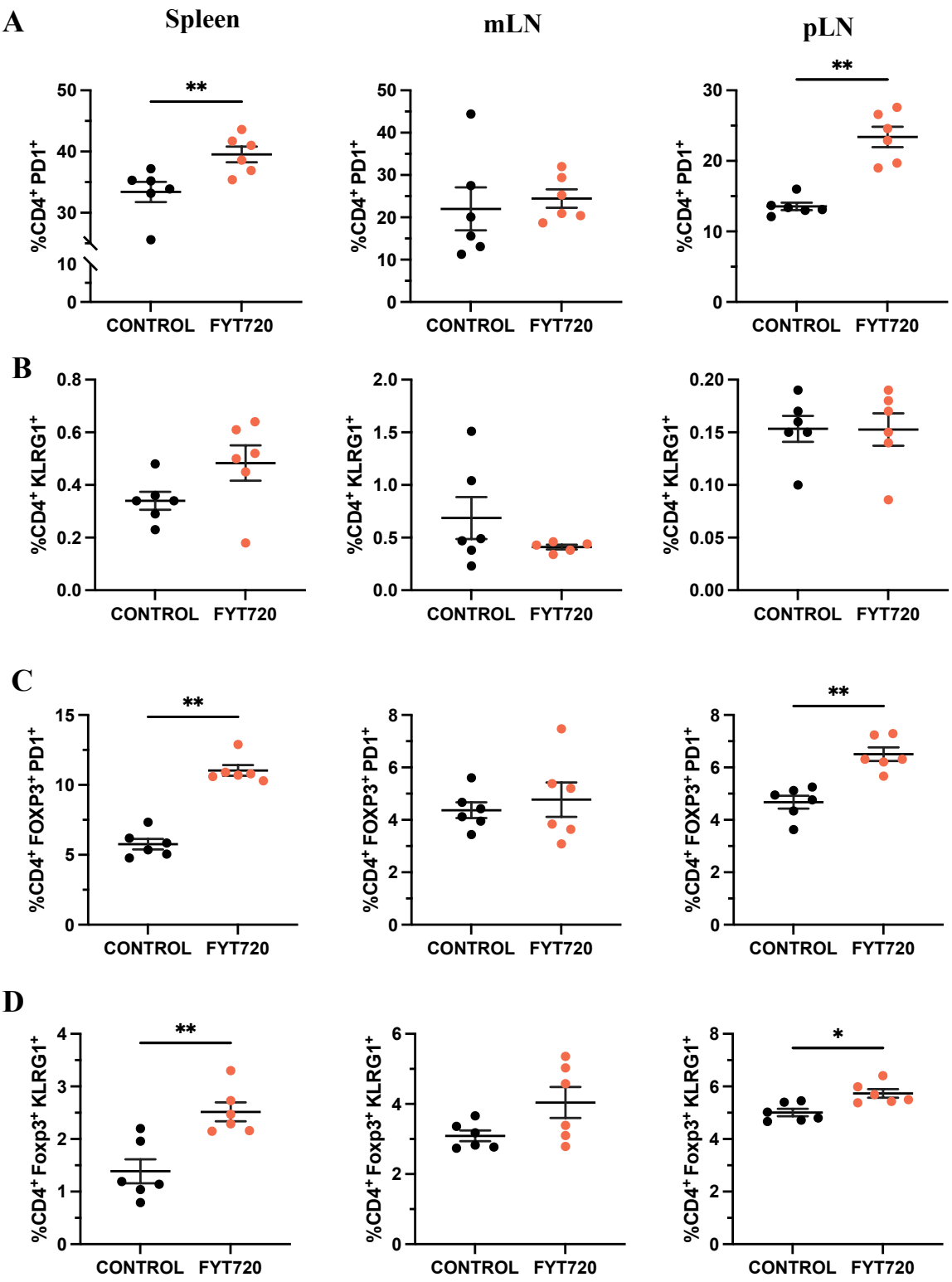
Supplementary Figure S1) Pharmacological inhibition of CerS2 via FTY720 did not attenuate the WD-induced distribution of memory CD8$^+$ T cell subsets

(A) Representative flow cytometry plots of CD44 and CD62L extracellular staining on CD4$^+$ T cells isolated from SLOs and fat tissues of female C57BL/6J mice fed on WD for 21 days and were given intraperitoneal injections of FTY720 (1 mg/ kg) three times (days 11, 14 and 18) (WD+FTY720) or three times PBS injections on respective time points (v.control). Both murine groups were also subjected to an allogenic immunization via intraperitoneal injections at day 14. Quantification of flow cytometry data on **(B)** naïve (CD44$^-$ and CD62L$^+$), **(C)** CM (CD44$^+$ and CD62L$^+$) and **(D)** EM (CD44$^+$ and CD62L$^-$) CD4$^+$ T cell populations within three different SLOs and fat tissues obtained from both groups. Each point represents an individual mouse in allocated diet groups (n=6). One-way ANOVA with Tukey's correction; Data presented as mean ± SEM, *p<0.05; ** p<0.01.



Supplementary Figure S2) Pharmacological inhibition of CerS2 via FTY720 did not attenuate the pro-inflammatory effector memory CD8$^+$ T cell phenotype induced by WD

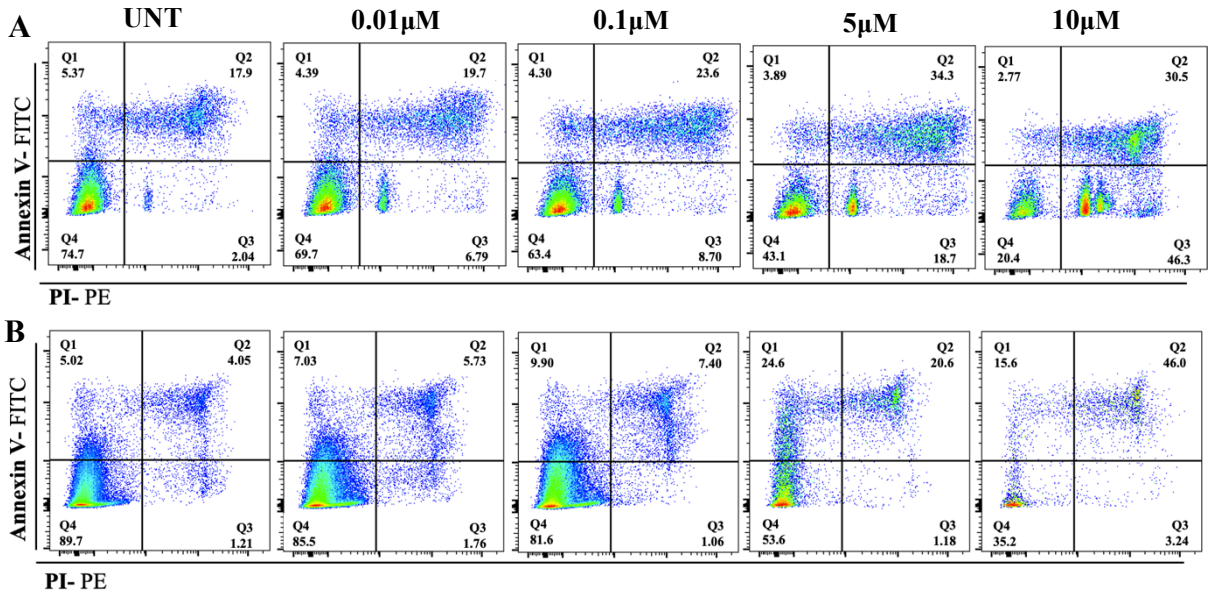
Quantification of flow cytometry data of **(A)** CD44$^+$ and LFA-1$^+$ and **(B)** CD44$^+$ and CXCR3$^+$ obesity-associated pro-inflammatory effector memory CD8$^+$ T cell populations in three main SLOs and two fat tissues obtained from female C57BL/6J mice fed on WD for 21 days and were given intraperitoneal injections of FTY720 (1 mg/ kg) three times (days 11, 14 and 18) (WD+FTY720) or three times PBS injections on respective time points (v.control). Both murine groups were also subjected to an allogenic immunization via intraperitoneal injections at day 14. Each point represents an individual mouse in allocated diet groups (n=6). One-way ANOVA with Tukey's correction; Data presented as mean ± SEM, *p<0.05; ** p<0.01.



Supplementary Figure S3) Effect of CerS2 inhibition on senescent T cell populations within SLOs

Quantification of flow cytometry data of **(A)** $PD1^+$ **(B)** $KLRG1^+$ total $CD4^+$ and **(C)** $Foxp3^+$ $PD1^+$ **(C)** $Foxp3^+$ $KLRG1^+$ $CD4^+$ Treg populations within SLO and fat tissues obtained from female C57BL/6J mice fed on WD for 21 days and were given intraperitoneal injections of FTY720 (1 mg/ kg) three times (days 11, 14 and 18) (WD+FTY720) or three times PBS injections on respective time points (v.control).

Both murine groups were also subjected to an allogenic immunization via intraperitoneal injections at day 14. Each point represents an individual mouse in allocated diet groups (n=6). One-way ANOVA with Tukey's correction; Data presented as mean ± SEM, *p<0.05; ** p<0.01.



Supplementary Figure S4) Representative flow cytometry gating strategy for Annexin V and PI staining.

$CD4^+$ T cells isolated from **(A)** human PBMCs (n = 3 donors) **(B)** murine spleen and LNs (n =3 mice) were untreated or treated with increasing concentration of C24; 0.01, 0.1, 5 and 10µM over 3-5 days of *in vitro* Treg differentiating cell culture conditions. All murine cell conditions were activated by CD3/CD28(1µg/mL) and human cell conditions by CD3/CD28 (1.5:2.5µg/mL) plate bound activation.

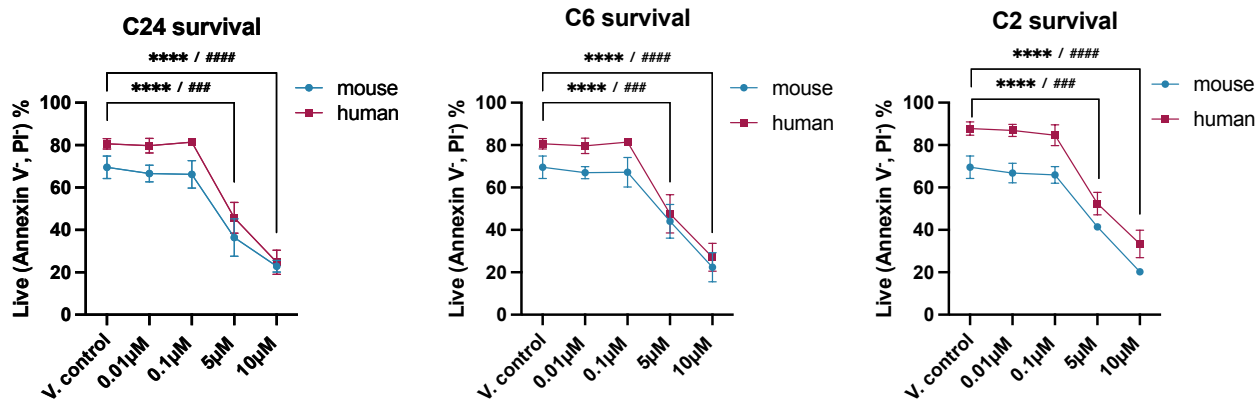
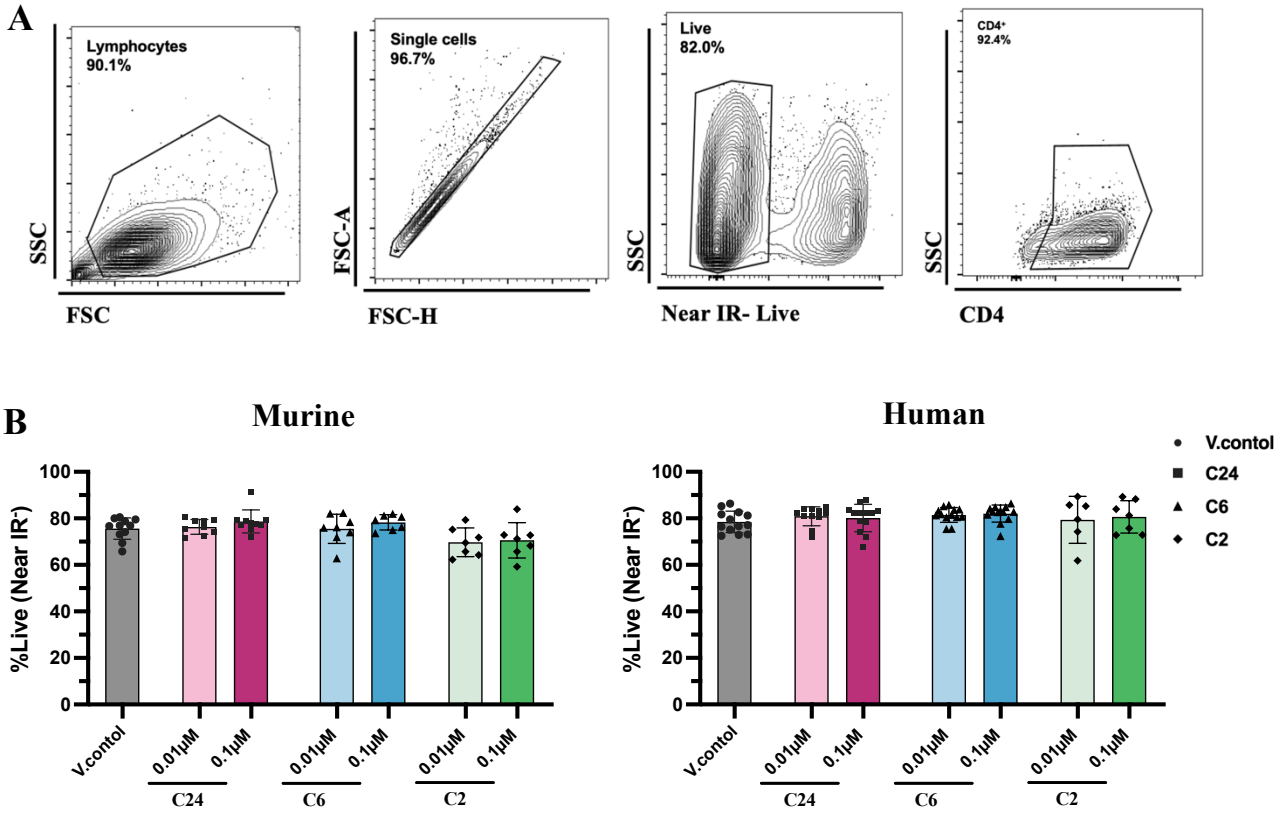


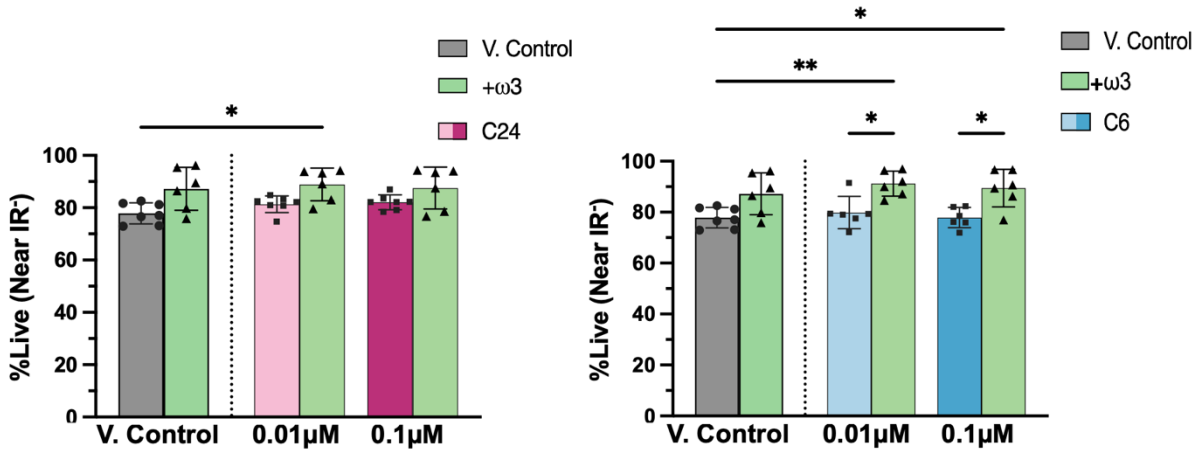
Figure Supplementary Figure S5) Survival plots of human and murine $CD4^+$ T cell for assessing the lipotoxicity of ceramides *in vitro* cultures

Quantification of the live percentage (Q4- PI^-, Annexin V^-) of both murine (blue) and human (pink) $CD4^+$ T cells treated with exogenous C24, C6 and C2 ceramides *in vitro* culture under Treg differentiation conditions for 3-5 days respectively. All murine cell conditions were activated by CD3/CD28(1µg/mL) and human cell conditions by CD3/CD28 (1.5:2.5µg/mL) plate bound activation. Both human and human treatment groups compared to untreated groups of the respective species. One-way ANOVA with Tukey's correction; Data presented as mean ± SEM (n=3), *p<0.05; ** p<0.01, ***p

< 0.001, ****p<0.0001 comparing mouse untreated vs mouse ceramide treated; #p<0.05,##p<0.01, ###p<0.001, ####p<0.0001 comparing human untreated vs human ceramide treated

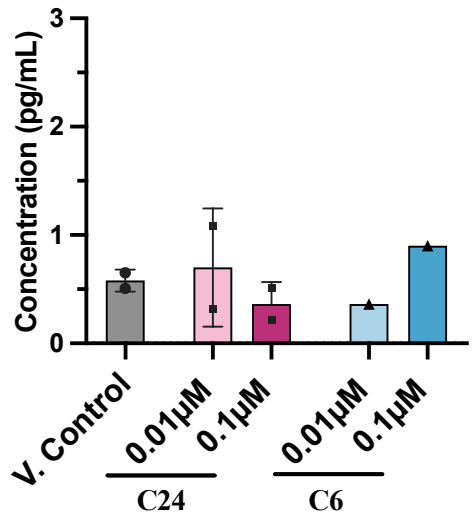


Supplementary Figure S6) Validation of AnnexinV/PI assay via Near IR live/dead marker
(A) Representative flow cytometry main gating strategy used in both human and murine *in vitro* $CD4^+$ T cell differentiation assays. **(B)** Quantification of Near IR^- Live cells $CD4^+$ T cells treated with C24, C6 and C2 (0.01 and 0.1 µM) or left untreated for 3-5 days. All murine cells were activated by CD3/CD28 (1µg/mL) plate bound activation under *in vitro* Treg differentiation conditions for 3 days (n=5-6 mice pooled together as naïve $CD4^+$ cells isolated from murine spleen and LNs). All human $CD4^+$ T cell were activated by CD3/CD28 (1.5/2.5µg/mL) plate bound activation under *in vitro* Treg differentiation conditions (IL-2: 46ng/ml, TGFβ: 10ng/ml) (n=4, naïve $CD4^+$ cells isolated from human PBMCs).



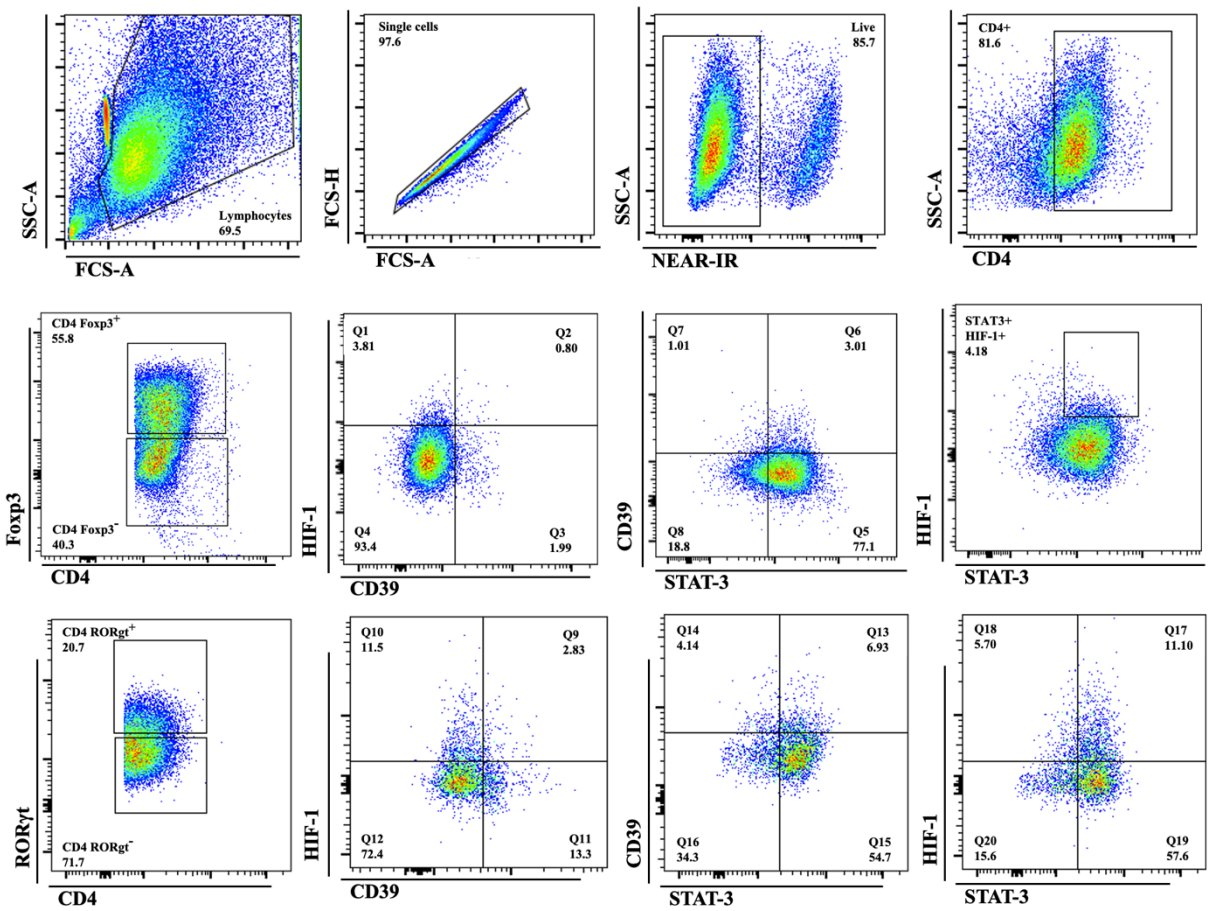
Supplementary Figure S7) Effect of exogenous EPA supplementation on the viability of human CD4$^+$ T cell *in* vitro ceramide treatment model

Quantification of the Near IR$^-$ (Live) cells within the human CD4$^+$ T cells monoculture treated with C24 or C6 ceramides (0.01 and 0.1µM) or candidate ceramides supplemented with EPA (50µM) as well as the untreated vehicle controls. All the cells were activated by CD3/CD28 (1.5/2.5µg/mL) plate bound activation under *in vitro* Treg differentiation conditions (IL-2: 46ng/ml and TGFβ: 10ng/ml) for 5 days. (n=3 with 2 technical replicated per donor, naïve CD4$^+$ cells isolated from human PBMCs). One-way ANOVA; Data presented as mean ± SEM, *p<0.05; ** p<0.01, *** p<0.001.



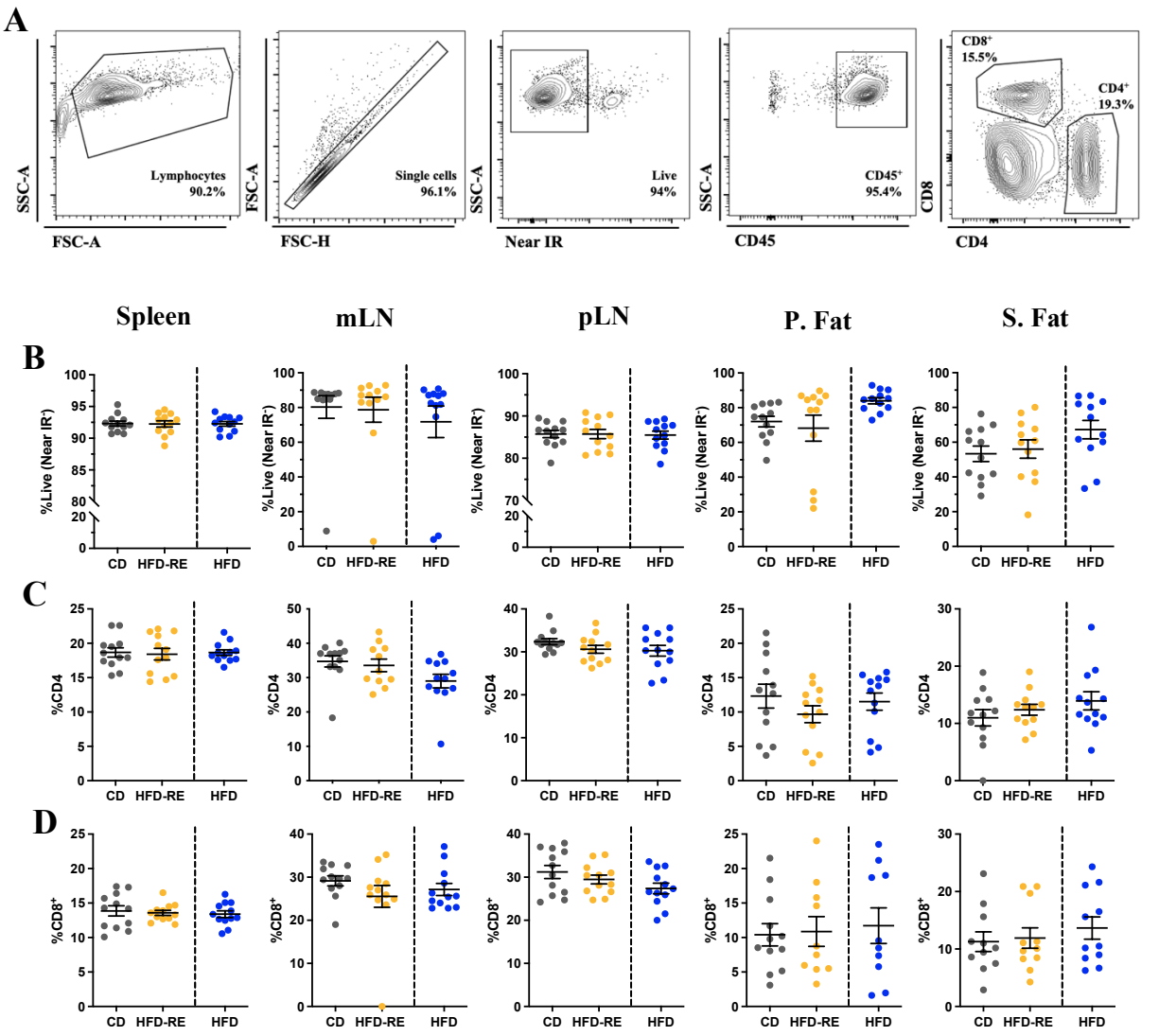
Supplementary Figure S8) IL-6 cytokine concentrations within *in vitro* C24-treated murine CD4$^+$ T cells under Treg differentiation conditions

IL-6 cytokine concentration (pg/ml) within the *in vitro* **(A)** murine (pooled naive CD4$^+$ T cells from n=5-6 mice) CD4$^+$ T cell monoculture media measured by ELISA. Cell culture media obtained from the corresponding *in vitro* samples as analysed by flow cytometry in **Figure 4.13-4.14**.



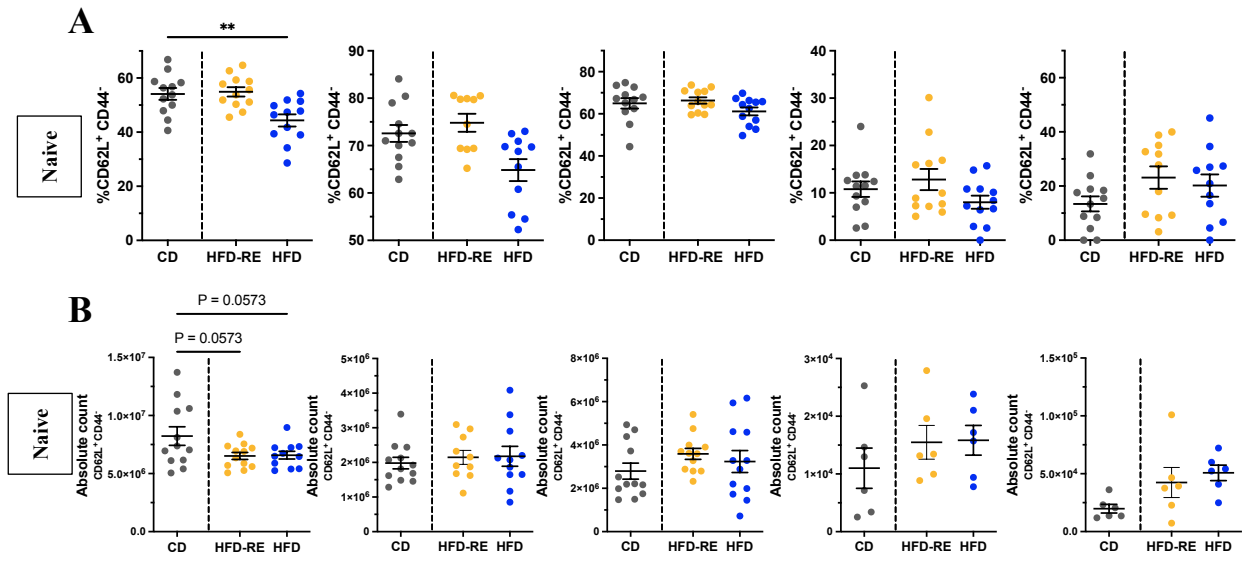
Supplementary Figure S9) Representative flow cytometry plots illustrating the full gating strategy utilised to analyse *in vitro* C24-treated human CD4$^+$ T cells under Treg differentiation condition model

All intracellular markers gated on live total CD4$^+$ T singlets obtained from vehicle control and C24 0.1μM groups, all conditions were activated by CD3/CD28 (1.5/2.5μg/mL) plate bound activation. Both vehicle control and C24 treated samples were kept under Treg differentiation conditions; Treg IL-2: 46ng/ml and TGFβ: 10ng/ml over 5 days *in vitro* ceramide treatment.



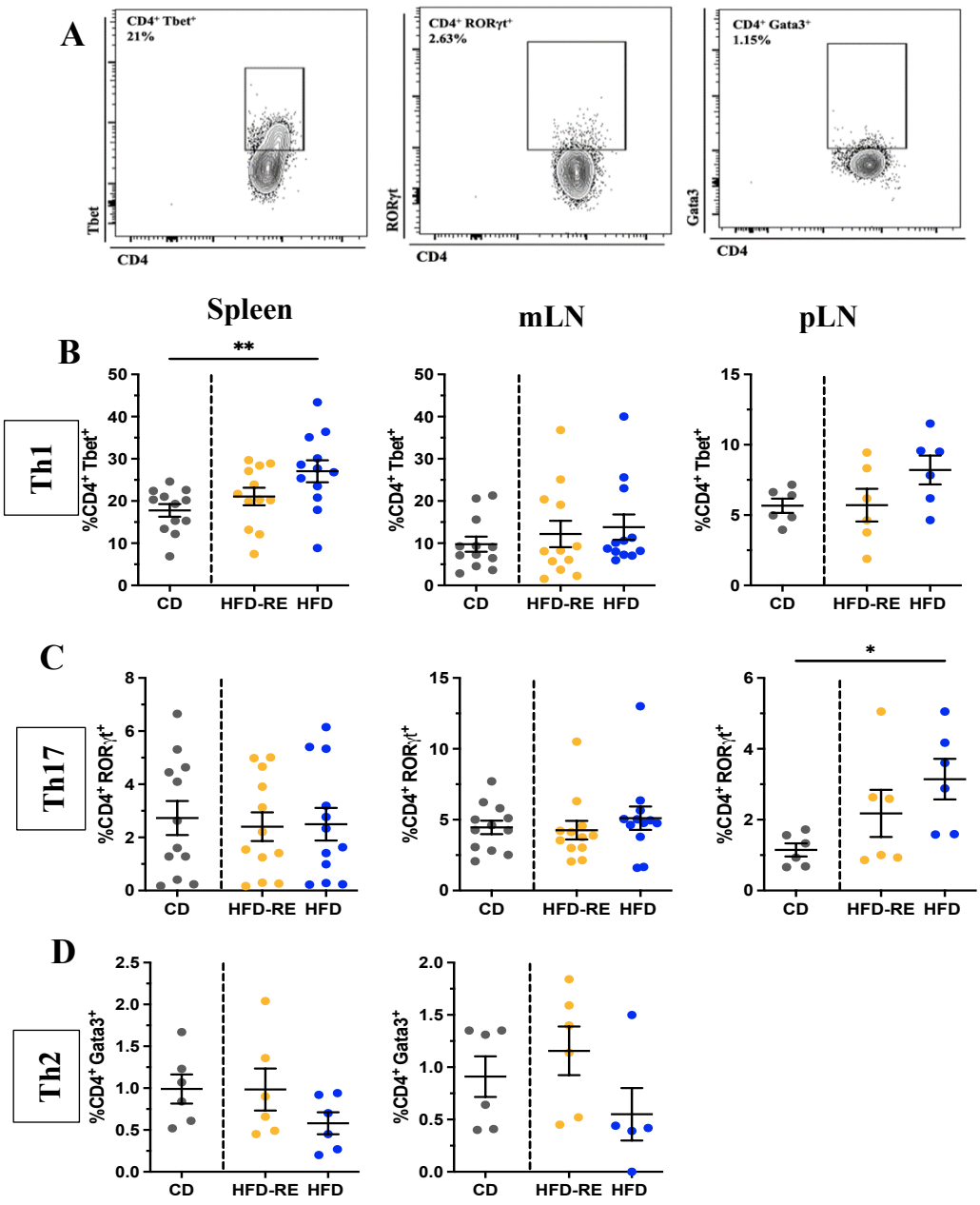
Supplementary Figure S10) Effects of HFD and HFD-RE (WGWL) on total live CD4$^+$ and CD8$^+$ T cell populations within SLOs and fat tissues

(A) Representative flow cytometry gating strategy used to gate on total live lymphocytes and then tissue CD45$^+$ CD4$^+$ and CD8$^+$ T cell populations of the SLOs and fat tissues analysed. **(B)** Quantification of total live lymphocyte as percentage isolated from SLOs (spleen, mLNs, pLNs) and fat tissues (p.fat and s.fat) tissues of female C57BL/6J mice fed on CD, HFD, and HFD-RE (8-wk HFD and 6-wk CD) for 14-weeks and were subjected to an allogeneic immunisation at 13.week with CBA and BALB/C splenocyte i.p injection. **(C)** Quantification of total live CD4$^+$ T cell percentage isolated from SLOs and fat tissues. **(D)** Quantification of total live CD8$^+$ T cell percentage isolated from SLOs and fat tissues. Each point represents an individual mouse in allocated diet groups (two *in vivo* experimental dataset with 6 mice per group shown together, n=12 in total). One-way ANOVA with Dunnett's correction; Data presented as mean ± SEM.

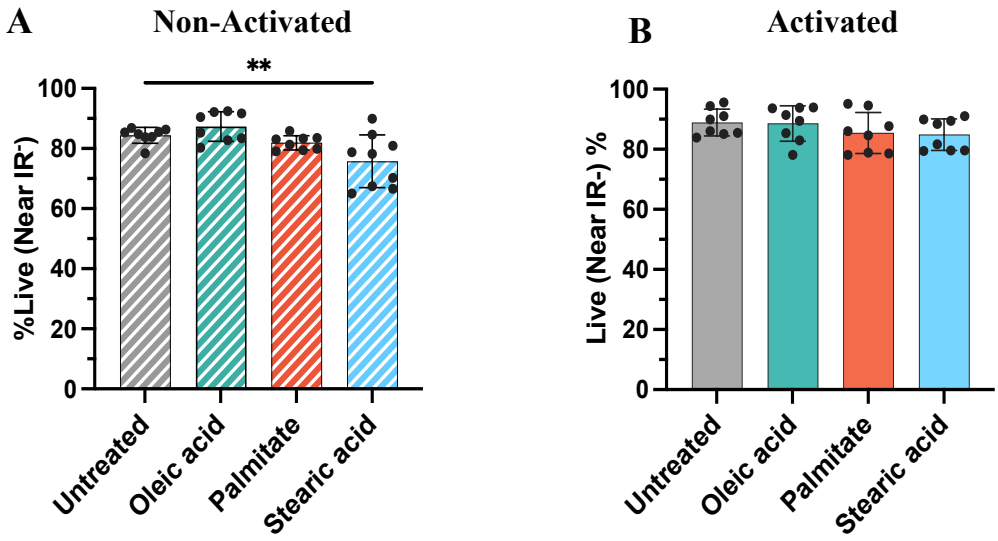


Supplementary Figure S11) Effects of HFD and HFD-RE (WGWL) on naive CD8$^+$ T cell populations within SLOs and fat tissues

Quantification of flow cytometry data on **(A)** naïve (CD44$^-$ and CD62L$^+$) frequencies and **(B)** absolute cell counts of naïve (CD44$^-$ and CD62L$^+$) CD8$^+$ T cells populations within three different SLOs and fat tissues obtained from different diet groups. Each point represents an individual mouse in allocated diet groups (two *in vivo* experimental dataset with 6 mice per group shown together, n=12 in total). One-way ANOVA with Dunnett's correction; Data presented as mean ± SEM, *p<0.05; ** p<0.01, *** p<0.001.

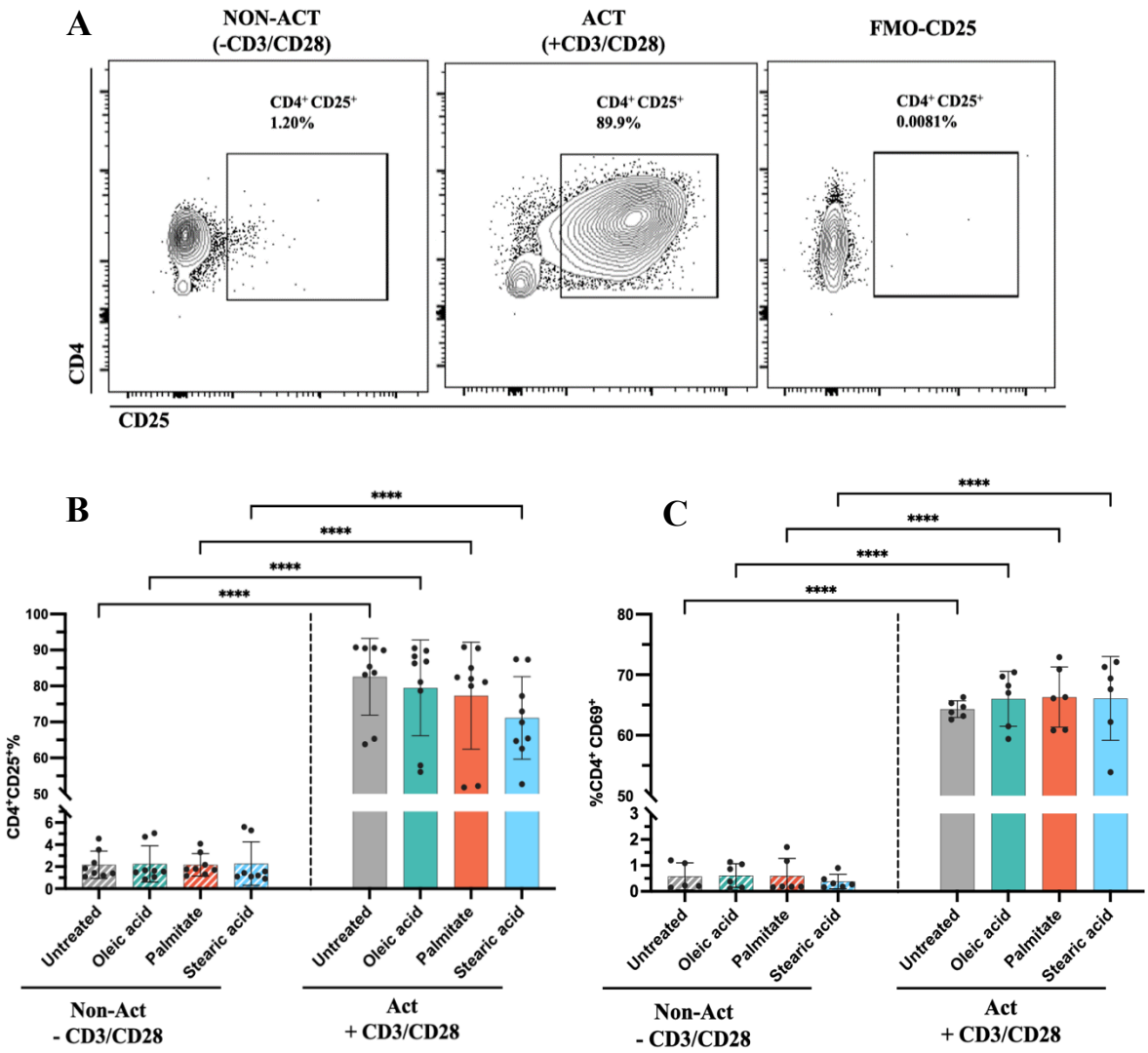


Supplementary Figure S12) HFD feeding induced alterations in main effector CD4$^+$ T cell subsets **(A)** Representative flow figures of the key intracellular transcription markers for distinct CD4$^+$ effector T cell subsets; Tbet$^+$, RORγt$^+$, Gata3$^+$ on spleen tissue of female C57BL/6J mice fed on CD control group, subjected to an allogeneic immunisation at week 13. Quantification of flow cytometry data of **(B)** Tbet$^+$ for Th1 **(C)** RORγt$^+$ for Th17 and **(D)** Gata3$^+$ for Th2 effector CD4$^+$ T cell populations within SLO tissues obtained from female C57BL/6J mice fed on CD, HFD, and HFD-RE (8-wk HFD and 6-wk CD) for 14-weeks and were subjected to an allogeneic immunisation at 13.week with CBA and BALB/C splenocyte i.p injection.. Each point represents an individual mouse in allocated diet groups (two *in vivo* experimental dataset with 6 mice per group shown together, n=12 in total). One-way ANOVA with Dunnett's correction; Data presented as mean ± SEM, *p<0.05; ** p<0.01, *** p<0.001. § Due to the experimental limitations encountered during the second *in vivo* experiment (n=6) cells from pLN were prioritised for other analysis methods.



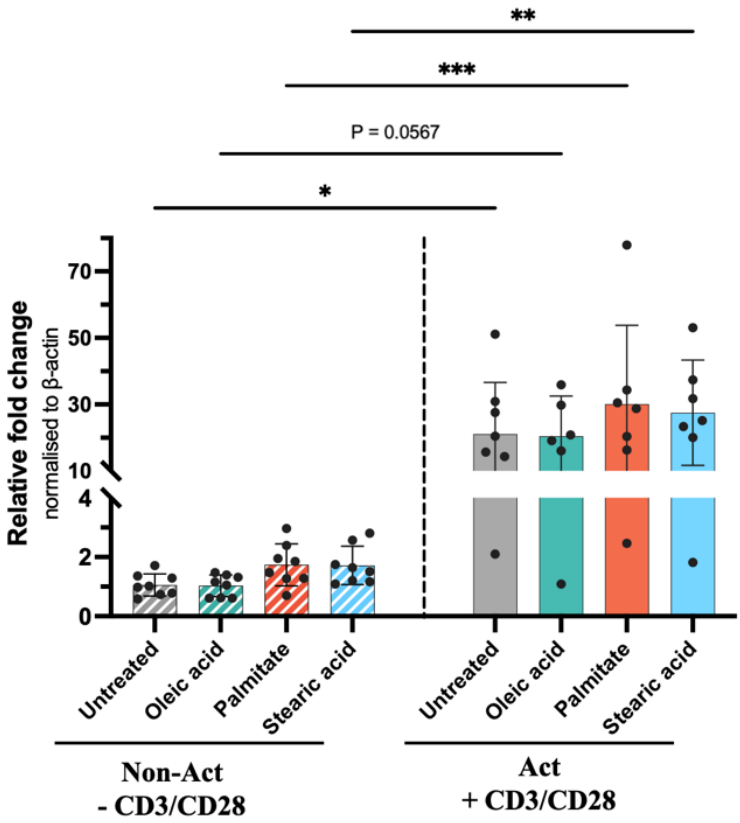
Supplementary Figure S13) Cell viability of human CD4$^+$ T cells on 3-day *in vitro* lipid treatment assay

Quantification of Near IR$^-$ Live human CD4$^+$ T cell frequencies pre-treated with 50µM of Oleic acid, Palmitate, stearic acid overnight without any activation signal. Cells were then **(A)** either left non-activated or **(B)** activated with CD3 (2.5µg/mL) and CD28 (1.5µg/mL) for 48 hours following the overnight lipid pre-treatment. The untreated control group represents the vehicle control group and received the ethanol: BSA (1:4) solution used for the solubilisation of lipid groups. Each point represents an individual technical replicate of the treatment group (n=4). Kruskal-Wallis with Dunnett's correction; Data presented as mean ± SEM, *p<0.05, ** p<0.01, *** p<0.001.



Supplementary Figure S14) Activation status of human CD4$^+$ T cells on 3-day *in vitro* lipid treatment assay with 48hrs of CD3 and CD28 stimulation

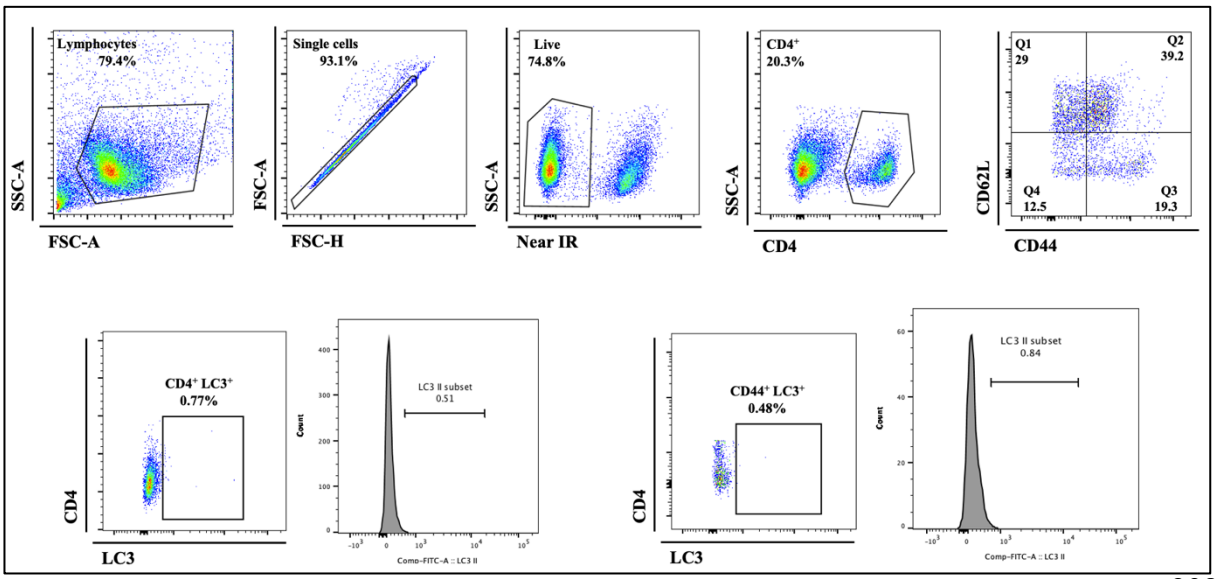
(A) Representative flow cytometry plots of CD25 (IL-2 receptor α chain- IL-2RA) activation marker expression on non-activated, activated and the FMO control (used to place the gating) in the untreated human CD4$^+$ T cell (vehicle control group). Quantification of **(B)** CD25$^+$ and **(C)** CD69$^+$ expression on human CD4$^+$ T cell pre-treated with 50µM of Oleic acid, Palmitate, stearic acid overnight without any activation signal. Cells were then either left non-activated or activated with plate bound CD3 (2.5µg/mL) and CD28 (1.5µg/mL) for 48 hours following the overnight lipid pre-treatment. The untreated control group represents the vehicle control group and received the ethanol: BSA (1:4) solution used for the solubilisation of lipid groups. Each point represents an individual technical replicate of the treatment group (n=4). Kruskal-Wallis with Dunnett's correction; Data presented as mean ± SEM, *p<0.05, ** p<0.01, *** p<0.001.



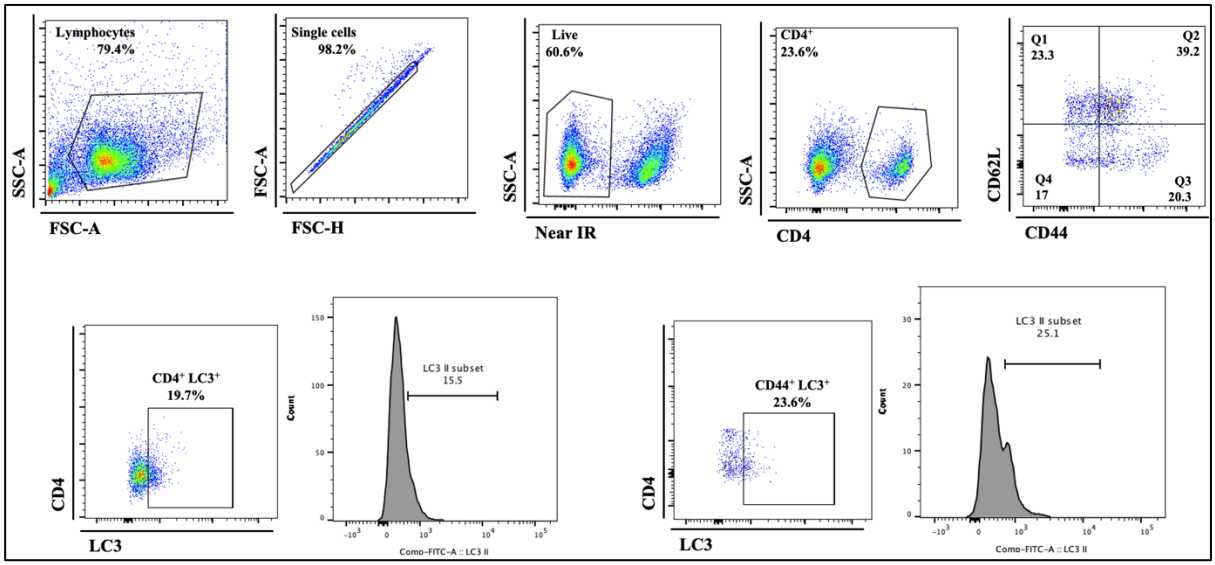
Supplementary Figure S15) IL-2Rα (CD25) mRNA expression within human CD4$^+$ T cells on 3-day *in vitro* lipid treatment assay

IL-2Rα mRNA expression within the human CD4$^+$ T cells pre-treated with 50µM of Oleic acid, palmitate, stearic acid overnight without any activation signal. Cells were then either left non-activated or activated with plate bound CD3 (2.5µg/mL) and CD28 (1.5µg/mL) for 48 hours following the overnight lipid pre-treatment. The untreated control group represents the vehicle control group and received the ethanol: BSA (1:4) solution used for the solubilisation of lipid groups. Each point represents an individual technical replicate of the treatment group (n=3). Kruskal-Wallis with Dunnett's correction; Data presented as mean ± SEM, *p<0.05, ** p<0.01, *** p<0.001.

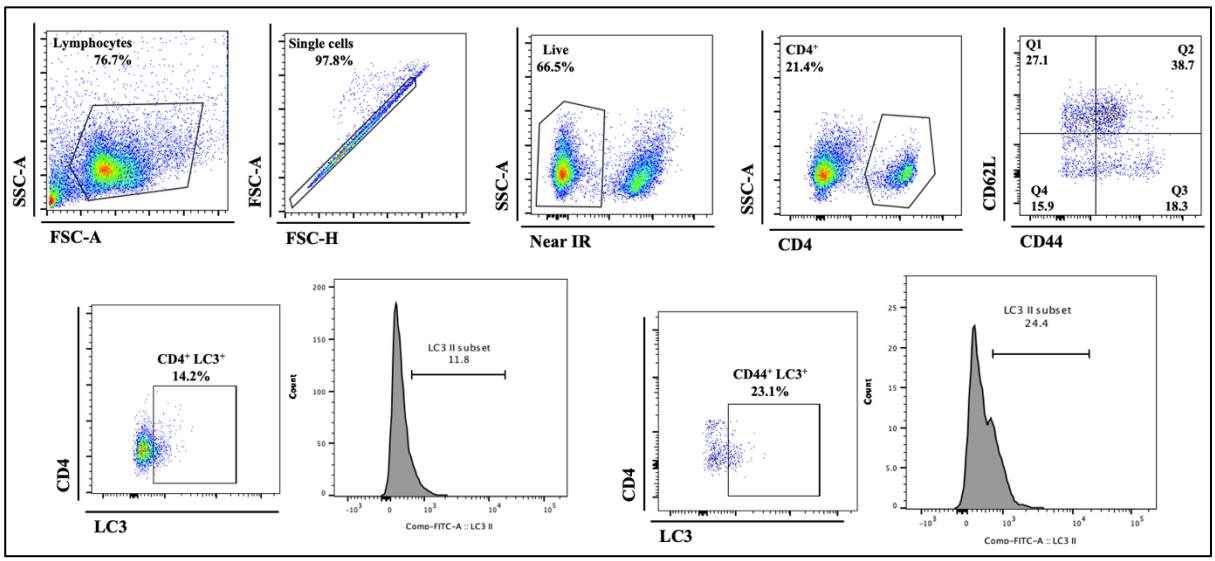
A - CQ (V. control)



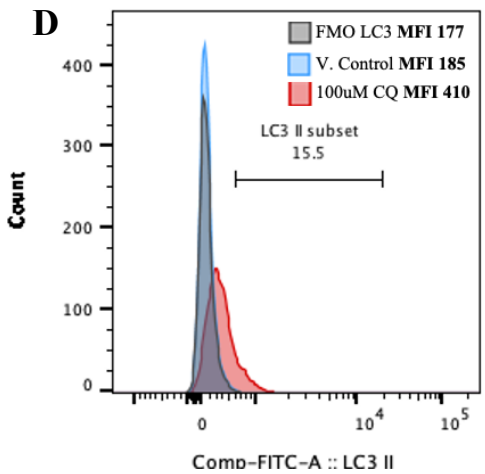
B **100μM CQ**



C **100μM CQ + Starvation**

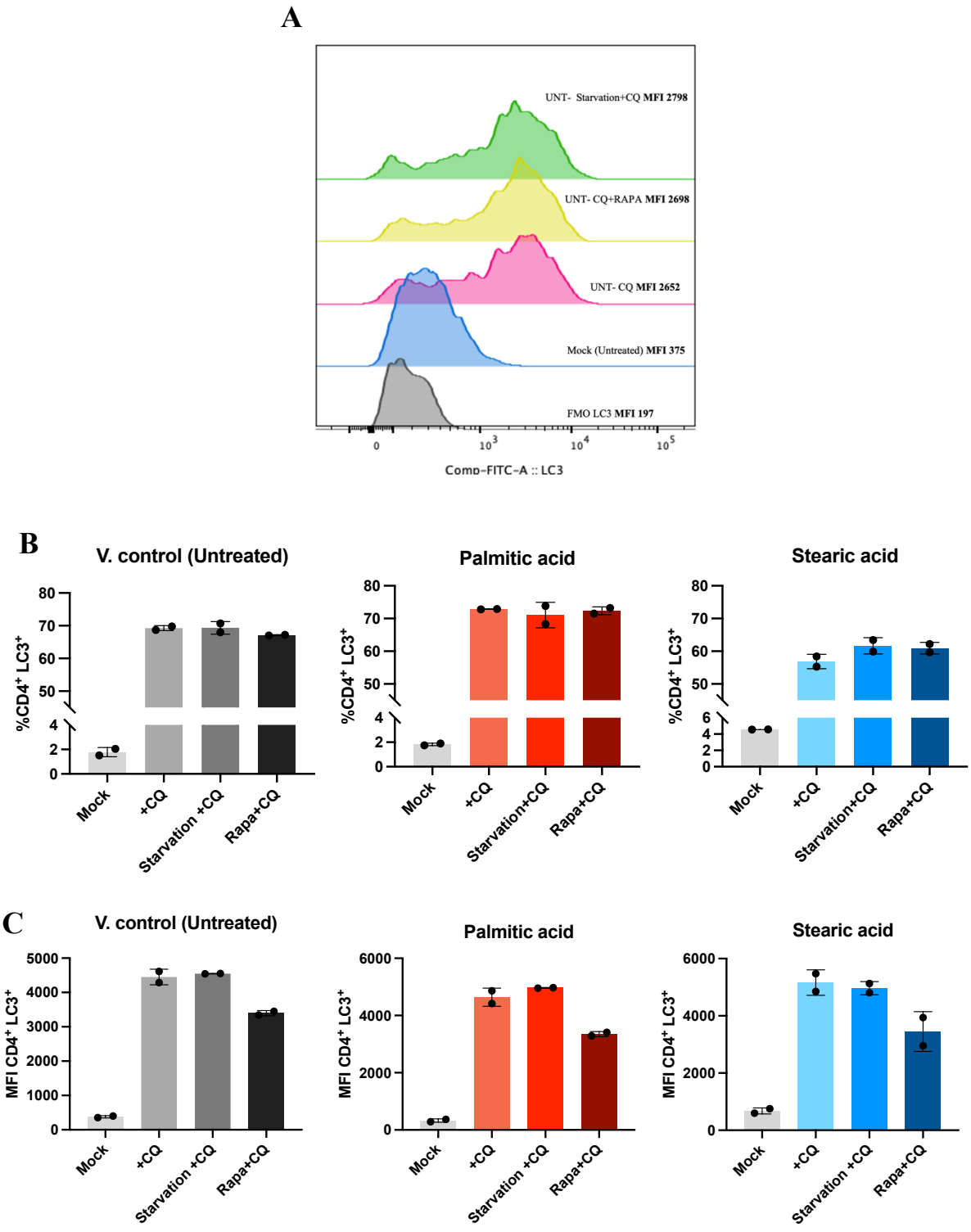


D



Supplementary Figure S16) Optimisation of autophagy flux detection within mouse splenocytes by quantifying autophagosome -bound intracellular LC3-II via Guava kit

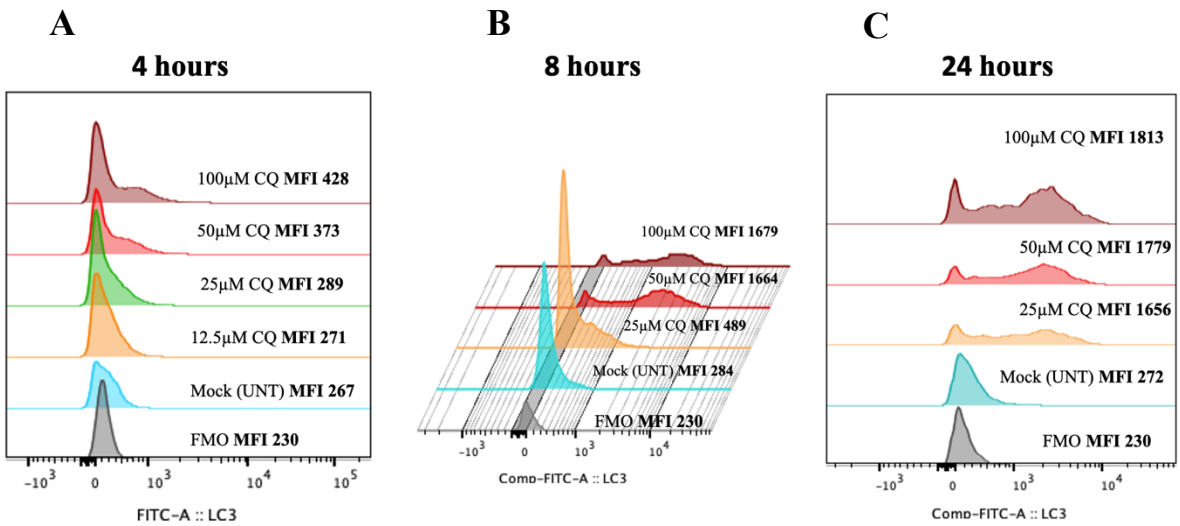
Representative flow cytometry plots and the complete gating strategy used on murine $CD4^+$ T cells isolated from female WT C57BL/6J mice (fed on CD) spleen. Splenocytes were incubated for 4hrs within **(A)** vehicle control solution used to solubilise chloroquine (CQ) **(B)** 100µM of CQ within RPMI media with 2% FCS and **(C)** 100µM of CQ within HBSS. All the conditions were initially stained for extracellular markers such as Live/Dear marker Near IR, CD4, CD44, CD62L and the stained for LC3-II by following the Guava's specific protocol as detailed in **Section 2.14.4**. **(D)** Histogram representation of shift in LC3-II MFI levels between FMO gating control (grey), CQ vehicle control (blue) and 100µM of CQ in RPMI media.



Supplementary Figure S17) Optimisation of autophagy flux detection within human PBMCs by quantifying autophagosome-bound intracellular LC3-II via Guava kit

(A) Representative flow cytometry histogram plots illustrating the shift in LC3-II MFI within FMO gating control (grey), CQ Mock vehicle control (blue), 100µM CQ in RPMI media (pink), 100µM CQ+ 0.1µM Rapamycin in RPMI media (yellow) and starvation conditions in HBSS (green). Quantification of $LC3^+$ $CD4^+$ T cell **(B)** frequencies in percentage and **(C)** MFI levels of conditions within human $CD4^+$

T cells pre-treated with 50µM of Palmitate, stearic acid and untreated vehicle control (for lipid treatment) overnight without any activation signal. Cells were then activated with plate bound CD3 (2.5µg/mL) and CD28 (1.5µg/mL) for 48 hours following the overnight lipid pre-treatment.



Supplementary Figure S18) Optimisation the dose- and time- response of CQ in autophagy flux detection within human PBMCs by quantifying autophagosome-bound intracellular LC3-II via Guava kit

(A) Representative flow cytometry histogram plots illustrating the shift in LC3-II MFI within FMO gating control (grey), CQ Mock vehicle control (blue), 12.5µM CQ (orange), 25µM CQ (green), 50µM CQ (red) and 100µM CQ (dark-red) non-lipid treated (untreated) human PBMC samples incubated *in vitro* for **(A)** 4 hours **(B)** 8 hours and **(C)** 24 hours. All cells were activated with plate bound CD3 (2.5µg/mL) and CD28 (1.5µg/mL) for 48 hours.